EDITED BY
PARDEEP SINGH
ANWESHA BORTHAKUR
P.K. MISHRA
DHANESH TIWARY

Nano-Materials as Photocatalysts for Degradation of Environmental Pollutants

CHALLENGES AND POSSIBILITIES

ELSEVIER

Nano-Materials as Photocatalysts for Degradation of Environmental Pollutants

This book belongs to

Central Library

BADJI Mokhtar-ANNABA UNIVERSITY

Copyright Elsevier 2024

This page intentionally left blank

This book belongs to Central Library BADJI Mokhtar-ANNABA UNIVERSITY

Copyright Elsevier 2024

Nano-Materials as Photocatalysts for Degradation of Environmental Pollutants

Challenges and Possibilities

Edited by

Pardeep Singh
Anwesha Borthakur
P.K. Mishra
Dhanesh Tiwary

ELSEVIER

This book belongs to Central Library BADJI Mokhtar-ANNABA UNIVERSITY

Copyright Elsevier 2024

Elsevier
Radarweg 29, PO Box 211, 1000 AE Amsterdam, Netherlands
The Boulevard, Langford Lane, Kidlington, Oxford OX5 1GB, United Kingdom
50 Hampshire Street, 5th Floor, Cambridge, MA 02139, United States

© 2020 Elsevier Inc. All rights reserved.

No part of this publication may be reproduced or transmitted in any form or by any means, electronic or mechanical, including photocopying, recording, or any information storage and retrieval system, without permission in writing from the publisher. Details on how to seek permission, further information about the Publisher's permissions policies and our arrangements with organizations such as the Copyright Clearance Center and the Copyright Licensing Agency, can be found at our website: www.elsevier.com/permissions.

This book and the individual contributions contained in it are protected under copyright by the Publisher (other than as may be noted herein).

Notices
Knowledge and best practice in this field are constantly changing. As new research and experience broaden our understanding, changes in research methods, professional practices, or medical treatment may become necessary.

Practitioners and researchers must always rely on their own experience and knowledge in evaluating and using any information, methods, compounds, or experiments described herein. In using such information or methods they should be mindful of their own safety and the safety of others, including parties for whom they have a professional responsibility.

To the fullest extent of the law, neither the Publisher nor the authors, contributors, or editors, assume any liability for any injury and/or damage to persons or property as a matter of products liability, negligence or otherwise, or from any use or operation of any methods, products, instructions, or ideas contained in the material herein.

Library of Congress Cataloging-in-Publication Data
A catalog record for this book is available from the Library of Congress

British Library Cataloguing-in-Publication Data
A catalogue record for this book is available from the British Library

ISBN: 978-0-12-818598-8

For information on all Elsevier publications
visit our website at https://www.elsevier.com/books-and-journals

Publisher: Susan Dennis
Acquisition Editor: Kostas KI Marinakis
Editorial Project Manager: Laura Okidi
Production Project Manager: Vignesh Tamil
Cover Designer: Miles Hitchen

Typeset by SPi Global, India

ELSEVIER Book Aid International Working together to grow libraries in developing countries
www.elsevier.com • www.bookaid.org

This book belongs to Central Library BADJI Mokhtar-ANNABA UNIVERSITY

Copyright Elsevier 2024

Contents

Contributors xv

CHAPTER 1 An overview of synthesis techniques for preparing doped photocatalysts 1
Indrajit Sinha and Arup Kumar De

1 General introduction 1
2 Doped semiconductors: An introduction 3
2.1 Synthesis techniques used prepare doped semiconductors: 3
3 Sonochemical synthesis 6
4 Reverse micelles 7
5 Conclusions 8
References 9
Further reading 13

CHAPTER 2 Low-dimensional nanomaterials for the photocatalytic degradation of organic pollutants 15
Debabrata Mishra and Manish Srivastava

1 Introduction 15
2 Methods of degradation of organic pollutants 16
3 Photocatalytic degradation using graphene-based nanostructures 18
3.1 Fe/Co/Ni-based graphene composites 18
3.2 (Zn/Ti/W/Ce)O-based graphene composites 21
3.3 Metal-/nonmetal (N)-based graphene nanocomposites 25
4 Photoelectrochemical technique 25
4.1 Mechanism of photoelectrocatalysis 26
5 Conclusions 31
Acknowledgments 31
References 31

CHAPTER 3 Recent advances in functionalized polymer-based composite photocatalysts for wastewater treatment 39
Zeenat Arif, Naresh K. Sethy, Lata Kumari, P.K. Mishra, and S.N. Upadhyay

1 Wastewater: Problems, environmental effect 39
2 Photocatalyst 42
2.1 Principles of photocatalysis 42
3 Need of supported system 46
3.1 Drawbacks of NPs in powder form 46

This book belongs to Central Library BADJI Mokhtar-ANNABA UNIVERSITY

Copyright Elsevier 2024

3.2 Immobilization of NPs has the following advantages 46
3.3 Polymer as a support 47
3.4 Various polymeric substrates 47
3.5 Different methods for supporting NPs on polymer substrate 48
4 Characterization of polymer nanocomposite 52
5 Photoreactor: Evaluation of photocatalytic activity 52
6 Surface modification of polymeric nanocomposite 54
7 Future research 57
8 Conclusion 58
References 58
Further reading 64

CHAPTER 4 Solar light-induced photocatalytic degradation of pharmaceuticals in wastewater treatment 65
Snehamol Mathew, Priyanka Ganguly, Vignesh Kumaravel, John Bartlett, and Suresh C. Pillai

1 Introduction 65
2 Pharmaceutical waste in water resources 65
3 Health effects of pharmaceutical waste 66
4 Solar active photocatalytic degradation of pharmaceuticals 68
4.1 Photocatalytic degradation mechanism 68
4.2 Titania-based materials 69
4.3 Graphene-based materials 70
4.4 Metal-organic frameworks (MOFs) 71
4.5 Novel composites 73
5 The scope of photocatalysis for wastewater treatment 74
6 Conclusions 74
Acknowledgment 75
References 75

CHAPTER 5 Hydrotalcite-like compounds and related materials as catalysts for the photodegradation of pharmaceutical compounds: Synthesis and catalytic performances 79
Leticia Santamaría, Antonio Gil, Miguel Angel Vicente, and Sophia A. Korili

1 Introduction 79
2 Structure of hydrotalcites 81
3 Preparation of hydrotalcites 83
4 Hydrotalcites in the photodegradation of pharmaceuticals 85
5 Conclusions and perspectives 88
Acknowledgments 88
References 88

This book belongs to Central Library BADJI Mokhtar-ANNABA UNIVERSITY Copyright Elsevier 2024

CHAPTER 6 Metal-organic frameworks for photocatalytic degradation of pollutants ... 91
Harpreet Kaur, Ajay Kumar, Rik Rani Koner, and Venkata Krishnan

1 Introduction ... 91
2 Metal-organic frameworks: Design, synthesis strategies, and characterizations ... 94
2.1 Design considerations ... 96
2.2 Synthesis strategies ... 97
2.3 Characterizations ... 100
3 Photocatalytic pollutant degradation using metal-organic frameworks ... 108
3.1 Fe-based MOFs ... 108
3.2 Co- and Ni-based MOFs ... 109
3.3 Zn-based MOFs ... 111
3.4 Cd-based MOFs ... 114
3.5 Other metal-based MOFs ... 115
4 Summary and perspectives ... 116
References ... 118
Further reading ... 126

CHAPTER 7 Photocatalytic degradation of petrochemical pollutants ... 127
Anupma Thakur, Praveen Kumar, Pardeep Singh, and Pooja Devi

1 Introduction: Petrochemical industry ... 127
2 Petrochemical pollutants: Geological spread, toxicity, regulation, and environmental stress ... 128
3 Methods of petrochemical pollutants degradation ... 131
4 Photocatalytic degradation of petrochemical pollutants: Principles and kinetic concepts of photo catalysis ... 131
5 Perspectives and advances in photocatalysts for petrochemical degradation ... 133
5.1 UV/Visible light-driven photocatalysts ... 134
5.2 Heterogeneous photocatalysts (binary, ternary, etc.) ... 136
6 Summary ... 137
Acknowledgements ... 137
References ... 138

CHAPTER 8 Photodegradation of pharmaceutical waste by nano-materials as photocatalysts ... 143
Yong Chen

1 Introduction ... 143
2 Pharmaceuticals ... 144
3 Nanotechnology for pharmaceutical waste treatment ... 145
4 Photodegradation of pharmaceuticals ... 145
5 Degradation pathways for pharmaceuticals and eco toxicity of photoproducts ... 145
6 Nanophotocatalysts ... 146

This book belongs to Central Library BADJI Mokhtar-ANNABA UNIVERSITY Copyright Elsevier 2024

7 Metal/metal oxide nanoparticles ... 146
8 Carbon-based nanomaterials ... 147
9 Zeolites ... 147
10 Heterogeneous photocatalysis ... 147
11 Semiconductor nanophotocatalyst ... 148
12 Current scenario and future prospectus ... 149
13 Conclusion ... 150
References ... 150

CHAPTER 9 Photocatalytical degradation of pesticides ... 153
Deepak Pathania, Manita Thakur, and Arush Sharma

1 Introduction ... 153
2 Entry of pesticides into animals ... 154
2.1 Dermal entry ... 154
2.2 Oral entry ... 154
2.3 Respiratory entry ... 155
3 Types of insecticides ... 155
3.1 Classification based on types of pests that they kill ... 155
3.2 Classification based on biodegradability ... 155
3.3 Chemically related pesticides ... 156
4 Usage of pesticides in India ... 157
5 Harmful effects of pesticides ... 158
5.1 Effect on human ... 159
5.2 Effect on biodiversity ... 159
5.3 Soil contamination ... 160
6 Different methods for the degradation of pesticides ... 161
6.1 Physical processes for remediation of pesticides ... 162
6.2 Chemical treatment for removal of pesticides ... 163
6.3 Adsorption ... 165
6.4 Biological treatment ... 165
6.5 Photocatalysis ... 167
7 Conclusions ... 168
References ... 168

CHAPTER 10 Imidazole framework based metal oxide nanoparticles photocatalysts: An approach towards amputation of organic pollutants from water ... 173
Benjamin Raj, Arun Kumar Padhy, Gajendra Prasad Singh, Ratan Kumar Dey, and Ramesh Oraon

1 Introduction ... 173
1.1 Classification of dye ... 174
1.2 Definition of photocatalysis ... 176

This book belongs to Central Library BADJI Mokhtar-ANNABA UNIVERSITY Copyright Elsevier 2024

2 Photocatalysis for pollutant degradation 177
3 Imidazole and imidazole-derived metal oxide photocatalyst 182
3.1 Structure, reactivity, and properties 182
3.2 Literature review on imidazole-based metal complexes and metal oxides 182
4 Prospects and challenges of imidazole framework-based metal oxide photocatalyst 186
5 Summary 188
References 188

CHAPTER 11 Exploitation of antibiotics: Mechanism of resistance, consequences, challenges of conventional remediation, and promise of nanomaterials in mitigation 195
Niloy Sarkar, Radhey Shyam Sharma, and Mahima Kaushik

1 Introduction 195
2 Classes of antibiotics and their mechanism of action 196
3 Sources of antibiotic pollutants 196
3.1 Pharmaceutical 196
3.2 Animal husbandry 198
4 Percolation of antibiotics into the environment 198
5 Environmental consequences of antibiotic pollution 199
6 Development of antibiotic-resistant genes (ARGs) and bacteria (ARB) 199
6.1 Intrinsic 200
6.2 Acquired 201
7 Consequences on human health 202
8 Challenges in conventional wastewater treatment methods in remediation of antibiotic pollutants 202
9 Nanomaterials in antibiotic pollution mitigation 205
9.1 Detection 205
9.2 Degradation 206
10 Conclusions 206
Acknowledgments 207
References 207

CHAPTER 12 Photochemical and photocatalytical degradation of antibiotics in water promoted by solar irradiation 211
Ricardo A. Torres-Palma, Efraím A. Serna-Galvis, and Yenny P. Ávila-Torres

1 Introduction 211
1.1 Environmental concern of antibiotics 211
1.2 Antibiotics classification and their presence in waters 211
2 Photochemical degradation of antibiotics by solar light 212

This book belongs to Central Library BADJI Mokhtar-ANNABA UNIVERSITY
Copyright Elsevier 2024

2.1 Sunlight action on antibiotics 212
2.2 Environmental implications of photodegradation using sunlight 224
3 Heterogeneous photocatalysis for antibiotics degradation 225
3.1 Photocatalytic process based on TiO_2 225
3.2 Photocatalytic process using nanomaterials for antibiotics degradation 230
4 Concluding remarks 236
References 237
Further reading 243

CHAPTER 13 Carbon-supported semiconductor nanoparticles as effective photocatalysts for water and wastewater treatment 245
Jaimy Scaria, Ansaf V. Karim, G. Divyapriya, P.V. Nidheesh, and M. Suresh Kumar

1 Introduction 245
2 Various carbonaceous materials as support for semiconductor photocatalysts 246
2.1 Activated carbon 247
2.2 Mesoporous carbon 248
2.3 Fullerene 248
2.4 Carbon nanotubes 250
2.5 Graphene 252
2.6 Carbon quantum dots 262
2.7 Carbon nanofibers 264
2.8 Carbon black 265
2.9 Graphitic carbon nitride 265
3 Conclusion and future perspectives 266
References 267

CHAPTER 14 Synthesis of graphitic carbon nitride—Nanostructured photocatalyst 279
Bin Xue

1 Introduction 279
2 Synthesis of bulk g-C_3N_4 281
3 Synthesis of g-C_3N_4 QDs 281
4 Synthesis of 1D g-C_3N_4 285
5 Synthesis of g-C_3N_4 nanosheets 287
6 Synthesis of 3D g-C_3N_4 294
7 Conclusion and outlook 297
Acknowledgments 299
References 299

This book belongs to Central Library BADJI Mokhtar-ANNABA UNIVERSITY Copyright Elsevier 2024

CHAPTER 15 Advancement and modification in photoreactor used for degradation processes 305
Gyanendra Tripathi, Dhirendra Kumar Srivastava, Jyoti Singh, and Vishal Mishra

1 Introduction 305
2 Remediation 306
3 Photoremediation 306
4 Semiconductor nanoparticles as a photocatalyst 307
5 Advancement of photocatalyst/auxiliary structure and properties of photocatalysts 308
5.1 Zero-dimensional 308
5.2 One-dimensional 309
5.3 Two-dimensional 311
5.4 Three-dimensional 312
6 Advancement of photoreactor in terms of applications for the degradation of the following contaminants 313
6.1 Dye 313
6.2 Drugs 316
6.3 Organic and microorganism 317
7 Conclusion 318
References 318

CHAPTER 16 Nanocatalyst types and their potential impacts in agroecosystems: An overview 323
Rahul Bhadouria, Disha Mishra, Vipin Kumar Singh, Pardeep Singh, Pratap Srivastava, Sachchidanand Tripathi, and Rishikesh Singh

1 Introduction 323
2 Metal-based nanocatalysts 324
2.1 Core-shell nanocatalyst 325
2.2 Silica nanomaterials 325
2.3 Layered double hydroxides 326
2.4 Nanocarbon catalysts 326
2.5 Quantum dots 327
2.6 Polymeric nanomaterials 327
3 Nanocatalysts in agriculture 327
4 Fate and transport of nanocatalysts in agroecosystems 330
5 Multifaceted benefits of nanocatalysts application on soil, plant, and microorganisms 332
6 Role of nanoparticles in agrowaste management 332

This book belongs to Central Library BADJI Mokhtar-ANNABA UNIVERSITY
Copyright Elsevier 2024

7 Unprecedented negative impacts of nanocatalysts in agriculture: Effect on soil, plant, and microorganisms ... 334
8 Nanocatalysts in agriculture: Boon or bane ... 336
9 Conclusion and future recommendations ... 336
Acknowledgments ... 337
References ... 337
Further reading ... 344

CHAPTER 17 Nanotechnology for soil remediation: Revitalizing the tarnished resource ... 345
Mansi Bakshi and P.C. Abhilash

1 Introduction ... 345
1.1 Soil contamination: Current scenario ... 345
1.2 Nanotechnology: Uses and applications in soil remediation ... 346
2 Role of nanomaterials in heavy metal removal from soil ... 348
3 Nanotechnology for pesticides and persistent organic pollutant (POP) remediation ... 351
3.1 Nanoremediation of pesticides and persistent organic pollutants (POPs) ... 351
3.2 Nanotechnology-based biosensing systems for pesticide residue detection ... 355
4 Role of nanotechnology for enhancing phytoremediation and bioremediation ... 357
5 Hopes, uncertainties, and future research needs ... 362
Acknowledgments ... 363
References ... 363
Further reading ... 370

CHAPTER 18 Overview of nanomaterials synthesis methods, characterization techniques and effect on seed germination ... 371
Somenath Das, Arpan Mukherjee, Gereraj Sengupta, and Vipin Kumar Singh

1 Introduction ... 371
2 Methods of nanomaterial synthesis ... 373
3 Characterization techniques for nanoparticles ... 375
3.1 Microscopic techniques ... 379
4 X-ray methods: X-ray photoelectron spectroscopy (XPC) and X-ray diffractometry (XRD) ... 380
5 Spectroscopic analysis ... 380
5.1 UV-visible spectroscopy ... 380
5.2 Dynamic light scattering (DLS) ... 381
5.3 Fourier transform infrared spectroscopy (FTIR) ... 381

This book belongs to Central Library BADJI Mokhtar-ANNABA UNIVERSITY Copyright Elsevier 2024

6 Nanoparticle filtration techniques 381
7 Characterization of magnetic features of nanoparticles 382
8 Effect of nanomaterials on seed germination 382
9 Mechanism of nanoparticle action 385
10 Conclusion 391
Acknowledgment 392
References 392
Further reading 401

Index 403

This book belongs to Central Library BADJI Mokhtar-ANNABA UNIVERSITY

Copyright Elsevier 2024

This page intentionally left blank

This book belongs to Central Library BADJI Mokhtar-ANNABA UNIVERSITY

Copyright Elsevier 2024

Contributors

P.C. Abhilash
Institute of Environment & Sustainable Development (IESD), Banaras Hindu University, Varanasi, India

Zeenat Arif
Department of Chemical Engineering and Technology, IIT (BHU) Varanasi, Varanasi, India

Yenny P. Ávila-Torres
Grupo de Investigación Química y Biotecnología (QUIBIO), Facultad de Ciencias Básicas, Universidad Santiago de Cali, Santiago de Cali, Colombia

Mansi Bakshi
Institute of Environment & Sustainable Development (IESD), Banaras Hindu University, Varanasi, India

John Bartlett
Nanotechnology and Bio-Engineering Research Group, Department of Environmental Science, School of Science; Centre for Precision Engineering, Materials and Manufacturing Research (PEM), Institute of Technology Sligo, Sligo, Ireland

Rahul Bhadouria
Department of Botany, University of Delhi, New Delhi, India

Yong Chen
School of Environmental Science and Engineering, Huazhong University of Science and Technology, Wuhan, China

Somenath Das
Department of Botany, Centre of Advanced Study (CAS), Institute of Science, Banaras Hindu University, Varanasi, India

Arup Kumar De
Department of Chemistry, Indian Institute of Technology (Banaras Hindu University), Varanasi, India

Pooja Devi
CSIR-Central Scientific Instruments Organisation, Chandigarh, India

Ratan Kumar Dey
Department of Chemistry, Central University of Jharkhand, Ranchi, Jharkhand, India

G. Divyapriya
Environmental Water Resources Engineering Division, Department of Civil Engineering, Indian Institute of Technology Madras, Chennai, India

Priyanka Ganguly
Nanotechnology and Bio-Engineering Research Group, Department of Environmental Science, School of Science; Centre for Precision Engineering, Materials and Manufacturing Research (PEM), Institute of Technology Sligo, Sligo, Ireland

This book belongs to Central Library BADJI Mokhtar-ANNABA UNIVERSITY

Copyright Elsevier 2024

Antonio Gil
INAMAT, Science Department, Public University of Navarre, Pamplona, Spain

Ansaf V. Karim
Center for Environmental Science and Engineering, Indian Institute of Technology Bombay, Mumbai, India

Harpreet Kaur
School of Basic Sciences, School of Engineering and Advanced Materials Research Center, Indian Institute of Technology Mandi, Mandi, India

Mahima Kaushik
Cluster Innovation Centre, University of Delhi, Delhi, India

Rik Rani Koner
School of Basic Sciences, School of Engineering and Advanced Materials Research Center, Indian Institute of Technology Mandi, Mandi, India

Sophia A. Korili
INAMAT, Science Department, Public University of Navarre, Pamplona, Spain

Venkata Krishnan
School of Basic Sciences, School of Engineering and Advanced Materials Research Center, Indian Institute of Technology Mandi, Mandi, India

Ajay Kumar
School of Basic Sciences, School of Engineering and Advanced Materials Research Center, Indian Institute of Technology Mandi, Mandi, India

Praveen Kumar
School of Material Science, Indian Association for the Cultivation of Science, Kolkata, India

Vignesh Kumaravel
Nanotechnology and Bio-Engineering Research Group, Department of Environmental Science, School of Science; Centre for Precision Engineering, Materials and Manufacturing Research (PEM), Institute of Technology Sligo, Sligo, Ireland

Lata Kumari
Department of Chemistry, IIT (BHU) Varanasi, Varanasi, India

Snehamol Mathew
Nanotechnology and Bio-Engineering Research Group, Department of Environmental Science, School of Science; Centre for Precision Engineering, Materials and Manufacturing Research (PEM), Institute of Technology Sligo, Sligo, Ireland

Debabrata Mishra
Department of Physics and Astrophysics, University of Delhi, Delhi, India

Disha Mishra
Central Institute of Medicinal and Aromatic Plants (CIMAP), Lucknow, India

P.K. Mishra
Department of Chemical Engineering and Technology, IIT (BHU) Varanasi, Varanasi, India

This book belongs to Central Library BADJI Mokhtar-ANNABA UNIVERSITY Copyright Elsevier 2024

Vishal Mishra
School of Biochemical Engineering, IIT (BHU) Varanasi, Varanasi, India

Arpan Mukherjee
Institute of Environment and Sustainable Development, Banaras Hindu University, Varanasi, India

P.V. Nidheesh
Environmental Impact and Sustainability Division, CSIR-National Environmental Engineering Research Institute, Nagpur, India

Ramesh Oraon
Department of Nanoscience and Technology, Central University of Jharkhand, Ranchi, Jharkhand, India

Arun Kumar Padhy
Department of Chemistry, Central University of Jharkhand, Ranchi, Jharkhand, India

Deepak Pathania
Department of Environmental Sciences, Central University of Jammu, Samba, India

Suresh C. Pillai
Nanotechnology and Bio-Engineering Research Group, Department of Environmental Science, School of Science; Centre for Precision Engineering, Materials and Manufacturing Research (PEM), Institute of Technology Sligo, Sligo, Ireland

Benjamin Raj
Department of Chemistry, Central University of Jharkhand, Ranchi, Jharkhand, India

Leticia Santamaría
INAMAT, Science Department, Public University of Navarre, Pamplona, Spain

Niloy Sarkar
Cluster Innovation Centre; Department of Environmental Studies, University of Delhi, Delhi, India

Jaimy Scaria
Academy of Scientific and Innovative Research (AcSIR), Ghaziabad, India

Gereraj Sengupta
Department of Botany, Centre of Advanced Study (CAS), Institute of Science, Banaras Hindu University, Varanasi, India

Efraím A. Serna-Galvis
Grupo de Investigación en Remediación Ambiental y Biocatálisis (GIRAB), Instituto de Química, Facultad de Ciencias Exactas y Naturales, Universidad de Antioquia UdeA, Medellin, Colombia

Naresh K. Sethy
Department of Chemical Engineering and Technology, IIT (BHU) Varanasi, Varanasi, India

Arush Sharma
School of Sciences, Baddi University of Emerging Sciences and Technology (BUEST), Solan, India

Radhey Shyam Sharma
Department of Environmental Studies, University of Delhi, Delhi, India

This book belongs to Central Library BADJI Mokhtar-ANNABA UNIVERSITY Copyright Elsevier 2024

Gajendra Prasad Singh
Department of Nanoscience and Technology, Central University of Jharkhand, Ranchi, Jharkhand, India

Jyoti Singh
School of Biochemical Engineering, IIT (BHU) Varanasi, Varanasi, India

Pardeep Singh
Department of Environmental Studies, PGDAV College, University of Delhi, New Delhi, India

Rishikesh Singh
Institute of Environment & Sustainable Development (IESD), Banaras Hindu University, Varanasi, India

Vipin Kumar Singh
Department of Botany, Centre of Advanced Study (CAS), Institute of Science, Banaras Hindu University, Varanasi, India

Indrajit Sinha
Department of Chemistry, Indian Institute of Technology (Banaras Hindu University), Varanasi, India

Dhirendra Kumar Srivastava
Council of Science and Technology, Lucknow, India

Manish Srivastava
Department of Physics and Astrophysics, University of Delhi, Delhi; Department of Chemical Engineering & Technology, IIT (BHU), Varanasi, India

Pratap Srivastava
Department of Botany, Shyama Prasad Mukherjee Post-graduate College, University of Allahabad, Prayagraj, India

M. Suresh Kumar
Academy of Scientific and Innovative Research (AcSIR), Ghaziabad; Environmental Impact and Sustainability Division, CSIR-National Environmental Engineering Research Institute, Nagpur, India

Anupma Thakur
Academy of Scientific and Innovative Research (AcSIR), Ghaziabad; CSIR-Central Scientific Instruments Organisation, Chandigarh, India

Manita Thakur
Department of Chemistry, IEC University Baddi, Solan, India

Ricardo A. Torres-Palma
Grupo de Investigación en Remediación Ambiental y Biocatálisis (GIRAB), Instituto de Química, Facultad de Ciencias Exactas y Naturales, Universidad de Antioquia UdeA, Medellin, Colombia

Gyanendra Tripathi
Department of Bioengineering, Integral University, Lucknow, India

Sachchidanand Tripathi
Department of Botany, Deen Dayal Upadhyaya College, University of Delhi, New Delhi, India

This book belongs to Central Library BADJI Mokhtar-ANNABA UNIVERSITY

Copyright Elsevier 2024

S.N. Upadhyay
Department of Chemical Engineering and Technology, IIT (BHU) Varanasi, Varanasi, India

Miguel Angel Vicente
GIR-QUESCAT, Inorganic Chemistry Department, University of Salamanca, Salamanca, Spain

Bin Xue
Department of Chemistry, College of Food Science and Technology, Shanghai Ocean University; Quality Supervision, Inspection and Testing Center for Cold Storage and Refrigeration Equipment (Shanghai), Ministry of Agriculture; National Experimental Teaching Demonstration Center for Food Science and Engineering (Shanghai Ocean University), Shanghai, China

This book belongs to Central Library BADJI Mokhtar-ANNABA UNIVERSITY

Copyright Elsevier 2024

This page intentionally left blank

This book belongs to Central Library BADJI Mokhtar-ANNABA UNIVERSITY

Copyright Elsevier 2024

CHAPTER

An overview of synthesis techniques for preparing doped photocatalysts

1

Indrajit Sinha, Arup Kumar De

Department of Chemistry, Indian Institute of Technology (Banaras Hindu University), Varanasi, India

1 General introduction

Energy and environmental problems are the most pressing topical issues of our planet today (Umezawa & Ye, 2012). The two topics go in a cycle. Fossil fuels are the mainstay of most technologies in fashion currently, and their excessive use is also the primary reason for many of the environmental problems that are being encountered (Marschall & Wang, 2014). Jettisoning fossil fuels and shifting focus to renewable energy technologies are the apparent solution to this vicious circle (Jiang et al., 2017; Marschall & Wang, 2014). One major renewable energy technology is photocatalysis, which requires only solar radiation for energy production by artificial photosynthetic reactions like water splitting and CO_2 reduction (Ong, Tan, Ng, Yong, & Chai, 2016). Additionally, it is a technique that can degrade environmental pollutants to less harmful fractions using only sunlight (Khaki, Shafeeyan, Raman, & Daud, 2017; Ong et al., 2016). Discovery of semiconductors and their science was the first step to the realization of the phenomenon of photocatalysis (Hashimoto, Irie, & Fujishima, 2005). The oil crisis of the 1970s spurred the governments of developed countries to sponsor extensive research on renewable energy sources and technologies (Meng, Xing, Li, & Li, 2015; Ong et al., 2016). Another key stepping stone was the first paper on photocatalytic water splitting by Honda and Fujishima (Fujishima & Honda, 1972).

Today, we know that there are several requirements for the design of an active photocatalyst for a target reaction. The starting point is efficient light absorption for exciting electrons from the valence band (VB) to the conduction band (CB) of the semiconductor (Asahi, Morikawa, Ohwaki, Aoki, & Taga, 2001). Most of the traditional photocatalysts like TiO_2, ZnO, and ZnS are wide bandgap (WBG) semiconductors, and therefore, photoexcitation requires irradiation by short-wavelength UV radiation (Kedziora, Strek, Kepinski, Bugla-Ploskonska, & Doroszkiewicz, 2012). On the other hand the visible range of radiation constitutes a significant part of the solar spectrum. Consequently the use of UV radiation by WBG photocatalysts results in inefficient use of solar energy resources (Kumar, Verma, Pal, & Sinha, 2018). Naturally, a large amount of current photocatalysis research is on designing nanocomposites that can utilize visible light (Wang et al., 2014). Another vital issue related to the absorption of light is the photoefficiency of the photocatalyst. Generally the photoefficiency of most photocatalysts is very poor and is ~1% in most cases (Ge, Han, & Liu, 2011; Li et al., 2011).

Nano-Materials as Photocatalysts for Degradation of Environmental Pollutants. https://doi.org/10.1016/B978-0-12-818598-8.00001-8
© 2020 Elsevier Inc. All rights reserved.

This book belongs to Central Library BADJI Mokhtar-ANNABA UNIVERSITY

Copyright Elsevier 2024

The next issue is the fate of the photogenerated electron–hole pair (or exciton) excited species. The electrons and holes thus formed travel to the surface of the catalyst, or they may recombine (Pesci, Wang, Klug, Li, & Cowan, 2013). The energy that has been absorbed could be released by various phenomena included in photoluminescence and also by energy release in the form of heat (Wojcieszak, Kaczmarek, Domaradzki, & Mazur, 2013; Zhang & Mu, 2007). Overall the increase in photocatalytic efficiency can be achieved by ensuring that excitons do go to the photocatalyst surface and survive long enough to harness their redox ability (Takanabe, 2017). In other words, it is vital to design photocatalysts with increased lifetime or charge separation of the photogenerated electron–hole species (Jiang et al., 2018). A crucial point is the VB and CB positions of the photocatalyst. The redox potential of the targeted oxidation or reduction reaction needs to be lesser or more than the VB and CB positions of the photocatalyst, respectively. However, semiconductors with good driving force due to valence band (VB) and conduction band (CB) positions also may not show good efficiency (Jiang et al., 2018; Schoonen & Xu, 2000). The main reason for this is the weak adsorption of reactants on the catalyst surface. Thus the adsorption characteristics of different components making up the photocatalyst concerning the target reactants also need to be taken into account (Crittenden, Suri, Perram, & Hand, 1997; Nguyen-Phan et al., 2011).

From the previous discussion, it is clear that the photocatalytic efficiency of a material is dependent on two types of characteristics. The first set of requirements is not specific to any reactant. In contrast to this the second set of conditions depends on the reactant. Photocatalytic material characteristics (which are not reactant dependent) include bandgap (visible or UV range), charge separation, and photoefficiency. On the other hand, fabricating materials with tailored band positions and having compatible adsorption properties are aspects specific to the reaction being considered.

It is evident that there are two contradictory requirements in photocatalyst development. Thus the CB and VB positions should be sufficiently negative and positive, respectively to induce the required the reduction and oxidation reactions for the process to be sustained only by light irradiation (Jafari et al., 2016). The required band positions indicate that a wide band gap (WBG) semiconductor should be used. But a wide band semiconductor would either be an insulator or its absorption would in the UV range (Yan, Wang, Yao, & Yao, 2013). Since the UV range is only 4% of the solar radiation, therefore, this would result in poor utilization of this natural resource. Thus, proper exploitation of solar resources necessitates photocatalysts that can operate using visible light. Hence, proper energy utilization requires small band gap semiconductors (Fox & Dulay, 1993), while required band positions dictate a wide bandgap photocatalysts.

Wide bandgap photocatalysts also face the problem of relatively easy recombination of photoinduced holes and electron (Fox & Dulay, 1993; Johar, Afzal, Alazba, & Manzoor, 2015). The recombination problem can be reduced by taking recourse to one of the following methods. A major path followed involves designing of new heterostructure nanocomposites (Johar et al., 2015). Thus two semiconductors may be combined in such manner that the (VB and CB) band positions of two photocatalysts have staggered alignment with respect to each other. In such cases, semiconductor heterojunction is formed, and such composites may be Z-scheme or p-n junction-type photocatalysts (Maeda, 2013; Sun et al., 2018). Both types of heterojunctions have their advantages. In both cases, charge separation is achieved, but in Z-scheme, the photocatalytic driving forces due to (lower) VB and (higher) CB positions are better. Such semiconductor heterostructures are generally made up of two visible range semiconductors. Similarly, deposition of a noble metal cocatalyst can also lead to the utilization

This book belongs to Central Library BADJI Mokhtar-ANNABA UNIVERSITY Copyright Elsevier 2024

of visible light range (Sakthivel et al., 2004). Other techniques include sensitization by organic dyes or inorganic complexes (Zhang, Peng, & Song, 2016).

An extensively used technique to tackle many of the problems listed previously as impediments to efficient photocatalyst construction is doping the crystal lattice of the native semiconductor by a metal or nonmetal ions. Doping, thus, introduces defects into the ideal crystal lattice of the native semiconductor, and this technique has been extensively used to improve the activity of the photocatalysts by modifying their electronic structures (Shao, Wang, & Zhang, 2018). Such defects introduce sites that can entrap (also known as trap sites) electrons or holes formed during the photoexcitation process. Another important function of the defect sites like vacancies is to increase the catalytic activation of strong bonds kinetically facilitating reactions. For instance, in many cases, oxygen vacancies have been found to catalytically activate the strong first bond of dinitrogen (Chen, Li, Kong, Ong, & Zhao, 2018 and references therein). Doping could also lead to additional charge carriers in the photocatalyst. Formation of extra bands that may narrow or widen the bandgap of the original photocatalyst is also possible. Therefore doping can affect light absorption, reduce recombination through trap sites, and alter VB or CB positions to change the photocatalytic activity toward a substrate molecule or reaction.

2 Doped semiconductors: An introduction

Doping is the inclusion of foreign metal or nonmetal ions in the crystal lattice of a semiconductor (Cargnello et al., 2015; Norris, Efros, & Erwin, 2008). It could be p-type or n-type. Thus if the dopant is one with higher valency than that being doped, then it is called n-type. Conversely, doping by lower valence element means that p-type semiconductor will be formed (Oba, Tatsumi, Adachi, & Tanaka, 2001). Doping could be by substituting the cation or the anion in the semiconductor (Baerends & Gritsenko, 1997; Zhang, Tse, Wong, Zhang, & Zhu, 2016). In general the atomic size of the dopant should be similar to that being substituted, otherwise the lattice gets distorted and the percentage of doping will also very low (Kudo & Sekizawa, 2008). Interstitial position could also be occupied by dopants. In this case the size of the dopant ions should be such that it can occupy interstitial positions such as tetrahedral or octahedral holes without much distortion (Kudo & Sekizawa, 2008; Zhang, Tse, et al., 2016).

2.1 Synthesis techniques used prepare doped semiconductors:

The present chapter attempts to give a concise review of the synthesis techniques used to produce doped WBG semiconductors. The method of preparation of doped semiconductors determines the amount of doping possible and the nanostructure formed. One can introduce the dopant into the native metal oxide lattice in a number of ways. Mostly, examples of semiconducting oxides are considered. It is important to mention that only those research works, which report shift in XRD peaks of the original phase due to doping, have been discussed in this chapter. Shift in XRD peak implies that the dopant cation or anion has been incorporated in the crystal lattice of the native semiconductor (Aydin, Yakuphanoglu, & Aydin, 2019; Kudo & Sekizawa, 2008) and hence such a preparation conforms to the definition of doped semiconductors mentioned previously. While a large number of papers have been published in the area of doped photocatalysts, the discussion in the succeeding text uses few typical examples to illustrate the features of different preparation protocols.

This book belongs to Central Library BADJI Mokhtar-ANNABA UNIVERSITY
Copyright Elsevier 2024

(i) Coprecipitation followed by calcination

In this method the salt solutions of the major and the dopant components are mixed together in a common solvent (Arai et al., 2008; Burda et al., 2003; Karakitsou & Verykios, 2005; Kwon et al., 2016; Verma, Patel, Ram, & Barbar, 2016). The solvent is selected such that the component salts are soluble in it (Parveen, Agrawal, & Azam, 2016). Thus a clear solution should be obtained after the mixing of the component salt solutions in the same solvent (Iqbal & Ashiq, 2008; Parveen et al., 2016). Thereafter, the some intensive experimental parameter like pH and temperature is varied to precipitate the semiconductor phase (Mittal, Sharma, & Pandey, 2014). For example, cation-doped ZnO has been prepared by many groups by first dissolving the Zn salt and dopant salt in methanol (or some suitable solvent) (Devi & Velu, 2016; Mittal et al., 2014). In next step the pH of the obtained solution was increased by adding NaOH. Precipitate of ZnO is formed, which is then dried and generally subjected to calcination to improve the crystallinity of the major phase formed (Devi & Velu, 2016).

Similarly, in-doped ZnO nanoparticles were prepared by Raj et al. (Pradeev Raj, Sadaiyandi, Kennedy, & Sagadevan, 2017). They mixed $ZnCl_2$ and $InCl_2$ in deionized water. Sodium hydroxide was then added until doped $Zn(OH)_2$ precipitate was formed, which was then dried and calcined at 600C to obtain In-doped ZnO nanoparticles. Nearly 1 mol% of In could be doped into ZnO in this way. The doped ZnO nanoparticles had finer sizes with slight change in lattice parameters. Moreover, there was marked increase in photocatalytic degradation rate of RhB dye with the higher In-doped sample. The authors proposed that this could be due to the finer particle size (thereby larger surface area) and also due to new trapping center in the doped samples.

In another recent publication, Mansour, Bargougui, Autret-Lambert, Gadri, and Ammar (2018) prepared hematite nanoparticles doped with Sn using a simple coprecipitation method. These workers added different amounts of $SnCl_2$ to aqueous solutions of $FeCl_3$. Appropriate amount of NH_3 was added to induce precipitation. Authors reported change in lattice parameters with increase in Sn ion content. Photocatalytic degradation of efficiency of methylene blue (MB) increased with doping due to decrease in exciton recombination.

(ii) Sol–gel synthesis

The sol–gel technique is another very extensively used method for the preparation of doped photocatalysts (Marami & Farahmandjou, 2018; Pathak, Kroon, & Swart, 2018). It is also a low-temperature solution route technique. The input compounds could be costly since many times it involves the mixing of precursor metal alkoxides to form a clear solution, followed by hydrolysis to convert the alkoxides into metal hydroxides (Guglielmi & Carturan, 1988). Latter undergo immediate condensation to form gels that are dried to obtain xerogel or aerogels. The highly porous and lightweight gels are then sintered at relatively high temperature for densification to nanosized powders. It must be mentioned that it is not necessary that the alkoxide precursor be used.

Hydrolysis and condensation may also occur almost concurrently, making control of the process difficult. In this respect, nonaqueous sol–gel processes give access to better control over the kinetics of the process (Niederberger, 2007). As a consequence, more crystalline products with better particle size distribution are often obtained. In general, sol–gel method gives more control over shape and size of the nanoparticles formed. Thus Nithya, Bhoopathi, Magesh, & Kumar (2018) were able to prepare Nd-doped TiO_2 by the nonaqueous sol–gel route. They dissolved titanium isopropoxide and neodymium acetate in isopropyl alcohol along with suitable amount acetic acid. Latter helped complete the

This book belongs to Central Library BADJI Mokhtar-ANNABA UNIVERSITY Copyright Elsevier 2024

hydrolysis part. The sol pH was raised to 9 by addition of NaOH. After ageing and washing the precipitate was dried and finally annealed at 600°C. While the pure TiO_2 powder is prepared by the same sol–gel method consisted only of anatase phase, the doped TiO_2 was a mixture of rutile, brookite, and anatase phases. Doping enhanced the photocatalytic properties of TiO_2 for Congo red dye degradation, although very little change in bandgap was observed.

An interesting variation is provided to the sol–gel method by combining it with the combustion method. Thus Fe- and Cr-doped ZnO have been prepared by sol–gel auto combustion method (Irshad, Khan, & Murtaza, 2018). In this protocol, aqueous solutions of zinc nitrate and the dopant metal nitrate were prepared. The solutions were then subjected to combustion with glycine as the fuel. On complete evaporation of the water, the sol changed into gel, which was then calcined to get the final doped product powder. XRD peak shifting was observed because of substitutional doping.

Some papers have reported that inclusion of transition metal dopants like Mn, V, and Ru in ZnO decreases its thermal instability (Macías-Sánchez et al., 2015; Nikam, Sabale, Jadhav, & Chikode, 2019). It was found that this could be avoided by doping nonmetal anions that substitute for oxygen in such WBG semiconductors. Macías-Sánchez et al. used zinc acetate and urea as the precursors for prepared N-doped ZnO (Macías-Sánchez et al., 2015). Ammonium hydroxide was used to raise the pH to ~8.5, and then, sol was aged for 24 h for the condensation process to be completed. The solvent was evaporated, and the gel was subjected to calcination at 400°C. N-doped ZnO demonstrated lower bandgaps and finer particle sizes. The doped ZnO photocatalysts exhibited better activity for oxidation of picloram.

(iii) Hydrothermal and solvothermal synthesis

Nowadays, hydrothermal or solvothermal techniques are frequently used to prepare nanoparticles, especially when nonequilibrium phases or varied nanomorphologies may be desired (Li et al., 2017; Nikam et al., 2019). In this method the precursor salt solutions and other reactants are mixed in an autoclave such that at least 20%–30% of the reaction vessel is left vacant. The precursors could also be in gel or suspension form (Nguyen, Nguyen, & Nguyen, 2011). Small amounts of stabilizers and crystal growth directing agents can also be added (Cao et al., 2015). The autoclave is sealed and subjected to thermal treatment at temperatures ranging from 120°C to 260°C, depending on the solvent. If the solvent is water, then the reaction temperature would not exceed 170°C, and moreover, in that case, the technique is referred to as the hydrothermal method (Aliofkhazraei, 2015). On the other hand, if a higher boiling solvent is used, then the preparation technique is known as the solvothermal method. In this case the reaction temperature can go up to 260°C (Aliofkhazraei, 2015; Li et al., 2017). Since the temperatures used are typically higher than the boiling temperatures of the solvent, therefore, the boiling of the solvent results in self-generated or autogenous pressure (Wang, Jia, Wu, Lu, & Xu, 2012). Because of such high pressures, the viscosity of the solvent is significantly lesser than the normal, increasing the diffusion rates of the precursor (Pathak, Swart, & Kroon, 2018). Such enhanced pressures also solubilize the precursors introduced in sol or gel forms as well. Moreover, the kinetics of metal salt hydrolysis also increases with pressure. The high-pressure and high-temperature conditions provide nonequilibrium condition leading to crystallization of kinetically stable phases (Lupan et al., 2010). Nanoparticles with different morphological features can be obtained by varying parameters like pH, pressure, and temperature. It is important to remember that pressure is autogenous, depending on the filled volume and temperature of reaction vessel.

This book belongs to Central Library BADJI Mokhtar-ANNABA UNIVERSITY Copyright Elsevier 2024

As mentioned previously, whenever nonequilibrium or a product is desired, then hydrothermal or solvothermal processes are preferred. Thus Türkyılmaz, Güy, and Özacar (2017) reported the hydrothermal synthesis of Ni-, Mn-, Fe-, and Ag-doped ZnO nanoparticles. It may be noted that while the cations of Ni, Mn, and Fe have sizes similar to Zn ions, the size of Ag ions is significantly larger. The procedure involved the mixing of the respective dopant solution with the zinc acetate solution, followed by the addition of NaOH for hydrolysis. The reaction mixture was then transferred to the autoclave and subjected to heat treatment for 20 h at ~120°C. The XRD patterns of the doped samples revealed that the diffraction plots corresponding to Mn, Fe, and Ni dopants match very well with that of the typical wurtzite crystal structure data of ZnO. No peaks of dopant metal oxide could be found. However, Ag peaks were observed in case of attempted ZnO doping. The result obtained is expected, since the Ag ion is much larger than the Zn cation. Ni-doped ZnO exhibited the best photocatalytic degradation of tartrazine. Authors concluded that higher dopant concentrations led to their agglomeration, which increased exciton recombination. In another example, smaller Yb^{3+}/Ho^{3+} ions (radii:101/90 pm) were substituted for Bi^{3+} ion (radii:117 pm) (Li, Hao, et al., 2017). The XRD of the prepared powders displayed peaks corresponding to pure Bi_2WO_6, phase only. However, the peaks shift slightly toward higher 2θ values due to decrease in cell volume by smaller cation substitution. Formation of finer crystallite sizes in doped samples was also reported by the authors. Yb^{3+}-/Ho^{3+}-Bi_2WO_6_ doped semiconductors were found to be very good photocatalysts for visible light aerobic degradation of RhB (Cao et al., 2015; Li, Hao, et al., 2017). The improved activities were credited to the IR to visible upconversion phenomenon.

Wang et al. (Wang et al., 2012) reported another interesting hydrothermal synthesis for the preparation of N-doped TiO2/C nanocomposites. They resorted the addition of L-lysine to an aqueous solution of $TiCl_4$. The former was the source of N and C. After adjustment of pH the reaction mixture was subjected to hydrothermal treatment at 180°C for 12 h. The N-doped TiO_2 corresponds to the anatase phase and also exhibited very fine nanoparticle sizes. The doped TiO_2 demonstrated good aerobic photocatalytic degradation of methyl orange. The authors also demonstrated that N-doping led to Ti^{3+} formation, which was responsible for visible light absorption.

3 Sonochemical synthesis

Sonochemical synthesis involves irradiating the reaction mixture with high-frequency ultrasonic waves. The ultrasound wavelength range ranges from 20 kHz to 1 GHz, and the wavelength corresponding to this is from 10 to 10^{-4} cm (Shchukin, Radziuk, & Möhwald, 2010). Since the wavelength range is much bigger than the atomic or molecular dimensions, therefore, ultrasound does not directly interact with these entities. Sonochemical processes take place due to acoustic cavitation (Gedanken & Perelshtein, 2014; Shchukin et al., 2010). A liquid expansion–compression cycle results in germination of bubbles when sonochemical waves interact with the reaction medium. Size of the bubble formed depends on the wave frequency. The collapse of these cavities (or bubbles) leads to generation of very high local temperatures (>5000 K) and pressures (~20 MPa), which are also known as local hot spots (Kim et al., 2013; Zhou, Yu, & Cheng, 2006). Thus extreme temperature and pressure conditions can be generated at the liquid–gas interface due to cavitation but at overall ambient reaction temperature conditions. Such extreme nonequilibrium conditions can cause the formation of metastable or kinetically stable nanostructures (Yayapao, Thongtem, Phuruangrat, & Thongtem, 2013).

This book belongs to Central Library BADJI Mokhtar-ANNABA UNIVERSITY Copyright Elsevier 2024

A recent paper by Fulekar et al. (2014) illustrates some of the key factors involved in sonochemical synthesis. Aqueous solutions of $Bi(NO_3)_3$ and $(NH_4)H_2PO_4$ were mixed with stoichiometric amount of $AgNO_3$ and subjected to ultrasonic probe at 40 KHz. The precipitate formed was dried and characterized by XRD and other techniques. Ag^+ could be incorporated in the $BiPO_4$ lattice up to 10 mol% without phase separation. Doping led to stabilization of the monoclinic $BiPO_4$ at lower annealing temperatures than usual. While the undoped $BiPO_4$ acts as a photocatalyst only on UV irradiation, the Ag-doped samples demonstrated good visible light photocatalytic degradation of RhB.

Another example is the successful N-doping of TiO_2 (Jia et al., 2014). Urea was the source of N, and $TiCl_4$ was the main precursors. The alkaline aqueous reaction mixture was subjected to ultrasound and aged for 24 h. The XRD of the precipitated powder showed the formation of finer crystallite size for N-doped cases. The N-doped TiO_2 nanoparticles have very good RhB photocatalytic degradation properties. In a recent publication, Ambati and Gogate (2018) claimed the formation of Fe-doped TiO_2 by this technique. Titanium isopropoxide and isopropanol were the initial precursors subjected to few minutes of ultrasound. Later, NaOH and $Fe(NO_3)_3$ solutions were added with prolonged ultrasonic bath treatment. However, this protocol resulted separate formation of hematite phase besides TiO_2.

4 Reverse micelles

Surfactant molecules reduce the surface tension between two immiscible liquid phases by suitably orienting their hydrophilic head toward the aqueous phase and the hydrophobic tail (alkyl chain) part toward nonpolar phase. When the concentration of such surfactant molecules is low, then they may be soluble in the aqueous phase. On increasing the surfactant concentration when a critical value is reached, the surfactant molecules arrange themselves (or aggregate) into micelles. Since the aqueous part is the major phase, therefore, in micelles, the hydrophobic tail points toward the center of the micelle, while the hydrophilic head functional group points outward. Therefore micelles can capture nonpolar molecules in their cores and solubilize them in the major aqueous phase. On the other hand the surfactants that organize themselves in nonpolar solvents can trap and solubilize polar entities in the former. These surfactant aggregates are exactly the reverse of micelles and hence are known as reverse or inverted micelles (Eastoe, Hollamby, & Hudson, 2006; Ganguli, Ganguly, & Vaidya, 2010). The size of the cavity of a spherical micelle cannot exceed a certain value, and hence, preparation of nanoparticles by this technique ensures nearly monodisperse particle distribution. Semiconducting oxide nanoparticles have been prepared by the reverse micelle technique. The reverse micelles diffuse, collide with each other, and then again come apart. During the collision, they can exchange polar reactant molecules protected in the inner spherical enclosure. The reactions occur during this temporary coalescence process. A typical example of the preparation of doped semiconductors is given in the publication of Gavrilović, Jovanović, Lojpur, and Dramićanin (2014). These authors prepared Eu^{3+}- and Er^{3+}/Yb^{3+}-doped $GdVO_4$ nanoparticles by the reverse micelle method. They first prepared the nonpolar (or the oil) phase by mixing appropriate volumes of cyclohexane, Triton X-100, and n-pentanol. Then, they mixed small volumes of aqueous solution of $NaVO_4$ and the dopant salt solutions with continuous stirring and in a drop wise manner. A yellowish colloidal sol was obtained, which was further aged for 24 h. Finally, methanol was added to destabilize the sol, and the precipitate formed was separated by centrifuge. The XRD pattern of the dried powder showed the formation of only tetragonal phase of $GdVO_4$, meaning the dopants had been incorporated in the crystal lattice of this phase.

This book belongs to Central Library BADJI Mokhtar-ANNABA UNIVERSITY Copyright Elsevier 2024

In another recent publication, Nasi et al. (2019) have demonstrated the preparation of Mo-doped TiO_2 NPs by the sol–gel reverse micelle microemulsion protocol. The surfactant, polyoxyethylene (20) oleyl ether (Brij O20), was dispersed in cyclohexane. Concurrently the dopant and the native salt precursors were dissolved in MilliQ water. The prepared solutions were mixed at the same temperature with the formation of a water-in-oil (w/o) microemulsion of surfactant nanoreactors. Then Ti-$(BuO)_4$ component was then added dropwise to the prepared microemulsion. After ageing for 2 h the emulsion was destabilized by adding two propanol. The solid product was isolated and then calcined at 500°C to remove the surfactant. Anatase phase pure TiO_2 was prepared by this method. On doping additional rutile phase, peaks were also observed in the XRD of the doped samples. No peaks due to MoO_x were detected showing that substitutional doping had occurred. Mo-doped TiO_2 exhibited better photocatalytic activity for RhB degradation than the pure TiO_2.

Interestingly, Elghniji, Ksibi, and Elaloui (2012) could successfully combine the sol–gel and the reverse micelle methods to prepare N-doped TiO_2 nanoparticles. These authors prepared a reverse micelle sol with cyclohexane and aqueous solution of Na_2EDTA. Triton X-100 was used as the surfactant. The prepared reverse micelle sol was added in a drop wise manner to titanium (IV) 2-ethyl-1,3-hexanediolate diluted in 30 mL of isopropyl alcohol. Excess solvent was evaporated. Additionally the heating process accelerated the process of hydrolysis. After ageing for 1 h the gel was calcined at 500°C. The XRD of the prepared powder showed the formation of only one pure phase of TiO_2. No impurity phases were formed. Thus it was concluded that the doped N had substituted O atoms in the crystal lattice of TiO_2. Moreover, the doped sample crystallite sizes were finer than those observed for pure phases.

5 Conclusions

In the last two decades, photocatalysts with different types of nanostructures have been designed for decreasing recombination through charge separation, increased use of visible light for photoexcitation, bandgap, and band position modulations. Among different nanostructure design strategies available, a frequent technique used by researchers of this area is the doping of the original semiconductor with metal or nonmetal ions. Besides introducing additional dopant levels in the band structure of the photocatalyst, doping can also lead to creation of vacancies and defects in the nanostructure. Latter can foster catalytic bond activation or act as trapping sites for photoexcited electrons and holes, preventing their recombination. The synthesis techniques used to prepare doped photocatalysts determine their nanostructures. In the present article, an overview of different liquid phase synthesis techniques has been presented. The discussion begins with the ambient temperature coprecipitation technique. Only small percentage of doping can be achieved by this method. The sol–gel technique, another popular low-temperature method, involves hydrolysis of metal salts, followed by their condensation and gelation. Nonaqueous sol–gel processing gives better control over the kinetics of the method. Hydrothermal and solvothermal use high autogenous pressure and temperatures. In contrast to the coprecipitation and sol–gel techniques, here, all precursors need not be soluble in the initial reaction mixture. While the methods discussed earlier are basically suitable for substitutional type of doping only, nonequilibrium interstitial site doping has also been performed successfully by this method. The sonochemical method is another useful nonequilibrium technique for prepared doped photocatalysts. However, not many workers have used this technique for preparing doped semiconductors. Reverse micelle technique gives

This book belongs to Central Library BADJI Mokhtar-ANNABA UNIVERSITY Copyright Elsevier 2024

access to almost monodisperse particle size distributions. For every technique, there are some examples where workers have tried to smartly combine two techniques in a complementary manner. We believe that in future, more such attempts will made to flexibly combine different preparation techniques for synthesis of novel and more controlled nanostructures.

References

Aliofkhazraei, M. (Ed.), (2015). *Handbook of nanoparticles*. Springer International Publishing ISBN: 978-3-319-15339-1.

Ambati, R., & Gogate, P. R. (2018). Ultrasound assisted synthesis of iron doped TiO_2 catalyst. *Ultrasonics Sonochemistry*, *40*, 91–100.

Arai, T., Senda, S. I., Sato, Y., Takahashi, H., Shinoda, K., Jeyadevan, B., et al. (2008). Cu-doped ZnS hollow particle with high activity for hydrogen generation from alkaline sulfide solution under visible light. *Chemistry of Materials*, *20*, 1997–2000.

Asahi, R., Morikawa, T., Ohwaki, T., Aoki, K., & Taga, Y. (2001). Visible-light photocatalysis in nitrogen-doped titanium oxides. *Science*, *293*, 269–271.

Aydin, H., Yakuphanoglu, F., & Aydin, C. (2019). Al-doped ZnO as a multifunctional nanomaterial: Structural, morphological, optical and low-temperature gas sensing properties. *Journal of Alloys and Compounds*, *773*, 802–811.

Baerends, E. J., & Gritsenko, O. V. (1997). Feature article. *The Journal of Physical Chemistry. A*, *101*, 24287–24293.

Burda, C., Lou, Y., Chen, X., Samia, A. C. S., Stout, J., & Gole, J. L. (2003). Enhanced nitrogen doping in TiO_2 nanoparticles. *Nano Letters*, *3*, 1049–1051.

Cao, R., Huang, H., Tian, N., Zhang, Y., Guo, Y., & Zhang, T. (2015). Novel Y doped Bi_2WO_6 photocatalyst: Hydrothermal fabrication, characterization and enhanced visible-light-driven photocatalytic activity for rhodamine B degradation and photocurrent generation. *Materials Characterization*, *101*, 166–172.

Cargnello, M., Johnston-Peck, A. C., Diroll, B. T., Wong, E., Datta, B., Damodhar, D., et al. (2015). Substitutional doping in nanocrystal superlattices. *Nature*, *524*, 450–453.

Chen, X., Li, N., Kong, Z., Ong, W., & Zhao, X. (2018). Photocatalytic fixation of nitrogen to ammonia: State-of-the-art advancements and future prospects. *Materials Horizons*, *5*, 9–27.

Crittenden, J. C., Suri, R. P. S., Perram, D. L., & Hand, D. W. (1997). Decontamination of water using adsorption and photocatalysis. *Water Research*, *31*, 411–418.

Devi, P. G., & Velu, A. S. (2016). Synthesis, structural and optical properties of pure ZnO and co doped ZnO nanoparticles prepared by the co-precipitation method. *Journal of Theoretical and Applied Physics*, *10*, 233–240.

Eastoe, J., Hollamby, M. J., & Hudson, L. (2006). Recent advances in nanoparticle synthesis with reversed micelles. *Advances in Colloid and Interface Science*, *128–130*, 5–15.

Elghniji, K., Ksibi, M., & Elaloui, E. (2012). Sol-gel reverse micelle preparation and characterization of n-doped TiO_2: Efficient photocatalytic degradation of methylene blue in water under visible light. *Journal of Industrial and Engineering Chemistry*, *18*, 178–182.

Fox, M. A., & Dulay, M. T. (1993). Heterogeneous photocatalysis. *Chemical Reviews*, *93*, 341–357.

Fujishima, A., & Honda, K. (1972). Electrochemical photolysis of water at a semiconductor electrode. *Nature*, *238*, 37–38.

Fulekar, M. H., Singh, A., Dutta, D. P., Roy, M., Ballal, A., & Tyagi, A. K. (2014). Ag incorporated nano $BiPO_4$: Sonochemical synthesis, characterization and improved visible light photocatalytic properties. *RSC Advances*, *4*, 10097–10107.

This book belongs to Central Library BADJI Mokhtar-ANNABA UNIVERSITY

Copyright Elsevier 2024

Ganguli, A. K., Ganguly, A., & Vaidya, S. (2010). Microemulsion-based synthesis of nanocrystalline materials. *Chemical Society Reviews*, *39*, 474–485.

Gavrilović, T. V., Jovanović, D. J., Lojpur, V., & Dramićanin, M. D. (2014). Multifunctional Eu^{3+}- and Er^{3+}/Yb^{3+}-doped $GdVO_4$ nanoparticles synthesized by reverse micelle method. *Scientific Reports*, *4*, 1–9.

Ge, L., Han, C., & Liu, J. (2011). Novel visible light-induced g-C_3N_4/Bi_2WO_6 composite photocatalysts for efficient degradation of methyl orange. *Applied Catalysis B: Environmental*, *108–109*, 100–107.

Gedanken, A., & Perelshtein, I. (2014). *Power ultrasound for the production of nanomaterials*. Elsevier Ltd.

Guglielmi, M., & Carturan, G. (1988). Precursors for sol-gel preparations. *Journal of Non-crystalline Solids*, *100*, 16–30.

Hashimoto, K., Irie, H., & Fujishima, A. (2005). TiO_2 photocatalysis: A historical overview and future prospects. *Japanese Journal of Applied Physics*, *44*, 8269–8285.

Iqbal, M. J., & Ashiq, M. N. (2008). Physical and electrical properties of Zr-cu substituted strontium hexaferrite nanoparticles synthesized by co-precipitation method. *Chemical Engineering Journal*, *136*, 383–389.

Irshad, K., Khan, M. T., & Murtaza, A. (2018). Synthesis and characterization of transition-metals-doped ZnO nanoparticles by sol-gel auto-combustion method. *Physica B: Condensed Matter*, *543*, 1–6.

Jafari, T., Moharreri, E., Amin, A. S., Miao, R., Song, W., & Suib, S. L. (2016). Photocatalytic water splitting—The untamed dream: A review of recent advances. *Molecules*, *21*, 1–29.

Jia, T., Fu, F., Zhao, J., Chen, J., Wang, X., Fan, Z., et al. (2014). Sonochemical synthesis, characterization, and photocatalytic activity of N-doped TiO_2 nanocrystals with mesoporous structure. *International Journal of Photoenergy*, *2014*, 1–7.

Jiang, L., Yuan, X., Pan, Y., Liang, J., Zeng, G., Wu, Z., et al. (2017). Doping of graphitic carbon nitride for photocatalysis: A review. *Applied Catalysis B: Environmental*, *217*, 388–406.

Jiang, L., Yuan, X., Zeng, G., Liang, J., Wu, Z., & Wang, H. (2018). Construction of an all-solid-state Z-scheme photocatalyst based on graphite carbon nitride and its enhancement to catalytic activity. *Environmental Science. Nano*, *5*, 599–615.

Johar, M. A., Afzal, R. A., Alazba, A. A., & Manzoor, U. (2015). Photocatalysis and bandgap engineering using ZnO nanocomposites. *Advances in Materials Science and Engineering*, *2015*, 1–22.

Karakitsou, K. E., & Verykios, X. E. (2005). Effects of altervalent cation doping of titania on its performance as a photocatalyst for water cleavage. *The Journal of Physical Chemistry*, *97*, 1184–1189.

Kedziora, A., Strek, W., Kepinski, L., Bugla-Ploskonska, G., & Doroszkiewicz, W. (2012). Synthesis and antibacterial activity of novel titanium dioxide doped with silver. *Journal of Sol-Gel Science and Technology*, *62*, 79–86.

Khaki, M. R. D., Shafeeyan, M. S., Raman, A. A. A., & Daud, W. M. A. W. (2017). Application od doped photocatalysts for organic pollutant degradation—A review. *Journal of Environmental Management*, *198*, 78–94.

Kim, T. H., Rodríguez-González, V., Gyawali, G., Cho, S. H., Sekino, T., & Lee, S. W. (2013). Synthesis of solar light responsive Fe, N co-doped TiO_2 photocatalyst by sonochemical method. *Catalysis Today*, *212*, 75–80.

Kudo, A., & Sekizawa, M. (2008). Photocatalytic H_2 evolution under visible light irradiation on Zn_{1-X} Cu_X S solid solution. *ACS Catalysis*, *58*, 241–243.

Kumar, S., Verma, A., Pal, S., & Sinha, I. (2018). Curcumin-functionalized ag/Ag2O nanocomposites: Efficient visible-light Z-scheme photocatalysts. *Photochemistry and Photobiology*, *94*, 641–649.

Kwon, S. G., Chattopadhyay, S., Koo, B., Dos Santos Claro, P. C., Shibata, T., Requejo, F. G., et al. (2016). Oxidation induced doping of nanoparticles revealed by in situ X-ray absorption studies. *Nano Letters*, *16*, 3738–3747.

Li, H., Hao, H., Jin, S., Guo, W., Hu, X., Hou, H., et al. (2017). Synthesis of Yb3+/Ho3+ co-doped Bi2WO6 upconversion photocatalyst with highly improved visible light photocatalytic activity. *Catalysis Communications*, *97*, 60–64.

This book belongs to Central Library BADJI Mokhtar-ANNABA UNIVERSITY

Copyright Elsevier 2024

Li, H., Wang, D., Fan, H., Wang, P., Jiang, T., & Xie, T. (2011). Synthesis of highly efficient C-doped TiO_2 photocatalyst and its photo-generated charge-transfer properties. *Journal of Colloid and Interface Science*, *354*, 175–180.

Li, H., Zhang, J., Huang, G., Fu, S., Ma, C., Wang, B., et al. (2017). Hydrothermal synthesis and enhanced photocatalytic activity of hierarchical flower-like Fe-doped $BiVO_4$. *Transactions of Nonferrous Metals Society of China*, *27*, 868–875.

Lupan, O., Chow, L., Ono, L. K., Cuenya, B. R., Chai, G., Khallaf, H., et al. (2010). Synthesis and characterization of Ag- or Sb-doped ZnO nanorods by a facile hydrothermal route. *The Journal of Physical Chemistry C*, *114*, 12401–12408.

Macías-Sánchez, J. J., Hinojosa-Reyes, L., Caballero-Quintero, A., De La Cruz, W., Ruiz-Ruiz, E., Hernández-Ramírez, A., et al. (2015). Synthesis of nitrogen-doped ZnO by sol-gel method: Characterization and its application on visible photocatalytic degradation of 2,4-D and picloram herbicides. *Photochemical and Photobiological Sciences*, *14*, 536–542.

Maeda, K. (2013). Z- scheme water splitting using two different semiconductor Photocatalysts. *ACS Catalysis*, *3*, 1486–1503.

Mansour, H., Bargougui, R., Autret-Lambert, C., Gadri, A., & Ammar, S. (2018). Co-precipitation synthesis and characterization of tin-doped α-Fe_2O_3 nanoparticles with enhanced photocatalytic activities. *Journal of Physics and Chemistry of Solids*, *114*, 1–7.

Marami, M. B., & Farahmandjou, M. (2018). Sol-gel synthesis of Fe-doped TiO_2 nanocrystals. *Journal of Electronic Materials*, *47*, 3741–3748.

Marschall, R., & Wang, L. (2014). Non-metal doping of transition metal oxides for visible-light photocatalysis. *Catalysis Today*, *225*, 111–135.

Meng, A., Xing, J., Li, Z., & Li, Q. (2015). Cr-doped ZnO nanoparticles: Synthesis, characterization, adsorption property, and recyclability. *ACS Applied Materials & Interfaces*, *7*, 27449–27457.

Mittal, M., Sharma, M., & Pandey, O. P. (2014). UV-visible light induced photocatalytic studies of cu doped ZnO nanoparticles prepared by co-precipitation method. *Solar Energy*, *110*, 386–397.

Nasi, R., Esposito, S., Freyria, F. S., Armandi, M., Gadhi, T. A., Hernandez, S., et al. (2019). Application of reverse micelle sol-gel synthesis for bulk doping and heteroatoms surface enrichment in Mo-doped TiO_2 nanoparticles. *Materials (Basel)*, *12*, 937.

Nguyen, V. N., Nguyen, N. K. T., & Nguyen, P. H. (2011). Hydrothermal synthesis of Fe-doped TiO_2 nanostructure photocatalyst. *Advances in Natural Sciences: Nanoscience and Nanotechnology*, *2*.

Nguyen-Phan, T. D., Pham, V. H., Shin, E. W., Pham, H. D., Kim, S., Chung, J. S., et al. (2011). The role of graphene oxide content on the adsorption-enhanced photocatalysis of titanium dioxide/graphene oxide composites. *Chemical Engineering Journal*, *170*, 226–232.

Niederberger, M. (2007). Nonaqueous Sol-Gel Routes to Metal Oxide Nanoparticles. *Accounts of Chemical Research*, *40*, 793–800.

Nikam, G., Sabale, S., Jadhav, V., & Chikode, P. (2019). Polyol synthesis and characterization of ZnO@$CoFe_2O_4$MNP's to study the photodegradation rate of azo and diphenyl type dye. *Materials Today: Proceedings*, *3*, 4121–4127.

Nithya, N., Bhoopathi, G., Magesh, G., & Kumar, C. D. N. (2018). Neodymium doped TiO_2 nanoparticles by sol-gel method for antibacterial and photocatalytic activity. *Materials Science in Semiconductor Processing*, *83*, 70–82.

Norris, D. J., Efros, A. L., & Erwin, S. C. (2008). ChemInform abstract: Doped nanocrystals. *ChemInform*, *39*, 1776–1780.

Oba, F., Tatsumi, K., Adachi, H., & Tanaka, I. (2001). N- and p-type dopants for cubic silicon nitride. *Applied Physics Letters*, *78*, 1577–1579.

This book belongs to Central Library BADJI Mokhtar-ANNABA UNIVERSITY

Copyright Elsevier 2024

Ong, W. J., Tan, L. L., Ng, Y. H., Yong, S. T., & Chai, S. P. (2016). Graphitic carbon nitride (g-C_3N_4)-based Photocatalysts for artificial photosynthesis and environmental remediation: Are we a step closer to achieving sustainability? *Chemical Reviews*, *116*, 7159–7329.

Parveen, A., Agrawal, S., & Azam, A. (2016). Thermal properties of transition metals doped (a: Co, Ni and cu) $BiFe_{0.9}A_{0.1}O_3$, AIP Conf. *Proc*, *1728*, 1956–1968.

Pathak, T. K., Kroon, R. E., & Swart, H. C. (2018). Photocatalytic and biological applications of ag and au doped ZnO nanomaterial synthesized by combustion. *Vacuum*, *157*, 508–513.

Pathak, T. K., Swart, H. C., & Kroon, R. E. (2018). Structural and plasmonic properties of noble metal doped ZnO nanomaterials. *Physics B*, *535*, 114–118.

Pesci, F. M., Wang, G., Klug, D. R., Li, Y., & Cowan, A. J. (2013). Efficient suppression of Electron – hole recombination in oxygen-deficient hydrogen-treated TiO_2 nanowires for Photoelectrochemical water splitting. *Journal of Physical Chemistry C*, *117*, 25837–25844.

Pradeev Raj, K., Sadaiyandi, K., Kennedy, A., & Sagadevan, S. (2017). Photocatalytic and antibacterial studies of indium-doped ZnO nanoparticles synthesized by co-precipitation technique. *Journal of Materials Science: Materials in Electronics*, *28*, 19025–19037.

Sakthivel, S., Shankar, M. V., Palanichamy, M., Arabindoo, B., Bahnemann, D. W., & Murugesan, V. (2004). Enhancement of photocatalytic activity by metal deposition: Characterisation and photonic efficiency of Pt, au and Pd deposited on TiO_2 catalyst. *Water Research*, *38*, 3001–3008.

Schoonen, M. A. A., & Xu, Y. (2000). The absolute energy positions of conduction and valence bands of selected semiconducting minerals. *American Mineralogist*, *85*, 543–556.

Shao, W., Wang, H., & Zhang, X. (2018). Elemental doping for optimizing photocatalysis in semiconductors. *Dalton Transactions*, *47*, 12642–12646.

Shchukin, D. G., Radziuk, D., & Möhwald, H. (2010). Ultrasonic fabrication of metallic nanomaterials and nanoalloys. *Annual Review of Materials Research*, *40*, 345–362.

Sun, S., Hisatomi, T., Wang, Q., Chen, S., Ma, G., Liu, J., et al. (2018). Efficient redox-mediator-free Z-scheme water splitting employing oxysulfide photocatalysts under visible light. *ACS Catalysis*, *8*, 1690–1696.

Takanabe, K. (2017). Photocatalytic water splitting: Quantitative approaches toward Photocatalyst by design. *ACS Catalysis*, *7*, 8006–8022.

Türkyılmaz, Ş. Ş., Güy, N., & Özacar, M. (2017). Photocatalytic efficiencies of Ni, Mn, Fe and ag doped ZnO nanostructures synthesized by hydrothermal method: The synergistic/antagonistic effect between ZnO and metals. *Journal of Photochemistry and Photobiology A: Chemistry*, *341*, 39–50.

Umezawa, N., & Ye, J. (2012). Role of complex defects in photocatalytic activities of nitrogen-doped anatase TiO_2. *Physical Chemistry Chemical Physics*, *14*, 5924–5934.

Verma, K., Patel, K. R., Ram, S., & Barbar, S. K. (2016). Synthesis and characterization of Cr doped $CoFe_2O_4$. *AIP Conf. Proc.*, *1728*, 208–211.

Wang, D. H., Jia, L., Wu, X. L., Lu, L. Q., & Xu, A. W. (2012). One-step hydrothermal synthesis of N-doped TiO_2/C nanocomposites with high visible light photocatalytic activity. *Nanoscale*, *4*, 576–584.

Wang, H., Zhang, L., Chen, Z., Hu, J., Li, S., Wang, Z., et al. (2014). Semiconductor heterojunction photocatalysts: Design, construction, and photocatalytic performances. *Chemical Society Reviews*, *43*, 5234–5244.

Wojcieszak, D., Kaczmarek, D., Domaradzki, J., & Mazur, M. (2013). Correlation of photocatalysis and photoluminescence effect in relation to the surface properties of TiO_2:Tb thin films. *International Journal of Photoenergy*, *2013*, 1–9.

Yan, H., Wang, X., Yao, M., & Yao, X. (2013). Progress in natural science: Materials international band structure design of semiconductors for enhanced photocatalytic activity: The case of TiO_2. *Progress in Natural Science: Materials International*, *23*, 402–407.

Yayapao, O., Thongtem, T., Phuruangrat, A., & Thongtem, S. (2013). Sonochemical synthesis of Dy-doped ZnO nanostructures and their photocatalytic properties. *Journal of Alloys and Compounds*, *576*, 72–79.

This book belongs to Central Library BADJI Mokhtar-ANNABA UNIVERSITY

Copyright Elsevier 2024

Zhang, Y., & Mu, J. (2007). One-pot synthesis, photoluminescence, and photocatalysis of ag/ZnO composites. *Journal of Colloid and Interface Science*, *309*, 478–484.

Zhang, X., Peng, T., & Song, S. (2016). Recent advances in dye-sensitized semiconductor systems for photocatalytic hydrogen production. *Journal of Materials Chemistry A*, *4*, 2365–2402.

Zhang, J., Tse, K., Wong, M., Zhang, Y., & Zhu, J. (2016). A brief review of co-doping. *Frontiers of Physics*, *11* 117405.

Zhou, M., Yu, J., & Cheng, B. (2006). Effects of Fe-doping on the photocatalytic activity of mesoporous TiO2 powders prepared by an ultrasonic method. *Journal of Hazardous Materials*, *137*, 1838–1847.

Further reading

Marwah, K., & Tavakoli, A. (2004). The effect of foreign capital and imports on economic growth: Further evidence from four Asian countries (1970-1998). *Journal of Asian Economics*, *15*, 399–413.

This book belongs to Central Library BADJI Mokhtar-ANNABA UNIVERSITY

Copyright Elsevier 2024

This page intentionally left blank

This book belongs to Central Library BADJI Mokhtar-ANNABA UNIVERSITY

Copyright Elsevier 2024

CHAPTER

Low-dimensional nanomaterials for the photocatalytic degradation of organic pollutants

2

Debabrata Mishra[a], Manish Srivastava[a,b]

Department of Physics and Astrophysics, University of Delhi, Delhi, India[a] Department of Chemical Engineering & Technology, IIT (BHU), Varanasi, India[b]

1 Introduction

One of the most important challenges that has posed a serious threat to the existence of living being on earth is environmental pollution. There is a deleterious effect on the health of human being, and many species are in danger owing to the hazardous effect of pollutants (Brulle & Pellow, 2006; Cabello, 2006; Kampa & Castanas, 2008; Martinez, 2009). In general, there are two kinds of contributions to the environmental pollution. One is natural and the other artificial. Among the natural pollution, volcanoes, hurricanes, and earthquake contribute to the maximum effect, while industry and agriculture are mainly responsible for artificial pollution (Aiuppa, Bellomo, Brusca, D'Alessandro, & Federico, 2003; Hettige, Mani, & Wheeler, 2000; Rozell & Reaven, 2012; Tarzia et al., 2002). The environmental pollution is the sum total of the pollution that exists in water, air, and on soil. Environmental pollution is categorically divided into two types. One is organic and the other inorganic. Among the various sources of pollutants, physical, chemical, and biological pollutants are the prime sources of pollution, which varies in different degree for the contribution toward the same. The inorganic pollutants belong to the category of chemical pollutants. Among the different types of inorganic pollutants, sulfur- and nitrogen-based compounds contribute to the maximum contamination. Few examples are NO_2, SO_2, HS, HCl, HF, Cl, Pb, and Zn (Bosco, Varrica, & Dongarrà, 2005; Brown, 1999; Seiler & Sigel, 1988; Wang, 1987). A detailed study of the inorganic pollutants can be found elsewhere and is beyond the scope of this chapter (Manahan, 2001, 2013).

It has been widely recognized that pesticides, synthetic dyes, and pharmaceutical compounds are the prime contributor of organic pollutions (Dietz & Schnoor, 2001; Ghasemi, Rasoul-Amini, & Fotooh-Abadi, 2011; Kolpin et al., 2002; Manahan, 2013; Semrany, Favier, Djelal, Taha, & Amrane, 2012; Teh & Mohamed, 2011). Various industries including paper industry, textile industry, and hair coloring use synthetic organic dyes extensively and cause many health hazards upon consumption directly or indirectly. Serious health risk factors crop up when large-scale production of these materials are disposed of untreated in aquatic environment. Organic dyes mainly contain either chromophores (—C═C—, —C═N—) or auxochrome (—NH3, —COOH) that generate coloring.

Nano-Materials as Photocatalysts for Degradation of Environmental Pollutants. https://doi.org/10.1016/B978-0-12-818598-8.00002-X
© 2020 Elsevier Inc. All rights reserved.

This book belongs to Central Library BADJI Mokhtar-ANNABA UNIVERSITY

Copyright Elsevier 2024

Different classes of dyes are available in the market depending on their chemical structure such as azo, anthraquinone, and phthalocyanine (Hunger, 2002; Moussavi & Mahmoudi, 2009). Mostly, azo and anthraquinone constitute nearly 80% of organic dyes found commercially. Pesticides are another source of organic pollutants that are mainly used to control and prevent plant diseases and are used in food industries and in agriculture. They are classified as per their biological activity, which include fungicides, herbicides, insecticides, and molluscicides (Dirinck et al., 2011). Chemically, they contain phosphates and chlorine that produce hazardous effect when contaminated. Phenols are another class of organic pollutants that find many applications including in petroleum refining, paper and pulp mills, disinfectants, and preservatives (Lacorte et al., 2003). Apart from that, pharmaceutical residues also cause a potential impact on human health drastically and need to be checked urgently (Nicolopoulou-Stamati, Maipas, Kotampasi, Stamatis, & Hens, 2016).

2 Methods of degradation of organic pollutants

There exist various methods for the degradation of organic pollutants, which may be physical, chemical, biological, or natural in nature (Schell, Knutson, & Bailey, 2012). In physical processes, degradation is done by photocatalytic activity of a semiconductor such as TiO_2 or its composites with other materials, for example, graphene, to accelerate the process of degradation of the organic pollutants. TiO_2 is chosen for its nontoxicity and cheap market value as well as abundance. It is also easy to prepare TiO_2 nanoparticles of varying sizes (Xiong, Zhang, Ma, & Zhao, 2010; Zhang, Tang, Fu, & Xu, 2010). Dehalogenation of chlorinated benzene is an example of chemical degradation of organic pollutants. A detailed description of its various processes can be found in the literature (Fennell, Nijenhuis, Wilson, Zinder, & Häggblom, 2004; Wada, Kitamura, Yanagida, & Yin, 1998; Yin, Wada, Kitamura, & Yanagida, 2001). Mineralization of various dyes such as rhodamine B is also an example of chemical process of degradation. Nevertheless, microorganisms present on earth degrade many organic pollutants slowly but steadily. They convert a particular composition of the target molecule to a different one and reduce its toxic or hazardous effect naturally. Ozonization and oxidation of various species yield to the degradation of their basic pollutant character. Coagulation is a method of treating wastewater in a large scale. In this method, fine particles are coagulated using suitable chemicals to remove the pollutants present, if any, in aqueous medium (DeLuca, Chao, & Smallwood, 1983; Matilainen, Vepsäläinen, & Sillanpää, 2010; Poznyak, Bautista, Chaírez, Córdova, & Ríos, 2008; Renault, Sancey, Badot, & Crini, 2009). Similarly, water oxidation is another effective method of degradation of pollutants present in water. Photocatalytic degradation is a physicochemical process that has drawn lot of attention due to its effective remediation of organic pollutants present in water or in the liquid medium (Akpan & Hameed, 2009; Daneshvar, Salari, & Khataee, 2004; Gaya & Abdullah, 2008). The low cost and high efficiency of photocatalyst method have made TiO_2 more attractive and were discovered by Fujishima and Honda in 1972 during the photocatalytic splitting of water on a TiO_2 electrode under UV irradiation. In the photocatalytic process, both light and catalyst contribute to the enhancement of the rate of chemical reaction (Fujishima & Honda, 1972). Photocatalysts can be either homogeneous or heterogeneous in nature. In homogeneous photocatalysis, metal ions produce hydroxyl ions, which react with the organic pollutants to reduce it. However, in heterogeneous photocatalysis, semiconductors like ZnO and TiO_2 participate in the reaction. Due to the photoabsorption properties of these semiconductors, conduction and

This book belongs to Central Library BADJI Mokhtar-ANNABA UNIVERSITY
Copyright Elsevier 2024

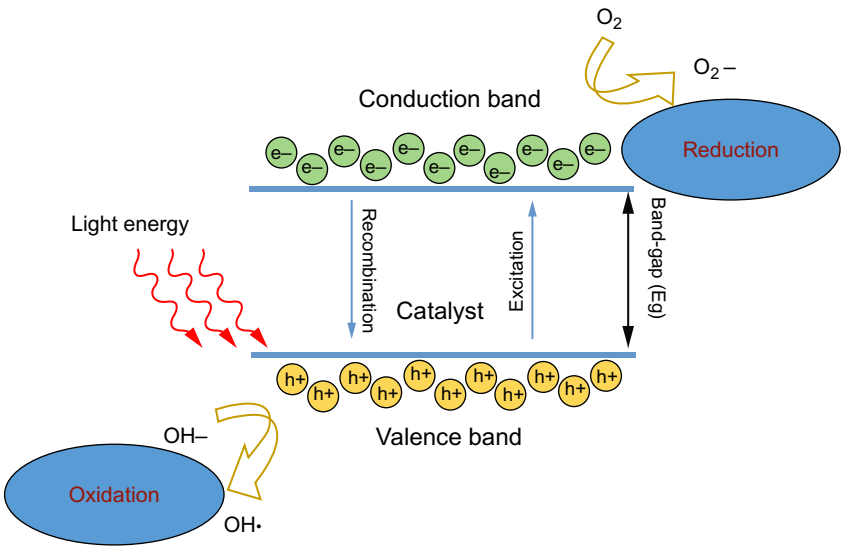

FIG. 1

Schematic representation of the mechanism of photocatalysis.

valence band participate in the conduction of electrons, and the lifetime of excited photoelectrons is used to carry out the necessary chemical reaction for the degradation of organic pollutants. The main characteristics of semiconductors are nontoxicity, chemically inertness, cheap, and their abundance.

Fig. 1 represents the mechanism of a typical photocatalytic process. A semiconductor has valence band and conduction band separated by an energy gap called bandgap. When the light of sufficient energy is irradiated on the surface of a semiconductor, an electron–hole pair is created. The electrons move to the conduction band, while the holes reside in the valence band of the semiconductor. These holes oxidize the donor molecule and react with water to produce hydroxyl radicals. These radicals are strong oxidizing agents to reduce the organic pollutants. Electrons of the conduction band react with the adsorbed oxygen species to make superoxide ions and cause redox reactions. The main advantage of photocatalysis is the formation of nontoxic products, and it uses the renewable energy like sunlight to carry out the reaction. It is mainly used to treat the wastewater for purification. Nonetheless, there are also certain limitations of the photocatalytic process. The recombination rate of electron–hole pair is quite high for semiconductors; as a result, an effective charge separation is needed to carry out the necessary reaction (Aulbur, Jönsson, & Wilkins, 2000). Therefore, alternative materials/composites should be prepared to combat the effect of organic pollutants. In other words, efficient charge separation and reduced recombination of electron–hole pair is needed to increase the efficiency of the photocatalytic activities. To achieve this 2D materials like graphene, MoS_2 can be useful in photocatalysis due to their better conductivity and high active surface area for photocatalytic activity.

This book belongs to Central Library BADJI Mokhtar-ANNABA UNIVERSITY Copyright Elsevier 2024

3 Photocatalytic degradation using graphene-based nanostructures

Scientists across the globe have developed many physical/chemical techniques such as adsorption and membrane separation for the removal of contaminants from the aquatic system (Barakat, 2011; Rajasulochana & Preethy, 2016; Sharma & Bhattacharya, 2017). However, these methods are as cost intensive and tedious restricting their use. Nevertheless, a detailed discussion about these methods is beyond the scope of this chapter. In view of the aforementioned facts, novel techniques are needed to overcome these difficulties and might offer a better avenue for the treatment of organic pollutants in an efficient way. As it has been mentioned earlier for the case of TiO_2 nanomaterials, 2D materials such as graphene can also play an important role in enhancing the rate of biodegradation of organic pollutants. The combination of graphene and a photocatalytic material has emerged as an alternative route to treat wastewater remediation (An & Yu, 2011). Separation and transfer of photogenerated charges are important in photocatalytic processes for successful degradation of organic pollutants. Hence, organic chromophores with visible-light absorption properties with the charge transfer properties of graphene-based materials (graphene, graphene oxide, and reduced graphene oxide) have been established as the state-of-the-art technique for wastewater management. In addition to these, abundance, proecofriendly, and tunable functional behavior of graphene offer to develop the next-generation material for photocatalytic processes (Liu, Cai, & Li, 2015; Toth, Ramasse, Velický, & Dryfe, 2015). It is well known that graphene has numerous fascinating properties most notably high specific surface area and charge transfer characteristics. Further, graphene forms the basis of reactivity with the other moieties and can be a promising candidate for pollutant removal/reduction. In addition to this, graphene can also be functionalized with many other functional (chemical) groups needed for the multifunctional reduction of the pollutants. The extremely small size of graphene makes it a fundamental material and can be used to make multifunctional composite with other materials. It is also biocompatible and highly conductive, thus enhancing the reactivity of the final product. Anchoring different photoresponsive material onto graphene-based materials via covalent and noncovalent interactions (van der Waals and/or electrostatic interactions) allows to bind molecules together (Georgakilas et al., 2012).

Recently, several studies have contributed to the investigation of the catalytic or photocatalytic properties of graphene or reduced graphene oxide (rGO) (Zhang, Lv, Li, Wang, & Li, 2010; Zhang, Tang, et al., 2010). The oxidized derivative of graphene, such as graphene oxide (GO), contains various functional groups such as carboxyl, hydroxyl, and epoxide on its surface, which makes it highly hydrophilic and water soluble. This makes it applicable for supporting metal/metal oxide particles. Compared with GO, rGO has higher electrical conductivity and thermal stability, which may promote better electron transportation in the Fenton process (Yu, Tian, Chen, Wang, & Wang, 2015).

3.1 Fe/Co/Ni-based graphene composites

Metal–organic frameworks (MOFs) possess unique properties including high surface area, tunability, and functionalities. They are generally constructed from the self-assembled metals, organic ligands, or ions. Due to their multifunctional behavior, they find applications in many important areas including in gas storage, sensors, drug delivery, and catalysis (Farrusseng, Aguado, & Pinel, 2009; Sun et al., 2017; Xia, Mahmood, Zou, & Xu, 2015). Moreover, the compact arrangements of ions and their affinity with the reaction environment make them a better catalyst. Recently, some Fe-based MOFs have been studied in heterogeneous Fenton degradation of organic pollutants (Lv et al., 2015; Tang & Wang, 2017).

This book belongs to Central Library BADJI Mokhtar-ANNABA UNIVERSITY Copyright Elsevier 2024

Note that the Fenton reaction has great potential to purify organic contaminants in water (Brillas, Sirés, & Oturan, 2009; Wang, Chen, Ma, & Zhao, 2012). In the Fenton system, benign H_2O_2 and Fe^{2+} ions are used as the oxidant and the catalyst, respectively. The oxidative intermediates occurred during the reaction such as OH, ·OOH, and Fe ions help in the degradation of organic pollutants. Jiang et al. used MIL-53(Fe) as Fenton-like catalysts to decompose rhodamine B in the presence of H_2O_2 (Ai, Zhang, Li, & Jiang, 2014). MIL-100(Fe)/GO nanocomposite was synthesized by Tang et al. via hydrothermal method, and the content of GO in the MIL-100(Fe)/GO nanocomposite was set to be 5 wt% (Tang & Wang, 2017). The synthesized nanocomposite was characterized by different techniques including XRD, FT-IR, XPS, and TGA. These characterizations confirmed the formation of the nanocomposites as desired. The catalytic activity was monitored in a 100-mL sealed serum bottles within a shaking incubator. The MIL-100(Fe)/GO nanocomposite was dispersed in MO solution (50 mg L^{-1}, 40 mL) while keeping the pH constant. Subsequently, a known dosage of H_2O_2 was immediately added to the solution to initiate the reaction. It was observed that complete decomposition of MO occurred after 240 min.

Yao et al. prepared a hybrid rGS/Fe_xO_y/NCL (nitrogen-doped carbon layer) aerogel having 3D hierarchical porous structure by tandem reaction followed by pyrolysis process as shown in Fig. 2 (Yao et al., 2019). Subsequently, photo-Fenton reaction was carried out to degrade rhodamine B. It was found that the rate constant, k, and TOC (mineral efficiency) value reached 2.37×10^{-2} min^{-1} and

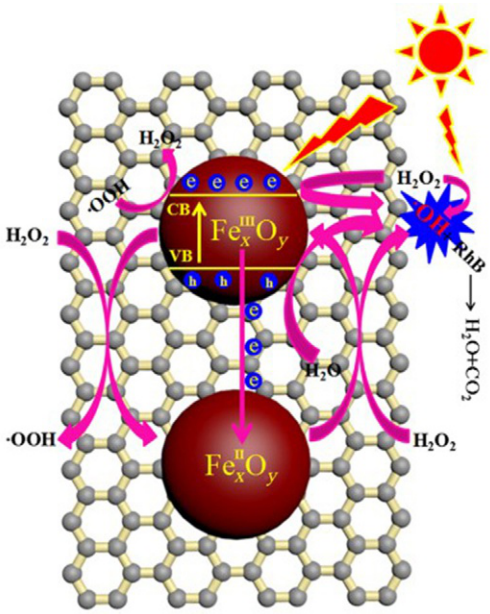

FIG. 2

Schematic representation for the rGS/Fe_xO_y/NCL aerogel toward photo-Fenton degradation of RhB.

Fig. 12 of Yao, T., Jia, W., Feng, Y., Zhang, J., Lian, Y., Wu, J., & Zhang, X. (2019). Preparation of reduced graphene oxide nanosheet/FexOy/nitrogen-doped carbon layer aerogel as photo-Fenton catalyst with enhanced degradation activity and reusability. Journal of Hazardous Materials, 362, *62–71. https://doi.org/10.1016/j.jhazmat.2018.08.084, reproduced with permission.*

This book belongs to Central Library BADJI Mokhtar-ANNABA UNIVERSITY Copyright Elsevier 2024

76.1%, respectively. The enhanced catalytic activity has been attributed to the sandwiching Fe_xO_y nanoparticles between rGS and NCL. In addition to this, reusability was good up to five cycles. In another work, Huang et al. investigated the degradation of rhodamine 6G using Fe nanoparticle–based nanocomposite with graphene in a Fenton reaction (Huang, Niu, & Hu, 2017). The Fe/Fe_3C nanoparticles were decorated on Fe-/N-doped graphene nanosheet and were used to degrade Rh-6G. Excellent catalytic activity was observed with efficient durability. The degradation time was found to be 40 min, and it could also be used for 13 repeated cycles. Thus, the reproducibility was noticed to be very high. A thin layer of carbon acts as a shell for the Fe/Fe3C nanoparticles, which prevented possible aggregation. It was claimed that the porosity provided a surface area to Fe for active reaction, which could easily degraded organic pollutant (Rh-6G) (Huang et al., 2017).

Boruha et al. prepared a nanocomposite of Fe_3O_4/rGO and studied degradation of various organic dyes including methyl green (MG), methyl blue (MB), and rhodamine B (RhB) in the presence of sunlight (Boruah et al., 2016). The photocatalytic processes start with the absorption of a photon by Fe_3O_4/rGO nanocomposites. As a result, electron transfer takes place from the valence band to the conduction band of Fe_3O_4. Further, this electron is captured by rGO and helps in the conduction of electrons. This is readily captured by the dissolved oxygen and forms O^{2-} radical. In aqueous solution, holes form hydroxyl ions, which is the main cause of the degradation of dyes. Apart from that, another important characteristic is that, due to the presence of magnetic nanoparticles, it can also be separated after the reaction is completed and can be reused. This shows that Fe_3O_4/rGO nanocomposite can be a suitable candidate for the degradation of organic pollutants present in water. Jaihindh et al. prepared rGO-/Ag-/Fe-doped TiO_2 by a simple chemical reduction and the hydrothermal method (Jaihindh, Chen, & Fu, 2018). Further, photocatalytic MB degradation was examined under a 35 W Xe arc lamp. The rGO-/Ag-/Fe-doped TiO_2 degraded MB in 150 min with the conversion efficiency >95.33%. The rate of degradation constant, k, was found to be $0.020\,min^{-1}$. Moreover, the oxygen evolution reaction was maintained during the photodegradation of MB. Sulfate radicals are better candidates for the degradation of refractory organic pollutants than their hydroxyl counterparts. They have a higher oxidation potential (2.5–3.1 V) with a longer half-life than OH^-, which is close to 2.7 V (Wang, Kang, et al., 2016; Zhao et al., 2017). Compared with hydroxyl radical (OH^-)–based advanced oxidation processes (AOPs), sulfate radical (SO_4^-)–based AOPs exhibited additional advantages to treat refractory organic pollutants, including higher oxidative potential of SO_4^- (2.5–3.1 V) than OH (2.7 V), much longer half-life of SO_4^- (30–40 ms) than OH (<1 ms) and broader application range of pH values (2.0–8.0).

Yuan et al. prepared 3D porous $Co_3O_4^-$/nitrogen-doped graphene aerogel (NGA) hybrid for the activation of peroxymonosulfate (PMS) (Yuan et al., 2018). This hybrid was prepared by hydrothermal method followed by freeze-drying methods. The morphology of the composites as probed by scanning electron microscope is shown in Fig. 3. It was noticed that Co_3O_4/NGA hybrid could degrade acid orange 7 (AO7) within 30 min. In addition, it was found that moderate concentration of PMS, high temperature, and low PH value facilitated the degradation of AO7. It is anticipated that Co_3O_4 nanoparticles embedded on NGA surface acted as main facilitator for catalytic degradation. The formation of $CoOH^+$ on Co_3O_4 will bring an electron transfer to PMS to make SO_4^+ ions. At the same time, the formation of OH^- by the reaction of SO_4^- and water molecules starts the degradation of AO7 molecules and their intermediates. Graphene contains many electron-rich functional groups including carboxylic and quinone group and have high affinity to chemical reactivity for PMS (Duan et al., 2015; Qin et al., 2017). Charge density of the carbon atoms in NGA can also be altered by N doping, which might create new sites of chemical activity. This can be achieved by bringing a change to the sp^2-hybridized carbon

This book belongs to Central Library BADJI Mokhtar-ANNABA UNIVERSITY Copyright Elsevier 2024

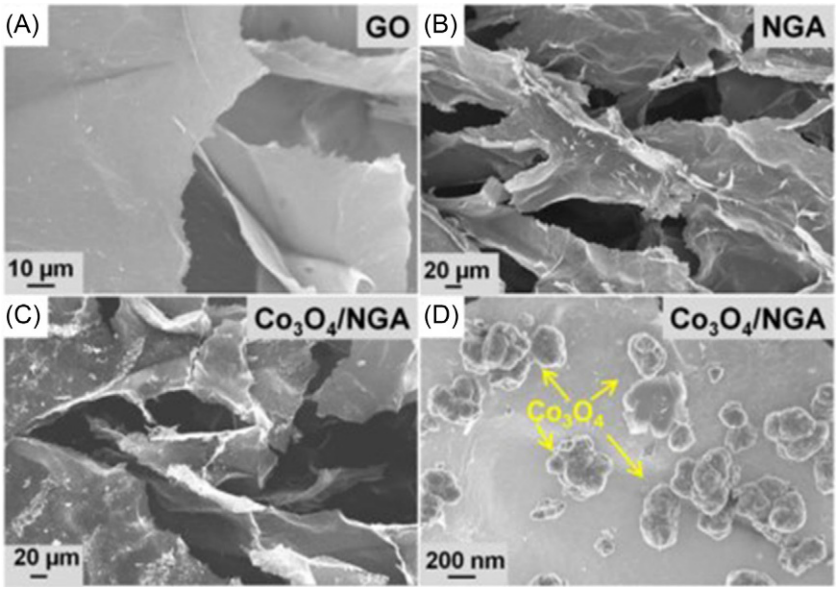

FIG. 3

SEM of (A) GO nanosheets, (B) NGA, and (C and D) Co_3O_4/NGA.

Fig. 2 of Yuan, R., Hu, L., Yu, P., Wang, Z., Wang, H., & Fang, J. (2018). Co_3O_4 nanocrystals/3D nitrogen-doped graphene aerogel: A synergistic hybrid for peroxymonosulfate activation toward the degradation of organic pollutants. Chemosphere, 210, *877–888. https://doi.org/10.1016/j.chemosphere.2018.07.065 reproduced with permission.*

configuration. Sulfate ion radicals can be produced when there is an electron transfer from PMS to NGA layer. This leads finally to elevate catalytic activity of Co_3O_4/NGA nanocomposite (Ren et al., 2018). In this process, organic pollutants and their intermediates degrade to harmless CO_2 and H_2O. Zhao et al. reported that the Ag_3PO_4/GO/$NiFe_2O_4$ nanocomposites prepared by ion-exchange deposition method showed excellent photocatalytic degradation of rhodamine B (Zhou et al., 2018). The photocatalytic degradation efficiency was calculated to be 96% with 15 min of light irradiation. Both the electrochemical and fluorescence measurements were performed on this nanocomposite, and it was found that large transient photocurrent associated with fluorescence lifetime (7.82 ns) could be achievable. The photocatalytic degradation was explained on the basis of fast electron transfer from Ag_3PO_4 to $NiFe_2O_4$ through GO sheet and can be useful in wastewater treatment.

3.2 (Zn/Ti/W/Ce)O-based graphene composites

ZnO nanostructures possess a number of superior physical properties including abundance, low cost, nontoxicity, and semiconducting properties. It also possesses high rate of reactivity, which is particularly useful for photocatalytic activity. Nevertheless, one of the major drawbacks of ZnO nanostructure is that the recombination rate of electron-hole pair is very high. This results in low conversion efficiency and poor catalytic activity. The photocatalytic activity can be further improved by creating defects and oxygen vacancy in ZnO nanostructure. To achieve this, materials with similar radius such

This book belongs to Central Library BADJI Mokhtar-ANNABA UNIVERSITY Copyright Elsevier 2024

as Mg can be doped in to the matrix of ZnO selectively. But this may not guarantee to suppress the recombination rate (Chen et al., 2018; Labhane, Sonawane, Sonawane, Patil, & Huse, 2018). Therefore, it can be combined with other materials to form a nanocomposite that can prevent recombination rate by rapidly transferring the photoinduced electrons. One of the advanced materials for this purpose is graphene. Due to the high carrier mobility and large surface area, graphene is capable to hinder aggregation of ZnO nanoparticles and thus enhances the electron transfer through its matrix (Lei, Wang, Zhu, Xie, & Tang, 2014). Chen et al. prepared GO/MoS_2/Mg-ZnO nanocomposites by mean of electrostatic interactions (Fig. 4). Further, the inclusion of MoS_2 in the nanocomposite is mainly because it

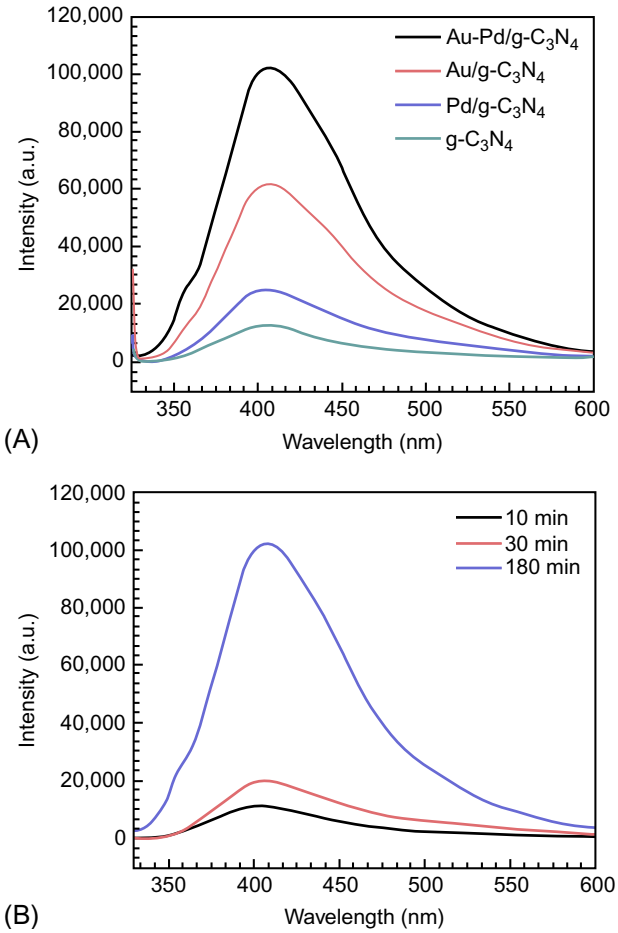

FIG. 4

PL spectra of (A) different catalysts (B) Au-Pd/g-C_3N_4.

Fig. 5 of Darabdhara, G., & Das, M. R. (2018). Bimetallic Au-Pd nanoparticles on 2D supported graphitic carbon nitride and reduced graphene oxide sheets: A comparative photocatalytic degradation study of organic pollutants in water. Chemosphere, 197, *817–829. https://doi.org/10.1016/j.chemosphere.2018.01.073 reproduced with permission.*

This book belongs to Central Library BADJI Mokhtar-ANNABA UNIVERSITY Copyright Elsevier 2024

is a p-type semiconductor and has good photoactivity due to the presence of narrow energy bandgap. These authors reported that the excellent photocatalytic activity and quantum yield are due to the synergistic effect between GO and MoS_2 nanosheets (Chen et al., 2018). Liu et al. prepared a nanocomposite (ZnO/rGO) that was incorporated into graphene to form hydrogels (ZnO/rGO–rGH) hybrid having three-dimensional (3D) network structures (Liu, Yue, Liu, Rui, & Cui, 2018). The ZnO/rGO–rGH nanohybrid possessed the ability of fast adsorption and desorption due to the presence of graphene. The nanocomposite of ZnO and rGO improves the photocatalytic activity by lowering the recombination rate of electron and hole pairs. The photocatalytic activity suggested that phenol and bisphenol A (BPA) could be removed 100% within 20 min under the UV irradiation. Further, it was found that the purification efficiency of ZnO/rGO–rGH nanohybrid could be achieved ~90% even after five cycles. Moreover, these authors followed the same experiment in flow condition of BPA and found that it takes 16 h to completely remove BPA under the flow condition. Nevertheless, there was a decline of adsorption capacity of the nanocomposite after few cycles of use but could still performed the photocatalytic reaction effectively. Moreover, ZnO/rGO–rGH nanocomposite could be separated using a filter due to the micron size of the composite and can be reused with the same efficiency. In summary, ZnO/rGO–rGH composite possesses high degree of adsorption and photocatalytic degradation, and therefore, it can be a useful candidate to remove BPA from sewage. Sun et al. prepared a series of graphene-based nanocomposites using TiO_2 nanoparticles (Sun et al., 2018). The authors used different functional groups of graphene and investigated the photocatalytic activity of the nanocomposites. Further, it was found that carboxylic functional group plays very important role in efficient photocatalysis. Adsorption and photocatalytic activities strongly depend on the functional groups attached to the graphene. This was probed by electron paramagnetic resonance (EPR) techniques, infrared spectroscopy (IR), and electron lifetime measurements. The carboxylic group facilitates to form a strong chemical bond with the TiO_2 nanoparticles. Due to this, there is an efficient conduction of electrons that increases the lifetime of photoinduced electrons. In addition, it was highly stable and can be reused after many cycles of operation. There is a strong limitation of ZnO nanoparticles/nanorods for photocatalytic use due to its fast recombination rate. However, this can be overcome by making composites with other materials such as light harvesting material, $CuInS_2$. Ternary copper indium disulfide is a photosensitizer (bandgap of 1.5 eV) and exhibits high extinction efficiency (Torimoto et al., 2016; Xu et al., 2018). Xu et al. prepared a ternary alloy of ZnO nanorod/rGO/$CuInS_2$ quantum dots and investigated photocatalytic degradation of rhodamine B under the visible-light irradiation (Xu et al., 2018). In this alloy, $CuInS_2$ was kept at 10 at.% having an optimized value. The 100% degradation of rhodamine B in 120 min could be achieved, which was much higher than the mere 20% degradation of rhodamine B using ZnO alone. Chouhan et al. prepared zinc oxide (ZnO) nanoflowers/graphene oxide (GO) composite, which was uniformly grown over silicon (Si) substrate. In this approach, ZnO nanoseeds and graphene oxide (GO) were prepared by chemical and Hummer's method, respectively (Chauhan, Kant, Rai, Gupta, & Bhattacharya, 2019). The as-prepared ZnO/GO nanocomposite was used to degrade the methylene blue (MB) dye under the sunlight. It was found that 99% of MB was degraded using this nanocomposite, ~30% more than that achieved by bare ZnO. The enhanced photocatalytic activity was attributed to the excess of carboxylic ions provided by GO. A detailed list of different shapes of ZnO is also listed in Table 1.

Anshuman et al. studied the degradation behavior of orange-G azo dye under the microwave irradiation (Anshuman, Saremi-Yarahmadi, & Vaidhyanathan, 2018). Orange-G azo dye or colorant finds large-scale applications in industry. It disturbs the aquatic ecosystem and is also resistant to microbial

This book belongs to Central Library BADJI Mokhtar-ANNABA UNIVERSITY Copyright Elsevier 2024

Table 1 Comparison of ZnO/GO nanocomposite with other studies for decolorization of MB dye.

S. no.	Photocatalyst	MB concentration (M)	Light source	Dosage and decolorization time	Reference
1	Graphene–ZnO thin films	5×10^{-3}	UV light ($\lambda = 254$ nm)	Thin film (size or weight of photocatalyst not mentioned) degraded 68% dye in 120 min	Joshi, Yoon, Na, Choi, and Yoon (2014)
2	Graphene–ZnO nanoparticles	1	Sunlight	1645 mg of the material degraded 99.8% MB in 25 min	Bu, Chen, Li, and Hou (2013)
3	Electrospun graphene–ZnO	5×10^{-3}	UV light ($\lambda = 365$ nm)	Thin film (5 cm^2) of photocatalyst degraded 64% MB in 240 min	An, Joshi, Lee, Kim, and Yoon (2014)
4	Graphene-wrapped ZnO nanospheres	5×10^{-5}	Xenon lamp (300 W)	Thin film (0.1 wt%) degraded 81.9% of MB in 140 min	Chen et al. (2015)
5	ZnO nanoflowers at GO sheet on Si substrate	6.25×10^{-5}	Sunlight	Thin film (1 in.2) (~10 mg in 50-mL dye) degraded 99% of MB in 80 min	Chauhan et al. (2019)

Table 3 of Chauhan, P. S., Kant, R., Rai, A., Gupta, A., & Bhattacharya, S. (2019). Facile synthesis of ZnO/GO nanoflowers over Si substrate for improved photocatalytic decolorization of MB dye and industrial wastewater under solar irradiation. Materials Science in Semiconductor Processing, 89, *6–17. https://doi.org/10.1016/j.mssp.2018.08.022 reproduced with permission.*

degradation when present in water. In view of the aforementioned fact, Anshuman et al. prepared a reduced graphene oxide–titania (rGO–TiO_2) nanocomposite by chemical reduction technique (Anshuman et al., 2018). The catalytic activity under the microwave irradiation and heat treatment showed degradation of 88% dye within 20 min of treatment at 120°C. It was also noticed that 65% of the dye was degraded in only 5 min of microwave irradiation compared with 18% decomposition achieved during conventional heating technique. High-resolution transmission electron microscope (HR-TEM) imaging and UV–vis spectra confirmed the formation of hot spots in the nanostructure due to the absorption of microwave by reduced graphene oxide. The origin of such local hot spots triggers more electron/hole pairs at the surface of the hybrid nanocatalysts. As a result, it reacts with O_2 and H_2O to form ·OH and superoxide radical anion (O_2^{-2}), and thus, the rate of decomposition increases by many folds. Tie et al. prepared a nanocomposite made up of tungsten trioxide (WO_3) nanorods on rGO sheets by in situ solvothermal method (Tie et al., 2018). Photocatalytic activity of as-prepared WO_3 and WO_3/rGO nanocomposites was monitored separately by applying it to methylthionine chloride (MB)–contained wastewater under the visible-light irradiation. It was found that >94% photocatalytic degradation efficiency could be achieved within 150 min, which was 71.8% greater than WO_3 alone. Such a large difference in the efficiency was attributed to the strong interfacial activity of graphene and WO_3, which hinders the recombination rate upon light irradiation. Choi et al. significantly increased the dye absorption capacity of CeO_2 by functionalizing it with reduced graphene oxide aerogels (RGAs)

This book belongs to Central Library BADJI Mokhtar-ANNABA UNIVERSITY Copyright Elsevier 2024

following chemical route (Choi, Reddy, Islam, Ma, & Kim, 2016). It was observed that the self-assembly of RGA-functionalized CeO_2 enhanced the charge transfer and separation of electron–hole pairs because of their similar band positions. Further, the photocatalytic study was performed on the degradation of rhodamine B in aqueous solution. Owing to excellent photocatalytic activity, this nanocomposite can be a promising candidate for wastewater treatment.

3.3 Metal-/nonmetal (N)-based graphene nanocomposites

The presence of bimetallic nanoparticles in photocatalytic process is very useful as it hinders the recombination rate and enhances the photocatalytic activity due to the synergistic effect of these nanoparticles when made of composites with graphene or any other 2D materials such as graphitic carbon nitride (g-C_3N_4), transition metal chalcogenides, and hexagonal boron nitrides (see Fig. 4). Darabdhara et al. prepared Au-Pd/g-C_3N_4 and Au-Pd/rGO nanocomposites by chemical route (Darabdhara & Das, 2018). These nanocomposites were then used as active photocatalyst for the degradation of phenolic compounds in water. Both the experiments were performed under the sunlight and UV-light irradiation. It was found that >95% of degradation was achieved using Au-Pd/g-C_3N_4 nanocomposite in 180 min. The decomposition efficiency of Au-Pd/g-C_3N_4 nanocomposite was found to be greater than Au-Pd/rGO. This might be due to the presence of nitrogen atoms in the nanocomposites. However, these authors noticed no significant change in the size or crystalline structure after using it as the photocatalyst. This ensures the stability of the nanocomposites and promotes other 2D material to be used as a photocatalyst. Sewage contamination by organic dyes is detrimental to the hazardous nature of the water and hence various absorbing materials including charcoal, silica, wool fiber, etc. are generally used to remove these pollutants. However, one of the most intriguing challenges is the regeneration of adsorbent. To avoid this issue, Liu et al. prepared a nanocomposite with porous diamine-functionalized graphene oxide (GO) embedded with photocatalytically active polyoxometalates (POMs) (Liu et al., 2017). These two components work synergistically to degrade certain organic dyes. These authors reported that, due to the encapsulation, POM stabilizes the photogenerated electron–hole pairs in the GO matrix by trapping it. In this way, oxidative degradation was enhanced mutually by GO and POM. The enhanced adsorption may be due to the combination of strong hydrophobic and π–π interactions between the organic pollutants and the graphene-based nanocomposite (Chabot et al., 2014). However, this strong interaction may hinder the photoregeneration. Therefore, a suitable choice of host with graphene matrix is prerequisite for the photocatalytic activity to be carried out.

4 Photoelectrochemical technique

Another important process that has gained widespread attention is the use of electrophotocatalysis. This technique is the combination of heterogeneous photocatalysis and electrochemistry. It can also be viewed as an interdisciplinary area where surface science, physical chemistry, solid-state physics, and biology meet. In this technique, light is irradiated on a semiconductor electrode followed by an applied electrical potential gradient across the electrodes, which degrades the organic pollutants. This technique is widely used in the deactivation of microorganism and oxidation of organic compounds (Delegan, Daghrir, Drogui, & Khakani, 2014; Garcia-Segura & Brillas, 2017; Lewerenz et al., 2010; Wu, Pan, & Chen, 2012).

This book belongs to Central Library BADJI Mokhtar-ANNABA UNIVERSITY Copyright Elsevier 2024

4.1 Mechanism of photoelectrocatalysis

Energy bands are formed in a semiconductor due to the overlapping of atomic orbitals. Two types of bands are created, namely, valence band and conduction band with an energy gap between them (ΔE). Fermi energy (E_f) is the energy of the highest filled orbital at 0 K and lies between valence and conduction band. To make the semiconductor conductive, electrons need to be pushed to the conduction band. This is done with the photon energy. When the light is irradiated on semiconductor surface, it creates electron-hole pair. But due to the high affinity to recombination behavior, they are less efficient in making any impact (see Fig. 5). This can be removed by combining the electrochemical reaction with photocatalytic processes. This way, the charge separation can be enhanced. When the electrodes are bare, the energy bands of the semiconductor electrode are flat. But when it comes in contact with the electrolyte, a junction is formed (Schottky junction), and there is a shift in the Fermi level that tries to equilibrate it with respect to the electrolyte. As a result, there is a band bending, and the region near the bend bending is called space charge layer or depletion layer (see Fig. 6). Majority charge carrier that is electrons for N-type or holes for p-type semiconductors are depleted in this region (Ashcroft, Mermin, & Brooks/Cole Publishing, 2018; Neamen, 2012). Due to the depletion of majority charge carriers, charge separation is enhanced, and minority carriers participate in the chemical reaction near the surface. They bring about the formation of hydroxyl radicals, which can then degrade organic pollutants. When the light is irradiated and the external potential applied is greater than the flat band energy, there is an increase in the band bending; as a result, there is an accumulation of more minority charge carriers on the surface, which is good for causing redox reaction. The recombination rate of electron-hole pair is minimized, which improves the photocatalytic properties. TiO_2 is one of the promising candidates being used for the degradation of organic pollutants. This is due to its low-cost availability and inert behavior that enable to find wide applications mainly in wastewater management. Mostly, studies have been reported on TiO_2 in its nanoparticle form. Researchers also doped many

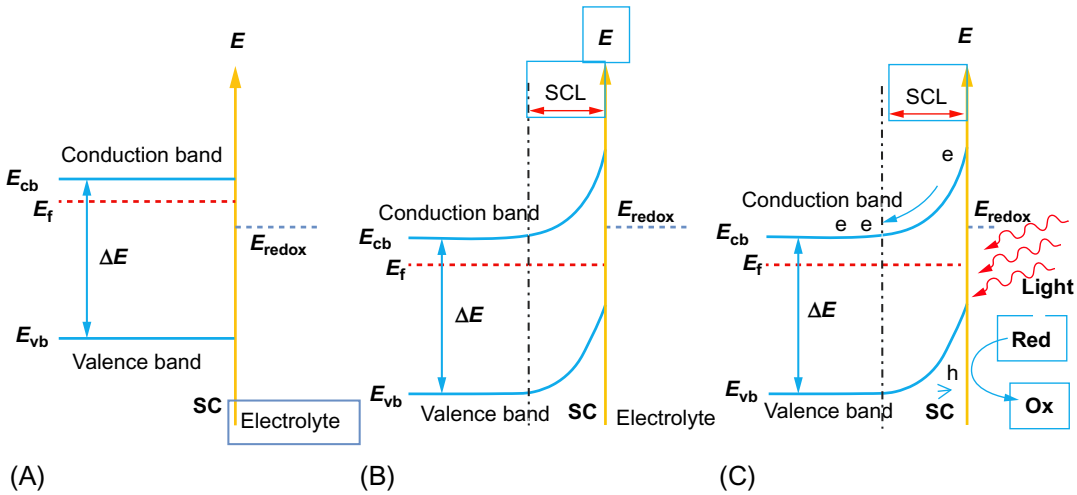

FIG. 5

Schematic diagram of band bending in a semiconductor.

This book belongs to Central Library BADJI Mokhtar-ANNABA UNIVERSITY
Copyright Elsevier 2024

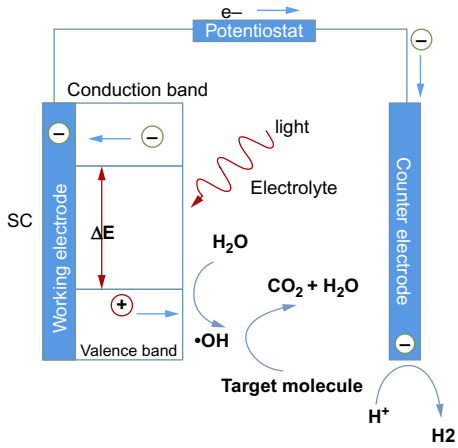

FIG. 6

Schematic diagram of photoelectrocatalysis by an n-type semiconductor.

metals and nonmetals in the matrix of TiO_2 nanoparticle. However, this form of TiO_2 severely restricts its benefits for the optimal use as the photogenerated electrons and holes recombine very fast and is hydrophobic therefore unsuited for water treatment and poorly adsorbs pollutants. Nevertheless, the utilization of visible light is severely restricted owing to the fast recombination rate, and consequently, photodegradation is badly affected, resulting in the creation of secondary pollutants (Dong et al., 2015). To overcome the aforementioned difficulties, one-dimensional (1D) TiO_2 nanomaterials in the form of nanotubes, nanowires, nanorods, and/or nanobundles can be considered for the photocatalytic activities. The 1D structure of TiO_2 possesses many advantages including large aspect ratio, surface area, and nonagglomeration properties, which can be used for the wastewater management (Lee, Mazare, & Schmuki, 2014; Wang, Li, Shi, & Yu, 2014). Due to its free-standing nature, these 1D TiO_2 structure can be used for the efficient photodegradation (Wu, Si, Yu, & Ding, 2018). Photoelectrocatalysis is a powerful technique that combines both heterogeneous photocatalysis and electrochemical techniques. In this technique, a semiconductor is used that creates electron-hole pair upon irradiation of light where the photon energy should be greater than the energy bandgap of the semiconductor used therein. In this context, TiO_2 is a well-known semiconductor widely used as an effective photocatalyst since long back (Hashimoto, Irie, & Fujishima, 2005). However, it is the great work done by Fujishima and Honda in 1972 that begins the photoelectrocatalytic water splitting by using n-type TiO_2 electrode as anode and Pt electrode as cathode (Fujishima and Honda, 1972). Photoelectrocatalysis in recent times finds many applications in organic compound oxidation (Brugnera, Rajeshwar, Cardoso, & Zanoni, 2010; Cardoso, Lizier, & Zanoni, 2010) and CO_2 reduction (LaTempa, Rani, Bao, & Grimes, 2012). Wang et al. prepared TiO_2 nanotube array electrodes (CdSe/TNTAs) decorated with CdSe quantum dots (see Fig. 7). This photoanode was used for the photoelectrocatalytic (PEC) degradation of organic pollutants. A three-electrode system was taken in an electrolytic cell under the visible-light ($\lambda > 400$ nm) irradiation. These authors found that the CdSe/TiO_2-based PEC system was effective in the oxidation of methyl orange (MO). Such an efficient catalytic ability was attributed to the high dispersion of CdSe nanoparticles around the pore walls of TiO_2 nanotube arrays. Moreover, the formation of

This book belongs to Central Library BADJI Mokhtar-ANNABA UNIVERSITY
Copyright Elsevier 2024

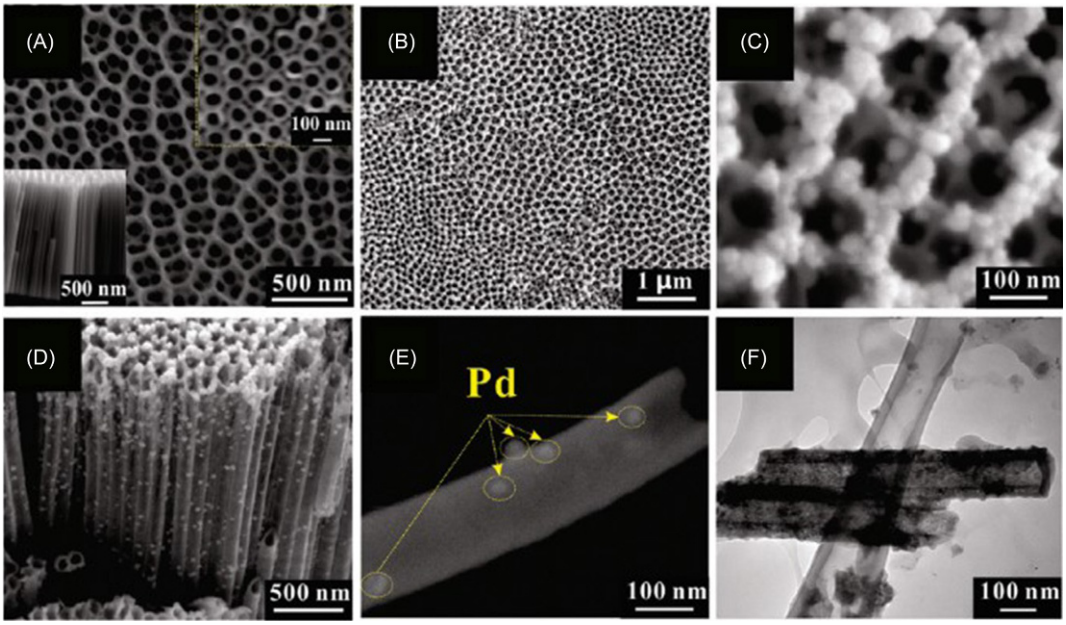

FIG. 7

(A) SEM top-view image of top-porous and bottom-tubular TiO_2 NTs, the top right inset shows the TiO_2 NTs with the top-porous structure removed, and the bottom left inset shows a cross-sectional view of TiO_2 NTs; (B) SEM top-view image of Pd/TiO_2 NTs; (C) high magnification of Pd nanoparticles associated with Pd/TiO2 NTs; (D) cross-sectional SEM image of Pd/TiO_2 NTs; (E) SEM image of single TiO_2 NT with Pd nanoparticles on its outer surface; and (F) TEM image of TiO_2 NTs with Pd nanoparticles inside the tubes.

Fig. 1 of Zhang, Z., Yu, Y., & Wang, P. (2012). Hierarchical top-porous/bottom-tubular TiO_2 nanostructures decorated with Pd nanoparticles for efficient photoelectrocatalytic decomposition of synergistic pollutants. ACS Applied Materials & Interfaces, 4*(2), 990–996. https://doi.org/10.1021/am201630s reproduced with permission.*

heterojunctions between CdSe and TiO_2 through CdO bonds can be responsible for such an effect (Wang, Li, Zhang, Leung, & Li, 2016).

In one of the studies, Zhang et al. fabricated Pd-loaded TiO_2 nanotubes (TiO_2 NTs) and utilized it for the degradation of organic dye. In this method, TiO_2 nanotubes were deposited by photoreduction process (Zhang et al., 2012). Decomposition of methylene blue (MB) and rhodamine B (RhB) was tested using this photoelectrode. Since there is a formation of Schottky junctions between TiO_2 and Pd, the Pd/TiO_2 nanotube electrode performed better degradation than bare TiO_2 nanotube electrode. Due to the earlier combination, transfer of electrons and holes is facilitated as a result of a readjustment of energy levels (Zhang et al., 2012).

In a recent study, Rajput prepared a TiO_2 nanotube electrode and decorated it with Cs. This was achieved by anodic oxidation by means of electrochemical processes (Rajput et al., 2019). The as-prepared Cs/TiO_2NTs electrode showed visible-light absorption ranging from 390 to 700 nm, and the decomposition of 4-chloroguaiacol was also monitored. Effect of various combination of parameters including cesium, sulfate concentration, current, and pH on 4-chloroguaiacol degradation is

This book belongs to Central Library BADJI Mokhtar-ANNABA UNIVERSITY Copyright Elsevier 2024

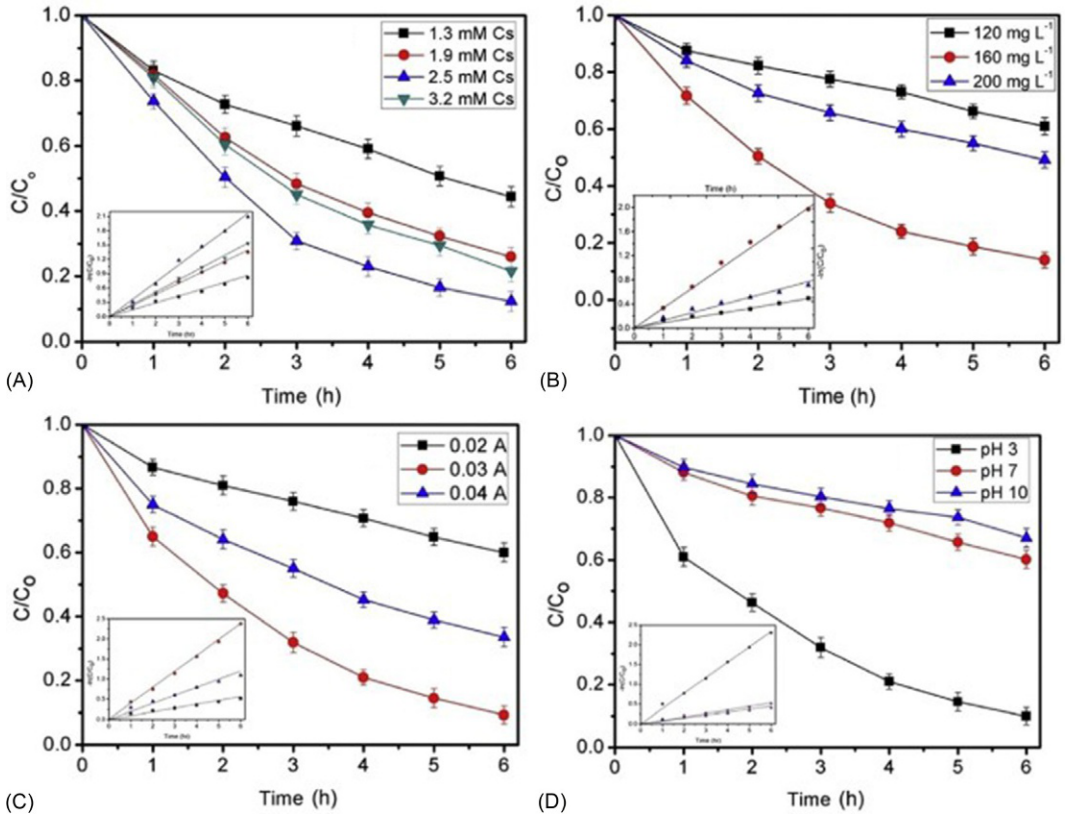

FIG. 8

Effect of operating parameters: (A) cesium concentration (0.02 A current, 150 mg/L Na_2SO_4 and pH 3) (B) sulfate concentration (2.5 mM Cs, 0.02 A current and pH 3) (C) current (2.5 mM Cs, 160 mg L^{-1} Na_2SO_4 and pH 3), and (D) pH (2.5 mM Cs, 160 mg/L Na_2SO_4 and 0.03 A current) on PEC degradation of 4-CG with their respective rate kinetics study (inset).

Fig. 4 of Rajput, H., Changotra, R., Sangal, V. K., Mahla, S. K., & Dhir, A. (2019). A facile synthesis of Cs loaded TiO2 nanotube photoelectrode for the removal of 4-chloroguaiacol. Chemosphere, 218, 687–695. https://doi.org/10.1016/j.chemosphere.2018.11.157 reproduced with permission.

depicted in Fig. 8. It showed better photocatalytic degradation and mineralization of organic pollutants compared with bare TiO_2. In addition, Cs/TiO_2NT electrode was capable to generate more OH radicals. It is well known that oxygen vacancies are formed by light irradiation or by vacuum annealing in semiconductor oxides including In_2O_3 and TiO_2. The PEC degradation was attributed to the rapid formation of oxygen vacancies in TiO_2NTs. The cytotoxicity and hydroxyl radicals were also removed with enhanced performance. This study presents a better way to fabricate highly efficient nanocomposites for wastewater treatment and solar energy conversion at nominal cost. *J*. Qui reported a novel method to

This book belongs to Central Library BADJI Mokhtar-ANNABA UNIVERSITY Copyright Elsevier 2024

prepare nanosheet of Mo/N-codoped TiO_2 nanorods immobilized on carbon nanoflowers synthesized by chemical method. These authors noticed that dispersion of nanoflower sheet did not disturb the morphology of the of TiO_2 nanorods. This was possible due to the network-type structure of CNFs, which facilitated the in situ growth of TiO_2 nanorods. The as-prepared nanocomposites showed enhanced photodegradation of methylene blue under sunlight. Nearly 79.8% of TOC removal was observed, which was much higher than the bare TiO_2 nanoparticles. Nitrate and carbonate contributed to the photodegradation process. This novel technique can be used to treat wastewater management. The experiments verified that h^+ was mainly responsible for the photodegradation process (Qiu, Liu, Yue, Ling, & Li, 2019). Qi et al. reported both photoelectrochemical and spectroelectrochemical techniques for the degradation of small colorless organic pollutants attached to the rutile TiO_2 (Qi et al., 2016). It has been observed that the exposed (110) plane of the r-TiO_2 crystals is very robust and stable and interacts efficiently with organic compounds including alcohols (e.g., methanol) and phenols (e.g., 4-chlorophenol) (Kim, Barteau, & Farneth, 1988; Tunesi & Anderson, 1991). A three-electrode system was taken with Ag/AgCl and Pt as reference and counterelectrode, respectively. The measurements were performed using an electrochemical analyzer. The spectrochemical measurements were done with a cuvette. Further, benzene derivatives with —OH and —COOH groups (such as catechol, salicylic acid, phthalic acid, and terephthalic acid) were selected as model colorless pollutants. It was also found that OH favors one-step electron transfer process, while COOH exhibits two-step electron transfer processes. The decomposition efficiency was found to be decreased in the order: (—OH, —OH) > (—OH, —COOH) > (—COOH, —COOH). This result agrees well with the theoretical and experimental predictions. In another study, Kim et al. investigated the effect of calcination temperature and copper oxide loading over rhodium–antimony-codoped TiO_2 nanorods and titanate nanotube (RS-TONR/TNT) composite, which was hydrothermally synthesized from rhodium–antimony-codoped TiO_2 nanorod (RS-TONR) (Kim et al., 2018). They found that RS-TONR/TNT nanocomposite was effective in the photocatalytic degradation of orange (II) dye and bisphenol A and disinfection of pathogenic bacteria under the visible-light irradiation. When calcination temperature of the nanocomposite was elevated to 400°C, there was a significant improvement in the photocatalytic degradation. In composite form, rutile phase of TiO_2 nanorods contains rhodium–antimony that could generate electron–hole pairs under the visible-light irradiation. Song et al. prepared rGO/TiO_2 nanocomposites by one-step solvothermal method. The interface formed was chemically bonded Ti-O-C (Jianhua, Yun, Yu, Lianjun, & Huihua, 2018). The interface formed highly depended on the content of rGO, solvothermal reaction time, and solvent ratio. About 25% of TiO_2 particles was evenly dispersed, and a shell was formed by rGO sheets, which created a large surface area. The as-prepared rGO/TiO_2 nanocomposite was tested for the degradation of MO. A two-step process was followed: adsorption in the dark subsequently and photocatalytic degradation after it attained adsorption–desorption equilibrium. It is known that both TiO_2 and commercial Degussa P25 have negligible effect of MO adsorption in the dark. However, under light irradiation, MO was completely degraded after 80–90 min of the experiment. It confirmed that TiO_2 primarily acted as a photocatalyst but not as an adsorbent. On the other hand, mineralization of MO by TiO_2 was slow when only TiO_2 was used. The interface sheltered organic pollutants and also enhanced charge transfer from TiO_2 to rGO. Overall, 25 wt% of rGO/TiO_2 nanocomposite showed higher adsorption efficiency (25%) and four times faster photodegradation rate ($k = 0.119\,min^{-1}$) than bare TiO_2 (0%, $k = 0.023\,min^{-1}$) (Jianhua et al., 2018). The nanocomposite could also be repeatedly used up to 30 cycles. The integration of adsorption/photodegradation approach enables a new insight into the field of water treatment. Humic acids (HA) create metal complexes and

This book belongs to Central Library BADJI Mokhtar-ANNABA UNIVERSITY Copyright Elsevier 2024

organic pollutants (Wei et al., 2011), destroy free radicals (^{-}OH) in advanced oxidation processes (AOP) (Imai et al., 2009). Ozone–ultraviolet (O3/UV) photocatalytic oxidation is highly efficient in generating ^{-}OH for the degradation of pollutants (Lin & Lin, 2007). To remove HA, various methods have been proposed, and one of them is ion-doped TiO_2. Various ions including Ag^{+}, Al^{3+}, Cu^{2+}, Fe^{3+}, V^{5+}, and Zn^{2+} were incorporated in to the TiO_2 lattice. As a result, the energy bandgap of TiO_2 becomes narrower. It was found that Fe^{+3} ion showed best result but Mn^{+2} and Ni^{+2} downgraded the photocatalytic activity. It was found that the hydroxyl radicals react with HA near the surface of TiO_2. The formation of OH radicals can be amplified by UV light. Gu et al. prepared a composite made up of carbon nanofibers (CN) and TiO_2 nanorod bundles assisted by dipcoating and hydrothermal growth (Gu et al., 2015). The size of the nanorods was found to be 340–400 nm, whereas the diameter was ~30 nm. A bias of 0.6 V was applied versus saturated calomel electrode. The results confirmed that CFs/TiO_2 nanocomposite was capable to decompose 94.0% RhB in 100 min by photoelectrocatalysis. On the contrary, only 5.6% degradation was found to be in the case of photocatalytic process. This concludes that CFs/TiO_2 could serve as an excellent photoelectrode for the degradation of organic pollutants.

5 Conclusions

In summary, both 1D– and 2D–based nanomaterials including TiO_2 and graphene play an important role in the degradation of organic pollutants. By combining with different techniques such as photoelectrochemical process, organic pollutants can be degraded efficiently.

Acknowledgments

DM acknowledges the University Grants Commission, New Delhi, for providing research support through Faculty Recharge Program (Letter No. F.4-5(202-FRP)/2015/BSR), financial support by MHRD-DST, India through grant No. IMP/2018/001668, financial support by SERB through grant No. CRG/2018/004264. Author M.S. acknowledges the DST, Government of India, for awarding the DST-INSPIRE Faculty Award [IFA13-MS-02] 2014. M.S. also acknowledges Science and Engineering Research Board for SERB-Research Scientist (SRS) award.

References

Ai, L., Zhang, C., Li, L., & Jiang, J. (2014). Iron terephthalate metal–organic framework: Revealing the effective activation of hydrogen peroxide for the degradation of organic dye under visible light irradiation. *Applied Catalysis B: Environmental*, *148–149*, 191–200. https://doi.org/10.1016/j.apcatb.2013.10.056.

Aiuppa, A., Bellomo, S., Brusca, L., D'Alessandro, W., & Federico, C. (2003). Natural and anthropogenic factors affecting groundwater quality of an active volcano (Mt. Etna, Italy). *Applied Geochemistry*, *18*(6), 863–882. https://doi.org/10.1016/S0883-2927(02)00182-8.

Akpan, U. G., & Hameed, B. H. (2009). Parameters affecting the photocatalytic degradation of dyes using TiO2-based photocatalysts: A review. *Journal of Hazardous Materials*, *170*(2), 520–529. https://doi.org/10.1016/j.jhazmat.2009.05.039.

This book belongs to Central Library BADJI Mokhtar-ANNABA UNIVERSITY

Copyright Elsevier 2024

An, S., Joshi, B. N., Lee, M. W., Kim, N. Y., & Yoon, S. S. (2014). Electrospun graphene-ZnO nanofiber mats for photocatalysis applications. *Applied Surface Science*, *294*, 24–28. https://doi.org/10.1016/j.apsusc.2013.12.159.

An, X., & Yu, J. C. (2011). Graphene-based photocatalytic composites. *RSC Advances*, *1*(8), 1426–1434. https://doi.org/10.1039/c1ra00382h.

Anshuman, A., Saremi-Yarahmadi, S., & Vaidhyanathan, B. (2018). Enhanced catalytic performance of reduced graphene oxide–TiO2 hybrids for efficient water treatment using microwave irradiation. *RSC Advances*, *8*(14), 7709–7715. https://doi.org/10.1039/c8ra00031j.

Ashcroft, N. W., Mermin, N. D., & Brooks/Cole Publishing, C. (2018). *Solid state physics*. Singapore: Brooks/Cole Cengage Learning Learning [i pozostale].

Aulbur, W. G., Jönsson, L., & Wilkins, J. W. (2000). Quasiparticle calculations in solids. H. Ehrenreich & F. Spaepen (Eds.), *Solid State Physics* (pp. 1–218). *54*(pp. 1–218). Academic Press.

Barakat, M. A. (2011). New trends in removing heavy metals from industrial wastewater. *Arabian Journal of Chemistry*, *4*(4), 361–377. https://doi.org/10.1016/j.arabjc.2010.07.019.

Boruah, P. K., Borthakur, P., Darabdhara, G., Kamaja, C. K., Karbhal, I., Shelke, M. V., et al. (2016). Sunlight assisted degradation of dye molecules and reduction of toxic Cr(vi) in aqueous medium using magnetically recoverable Fe3O4/reduced graphene oxide nanocomposite. *RSC Advances*, *6*(13), 11049–11063. https://doi.org/10.1039/c5ra25035h.

Bosco, M. L., Varrica, D., & Dongarrà, G. (2005). Case study: Inorganic pollutants associated with particulate matter from an area near a petrochemical plant. *Environmental Research*, *99*(1), 18–30. https://doi.org/10.1016/j.envres.2004.09.011.

Brillas, E., Sirés, I., & Oturan, M. A. (2009). Electro-Fenton process and related electrochemical technologies based on Fenton's Reaction Chemistry. *Chemical Reviews*, *109*(12), 6570–6631. https://doi.org/10.1021/cr900136g.

Brown, C. A. (1999). Rapid guide to hazardous air pollutants. Howard J. Beim, Jennifer Spero, Louis Theodore, Van Nostrand Reinhold and international thomson publishing company, New York, NY, (1998),582 pages, [ISBN No.: 0–442–02515-7], U.S. list price: $34.95. *Environmental Progress*, *18*(3), F7–F8. https://doi.org/10.1002/ep.670180306.

Brugnera, M. F., Rajeshwar, K., Cardoso, J. C., & Zanoni, M. V. B. (2010). Bisphenol A removal from wastewater using self-organized TIO2 nanotubular array electrodes. *Chemosphere*, *78*(5), 569–575. https://doi.org/10.1016/j.chemosphere.2009.10.058.

Brulle, R. J., & Pellow, D. N. (2006). Environmental justice: Human health and environmental inequalities. *Annual Review of Public Health*, *27*(1), 103–124. https://doi.org/10.1146/annurev.publhealth.27.021405.102124.

Bu, Y., Chen, Z., Li, W., & Hou, B. (2013). Highly efficient photocatalytic performance of graphene–ZnO quasi-shell–core composite material. *ACS Applied Materials & Interfaces*, *5*(23), 12361–12368. https://doi.org/10.1021/am403149g.

Cabello, F. C. (2006). Heavy use of prophylactic antibiotics in aquaculture: a growing problem for human and animal health and for the environment. *Environmental Microbiology*, *8*(7), 1137–1144. https://doi.org/10.1111/j.1462-2920.2006.01054.x.

Cardoso, J. C., Lizier, T. M., & Zanoni, M. V. B. (2010). Highly ordered TiO2 nanotube arrays and photoelectrocatalytic oxidation of aromatic amine. *Applied Catalysis B: Environmental*, *99*(1), 96–102. https://doi.org/10.1016/j.apcatb.2010.06.005.

Chabot, V., Higgins, D., Yu, A., Xiao, X., Chen, Z., & Zhang, J. (2014). A review of graphene and graphene oxide sponge: material synthesis and applications to energy and the environment. *Energy & Environmental Science*, *7*(5), 1564–1596. https://doi.org/10.1039/c3ee43385d.

Chauhan, P. S., Kant, R., Rai, A., Gupta, A., & Bhattacharya, S. (2019). Facile synthesis of ZnO/GO nanoflowers over Si substrate for improved photocatalytic decolorization of MB dye and industrial wastewater under solar

This book belongs to Central Library BADJI Mokhtar-ANNABA UNIVERSITY Copyright Elsevier 2024

irradiation. *Materials Science in Semiconductor Processing*, *89*, 6–17. https://doi.org/10.1016/j.mssp.2018.08.022.

Chen, C., Mei, W., Yu, W., Chen, X. a., Zeng, L., Tsang, Y., et al. (2018). Enhanced sunlight-driven photocatalytic property of Mg-doped ZnO nanocomposites with three-dimensional graphene oxide/MoS2 nanosheet composites. *RSC Advances*, *8*(31), 17399–17409. https://doi.org/10.1039/c8ra02382d.

Chen, D., Wang, D., Ge, Q., Ping, G., Fan, M., Qin, L., et al. (2015). Graphene-wrapped ZnO nanospheres as a photocatalyst for high performance photocatalysis. *Thin Solid Films*, *574*, 1–9. https://doi.org/10.1016/j.tsf.2014.11.051.

Choi, J., Reddy, D. A., Islam, M. J., Ma, R., & Kim, T. K. (2016). Self-assembly of CeO2 nanostructures/reduced graphene oxide composite aerogels for efficient photocatalytic degradation of organic pollutants in water. *Journal of Alloys and Compounds*, *688*, 527–536. https://doi.org/10.1016/j.jallcom.2016.07.236.

Daneshvar, N., Salari, D., & Khataee, A. R. (2004). Photocatalytic degradation of azo dye acid red 14 in water on ZnO as an alternative catalyst to TiO2. *Journal of Photochemistry and Photobiology A: Chemistry*, *162*(2), 317–322. https://doi.org/10.1016/S1010-6030(03)00378-2.

Darabdhara, G., & Das, M. R. (2018). Bimetallic Au-Pd nanoparticles on 2D supported graphitic carbon nitride and reduced graphene oxide sheets: A comparative photocatalytic degradation study of organic pollutants in water. *Chemosphere*, *197*, 817–829. https://doi.org/10.1016/j.chemosphere.2018.01.073.

Delegan, N., Daghrir, R., Drogui, P., & Khakani, M. A. E. (2014). Bandgap tailoring of in-situ nitrogen-doped TiO2 sputtered films intended for electrophotocatalytic applications under solar light. *Journal of Applied Physics*, *116*(15), 153510. https://doi.org/10.1063/1.4898589.

DeLuca, S. J., Chao, A. C., & Smallwood, C. (1983). Removal of Organic Priority Pollutants by Oxidation‐ Coagulation. *Journal of Environmental Engineering*, *109*(1), 36–46. https://doi.org/10.1061/(ASCE)0733-9372(1983)109:1(36.

Dietz, A. C., & Schnoor, J. L. (2001). Advances in phytoremediation. *Environmental Health Perspectives*, *109* (suppl 1), 163–168. https://doi.org/10.1289/ehp.01109s1163.

Dirinck, E., Jorens, P. G., Covaci, A., Geens, T., Roosens, L., Neels, H., et al. (2011). Obesity and persistent organic pollutants: Possible obesogenic effect of organochlorine pesticides and polychlorinated biphenyls. *Obesity*, *19*(4), 709–714. https://doi.org/10.1038/oby.2010.133.

Dong, H., Zeng, G., Tang, L., Fan, C., Zhang, C., He, X., et al. (2015). An overview on limitations of TiO2-based particles for photocatalytic degradation of organic pollutants and the corresponding countermeasures. *Water Research*, *79*, 128–146. https://doi.org/10.1016/j.watres.2015.04.038.

Duan, X., Ao, Z., Sun, H., Indrawirawan, S., Wang, Y., Kang, J., et al. (2015). Nitrogen-doped graphene for generation and evolution of reactive radicals by metal-free catalysis. *ACS Applied Materials & Interfaces*, *7*(7), 4169–4178. https://doi.org/10.1021/am508416n.

Farrusseng, D., Aguado, S., & Pinel, C. (2009). Metal–organic frameworks: Opportunities for catalysis. *Angewandte Chemie International Edition*, *48*(41), 7502–7513. https://doi.org/10.1002/anie.200806063.

Fennell, D. E., Nijenhuis, I., Wilson, S. F., Zinder, S. H., & Häggblom, M. M. (2004). Dehalococcoides ethenogenes Strain 195 reductively dechlorinates diverse chlorinated aromatic pollutants. *Environmental Science & Technology*, *38*(7), 2075–2081. https://doi.org/10.1021/es034989b.

Fujishima, A., & Honda, K. (1972). Electrochemical photolysis of water at a semiconductor electrode. *Nature*, *238* (5358), 37–38. https://doi.org/10.1038/238037a0.

Garcia-Segura, S., & Brillas, E. (2017). Applied photoelectrocatalysis on the degradation of organic pollutants in wastewaters. *Journal of Photochemistry and Photobiology C: Photochemistry Reviews*, *31*, 1–35. https://doi.org/10.1016/j.jphotochemrev.2017.01.005.

Gaya, U. I., & Abdullah, A. H. (2008). Heterogeneous photocatalytic degradation of organic contaminants over titanium dioxide: A review of fundamentals, progress and problems. *Journal of Photochemistry and Photobiology C: Photochemistry Reviews*, *9*(1), 1–12. https://doi.org/10.1016/j.jphotochemrev.2007.12.003.

This book belongs to Central Library BADJI Mokhtar-ANNABA UNIVERSITY

Copyright Elsevier 2024

Georgakilas, V., Otyepka, M., Bourlinos, A. B., Chandra, V., Kim, N., Kemp, K. C., et al. (2012). Functionalization of graphene: Covalent and non-covalent approaches, derivatives and applications. *Chemical Reviews*, *112*(11), 6156–6214. https://doi.org/10.1021/cr3000412.

Ghasemi, Y., Rasoul-Amini, S., & Fotooh-Abadi, E. (2011). The Biotransformation, Biodegradation, and Bioremediation of Organic Compounds by Microalgae1. *Journal of Phycology*, *47*(5), 969–980. https://doi.org/10.1111/j.1529-8817.2011.01051.x.

Gu, X., Yu, N., Zhang, L., Yang, J., Hu, J., & Chen, Z. (2015). Growth of TiO2 nanorod bundles on carbon fibers as flexible and weaveable photocatalyst/photoelectrode. *RSC Advances*, *5*(124), 102868–102876. https://doi.org/10.1039/c5ra21344d.

Hashimoto, K., Irie, H., & Fujishima, A. (2005). *TiO_2 photocatalysis: A historical overview and future prospects*. *Japanese Journal of Applied Physics*, ***44***, 8269–8285. https://doi.org/10.1143/JJAP.44.8269.

Hettige, H., Mani, M., & Wheeler, D. (2000). Industrial pollution in economic development: the environmental Kuznets curve revisited. *Journal of Development Economics*, *62*(2), 445–476. https://doi.org/10.1016/S0304-3878(00)00092-4.

Huang, X., Niu, Y., & Hu, W. (2017). Fe/Fe3C nanoparticles loaded on Fe/N-doped graphene as an efficient heterogeneous Fenton catalyst for degradation of organic pollutants. *Colloids and Surfaces A: Physicochemical and Engineering Aspects*, *518*, 145–150. https://doi.org/10.1016/j.colsurfa.2017.01.039.

Hunger, K. (2002). *Industrial dyes chemistry, properties, applications.* Wiley-VCH Verlag GmbH & Co. KGaA.

Imai, D., Dabwan, A. H. A., Kaneco, S., Katsumata, H., Suzuki, T., Kato, T., et al. (2009). Degradation of marine humic acids by ozone-initiated radical reactions. *Chemical Engineering Journal*, *148*(2), 336–341. https://doi.org/10.1016/j.cej.2008.09.013.

Jaihindh, D. P., Chen, C.-C., & Fu, Y.-P. (2018). Reduced graphene oxide-supported Ag-loaded Fe-doped TiO2 for the degradation mechanism of methylene blue and its electrochemical properties. *RSC Advances*, *8*(12), 6488–6501. https://doi.org/10.1039/c7ra13418e.

Jianhua, S., Yun, L., Yu, X., Lianjun, L., & Huihua, Z. (2018). One-pot engineering TiO2/graphene interface for enhanced adsorption and photocatalytic degradation of multiple organics. *Nanotechnology*, *29*(39), 395701.

Joshi, B. N., Yoon, H., Na, S.-H., Choi, J.-Y., & Yoon, S. S. (2014). Enhanced photocatalytic performance of graphene–ZnO nanoplatelet composite thin films prepared by electrostatic spray deposition. *Ceramics International*, *40*(2), 3647–3654. https://doi.org/10.1016/j.ceramint.2013.09.060.

Kampa, M., & Castanas, E. (2008). Human health effects of air pollution. *Environmental Pollution*, *151*(2), 362–367. https://doi.org/10.1016/j.envpol.2007.06.012.

Kim, K. S., Barteau, M. A., & Farneth, W. E. (1988). Adsorption and decomposition of aliphatic alcohols on titania. *Langmuir*, *4*(3), 533–543. https://doi.org/10.1021/la00081a007.

Kim, S.-G., Dhandole, L. K., Seo, Y.-S., Chung, H.-S., Chae, W.-S., Cho, M., et al. (2018). Active composite photocatalyst synthesized from inactive Rh & Sb doped TiO2 nanorods: Enhanced degradation of organic pollutants & antibacterial activity under visible light irradiation. *Applied Catalysis A: General*, *564*, 43–55. https://doi.org/10.1016/j.apcata.2018.07.016.

Kolpin, D. W., Furlong, E. T., Meyer, M. T., Thurman, E. M., Zaugg, S. D., Barber, L. B., et al. (2002). Pharmaceuticals, hormones, and other organic wastewater contaminants in U.S. streams, 1999–2000: A National Reconnaissance. *Environmental Science & Technology*, *36*(6), 1202–1211. https://doi.org/10.1021/es011055j.

Labhane, P. K., Sonawane, S. H., Sonawane, G. H., Patil, S. P., & Huse, V. R. (2018). Influence of Mg doping on ZnO nanoparticles decorated on graphene oxide (GO) crumpled paper like sheet and its high photo catalytic performance under sunlight. *Journal of Physics and Chemistry of Solids*, *114*, 71–82. https://doi.org/10.1016/j.jpcs.2017.11.017.

Lacorte, S., Latorre, A., Barceló, D., Rigol, A., Malmqvist, A., & Welander, T. (2003). Organic compounds in paper-mill process waters and effluents. *TrAC Trends in Analytical Chemistry*, *22*(10), 725–737. https://doi.org/10.1016/S0165-9936(03)01009-4.

This book belongs to Central Library BADJI Mokhtar-ANNABA UNIVERSITY

Copyright Elsevier 2024

LaTempa, T. J., Rani, S., Bao, N., & Grimes, C. A. (2012). Generation of fuel from CO2 saturated liquids using a p-Si nanowire || n-TiO_2 nanotube array photoelectrochemical cell. *Nanoscale*, *4*(7), 2245–2250. https://doi.org/10.1039/c2nr00052k.

Lee, K., Mazare, A., & Schmuki, P. (2014). One-dimensional titanium dioxide nanomaterials: Nanotubes. *Chemical Reviews*, *114*(19), 9385–9454. https://doi.org/10.1021/cr500061m.

Lei, M., Wang, N., Zhu, L., Xie, C., & Tang, H. (2014). A peculiar mechanism for the photocatalytic reduction of decabromodiphenyl ether over reduced graphene oxide–TiO2 photocatalyst. *Chemical Engineering Journal*, *241*, 207–215. https://doi.org/10.1016/j.cej.2013.12.032.

Lewerenz, H. J., Heine, C., Skorupska, K., Szabo, N., Hannappel, T., Vo-Dinh, T., et al. (2010). Photoelectrocatalysis: principles, nanoemitter applications and routes to bio-inspired systems. *Energy & Environmental Science*, *3*(6), 748–760. https://doi.org/10.1039/b915922n.

Lin, C., & Lin, K.-S. (2007). Photocatalytic oxidation of toxic organohalides with TiO2/UV: the effects of humic substances and organic mixtures. *Chemosphere*, *66*(10), 1872–1877. https://doi.org/10.1016/j.chemosphere.2006.08.027.

Liu, W., Cai, J., & Li, Z. (2015). Self-assembly of semiconductor nanoparticles/reduced graphene oxide (RGO) composite aerogels for enhanced photocatalytic performance and facile recycling in aqueous photocatalysis. *ACS Sustainable Chemistry & Engineering*, *3*(2), 277–282. https://doi.org/10.1021/sc5006473.

Liu, Y., Luo, F., Liu, S., Liu, S., Lai, X., Li, X., et al. (2017). Aminated graphene oxide impregnated with photocatalytic polyoxometalate for efficient adsorption of dye pollutants and its facile and complete photoregeneration. *Small*, *13*(14), 1603174. https://doi.org/10.1002/smll.201603174.

Liu, C., Yue, M., Liu, L., Rui, Y., & Cui, W. (2018). A separation-free 3D network ZnO/rGO–rGH hydrogel: adsorption enriched photocatalysis for environmental applications. *RSC Advances*, *8*(40), 22402–22410. https://doi.org/10.1039/c8ra03873b.

Lv, H., Zhao, H., Cao, T., Qian, L., Wang, Y., & Zhao, G. (2015). Efficient degradation of high concentration azo-dye wastewater by heterogeneous Fenton process with iron-based metal-organic framework. *Journal of Molecular Catalysis A: Chemical*, *400*, 81–89. https://doi.org/10.1016/j.molcata.2015.02.007.

Manahan, S. E. (2001). *Fundamentals of environmental chemistry*. Boca Raton, FL: Lewis Publishers.

Manahan, S. E. (2013). *Fundamentals of environmental and toxicological chemistry: Sustainable science* (4th ed.). Hoboken: CRC Press.

Martinez, J. L. (2009). Environmental pollution by antibiotics and by antibiotic resistance determinants. *Environmental Pollution*, *157*(11), 2893–2902. https://doi.org/10.1016/j.envpol.2009.05.051.

Matilainen, A., Vepsäläinen, M., & Sillanpää, M. (2010). Natural organic matter removal by coagulation during drinking water treatment: A review. *Advances in Colloid and Interface Science*, *159*(2), 189–197. https://doi.org/10.1016/j.cis.2010.06.007.

Moussavi, G., & Mahmoudi, M. (2009). Removal of azo and anthraquinone reactive dyes from industrial wastewaters using MgO nanoparticles. *Journal of Hazardous Materials*, *168*(2), 806–812. https://doi.org/10.1016/j.jhazmat.2009.02.097.

Neamen, D. A. (2012). *Semiconductor physics and devices: basic principles*. New York: McGraw-Hill Higher Education.

Nicolopoulou-Stamati, P., Maipas, S., Kotampasi, C., Stamatis, P., & Hens, L. (2016). Chemical pesticides and human health: The urgent need for a new concept in agriculture [Review]. *Frontiers in Public Health*. 4 (148)https://doi.org/10.3389/fpubh.2016.00148.

Poznyak, T., Bautista, G. L., Chaírez, I., Córdova, R. I., & Ríos, L. E. (2008). Decomposition of toxic pollutants in landfill leachate by ozone after coagulation treatment. *Journal of Hazardous Materials*, *152*(3), 1108–1114. https://doi.org/10.1016/j.jhazmat.2007.07.098.

This book belongs to Central Library BADJI Mokhtar-ANNABA UNIVERSITY

Copyright Elsevier 2024

Qi, K., Zasada, F., Piskorz, W., Indyka, P., Gryboś, J., Trochowski, M., et al. (2016). Self-sensitized photocatalytic degradation of colorless organic pollutants attached to rutile nanorods—Experimental and theoretical DFT+D studies. *The Journal of Physical Chemistry C*, *120*(10), 5442–5456. https://doi.org/10.1021/acs.jpcc.5b10983.

Qin, X., Fang, S., Zhao, L., Shi, P., Fan, J., Min, Y., et al. (2017). Cobalt super-microparticles anchored on nitrogen-doped graphene for aniline oxidation based on sulfate radicals. *Science of the Total Environment*, *601–602*, 99–108. https://doi.org/10.1016/j.scitotenv.2017.05.198.

Qiu, J., Liu, F., Yue, C., Ling, C., & Li, A. (2019). A recyclable nanosheet of Mo/N-doped TiO2 nanorods decorated on carbon nanofibers for organic pollutants degradation under simulated sunlight irradiation. *Chemosphere*, *215*, 280–293. https://doi.org/10.1016/j.chemosphere.2018.09.182.

Rajasulochana, P., & Preethy, V. (2016). Comparison on efficiency of various techniques in treatment of waste and sewage water—A comprehensive review. *Resource-Efficient Technologies*, *2*(4), 175–184. https://doi.org/10.1016/j.reffit.2016.09.004.

Rajput, H., Changotra, R., Sangal, V. K., Mahla, S. K., & Dhir, A. (2019). A facile synthesis of Cs loaded TiO2 nanotube photoelectrode for the removal of 4-chloroguaiacol. *Chemosphere*, *218*, 687–695. https://doi.org/10.1016/j.chemosphere.2018.11.157.

Ren, X., Guo, H., Feng, J., Si, P., Zhang, L., & Ci, L. (2018). Synergic mechanism of adsorption and metal-free catalysis for phenol degradation by N-doped graphene aerogel. *Chemosphere*, *191*, 389–399. https://doi.org/10.1016/j.chemosphere.2017.10.076.

Renault, F., Sancey, B., Badot, P. M., & Crini, G. (2009). Chitosan for coagulation/flocculation processes—An eco-friendly approach. *European Polymer Journal*, *45*(5), 1337–1348. https://doi.org/10.1016/j.eurpolymj.2008.12.027.

Rozell, D. J., & Reaven, S. J. (2012). Water pollution risk associated with natural gas extraction from the Marcellus Shale. *Risk Analysis*, *32*(8), 1382–1393. https://doi.org/10.1111/j.1539-6924.2011.01757.x.

Schell, L. M., Knutson, K. L., & Bailey, S. (2012). Environmental effects on growth. In N. Cameron & B. Bogin (Eds.), *Human Growth and Development* (pp. 245–286). (2nd ed.). Boston: Academic Press [chapter 10].

Seiler, H. G., & Sigel, H. (1988). *Handbook on toxicity of inorganic compounds.* United States: Marcel Dekker.

Semrany, S., Favier, L., Djelal, H., Taha, S., & Amrane, A. (2012). Bioaugmentation: Possible solution in the treatment of Bio-Refractory Organic Compounds (Bio-ROCs). *Biochemical Engineering Journal*, *69*, 75–86. https://doi.org/10.1016/j.bej.2012.08.017.

Sharma, S., & Bhattacharya, A. (2017). Drinking water contamination and treatment techniques. *Applied Water Science*, *7*(3), 1043–1067. https://doi.org/10.1007/s13201-016-0455-7.

Sun, Y., He, Y., Tang, B., Wu, Z., Tao, C., Ban, J., et al. (2018). Selective adsorption and decomposition of pollutants using RGO-TiO2 with optimized surface functional groups. *RSC Advances*, *8*(56), 31996–32002. https://doi.org/10.1039/c8ra05345f.

Sun, Q., Liu, M., Li, K., Han, Y., Zuo, Y., Chai, F., et al. (2017). Synthesis of Fe/M (M = Mn, Co, Ni) bimetallic metal organic frameworks and their catalytic activity for phenol degradation under mild conditions. *Inorganic Chemistry Frontiers*, *4*(1), 144–153. https://doi.org/10.1039/c6qi00441e.

Tang, J., & Wang, J. (2017). Fe-based metal organic framework/graphene oxide composite as an efficient catalyst for Fenton-like degradation of methyl orange. *RSC Advances*, *7*(80), 50829–50837. https://doi.org/10.1039/c7ra10145g.

Tarzia, M., De Vivo, B., Somma, R., Ayuso, R. A., McGill, R. A. R., & Parrish, R. R. (2002). Anthropogenic vs. natural pollution: an environmental study of an industrial site under remediation (Naples, Italy). *Geochemistry: Exploration, Environment, Analysis*, *2*(1), 45. https://doi.org/10.1144/1467-787302-006.

Teh, C. M., & Mohamed, A. R. (2011). Roles of titanium dioxide and ion-doped titanium dioxide on photocatalytic degradation of organic pollutants (phenolic compounds and dyes) in aqueous solutions: A review. *Journal of Alloys and Compounds*, *509*(5), 1648–1660. https://doi.org/10.1016/j.jallcom.2010.10.181.

Tie, L., Yu, C., Zhao, Y., Chen, H., Yang, S., Sun, J., et al. (2018). Fabrication of WO3 nanorods on reduced graphene oxide sheets with augmented visible light photocatalytic activity for efficient mineralization of dye. *Journal of Alloys and Compounds*, *769*, 83–91. https://doi.org/10.1016/j.jallcom.2018.07.176.

This book belongs to Central Library BADJI Mokhtar-ANNABA UNIVERSITY Copyright Elsevier 2024

Torimoto, T., Kamiya, Y., Kameyama, T., Nishi, H., Uematsu, T., Kuwabata, S., et al. (2016). Controlling shape anisotropy of ZnS–AgInS2 solid solution nanoparticles for improving photocatalytic activity. *ACS Applied Materials & Interfaces*, *8*(40), 27151–27161. https://doi.org/10.1021/acsami.6b10408.

Toth, P. S., Ramasse, Q. M., Velický, M., & Dryfe, R. A. W. (2015). Functionalization of graphene at the organic/water interface. *Chemical Science*, *6*(2), 1316–1323. https://doi.org/10.1039/c4sc03504f.

Tunesi, S., & Anderson, M. (1991). Influence of chemisorption on the photodecomposition of salicylic acid and related compounds using suspended titania ceramic membranes. *The Journal of Physical Chemistry*, *95*(8), 3399–3405. https://doi.org/10.1021/j100161a078.

Wada, Y., Kitamura, T., Yanagida, S., & Yin, H. (1998). Photoreductive dechlorination of chlorinated benzene derivatives catalyzed by ZnS nanocrystallites. *Chemical Communications*, *24*, 2683–2684. https://doi.org/10.1039/a806035e.

Wang, W. (1987). Root elongation method for toxicity testing of organic and inorganic pollutants. *Environmental Toxicology and Chemistry*, *6*(5), 409–414. https://doi.org/10.1002/etc.5620060509.

Wang, Z., Chen, C., Ma, W., & Zhao, J. (2012). Photochemical coupling of iron redox reactions and transformation of low-molecular-weight organic matter. *The Journal of Physical Chemistry Letters*, *3*(15), 2044–2051. https://doi.org/10.1021/jz3005333.

Wang, C., Kang, J., Sun, H., Ang, H. M., Tadé, M. O., & Wang, S. (2016). One-pot synthesis of N-doped graphene for metal-free advanced oxidation processes. *Carbon*, *102*, 279–287. https://doi.org/10.1016/j.carbon.2016.02.048.

Wang, X., Li, Z., Shi, J., & Yu, Y. (2014). One-dimensional titanium dioxide nanomaterials: Nanowires, nanorods, and nanobelts. *Chemical Reviews*, *114*(19), 9346–9384. https://doi.org/10.1021/cr400633s.

Wang, W., Li, F., Zhang, D., Leung, D. Y. C., & Li, G. (2016). Photoelectrocatalytic hydrogen generation and simultaneous degradation of organic pollutant via CdSe/TiO2 nanotube arrays. *Applied Surface Science*, *362*, 490–497. https://doi.org/10.1016/j.apsusc.2015.11.228.

Wei, M.-C., Wang, K.-S., Hsiao, T.-E., Lin, I. C., Wu, H.-J., Wu, Y.-L., et al. (2011). Effects of UV irradiation on humic acid removal by ozonation, Fenton and Fe0/air treatment: THMFP and biotoxicity evaluation. *Journal of Hazardous Materials*, *195*, 324–331. https://doi.org/10.1016/j.jhazmat.2011.08.044.

Wu, T.-N., Pan, T.-C., & Chen, L.-C. (2012). Electrophotocatalysis of aqueous methyl tert-butyl ether on a titanium dioxide coated electrode. *Electrochimica Acta*, *86*, 170–176. https://doi.org/10.1016/j.electacta.2012.02.075.

Wu, X., Si, Y., Yu, J., & Ding, B. (2018). Titania-based electrospun nanofibrous materials: a new model for organic pollutants degradation. *MRS Communications*, *8*(3), 765–781. https://doi.org/10.1557/mrc.2018.139.

Xia, W., Mahmood, A., Zou, R., & Xu, Q. (2015). Metal–organic frameworks and their derived nanostructures for electrochemical energy storage and conversion. *Energy & Environmental Science*, *8*(7), 1837–1866. https://doi.org/10.1039/c5ee00762c.

Xiong, Z., Zhang, L. L., Ma, J., & Zhao, X. S. (2010). Photocatalytic degradation of dyes over graphene–gold nanocomposites under visible light irradiation. *Chemical Communications*, *46*(33), 6099–6101. https://doi.org/10.1039/c0cc01259a.

Xu, T., Hu, J., Yang, Y., Que, W., Yin, X., Wu, H., et al. (2018). Ternary system of ZnO nanorods/reduced graphene oxide/CuInS2 quantum dots for enhanced photocatalytic performance. *Journal of Alloys and Compounds*, *734*, 196–203. https://doi.org/10.1016/j.jallcom.2017.10.275.

Yao, T., Jia, W., Feng, Y., Zhang, J., Lian, Y., Wu, J., et al. (2019). Preparation of reduced graphene oxide nanosheet/FexOy/nitrogen-doped carbon layer aerogel as photo-Fenton catalyst with enhanced degradation activity and reusability. *Journal of Hazardous Materials*, *362*, 62–71. https://doi.org/10.1016/j.jhazmat.2018.08.084.

Yin, H., Wada, Y., Kitamura, T., & Yanagida, S. (2001). Photoreductive dehalogenation of halogenated benzene derivatives using ZnS or CdS nanocrystallites as photocatalysts. *Environmental Science & Technology*, *35*(1), 227–231. https://doi.org/10.1021/es001114d.

This book belongs to Central Library BADJI Mokhtar-ANNABA UNIVERSITY

Copyright Elsevier 2024

Yu, H., Tian, J., Chen, F., Wang, P., & Wang, X. (2015). Synergistic effect of dual electron-cocatalysts for enhanced photocatalytic activity: rGO as electron-transfer mediator and Fe(III) as oxygen-reduction active site [Article]. *Scientific Reports*, 5, 13083. https://doi.org/10.1038/srep13083. https://www.nature.com/articles/srep13083#supplementary-information.

Yuan, R., Hu, L., Yu, P., Wang, Z., Wang, H., & Fang, J. (2018). Co3O4 nanocrystals/3D nitrogen-doped graphene aerogel: A synergistic hybrid for peroxymonosulfate activation toward the degradation of organic pollutants. *Chemosphere*, *210*, 877–888. https://doi.org/10.1016/j.chemosphere.2018.07.065.

Zhang, H., Lv, X., Li, Y., Wang, Y., & Li, J. (2010). P25-graphene composite as a high performance photocatalyst. *ACS Nano*, *4*(1), 380–386. https://doi.org/10.1021/nn901221k.

Zhang, Y., Tang, Z.-R., Fu, X., & Xu, Y.-J. (2010). TiO_2 – Graphene nanocomposites for gas-phase photocatalytic degradation of volatile aromatic pollutant: Is TiO2 – graphene truly different from other TiO2 – carbon composite materials? *ACS Nano*, *4*(12), 7303–7314. https://doi.org/10.1021/nn1024219.

Zhang, Z., Yu, Y., & Wang, P. (2012). Hierarchical top-porous/bottom-tubular TiO2 nanostructures decorated with Pd nanoparticles for efficient photoelectrocatalytic decomposition of synergistic pollutants. *ACS Applied Materials & Interfaces*, *4*(2), 990–996. https://doi.org/10.1021/am201630s.

Zhao, Q., Mao, Q., Zhou, Y., Wei, J., Liu, X., Yang, J., et al. (2017). Metal-free carbon materials-catalyzed sulfate radical-based advanced oxidation processes: A review on heterogeneous catalysts and applications. *Chemosphere*, *189*, 224–238. https://doi.org/10.1016/j.chemosphere.2017.09.042.

Zhou, T., Zhang, G., Yang, H., Zhang, H., Suo, R., Xie, Y., et al. (2018). Fabrication of Ag3PO4/GO/NiFe2O4 composites with highly efficient and stable visible-light-driven photocatalytic degradation of rhodamine B. *RSC Advances*, *8*(49), 28179–28188. https://doi.org/10.1039/c8ra02962h.

This book belongs to Central Library BADJI Mokhtar-ANNABA UNIVERSITY

Copyright Elsevier 2024

CHAPTER

Recent advances in functionalized polymer-based composite photocatalysts for wastewater treatment

3

Zeenat Arif[a], Naresh K. Sethy[a], Lata Kumari[b], P.K. Mishra[a], S.N. Upadhyay[a]

Department of Chemical Engineering and Technology, IIT (BHU) Varanasi, Varanasi, India[a] Department of Chemistry, IIT (BHU) Varanasi, Varanasi, India[b]

1 Wastewater: Problems, environmental effect

Water accounts for 70% on the earth surface, but only 2.5% is considered as clean water. It is a precious source for every living thing in the world. The existence of minor clean water is used, recycled, and treated so as to fulfill the demands of living organism. Water usage is not only applicable to domestic purpose but also in other areas of application that include industrial and agriculture sector (Yahya et al., 2018). Fig. 1A and B shows the global usage of water across the world based on the group and water usage trend in India, respectively. Rapid urbanization and industrialization generate large volumes of wastewater and water scarcity (Rajasulochana & Preethy, 2016). The fast-growing problem of water scarcity creates negative impact on economic development, human, and aquatic life, throughout the world. The World Survey reported that 21% of the communicable diseases, in India, is waterborne disease. One such disease, namely, diarrhea, is estimated to have killing rate over 535,000 Indians in 2004 (Rajasulochana & Preethy, 2016). The major microbial organisms found in wastewater are bacteria, protozoa, viruses, fungi, and algae. Their presence in water leads to the spread of diseases. The effluent generated from industries like textile, food beverage, and paper leads to large quantities of dye pollutants, thereby creating severe water contamination problems (Ahmad, Razali, Mamat, Kassim, & Amin, 2018). Hence, it has become significantly important for today's environment to take a step to protect water against pollution and also to develop cost-effective method to treat and reuse it.

Conventional wastewater treatment involves costly techniques to remove the contaminant of wastewater effectively so that it can be reuse again safely. The conventional methods include biological and physical treatments but require further advanced technology to work efficiently at lower cost within short duration (Saleh, 2015). In earlier 1970s, different methods employed for wastewater treatment include metal removal by filtration, flocculation, and activated charcoal (Karthikeyan, Rajgopal, & Miranda, 2005; Vijayaraghavan, Ahmad, & Abdul Aziz, 2007; Wang & Chen, 2009). Since 1990 due to the increased scientific knowledge and increased understanding of adverse effect caused by

Nano-Materials as Photocatalysts for Degradation of Environmental Pollutants. https://doi.org/10.1016/B978-0-12-818598-8.00003-1
© 2020 Elsevier Inc. All rights reserved.

This book belongs to Central Library BADJI Mokhtar-ANNABA UNIVERSITY

Copyright Elsevier 2024

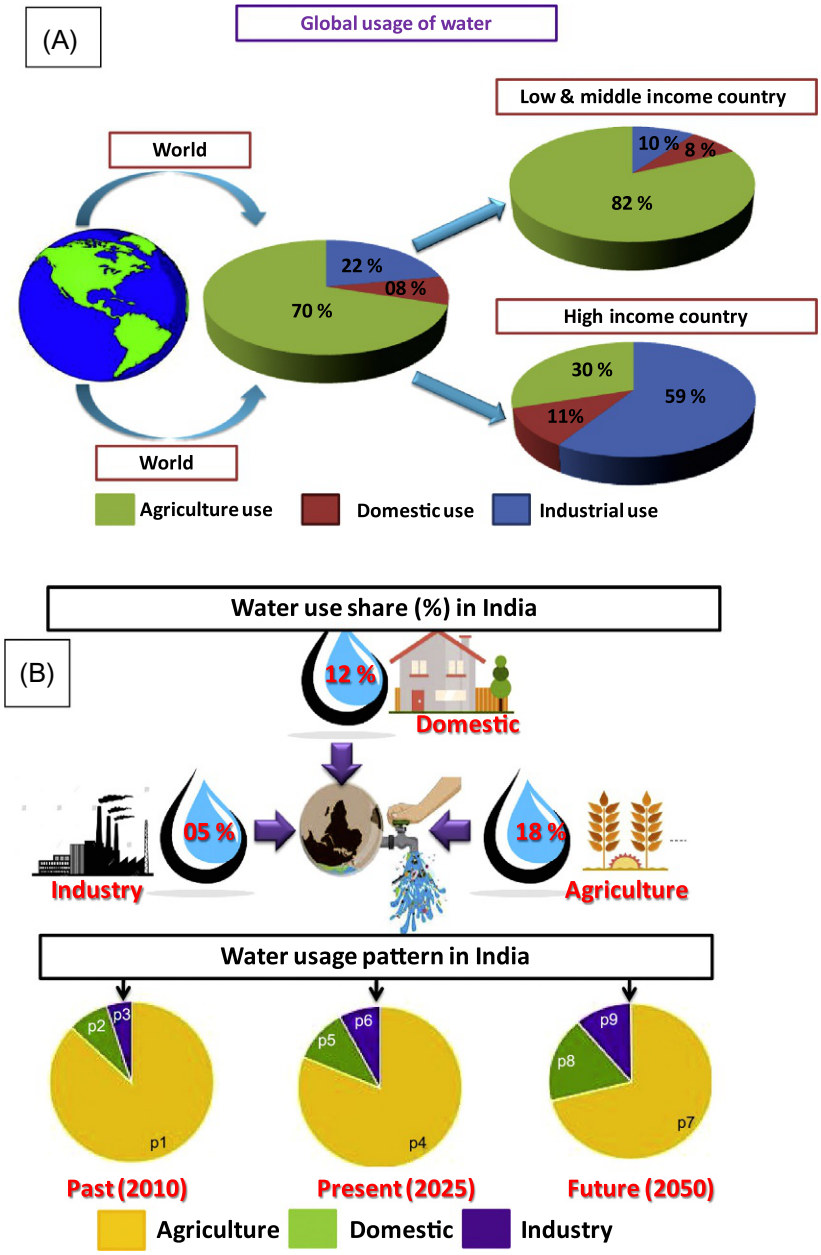

FIG. 1

(A) Water usage at different fields across the world and (B) water usage pattern in India.

This book belongs to Central Library BADJI Mokhtar-ANNABA UNIVERSITY

Copyright Elsevier 2024

water pollution, a typical DEWATS system includes primary and secondary treatments and solid waste disposal. The primary treatment is done to remove settleable solids. The process is cheap and little maintenance is required, it may leave a pathogen-rich waste stream even if operated effectively. The problem of primary treatment is overcome by the use of secondary treatment options, but they are ineffective in highly permeable soil type (Rajasulochana & Preethy, 2016).

There are several other physical and chemical methods available for the removal of pollutants from water (Fig. 2). The selection of treatment is dependent on various factors like type and concentration of waste, effluent heterogeneity, and level of cleanup. Table 1 enlists the several conventional treatments with their advantage and disadvantage (Crin, 2006).

Biological treatment is economic alternative and uses microorganisms to remove toxic and to recover precious metals from wastewater. It has gained popularity over the years because of increased performance and low cost of raw materials (Ahluwalia & Goyal, 2007; Benaissa & Elouchdi, 2007; Bunluesin, Kruatrachue, Pokethitiyook, Upatham, & Lanza, 2007). The demerits of biological treatment include large land area requirement and constrained sensitivity toward diurnal variation and less

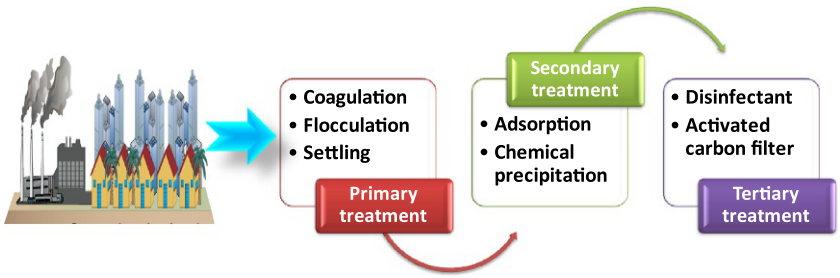

FIG. 2

Flowsheet for conventional treatment of wastewater.

Table 1 Conventional treatment process: advantages and disadvantages.

Technology	Advantage	Disadvantage
Conventional treatment process		
Coagulation	Economically feasible and simple technique	Large volume of sludge production Handling and disposable problem
Flocculation	Economically feasible and simple technique	Large volume of sludge production Handling and disposable problem
Biodegradation	Economically acceptable treatment	Very slow process High maintenance requirement
Adsorption	Produce a high quality of treated water	Regeneration of adsorbent is inexpensive Nondestructive process
Ion exchange	Rapid and efficient process No loss during regeneration process	High energy cost Require chemicals

This book belongs to Central Library BADJI Mokhtar-ANNABA UNIVERSITY Copyright Elsevier 2024

flexibility in designing and operation. The conventional technologies do not completely eliminate the pollutants. Somehow, these pollutants were simply being transferred to another phase. Thus, it becomes necessary to find the best practices/strategies for the treatment of wastewater for our environment and sustainable development.

2 Photocatalyst

As stated earlier, the treatment of organic pollutants is generally a costly proposition, so researchers are focusing on the utilization of cost-effective energy source. The concept of utilizing huge availability and clean solar energy for different application is gaining interest (Bora & Mewada, 2017). The spectrum of solar constitutes of 3%–5% UV ($\lambda < 400$ nm) and 47% visible light ($400 > \lambda < 700$ nm). It is stated about 89,300 TW of solar insolation is received by the earth (Tsao, 2006). The huge gap between solar availability and application should be reduced to effectively utilize the cost-effective source. Researchers and environmentalists are searching to harvest it for treatment purpose.

Advanced oxidation processes (AOPs) are a recently developed technology to degrade organic pollutants by generating hydroxyl radicals. Due to the strong oxidative power of the hydroxyl radicals, they almost oxidize and mineralize the organic molecule, yielding final product as CO_2 and inorganic ions (Miranda-García, Maldonado, Coronado, & Malato, 2010). Among AOP photocatalysis, an environment-friendly chemistry technology is an interesting alternative process that has drawn much attention to remove the contaminants at ambient temperature by oxidation (Cao, Jiao, Chen, Jiang, & Wang, 2018). In 1972, Fujishima and Honda have found photocatalyst when they discovered titanium dioxide (TiO_2) (Chen, Guan-Ping, Su, & Feng, 2016), which were used for splitting of water into hydrogen and oxygen. In 1991, Bahnemann, Bockelmann, and Goslich (1991) reported the influence of light for degradation of halogenated hydrocarbon and concluded that this technology has bright future for treatment technology. Heterogeneous photocatalysis is sustainable AOP for the removal of organic pollutant. This is due to the fact that visible/solar light active photocatalysts are nontoxic in nature; they are relatively inexpensive having high surface area with broad absorption spectra from UV region to visible region (Herrmann, 1995).

2.1 Principles of photocatalysis

It is a five-step process that includes pollutant transport from bulk fluid onto the photocatalyst surface for adsorption, followed by photoreaction, and finally desorption of final and by-products from the surface to the bulk fluid. The simplified mechanism is shown in Fig. 3.

2.1.1 Basic mechanism

The basic photocatalyst mechanism includes photon absorption by photocatalyst having energy greater than its bandgap (BG). This adsorption enables excitation and transfer of electrons (e^-) from the valence band (VB) to the conduction band (CB), thus generating hole (h^+), a positive charge in the valence band. This stage is referred as "semiconductor's photoexcitation" (Safarpour, Khataee, & Vatanpour, 2014), but there may be chances of recombination of the electron and the hole that must be avoided because this excitation will not participate in the reaction and will directly affect the photocatalyst

This book belongs to Central Library BADJI Mokhtar-ANNABA UNIVERSITY
Copyright Elsevier 2024

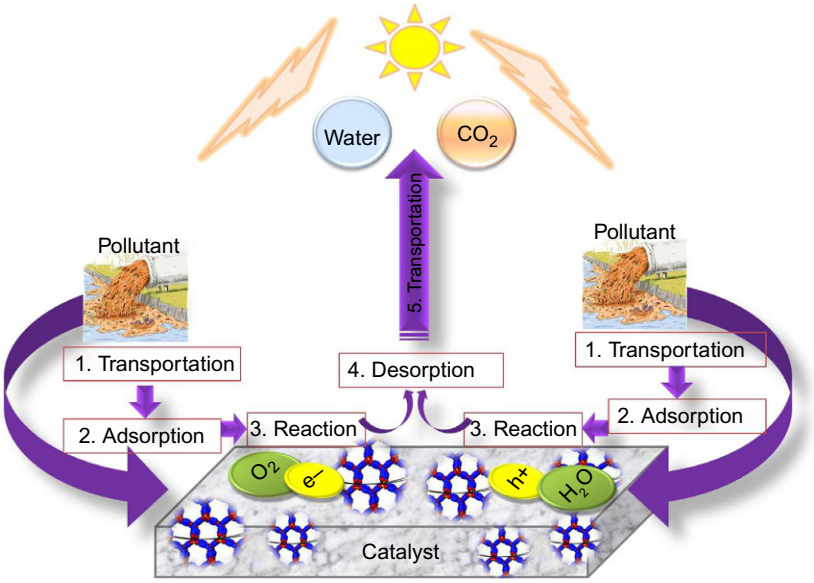

FIG. 3

Representation of steps involved in heterogeneous photocatalysis.

efficiency. The photogenerated e^- will react with available organic species (oxidants), and h^+ will react with reductants to yield powerful unstable radicals, which react further with the pollutant and mineralize it to carbon dioxide and water. The generalized photocatalytic reactions are summarized as follows:

$$\text{Photocatalyst} + h\nu \rightarrow h^+ + e^- \tag{1}$$

$$h^+ + e^- \rightarrow \text{energy (heat)} \tag{2}$$

$$H_2O + h^+ \rightarrow {}^*OH\ (\text{hydroxyl radical}) + H^+ \tag{3}$$

$$O_2 + e^- \rightarrow O_2{}^{*-}\ (\text{superoxide radical}) \tag{4}$$

$$^*OH + \text{pollutant} \rightarrow \text{Intermediates} \rightarrow H_2O + CO_2 \tag{5}$$

$$O_2{}^{*-} + \text{pollutant} \rightarrow \text{Intermediates} \rightarrow H_2O + CO_2 \tag{6}$$

The unique property of transition metal and their oxide nanoparticles (NPs) are widely used to remove pollutants present in wastewater. To date, various semiconductor photocatalysts have been reported for photodegradation of organic and inorganic contaminants (Chen et al., 2016). Titanium dioxide (TiO_2) (Miranda-García et al., 2010; Safarpour et al., 2014), graphene oxide (GO) (Upadhyay, Soin, & Roy, 2014; Zhao, Xu, Chen, Wang, & Yang, 2014), zinc oxide (ZnO) (Ramesha, Kumara, Muralidhara, & Sampath, 2011; Xu, Chen, Guo, Lei, & Ni, 2012), and TiO_2/ZnO (Ji et al., 2012) are some of the widely used and known photocatalyst material. A comprehensive study of the different types of transition nanomaterials used as photocatalyst that are listed for the removal of organic, inorganic, and heavy metal is shown in Tables 2 and 3, respectively.

This book belongs to Central Library BADJI Mokhtar-ANNABA UNIVERSITY
Copyright Elsevier 2024

Table 2 Removal of organic pollutant using different nanoparticles

Transition metal nanomaterials	Pollutant	Structure	Result	Ref.
Au/Au_3^+-TiO_2	Methylene blue (MB)	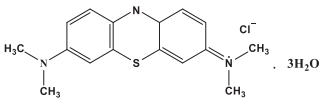	TOC removals is 73.6%	Li and Li (2001)
TiO_2	Phenol		Optimum loading = 2 g/L 92% degradation achieved in 6 h	Salah, Bouhelassa, Bekkouche, and Boultif (2004)
ZnO	Phenol, dichloro phenol (DCP), trichloro phenol (TCP)	DCP: 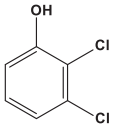 TCP: 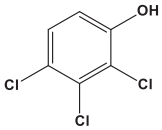	Optimum loading = 0.4 g/L 85%, 90%, and 93% degradation of TNP, DCP, and phenol in 2.5 h, respectively	Shukla, Wang, Ang, and Tade (2010)
ZnO	4-Nitrophenol	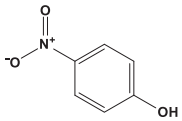	Optimum loading = 0.6 g/L Optimum pH = 6 Degradation > 90% was achieved	Parida, Dash, and Das (2006)
Au/graphene	Rhodamine B	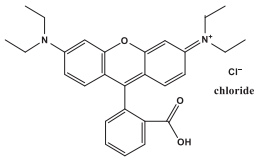	Removal efficiency (%) = 100 in 3.5 h Removal capacity = 40.3 mg/g	Xiong, Zhang, Ma, and Zhao (2010)
Ag/TiO_2	Methyl orange	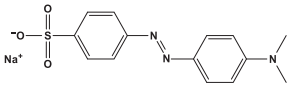	Removal efficiency (%) = 90 in 0.8 h Removal capacity = 135 mg/g	Yang, Fu, Wong, Jiang, and Yu (2013)
Reduced graphene oxide (rGO) Multiwalled carbon nanotubes (MWCNTs)	Bisphenol-A	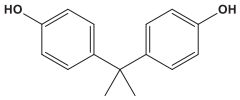	Removal capacity = 150 mg/g using rGO and 59 mg/g using MWCNTs	Liu, Zhao, Wang, Du, and Xing (2014)

This book belongs to Central Library BADJI Mokhtar-ANNABA UNIVERSITY

Copyright Elsevier 2024

Table 2 Removal of organic pollutant using different nanoparticles—cont'd

Transition metal nanomaterials	Pollutant	Structure	Result	Ref.
Ag/nZVI	Chloramphenicol	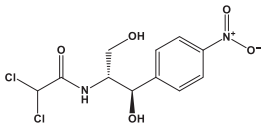	Removal capacity = 57 mg/g	Singh, Singh, Gupta, and Rai (2012)
TiO_2	Chlorohexa-dine	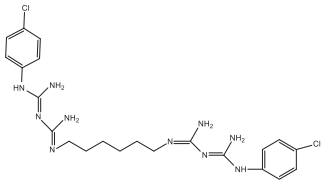	Removal efficiency (%) = 64 in 1 h Removal capacity = 32000 mg/g	Das, Sarkar, Chakraborty, Choi, and Bhattacharjee (2014)
$Al_2O_3/MgO + C$ nanofibers	Diazinon	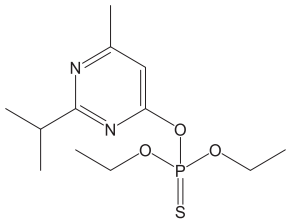	Removal efficiency (%) = 55 in 0.5 h	Behnam, Morshed, Tavanai, and Ghiaci (2013)

Table 3 Removal of heavy and inorganic nonmetals using different nanoparticles.

	Pollutant	Nanoparticle	Result	Ref.
Heavy metal	Lead	ZrO_2	Removal efficiency (%) = 25 in 1.7 h Removal capacity = 320 mg/g	Hua et al. (2013)
	Copper	MWCNTs/ Fe_3O_4	Removal capacity = 39 mg/g	Hu, Zhao, and Wang (2011)
	Cadmium	ZrO_2	Removal efficiency (%) = 30 in 1.7 h Removal capacity = 215 mg/g	Hua et al. (2013)
	Mercury	Fe_3O_4/SiO_2	Removal efficiency (%) = 50 Removal capacity = 17 mg/g	Girginova et al. (2010)
	Chromium	CeO_2 composite	Removal efficiency (%) = 60 in 5 h Removal capacity = 5.9 mg/g	Zhong et al. (2007)
Inorganic nonmetals	Arsenic	Reduced GO/ nZVI	Removal capacity (mg/g) As(III) = 36, As(V) = 29	Wang et al. (2014)
		Mn/Al oxide	Removal efficiency (%) = 65 in 5 h. Removal capacity = 140 mg/g	Wu, Liu, Xue, and Wang (2012)
	Phosphate	ZrO_2/graphite oxide	Removal capacity = 18 mg/g	Zong et al. (2013)
		Mn/Al oxide	Removal efficiency (%) = 100 in 5 h. Removal capacity = 60 mg/g	Wu et al. (2014)
	Nitrate	CNT sheets	Removal capacity = 140 mg/g	Tofighy and Mohammadi (2012)

This book belongs to Central Library BADJI Mokhtar-ANNABA UNIVERSITY

Copyright Elsevier 2024

3 Need of supported system

3.1 Drawbacks of NPs in powder form

(i) The direct application of NPs for photocatalytic degradation suffers from aggregation of NPs. As a result, it affects the stability and recyclability of NPs (Astruc, Lu, & Aranzaes, 2005).
(ii) The attenuation loss suffered by light rays leads to low quantum utilization by suspended NPs. Researchers reported that <1% of UV light or only 20% of visible light actually penetrates to 0.5-m depth under the water surface (Han & Bai, 2010).
(iii) Reusability and regeneration are important cost-effective factors. It was also reported that, in some systems, the use of sedimentation, centrifugation, and filtration technique to reclaim the dispersed and suspended catalyst from the treated water is a time-consuming process. These techniques are also increasingly inefficient due to smaller size particle to remain suspended in the water and may penetrate and clog through the filter material (Bao, Feng, Yang, Shen, & Lu, 2004; Malato et al., 2003).
(iv) Human health problems due to powder form mobility (Sriwong, Wongnawa, & Patarapaiboolchai, 2008).

The limited photocatalytic activity, low adsorption capacity, and difficulty in recovery restrict their practical application. To minimize the catalyst retrieval problem, they have been immobilized on solid supports/dopants. The use of immobilization or dopant creates a new orbital between the VB and the CB, thereby reducing the bandgap. Thus, electrons now require less energy for excitation to reach the conduction band (Seery, George, Floris, & Pillai, 2007). The incorporation of nanoparticles into a polymer, metal, or ceramic matrix to upgrade their novel properties—mechanical stability, good optical features, low water/gas permeability, and high electrothermal conductivity—is termed as nanocomposite (Han & Bai, 2010).

3.2 Immobilization of NPs has the following advantages (Han & Bai, 2010; Seery et al., 2007)

(i) High quantum utilization efficiency compared with powder photocatalyst
(ii) Comparatively low operational cost than suspended system due to ease of posttreatment recovery for large applications
(iii) Reduced catalyst loss during regeneration process
(iv) Longer time of contact of the photocatalyst with pollutants

Immobilization has its own sets of drawbacks too, such as the following:

(i) Reduced surface area available for reaction (Byrne, Eggins, Brown, McKinney, & Rouse, 1998)
(ii) Require suitable techniques with well-defined procedures and equipment to make them available in "ready to be used form."

However, the advantages of immobilized supersede the disadvantages, and thus, researchers are focusing to develop simple and efficient technique to coat NPs on suitable substrate.

This book belongs to Central Library BADJI Mokhtar-ANNABA UNIVERSITY Copyright Elsevier 2024

Supports available:

The different types of supports that have been reported include glass mats (Dhananjeyan, Kiwi, Albers, & Enea, 2001), inorganic carbon fabrics (Yuranova et al., 2004), plastics (Kwon, Shin, Kim, Choi, & Yoon, 2004), natural fabrics (Yuranova, Mosteo, Bandara, Laub, & Kiwi, 2006), polymers (Yang, Han, & Choy, 2006), fly ash, ceramic membranes and monoliths, stainless steel, and polystyrene (Fabiyi & Skelton, 2000). The polymer nanocomposites have attracted significant interest because of their significant potential to advance engineering applications.

3.3 Polymer as a support

The following property of the polymers makes them suitable for application as a support for photocatalysts

(i) They are nontoxic materials and are chemically inert, mechanically stable with long durability (Magalhaes, Moura, & Lago, 2011; Shan, Ghazi, & Rashid, 2010).
(ii) The hydrophobic polymer adds an advantage to preconcentrate the organic pollutants, thereby increasing the adsorption efficiency and subsequent oxidation (Magalhaes et al., 2011).
(iii) Inexpensive and easy availability (Shan et al., 2010).
(iv) The thermoplastic feature provides thermosoftening properties and provides the ease of coating NPs on them by simple thermal treatment technique (Shan et al., 2010).
(v) Many of the polymers are having high UV resistance; as a result, they do not undergo oxidation readily (Fabiyi & Skelton, 2000).

3.4 Various polymeric substrates

A lot of polymeric substrates have been used for anchoring photocatalyst.

In polymeric nanocomposites, filler or additives at the nanometer scale are incorporated into a polymer matrix in a small ratio or volume (<5%) to affect their optical/mechanical properties and other such property (Yang et al., 2006). The choice of polymer matrix strongly affects the physiochemical properties for different applications.

Some of the widely used polymers are polythene $(C_2H_4)_n$ (Naskar, Pillay, & Chanda, 1998), polystyrene $(C_8H_8)_n$ (PS) (Fabiyi & Skelton, 2000), cellulose $(C_6H_{10}O_5)_n$, microspheres (Nagaoka et al., 2002), fluoropolymer resins (Sopyan, Watanabe, Murasawa, Hashimoto, & Fujishima, 1996), polyethylene terephthalate (PET) $(C_{10}H_8O_4)_n$ (Fostier, Pereira, Rath, & Guimaraes, 2008), cellulose fibers (Mounir, Pons, Zahraa, Yaacoubi, & Benhammou, 2007), polyvinyl chloride (PVC) $(C_2H_3Cl)_n$ (Cho & Choi, 2001), polyvinyl alcohol (PVA) $(C_2H_4O)x$ (El-Rehim, Hegazy, & Diaa, 2012), polyaniline (PANI) (Yu, Wu, Fu, Dong, & Ma, 2012), polycarbonate (PC), poly(methyl methacrylate) (PMMA) $(C_5O_2H_8)_n$ (Langlet, Kim, Audier, & Herrmann, 2002), polyvinyl acetate (PVAc) $(C_4H_6O_2)_n$ (Brezova et al., 1994), and rubber latex (an elastic hydrocarbon polymer) (Sriwong et al., 2008).

This book belongs to Central Library BADJI Mokhtar-ANNABA UNIVERSITY
Copyright Elsevier 2024

3.5 Different methods for supporting NPs on polymer substrate

The method for selecting the support is dependent on the substrate type and pollutant to be degraded as it affects the photocatalytic activity (PCA). The approach selected to combine the beneficial characteristics of inorganic fillers within the polymer matrix should not lead to any reduction in the PCA of NPs. The different fabrication methods for polymeric nanocomposites are shown in Fig. 4.

Some other different methods are also available such as sol-gel method (Chen, Stathatos, & Dionysiou, 2008), dipcoating (Balasubramanian, Dionysiou, Suidan, Baudin, & Laıne, 2004), chemical vapor deposition (CVD) (Kuo, Tseng, Huang, & Li, 2007), plasma-enhanced chemical vapor deposition (PECVD) (Nizard et al., 2008), metal–organic chemical vapor deposition (MOCVD), thermal treatment method (Fabiyi & Skelton, 2000), hydrothermal methods (Liu & Chen, 2007), and sol-spray methods (Shan et al., 2010). A comparative study of different methods for the synthesis of nanocomposites is given in Table 4.

The choice of the polymeric matrix to be used as support system is dependent on factors like mechanical and thermal behavior, chemical stability, biocompatibility, and chemical functionalities (i.e., solvation and wettability) to select the appropriate organic host. Table 5 summarizes the different types of polymer-based nanocomposite material prepared by different methods for photocatalytic degradation.

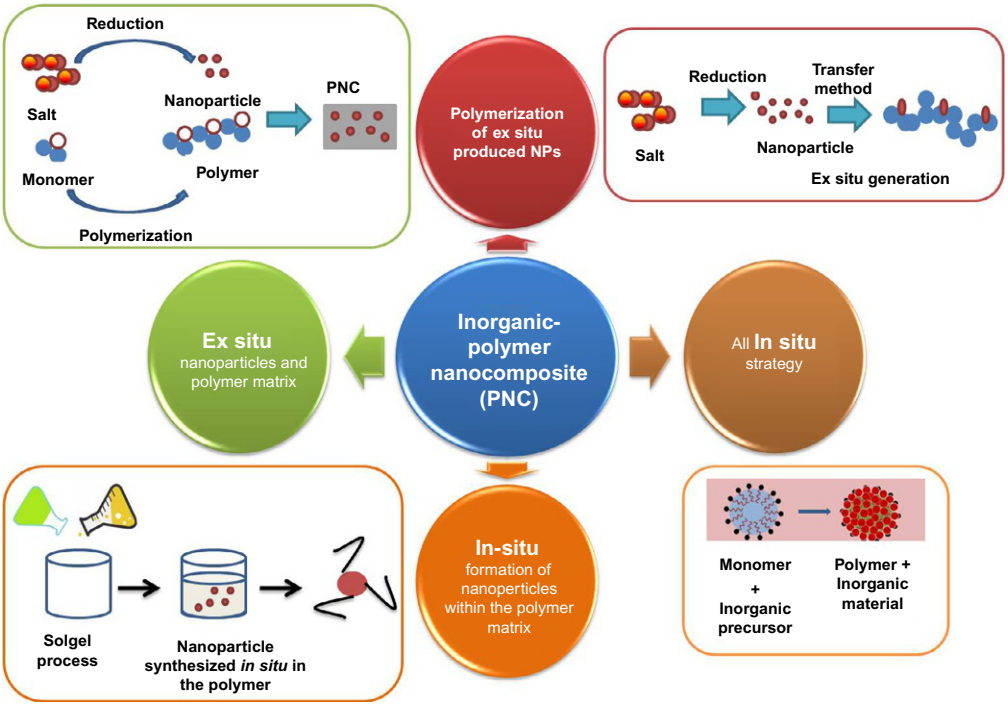

FIG. 4

Fabrication method for polymeric nanocomposites.

This book belongs to Central Library BADJI Mokhtar-ANNABA UNIVERSITY
Copyright Elsevier 2024

Table 4 Polymers used in the synthesis nanocomposites.

Preparation technique	Polymer nanocomposite	Advantage	Disadvantage	Ref.
Solution casting	PMMA/titanium dioxide nanotube	Easy scale-up	Impurity	Langlet, Kim, Audier, and Herrmann (2002)
Intercalation	Poly(glycidyl methacrylate) (PGMA)/ poly(glycidyl methacrylate) (PGMA)/Fe_3O_4 nanocomposite	Organized structure	Nonuniform dispersion	Fu et al. (2015)
In situ polymerization	Carbon nanotube (CNT) polymer composite	Liquid-phase processing Polymer matrix free of agglomeration	Costly and time-consuming technique	Shawky, Chae, Lin, and Wiesner (2011)
Sol-gel	Polyethylene-octene elastomer (POE)	Compatibility and unique properties	High reactivity	Rahmat and Hubert (2011)
Template synthesis	PMMA/carbon nanotube (CNT)	Synergistic effects	Control dispersion	Arash, Park, and Rabczuk (2015)
Phase separation	Polyaniline/tin oxide	Functionalization	Uncontrolled formation	Shukla, Shukla, Govender, and Agorku (2016)
Electrochemical synthesis	polyurethane/ montmorillonite	Synthesized under moderate conditions	Reactions are confined to the surfaces	David, Drobota, and Simionescu (2015)
Hydrothermal synthesis	$Mn^0.6Zn^0.4Fe_2O_4$-CNTs/ PANI nanocomposites	High conductivity and strong saturated magnetization	High temperature and high vapor pressure	Kundu, Satpati, Mukherjee, Kar, and Pradhan (2017)
Melt intercalation technique	Polypropylene-based nanocomposites	Environmentally friendly technique. Flexible in terms of formulation, price, and compatibility		Normand, Mija, Pagnotta, Peuvrel-Disdier, and Vergnes (2017)
Spinning	Ethylene vinyl acetate/ graphene oxide	Good interfacial interaction	Costly technique	Hussain, Hojjati, Okamoto, and Gorga (2006)

This book belongs to Central Library BADJI Mokhtar-ANNABA UNIVERSITY
Copyright Elsevier 2024

Table 5 List of polymer-based nanocomposites (PNCs) for degradation of pollutants

NPs	Polymer	Structure	Method	Pollutant	Result	Ref.
TiO_2	Polypropylene (PP)	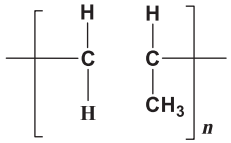	Hot pressing	Paraquat	TiO_2 coverage 8.8 $\times 10^{-5}$ g cm^{-2} (PP) achieved optimum PCA under UV and sunlight	Tennakone and Kottegoda (1996)
	Poly (tetrafluoro-ethylene) (PTFE)	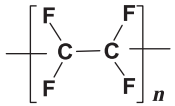	Electrophoretic deposition	Trichlorobenzene (TCB)	100% mineralization in 2 h under UV light	Uchida, Katoh, and Watanabe (1998)
	Polythene (PE) pellets	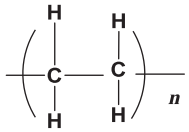	Thermal treatment method	4-Chlorophenol (4-CP)	58% degradation by PE-TiO_2 in 6 h	Velasquez, Valencia, Rios, Restrepo, and Marin (2012)
	Poly(di-methylsiloxane) (PDMS)	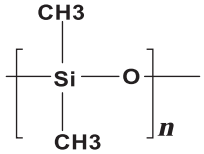	Sol-gel	Methylene blue and acetaldehyde	The MB and acetaldehyde were decomposed at PDMS content less than 60% under UV irradiation	Iketania, Sunb, Tokib, Hirotaa, and Yamaguchi (2003)
	Polyhydroxy-butyrate (PHB)	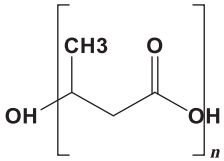	Solvent-cast	Methylene blue	96% of the MB solution degraded in 1 h under solar illumination	Yew, Tang, and Sudesh (2006)
CdS	Chitosan	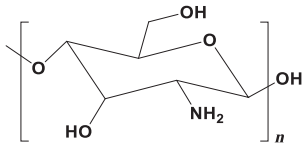	Simulating bio-mineralization	Congo red	85.9% of degradation rate achieved within 180 min	Zhu et al. (2009)

This book belongs to Central Library BADJI Mokhtar-ANNABA UNIVERSITY

Copyright Elsevier 2024

Table 5 List of polymer-based nanocomposites (PNCs) for degradation of pollutants—cont'd

NPs	Polymer	Structure	Method	Pollutant	Result	Ref.
Fe	Poly(vinyl pyrrolidone) (PVP)	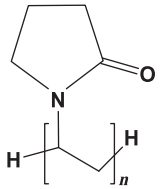	Electrospinning	Bromate	90% of activity of fresh bare Fe was observed	Xu, Wang, and Choi (2010)
	Poly(methyl methacrylate) (PMMA)	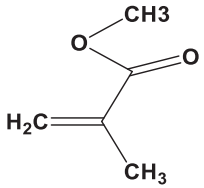	In situ synthesis	Trichloroethene	Dechlorination efficiency was 62.3%, with rate constant was 0.0034 h^{-1}	Wang, Zhao, and Jin (2010)
	Carboxy-methyl Cellulose (CMC)	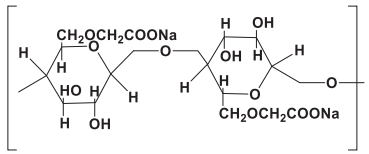	In situ synthesis	Cr(VI)	Removal efficiency was 22% and 94% for Fe NPs and CMC-Fe0 after 60 min	Wang, Qian, et al. (2010)
Cu	Chitosan	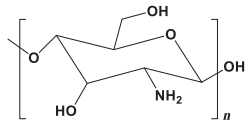	In situ synthesis	Cr(VI)	Degraded from 50 mg/L to 2.21 mg/L (pH 2.85), and at 5 mg/L, the removal efficiency > 99%	Wu, Liou, and Mi (2009)
Ni/Fe	Cellulose acetate	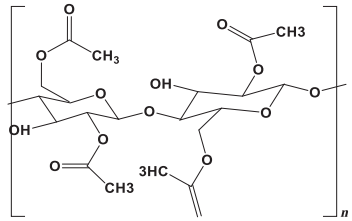	Solvent cast	Trichloroethylene	Reduction rate constant was proportional to the Ni content	Wu and Ritchie (2006)
Fe/Pd	Poly(vinylidene fluoride) (PVDF)	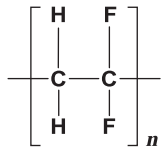	Reduction-deposition	Trichloroacetic acid	Dechlorinated within 180 min	Wang, Chen, Liu, and Ma (2008)

This book belongs to Central Library BADJI Mokhtar-ANNABA UNIVERSITY

Copyright Elsevier 2024

4 Characterization of polymer nanocomposite

The commonly used techniques for the characterizations of PNCs include the following:

(i) **Thermal analysis**—thermal gravimetric analysis (TGA), differential thermal analysis (DTA), differential scanning calorimetry (DSC), and thermomechanical analysis (TMA)
(ii) **Microscopic techniques**—scanning electron microscope (SEM), transmission electron microscope (TEM), and atomic force microscope (AFM)
(iii) **Spectroscopic techniques**—Fourier transform infrared (FTIR), Raman spectroscopy, and X-ray diffraction techniques

The processability of a nonpolymeric component improves significantly due to the presence of polymeric matrix, and at the same time, the thermal stability of polymer is also improved by the nonpolymeric significantly. So, they have frequently been used for thermal stability analysis (Meneghetti & Qutubuddin, 2006). The homogeneity, porosity, and roughness of the surface were analyzed using SEM and AFM. The transmission electron microscopy (TEM) provides qualitative information about the internal structure, spatial distribution, and defective structure. XRD analysis reveals the crystallinity and lattice structure. FTIR and Raman spectra are used to study the physical and chemical interaction in dispersed phase matrix responsible for newer physical and chemical properties (Kumar et al., 2018).

5 Photoreactor: Evaluation of photocatalytic activity

Photocatalytic activity was evaluated by carrying out the experiment in photoreactor setup. Generalized photoreactor setup consists of Pyrex glass column of specific dimension surrounded by UV lamps with an emission at 365 nm. The column top was open to air. Air pump was used to provide aeration so as to ensure a constant supply of O_2 and to promote a complete mixing of solution during photoreaction. The schematic representation of photoreactor setup is shown in Fig. 5. Initially, the adsorption procedure was carried for 30 min to achieve equilibrium in the dark. After equilibrium, UV lights were turned on and were sampled at different time interval and were analyzed to evaluate concentration.

The photocatalytic efficiency was evaluated using Eq. (7) (Yu et al., 2005):

$$\text{Color removal} = C_0 - C_t / C_0 \times 100 \tag{7}$$

where C_o and C_t (mg/L) are initial and final concentration of pollutant.

It was reported in the literature that the photodegradation by UV irradiation follows the pseudo-first-order kinetics with respect to the concentration of pollutant and is due its simplicity (Li, Sun, Ma, Ouyang, & Yan, 2008; Wang, Min, et al., 2010; Wang, Qian, et al., 2010; Wang, Zhou, et al., 2010). It is expressed as

$$r = -dC/dt = k_{\text{app}}\, C \tag{8}$$

This book belongs to Central Library BADJI Mokhtar-ANNABA UNIVERSITY
Copyright Elsevier 2024

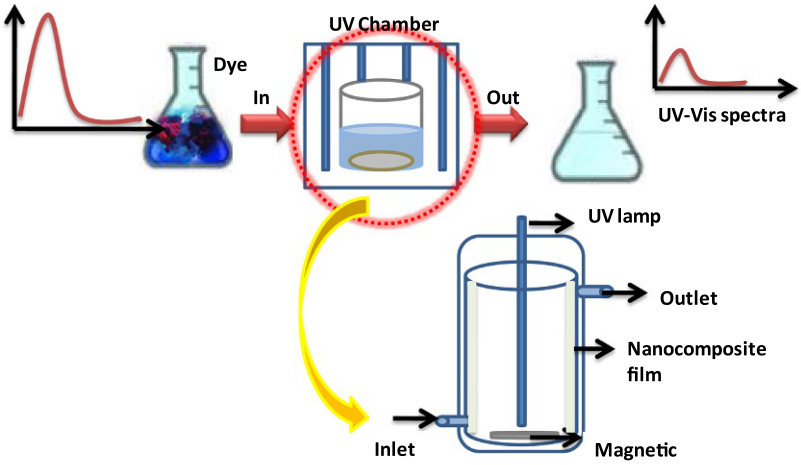

FIG. 5

Photoreactor setup.

where k_{app} is the pseudo-first-order rate constant and the relationship between them is explained by Langmuir-Hinshelwood (L-H) model (Kesselman, Lewis, & Hoffmann, 1997; Tennakone, Tilakaratne, & Kottegoda, 1997; Xu & Langford, 2000).

The kinetic rate constant of the photocatalytic degradation was evaluated by integrating Eq. (8):

$$\ln (C/C_0) = k_{app}\,\mathrm{C} \tag{10}$$

where the slope of ln (C/C_0) versus t will give rate constant k_{app}.

Based on the derived photocatalyst rate equation, the parameter affecting the photocatalyst activity is as follows:

(i) *Effect of catalyst dosing* (Jawad & Nawi, 2012; Li et al., 2008)

The optimization of NPs loading in polymeric matrix is an important and significant parameter to avoid the excess use of NPs and maximum absorption of light by them. It was studied that pseudo-first-order rate increases with increase in loading at optimal loading. Above optimal loading, no further change in rate constant value was observed.

(ii) *Effect of pH*

pH parameter influences the surface state of NPs and the ionization state of organic pollutant. It was concluded that pH has direct influence on the rate constant value. Any change in pH will affect the isoelectric point (PZC) of NPs. When pH < PZC, the catalyst surface becomes positively charge and hence exerts an electrostatic attraction force to the negatively charged compounds. Such interactions intensify the adsorption rate and vice versa.

(iii) *Effect of organic pollutant*

The increase in concentration of pollutant leads to the absorption of UV light, thereby lowering the light intensity available for photocatalytic degradation and hence decreasing the photocatalytic activity. Since the concentration of active centers is finite, the organic molecules

This book belongs to Central Library BADJI Mokhtar-ANNABA UNIVERSITY Copyright Elsevier 2024

are excessive in comparison with the active centers; thereby, UV adsorption capability by active centers diminishes. Thus, the initial concentration of pollutant strongly affects the photocatalytic process (Li et al., 2008).

(iv) *Effect of light Intensity*

Light intensity is also important parameter affecting the efficiency of photocatalytic reaction. The generation of electron-hole pair is due to light intensity. It was stated that higher light intensity provides higher energy for the generation of electron-hole pair, so k_{app} increases with increase in light intensity, and the decomposition is also faster at high intensity (Li et al., 2008). Table 6 summarizes the effect of operating parameter on photocatalyst activity for different polymer nanocomposites.

(v) *Temperature effect*

Several investigations have been carried out to study the temperature effect on photocatalytic reaction. The studies reported that reaction temperature (>80 °C) disfavors the adsorption phenomenon and also accelerates the recombination of electron-hole pair, thus drastically reducing the photocatalytic activity with increasing reaction temperature.

6 Surface modification of polymeric nanocomposite

Nowadays, surface modification has become a spotlight of research due to particle agglomeration because of specific area and specific volume effects. The modification improves the polymer-particle interaction. Modification can be carried out in two ways: (i) surface absorption with coupling agents and (ii) grafting polymerization. Different modification techniques to enhance the dispersion stability of NPs to increase the interfacial adhesion are shown in Fig. 6.

(i) Chemical treatment

The surface modification of organic nanocomposite using chemical treatments like nanomaterial functionalization is an attractive research topic regarding aqueous solutions. Alam, Wan, and McNally (2017) reported the carbon nanoparticle surface functionalization to overcome the problem associated with the interaction and dispersion within the polymer matrices. Graphene surfaces were functionalized to provide chemical stability between fillers and polymer matrix (Sainsbury et al., 2017). Chu et al. (2017) enhanced the properties of epoxy nanocomposites by functionalization of the surface-modified silica nanoparticles.

(ii) Ligand exchange technique

This technique is a combination of two techniques, namely, ion exchange and coordination chemistry, used to accomplish a task that cannot be done alone. Zeng et al. (2017) used adenosine monophosphate as a capping ligand to develop the poly PEGyl hydrox-yapatite (HA) nanorods to enhance their dispersion stability for biomedical field. Similarly, the surface of ZIF-8 powders was modified using 5,6-dimethylbenzimidazole (DMBIM) as a capping agent by ligand exchange techniques (Zhang, Ding, et al., 2017; Zhang, James, et al., 2017).

This book belongs to Central Library BADJI Mokhtar-ANNABA UNIVERSITY Copyright Elsevier 2024

Table 6 Effect of parameter on photocatalyst activity.

Nanocomposite	Pollutant	Operating parameter		Result	Ref.
Epoxidized natural rubber/ TiO_2	MB	NP loading	0.65–3.93 mg cm^{-2}	k_{app} 2.8 times faster 0.65–3.93 mg cm^{-2}	Jawad and Nawi (2012)
		pH	2–10	k_{app} five times faster from two to eight	
PANI/TiO_2	MB	Ratio (PANI/ TiO_2)	1:500 to 1:200	Maximum absorption for 1:500 Degradation efficiency increases from 31% to 81.74% from 1:200 to 1:500	Wang, Min, et al. (2010), Wang, Qian, et al. (2010), Wang, Zhou, et al. (2010)
Polyaniline/ZnO	MB and MG (malachite green)	At 0.4 mg/mL		Decolorization efficiency of MB and MG in 94% and 95%, respectively, and three times higher than that pure polyaniline	Eskizeybek, Sari, Gülce, Gülce, and Avci (2012)
		ZnO loading	0.2–1.6 mg/mL	The degradation efficiency increased with increasing the amounts up to 0.4 mg/mL	
SnS_2/PANI composite	Cr(VI)	SnS_2/PANI = 100:7		Photocatalytic reduction of Cr (VI) nearly 4.2 times that by SnS_2	Zhang, Ding, Zhang, Yang, and Xue (2017)
Polyacrylamide Zr(IV) vanadophosphate (PAM/ZVP)	Congo red dye			96% degradation for (PAM/ZVP) and only 64% for ZVP	Sharma, Kumar, Naushad, Pathania, and Sillanpää (2016)
PVA-assisted Bi2WO6–CdS	Metronidazole and methylene blue			PVA-assisted Bi_2WO_6–CdS 1.7142, 1.333 and 1.0909 times higher than CdS, Bi_2WO_6 and Bi_2WO_6–CdS for metronidazole Degradation efficiency is 92%, 72%, and 86% for PVA-assisted Bi_2WO_6, CdS, Bi_2WO_6, respectively	Rajendran, Varadharajan, Jayaraman, Singaram, and Jeyaram (2018)
Grapheme (Gr)/ polyaniline	Rose bengal dye	Gr loading	0–3 wt%	Degradation percentage increases from 15% to 59%	Ameen, Seo, Akhtar, and Shin (2012)
Gelatin/CuS/PVA	Rhodamine B	Catalyst amount	0.1–0.35 g	k_{app} increases from 1.383 to 2.614 $*10^{-3}$ (min^{-1})	Al-Kahtani (2017)
		Dye concentration	25–100 ppm	Degradation percentage from 100% to 80%	
		pH	2–11	Efficiency of the degradation up to pH 10	

Continued

This book belongs to Central Library BADJI Mokhtar-ANNABA UNIVERSITY

Copyright Elsevier 2024

Table 6 Effect of parameter on photocatalyst activity—cont'd

Nanocomposite	Pollutant	Operating parameter		Result	Ref.
PANI/CdO	MB	Catalyst amount	0.01–0.04 mmol	Decolorization efficiency from 39% to 73%	Tadjarodi, Imani, and Kerdari (2013)
Polyaniline/ CoFe2O4	MO	Catalyst amount	1:0 to 1:2	Degradation percentage approximately 30%–95%	Khan et al. (2013)
		Dye concentration	10–40 μg/mL	Degradation percentage approximately from 95% to 50%	
PNA (poly(1-naphthylamine))/ bent (bentonite)	MB	Catalyst amount	1:0 to 1:0.5	Degradation efficiency increases from 35% to 73%	Riaz, Ashraf, and Ruhela (2015)

This book belongs to Central Library BADJI Mokhtar-ANNABA UNIVERSITY

Copyright Elsevier 2024

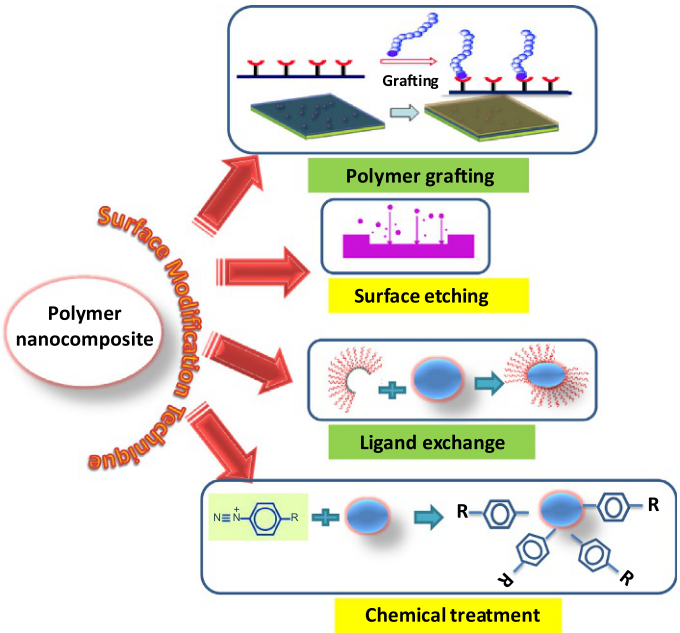

FIG. 6

Surface modification techniques of the nanocomposite.

(iii) Grafting of synthetic polymers

Grafting is one of the promising methods to modify the polymer. It imparts different functional group to the polymer. In grafting, the monomers are covalently bonded onto the polymer chain. The grafting of poly[(dimethylamino)ethyl methacrylate] (PDMAEMA) onto graphene oxide sheets was done using noncovalent modification followed by in situ surface-initiated ATRP (SI-ATRP) (Gao, Ye, Pei, Xia, & Zhou, 2013).

7 Future research

The chapter clearly reflects the increasing research interest on polymer nanocomposite and to make efficient and cost-effective polymer nanocomposites for wastewater treatment, a lot of work is still needed because there are still few drawbacks to be negotiated. Recent fabrication techniques of polymer nanocomposites have been studied by many researchers, but at commercial level, the large-scale production is required, which is a crucial issue due to the involvement of complex fabrication steps during synthesis. And also, several parameters must be focused on such as uniform dispersion and stability of NPs within the polymer matrix (the standards for analyzing the toxicity of nanomaterials are insufficient at present), surface charge, proper interaction between polymer and nanofiller since nanoparticles might release polymer chain flexibility, and the crystallization ability of the nanomaterials. Another important challenge is the proper designing of photoreactor and its scale-up. The basic

This book belongs to Central Library BADJI Mokhtar-ANNABA UNIVERSITY Copyright Elsevier 2024

requirement for proper designing provides an effective contact between pollutants, photocatalyst, and oxygen along with proper supply of solar radiation by providing a parabolic solar collector for maximum utilization of solar energy and thus reducing the electricity costs. Therefore, a detailed study is required to overcome the gap between laboratory scale and industrial applications. The other limitation includes photocatalyst degradation that is more effective on dyes and is susceptible to fluctuations in solar intensity, to ensure proper contact with the effluent and photons. For commercial viability and effective optimization, extensive research is required to use visible/solar active photocatalysts coupled with large-scale applications. Further investigation on the development of the host metal oxides and conducting polymers is required to design photochemically active hybrid materials for effective technological development.

8 Conclusion

Water is one of the most important abundant resources available on earth, but the growing world population and global climatic change have raised considerable attention around the world. The demand for fresh water is increasing dramatically. Traditional treatment technologies are not cost effective and may not efficiently remove pollutant present in low concentration but are harmful to the living organism. These technologies also suffer some limitation and thereby unable to meet stringent water quality standards. In addition, they also generate large quantity of sludge and hazardous wastes and are energy-intensive technique. Recently, the use of nanobased technique becomes very important in water remediation. Their unique size-dependent properties allow the development of materials that can provide lesser amount of space and reduced intermediate formation that are toxic in nature and show excellent performance compared with conventional treatment technology. Apart from many advantageous features, the agglomeration and instability problems due to high surface energy as a result of immobilized system are now being more preferred. The polymer nanocomposites have a great deal of future promise because of the efficient decontamination of metal ions, dye degradation from water, their regeneration, and cost effectiveness. They have gained significant interest due to their novel properties including large ratio of surface area to volume and good strength with high elastic modulus through the addition of nanomaterials in smaller amount into the polymer matrix. In this chapter, different functionalization techniques were also studied based on schemes like covalent and noncovalent bonding to improve the dispersion and stability of NPs in the polymer matrices. The kinetic characteristics of the photocatalytic degradation were also explained to study the factor influencing the photocatalytic activity. It was mentioned that pH and catalyst dosing have direct relationship with photocatalyst activity, while it shows an inverse relation with pollutant concentration. However, beyond optimal condition, further change in this parameter will not affect the degradation efficiency.

References

Ahluwalia, S. S., & Goyal, D. (2007). Microbial and plant derived biomass for removal of heavy metals from wastewater. *Bioresource Technology*, *98*, 2243–2257.

Ahmad, A., Razali, H., Mamat, M., Kassim, K., & Amin, K. A. M. (2018). Physiochemical properties of TiO_2 nanoparticle loaded APTES-functionalized MWCNTs composites and their photocatalytic activity with kinetic study. *Arabian Journal of Chemistry*. https://doi.org/10.1016/j.arabjc.2018.07.009.

This book belongs to Central Library BADJI Mokhtar-ANNABA UNIVERSITY Copyright Elsevier 2024

Alam, A., Wan, C., & McNally, T. (2017). Surface amination of carbon nanoparticles formodification of epoxy resins: Plasma-treatment vs wet-chemistry approach. *European Polymer Journal*, *87*, 422–448.

Al-Kahtani, A. A. (2017). Photocatalytic degradation of rhodamine B dye in wastewater using gelatin/CuS/PVA nanocomposites under solar light irradiation. *Journal of Biomaterials and Nanobiotechnology*, *8*, 66–82.

Ameen, S., Seo, H., Akhtar, M. S., & Shin, H. S. (2012). Novel graphene/polyaniline nanocomposites and its photocatalytic activity toward the degradation of rose Bengal dye. *Chemical Engineering Journal*, *210*, 220–228.

Arash, B., Park, H. S., & Rabczuk, T. (2015). Mechanical properties of carbon nanotube reinforced polymer nanocomposites: A coarse-grained model. *Composites Part B: Engineering*, *80*, 92–100.

Astruc, D., Lu, F., & Aranzaes, J. R. (2005). Nanoparticles as recyclable catalysts: The frontier between homogeneous and heterogeneous catalysis. *Angewandte Chemie International Edition*, *44*, 7852–7872.

Bahnemann, D., Bockelmann, D., & Goslich, R. (1991). Mechanistic studies of water detoxification in illuminated TiO_2 suspensions. *Solar Energy Materials*, *24*(1–4), 564–583.

Balasubramanian, G., Dionysiou, D. D., Suidan, M. T., Baudin, I., & Laıne, J.-M. (2004). Evaluating the activities of immobilized TiO_2 powder films for the photocatalytic degradation of organic contaminants in water. *Applied Catalysis B: Environmental*, *47*(2), 73–84.

Bao, N., Feng, X., Yang, Z., Shen, L., & Lu, X. (2004). Highly efficient liquid-phase photooxidation of an azo dye methyl Orange over novel nanostructured porous Titanate-based Fiber of self-supported radially aligned $H_2Ti_8O_{17}{\cdot}1.5H_2O$ nanorods. *Environmental Science & Technology*, *38*, 2729–2736.

Behnam, R., Morshed, M., Tavanai, H., & Ghiaci, M. (2013). Destructive adsorption of diazinon pesticide by activated carbon nanofibers containing Al_2O_3 and MgO nanoparticles. *Bulletin of the Environmental Contamination and Toxicology*, *91*, 475–480.

Benaissa, H., & Elouchdi, M. A. (2007). Removal of copper ions from aqueous solutions by dried sunflower leaves. *Chemical Engineering and Processing*, *46*, 614–622.

Bora, L. V., & Mewada, R. K. (2017). Visible/solar light active photocatalysts for organic effluent treatment: Fundamentals, mechanisms and parametric review. *Renewable and Sustainable Energy Reviews*, *76*, 1393–1421.

Brezova, V., Jankovikova, M., Soldan, M., Blazkova, A., Rehakova, M., Surina, I., et al. (1994). Photocatalytic degradation of p-toluenesulphonic acid in aqueous systems containing powdered and immobilized titanium dioxide. *Journal of Photochemistry and Photobiology A*, *83*, 69–75.

Bunluesin, S., Kruatrachue, M., Pokethitiyook, P., Upatham, S., & Lanza, G. R. (2007). Batch and continuous packed column studies of cadmium biosorption by Hydrilla verticillata biomass. *Journal of Bioscience and Bioengineering*, *103*, 509–513.

Byrne, J. A., Eggins, B. R., Brown, N. M. D., McKinney, B., & Rouse, M. (1998). Immobilisation of TiO_2 powder for the treatment of polluted water. *Applied Catalysis B: Environmental*, *17*, 25–36.

Cao, S., Jiao, Z., Chen, H., Jiang, F., & Wang, X. (2018). Carboxylic acid-functionalized cadmium sulfide/graphitic carbon nitride composite photocatalyst with well-combined interface for sulfamethazine degradation. *Journal of Photochemistry and Photobiology A: Chemistry*, *364*, 22–31.

Chen, F. P., Guan-Ping, J., Su, J., & Feng, X. (2016). Electrochemical preparation of uniform CuO/Cu_2O heterojunction on beta-cyclodextrin-modified carbon fibers. *Journal of Applied Electrochemistry*, *46*(3), 379–388.

Chen, Y., Stathatos, E., & Dionysiou, D. D. (2008). Microstructure characterization and photocatalytic activity of mesoporous TiO_2 films with ultrafine anatase nanocrystallites. *Surface and Coating Technology*, *202*, 1944–1950.

Cho, S., & Choi, W. (2001). Solid-phase photocatalytic degradation of PVC–TiO_2 polymer composites. *Journal of Photochemistry and Photobiology A*, *143*, 221–228.

Chu, P., Zhang, H., Zhao, J., Gao, F., Guo, Y., Dang, B., et al. (2017). On the volume resistivity of silica nanoparticle filled epoxy with different surface modifications. *Composites Part A Applied Science and Manufacturing*, *99*, 139–148.

Crin, G. (2006). Non-conventional low-cost adsorbents for dye removal: A review. *Bioresource Technology*, *97*, 1061–1085.

This book belongs to Central Library BADJI Mokhtar-ANNABA UNIVERSITY

Copyright Elsevier 2024

Das, R., Sarkar, S., Chakraborty, S., Choi, H., & Bhattacharjee, C. (2014). Remediation of antiseptic components in wastewater by photocatalysis using TiO_2 nanoparticles. *Industrial and Engineering Chemistry Research*, *53*, 3012–3020.

David, G., Drobota, M., & Simionescu, B. C. (2015). Preparation approach effect on polyurethane/montmorillonite nanocomposites characteristics. *High Performance Polymers*, *27*(2015), 555–562.

Dhananjeyan, M., Kiwi, J., Albers, P., & Enea, O. (2001). Photo-assisted immobilized *Fenton* degradation up to pH 8 of azo dye Orange II mediated by Fe^{3+}/*Nafion*/glass fibers. *Helvetica Chimca Acta*, *84*, 3433–3445.

El-Rehim, H. A. A., Hegazy, E.-S. A., & Diaa, D. A. (2012). Photo-catalytic degradation of Metanil yellow dye using TiO_2 immobilized into polyvinyl alcohol/acrylic acid microgels prepared by ionizing radiation. *Reactive and Functional Polymers*, *72*, 823–831.

Eskizeybek, V., Sari, F., Gülce, H., Gülce, A., & Avci, A. (2012). Preparation of the new polyaniline/ZnO nanocomposite and its photocatalytic activity for degradation of methylene blue and malachite green dyes under UV and natural sun lights irradiations. *Applied Catalysis B: Environmental*, *119–120*, 197–206.

Fabiyi, M. E., & Skelton, R. L. (2000). Skelton, photocatalytic mineralisation of methylene blue using buoyant TiO_2-coated polystyrene beads. *Journal of Photochemistry and Photobiology A*, *132*, 121–128.

Fostier, A. H., Pereira, M. S. S., Rath, S., & Guimaraes, J. R. (2008). Arsenic removal from water employing heterogeneous photocatalysis with TiO_2 immobilized in PET bottles. *Chemosphere*, *72*, 319–324.

Fu, Z., He, C., Li, H., Yan, C., Chen, L., Huang, J., et al. (2015). A novel hydrophilic hydrophobic magnetic interpenetrating polymer networks (IPNs) and its adsorption towards salicylic acid from aqueous solution. *Chemical Engineering Journal*, *279*, 250–257.

Gao, T., Ye, Q., Pei, X., Xia, Y., & Zhou, F. (2013). Grafting polymer brushes on grapheneoxide for controlling surface charge states and templated synthesis of metalnanoparticles. *Journal of Applied Polymer Science*, *127*, 3074–3083.

Girginova, P. I., Daniel-da-Silva, A. L., Lopes, C. B., Figueira, P., Otero, M., Amaral, V. S., et al. (2010). Silica coated magnetite particles for magnetic removal of Hg^{2+} from water. *Journal of Colloid and Interface Science*, *345*, 234–240.

Han, H., & Bai, R. (2010). Highly effective buoyant photocatalyst prepared with a novel layered-TiO_2 configuration on polypropylene fabric and the degradation performance for methyl orange dye under UV–vis and Vis lights. *Separation and Purification Technology*, *73*, 142–150.

Herrmann, J.-M. (1995). Heterogeneous photocatalysis: An emerging discipline involving multiphase systems. *Catalysis Today*, *24*(1–2), 157–164.

Hu, J., Zhao, X., & Wang, D. (2011). Removal of Pb (II) and cu (II) from aqueous solution using multiwalled carbon nanotubes/iron oxide magnetic composites. *Water Science and Technology*, *63*, 918–924.

Hua, M., Jiang, Y. N., Wu, B., Pan, B. C., Zhao, X., & Zhang, Q. X. (2013). Fabrication of a new hydrous Zr(IV) oxide-based nanocomposite for enhanced Pb(II) and cd(II) removal from waters. *ACS Applied Materials and Interfaces*, *5*, 12135–12142.

Hussain, F., Hojjati, M., Okamoto, M., & Gorga, R. E. (2006). Review article: Polymer-matrix nanocomposites, processing, manufacturing, and application: An overview. *Journal of Composite Materials*, *40*, 1511–1575.

Iketania, K., Sunb, R. D., Tokib, M., Hirotaa, K., & Yamaguchi, K. (2003). Sol–gel-derived TiO2/poly(dimethylsiloxane) hybrid films and their photocatalytic activities. *Journal of Physics and Chemistry of Solids*, *64*(3), 507–513.

Jawad, A. H., & Nawi, M. A. (2012). Fabrication, optimization and application of an immobilized layer-by-layer TiO_2/chitosan system for the removal of phenol and its intermediates under 45-W fluorescent lamp. *Reaction Kinetics, Mechanisms and Catalysis*, *106*, 49–65.

Ji, I. A., Park, M. J., Jung, J. Y., Choi, M. J., Lee, Y.-W., Lee, J.-H., et al. (2012). One-dimensional Core/Shell structured TiO_2/ZnO heterojunction for improved photoelectrochemical performance. *Bulletin of the Korean Chemical Society*, *33*, 2200–2206.

Karthikeyan, T., Rajgopal, S., & Miranda, L. R. (2005). Chromium (VI) adsorption from aqueous solution by Hevea brasiliensis sawdust activated carbon. *Journal of Hazardous Materials*, *124*, 192–199.

This book belongs to Central Library BADJI Mokhtar-ANNABA UNIVERSITY

Copyright Elsevier 2024

Kesselman, J. M., Lewis, N. S., & Hoffmann, M. R. (1997). Photoelectrochemical degradation of 4-chlorocatechol at TiO_2 electrodes: Comparison between sorption and photoreactivity. *Environmental Science and Technology*, *31*, 2298–2302.

Khan, J. A., Qasim, M., Singh, B. R., Singh, S., Shoeb, M., Khan, W., et al. (2013). Synthesis and characterization of structural, optical, thermal and dielectric properties of polyaniline/$CoFe_2O_4$ nanocomposites with special reference to photocatalytic activity. *Spectrochimica Acta Part A: Molecular and Biomolecular Spectroscopy*, *109*, 313–321.

Kumar, S., Sarita., Nehra, M., Dilbaghi, N., Tankeshwar, K., & Kim, K.-H. (2018). Recent advances and remaining challenges for polymeric nanocomposites in healthcare applications. *Progress in Polymer Science*, *80*, 1–38.

Kundu, S., Satpati, B., Mukherjee, M., Kar, T., & Pradhan, S. K. (2017). Hydrothermal synthesis of polyaniline intercalated vanadium oxide xerogel hybrid nanocomposites: Effective control of morphology and structural characterization. *The New Journal of Chemistry*, *41*, 3634–3645.

Kuo, C., Tseng, Y., Huang, C., & Li, Y. (2007). Carbon-containing nano-titania prepared by chemical vapor deposition and its visible-light-responsive photocatalytic activity. *Journal of Molecular Catalysis A: Chemical*, *270*(1–2), 93–100.

Kwon, C. H., Shin, H., Kim, J. H., Choi, W. S., & Yoon, K. H. (2004). Degradation of methylene blue via photocatalysis of titanium dioxide. *Materials Chemistry and Physics*, *86*, 78–82.

Langlet, M., Kim, A., Audier, M., & Herrmann, J. M. (2002). Sol-gel preparation of photocatalytic TiO_2 films on polymer substrates. *Journal of Sol-Gel Science and Technology*, *25*, 223–234.

Li, X. Z., & Li, F. B. (2001). Study of au/Au_3^+-TiO_2 Photocatalysts toward visible Photooxidation for water and wastewater treatment. *Environmental Science and Technology*, *35*, 2381–2387.

Li, Y., Sun, S., Ma, M., Ouyang, Y., & Yan, W. (2008). Kinetic study and model of the photocatalytic degradation of rhodamine B (RhB) by a TiO_2-coated activated carbon catalyst: Effects of initial RhB content, light intensity and TiO_2 content in the catalyst. *Chemical Engineering Journal*, *142*, 147–155.

Liu, S., & Chen, X. (2007). Preparation and characterization of a novel activated carbon-supported N-doped visible light response photocatalyst ($TiO_{2-x}N_y$/AC). *The. Journal of Chemical Technology & Biotechnology*, *82*, 453–459.

Liu, F.-F., Zhao, J., Wang, S., Du, P., & Xing, B. (2014). Effects of solution chemistry on adsorption of selected pharmaceuticals and personal care products (PPCPs) by graphenes and carbon nanotubes. *Environmental Science and Technology*, *48*, 13197–13206.

Magalhaes, F., Moura, F. C. C., & Lago, R. M. (2011). TiO_2/LDPE composites: A new floating photocatalyst for solar degradation of organic contaminants. *Desalination*, *276*(2011), 266–271.

Malato, S., Blanco, J., Campos, A., Ca'eres, J., Guillard, C., Herrmann, J. M., et al. (2003). Effect of operating parameters on the testing of new industrial titania catalysts at solar pilot plant scale. *Applied Catalysis B: Environmental*, *42*, 349–357.

Meneghetti, P., & Qutubuddin, S. (2006). Synthesis, thermal properties and applications of polymer–clay nanocomposites. *Thermochimica Acta*, *42*, 74–77.

Miranda-García, N., Maldonado, M. I., Coronado, J. M., & Malato, S. (2010). Degradation study of 15 emerging contaminants at low concentration by immobilized TiO2 in a pilot plant. *Catalysis Today*, *151*(1–2), 107–113.

Mounir, B., Pons, M. N., Zahraa, O., Yaacoubi, A., & Benhammou, A. (2007). Discoloration of a red cationic dye by supported TiO_2 photocatalysis. *Journal of Hazardous Materials*, *148*, 513–520.

Nagaoka, S., Hamasaki, Y., Ishihara, S., Nagata, M., Iio, K., Nagasawa, C., et al. (2002). Preparation of carbon/TiO_2 microsphere composites from cellulose/TiO_2 microsphere composites and their evaluation. *Journal of Molecular Catalysis A: Chemical*, *177*, 255–263.

Naskar, S., Pillay, S. A., & Chanda, M. (1998). Photocatalytic degradation of organic dyes in aqueous solution with TiO_2 nanoparticles immobilized on foamed polyethylene sheet. *Journal of Photochemistry and Photobiology A*, *113*, 257–264.

Nizard, H., Kosinova, M. L., Fainer, N. I., Rumyantsev, Y. M., Ayupov, B. M., & Shubin, Y. V. (2008). Deposition of titanium dioxide from TTIP by plasma enhanced and remote plasma enhanced chemical vapor deposition. *Surface and Coating Technology*, *202*, 4076–4085.

This book belongs to Central Library BADJI Mokhtar-ANNABA UNIVERSITY

Copyright Elsevier 2024

Normand, G., Mija, A., Pagnotta, S., Peuvrel-Disdier, E., & Vergnes, B. (2017). Preparation ofpolypropylene nanocomposites by melt-mixing: Comparison between three organoclays. *Journal of Applied Polymer Science*, *134*, 45053/1–8.

Parida, K. M., Dash, S. S., & Das, D. P. (2006). Physico-chemical characterization and photocatalytic activity of zinc oxide presented by various methods. *Journal of Colloid and Interface Science*, *298*, 787–793.

Rahmat, M., & Hubert, P. (2011). Carbon nanotube–polymer interactions in nanocomposites: A review. *Composites Science and Technology*, *72*, 72–84.

Rajasulochana, P., & Preethy, V. (2016). Comparison on efficiency of various techniques in treatment of waste and sewage water—A comprehensive review. *Resource-Efficient Technologies*, *2*, 175–184.

Rajendran, R., Varadharajan, K., Jayaraman, V., Singaram, B., & Jeyaram, J. (2018). Photocatalytic degradation of metronidazole and methylene blue by PVA-assisted Bi_2WO_6–CdS nanocomposite film under visible light irradiation. *Applied Nanoscience*, *8*, 61–78.

Ramesha, G. K., Kumara, A. V., Muralidhara, H. B., & Sampath, S. (2011). Graphene and graphene oxide as effective adsorbents towards anionic and cationic dyes. *Journal of Colloid and Interface Science*, *361*(1), 270–277.

Riaz, U., Ashraf, S. M., & Ruhela, A. (2015). Catalytic degradation of orange G under microwave irradiation with a novel nanohybrid catalyst. *Journal of Environmental Chemical Engineering*, *3*, 20–29.

Safarpour, M., Khataee, A., & Vatanpour, V. (2014). Preparation of a novel Polyvinylidene fluoride (PVDF) ultrafiltration membrane modified with reduced graphene oxide/titanium dioxide (TiO_2) nanocomposite with enhanced hydrophilicity and antifouling properties. *Industrial & Engineering Chemistry Research*, *53*, 13370–13382.

Sainsbury, T., Gnaniah, S., Spencer, S. J., Mignuzzi, S., Belsey, N. A., Paton, K. R., et al. (2017). Extreme mechanical reinforcement in graphene oxide based thin-film nanocomposites via covalently tailored nanofiller matrix compatibilization. *Carbon*, *114*, 367–376.

Salah, N. H., Bouhelassa, M., Bekkouche, S., & Boultif, A. (2004). Study of photocatalytic degradation of phenol. *Desalination*, *166*, 347–354.

Saleh, T. A. (2015). Mercury sorption by silica/carbon nanotubes and silica/activated carbon: A comparison study. *Journal of Water Supply: Research and Technology—AQUA*, *64*(8), 892.

Seery, M. K., George, R., Floris, P., & Pillai, S. C. (2007). Silver doped titanium dioxide nanomaterials for enhanced visible light photocatalysis. *Journal of Photochemistry and Photobiology A: Chemistry*, *189*(2–3), 258–263.

Shan, A. Y., Ghazi, T. I. M., & Rashid, S. A. (2010). Immobilisation of titanium dioxide onto supporting materials in heterogeneous photocatalysis: A review. *Applied Catalysis A: General*, *389*, 1–8.

Sharma, G., Kumar, A., Naushad, M., Pathania, D., & Sillanpää, M. (2016). Polyacrylamide@Zr(IV) vanadophosphate nanocomposite: Ion exchange properties, antibacterial activity, and photocatalytic behaviour. *Journal of Industrial and Engineering Chemistry*, *33*, 201–208.

Shawky, H. A., Chae, S.-R., Lin, S., & Wiesner, M. R. (2011). Synthesis and characterization of a carbon nanotube/polymer nanocomposite membrane for water treatment. *Desalination*, *272*, 46–50.

Shukla, S. K., Shukla, S. K., Govender, P. P., & Agorku, E. S. (2016). A resistive type humidity sensor based on crystalline tin oxide nanoparticles encapsulated in polyaniline matrix. *Microchimica Acta*, *183*, 573–580.

Shukla, P. R., Wang, S., Ang, H. M., & Tade, M. O. (2010). Photocatalytic oxidation of phenolic compounds using zinc oxide and sulphate radicals under artificial solar light. *Separation and Purification Technology*, *70*, 338–344.

Singh, K., Singh, A., Gupta, S., & Rai, P. (2012). Modeling and optimization of reductive degradation of chloramphenicol in aqueous solution by zero-valent bimetallic nanoparticles. *Environmental Science and Pollution Research*, *19*, 2063–2078.

Sopyan, I., Watanabe, M., Murasawa, S., Hashimoto, K., & Fujishima, A. (1996). A film-type photocatalyst incorporating highly active TiO_2 powder and fluororesin binder: Photocatalytic activity and long-term stability. *Journal of Electroanalytical Chemistry*, *415*, 183–186.

This book belongs to Central Library BADJI Mokhtar-ANNABA UNIVERSITY

Copyright Elsevier 2024

Sriwong, C., Wongnawa, S., & Patarapaiboolchai, O. (2008). Photocatalytic activity of rubber sheet impregnated with TiO_2 particles and its recyclability. *Catalysis Communication*, *9*, 213–218.

Tadjarodi, A., Imani, M., & Kerdari, H. (2013). Experimental design to optimize the synthesis of CdO cauliflower-like nanostructure and high performance in photodegradation of toxic azo dyes. *Materials Research Bulletin*, *48*, 935–942.

Tennakone, K., & Kottegoda, I. R. M. (1996). Photocatalytic mineralization of paraquat dissolved in water by TiO_2 supported on polythene and polypropylene films. *Journal of Photochemistry & Photobiology*, *93*(1), 79–81.

Tennakone, K., Tilakaratne, C. T. K., & Kottegoda, I. R. M. (1997). Photomineralization of carbofuran by TiO_2-supported catalyst. *Water Research*, *31*, 1909–1912.

Tofighy, M. A., & Mohammadi, T. (2012). Nitrate removal from water using functionalized carbon nanotube sheets. *Chemical Engineering Research and Design*, *90*, 1815–1822.

Tsao, J. (2006). *Solar FAQs. 2006*. [online] Available: http://www.sandia.gov/~jytsao/Solar%20FAQs.pdf (Accessed 05 January 2015).

Uchida, H., Katoh, S., & Watanabe, M. (1998). Photocatalytic degradation of trichlorobenzene using immobilized TiO_2 films containing poly(tetrafluoroethylene) and platinum metal catalyst. *Electrochimica Acta*, *43*(14–15), 2111–2116.

Upadhyay, R. K., Soin, N., & Roy, S. S. (2014). Role of graphene/metal oxide composites as photocatalysts, adsorbents and disinfectants in water treatment: A review. *RSC Advances*, *4*(8), 3823–3851.

Velasquez, J., Valencia, S., Rios, L., Restrepo, G., & Marin, J. (2012). Characterization and photocatalytic evaluation of polypropylene and polyethylene pellets coated with P25 TiO_2 using the controlled-temperature embedding method. *Chemical Engineering Journal*, *203*, 398–405.

Vijayaraghavan, K., Ahmad, D., & Abdul Aziz, M. E. (2007). Aerobic treatment of palm oil mill effluent. *Journal of Environmental Management*, *82*, 24–31.

Wang, J., & Chen, C. (2009). Biosorbents for heavy metals removal and their future. *Biotechnoly Advances*, *27*, 195–226.

Wang, X., Chen, C., Liu, H., & Ma, J. (2008). Preparation and characterization of PAA/PVDF membrane-immobilized Pd/Fe nanoparticles for dechlorination of trichloroacetic acid. *Water Research*, *42*(18), 4656–4664.

Wang, C., Luo, H., Zhang, Z., Wu, Y., Zhang, J., & Chen, S. (2014). Removal of as(III) and as (V) from aqueous solutions using nanoscale zero valent iron-reduced graphite oxide modified composites. *Journal of Hazardous Materials*, *268*, 124–131.

Wang, F., Min, S., Han, Y., & Feng, L. (2010). Visible-light-induced photocatalytic degradation of methylene blue with polyaniline-sensitized TiO_2 composite photocatalysts. *Superlattices and Microstructures*, *48*, 170–180.

Wang, Q., Qian, H. J., Yang, Y. P., Zhang, Z., Naman, C., & Xu, X. H. (2010). Reduction of hexavalent chromium by carboxymethyl cellulose-stabilized zero-valent iron nanoparticles. *Journal of Contaminant Hydrology*, *114*, 35–42.

Wang, W., Zhou, M., & Jin, Z. (2010). Reactivity characteristics of poly(methyl methacrylate) coated nanoscale iron particles for trichloroethylene remediation. *Journal of Hazardous Materials*, *173*(1–3), 724–730.

Wu, K., Liu, T., Ma, C., Chang, B., Chen, R., & Wang, X. C. (2014). The role of Mn oxide doping in phosphate removal by Al-based bimetal oxides: Adsorption behaviors and mechanisms. *Environmental Science and Pollution Research*, *21*, 620–630.

Wu, K., Liu, T., Xue, W., & Wang, X. C. (2012). Arsenic(III) oxidation/adsorption behaviours on a new bimetal adsorbent of Mn-oxide-doped Al oxide. *Chemical Engineering Journal*, *192*, 343–349.

Wu, L. F., & Ritchie, S. M. C. (2006). Removal of trichloroethylene from water by cellulose acetate supported bimetallic Ni/Fe nanoparticles. *Chemosphere*, *63*(2), 285–292.

Xiong, Z. G., Zhang, L. L., Ma, J. Z., & Zhao, X. S. (2010). Photocatalytic degradation of dyes over graphene-gold nanocomposites under visible light irradiation. *Chemical Communications*, *46*, 6099–6101.

Xu, F., Chen, J., Guo, L., Lei, S., & Ni, Y. (2012). In situ electrochemically etching-derived ZnO nanotube arrays for highly efficient and facilely recyclable photocatalyst. *Applied Surface Science*, *258*, 8160–8165.

This book belongs to Central Library BADJI Mokhtar-ANNABA UNIVERSITY

Copyright Elsevier 2024

Xu, Y. M., & Langford, C. H. (2000). Variation of Langmuir adsorption constant determined for TiO_2-photocatalyzed degradation of acetophenone under different light intensity. *Journal of Photochemistry and Photobiology, A: Chemistry*, *133*, 67–71.

Xu, X., Wang, Q., & Choi, H. C. (2010). Encapsulation of iron nanoparticles with PVP nanofibrous membranes to maintain their catalytic activity. *Journal of Membrane Science*, *348*, 231–237.

Yahya, N., Aziz, F., Jamaludin, N. A., Mutalib, M. A., Ismail, A. F., Salleh, W. N. W., et al. (2018). A review of integrated photocatalyst adsorbents for wastewater treatment. *Journal of Environmental Chemical Engineering*, *6*, 7411–7425.

Yang, X. H., Fu, H. T., Wong, K., Jiang, X. C., & Yu, A. B. (2013). Hybrid ag@ TiO_2 core–shell nanostructures with highly enhanced photocatalytic performance. *Nanotechnology*, *24*, 415601–415610.

Yang, J. H., Han, Y. S., & Choy, J. H. (2006). TiO_2 thin-films on polymer substrates and their photocatalytic activity. *Thin Solid Films*, *495*, 266–271.

Yew, S. P., Tang, H. Y., & Sudesh, K. (2006). Photocatalytic activity and biodegradation of polyhydroxybutyrate films containing titanium dioxide. *Polymer Degradation and Stability*, *91*(8), 1800–1807.

Yu, C., Wu, R., Fu, Y., Dong, X., & Ma, H. (2012). Preparation of polyaniline supported TiO_2 photocatalyst and its photocatalytic property. *Advances in Materials Research*, 356–*360*, 524–528.

Yu, Y., Yu, J. C., Chan, C., Che, Y., Zhao, J., Ding, L., et al. (2005). Enhancement of adsorption and photocatalytic activity of TiO_2 by using carbon nanotubes for the treatment of azo dye. *Applied Catalysis B: Environmental*, *61*, 1–11.

Yuranova, T., Enea, O., Mielczarski, E., Mielczarski, J., Albers, P., & Kiwi, J. (2004). Fenton immobilized photo-assisted catalysis through a Fe/C structured fabric. *Applied Catalysis B: Environmental*, *49*, 39 50.

Yuranova, T., Mosteo, R., Bandara, J., Laub, D., & Kiwi, J. (2006). Self-cleaning cotton textiles surfaces modified by photoactive SiO_2/TiO_2 coating. *Journal of Molecular Catalysis A*, *244*, 160–167.

Zeng, G., Liu, M., Heng, C., Huang, Q., Mao, L., Huang, H., et al. (2017). Surface polyPEGylation of Eu^{3+} doped luminescent hydroxyapatite nanorods through the combination of ligand exchange and metal free surface initiated atom transfer radical polymerization. *Applied Surface Science*, *399*, 499–505.

Zhang, F., Ding, T., Zhang, Y., Yang, Z., & Xue, H. (2017). Polyaniline modified SnS_2 as a novel efficient visible-light-driven photocatalyst. *Materials Letters*, *192*, 149–152.

Zhang, H., James, J., Zhao, M., Yao, Y., Zhang, Y., Zhang, B., et al. (2017). Improving hydrostability of ZIF-8 membranes via surface ligand exchange. *Journal of Membrane Science*, *532*, 1–8.

Zhao, C., Xu, X., Chen, J., Wang, G., & Yang, F. (2014). Highly effective antifouling performance of PVDF/graphene oxide composite membrane in membrane bioreactor (MBR) system. *Desalination*, *340*, 59–66.

Zhong, L. S., Hu, J. S., Cao, A. M., Liu, Q., Song, W. G., & Wan, L. J. (2007). 3D flowerlike ceria micro/nanocomposite structure and its application for water treatment and CO removal. *Chemistry of Materials*, *19*(2007), 1648–1655.

Zhu, H., Jiang, R., Xiao, L., Chang, Y., Guan, Y., Li, X., et al. (2009). Photocatalytic decolorization and degradation of Congo red on innovative crosslinked chitosan/nano-CdS composite catalyst under visible light irradiation. *Journal of Hazardous Materials*, *169*(1–3), 933–940.

Zong, E. M., Wei, D., Wan, H. Q., Zheng, S. R., Xu, Z. Y., & Zhu, D. Q. (2013). Adsorptive removal of phosphate ions from aqueous solution using zirconia-functionalized graphite oxide. *Chemical Engineering Journal*, *221*, 193–203.

Further reading

Li, C., Bai, H., & Shi, G. (2009). Conducting polymer nanomaterials: Electrosynthesis and applications. *Chemical Society Reviews*, *38*, 2397–2409.

Wu, S. J., Liou, T. H., & Mi, F. L. (2009). Synthesis of zero-valent copper-chitosan nanocomposites and their application for treatment of hexavalent chromium. *Bioresource Technology*, *100*(19), 4348–4353.

This book belongs to Central Library BADJI Mokhtar-ANNABA UNIVERSITY

Copyright Elsevier 2024

CHAPTER

Solar light-induced photocatalytic degradation of pharmaceuticals in wastewater treatment

4

Snehamol Mathew[a,b], Priyanka Ganguly[a,b], Vignesh Kumaravel[a,b], John Bartlett[a,b], Suresh C. Pillai[a,b]

Nanotechnology and Bio-Engineering Research Group, Department of Environmental Science, School of Science, Institute of Technology Sligo, Sligo, Ireland[a] Centre for Precision Engineering, Materials and Manufacturing Research (PEM), Institute of Technology Sligo, Sligo, Ireland[b]

1 Introduction

Declining water quality for a rapidly growing population has become a global issue. An emerging concern in this area is the impact of the overuse and discharge of pharmaceuticals and personal care products (PPCP), such as birth control pills, painkillers, and antibiotics, on aquatic ecosystems and human health (Jones, Voulvoulis, & Lester, 2005). Even at trace levels, these materials can have significant biological effects. Widespread use in human populations means that increasing amounts are reaching the environment through wastewater treatment discharges, and the academic literature shows increasing concern among scientists on the issue (WHO, 2001; Rizzo et al., 2013).

Antibiotics and hormones are also reaching the environment from a variety of food production sectors, including aquaculture, cattle farming, pig rearing, and the poultry sector (Kemper, 2008; Landers, Cohen, Wittum, & Larson, 2012). The potential exists for bioaccumulation in higher levels of the food chain (Chapman & Organization, 1996).

Photocatalysis is an important technology that is considered to have high potential as an effective, low-cost, green, and sustainable technology to remove pharmaceutical residues from effluents (Comninellis et al., 2008). The chapter aims to provide a comprehensive overview with a variety of semiconductor catalysts for the degradation of pharmaceutical effluents using solar light irradiation.

2 Pharmaceutical waste in water resources

Pharmaceutical products are mainly categorized based on their chemical structure, origin, or by their therapeutic use. Alkaloids are pharmaceuticals usually derived from plants, such as cocaine, quinine, and morphine. Other common pharmaceuticals are antibiotics, lipid regulators, nonsteroidal antiinflammatories, antidepressants, anticonvulsants, antineoplastics, and beta blockers (Renita, Kumar, Srinivas, Priyadharshini, & Karthika, 2017). These materials can be found in concentrations from

Nano-Materials as Photocatalysts for Degradation of Environmental Pollutants. https://doi.org/10.1016/B978-0-12-818598-8.00004-3
© 2020 Elsevier Inc. All rights reserved.

This book belongs to Central Library BADJI Mokhtar-ANNABA UNIVERSITY

Copyright Elsevier 2024

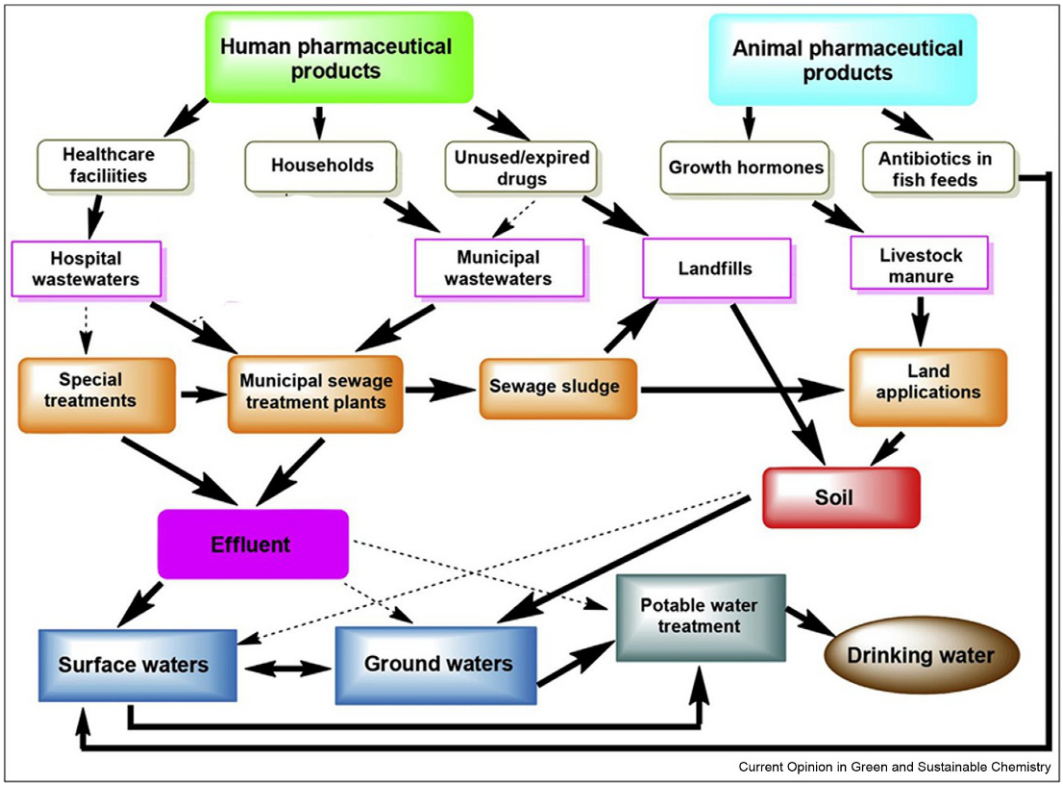

FIG. 1

Pathways of human and animal pharmaceutical products to contaminate water sources (Serpone et al., 2017).

nanograms per liter ($ng\,L^{-1}$) to micrograms per liter ($\mu g\,L^{-1}$) in the aquatic environment (Serpone, Artemev, Ryabchuk, Emeline, & Horikoshi, 2017).

The release of pharmaceutical residues to the aquatic environment happens via different routes. Fig. 1 illustrates various possible pathways. Even though pharmaceuticals are present in low concentrations, when compared with other organic pollutants in the environment, potency and potential bioaccumulation are factors that lead to a concern that organisms, including humans, may be at high risk from these discharges.

3 Health effects of pharmaceutical waste

Different categories of pharmaceutical materials can have different effects when exposure occurs from environmental sources. Antibiotics, for example, are a very important group of pharmaceuticals that make a considerable contribution to a wide variety of disease treatments (Dias, Urban, & Roessner, 2012; Dias et al., 2012; Fair & Tor, 2014; Lara, Ayala-Núnez, Turrent, & Padilla,

This book belongs to Central Library BADJI Mokhtar-ANNABA UNIVERSITY Copyright Elsevier 2024

2010; Mathur & Hoskins, 2017; O'Shea & Moser, 2008). They are consumed to mitigate any risk or infection associated with bacterial strains (Ventola, 2015). They are an effective potential cure against several infectious diseases in humans and animals (Perumal Samy & Gopalakrishnakone, 2010). The use of antibiotics has resulted in a significant decline in mortality rates among humans and animals (Hawkey, 2008).

However, their action is concentration dependent. At high concentration, antibiotics are extremely lethal to microbial cells. However, prolonged exposure to low concentrations can lead to the development of genetic and phenotypic variability or antibiotic resistance (Whitham et al., 2006). Antibiotics are partially metabolized inside the human body, and several active fragments are disseminated via urine and feces (Hsu et al., 2014). Thus wastewater from municipal sewage, as well as agricultural usage, are the common routes of antibiotic discharge to the environment (Strauch, 2011). The rate of contribution from each source varies from country to country. Asian countries, particularly developing economies, such as India and China, have seen an increase in pharmaceutical companies, while the European countries have seen a rise in the use of antibiotics in animal husbandry and aquaculture (Huttner et al., 2013). Studies have shown that the discharge of antibiotics to the environment has had a number of effects. Alterations to the pH, adsorption capacity, temperature, and texture of soils are some of the environmental impacts found (Sassman & Lee, 2005).

The introduction of antibiotics to soil affects the balance of microbial species in the overall microbial ecosystem. Studies have shown the loss of particular bacterial groups, such as those controlling the nitrogen fixation process (Kümmerer, 2009). Stress responses shown have included significant growth in some bacteria (Davies & Davies, 2010). Others have led to alteration of target sites with microbial cells, production of inactivating enzymes, changes to cellular permeability, and changes to transportation systems such as the efflux pumps (Wexler, 2007).

The emergence of antibiotic resistance has been the subject of many studies (Laxminarayan et al., 2013). It has been identified as one of the major threats to global health and food security (Berendonk et al., 2015). The rise in the cases of antibiotic resistances impacts the overall economy of a country (Malizos & Kirketerp-Møller, 2016; Ventola, 2015). It increases the duration of medical care, which increases the average medical cost of the population (Aslam et al., 2018). It also jeopardizes other critical treatments, such as organ transplant and chemotherapy (Lundholm, Hyltander, & Sandström, 1992).

In response to this the WHO has strategized a global action plan on antimicrobial resistance. It requires countries to identify the sources of antibiotic release to the environment and to develop standards to reduce the levels of discharge (Tiong, Loo, & Mai, 2016). The European Commission and many North American countries have also taken similar actions (Morgan, Okeke, Laxminarayan, Perencevich, & Weisenberg, 2011). However, conventional wastewater treatment plants are not designed for the removal of pharmaceutical products (Stackelberg et al., 2004). New technologies are being introduced in new treatment plants such as advanced oxidation processes (AOPs) and microfiltration utilizing membranes (Pérez-González, Urtiaga, Ibáñez, & Ortiz, 2012). These can lead to a significant increase in the cost of treatment.

Another category of pharmaceuticals of concern is endocrine disruptive compounds. These compounds can cause significant health threat by interfering with metabolism, and hormone biosynthesis can lead to congenital disabilities or developmental disorders in infants. They have also been shown to cause cancer (Diamanti-Kandarakis et al., 2009). Accumulation of such materials could interfere with the functioning of organs. Most of the pharmaceuticals can act as endocrine disruptive compounds (EDC) (Benotti et al., 2008).

This book belongs to Central Library BADJI Mokhtar-ANNABA UNIVERSITY Copyright Elsevier 2024

4 Solar active photocatalytic degradation of pharmaceuticals

4.1 Photocatalytic degradation mechanism

The development of photocatalysis technology can be traced back to the 1960s when the landmark work was done by Honda and Fujishima (Ganguly, Byrne, Breen, & Pillai, 2018). Initial studies investigated the use of TiO_2 for photoelectrochemical applications, and there are now many applications in energy and environmental remediation (Fujishima & Honda, 1972). In this chapter the use of photocatalysis for the degradation of pharmaceutical effluent is discussed. The role of a semiconductor photocatalyst is to provide active sites on the surface of a material for reduction and oxidation processes that result from irradiation by solar light (Mathew et al., 2018). When the energy of the incident photon matches with the bandgap of the semiconductor material, it results in the excitation of the electron-hole pairs (Ganguly et al., 2019). In general the valence band displays an oxidative potential of +1.0 eV to +3.5 eV versus NHE. Similarly the conduction band shows a reductive potential of +0.5 eV to −1.5 eV versus NHE (Tong et al., 2012). Thus the irradiated solar energy is utilized to generate charge carriers. These charge carriers have a minute timescale, of around few femtoseconds, to participate with the water and oxygen in the atmosphere to create potential reactive oxygen species (transform into chemical energy) (Panneri, Thomas, et al., 2017). A significant amount of the input energy is transferred back in the form of light and thermal energy, as a large proportion of the charge carriers (electron-hole pairs) recombine (Panneri et al., 2016) (Fig. 2). Several structural and chemical modifications have been introduced in the semiconductor surfaces to date to delay the recombination process (Panneri, Ganguly, et al., 2018). Defect formation, the introduction of cocatalysts, and the formation of different types of heterojunctions are some of the major routes investigated to enhance the photocatalytic efficiency (Mathew et al., 2018). These processes induce an internal electric field that causes the migration of the charge carriers from the conduction and the valence band of the semiconductor surface.

Notwithstanding the improved technologies and photocatalytic results observed, there still exists significant scope for growth and improvement. Firstly, in the case of photocatalytic efficiency, the major challenge is scale up to commercial scale. Secondly the stability and the cost of these semiconductor

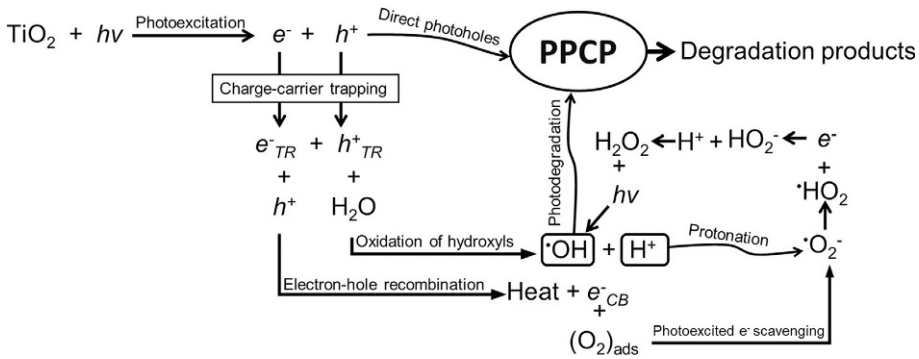

FIG. 2

Schematic illustration of photocatalytic reduction and oxidation mechanism of pharmaceutical and personal care products (Awfa, Ateia, Fujii, Johnson, & Yoshimura, 2018).

This book belongs to Central Library BADJI Mokhtar-ANNABA UNIVERSITY
Copyright Elsevier 2024

materials are significant concerns. Thirdly the toxicity profile and their impact on the ecosystem must be addressed. Fourthly, visible light absorption must be improved. Finally a better understanding of the surface-interface chemistry of the semiconductor surface, which is a key factor contributing to the transfer of electrons and overpotential of the redox reactions, is required (Tong et al., 2012). Thus engineering eco-friendly, cost-effective semiconductor systems with significant photocatalytic efficiency that illustrate thermal, structural, and chemical stability is a major target (Awfa et al., 2018).

4.2 Titania-based materials

TiO_2 is an ideal catalyst for photocatalytic degradation of waste materials because of its high photostability, nontoxicity, low cost, and photoreactivity. There are three polymorphs for TiO_2, namely, anatase, rutile, and brookite. Among these polymorphs, anatase exhibits the highest photocatalytic activity, most extended lifetime of photoexcited electron, and fastest migration of photoelectron (Malato, Fernández-Ibáñez, Maldonado, Blanco, & Gernjak, 2009). TiO_2 even shows catalytic activity under mild conditions with mild oxidants (Malato et al., 2009). However, in the presence of a high concentration of contamination, it shows low photoefficiencies and kinetics, which could lead to catalyst inactivation and unpredictable mechanisms. This needs to be addressed. Limitation of photocatalytic activity of unmodified TiO_2 within the UV range of spectra ($\lambda < 380$ nm) is another factor inhibiting its use in real-life applications. Reactor setup with artificial lamps for use in industrial applications could increase the cost of production at a large scale. Employing visible light radiation for catalytic degradation of pharmaceutical waste will be a sustainable solution for this. Modification of TiO_2 by doping noble metals or nonmetals or coupling with other semiconductor materials has been used in the activation of titania in the visible light region.

Doping of titania with various metals, nonmetals, and carbonaceous materials has been extensively studied previously. Belet et al. studied a comparison analysis on seven photocatalysts with TiO_2, ZnO, TiO_2+ P25, TiO_2+Ag, TiO_2+ MnO_2, TiO_2+Zn+, and TiO_2 (aqua) for degradation of 15 different pharmaceutical products. Ag-doped TiO_2 and P25-doped TiO_2 showed better performance in pharmaceutical waste degradation (Belet et al., 2019). Similarly, Rabhi et al. reported 100% efficiency demonstrated by 1 wt% Ag-TiO_2 in the degradation of amlodipine besylate within 100 min of irradiation. This efficiency is due to the introduction of more active sites by Ag doping and the presence of polymorphism of TiO_2 crystals with 47% of anatase phase and 53% of rutile phase. Several studies of N-doped TiO_2 for the removal of antibiotic ciprofloxacin (CIP) have been reported. The first report of CIP degradation with N-doped TiO_2 was by Shetty, Chavan, Kulkarni, Kulkarni, and Kamble (2017). Ninety-five percent degradation of antibiotic within 90 min of visible light irradiation at neutral pH was attained by N-doped catalyst. Xing et al. synthesized and immobilized N-doped TiO_2 on glass spheres. The removal efficiency of CIP by these materials was about 90% in 90 min under visible light irradiation. The recyclability of materials up to five cycles was also reported (Xing, Du, Zhuang, & Wang, 2018). Easy removal of these catalysts from the reactor and recyclability gives a new impetus to the use of these materials at the industrial application level. Tridoped anatase-brookite titania heterojunction catalyst was reported for complete degradation of ibuprofen under visible light irradiation. C-, N-, and S-tridoped mesoporous TiO_2 exhibited 40 times more reaction rate when compared with pristine TiO_2 (Khedr et al., 2017).

Namshah and Mohamed (2018) reported visible light photocatalytic degradation (100%) of paracetamol, using 3 wt% WO_3-TiO_2 as a catalyst, with 30 min of irradiation time. The coupling of tungsten

This book belongs to Central Library BADJI Mokhtar-ANNABA UNIVERSITY Copyright Elsevier 2024

trioxide with titanium dioxide increased the surface area of the materials, due to the insertion of tungsten ion into titania lattice. These enhanced surface area helped in increasing the number of active sites on the surface, which could enhance the paracetamol degradation. The coupling with WO_3 also enhanced the photogenerated charge separation in TiO_2.

To enhance the photocatalytic activity of titania, N-doped TiO_2 was coupled with graphene to form a 2D heterocatalyst. Zhao et al. studied the photocatalytic degradation of multiple antibiotics (norfloxacin, sulfamethazine, oxytetracycline, and chlortetracycline) using N-TiO_2/graphene. Inhibiting the recombination of generated electron-hole pairs is an efficient way to enhance the catalytic property of TiO_2. Graphene can work as an efficient "electron pump" for the photodegradation, which can promote the separation of carriers. (Zhao, Duan, Ji, Ma, & Yang, 2018). During UV light illumination the electrons in the VB of TiO_2 get excited to the CB, to generate electron-hole pairs. The holes are transferred from VB of exited TiO_2 to N-TiO_2, due to the comparable energy difference between the VB of TiO_2 and N-TiO_2. These holes react with hydroxyl groups (OH^-) to form the OH• radicals. These OH radicals are responsible for the decomposition of antibiotics during the photocatalytic process. The photogenerated electrons migrate to the graphene surface, where electrons are scavenged by molecular oxygen O_2 to yield $O_2^{\bullet-}$ superoxide radicals. This helps in decreasing the recombination of the electron-hole pairs, thus enhancing the photocatalytic efficiency of the material.

MoS_2 is a graphene-like two-dimensional (2D) transition metal dichalcogenide. MoS_2/TiO_2 composite for photocatalytic degradation for carbamazepine, an antiepilepsy drug, was reported by Cravanzola et al. The MoS_2/TiO_2 was obtained by thermal treatment under H_2S atmosphere. The photocatalytic activity was compared with P-25. Even though the surface area of P25 was larger than the composite, the synthesized MoS_2/TiO_2 showed enhanced catalytic activity. Small and thin MoS_2 slabs dispersed on the surface of TiO_2 nanoparticles; here the MoS_2 is acting as a photosensitizer. By using this composite in the mineralization of carbamazepine, the formation of a hazardous by-product (acridine derivatives), which is usually formed with other catalysts, was prevented (Cravanzola, Sarro, Cesano, Calza, & Scarano, 2018).

4.3 Graphene-based materials

Reduced graphene oxide (rGO) is a two-dimensional material that is widely explored due to its large surface area, excellent electrical and chemical stability, and greater carrier mobility. Dong et al. reported the visible light degradation of metronidazole by $ZnSnO_3$ hollow nanospheres/reduced graphene oxide (rGO). The composite $ZnSnO_3$/rGO showed better activity than other prepared samples, $ZnSnO_3$ hollow nanospheres, $ZnSnO_3$/rGO nanocomposites, pure rGO, and $ZnSnO_3$-rGO. The surface areas of the later three samples were kept to eliminate the enhancement in the photocatalytic activity due to the surface area of rGO. ZnSnO3/rGO showed 72.5% of the removal of metronidazole under visible light illumination. The addition of rGO resulted in enhanced absorption efficiency and visible light activity absorption of catalyst (Dong et al., 2014).

Lin et al. reported the removal of pharmaceutical wastes like carbamazepine, ibuprofen, and sulfamethoxazole using immobilized TiO_2-rGO on side-glowing optical fibers (SOFs). The coupling of TiO_2 with rGO helped in reducing the bandgap energy, thus increasing the visible light absorption efficiency. SOF is a fiber with quartz glass as inner core and silicone rubber as the coating. Light irradiation distribution of these fibers is uniform along the fiber length. It can act as catalyst support and simultaneously provide light illumination in the reactor (Lin, Wang, & Xu, 2017). As previously

This book belongs to Central Library BADJI Mokhtar-ANNABA UNIVERSITY Copyright Elsevier 2024

reported the photocatalytic activity increased by increasing rGO concentration from 0% to 2.7%. At 2.7%, rGO displayed carbamazepine (54%), ibuprofen (81%), and sulfamethoxazole (92%) degradation after 180 min of high-pressure UV irradiation. Similarly, Shinde et al. also reported TiO_2-rGO composite with Pt metals for the enhanced photocatalytic degradation and mineralization of pharmaceutical pollutant β-blocker propranolol under solar irradiation. Ternary composite in the ratio of 1Pt:10 rGO showed the enhanced photocatalytic degradation (94%) of propranolol using simulated solar light. In these reactions, rGO acts as an electron sink, and it provides more surface area to the catalyst to adsorb the pollutant to the catalyst surface. Pt nanoparticles help in reducing the recombination of photogenerated species and increasing the absorption in the visible spectra (Shinde, Wadhai, Ponkshe, Kapoor, & Thakur, 2018).

rGO/$AgInS_8$ composite was prepared for visible light active degradation of nitrophenol (2-nitrophenol and 4-nitrophenol) by Che et al. (2018). One percent rGO/AIS composite exhibited higher degradation efficiency than their parent compound. The coupling of $AgIn_5S_8$ (AIS) with rGO promoted the flow of photogenerated electrons from AIS to rGO. The catalyst showed 91% of 4NP and 93.2% of 2NP removal efficiency within 120 min of visible light irradiation. These could be attributed to the phenomenon of rGO acting as an electron acceptor, which helps in inhibiting the electron-hole recombination by enhancing the photogenerated charge separation. Meanwhile, by increasing the concentration of rGO, they found that the photocatalytic activity declined, due to the suppression of visible light absorption of AIS by excess rGO covering on its surface (Che et al., 2018).

4.4 Metal-organic frameworks (MOFs)

Metal-organic frameworks (MOFs) are the new class of hybrid materials with inorganic and organic components. The versatile physicochemical properties of these compounds make them superior candidates for the photocatalytic treatment of pharmaceutical waste, relative to other materials. Easily modifiable structure and high porosity help to act as a filter for organic pollutants by trapping the organic molecule in the pores. Crystalline structure, chemical/physical stability, and tunable bandgap help in the degradation of adsorbed contaminants in the pores in the presence of sunlight. MOFs with a loaded catalyst are a new area where a lot of studies are being undertaken in relation to wastewater treatment. The high surface area of these networks helps in absorbing the hazardous molecules onto its surface. This peculiarity is widely exploited, especially in the degradation of pharmaceutical waste, where most of them are not biodegradable.

Liang et al. reported an initial study, using metal-doped MOFs for the removal of pharmaceutical waste. Pd NPs @ MIL-100(Fe) nanocomposite was developed for the photocatalytic degradation of pharmaceutical contaminants like theophylline, ibuprofen, and bisphenol A under visible light irradiation (Liang et al., 2015). One weight percent Pd @ MIL-100(Fe) showed enhanced degradation efficiency over bare MIL-100(Fe). Pd NPs help in minimizing the recombination of photogenerated electron-hole pairs, thus leading to an increase in the photocatalytic activity. The efficiency in removing contaminants remained constant, even after an increase in the loading concentration of Pd NPs. The different contaminants behaved differently with the catalyst at varying pHs. By decreasing pH from 6 to 2, the adsorption of theophylline to the MOFs and degradation efficiency increased significantly from 65% to 100%. For ibuprofen and bisphenol A, it was observed that degradation efficiency was enhanced by increasing the pH of the system.

This book belongs to Central Library BADJI Mokhtar-ANNABA UNIVERSITY Copyright Elsevier 2024

Tetracycline removal by a simulated solar source using a novel composite, Co-doped UiO-66 synthesized by the solvothermal method, was reported by Cao et al. (2018). The CoUiO-66 with Zr/Co molar ratio of 1:1 displayed the highest photocatalytic activity (94%) and adsorption capacity. This adsorption can be ascribed due to the π–π and electrostatic interaction between the tetracycline molecule and catalyst. The doping of Co aided in the enhancement of visible light absorption and thus in an increase in photocatalytic degradation efficiency. TC was degraded into CO_2 and H_2O.

Wang et al. have done a comparative study for tetracycline degradation using Fe-based MOFs (Fe-MIL-101, Fe-MIL-100, and Fe-MIL-53). Fe-MIL 101 showed the highest degradation efficiency, with 96.6% removal, and also the highest visible light absorption efficiency. The concentration of TC stayed constant at 50 mg/L, and the efficiency was decreased relative to the increase in the TC concentration. Fe-based MOFs show visible light activity due to the presence of Fe—O clusters presents in the ligand. The photogenerated electrons react with adsorbed O_2 molecules to form $\bullet O_2^-$. With radicle, on the other hand, photogenerated holes react with an adsorbed water molecule to form hydroxyl radicles. These generated ROS help in the removal of tetracycline (Wang et al., 2018).

MIL(100)Fe-loaded N-TiO_2 for dye degradation in wastewater was firstly reported by Huang et al. (2017) (Fig. 3). Later, He et al. reported a magnetic MIL-101 (Fe)/TiO_2 for the degradation of tetracycline (TC) under solar light (He et al., 2019). The large surface area of the MOFs and photocatalytic activity of TiO_2 helped in the enhanced adsorption and degradation of TC 92.7% of TC degradation was achieved by 10 min of solar light irradiation. Additionally, due to the magnetic properties of the catalyst, it could also easily be recovered from the TC solution by using a magnet.

A novel visible light photocatalyst Fe_2O_3/TiO_2@MIL-101 was synthesized by Tilgner et al. MIL-101(Cr) was used as the support for Fe_2O_3 (hematite)/TiO_2 (anatase) heterojunction. The average size of crystallites was taken as 300 nm, large enough for the separation of generated charge carriers and small enough to have high surface area for the modification of catalysts. The visible light active degradation of antibiotics of as synthesized material was compared with Fe_2O_3@MIL-101, TiO_2@MIL-101, bare Fe_2O_3, TiO_2, and commercial TiO_2 (P25). The Fe_2O_3/TiO_2@MIL-101 material showed higher photocatalytic activity than their bare parent materials. This enhanced catalytic activity is due to the support and synergy effect of Fe_2O_3 and TiO_2 with MIL-101 crystallites. Fe_2O_3 acts as the visible light–absorbing component. Under illumination the excited electrons can be transferred from Fe_2O_3 to the conduction band of TiO_2, and this ensures the efficient charge separation, which

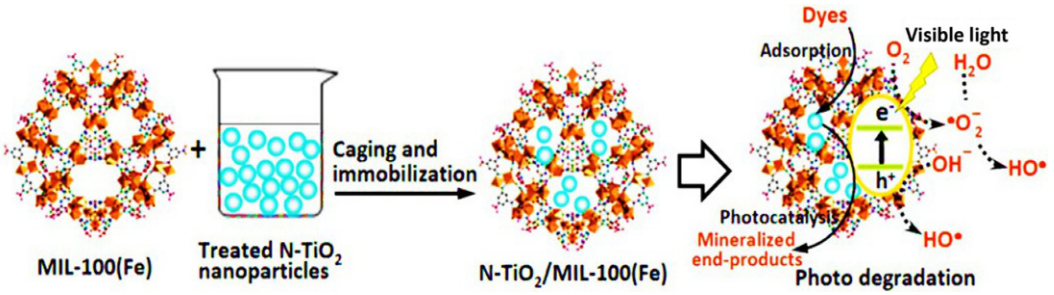

FIG. 3

Schematic illustration of photocatalytic degradation mechanism using MOFs (Huang et al., 2017).

This book belongs to Central Library BADJI Mokhtar-ANNABA UNIVERSITY Copyright Elsevier 2024

helps in the enhanced production of ROS for the degradation of organic components (Tilgner, Friedrich, Verch, de Jonge, & Kempe, 2018).

4.5 Novel composites

Recently, Ray et al. reported AgBr-α-$NiMoO_4$ composite photocatalyst for rapid degradation and mineralization of naproxen (a nonsteroidal antiinflammatory drug) in wastewater. $NiMoO_4$ is a low-cost and environmentally friendly photocatalyst with a bandgap of 2.8 eV, and it consists of low temperature α monoclinic structure. To increase the photocatalytic activity of $NiMoO_4$, material was coupled with AgBr with the bandgap of 2.5 eV. The prepared AgBr-α-$NiMoO_4$ composite exhibited 84% degradation of the drug within 20 min and achieved 100% mineralization after 100 min of visible light irradiation. This high photocatalytic activity is attributed to the efficient charge separation, due to matching energy levels of $NiMoO_4$ and AgBr and the surface plasmon resonance of silver particles (Ray, Dhakal, & Lee, 2018).

$BiVO_4$ is another visible light active photocatalytic semiconductor that has been widely investigated for treating wastewater. Even though it exhibits long-term stability, low separation of photogenerated electrons and poor electrical conductivity limit its application in practical situations. To enhance the photocatalytic activity of $BiVO_4$, Regmi et al. codoped the catalyst with nonmetal, sulfur (S), and a metal, tungsten (W), for the catalytic degradation of naproxen. Compared with undoped and S and W single-doped catalyst, codoped samples showed significant increases in efficiency (76.5%), up to 180 min of visible light radiation. The bandgap of the semiconductor was reduced by the insertion of S 3p orbitals with Bi 6s and O *2p* states. Thus the valence bandwidth increased, which caused the shortening of the bandgap (Regmi, Kshetri, Pandey, & Lee, 2018), increasing the surface area of the codoped catalyst, which enhanced the visible light absorption for the activation.

For harnessing broad brand spectrum, Kumar, Reddy, Kumar, Sharma, and Krishnan (2018) developed a novel quaternary plasmonic core-shell nanostructured photocatalyst. These catalysts are composed of La-doped $NaYF_4$@ CdS core-shell decorated with Au NPs supported on rGO nanosheets. $NaYF_4$:Yb/Er was used to obtain NIR photons, and to convert them to visible light, core-shell CdS was helpful in the direct absorption visible region of the spectra. Au NPs were added to exploit the plasmonic enhancement effect. The SPR effect of NPs can be effectively used to increase the adsorbent efficiency of semiconductors due to the tunability from UV to NIR. Au NPs act as cocatalysts to reduce the recombination of generated electron-hole pairs, while rGO acts as an electron acceptor, as an electron transporter, and also as an adsorbent of the pollutant (Kumar et al., 2018). Depending on the percentage of rGO incorporated, the photocatalytic degradation efficiency varied. The optimum value rGO for the highest degradation efficiency of 90% within 180 min under visible light was 4 wt%.

The use of clay-based photocatalysts for pharmaceutical waste treatment is another new area that is being explored. These materials are promising alternatives for traditional photocatalysts, due to their low cost, abundant availability, chemical stability, and nontoxicity. Degradation of antibiotics sulfamethoxazole and trimethoprim by UV and solar radiation using clay was recently reported by Martinez-Costa, Rivera-Utrilla, Leyva-Ramos, Sanchez-Polo, and Velo-Gala (2018). They used bentonite and vermiculite as photocatalysts. Doping ions present within the structure of these materials help to enhance the generation of electrons and holes and directly react with the antibiotics. Among them, vermiculite showed better efficiency due to the presence of a high concentration of Fe, Mn, Ti, and V relative to the bentonite. They reported 11.4 and 46.4 times increase in the reaction rate under UV radiation for sulfamethoxazole and trimethoprim.

This book belongs to Central Library BADJI Mokhtar-ANNABA UNIVERSITY Copyright Elsevier 2024

5 The scope of photocatalysis for wastewater treatment

Conventional means of wastewater treatments are done by using physical, chemical, and biological process. Based on the pollutant concentration in the effluent and the production cost of the process, different treatment methods can be chosen (Homem & Santos, 2011). In wastewater treatment plants (WWTP), there are three main stages of treatment, that is, primary, secondary, and tertiary treatments. The raw wastewater is pretreated/screened to remove grit, paper, plastic, fat, and grease. For the primary treatment the wastewater flows through a large sedimentation tank, where the heavy solids are settled using gravitational force. The effluent is transferred for secondary treatment, where dissolved and suspended biological matter is removed using aerobic digestion (activated sludge bacteria). Bacteria in the effluent form flocs; excess amounts of which are removed by sedimentation, which also produces the treated wastewater. In tertiary treatment (not used in all plants), effluent is treated with a variety of physical and chemical methods, which are normally focused on disinfection (as opposed to further removal of pollutant chemicals).

Following these treatments the treated water is released to the water bodies or, in some countries, can be used as reclaimed water. Reclaimed water or reused water is mainly used for irrigation in agricultural, for toilet flushing in households, and for replenishing the surface water or groundwater. It can be further treated to achieve the drinking water standard. Whether wastewater is disposed to surface water (which may be a source and downstream of water for treatment to drinking water) or it is used as reclaimed water, a significant concern is emerging that current wastewater and water treatment technologies and systems can lead to exposure PPCS from water and alteration of physicochemical and microbiological properties of the environment.

Over time, exposure to these harmful chemicals could lead to chronic diseases. A current lack of technologies for the complete removal of these substances is a significant issue today. The use of photocatalytic materials for the degradation of pharmaceutical and personal care substance could be an effective way of dealing with the issue.

Recently, many studies of photocatalytic treatment of outlet water from WWTP have been reported. Bernabeu et al. used solar photocatalysts for the removal of a pharmaceutical substance from treated water in WWTP in the southeast of Spain (Bernabeu et al., 2011). In a preliminary analysis of water from the outlet of the treatment plant, they found a significant amount of nine emerging pollutants (trimethoprim, ofloxacin, enrofloxacin, clarithromycin, acetaminophen, diclofenac, caffeine, thiabendazole, and carbamazepine). Irradiation of the wastewater with TiO_2 catalyst showed significant removal of these contaminants, and 100% fecal bacteria elimination was achieved. 0.2–0.5 g/L of TiO_2 was used and irradiated for 3 h. The complete removal of bacteria was achieved within 1 h. Similarly, Prieto et al. reported the removal of endocrine disruptive compounds with very low concentrations of TiO_2 from tertiary treated water (Prieto-Rodriguez et al., 2012). With the use of compound parabolic reactors (CPC) reactors of wide diameter under natural sunlight, 85% of these chemicals were degraded. Low concentrated TiO_2 is an effective, economical, and simple alternative for the tertiary treatment of WWTP effluent.

6 Conclusions

The development of more effective strategies for the removal of pharmaceutical waste from water has become a necessity, as these pollutants pose a significant threat to humans and the wider environment. The use of solar light active materials as catalysts for removing such wastes is an effective option, but

This book belongs to Central Library BADJI Mokhtar-ANNABA UNIVERSITY Copyright Elsevier 2024

the production of toxic by-products, scale-up issues, and difficulties with separation and recycling of heterocatalysts are the limitations to their use in real-world applications.

An ideal solution may be to use combined immobilized photocatalyst systems with membrane filtration or adsorption for the treatment of effluents containing pharmaceutical waste products and other organic materials. Further investigation is also required into up scaling of the proposed treatment technology from bench-scale to municipal/industrial applications.

Acknowledgment

The authors are grateful for the funding of the European Union's INTERREG VA Programme, Renewable Engine managed by the Special EU Programmes Body (SEUPB), with match funding provided by the Department for the Economy and Department of Jobs, Enterprise and Innovation in Dublin, Ireland.

References

Aslam, B., Wang, W., Arshad, M. I., Khurshid, M., Muzammil, S., Rasool, M. H., et al. (2018). Antibiotic resistance: A rundown of a global crisis. *Infection and Drug Resistance*, *11*, 1645.

Awfa, D., Ateia, M., Fujii, M., Johnson, M. S., & Yoshimura, C. (2018). Photodegradation of pharmaceuticals and personal care products in water treatment using carbonaceous-TiO2 composites: A critical review of recent literature. *Water Research*, *142*, 26–45.

Belet, A., Wolfs, C., Mahy, J. G., Poelman, D., Vreuls, C., Gillard, N., et al. (2019). Sol-gel syntheses of Photocatalysts for the removal of pharmaceutical products in water. *Nanomaterials*, *9*(1), 126.

Benotti, M. J., Trenholm, R. A., Vanderford, B. J., Holady, J. C., Stanford, B. D., & Snyder, S. A. (2008). Pharmaceuticals and endocrine disrupting compounds in US drinking water. *Environmental Science & Technology*, *43*(3), 597–603.

Berendonk, T. U., Manaia, C. M., Merlin, C., Fatta-Kassinos, D., Cytryn, E., Walsh, F., et al. (2015). Tackling antibiotic resistance: The environmental framework. *Nature Reviews Microbiology*, *13*(5), 310.

Bernabeu, A., Vercher, R., Santos-Juanes, L., Simón, P., Lardín, C., Martínez, M., et al. (2011). Solar photocatalysis as a tertiary treatment to remove emerging pollutants from wastewater treatment plant effluents. *Catalysis Today*, *161*(1), 235–240.

Cao, J., Yang, Z. H., Xiong, W. P., Zhou, Y. Y., Peng, Y. R., Li, X., et al. (2018). One-step synthesis of co-doped UiO-66 nanoparticle with enhanced removal efficiency of tetracycline: Simultaneous adsorption and photocatalysis. *Chemical Engineering Journal*, *353*, 126–137.

Chapman, D. V., & Organization, W. H. (1996). *Water quality assessments: A guide to the use of biota, sediments and water in environmental monitoring*.

Che, W. J., Luo, Y. B., Deng, F., Zhang, A. T., Zhao, L. N., Luo, X. B., et al. (2018). Facile solvothermal fabrication of cubic-like reduced graphene oxide/AgIn5S8 nanocomposites with anti-photocorrosion and high visible-light photocatalytic performance for highly-efficient treatment of nitrophenols and real pharmaceutical wastewater. *Applied Catalysis A: General*, *565*, 170–180.

Comninellis, C., Kapalka, A., Malato, S., Parsons, S. A., Poulios, I., & Mantzavinos, D. (2008). Advanced oxidation processes for water treatment: Advances and trends for R&D. *Journal of Chemical Technology & Biotechnology: International Research in Process, Environmental & Clean Technology*, *83*(6), 769–776.

Cravanzola, S., Sarro, M., Cesano, F., Calza, P., & Scarano, D. (2018). Few-layer MoS2 Nanodomains decorating TiO2 nanoparticles: A case study for the Photodegradation of carbamazepine. *Nanomaterials*, *8*(4), 207.

Davies, J., & Davies, D. (2010). Origins and evolution of antibiotic resistance. *Microbiology and Molecular Biology Reviews*, *74*(3), 417–433.

This book belongs to Central Library BADJI Mokhtar-ANNABA UNIVERSITY

Copyright Elsevier 2024

Diamanti-Kandarakis, E., Bourguignon, J.-P., Giudice, L. C., Hauser, R., Prins, G. S., Soto, A. M., et al. (2009). Endocrine-disrupting chemicals: An Endocrine Society scientific statement. *Endocrine Reviews*, *30*(4), 293–342.

Dias, D. A., Urban, S., & Roessner, U. (2012). A historical overview of natural products in drug discovery. *Metabolites*, *2*(2), 303–336.

Dong, S. Y., Sun, J. Y., Li, Y. K., Yu, C. F., Li, Y. H., & Sun, J. H. (2014). ZnSnO3 hollow nanospheres/reduced graphene oxide nanocomposites as high-performance photocatalysts for degradation of metronidazole. *Applied Catalysis B: Environmental*, *144*, 386–393.

Fair, R. J., & Tor, Y. (2014). Antibiotics and bacterial resistance in the 21st century. *Perspectives in Medicinal Chemistry*, *6*, S14459.

Fujishima, A., & Honda, K. (1972). Electrochemical photolysis of water at a semiconductor electrode. *Nature*, *238* (5358), 37.

Ganguly, P., Byrne, C., Breen, A., & Pillai, S. C. (2018). Antimicrobial activity of Photocatalysts: Fundamentals, mechanisms, kinetics and recent advances. *Applied Catalysis B: Environmental*, *225*, 51–75.

Ganguly, P., Mathew, S., Clarizia, L., R Kumar, S., Akande, A., Hinder, S., et al. (2019). Theoretical and experimental investigation of visible light responsive AgBiS 2-TiO2 heterojunctions for enhanced photocatalytic applications. *Applied Catalysis B*: *Environmental*, *253*, 401–418.

Hawkey, P. (2008). The growing burden of antimicrobial resistance. *The Journal of Antimicrobial Chemotherapy*, *62*(suppl_1), i1–i9.

He, L., Dong, Y. N., Zheng, Y. N., Jia, Q. M., Shan, S. Y., & Zhang, Y. Q. (2019). A novel magnetic MIL-101(Fe)/TiO2 composite for photo degradation of tetracycline under solar light. *Journal of Hazardous Materials*, *361*, 85–94.

Homem, V., & Santos, L. (2011). Degradation and removal methods of antibiotics from aqueous matrices–a review. *Journal of Environmental Management*, *92*(10), 2304–2347.

Hsu, J.-T., Chen, C.-Y., Young, C.-W., Chao, W.-L., Li, M.-H., Liu, Y.-H., et al. (2014). Prevalence of sulfonamide-resistant bacteria, resistance genes and integron-associated horizontal gene transfer in natural water bodies and soils adjacent to a swine feedlot in northern Taiwan. *Journal of Hazardous Materials*, *277*, 34–43.

Huang, J., Song, H. Y., Chen, C. X., Yang, Y., Xu, N. D., Ji, X. Z., et al. (2017). Facile synthesis of N-doped TiO2 nanoparticles caged in MIL-100(Fe) for photocatalytic degradation of organic dyes under visible light irradiation. *Journal of Environmental Chemical Engineering*, *5*(3), 2579–2585.

Huttner, A., Harbarth, S., Carlet, J., Cosgrove, S., Goossens, H., Holmes, A., et al. (2013). Antimicrobial resistance: A global view from the 2013 world healthcare-associated infections forum. *Antimicrobial Resistance and Infection Control*, *2*(1), 31.

Jones, H. O., Voulvoulis, N., & Lester, J. (2005). Human pharmaceuticals in wastewater treatment processes. *Critical Reviews in Environmental Science and Technology*, *35*(4), 401–427.

Kemper, N. (2008). Veterinary antibiotics in the aquatic and terrestrial environment. *Ecological Indicators*, *8*(1), 1–13.

Khedr, T. M., El-Sheikh, S. M., Hakki, A., Ismail, A. A., Badawy, W. A., & Bahnemann, D. W. (2017). Highly active non-metals doped mixed-phase TiO2 for photocatalytic oxidation of ibuprofen under visible light. *Journal of Photochemistry and Photobiology A: Chemistry*, *346*, 530–540.

Kumar, A., Reddy, K. L., Kumar, S., Sharma, V., & Krishnan, V. (2018). Rational design and development of lanthanide-doped NaYF4@CdS-au-RGO as quaternary Plasmonic Photocatalysts for harnessing visible-near-infrared broadband Spectrum. *ACS Applied Materials & Interfaces*, *10*(18), 15565–15581.

Kümmerer, K. (2009). Antibiotics in the aquatic environment–a review–part I. *Chemosphere*, *75*(4), 417–434.

Landers, T. F., Cohen, B., Wittum, T. E., & Larson, E. L. (2012). A review of antibiotic use in food animals: Perspective, policy, and potential. *Public Health Reports*, *127*(1), 4–22.

This book belongs to Central Library BADJI Mokhtar-ANNABA UNIVERSITY

Copyright Elsevier 2024

Lara, H. H., Ayala-Núnez, N. V., Turrent, L. d. C. I., & Padilla, C. R. (2010). Bactericidal effect of silver nanoparticles against multidrug-resistant bacteria. *World Journal of Microbiology and Biotechnology*, *26*, 615–621.

Laxminarayan, R., Duse, A., Wattal, C., Zaidi, A. K., Wertheim, H. F., Sumpradit, N., et al. (2013). Antibiotic resistance—The need for global solutions. *The Lancet Infectious Diseases*, *13*(12), 1057–1098.

Liang, R. W., Luo, S. G., Jing, F. F., Shen, L. J., Qin, N., & Wu, L. (2015). A simple strategy for fabrication of Pd@MIL-100(Fe) nanocomposite as a visible-light-driven photocatalyst for the treatment of pharmaceuticals and personal care products (PPCPs). *Applied Catalysis B: Environmental*, *176*, 240–248.

Lin, L., Wang, H. Y., & Xu, P. (2017). Immobilized TiO2-reduced graphene oxide nanocomposites on optical fibers as high performance photocatalysts for degradation of pharmaceuticals. *Chemical Engineering Journal*, *310*, 389–398.

Lundholm, K., Hyltander, A., & Sandström, R. (1992). Nutrition and multiple organ failure. *Nutrition Research Reviews*, *5*(1), 97–113.

Malato, S., Fernández-Ibáñez, P., Maldonado, M. I., Blanco, J., & Gernjak, W. (2009). Decontamination and disinfection of water by solar photocatalysis: Recent overview and trends. *Catalysis Today*, *147*(1), 1–59.

Malizos, K. N., & Kirketerp-Møller, K. (2016). *Incidence and socioeconomic impact of bone and joint infections (BJIs): The European perspective, periprosthetic joint infections* (pp. 3–18). Springer.

Martinez-Costa, J. I., Rivera-Utrilla, J., Leyva-Ramos, R., Sanchez-Polo, M., & Velo-Gala, I. (2018). Individual and simultaneous degradation of antibiotics sulfamethoxazole and trimethoprim by UV and solar radiation in aqueous solution using bentonite and vermiculite as photocatalysts. *Applied Clay Science*, *160*, 217–225.

Mathew, S., Ganguly, P., Rhatigan, S., Kumaravel, V., Byrne, C., Hinder, S., et al. (2018). Cu-doped TiO2: Visible light assisted photocatalytic antimicrobial activity. *Applied Sciences*, *8*(11), 2067.

Mathur, S., & Hoskins, C. (2017). Drug development: Lessons from nature. *Biomedical Reports*, *6*(6), 612–614.

Morgan, D. J., Okeke, I. N., Laxminarayan, R., Perencevich, E. N., & Weisenberg, S. (2011). Non-prescription antimicrobial use worldwide: A systematic review. *The Lancet Infectious Diseases*, *11*(9), 692–701.

Namshah, K. S., & Mohamed, R. M. (2018). WO3-TiO2 nanocomposites for paracetamol degradation under visible light. *Applied Nanoscience*, *8*(8), 2021–2030.

O'Shea, R., & Moser, H. E. (2008). Physicochemical properties of antibacterial compounds: Implications for drug discovery. *Journal of Medicinal Chemistry*, *51*(10), 2871–2878.

Panneri, S., Ganguly, P., Mohan, M., Nair, B. N., Mohamed, A. A. P., Warrier, K. G., et al. (2017). Photoregenerable, Bifunctional granules of carbon-doped g-C3N4 as adsorptive Photocatalyst for the efficient removal of tetracycline antibiotic. *ACS Sustainable Chemistry & Engineering*, *5*(2), 1610–1618.

Panneri, S., Ganguly, P., Nair, B. N., Mohamed, A. A. P., Warrier, K. G., & Hareesh, U. N. (2016). Copyrolysed C3N4-Ag/ZnO ternary heterostructure systems for enhanced adsorption and photocatalytic degradation of tetracycline. *European Journal of Inorganic Chemistry*, *2016*(31), 5068–5076.

Panneri, S., Thomas, M., Ganguly, P., Nair, B. N., Mohamed, A. P., Warrier, K., et al. (2017). C 3 N 4 anchored ZIF 8 composites: Photo-regenerable, high capacity sorbents as adsorptive photocatalysts for the effective removal of tetracycline from water. *Catalysis Science & Technology*, *7*(10), 2118–2128.

Pérez-González, A., Urtiaga, A., Ibáñez, R., & Ortiz, I. (2012). State of the art and review on the treatment technologies of water reverse osmosis concentrates. *Water Research*, *46*(2), 267–283.

Perumal Samy, R., & Gopalakrishnakone, P. (2010). Therapeutic potential of plants as anti-microbials for drug discovery. *Evidence-based Complementary and Alternative Medicine*, *7*(3), 283–294.

Prieto-Rodriguez, L., Miralles-Cuevas, S., Oller, I., Agüera, A., Puma, G. L., & Malato, S. (2012). Treatment of emerging contaminants in wastewater treatment plants (WWTP) effluents by solar photocatalysis using low TiO2 concentrations. *Journal of Hazardous Materials*, *211*, 131–137.

Ray, S. K., Dhakal, D., & Lee, S. W. (2018). Rapid degradation of naproxen by AgBr-α-NiMoO4 composite photocatalyst in visible light: Mechanism and pathways. *Chemical Engineering Journal*, *347*, 836–848.

This book belongs to Central Library BADJI Mokhtar-ANNABA UNIVERSITY

Copyright Elsevier 2024

Regmi, C., Kshetri, Y. K., Pandey, R. P., & Lee, S. W. (2018). Visible-light-driven S and W co-doped dendritic BiVO4 for efficient photocatalytic degradation of naproxen and its mechanistic analysis. *Molecular Catalysis*, *453*, 149–160.

Renita, A. A., Kumar, P. S., Srinivas, S., Priyadharshini, S., & Karthika, M. (2017). A review on analytical methods and treatment techniques of pharmaceutical wastewater. *Desalination and Water Treatment*, *87*, 160–178.

Rizzo, L., Manaia, C., Merlin, C., Schwartz, T., Dagot, C., Ploy, M., et al. (2013). Urban wastewater treatment plants as hotspots for antibiotic resistant bacteria and genes spread into the environment: A review. *Science of the Total Environment*, *447*, 345–360.

Sassman, S. A., & Lee, L. S. (2005). Sorption of three tetracyclines by several soils: Assessing the role of pH and cation exchange. *Environmental Science & Technology*, *39*(19), 7452–7459.

Serpone, N., Artemev, Y. M., Ryabchuk, V. K., Emeline, A. V., & Horikoshi, S. (2017). Light-driven advanced oxidation processes in the disposal of emerging pharmaceutical contaminants in aqueous media: A brief review. *Current Opinion in Green and Sustainable Chemistry*, *6*, 18–33.

Shetty, R., Chavan, V. B., Kulkarni, P. S., Kulkarni, B. D., & Kamble, S. P. (2017). Photocatalytic degradation of pharmaceuticals pollutants using N-doped TiO2 Photocatalyst: Identification of CFX degradation intermediates. *Indian Chemical Engineer*, *59*(3), 177–199.

Shinde, Y., Wadhai, S., Ponkshe, A., Kapoor, S., & Thakur, P. (2018). Decoration of Pt on the metal free RGO-TiO2 composite photocatalyst for the enhanced photocatalytic hydrogen evolution and photocatalytic degradation of pharmaceutical pollutant beta blocker. *International Journal of Hydrogen Energy*, *43*(8), 4015–4027.

Stackelberg, P. E., Furlong, E. T., Meyer, M. T., Zaugg, S. D., Henderson, A. K., & Reissman, D. B. (2004). Persistence of pharmaceutical compounds and other organic wastewater contaminants in a conventional drinking-water-treatment plant. *Science of the Total Environment*, *329*(1–3), 99–113.

Strauch, K. A. (2011). Invisible pollution: The impact of pharmaceuticals in the water supply. *AAOHN Journal*, *59*(12), 525–533.

Tilgner, D., Friedrich, M., Verch, A., de Jonge, N., & Kempe, R. (2018). A metal–organic framework supported nonprecious metal photocatalyst for visible-light-driven wastewater treatment. *ChemPhotoChem*, *2*(4), 349–352.

Tiong, J. J., Loo, J. S., & Mai, C.-W. (2016). Global antimicrobial stewardship: A closer look at the formidable implementation challenges. *Frontiers in Microbiology*, *7*, 1860.

Tong, H., Ouyang, S., Bi, Y., Umezawa, N., Oshikiri, M., & Ye, J. (2012). Nano-photocatalytic materials: Possibilities and challenges. *Advanced Materials*, *24*(2), 229–251.

Ventola, C. L. (2015). The antibiotic resistance crisis: Part 1: Causes and threats. *Pharmacy and Therapeutics*, *40*(4), 277.

Wang, D., Jia, F., Wang, H., Chen, F., Fang, Y., Dong, W., et al. (2018). Simultaneously efficient adsorption and photocatalytic degradation of tetracycline by Fe-based MOFs. *Journal of Colloid and Interface Science*, *519*, 273–284.

Wexler, H. M. (2007). Bacteroides: The good, the bad, and the nitty-gritty. *Clinical Microbiology Reviews*, *20*(4), 593–621.

Whitham, T. G., Bailey, J. K., Schweitzer, J. A., Shuster, S. M., Bangert, R. K., LeRoy, C. J., et al. (2006). A framework for community and ecosystem genetics: From genes to ecosystems. *Nature Reviews. Genetics*, *7*(7), 510.

World Health Organization. (2001). *WHO global strategy for containment of antimicrobial resistance*. Geneva: World Health Organization.

Xing, X. B., Du, Z. X., Zhuang, J. C., & Wang, D. (2018). Removal of ciprofloxacin from water by nitrogen doped TiO2 immobilized on glass spheres: Rapid screening of degradation products. *Journal of Photochemistry and Photobiology A: Chemistry*, *359*, 23–32.

Zhao, W., Duan, J., Ji, B., Ma, L., & Yang, Z. (2018). Novel formation of large area N-TiO2/graphene layered materials and enhanced photocatalytic degradation of antibiotics. *Journal of Environmental Chemical Engineering*, *9*, 2489.

This book belongs to Central Library BADJI Mokhtar-ANNABA UNIVERSITY

Copyright Elsevier 2024

CHAPTER

5

Hydrotalcite-like compounds and related materials as catalysts for the photodegradation of pharmaceutical compounds: Synthesis and catalytic performances

Leticia Santamaría[a], Antonio Gil[a], Miguel Angel Vicente[b], Sophia A. Korili[a]

INAMAT, Science Department, Public University of Navarre, Pamplona, Spain[a] GIR-QUESCAT, Inorganic Chemistry Department, University of Salamanca, Salamanca, Spain[b]

1 Introduction

At present, large amounts of pharmaceutical compounds are used in several areas, as medicine, industry, and cosmetics (Michael, Frontistis, & Fatta-Kassinos, 2013). This large intake may cause an increase in the presence of these compounds in natural environments, due to their discharge in untreated wastes or partially treated wastewater. This can hardly be avoided; for example, some medicines are excreted unmetabolized by living organisms in percentages that can reach even 90% of the ingested dose. Obviously, this may lead to the contamination of surface or underground waters (Bethi, Sonawane, Bhanvase, & Gumfekar, 2016).

Water is one of the more abundant compounds in nature, covering about three quarters of Earth surface. However, several factors limit its availability for human intake. Human activities strongly affect the quality of water, mainly by the discarding of pollutants, which can provoke very negative effects on vegetal and animal species in the ecosystems and on humankind itself (Qadir et al., 2010). In the last years, new contaminants have been detected in the environment, being denoted as emerging organic pollutants (EOPs), listed by NORMAN Network (NORMAN, 2019), and defined as synthetic or naturally occurring chemicals that are not commonly monitored in the environment, but have the potential to enter the environment and cause known or suspected adverse ecological and (or) human health effects. >700 EOPs pollutants and their metabolites and transformation products have been reported in European aquatic environments; among them are pharmaceutical products, drugs, pesticides, personal care products, and industrial additives; and some of them can also be considered as anthropogenic markers for wastewater contamination

Nano-Materials as Photocatalysts for Degradation of Environmental Pollutants. https://doi.org/10.1016/B978-0-12-818598-8.00005-5
© 2020 Elsevier Inc. All rights reserved.

This book belongs to Central Library BADJI Mokhtar-ANNABA UNIVERSITY

Copyright Elsevier 2024

(Geissen et al., 2015). In the case of medicines, particularly antibiotics, their increasing propagation in the environment is causing the development of strongly resistant bacteria, which is an additional and very important health problem (Marti, Variatza, & Balcazar, 2014). It is expected that in the next years the main cause of death, surpassing those produced by cancer, will be the presence of bacteria multiresistant to several families of antibiotic molecules. This situation has been generated by the abuse of antibiotics in human medicine and environmental pollution derived from agricultural and livestock production.

Thus the removal of these pollutants becomes mandatory. Several procedures have been proposed and are being used for such removal, as solvent extraction, reverse osmosis, or adsorption (Park, Vecitis, & Hoffmann, 2009; Williams, Hestekin, Smothers, & Bhattacharyya, 1999). Adsorption using materials from various porous families is probably the most popular method, as these materials have low cost, their use is simple and versatile, and they adsorb several types of pollutants (Khenniche & Aissani, 2010). The adsorption process is mainly controlled by the pH of the aqueous solution, the ionic characteristics of the adsorbent and the pollutants, and the ionic strength of the medium. However, this process is based on the change of the pollutants from one phase (water) to the other (adsorbent), but does not destroy them.

In this context, advanced oxidation processes (AOPs) constitute a group of techniques very attractive for the elimination of these pollutants. They cover chemical, photochemical, sonochemical, and electrochemical procedures, including Fenton, ozonation, plasma, photocatalysis, and wet air oxidation reactions, and almost all the processes are based on the production of •OH radicals (sulfate and chlorine radicals can also be used). Other common characteristics are the operation at ambient temperature and pressure conditions (or very close to them) and that they attack all the organic compounds, that is, as they are based on the generation of strong radicals, they are not selective to the pollutants. Under optimal conditions the process may lead to the complete mineralization of the pollutants (Miklos et al., 2018).

Several materials have been used for assisting heterogeneous photocatalytic processes. Titanium dioxide, TiO_2 under anatase structure, is the most used, functional, versatile, and effective photocatalyst, based on its excellent photoelectric properties, low cost, corrosion resistance, and nontoxicity for living organisms (Papoulis et al., 2013). However, TiO_2 has an important limitation, its energy bandgap is 3.2 eV, and this limits its efficiency to the ultraviolet wavelength of 387.5 nm, only 3%–5% of the solar radiation that reaches the Earth surface (Deng et al., 2016). This can be partially solved by dispersing TiO_2 on inorganic matrices or by modifying it with several dopants as noble metals, transition metal, nonmetals, etc., which can decrease the energy required for its activation.

A different strategy is to substitute TiO_2 by other catalyst. For example, clay minerals have received large attention (Garrido-Ramírez, Theng, & Mora, 2010; Praneeth & Paria, 2017; Ramírez, Vicente, & Madeira, 2010). However, hydrotalcites have received very little consideration, although these solids, also called layered double hydroxides, are structurally related to clays and exist with a great variety of composition. The use of these solids for photocatalytic removal of organic compounds has been recently reviewed (Mohapatra & Parida, 2016), but their use for the degradation of pharmaceutical pollutants has been scarcely reported. In this context the application of this family of solids for catalytic photodegradation of pharmaceutical pollutants is reviewed in this chapter. Before the structure and methods of preparation of these materials are briefly presented.

This book belongs to Central Library BADJI Mokhtar-ANNABA UNIVERSITY
Copyright Elsevier 2024

2 Structure of hydrotalcites

The hydrotalcite-like materials, or simply hydrotalcites, are a group of solids whose structure and composition are related to the mineral hydrotalcite, $Mg_6Al_2(CO_3)(OH)_{16}{\cdot}4(H_2O)$. These solids have a lamellar structure, with a form similar to that of brucite, $Mg(OH)_2$. As they are hydroxides of two cations, they are also called layered double hydroxides and abbreviated LDHs.

As indicated the structure and chemical composition of hydrotalcites can be considered derived from brucite. Brucite is formed by a hexagonal compact packing of hydroxyl anions, with Mg^{2+} cations occupying all the octahedral holes each two layers, thus generating a layered structure. Mg^{2+} can be substituted by trivalent cations, and each time that this substitution occurs, a positive charge is generated that must be balanced by the incorporation of compensating anions in the interlayer region. Thus the layers are positively charged, and compensating anions are located in the interlayer region, just the opposite than in clays, the reason why hydrotalcites are also known as anionic clays and can be seen as a *mirror* of clays. In the case of hydrotalcite, one-fourth of Mg^{2+} cations are substituted by Al^{3+}, that is, two of eight in the formula given before, and consequently, two positive charges are generated, compensated by the incorporation of a carbonate anion. So the hydroxyl anions in the formula are *structural*, that is, they form the octahedra of the structure, while carbonate anions are charge-balancing and located in the interlayer. Besides a certain amount of water also incorporates to the interlayer region, this amount depending on the ambient conditions (Mishra, Dash, & Pandey, 2018; Nalawade, Aware, Kadam, & Hirlekar, 2009; Rives, 2001; Rives, del Arco, & Martín, 2013; Rives & Ulibarri, 1999). The resultant structure is that shown in Fig. 1.

It is remarkable that hydrotalcite layers can stack on different ways, giving up to different polytypes (rhombohedral and hexagonal). More interesting for the application of these solids is the large variety of chemical composition that they can show. Thus a large amount of divalent and trivalent cations can occupy the positions that in the parent compound are occupied by Mg^{2+} and Al^{3+}, respectively. Strictly, *hydrotalcite* is the mineral referenced earlier, and *hydrotalcites* are the solids derived from it, considering the changes in composition we are commenting on now. Almost all the cations, both divalent and trivalent, with size similar to Mg^{2+} can occupy the octahedral holes maintaining the hydrotalcite structure, and hydrotalcites containing a large variety of cations have been prepared in the laboratory: divalent, such as Ca, Mn, Co, Ni, Cu, Zn, Pd, and Pt, and trivalent, such as Ga, In, Y, V, Cr, Mn, Fe, Co, Rh, Ir, Ru, and lanthanides, among others. The structure is maintained if two or more divalent cations and/or two or more trivalent cations enter the composition. Even more, when monovalent or tetravalent cations that can isomorphically occupy the octahedral positions, as Li^+ or Zr^{4+}, are incorporated into the composition, the structure is also maintained (Mishra et al., 2018; Nalawade et al., 2009; Rives, 2001; Rives et al., 2013; Rives & Ulibarri, 1999).

Besides the size of the cations, other limiting structural factor is the degree of substitution, that is, beginning from an ideal brucite structure the amount of trivalent cations that can substitute the divalent ones. The molar fraction of the trivalent cation must be ranged between 0.20 and 0.33; in other words the ratio M(II)/M(III) must range between 2 and 4. Theoretical calculations have found that the maximum stability is found when the degree of substitution is 0.25 (M(II)/M(III) = 3.0), that is, exactly the value present in the natural hydrotalcite. If the substitution degree is higher than 0.33, charged $[Al(OH)_6]$ octahedra must be neighbor among them, creating a repulsion that destabilizes the structure, while for a substitution degree lower than 0.25 the amount of compensating anions is very low and

This book belongs to Central Library BADJI Mokhtar-ANNABA UNIVERSITY
Copyright Elsevier 2024

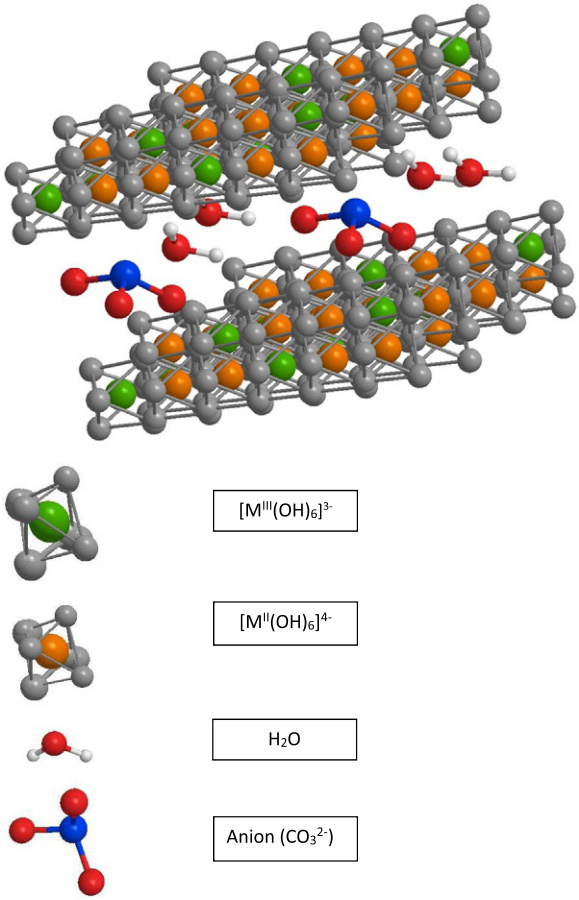

FIG. 1

Structure of hydrotalcites.

the distance among them is very large, also destabilizing the structure (Mishra et al., 2018; Nalawade et al., 2009; Rives, 2001; Rives et al., 2013; Rives & Ulibarri, 1999).

As indicated before the degree of substitution directly determines the charge of the layers, so it conditions the amount of compensating anions. This allows to define the *anion exchange capacity* (*AEC*) as the amount of anions that can be exchanged by a determined amount of hydrotalcite, by analogy with the well-known *cation exchange capacity* (*CEC*) of clays. In the natural hydrotalcite the compensating anion is carbonate, and due to its divalent charge, its amount is logically half of the substitution degree. When the hydrotalcites are prepared in the laboratory, other compensating anions can be incorporated to the structure, not only nitrate, halides, borates, hydroxyl (i.e., hydroxyls as compensating cations, besides of structural hydroxyls, the resultant hydrotalcite being known as meixnerite variety), phosphate, arsenate, sulfate, sulfonates, and carboxylates (lactate, terephthalate, acrylate,

This book belongs to Central Library BADJI Mokhtar-ANNABA UNIVERSITY Copyright Elsevier 2024

etc.), but also coordination compounds and polyoxometalates (polyvanadates, polymolibdates, polywolframates, etc.). In these last cases a new metal is incorporated to the structure, besides of those composing the layers.

With all these considerations the general formula of the hydrotalcite family can be expressed as $[M^{II}_{1-x}M^{III}_{x}(OH)_2]^{x+}(A^{n-})_{x/n} \bullet mH_2O$, where x is the degree of substitution of the divalent M^{II} cations by the trivalent M^{III} cations and consequently the charge of the layer, n is the charge of the anion A, and m is the degree of hydration (Mishra et al., 2018; Nalawade et al., 2009; Rives, 2001; Rives et al., 2013; Rives & Ulibarri, 1999).

When calcined, hydrotalcites tend to transform into oxides. As hydrotalcites are composed of divalent and trivalent cations, the calcination tends to form the spinels $M^{II}M^{III}_2O_4$, with an excess of the divalent oxide, as the ratio M(II)/M(III) in the hydrotalcites is higher than in the spinels. The degree of substitution allows to tailor the amount of spinel in the final oxide mixture, and if the compensating anions are coordination compounds or polyoxometalates, other metals are incorporated to the final mixtures of oxides, this strongly influencing their catalytic performance.

3 Preparation of hydrotalcites

The preparation of hydrotalcites is a relatively simple laboratory procedure, as the thermodynamic tendency to form these compounds is high when the adequate amount of cations and anions are present. Thus the following preparation procedures can be listed (Rives, 2001).

Coprecipitation: It is the simplest procedure. In summary, it consists in the preparation of aqueous solutions of the desired metal cations in the desired ratios, their mixture, and the increase of the pH up to the precipitation of the hydrotalcite. Usually the pH is increased by adding NaOH, Na_2CO_3, and/or $NaHCO_3$ solutions (or the metallic solutions are added over the alkaline solution). If not special precautions are taken, the interlayer anions should be carbonate, even if neither carbonate nor bicarbonate are used for the increase of pH; the reacting mixture, due to its strong alkaline pH, reacts with atmospheric CO_2, and the formed carbonate has a strong tendency to enter into the interlayer. With special precautions and selecting adequately the metallic salts used at the beginning of the process, nitrates, chlorides, etc., these anions can be incorporated into the interlayer.

This method has small modifications, which try to avoid the abrupt precipitation of the solid. The use of automatic titrators allows to modify the pH very slowly and to fix it very precisely to a predetermined value. Other possibility, widely used in the preparation of other families of solids, is to carry out the synthesis assisted by the hydrolysis of urea. A certain amount of urea is added to the mixture, and this is slowly heated, provoking the hydrolysis of the urea, which leads to the formation of ammonium carbonate, thus increasing the pH. Therefore the increase of the pH can be controlled by the intensity of the heating, with the advantage that the hydrolysis of urea is homogeneous in all the solution, and thus, the precipitation leads to more uniform and smaller particles (Fig. 2).

Anion exchange: This method allows to obtain a hydrotalcite with a certain interlayer anion from the solid containing other anion. The parent solid is put into a highly concentrated solution of the second anion, and the exchange proceeds. Carbonate hydrotalcite cannot be used as precursor, since the high affinity of this anion to the hydrotalcite interlayer avoids its exchange with other anions. The method is applicable for the intercalation of polyoxometallates and other large anions and also if

This book belongs to Central Library BADJI Mokhtar-ANNABA UNIVERSITY Copyright Elsevier 2024

FIG. 2

Laboratory procedure for the preparation of hydrotalcites by the coprecipitation method.

the desired anion is not stable in the initial alkaline conditions needed for the precipitation of the hydrotalcite.

Reconstruction: As indicated before, hydrotalcites are usually calcined to obtain mixtures of oxides. If this calcination is carried out at moderate temperatures, usually $\leq$500°C, the solids obtained show *memory effect*, that is, the solids are able to recover the hydrotalcite structure if they are dispersed in an anionic solution. Thus a *normal* hydrotalcite is obtained, usually containing carbonate and prepared by coprecipitation, and calcined. The calcined solid is then dispersed in a solution containing the final desired anion, and the hydrotalcite structure is now reconstructed with this desired anion in the interlayer. As in the previous method, this method is especially indicated for the preparation of hydrotalcites containing polyoxometallates and other large anions or if the desired anions are not stable under the conditions for coprecipitation synthesis.

In some cases the hydrotalcite synthesis is assisted by hydrothermal conditions, in recent years microwave treatments being frequent, allowing improvement in the crystallinity and homogeneity of the solids.

This book belongs to Central Library BADJI Mokhtar-ANNABA UNIVERSITY Copyright Elsevier 2024

4 Hydrotalcites in the photodegradation of pharmaceuticals

As indicated before, although the use of hydrotalcites as photocatalysts has been recently reviewed (Mohapatra & Parida, 2016), the use of these materials for the degradation of pharmaceutical pollutants has not been revised. A summary of the main conditions and results is included in Table 1.

The catalytic photodegradation of salicylic acid sodium under visible-light irradiation has been studied by Zhao et al. (2011). Other pollutants, although not pharmaceutical compounds, were also photodegraded, namely, sulforhodamine-B, Congo red, and chlorinated phenol. The catalysts were a series of MCr hydrotalcites (M = Cu, Ni, and Zn), prepared by mixing a solution containing the metallic nitrates with a NaOH solution and submitting the mixture to a colloid mill rotating at 3000 rpm for a short time, followed by a separate aging process at 100°C. Nitrate-containing hydrotalcites were thus obtained, the corresponding carbonate counterparts being obtained by anion exchange. These catalysts

Table 1 Applications and use conditions of hydrotalcite-like materials as catalysts for the photodegradation of pharmaceutical compounds

Composition of the hydrotalcite	Preparation method	Calcination temperature	Pharmaceutical pollutant	Radiation	Reference
Cu-Ni-Zn-Cr nitrate and carbonate	Mixture, colloid mill, and aging (nitrate solids) Anion exchange (carbonate solids)	NO (drying at 60°C)	Salicylic acid	Visible	Zhao et al. (2011)
Mg-Al carbonate	Co-precipitation	450°C	Sodium naproxen, oxytetracycline hydrochloride	UV	Jacome-Acatitla et al. (2014)
Ce-Zn-Al carbonate	Co-precipitation	450°C, 600°C, 750°C, 900°C	Paracetamol	Solar simulated	Zhu et al. (2016)
Zn-Al carbonate	Co-precipitation	200°C, 300°C, 400°C, 500°C	Ibuprofen	Solar simulated	Di et al. (2017)
Zn-Fe carbonate	Co-precipitation	300°C, 400°C, 500°C, 600°C, 800°C, 1000°C	Caffeine	UV	Elhalil et al. (2017)
Zn-Fe	Co-precipitation	550°C, 700°C	Tetraclycline	Visible	Yang et al. (2017)
Zn-Al chloride	Co-precipitation and anionic exchange	NO (drying at room temperature)	Tetracycline, oxytetracycline	UV	Bouaziz et al. (2018)
Zn-Fe[a]	Hydrothermal	450°C	Paracetamol	Solar simulated	Zhu et al. (2018)
Zn-Al-La carbonate[b]	Co-precipitation	300°C, 400°C, 500°C, 600°C, 800°C, 1000°C	Caffeine	UV	Elhalil et al. (2019)

[a]*Forming composites with graphene oxide.*
[b]*Forming composites with Ag.*

This book belongs to Central Library BADJI Mokhtar-ANNABA UNIVERSITY
Copyright Elsevier 2024

exhibited 20 times higher photocatalytic performance than Degussa P25, attributable to their low bandgap (1.6 eV) and their abundant surface OH groups. The authors claimed that the high dispersion of CrO_6 octahedra in the LDH layer played a key role in responding to visible light and photogenerating charge carriers. The LDH matrix provided an ordered dispersion of the CrO_6 octahedron in the layer, which promoted the efficiency of the excited electron and avoided the recombination of electron and hole. The solids showed high recyclable stability for three cycles.

Jacome-Acatitla et al. (2014) prepared MgAl hydrotalcites, with Mg/Al ratios of 2.0, 2.5, and 3.0 by the coprecipitation method (K_2CO_3/KOH, pH = 9). The resulting hydrotalcites were calcined at 450°C. The calcined solids were employed for the catalytic photodegradation of sodium naproxen and oxytetracycline hydrochloride, under 254-nm UV irradiation. About 90% of sodium naproxen and 70% of oxytetracycline hydrochloride were mineralized by the best catalyst (Mg/Al = 2.5) after 5 h of reaction, better behavior than that of commercial Degussa P25 TiO_2. Fluorescence spectroscopy study suggested the generation of hydroxyl radicals as the oxidative species, and bandgap energies were 3.054–3.083 eV.

Catalysts based on Zn-Al-Ce were prepared by calcination of Ce-doped Zn-Al hydrotalcite precursors and used in the photodegradation of paracetamol and rhodamine B dye in aqueous solutions under simulated solar light irradiation (Zhu et al., 2016). The results showed an increase of the catalytic photoactivity due to the presence of Ce. The optimal Ce content was studied and found to be of 5% mole ratio ($n_{Ce}/n_{(Zn+Al+Ce)}$), which could be attributed to the increase in the separation efficiency of electrons and holes. The most effective calcination temperature was also examined and found to be 750°C, which was attributed to the formation of well-crystallized metal oxides. After 240 min a 98.9% of paracetamol degradation efficiency was achieved (97.8% for rhodamine B), and the authors suggested the importance of hole, superoxide radical, and hydroxyl radical roles during the photocatalytic process. These catalysts were also proven to be stable and reusable up to 10 cycles.

Di et al. (2017) prepared Zn-Fe carbonate hydrotalcite by coprecipitation and calcined it at several temperatures, using the resultant solids for the degradation of ibuprofen. The solid with Zn/Fe ratio of 4 and calcined at 300°C exhibited the best efficiency in the degradation of the pharmaceutical (the amount degraded was not given, although, from the plot seems to be c. 95%, the rate constant was 1.584×10^{-2} 1/min). The solids were also used for the adsorption removal of As(III) (arsenite), obtaining a maximum adsorption capacity of 176.3 mg/g, and for the simultaneous removal of ibuprofen and arsenite, finding that the presence of ibuprofen did not affect the adsorption of arsenite but, in contrast, the presence of arsenic strongly influenced the degradation of ibuprofen, depending on the arsenic species and concentrations. The authors indicated that photogenerated h^+ played a major role in the process of ibuprofen degradation, while arsenic was removed by combined oxidation and adsorption. The reusability was also studied for six runs, with excellent behavior. The authors claimed that the process was effective using other pharmaceuticals, namely, acetaminophen and diclofenac, but no data on their degradation were given.

The degradation of caffeine using the solids derived from Zn—Al carbonate hydrotalcites has been studied by Elhalil et al. (2017). Various Zn/Al molar ratios were considered, namely 1, 3, and 5, and the resulting hydrotalcites were calcined at 300°C, 400°C, 500°C, 600°C, 800°C, and 1000°C for 6 h. As this calcination led to ZnO-$ZnAl_2O_4$ mixture, a pure ZnO sample was also prepared, and Degussa P-25 TiO_2 was also used as reference. The best caffeine removal efficiency (97.32%) was shown by the sample with Zn/Al = 3 calcined at 500°C, and caffeine photodegradation reaction always followed a pseudo–first order kinetics. The catalytic efficiency of the solids derived from the hydrotalcites,

This book belongs to Central Library BADJI Mokhtar-ANNABA UNIVERSITY Copyright Elsevier 2024

composed of mixtures $ZnO-ZnAl_2O_4$, strongly depended on the calcination temperature, attributed to the progressive formation of the active phase ZnO. These solids showed better behavior than pure ZnO and also than standard Degussa P25. The authors proposed that the crystallinity and good dispersion of ZnO on the surface of the solids were important factors in the catalytic performance.

The same authors (Elhalil et al., 2019) have used photocatalyst composites $Ag-ZnO-La_2O_2CO_3$ derived from hydrotalcites. The hydrotalcites were formed by the coprecipitation method, considering the ratios Zn/(Al+La) of 3 and La/Al of 0, 0.25, and 0.5. The pH was increased with Na_2CO_3/NaOH up to 8.5 when only Zn and Al formed the hydrotalcite and to 10 for the two samples containing La. The resulting hydrotalcites were calcined at 300°C, 400°C, 500°C, 600°C, 800°C, and 1000°C. The dried solids were composed of LDH and $LaCO_3OH$ phases, while ZnO, $ZnAl_2O_4$, $La_2O_2CO_3$, and $LaAlO_3$ were observed, in function of the temperature, in the calcined samples. Ag was deposited by a solvent-free ceramic process, grinding $AgNO_3$ and LDH in an agate mortar and then calcining them in air at 500°C for 6 h; 1%, 3%, and 5% Ag contents were considered. The solids were applied in the degradation of caffeine under a UV mercury lamp. The Ag-containing solids were much more active than undoped composites and also than reference ZnO and Degussa P-25 TiO_2. The best degradation result, 99.4% after 40 min of irradiation, was shown by the solids with La/Al = 0.25% and 5% Ag. The optimal catalyst dosage for the degradation of a 20 mg/L of caffeine solution was 0.3 g/L. The catalytic activity was mainly attributed to the interfacial heterostructure in the $Ag-ZnO-Al_2O_3$ surface and was observed to depend on the pH, 9.5 being the optimal value. The reusability was evaluated for the best catalyst, being excellent as it showed a degradation of 92.98% in the third cycle.

Yang et al. (2017) prepared a Zn/Fe hydrotalcite by the coprecipitation method, with molar ratio of Zn/Fe = 2.0. The anions should be nitrate and carbonate, as the nitrates were used as the source of the cations, and the pH was increased with NaOH, but no special precautions to avoid the carbonate incorporation were reported. The hydrotalcite was calcined at 550°C and 750°C to form the photocatalysts, denoted as Zn/Fe mixed metal oxide (Zn/Fe-MMO) nanocomposites by the authors, which were used for the degradation of the antibiotic tetracycline and also of the dye methylene blue, under visible-light irradiation. The catalysts were composed of wurtzite ZnO and spinel $ZnFe_2O_4$ phases. The hydrotalcite, not calcined, was also tested as catalyst, showing lower activity than the calcined composites. The degradation reached 90% after 60 min for the solid calcined at 700°C, following pseudo-first order kinetics. The improved catalytic performance of this solid was attributed to the visible-light adsorption and more production of photogenerated electron–hole pairs. Based on the trapping radical tests and ESR analysis, the authors suggested that the photodegradation occurred with the generation of active radicals ($\bullet O_2^-$ and •OH).

The preparation of ZnAl-chloride hydrotalcite (Zn/Al = 2) and its interaction with the antibiotics tetracycline and oxytetracycline was considered by Bouaziz et al. (2018). In this case, neither the hydrotalcite nor the oxides derived from its calcination were used for the degradation of the antibiotics, but the interaction between them was studied in a different way. First the antibiotic were intercalated into the interlayer of the hydrotalcite, and two methods were considered, the anionic exchange of the chloride anions of a previously prepared sample of the hydrotalcite by the antibiotics or the preparation of the hydrotalcite in the presence of the antibiotics, that is, having the antibiotics in the solution of the cations before increasing the pH for the coprecipitation process. Unfortunately, intercalation was not successful, and the antibiotics were located on the external surface of the hydrotalcite. The antibiotics were released after 10 h. The antibacterial activity of the solids was tested against *Escherichia coli* and *Staphylococcus epidermidis*, finding lower activity than for the free antibiotics. It is proposed that the

This book belongs to Central Library BADJI Mokhtar-ANNABA UNIVERSITY Copyright Elsevier 2024

antibiotics partially degraded in contact with the hydrotalcite. The degradation was confirmed under exposure of the solids to UV radiation or under storage at increasing temperatures (30°C, 60°C, and 120°C).

Zhu et al. (2018) prepared ZnFe carbonate hydrotalcite (Zn/Fe = 3) by the urea assisted coprecipitation. Composites graphene oxide/hydrotalcite were prepared by carrying out the hydrotalcite synthesis under the same conditions but in the presence of various amounts of graphene oxide, previously submitted to sonication for its delamination. The process was completed by hydrothermal treatment for 24 h at 120°C, centrifugation, drying, and calcination at 450°C under nitrogen atmosphere. The structure of well-crystallized hydrotalcite was observed in all the X-ray diffractograms. The calcined samples showed the presence of ZnO and $ZnFe_2O_4$. These composites were used toward the degradation of paracetamol under simulated solar light irradiation and exhibited a 3.5 times improved catalytic performance as compared with pristine ZnFe hydrotalcite sample. This behavior was attributed to the graphene oxide, which may increase pollutant adsorption capacity and enhance charge separation efficiency. These composites were also applied to the catalytic photooxidation of As(III) to As(V). Interestingly, paracetamol degradation was more efficient in the mixed system paracetamol/As(III) than in the single paracetamol system, while arsenic was also efficiently removed. The catalysts showed excellent reuse properties, showing a slight decrease of performance, 8.1%, after five successive experimental runs, with the advantage that can be easily separated and recovered by an external magnet.

5 Conclusions and perspectives

The presence of pharmaceutical compounds in natural water is an increasing problem as these compounds have environmental effects even at low concentrations. Hydrotalcite-like compounds, also known as layered double hydroxides (LDHs), although have been used as catalysts for the removal of some organic pollutants, have been very scarcely used for the photodegradation of pharmaceutical pollutants. The high versatility of these compounds in chemical composition, the easiness of their synthesis, and their good properties may strongly increase their use as photocatalysts in the next years.

Acknowledgments

The authors gratefully acknowledge the funding from the Spanish Ministry of Economy, Industry and Competitiveness (AEI/MINECO) and the European Regional Development Fund (ERDF) through project MAT2016-78863-C2-R. LS thanks Universidad Pública de Navarra for a predoctoral grant. AG also thanks Santander Bank for funding through the Research Intensification Program.

References

Bethi, B., Sonawane, S. H., Bhanvase, B. A., & Gumfekar, S. P. (2016). Nanomaterials-based advanced oxidation processes for wastewater treatment: A review. *Chemical Engineering and Processing*, *109*, 178–189.

Bouaziz, Z., Soussan, L., Janot, J. M., Jaber, M., Amara, A. B. H., & Balme, S. (2018). Dual role of layered double hydroxide nanocomposites on antibacterial activity and degradation of tetracycline and oxytetracyline. *Chemosphere*, *206*, 175–183.

This book belongs to Central Library BADJI Mokhtar-ANNABA UNIVERSITY Copyright Elsevier 2024

Deng, F., Zhao, X., Pei, X., Luo, X., Li, W., & Au, C. (2016). Sol-hydrothermal synthesis of inorganic-framework molecularly imprinted TiO_2 nanoparticle and its enhanced photocatalytic activity for degradation of target pollutant. *Science of Advanced Materials*, *8*, 1079–1085.

Di, G., Zhu, Z., Zhang, H., Zhu, J., Lu, H., Zhang, W., et al. (2017). Simultaneous removal of several pharmaceuticals and arsenic on Zn-Fe mixed metal oxides: Combination of photocatalysis and adsorption. *Chemical Engineering Journal*, *328*, 141–151.

Elhalil, A., Elmoubarki, R., Farnane, M., Machrouhi, A., Mahjoubi, F. Z., Sadiq, M., et al. (2019). Novel Ag-ZnO-$La_2O_2CO_3$ photocatalysts derived from the layered double hydroxide structure with excellent photocatalytic performance for the degradation of pharmaceutical compounds. *Journal of Science Advanced Materials and Devices*. https://doi.org/10.1016/j.jsamd.2019.01.002.

Elhalil, A., Elmoubarki, R., Machrouhi, A., Sadiq, M., Abdennouri, M., Qourzal, S., et al. (2017). Photocatalytic degradation of caffeine by ZnO-$ZnAl_2O_4$ nanoparticles derived from LDH structure. *Journal of Environmental Chemical Engineering*, *5*, 3719–3726.

Garrido-Ramírez, E. G., Theng, B. K. G., & Mora, M. L. (2010). Clays and oxide minerals as catalysts and nanocatalysts in Fenton-like reactions—A review. *Applied Clay Science*, *47*, 182–192.

Geissen, V., Mol, J. G. J., Klumpp, E., Umlauf, G., Nadal, M., van der Ploeg, M. J., et al. (2015). Emerging pollutants in the environment: A challenge for water resource management. *International Soil and Water Conservation Research*, *3*, 57–65.

Jacome-Acatitla, G., Tzompantzi, F., Lopez-Gonzalez, R., Garcia-Mendoza, C., Alvaro, J. M., & Gomez, R. (2014). Photodegradation of sodium naproxen and oxytetracycline hydrochloride in aqueous medium using as photocatalysts Mg-Al calcined hydrotalcites. *Journal of Photochemistry and Photobiology A: Chemistry*, *277*, 82–89.

Khenniche, L., & Aissani, F. (2010). Preparation and characterization of carbons from coffee residue: Adsorption of salicylic acid on the prepared carbons. *Journal of Chemical & Engineering Data*, *55*, 728–734.

Marti, E., Variatza, E., & Balcazar, J. L. (2014). The role of aquatic ecosystems as reservoirs of antibiotic resistance. *Trends in Microbiology*, *22*, 36–41.

Michael, I., Frontistis, Z., & Fatta-Kassinos, D. (2013). Removal of pharmaceuticals from environmentally relevant matrices by advanced oxidation processes (AOPs) (chapter 11). In M. Petrovic, D. Barcelo, & S. Pérez (Eds.), *Comprehensive Analytical Chemistry: Vol. 62. Analysis, Removal, Effects and Risk of Pharmaceuticals in the Water Cycle: Occurrence and Transformation in the Environment* (2nd ed., pp. 345–407): Elsevier

Miklos, D. B., Remy, C., Jeke, M., Linden, K. G., Drewes, J. E., & Hübner, U. (2018). Evaluation of advanced oxidation processes for water and wastewater treatment—A critical review. *Water Research*, *139*, 118–131.

Mishra, G., Dash, B., & Pandey, S. (2018). Layered double hydroxides: A brief review from fundamentals to application as evolving biomaterials. *Applied Clay Science*, *153*, 172–186.

Mohapatra, L., & Parida, K. (2016). A review on the recent progress, challenges and perspective of layered double hydroxides as promising photocatalysts. *Journal of Materials Chemistry A*, *4*, 10744–10766.

Nalawade, P., Aware, B., Kadam, V. J., & Hirlekar, R. S. (2009). Layered double hydroxides: A review. *Journal of Scientific and Industrial Research*, *68*, 267–272.

NORMAN. (2019). *NORMAN—Network of reference laboratories, research centres and related organisations for monitoring of emerging environmental substances*. *http://www.norman-network.net*.

Papoulis, D., Komarneni, S., Panagiotaras, D., Nikolopoulou, A., Li, H., Yin, S., et al. (2013). Palygorskite–TiO_2 nanocomposites: Part 1. Synthesis and characterization. *Applied Clay Science*, *83–84*, 191–197.

Park, H., Vecitis, C., & Hoffmann, M. R. (2009). Electrochemical water splitting coupled with organic compound oxidation: The role of active chlorine species. *Journal of Physical Chemistry C*, *113*, 7935–7945.

Praneeth, N. V. S., & Paria, S. (2017). Clay-semiconductor nanocomposites for photocatalytic applications (chapter 5). In T. K. Sen (Ed.), *Clay minerals: Properties, occurrence and uses* (pp. 143–184): Nova Science Publishers.

This book belongs to Central Library BADJI Mokhtar-ANNABA UNIVERSITY

Copyright Elsevier 2024

Qadir, M., Wichelns, D., Raschid-Sally, L., McCornick, P. G., Drechsel, P., Bahri, A., et al. (2010). The challenges of wastewater irrigation in developing countries. *Agricultural Water Management*, *97*, 561–568.

Ramírez, J. H., Vicente, M. A., & Madeira, M. (2010). Heterogeneous photo-Fenton oxidation with pillared clay-based catalysts for wastewater treatment: A review. *Applied Catalysis B: Environmental*, *98*, 10–26.

Rives, V. (Ed.), (2001). *Layered double hydroxides: Present and future*: Nova Science Publishers.

Rives, V., del Arco, M., & Martín, C. (2013). Layered double hydroxides as drug carriers and for controlled release of non-steroidal antiinflammatory drugs (NSAIDs): A review. *Journal of Controlled Release*, *169*, 28–39.

Rives, V., & Ulibarri, M. A. (1999). Layered double hydroxides (LDH) intercalated with metal coordination compounds and oxometalates. *Coordination Chemistry Reviews*, *181*, 61–120.

Williams, M. E., Hestekin, J. A., Smothers, C. N., & Bhattacharyya, D. (1999). Separation of organic pollutants by reverse osmosis and nanofiltration membranes: Mathematical models and experimental verification. *Industrial and Engineering Chemistry Research*, *38*, 3683–3695.

Yang, Q., Wang, S., Chen, F., Luo, K., Sun, J., Gong, C., et al. (2017). Enhanced visible-light-driven photocatalytic removal of refractory pollutants by Zn/Fe mixed metal oxide derived from layered double hydroxide. *Catalysis Communications*, *99*, 15–19.

Zhao, Y., Zhang, S., Li, B., Yan, H., He, S., Tian, L., et al. (2011). A family of visible-light responsive photocatalysts obtained by dispersing CrO_6 octahedra into a hydrotalcite matrix. *Chemistry—A European Journal*, *17*, 13175–13181.

Zhu, J., Zhu, Z., Zhang, H., Lu, H., Qiu, Y., Zhu, L., et al. (2016). Enhanced photocatalytic activity of Ce-doped Zn-Al multi-metal oxide composites derived from layered double hydroxide precursors. *Journal of Colloid and Interface Science*, *481*, 144–157.

Zhu, J., Zhu, Z., Zhang, H., Lu, H., Zhang, W., Qiu, Y., et al. (2018). Calcined layered double hydroxides/reduced graphene oxide composites with improved photocatalytic degradation of paracetamol and efficient oxidation-adsorption of as(III). *Applied Catalysis B: Environmental*, *225*, 550–562.

This book belongs to Central Library BADJI Mokhtar-ANNABA UNIVERSITY

Copyright Elsevier 2024

CHAPTER

Metal-organic frameworks for photocatalytic degradation of pollutants

6

Harpreet Kaur, Ajay Kumar, Rik Rani Koner, Venkata Krishnan

School of Basic Sciences, School of Engineering and Advanced Materials Research Center, Indian Institute of Technology Mandi, Mandi, India

1 Introduction

The wastewater generated from various industries (printing, textile, paper, plastic, etc.) and pharmaceutical effluents pollutes the water bodies and the ecosystem (Ho et al., 2012). Thus, the produced wastes from the industry as well as pharmacy have created serious threats to the human and aquatic life. The wastewaters produced in industrial processes generally contain nondegradable toxic organic compounds. Excessive accumulation of these waste organic compounds in the ecosystem has become one of the serious global environmental issues today. To balance the ecosystem and environment, complete degradation of these organic pollutants from the wastewater is of high importance and current interest in today's scenario (Shiying et al., 2009). There are a large number of organic pollutants that exist in wastewater, such as organic dyes, pesticides, fertilizers, plasticizers, hydrocarbons, oils, greases, carbohydrates, and proteins (Ali, Asim, & Khan, 2012). Most of these pollutants are highly toxic, quite stable, and potentially harmful to the environment. These pollutants once released into the water bodies can cause serious environmental problems such as it can adversely affect aquatic biota, clogging sewage treatment plants and increasing biochemical oxygen demand (Lin, Zhao, Hu, & Xing, 2014). Therefore, it is important to develop efficient and inexpensive technique to reduce the concentration of pollutants in wastewater before releasing them into other water bodies.

Different strategies have been adopted for complete removal of organic pollutants from wastewater. Generally, the traditional methods used for pollutant removal are classified into three categories: biological, chemical, and physical. The domestic and industrial wastewater can be treated by biological methods, which involve the aerobic and anaerobic processes (Olaopa, 2003). The chemical method involves either the adsorption or decomposition of the organic pollutants by oxidizing them using hydrogen peroxide or ozone (Kumar et al., 2018; Reddy, Kumar, Kumar, & Krishnan, 2019), whereas the physical processes include the removal of the suspended pollutants rather than dissolved pollutants. They allowed the suspended pollutants to settle down, thus helping in water purification. Chemical flocculation, ultrafiltration, and reverse osmosis are some other physical processes that are used to remove large and very fine unsettled particles (Tsai et al., 2007). In addition, the adsorption method is

Nano-Materials as Photocatalysts for Degradation of Environmental Pollutants. https://doi.org/10.1016/B978-0-12-818598-8.00006-7
© 2020 Elsevier Inc. All rights reserved.

This book belongs to Central Library BADJI Mokhtar-ANNABA UNIVERSITY

Copyright Elsevier 2024

well known for efficient removal of pollutants from wastewater (Chhabra, Kumar, Bahuguna, & Krishnan, 2019). This process can be categorized into two types: physical and chemical adsorption (Yenisoy-Karakaş, Aygün, Güneş, & Tahtasakal, 2004). The physical adsorption involves weak interactions, while chemical absorption method consists of very strong interactions between adsorbate and adsorbent. However, the adsorption process can be used only to separate the pollutants from wastewater. Also, these conventional wastewater treatment technologies (adsorption, membrane separation, and coagulation) suffer from very high operating expenses and also result in the formation of the secondary products (Snyder, Westerhoff, Yoon, & Sedlak, 2003). Sometimes, the secondary products thus formed are more hazardous than their primary products. To completely eliminate the secondary products, it is essential to degrade or destroy them into less toxic compounds or mineralize them to CO_2 and water molecules.

The advanced oxidation processes (AOPs) are composed of photocatalysis, ozonation, sonolysis, and Fenton reactions (Chakma, Das, & Moholkar, 2015; Parsons, 2004). These processes can degrade the organic pollutants effectively with high reproducibility in simpler way. AOPs include generation of very reactive oxidizing agents such as $OH^{\bullet}$, H_2O_2, O^{2-}, and O_3, which are responsible for the complete elimination of the organic pollutants from the wastewater. Under suitable reaction conditions, the complete mineralization of organic pollutants to CO_2 and H_2O is possible (Comninellis et al., 2008).

Heterogeneous photocatalysis is playing a crucial role for the degradation of organic pollutants by using semiconductor catalysts (Xiao, Xie, & Cao, 2015). Photocatalysis using the semiconducting materials, such as TiO_2, CdS, ZnO, ZnS, and Fe_2O_3, has gained a considerable attention by degrading a wide range of organic pollutants to less toxic or biodegradable organic compounds by using the natural solar light irradiations (Mrowetz & Selli, 2006). For wastewater treatment, the semiconductor photocatalysis has certain advantages such as low cost, ambient reaction conditions, and complete mineralization of the organic pollutant without leaving any secondary product. Kumar et al. have synthesized a semiconductor nanocomposite and utilize it for the degradation of various industrial pollutants (rhodamine B, thiabendazole, nitrobenzene, and tetracycline) under visible light irradiations (Kumar, Kumar, Kumar, Balaji, & Krishnan, 2018). The design and development of photocatalysts are also important for the efficient utilization of solar energy and thus for better photocatalytic activity (Kumar, Kumar, & Krishnan, 2019). A mechanistic pathway has been given to understand the secondary products obtained after fragmentation of the pollutants. In another study, a quaternary nanocomposite has been developed for the degradation of a pharmaceutical pollutant (ciprofloxacin), and the secondary products formed after degradation are identified by using mass spectrometry (Kumar, Reddy, et al., 2018). In addition, the complete mineralization of the organic pollutant with time is also monitored by UV–visible spectroscopy and total organic content (TOC) measurements. In the past two decades, a lot of work has been done on wastewater purification by degrading the organic pollutants using semiconducting materials (Kumar et al., 2016).

But still, there are certain drawbacks associated with the semiconductor photocatalysis:

(i) Some semiconductor photocatalysts are not stable under working conditions as these catalysts undergo photo corrosion while illuminated with light photons under aqueous media. Due to this reason, metal ion from the photocatalyst migrates into the aqueous solution, which ultimately results in dissolution of catalyst. Semiconductor photocatalysts, such as metal sulfides and some metal oxides are liable to photocorrosion (Wang et al., 2017; Zhang, Bosch, Gentle III, & Zhou, 2014).

This book belongs to Central Library BADJI Mokhtar-ANNABA UNIVERSITY
Copyright Elsevier 2024

(ii) The low separation efficiency of the semiconductor photocatalysts is also one of the major drawback associated with it. For example, the separation of some metal oxides, such as TiO_2, is very difficult (Pellegrino et al., 2017).

(iii) The very small particle size of the semiconductor photocatalyst leads to agglomeration because of its large surface area-to-volume ratio and high surface energy and thereby decreases the activity (Pellegrino et al., 2017).

Keeping in mind the aforementioned necessities, an efficient photocatalyst is required with improved properties.

In recent years, metal-organic frameworks (MOFs) have been emerged rapidly as a new class of porous inorganic-organic hybrid material (Das et al., 2011; Howarth et al., 2016; Wang, Li, Guo, & Wang, 2013). Yaghi et al. introduced the terminology "metal-organic framework" for the porous coordination polymers (MOFs) for the first time in 1995 (Yaghi, Li, & Li, 1995). Because of their 3D framework structures with porous nature along with free functional groups and due to several advantageous properties, MOFs are rising in demand day by day and are replacing other metal oxides and semiconductors.

In the recent decade, around 20,000 MOFs have been reported (Chong, Jin, Chow, & Saint, 2010). As MOFs are consist of variety of organic linkers and inorganic nodes, so structural possibilities are countless. The diversity in the coordination modes of organic linkers around inorganic metal ions and tunable properties has fueled the study of MOFs for a wide range of applications that include gas storage and separation, adsorption, catalysis, drug delivery, sensing, ion exchange, light harvesting and energy conversion, conductivity, and the removal of toxic chemicals from water and air (Eddaoudi et al., 2002; Farha et al., 2010; Lee et al., 2009; Murray, Dincă, & Long, 2009). The large surface area and porous nature, high stability, and reusability help MOFs to solve the issues that restrict the applications of other conventional photocatalysts and adsorbents used for wastewater treatment. For the removal of organic pollutants from wastewater, MOFs can be used for the adsorption and photocatalytic degradation process. Among the various applications of MOFs toward environmental remediation, the removal of organic pollutants by adsorption process has been explained in detail here. The mechanism involved in the process of adsorptive removal of organic pollutants is shown in Fig. 1 (Hasan & Jhung, 2015). The adsorption process mainly includes interactions starting from electrostatic, acid-base, and hydrophobic to hydrogen bonding. Although a large number of reports exist in literature for the removal of heavy metals from industry effluent wastewater, toxic gases, and other organic pollutants, however, the removal of these industrial contaminations (dyes) and agricultural pollutants (herbicides and pesticides) through adsorption process has not been explored much. An extensive range of catalytic studies have been reported recently for the removal of organic pollutants from wastewater through advanced oxidation processes (Fenton-based, photocatalysis, and $SO_4^{\bullet-}$-based oxidative systems) due to their simple use and reusability (Li, Xu, Ouyang, & Ye, 2016; Zhang & Lin, 2014). In the case of photocatalysis, two important mechanisms involved are ligand-to-metal charge transfer (LMCT) mechanism and absorption of incident photons and excitation of metal oxoclusters in MOFs when irradiated under UV or visible light (Wang, Wang, & Lin, 2012). MOFs behave as semiconductor materials when irradiated under light since organic linkers can absorb light and activate the metal sites through charge transition of LMCT.

In this process, photoinduced electrons and holes are generated, which then perform the heterogeneous photocatalysis. The low efficiency in the case of some of the MOFs is due to their UV light absorption ability and conduct reactions. It has been observed that the incorporation of amino group

This book belongs to Central Library BADJI Mokhtar-ANNABA UNIVERSITY Copyright Elsevier 2024

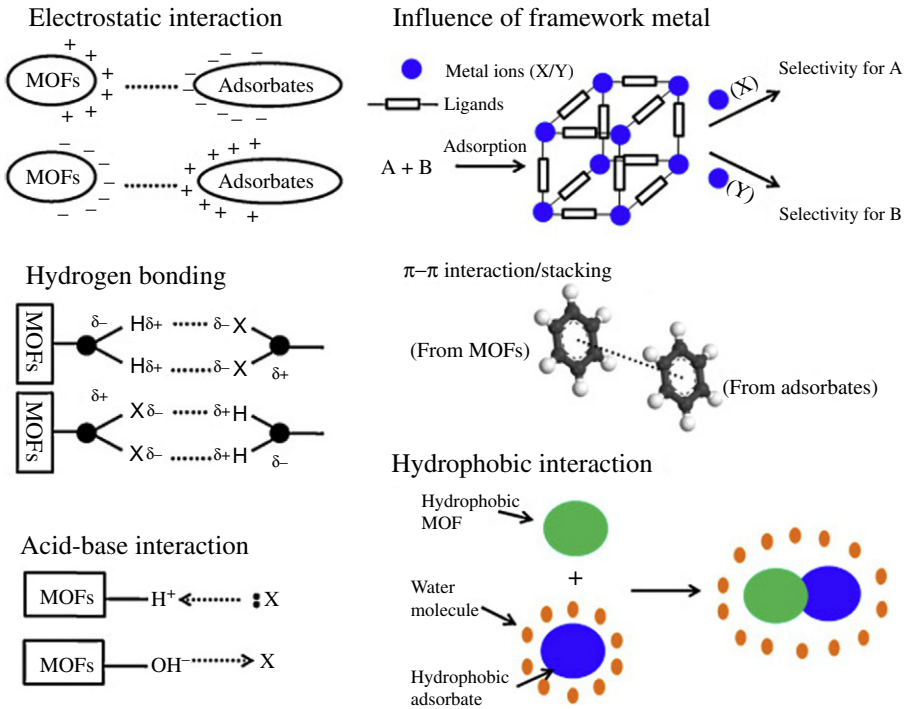

FIG. 1

Outline of various mechanisms involved in the adsorption of organic molecules on MOFs.

Reproduced from Hasan, Z., & Jhung, S. H. (2015). Removal of hazardous organics from water using metal-organic frameworks (MOFs): Plausible mechanisms for selective adsorptions. Journal of Hazardous Materials, 283, *329–339 with the permission of Elsevier publishers.*

onto the linker in the MOFs made the visible light active and hence more efficient toward photocatalytic degradation (Li et al., 2017; Lin, Kong, & Chen, 2016; Nguyen & Nguyen, 2014; Wang et al., 2012). Thus, it is possible to tune the properties of MOFs by functionalizing them and making them more efficient. Here, the entire aspects of MOFs as photocatalyst and research progress in the application area for the degradation of organic pollutants have been highlighted. In addition to this, the structural complexity, functional variation, and their impact on photocatalytic activity and future prospects has also been discussed.

2 Metal-organic frameworks: Design, synthesis strategies, and characterizations

Nearly all the MOFs are synthesized in laboratory conditions; therefore, the experimental research on MOFs begins with the rational design, selection, and synthesis of the organic linkers, which are considered as very much important and critical step. The synthesis of the MOFs emerges from two

This book belongs to Central Library BADJI Mokhtar-ANNABA UNIVERSITY Copyright Elsevier 2024

Table 1 Representations of the MOF structures, the corresponding metal node, and linker constituents.

MOF	Metal Node	Organic Linker
UiO-67	$Zr_6O_4(OH)_4$	BPDC
UiO-66	$Zr_6O_4(OH)_4$	BDC
PCN-600(M)	$Fe_3O(OH)_3$	M-TCPP
NU-1000	$Zr_6O_4(OH)_8(H_2O)_4$	TBAPy
Cr-MIL-101	$Cr_3O(OH)_3$	BDC
ZIF-8	Zn	MeIM
Mg-MOF-74	MgOH	$BDC\text{-}(OH)_2$
NU-125	Cu_2	LH_6
PCN-222(Fe)	$Zr_6O_4(OH)_8(H_2O)_4$	Fe-TCPP

Zr, *green;* Cr, *light purple;* Zn, *dark red;* Fe, *yellow;* Cu, *royal blue;* Mg, *blue;* C, *gray;* N, *light blue; O, red;* Cl, *pink. Reproduced from Howarth, A. J., Peters, A. W., Vermeulen, N. A., Wang, T. C., Hupp, J. T., & Farha, O. K. (2016). Best practices for the synthesis, activation, and characterization of metal–organic frameworks.* Chemistry of Materials, 29, *26–39 with the permission of ACS publishers.*

This book belongs to Central Library BADJI Mokhtar-ANNABA UNIVERSITY

Copyright Elsevier 2024

important branches of inorganic chemistry. It involves the solvothermal sol-gel method that corresponds to the use of minerals and reaction temperature above the boiling point of the solvent in closed reaction vessels. The other method comprises the clear solution of the reactants that upon mild heating or aging turns into the formation of MOFs.

2.1 Design considerations

MOFs are a class of porous materials with modular structure (Jiang, Zhao, & Yaghi, 2016). The development of MOFs involves assembly of two components including metal ion nodes or clusters, which are also known as "secondary building units (SBU)" and organic linkers. The structure of the MOFs can be tuned with the variation of SBU and organic linkers (Butova, Soldatov, Guda, Lomachenko, & Lamberti, 2016). The combination of different organic linkers with same SBU results in a large number of possible structures and thus different MOFs with tailored properties (Lin, Adhikari, Ku, Chiang, & Kuo, 2012). For example, HKUST-1 and MOF-5, the two much known MOFs, are synthesized using SBU and organic linkers: benzenetricarboxylate (BTC) and benzenedicarboxylate (BDC), respectively. The organic linkers are usually polytopic linkers, such as phosphonates, sulfates, carboxylates, azole, and heterocyclic compounds (Sharmin & Zafar, 2016). Some of the most commonly used SBUs (metal nodes) and organic linkers used for the formulation of MOFs are represented in Table 1. The successful design of rigid frameworks using such SBUs was first time demonstrated in MOF-5. The design principle engaged in MOF-5 has been discussed here to show that SBUs have inherent geometric properties that ease network design and help to tackle the issues of network synthesis in MOF-5. In this MOF, $Zn_4O(CO_2)_6$ units containing four ZnO_4 tetrahedra with six carboxylate C atoms define an octahedral SBU joined together by benzene links and a common vertex. This results in a cubic network where the vertices are the octahedral SBUs and the benzene struts are at the edges. Apart from this, a number of other examples are represented in Table 1 including Zr-based MOFs where $Zr_6O_4(OH)_4$ acts as SBU and along with different linkers results in different MOFs.

As there is a huge extent of variability of both organic linkers and SBUs, there is a possibility that a vast number of MOFs could be designed and synthesized. However, this makes it very difficult for researchers to focus on a rational way to design and synthesize MOFs with properties for specific use. In fact, the targeted syntheses of MOFs with specified properties and desired framework porosity have been very challenging. Thus, the rational design of novel MOFs is highly desirable in which the basic constructional units can depict the properties before the synthesis of the framework (Zhang et al., 2014). The purpose behind the rational design of the MOFs is to accomplish precise control of the framework functionality and porosity. Though it seems challenging, researchers have been trying for the solutions to overcome all these difficulties and are very close to achieve this goal due to convenient functionalizations and tunable nature of MOFs.

The synthesis of a Zr-based MOF (UiO-67) using the conventional approach involves the use of modulators benzoic acid and hydrochloric acid (Table 1). Although both the modulators result in compounds with same topology and were designated as UiO-67, both the compounds are not identical. The use of benzoic acid modulator typically results in an ideal structure comprising Zr_6 nodes of the framework connected to 12 structural linkers, whereas the process of using modulator hydrochloric acid ended into a defective structure in which some structural linkers are missing, thus forming defects sites (i.e., nodes concluded by hydroxyl or chloride ligands). A number of conventional MOF syntheses include the formation of metal clusters (nodes) or secondary building units (SBUs). For example, Férey

This book belongs to Central Library BADJI Mokhtar-ANNABA UNIVERSITY Copyright Elsevier 2024

et al. reported that replacing $ZrCl_4$ with a Zr_6 −methacrylate cluster $[Zr_6O_4(OH)_4(OMc)_{12}]$ (where OMc = methacrylate) can be an alternative route for the synthesis of UiO-66 and its derivatives (Table 1) (Abbasi, Geranmayeh, Skripkin, & Eriksson, 2012; Guillerm et al., 2010; Mondloch et al., 2013; Shearer et al., 2016).

2.2 Synthesis strategies

Normally, the synthesis of MOFs includes solvent and temperature with range from room temperature to 250°C (Sun & Zhou, 2015). The energy required for the reaction to take place is provided through conventional heating, that is, heat is transferred from heating source such as convection oven. Apart from this, other ways of providing energy include heat creators, which include electrochemical radiations, ultrasound, microwave assisted, and mechanical and electric potential. The energy source provided is strongly related to the parameters, like reaction pressure, duration, and energy per molecule in the system. All these parameters strongly influence the structural topology of the product. The synthesis of MOFs is composed of commonly used different approaches and synthetic conditions as shown in Fig. 2.

2.2.1 Conventional synthesis

The most commonly employed method is conventional synthesis (Farha & Hupp, 2010). In conventional synthesis, reaction temperature is one of the main parameters. The conventional method involves the reaction in liquid phase by mixing metal salt, organic ligands, and solvent for certain period of time.

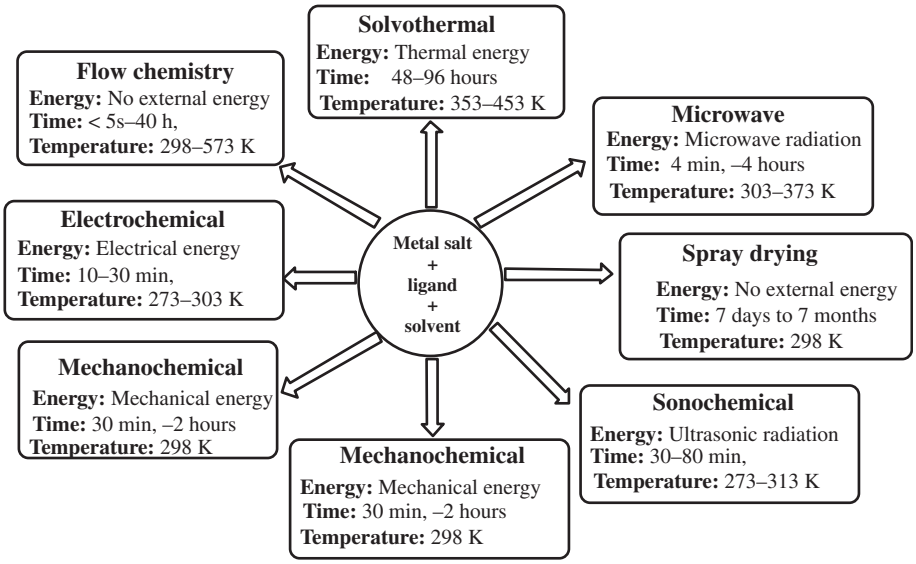

FIG. 2

Most common synthesis approach and conditions used for MOF synthesis.

Reproduced from Olajire, A. A. (2018). Synthesis chemistry of metal-organic frameworks for CO 2 capture and conversion for sustainable energy future. Renewable and Sustainable Energy Reviews, 92, *570–607 with the permission of Elsevier publishers.*

This book belongs to Central Library BADJI Mokhtar-ANNABA UNIVERSITY Copyright Elsevier 2024

Conventional method can further be divided into two categories: solvothermal and nonsolvothermal depending upon the reaction setup used. The solvothermal/hydrothermal method is the most commonly employed strategy for the synthesis of MOFs, and it involves the reaction in autoclave (closed vessel) at a controlled temperature. In solvothermal reactions, the high-solubility organic solvents are generally used, which includes dimethylformamide (DMF), dimethylamide (DMA), ethanol (EtOH), and methanol (MeOH) (Bedia et al., 2019). The mixture of solvents can also be used if there is solubility problem of reactants. Solvothermal reactions usually take place at different temperatures ranging from 60°C to 200°C. Here, the glass vials can be used if the reactions are performed at 80°C, whereas Teflon lined autoclave setups are required for high-temperature reaction (above 100°C) (Farha & Hupp, 2010).

Nonsolvothermal synthesis method involves the reaction below or at the boiling point under ambient pressure. Nonsolvothermal method further divided into two types either at elevated temperature or at room temperature. Conventional synthesis also comprises various methods, such as layering, evaporation, and slow diffusion method. All these lead to concentration gradient that results in the formation of MOFs. Temperature variation can also lead to concentration gradient, like slow cooling of reaction mixture. Even in some cases, mixing of starting materials simply forms MOFs at room temperature. Different approaches have also been utilized to synthesize MOFs using water as solvent as it is environment-friendly and inexpensive. So, a number of reports exist in literature where the concern about the Green synthesis has been discussed (Reinsch, 2016; Unterlass, 2016). In some cases, these types of reactions require longer time for the crystallization than conventional approaches.

However, to improve the crystallization and to accelerate the reaction, a number of other synthetic routes have been employed. These involve mechanochemical, electrochemical, sonochemical, and microwave-assisted routes of synthesis (Bedia et al., 2019). These synthesis methods lead to the formation of crystals with high quality in shorter time period. Apart from temperature, another important factor in liquid-phase reactions that affects the crystallization is the choice of solvents. The choice of solvent depends upon various factors like solubility, stability, redox potential, and reactivity. Moreover, the synthesis of MOFs in solid state has also been focused in various reports.

2.2.2 Microwave-assisted synthesis

Microwave-assisted (MW) synthesis describes a method for rapid synthesis of MOFs that allows the synthesis to be completed in just few minutes (Liang & D'Alessandro, 2013; Ni & Masel, 2006). This type of synthesis procedure has been used to produce metal and oxide particles involving heating of a solution with microwaves for a period of about an hour only. This synthetic approach have been used to prepare high-quality crystalline MOFs within a few minutes and has been named as "microwave-assisted solvothermal synthesis" (Klinowski, Paz, Silva, & Rocha, 2011). The crystals produced by this synthetic approach exhibit the same properties as that of crystals obtained by standard solvothermal process, except the point that synthesis is much more rapid in microwave-assisted process. MOFs synthesized by this process have been mainly focused on the following: to produce nanoscale product and to accelerate the crystallization for the selective synthesis of polymorphs. MW-assisted synthesis procedure has been used to synthesize several metal (Zhang et al., 2014) carboxylate-based MOFs (M = Cr, Fe, Zn, Ni, Mg, Al, V, and Ce) (Liu et al., 2008; Liu, Tsao, Zhang, & Lin, 2009; Wang, Zhang, Huang, Zhang, & Chen, 2008). The first MW synthesis of MOFs dealt with Cr-MIL-100 (Jhung, Lee, & Chang, 2005).

This book belongs to Central Library BADJI Mokhtar-ANNABA UNIVERSITY Copyright Elsevier 2024

2.2.3 Electrochemical synthesis

The first ever electrochemical synthesis of MOFs was reported by BASF in 2005 (Mueller, Puetter, Hesse, & Wessel, 2007). The motive to this synthetic method was to exclude the anionic part of the reaction mixture such as nitrates, perchlorates, or chlorides that is the main concern during the large-scale synthesis of MOFs. Instead of metal salts, this method includes the continuous introduction of metal ion through anodic dissolution into the synthesis mixture that contains electrolytes and dissolved organic linkers. This method provides a better way to produce thin films of MOFs over the surface at mild temperature conditions, thus reducing the cracking of films being observed in other synthesis methods (Martinez Joaristi, Juan-Alcañiz, Serra-Crespo, Kapteijn, & Gascon, 2012). The electrode is located in a solution containing an electrolyte and mixed organic linkers. Upon applying suitable voltage/current, metal dissolves and forms metal ions near the electrode surface that are required for the MOF's synthesis. The metal ions thus formed react immediately with the organic linkers present, and the formation of MOFs takes place on the electrode surface. Thus, in this method, there is no need of metal salts unlike other synthesis methods, and metal ions are provided by the oxidation of the electrolytes. Another advantage of this synthesis process is the possibility to run a continuous process and large-scale production at industrial scale that is not possible through other normal batch reactions. Till date, a number of microcrystalline powders and films have been reported using electrochemical synthesis process that includes a number of Zn- and Cu-based MOFs. $[Zn(MIm)_2]$, $[Zn(BIm)_2]$, and HKUST-1 are the most common MOFs synthesized using this electrochemical process (Schlesinger, Schulze, Hietschold, & Mehring, 2010; Yilmaz, Trukhan, & Mueller, 2012). Apart from this, the formation of films and patterned coating of HKUST-1 has also been reported.

2.2.4 Mechanochemical synthesis

The process of performing a chemical reaction by applying mechanical force is termed as mechanochemistry. Mechanochemical synthesis implies for solvent-free synthesis method of MOFs (Pichon, Lazuen-Garay, & James, 2006). Mechanochemical synthesis involves the breakage of intramolecular bonds followed by chemical transformation. Mechanochemical routes imply to the construction of bonds through simple, economical, and environment-friendly ways and have been of great interest in synthetic chemistry for a long time (Klimakow, Klobes, Thünemann, Rademann, & Emmerling, 2010). It has recently been employed in multicomponent reaction systems to form pharmaceutically active cocrystals, solid-state inorganic products, and polymer (Garay, Pichon, & James, 2007; Kaupp, 2009). The use of mechanochemical method for the synthesis of MOFs was first reported in 2006. The reasons behind the interest of mechanochemical synthesis of MOFs are multiple, which include environment-friendly synthesis at room temperature and solvent-free condition. Thus, the use of organic solvents can be avoided through this synthesis route, and reactions can be completed within 10–60 min, which results in quantitative yields. In some cases, metal salts can be replaced by metal oxides, which omit the production of anions as side products, and the only side product left is water. The first report on mechanochemical synthesis includes the solvent-free grinding of isonicotinic acid (INA) and $Cu(OAc)_2{\cdot}3H_2O$ (Pichon et al., 2006). The starting materials were treated for 10 min in a 20-mL steel reactor having a steel ball. This results in the formation of single phase and highly crystalline product of $[Cu(INA)_2]$ (Krishnakumar & Swaminathan, 2011) with water and acetic acid as guest molecules in the pores (Pichon et al., 2006). The guest molecules can be removed by thermal activation of the compound, and thus, solvent-free porous compound can be obtained. To initiate the reaction, only grinding was required; sample grounded for 1 min results in single-phase product in the course of 6 h as verified

This book belongs to Central Library BADJI Mokhtar-ANNABA UNIVERSITY Copyright Elsevier 2024

by powder X-ray diffraction (PXRD). A large number of other crystalline products were also obtained by using this solvent-free mechanochemical synthesis with metal ions Ni, Cu, and Zn and various others (Klimakow et al., 2010; Yang, Orefuwa, & Goudy, 2011).

2.2.5 Sonochemical synthesis

Sonochemistry refers to a phenomena in which molecules undergo chemical change upon implying high-energy ultrasound radiations (20 kHz–10 MHz) (Bang & Suslick, 2010; Mason & Peters, 2002). Ultrasound is a cyclic mechanical vibration that induces physical and chemical changes due to the formation of cavities that involves the formation, growth, and instant collapse of small bubble in the liquid phase, and it creates local hot spots for a short duration with high pressure and temperature. The intense conditions can trigger chemical reactions by immediately forming excess of crystalline nuclei and reduce the crystallization time. Sonochemical method can produce homogeneous nucleation centers and reduces the crystallization time considerably as compared with conventional hydrothermal synthesis. A number of parameters play an important role in this synthesis method like temperature, choice of liquid (depending on vapor pressure, chemical reactivity, and viscosity), and gas atmosphere. Volatile organic solvents are not preferred for the sonochemical synthesis because of the high pressure that reduces the cavitational collapse intensity. A number of MOFs have been synthesized using this method involving MOF-5, which was synthesized using sonochemical irradiation in 1-methyl-2-pyrrolidinone (NMP) and produces crystals of size 5–25 mm in just 30 min (Son, Kim, Kim, & Ahn, 2008). The structure MOF was the same when it was synthesized by microwave or solvothermal methods.

Other methods involve slow evaporation method, which is a conventional method for preparing MOFs and does not need any external energy source (Yoo, Varela-Guerrero, & Jeong, 2011). Although this method is preferred as this is a room-temperature process, the main drawback associated with this method is that it takes long time for the crystallization compared with other conventional methods. In this method, the initial reaction mixture is concentrated progressively by the slow evaporation of the solvent at a particular temperature, which is mostly room temperature. In some cases, a mixture of solvents is also used to increase the solubility of starting materials and to fasten up the evaporation of low-boiling solvents. Apart from this, the other few methods are diffusion method (Bian, Xiong, & Zhu, 2018), ionothermal method (Parnham & Morris, 2007), and spray-drying methods (Rubio-Martinez et al., 2017), which can also be employed for the MOF synthesis. These methods are less analyzed and are not used commonly.

2.3 Characterizations

The resulting MOFs that are being synthesized by various methods should be characterized properly using physiochemical techniques for determining their structural and other physical properties. From the photocatalysis point of view to use the MOFs, it is also important to determine its textural and structural properties while determining its electronic and photophysical properties. The various techniques required to determine all the aforementioned properties of MOFs include X-ray diffraction analyses (both single-crystal and powder X-ray diffraction), thermogravimetric analysis (TGA), light absorption properties (DRS), gas adsorption studies (BET), morphological studies (scanning electron microscopy and transmission electron microscopy), and surface charge analysis (zeta potential). These techniques are used extensively to characterize the MOFs and are described in the succeeding text.

This book belongs to Central Library BADJI Mokhtar-ANNABA UNIVERSITY Copyright Elsevier 2024

2.3.1 Powder X-ray diffraction

The high-resolution powder X-ray diffraction (PXRD) is the most commonly used technique to determine the crystallinity and structural parameters of MOFs in the bulk phase (Qin, Wang, & Wang, 2017), even though high-resolution crystal determination of MOFs is preferred to be determined by the traditional single-crystal X-ray diffraction (SCXRD). But for SCXRD measurements, uniform and undamaged crystals are required, which are rarely available than the microcrystalline ones. The obtained diffractogram from PXRD for the synthesized MOF can be compared either with the simulated pattern obtained from the single-crystal XRD or with the previous reports in literature included in database or through computational modeling. Using this technique, one can possibly identify the different polymorphic forms and crystalline structure, can differentiate between crystalline and amorphous materials, and also can determine the percentage crystallinity of the materials. After identifying the crystalline nature of the materials, one can find out the crystallographic parameters like unit cell, phases, crystallite size, and lattice parameters. After identifying the diffraction peaks, crystallite size can be found out by using the Scherrer equation (Holland & Redfern, 1997):

$$D = \frac{K \cdot \lambda}{\beta \cdot \mathrm{Cos}\,\theta}$$

Here, D is the crystallite size, K is the size factor (having value in between 0.84 and 0.98 depending on the equipment), β is the full width at half maximum height of the peak (FWHM), and θ is the Bragg's angle for the identified peak in the diffraction pattern. Apart from this, the same technique is also used to determine the stability of MOFs in the case of photocatalytic applications. In this case, the used MOF is recovered after the photocatalytic process from the reaction mixture, washed thoroughly, and dried. Its recorded diffraction pattern is then compared with that of the pristine MOF to check the change in structural property that proves the stability of the MOF structure (West, 2014). The X-ray absorption fine structure (XAFS) spectroscopy provides the information about valence state, energy band width, and the interatomic distances (Lee, Citrin, Eisenberger, & Kincaid, 1981). For example, Liang et al. synthesized In-based MOF using $In(NO_3)\cdot xH_2O$ and 1,4-benzenedicarboxylic acid, and it was assigned the name MIL-68(In) (Liang et al., 2015). The powder X-ray diffraction patterns of this synthesized MOF along with the simulated pattern extracted from single-crystal data are shown in Fig. 3A. It can be seen that the PXRD pattern of MIL-68(In) matches well with that of the simulated pattern, which means the MOF retains its crystalline structure to a good extent even in the bulk phase also. Apart from this, the amino-functionalized MIL-68(In) was also synthesized, and its PXRD pattern is also shown in Fig. 3A.

2.3.2 Single-crystal X-ray diffraction

Single-crystal X-ray diffraction (SCXRD) is considered to be the ultimate technique for structure determination of the crystalline materials (Volkringer et al., 2009). This technique has become readily accessible and is accompanied by the enormous improvements in the instrumentation. The recent developments and advancements in the instrument allow the single-crystal data collection to be performed routinely in the various laboratories within just few hours, even for the microsized crystals (Eddaoudi et al., 2002). The successful diffraction of a crystal sample entirely depends upon the quality of the crystal, so it is important to optimize the crystal growth process. There are very few reports that mainly focus on the optimization of the crystal growing process and aiming to obtain the large single

This book belongs to Central Library BADJI Mokhtar-ANNABA UNIVERSITY Copyright Elsevier 2024

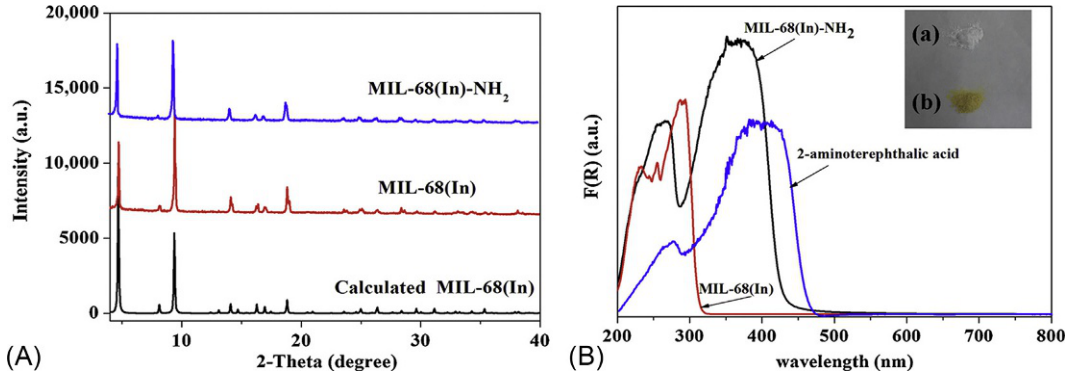

FIG. 3

(A) Powder X-ray diffraction patterns of simulated MIL-68(In), MIL-68(In), and MIL-68(In)-NH2;
(B) UV–vis DRS spectra of 2-aminoterephthalic acid, MIL-68(In), and MIL-68(In)-NH2. The inset images are of (A) MIL-68(In) and (B) MIL-68(In)-NH2.

Reproduced from Liang, R., Shen, L., Jing, F., Wu, W., Qin, N., Lin, R., & Wu, L. (2015). NH_2-mediated indium metal–organic framework as a novel visible-light-driven photocatalyst for reduction of the aqueous Cr (VI). Applied Catalysis B: Environmental, 162, *245–251 with the permission of Elsevier publishers.*

crystals of MOFs. Thus, there is need to optimize the synthetic conditions not only to obtain the desired phases but also to control the kinetics of the crystallization to improve the crystal quality and size. The introduction of small changes in the synthesis condition not only influences the crystallization but also results in emergence of other polymorphic phases. The structure obtained from the single crystal diffraction not only gives information about the asymmetric unit of the crystal but the presence of the guest solvent molecules can also be determined (Chae et al., 2004). The combined computational and experimental studies are being used extensively for the identification of the driving forces in the formation of the different crystal phases during the solvothermal synthesis of the MOFs. Kettner et al. reported a series of MOFs [M(tdc)(bpy)] with metal ions Zn, Cd, and Co and organic linkers tdc^{2-} = 2,5-thiophenedicarboxylate and bpy = 4.4′-bipyridine (Kettner et al., 2013). The structural unit of [Zn(tdc)(bpy)] is shown in Fig. 4. As shown in Fig. 4A, the carboxylate group of tdc^{2-} coordinated to metal ion using two different modes. In one case, both oxygen atoms of one carboxylic group of each tdc^{2-} moiety bind to different metal ion (μ^2-η^1:η^1), whereas the other carboxylic group behaves as a monodentate ligand (μ^1-η^1 or μ^1-η^2). This connectivity resulted in an extended planar 2D network as it leads to double nuclear motif of the metal ions. The M(tdc) planes are furthermore connected through the bpy (bridging ligands) and thus form a 3D network as shown in Fig. 4A.

2.3.3 Thermogravimetric analysis

Thermogravimetric analysis (TGA) is used extensively to measure the weight loss of a material as a function of the temperature. This technique is very useful in the determination of the thermal stability of the MOFs (Kaur, Kumar, Kumar, Krishnan, & Koner, 2019) and also helps to estimate the solvent accessed into the pore volume. Different carrier gases (N_2, O_2, or air) are used during the TGA analysis, and the product obtained after the decomposition of MOFs depends on these carrier gases used during analysis. The TGA curve represents the percentage weight loss of the MOF with temperature. From this

This book belongs to Central Library BADJI Mokhtar-ANNABA UNIVERSITY Copyright Elsevier 2024

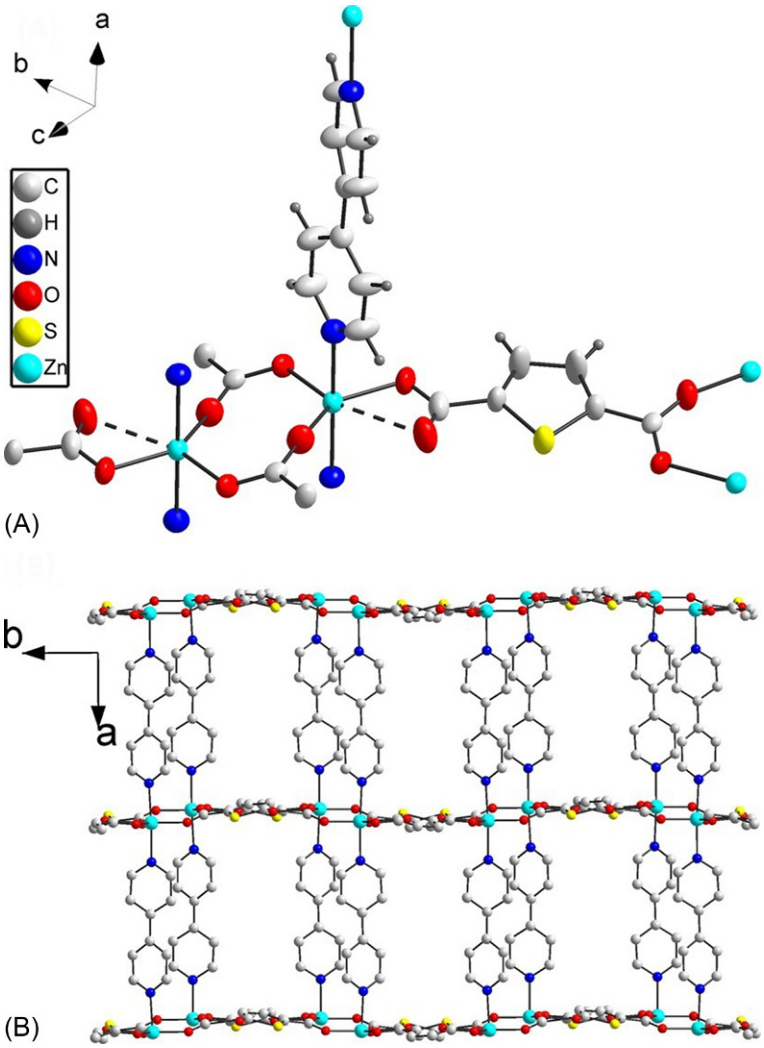

FIG. 4

(A) Structural unit of [M(tdc)(bpy)] for M = Zn^{2+}, tdc^{2-} = 2,5-thiophenedicarboxylate, and bpy = 4,4′-bipyridine (50% ellipsoids); (B) Overview of a single net of [M(tdc)(bpy)] with view along the crystallographic c-axis.

Reproduced from Kettner, F., Worch, C., Moellmer, J., Gläser, R., Staudt, R., & Krautscheid, H. (2013). Synthesis, crystal structure and catalytic behavior of Homo-and heteronuclear coordination polymers [M (tdc)(bpy)](M2+= Fe2+, Co2+, Zn2+, Cd2+; tdc2–= 2, 5-thiophenedicarboxylate). Inorganic Chemistry, 52, *8738–8742 with the permission of ACS publishers.*

TGA plot, the first weight loss in the region of 50–200°C depicts the removal of the solvent molecules, whereas the next weight loss in the temperature range of 300–600°C corresponds to the decomposition of the entire framework of MOFs and leftover corresponds to the metal oxides. To verify the structural changes upon the heat treatment process at various temperature, the XRD can be performed (Brunauer,

This book belongs to Central Library BADJI Mokhtar-ANNABA UNIVERSITY Copyright Elsevier 2024

Emmett, & Teller, 1938). In the TGA measurements of a series of MOFs [M(tdc)(bpy)] where M = Zn^{2+}, Cd^{2+} and Co^{2+}, a slight weight loss was observed in all the cases which can be assigned to the evaporation of the solvent molecules from the pores (Kettner et al., 2013).

2.3.4 Ultraviolet–visible diffuse reflectance spectroscopy

UV–vis diffuse reflectance spectroscopy (DRS) is used to determine the optical properties of the MOFs providing the wavelength range in which semiconductors absorbs the light; thus, this technique can be used to characterize the bandgap of the material. An absorption spectrum is recorded using this technique in the wavelength range of 200–800 nm appearing in the absorption band. Depending upon their compositions, MOFs can behave either as an inorganic semiconductor, organic, or both; thus, they represent an interesting type of semiconductors. When an inorganic semiconductor is excited by light of suitable energy, the electrons from valence band (VB) move to the conduction band (CB) leaving behind the holes in the VB; thus, there is formation of electron-hole pairs at the surface of the semiconductor. The similar type of mechanism is followed by the organic semiconductors except the point that, in the case of organic semiconductors, the electronic excitation is in between the highest occupied molecular orbital (HOMO) and lowest unoccupied molecular orbital (LUMO) of an organic compound (Sing, 2001). Since MOFs are the organometallic compounds consisting of metal oxoclusters and organic ligands, upon excitation by light of suitable energy, the electron transition occurs either between the VB and CB of the metal oxocluster and/or between the HOMO-LUMO of the organic ligands. Thus, the absorption spectrum can consist of several bands depending on the constituents, which will promote the electronic transition. To determine the bandgap energy (Pellegrino et al., 2017) of the material, Tauc plot approximation is used (Horiuchi et al., 2012; Tauc, 1970), which determines the value of E_g by using the following equation:

$$\alpha h\nu = A\left(h\nu - E_g\right)^{1/n}$$

where α is the absorption coefficient, h is Planck's constant, ν is the radiation frequency, E_g is the bandgap energy, and A is the constant. The value of n depends on the semiconductor type, being equal to 2 for indirect semiconductors and 0.5 for direct semiconductors. From this equation, one can plot $(\alpha h\nu)^{1/2}$ versus $h\nu$, which represents the Tauc plot. The plot with $n = 0.5$ shows a linear Tauc region just above the optical absorption edge, whereas $n = 2$ shows the Tauc region for the indirect semiconductors. On extrapolating this line to the photon energy axis, it yields the bandgap of the semiconductor that shows the efficiency of light harvesting when illuminated under light. For example, the UV–vis DRS spectra of MIL-68(In) and MIL-68(In)-NH_2 are shown in Fig. 3B in the previous text, and it reveals the semiconductor properties. The characteristic absorption peak at 360–380 nm in 2-aminoterephthalic acid (ATA) and MIL-68(In)-NH_2 can be attributed to the n–π* transition of the lone pair of electrons of the amino group in ATA (Kurihara & Nishihara, 2002). On the other hand, a blue shift of the absorption bands was found in the case of MIL-68(In)-NH_2 (360 nm) as compared with that in free ligand (390 nm) that could be ascribed to the transition perturbations by the metal center in the MOFs (Yam, Ko, & Zhu, 2004). MIL-68(In)-NH_2 shows an absorption edge at 440 nm, which corresponding to a bandgap of 2.82 eV, whereas the bandgap of MIL-68(In) comes out to be of 3.88 eV. These results also indicates that the shifting of absorption edge to the visible region in the case of MIL-68(In) by introducing the amino group (NH_2) to the organic linker is further confirmed by the color change from white to yellow (inset in Fig. 3B).

This book belongs to Central Library BADJI Mokhtar-ANNABA UNIVERSITY
Copyright Elsevier 2024

2.3.5 Nitrogen adsorption-desorption isotherms

The surface area analysis is one of the most widely used technique to characterize the porous materials using gas adsorption isotherms (Sing, 1985). The gas adsorption measurements are extensively used to determine the pore size distribution and surface area of different type of solid materials (Barrett, Joyner, & Halenda, 1951). This technique is used in the case of MOFs to characterize the textural parameters such as pore volume, surface area, average pore size, and pore size distribution. This technique is used to study the nitrogen adsorption over the surface of the material at the boiling temperature of the liquid nitrogen, that is, −196°C which results in an adsorption isotherm. The information about the homogeneity of the solid material can be obtained from the shape of the obtained isotherm (Alp, Mini, & Ramanathan, 1990). Earlier, the International Union of Pure and Applied Chemistry (IUPAC) classified the physisorption isotherms into six types (Thommes, 2010). Later on, each one of type I and IV was further classified into two subtypes by Thomas et al. (Sing, 1985). Similarly, six types of hysteresis loops were defined that gives information about the adsorption mechanism and pore structure (Sing, 1985). MOFs are a new class of porous crystalline materials having porosity and high surface area up to $7140\,m^2\,g^{-1}$, with most of the microporous MOFs describe type I isotherm (Farha et al., 2012). For N_2 adsorption/desorption isotherm studies, proper vacuum drying of MOFs is required. In some cases, pretreatment results in the reduction of surface area due to framework collapse. The reason behind this collapse can be attributed to the capillary forces and high surface stress that occurs in the interphase between confined solvent molecules and gas (Howarth et al., 2016). The Brunauer-Emmett-Teller (BET) is the most widely used approach to calculate the surface area of MOFs from nitrogen adsorption isotherms (Mondloch et al., 2014). It was derived originally for multilayer gas adsorption for flat surfaces, so special attention must be paid with highly porous 3D MOF frameworks. In some of the cases of MOFs, the adsorption occurs through a pore-filling mechanism instead of layer formation. Thus, it was doubtful whether the BET surface area numbers reported for certain MOFs were true or not. So, there was a need of critical test of the BET method to give the standard practices of reporting BET surface areas for porous materials. In this regard, grand canonical Monte Carlo simulations were used to see the nitrogen adsorption isotherms for a series of MOFs. These predicted isotherms were applied as pseudoexperimental data to check the applicability of the BET theory for obtaining the surface area for microporous MOFs. The surface area calculated from the crystal structure directly in a geometric fashion matches well with the BET surface area calculated from the simulated isotherms, which synchronize very well with the literature reports. So, all these results are in agreement for the strong validation of the BET theory, and it can be used to calculate the surface areas of the MOFs.

The t-plot method is used to determine the presence of micropores, as it compares the adsorption isotherm data of a nonporous material and that of porous sample (Howarth et al., 2016). The MOFs are classified into three types depending on their pore size according to IUPAC:

1. Pores with width $> 50\,nm$ are classified as macropores.
2. Pores with width in between 2 and 50 nm are classified as mesopores.
3. Pores with width $< 2\,nm$ are classified as micropores.

Thus, for the calculation of apparent surface area, the best practice is to use BET theory since the pore sizes of most of MOFs supports multilayer gas adsorption. Moreover, the surface area calculations also help in explaining the reason for the higher efficiency of MOFs with large surface areas.

This book belongs to Central Library BADJI Mokhtar-ANNABA UNIVERSITY
Copyright Elsevier 2024

2.3.6 Electron microscopy

Other basic technique for the characterization of MOFs includes scanning electron microscope (SEM) and transmission electron microscopy (TEM). SEM is used widely to characterize the surface morphology of MOFs, as it provides information about the morphology of the materials. SEM produces a beam of incident electron in an electron column above the sample chamber. The source of electron beam is thermal emission source that can be either a tungsten filament or field emission cathode. It generates high-resolution 2D images that display the shape of the material and its spatial variations that reveals the information about the external morphology, mixture of phases, and dispersion. MOFs upon being characterized give rise to different kind of morphologies such as rod shape, cubic, and rhombohedral. Sometimes, if the sample under analyses is insulating in nature, then, charging effect takes place on insulating material that affects the imaging. Depending upon the insulating nature of the MOFs and type of the SEM equipment used, the SEM characterization may require a pretreatment by coating the surface of the nonconducting material with some conducting material, usually gold (Brunauer et al., 1938). The coating can be done from 2 to 10 nm according to the need and nature of the sample being analyzed. To avoid this pretreatment, researchers have found out another advanced version called field emission scanning electron microscope (FESEM). In this technique, a field emission gun is used that provides an enormously focused electron beam that enhances the spatial resolution at low potentials. Thus, it decreases the charging effect on insulating materials and also avoids the damage to the sensitive MOFs that can be done by the electron beam.

Apart from this, TEM has been widely used to determine the particle and grain size and crystallographic data such as dislocations and plane indices. With this technique, it is possible to measure the different particle sizes and to create a histogram and the spacing between the crystallographic planes. This technique seems to be very helpful to characterize the nanoparticles (NPs)-incorporated MOFs, as the images collected can provide information about the dispersion and size of the NPs. Energy-dispersive X-ray analysis (EDAX or EDX) is another technique coupled with SEM/TEM, which can determine the qualitative and quantitative elemental compositions of MOFs. For example, Kelty et al. performed the SEM and TEM analyses for the series of porphyrinic zirconium MOFs, resulting in the isolation of MOF-525, MOF-545, and PCN-223 on the nanoscale. The SEM/TEM techniques were then used to analyze the pure-phase crystalline products to determine the average size and polydispersity of the nanocrystals. For example, the FESEM images of an iron-based MOF synthesized by Gao et al. are shown in Fig. 5A (Gao et al., 2018), which represents its uniform spindle-like morphology. It also indicates about the complete reaction of all the reactants that are linked together and results in the formation of Fe-MOFs under given reaction condition. The TEM images also show the uniform microstructure of the Fe-MOFs (Fig. 5B). High-resolution TEM (HRTEM) image is also shown in Fig. 5C, which reveals the irregularity in its lattice structure. Fig. 5D–E shows the EDX element mapping and gives the confirmation of the uniform existence of Fe, C, and O elements present in the Fe-MOFs structure (Gao et al., 2018).

2.3.7 Other characterization techniques

X-ray photoelectron spectroscopy (XPS) is a technique used for analyzing the surface chemistry of the materials. Since the material surface is the interaction point with the other materials and external environment, this technique can be used to understand the chemical and physical interactions that occur at the surface of the materials. XPS can be used to measure the empirical formula, elemental composition, and electronic and chemical state of the elements within the material. XPS spectra are obtained by

This book belongs to Central Library BADJI Mokhtar-ANNABA UNIVERSITY
Copyright Elsevier 2024

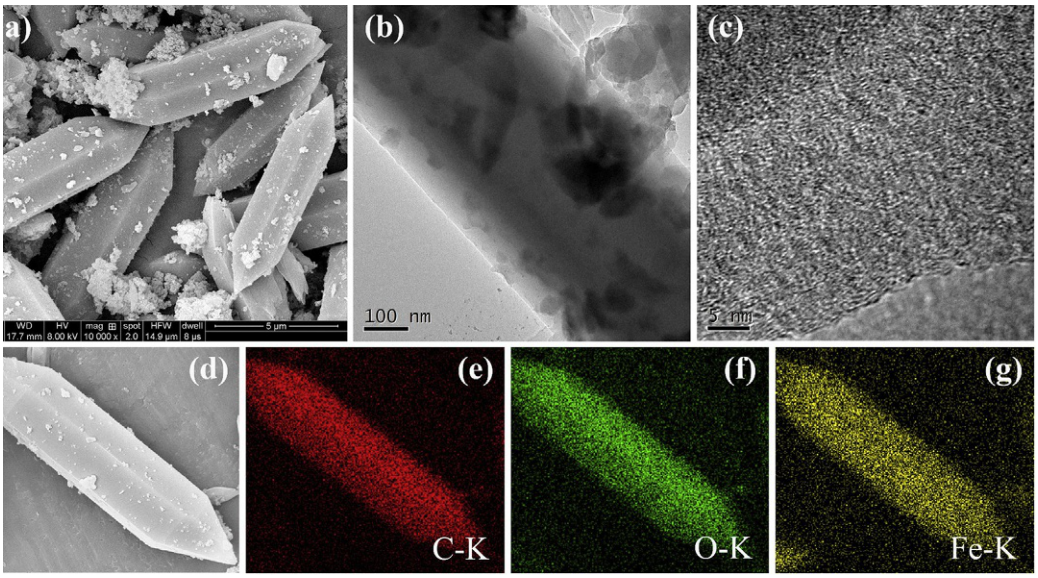

FIG. 5

(A) FESEM image of Fe-MOF; (B) TEM image of Fe-MOF; (C) HRTEM image of Fe-MOF; and (E–G) the element mapping of Fe, C and O and Fe elements present in the Fe-MOF obtained from (D).

Reproduced from Gao, G., Nie, L., Yang, S., Jin, P., Chen, R., Ding, D., Wang, X. C., Wang, W., Wu, K., & Zhang, Q. (2018). Well-defined strategy for development of adsorbent using metal organic frameworks (MOF) template for high performance removal of hexavalent chromium. Applied Surface Science, 457, *1208–1217 with the permission of Elsevier publishers.*

irradiating the surface of the material with X-ray beam and simultaneously measuring the kinetic energy and electrons escaping from the top 10-nm layer of the material surface. It requires high vacuum or ultrahigh vacuum conditions, although the current advancement in this technique is the development of ambient pressure XPS. The ejected electrons are counted over a range of electron kinetic energies to record a photoelectron spectrum. In the case of a number of MOFs, this technique have been used widely to determine the elemental composition and oxidation state of various metal ions present in the materials (Juan-Alcañiz et al., 2013; Kaur, Venkateswarulu, Kumar, Krishnan, & Koner, 2018; Khan & Jhung, 2012).

Photoluminescence (PL) spectroscopy is yet another important characterization technique for the determination of the electronic properties of the material (Lee, Chen, Liao, Wu, & Chueh, 2019). In this technique, the material is excited by the light irradiations produced from the xenon lamp. The excess energy that is not absorbed by the material and is dissipated in the form of light is known as PL. The emitted energy can be correlated with the bandgap energy of the material with localized defect levels. Thus, PL can provide the information about recombination of charge carriers, structural defects, and oxygen vacancies in the material. The most important information that PL provide is the number of recombination centers that are present in MOF (Wang & Wang, 2015). The efficient separation and the longer lifetime of photogenerated charge carriers are indicated by the higher photocurrent response. Sofi and coworkers investigated the photoresponse of the charge carriers in Ag/Ag_3PO_4/HKUST-1

This book belongs to Central Library BADJI Mokhtar-ANNABA UNIVERSITY Copyright Elsevier 2024

heterostructure (Sofi, Majid, & Mehraj, 2018). The authors described the decrease in intensity as the effective separation of the photoinduced charge carriers. Thus, this technique is very useful to understand the charge carrier separation and thus their photocatalytic activity.

3 Photocatalytic pollutant degradation using metal-organic frameworks

In the past decade, numerous efforts have been made to develop new photocatalysts based on MOFs to treat wastewater contaminated by organic pollutants discharged from industries. Due to the potential activity of the MOFs toward the photocatalytic degradation of organic pollutants, they have attracted much attention for exploring its photocatalytic activity for degradation of different types of pollutants. The first consideration of MOFs as a photocatalytic material started with the work of Hoskins and Robson in 1990, where a different approach was presented by the authors to construct 3D MOFs using metal ions and organic building blocks (Hoskins & Robson, 1989; Hoskins & Robson, 1990).

3.1 Fe-based MOFs

Jing Du et al. studied the photocatalytic degradation of methylene blue dye using MIL-53(Fe) MOF, which was prepared by using iron chloride, terephthalic acid, and *N*,*N′*-dimethylformamide (Du et al., 2011). The aqueous solution of MB dye was irradiated under UV–vis light and visible light in the presence of MIL-53(Fe). The results depict that MOF exhibits very low photocatalytic activity toward MB dye degradation both under UV–vis and visible light irradiations and this photocatalytic degradation process follows the first-order kinetics. The mechanism of photocatalytic dye degradation initiates with the generation of electron-hole pair and electron transition from the VB to the CB. The photogenerated holes (h^+) react with water molecules or organic molecules or hydroxyl ion to generate hydroxyl radical ($^{\bullet}OH$). These hydroxyl radicals ($^{\bullet}OH$) are known to have very strong oxidizing ability and thus react with the organic molecules adsorbed on the surface of the photocatalyst. However, the recombination of these photoinduced electron and holes always results in lesser decolorization of dyes due to the reduced number of holes. The addition of external electron acceptor was anticipated to enhance the activity of MIL-53(Fe). The effect of adding electron acceptor like $KBrO_3$, H_2O_2, and $(NH_4)_2S_2O_8$ onto the MOF for the photocatalytic activity was also studied. As the addition of these electron acceptors can suppress the recombination of electron-hole pairs and thus produces more number of hydroxyl radicals ($^{\bullet}OH$). A sharp enhancement in the photocatalytic activity of MIL-53(Fe) was observed on the addition of the different electron acceptors (see Fig. 6). The rate of enhancement follows the order of $(NH_4)_2S_2O_8 > H_2O_2 > KBrO_3$ under visible light irradiations, while the order was $H_2O_2 > (NH_4)_2S_2O_8 > KBrO_3$ under UV–vis light irradiation. Moreover, the reusability of the recovered MOF was also examined, and no obvious loss was found in its activity up to five cycles. The photocatalytic activity of the isostructural MOF of the same series MIL-53(M) with metal ions M = Al was also studied, and it was found that there was no effect of the metal center on the photocatalytic activity (Du et al., 2011).

Ran et al. reported another iron-based MOF and studied it for the photocatalytic degradation of two most commonly employed organic pollutants (RhB and MO) (Ran, Liu, Wu, & Pei, 2013). A new iron-based complex Fe_2(bhbdh) (where bhbdh = bis [2-hydroxybenzaldehyde]hydrazone) was synthesized and used for the photocatalytic degradation of RhB and MO in aqueous media under visible light

This book belongs to Central Library BADJI Mokhtar-ANNABA UNIVERSITY Copyright Elsevier 2024

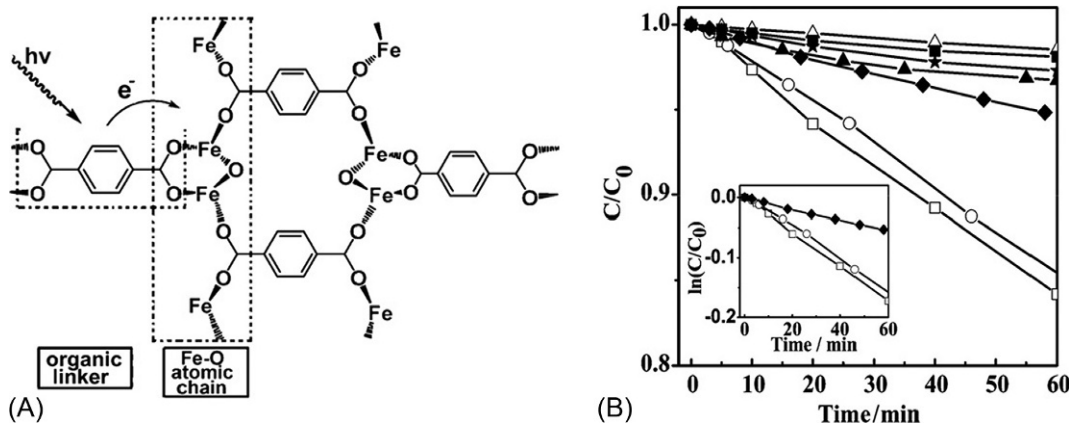

FIG. 6

(A) The chemical structure view of MIL-53(Fe) along with the mechanism of electron transfer that occurs in MIL-53(Fe) upon light irradiation. (B) The degradation profile of MB under different conditions. The inset represents the reaction kinetics using MIL-53(Fe) photocatalysts when irradiated under UV–vis light and visible light, respectively.

Reproduced from Du, J.-J., Yuan, Y.-P., Sun, J.-X., Peng, F.-M., Jiang, X., Qiu, L.-G., Xie, A.-J., Shen, Y.-H., & Zhu, J.-F. (2011). New photocatalysts based on MIL-53 metal–organic frameworks for the decolorization of methylene blue dye. Journal of Hazardous Materials, 190, *945–951 with the permission of Elsevier publishers.*

irradiation. Apart from this, the degradation rate was found to be faster with the introduction of H_2O_2. Subsequently, a number of other iron-based were synthesized and utilized for the photocatalytic degradation of organic pollutants (Wang & Li, 2019; Wang, Wang, Liang, Dong, & Zhang, 2019; Wu, Luo, & Wang, 2014).

3.2 Co- and Ni-based MOFs

Natarajan et al. used a series of MOFs using metal ions Zn, Co, and Ni to clarify the relationship between the bandgap values of the photocatalyst and degradation efficiency toward different organic pollutants (Mahata, Madras, & Natarajan, 2006). They used a series of MOFs $[Zn_2(4,4'\text{-bpy})](4,4'\text{-obb})_2$, $[Co_2(4,4'\text{-bpy})](4,4'\text{-obb})_2{\cdot}H_2O$, and $[Ni_2(4,4'\text{-bpy})_2](4,4'\text{-obb})_2{\cdot}H_2O$ with bandgap values of 4.02, 3.11, and 3.89 eV respectively. The 3D framework of the $[Co_2(4,4'\text{-bpy})](4,4'\text{-obb})_2{\cdot}H_2O$ is shown in Fig. 7A and B.

These MOFs were used as photocatalysts to degrade four widely used organic dyes orange G (OG), rhodamine B (RhB), methylene blue (MB), and brilliant blue R (BR). In the case of these three MOFs, it was found that the efficiency/activity of photocatalytic degradation of all these dyes was exactly reverse to their bandgap values. The Langmuir-Hinshelwood kinetic curves have been used successfully for the heterogeneous photocatalytic degradation to determine the relationship between the initial concentration of the organic substrate and the initial rate of degradation (Krishnakumar & Swaminathan, 2011; Kumar, Porkodi, & Selvaganapathi, 2007; Saien & Khezrianjoo, 2008). The equation used here is $r_0 = k_0C_0/(1 + K_0C_0)$ where r_0 represented the initial rate, k_0 was the rate

This book belongs to Central Library BADJI Mokhtar-ANNABA UNIVERSITY Copyright Elsevier 2024

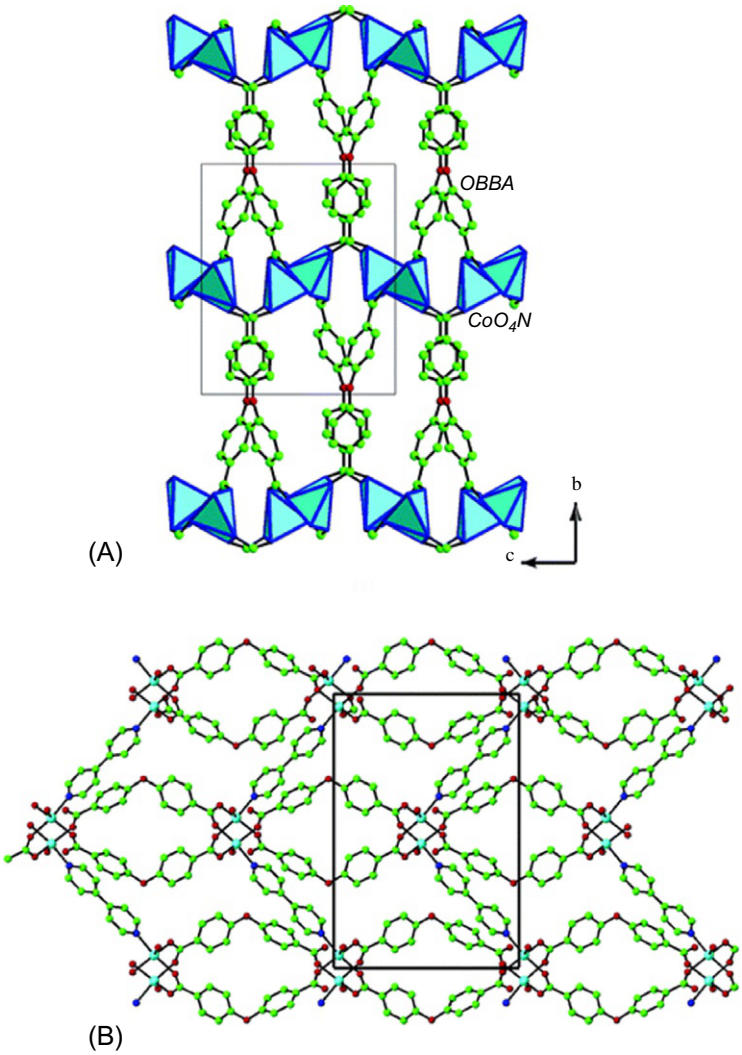

FIG. 7

(A) Connectivity between the Co^{2+} and obb anions and (B) connectivity along the *c*-axis.

Reproduced from Mahata, P., Madras, G., & Natarajan, S. (2006). Novel photocatalysts for the decomposition of organic dyes based on metal-organic framework compounds. The Journal of Physical Chemistry B, 110*, 13759–13768 with the permission of ACS publishers.*

constant, C_0 was the initial concentration of the dyes, and K_0 was the equivalent adsorption coefficient. The values of K_0 and k_0 in the case of all the three MOFs for all four dyes are given in Table 2. The value of K_0 was found to be very small in all these reactions. As K_0 stands for adsorption equilibrium, the low value of K_0 can be ascribed to the low adsorption. The photocatalytic performances

This book belongs to Central Library BADJI Mokhtar-ANNABA UNIVERSITY Copyright Elsevier 2024

Table 2 Kinetic parameters for the degradation of different dyes using $[Co_2(4,4'\text{-bpy})](4,4'\text{-obb})_2$, $[Zn_2(4,4'\text{-bpy})](4,4'\text{-obb})_2$, and $[Ni_2(4,4'\text{-bpy})_2](4,4'\text{-obb})_2 \cdot H_2O$ (Mahata et al., 2006).

MOFs	Organic pollutant	k_0 (min^{-1})	K_0 ($L\,mg^{-1}$)
$[Co_2(4,4'\text{-bpy})](4,4'\text{-obb})_2$	OG	0.031	0.0022
$[Co_2(4,4'\text{-bpy})](4,4'\text{-obb})_2$	RhB	0.013	0.0035
$[Co_2(4,4'\text{-bpy})](4,4'\text{-obb})_2$	RBBR	0.033	0.0007
$[Co_2(4,4'\text{-bpy})](4,4'\text{-obb})_2$	MB	0.032	0.0064
$[Zn_2(4,4'\text{-bpy})](4,4'\text{-obb})_2$	OG	0.020	0.0029
$[Zn_2(4,4'\text{-bpy})](4,4'\text{-obb})_2$	RhB	0.007	0.0020
$[Zn_2(4,4'\text{-bpy})](4,4'\text{-obb})_2$	RBBR	0.028	0.0069
$[Zn_2(4,4'\text{-bpy})](4,4'\text{-obb})_2$	MB	0.023	0.0029
$[Ni_2(4,4'\text{-bpy})_2](4,4'\text{-obb})_2 \cdot H_2O$	OG	0.029	0.0049
$[Ni_2(4,4'\text{-bpy})_2](4,4'\text{-obb})_2 \cdot H_2O$	RhB	0.008	0.0023
$[Ni_2(4,4'\text{-bpy})_2](4,4'\text{-obb})_2 \cdot H_2O$	RBBR	0.029	0.0015
$[Ni_2(4,4'\text{-bpy})_2](4,4'\text{-obb})_2 \cdot H_2O$	MB	0.027	0.0027

of all these MOFs were also found to be superior to that of the commercially available TiO_2 under the same experimental conditions.

Wen et al. synthesized a series of MOFs $[M(btec)_{0.5}(bimb)]_n$ including Co and Ni using ligands 4,4′-bis(1-imidazolyl)biphenyl (bimb) and 1,2,4,5-benzenetetracarboxylic acid (H_4btec) using solvothermal process (Wen et al., 2012). Co-MOF exhibits a 3D network, whereas Ni-MOF represents 2D layer structure. Both the MOFs were thoroughly characterized using various techniques, and they represent a rare MOF-based example of visible light-active photocatalyst and showed good photocatalytic activity. To evaluate the photocatalytic performance of both these MOFs, an anionic organic dye X3B was selected as a target pollutant. X3B is out of the widespread organic dyes that are difficult to decompose in waste stream under UV and visible light irradiation. This study showed a good photocatalytic efficiency of 90% and 80% in the degradation of X3B using Co and Ni MOFs in 9 h, respectively. Interestingly, the same photocatalytic efficiency was observed in just 5 h on the introduction of electron acceptor (H_2O_2). A number of other Co- and Ni-based MOFs are reported, which are used efficiently for the photocatalytic degradation of organic pollutants and are included in Table 3.

3.3 Zn-based MOFs

In 1999, Yaghi et al. reported MOF-5 having cubic crystal with formula $Zn_4O(BDC)_3.(DMF)_8.(C_6H_5Cl)$ synthesized using zinc nitrate, 1,4-BDC, DMF, and chlorobenzene (Li, Eddaoudi, O'Keeffe, & Yaghi, 1999). This MOF consists of Zn_4O clusters at the corners of the cubic framework connected orthogonally by 1,4-BDC ligand. Later on, in 2007, Garcia et al. for the first time examined the photocatalytic activity of the MOF-5 for degradation of phenol in aqueous solution. The MOF was found to exhibit a broad absorption band in the region of 500–840 nm with a bandgap of 3.4 eV. The activity of this MOF for the degradation of phenol in aqueous solution was found to be comparable with the commercial TiO_2, confirmed the highly efficient nature of MOF-5. The proposed mechanism suggests that the photodegradation of phenol occurs through a set of the reactions that include the

This book belongs to Central Library BADJI Mokhtar-ANNABA UNIVERSITY Copyright Elsevier 2024

Table 3 Performances of some d-block metal-based MOFs as photocatalysts for the photocatalytic degradation of organic pollutants in aqueous media.

MOFs	Organic pollutants	Light irradiation	Degradation (%)	Time (min)	Ref.
Zn-based MOFs					
{[Zn(4-bpah)(1,3-BDC)(H_2O)]}n	MB	UV	40	240	Wang et al. (2013)
[Zn(1,4-biyb)(adtz)]·H_2O	MB	UV	62	180	Wang et al. (2014)
MOF-5	Phenol	UV	50	180	Alvaro et al. (2007)
MOF-5	DTBP	UV	100	180	Llabrés I Xamena, Corma, and Garcia (2007)
[Zn_2(4,4′-bpy)](4,4′-obb)$_2$	MB	UV	70	90	Mahata et al. (2006)
[Zn_2(4,4′-bpy)](4,4′-obb)$_2$	RhB	UV	40	90	Mahata et al. (2006)
(UTSA-38)	MO	UV–vis	100	120	Das et al. (2011)
Fe-based MOFs					
MIL-53(Fe)	MB	UV–vis	11	40	Du et al. (2011)
MIL-53(Fe)	MB	Vis	30	40	Du et al. (2011)
MIL-53(Fe)	MB(H_2O_2)	UV–vis	99	20	Du et al. (2011)
MIL-53(Fe)	MB(H_2O_2)	Vis	20	20	Du et al. (2011)
Fe_2(bhbdh)	RhB(H_2O_2)	Vis	90	15	Ran et al. (2013)
Fe_2(bhbdh)	MO(H_2O_2)	Vis	90	15	Ran et al. (2013)
Cu-based MOFs					
{[Cu_2(3-bpah)(1,3-BDC)$_2$]·H_2O}$_n$	MB	UV	70	240	Wang, Luan, Lin, et al. (2013)
Cu(dm-bim)	MB	Vis	96	20	Wen, Zhang, Liu, Lin, & Zhang (2013)
Cu(dm-bim)	RhB	Vis	100	34	Wen et al. (2013)
Cu(dm-bim)	MO	Vis	95	45	Wen et al. (2013)
[Cu_3(3-dpsea)(1,3,5-btc)$_2$(H_2O)$_5$]	MB	UV	56	120	Wang et al. (2013)
[Cu(3-dpyh)$_{0.5}$(1,4-ndc)]·H_2O	MB	UV	67	120	Wang, Luan, Sui, et al. (2013)
Cu(ptz)(I)	MB(H_2O_2)	Vis	98	24	Wen, Zhang, and Zhang (2012)
Cu(ptz)(I)	RhB(H_2O_2)	Vis	100	35	Wen, Zhang, and Zhang (2012)
Cd-based MOFs					
[Cd(4,4′-bpy)(H_2O)$_2$(S_2O_3)]·2H_2O	MB	UV	86	60	Paul, Madras, & Natarajan (2009)
Cd_2(4,4′-bpy)$_3$(S_2O_3)$_2$	MB	UV	84	60	Paul et al. (2009)

This book belongs to Central Library BADJI Mokhtar-ANNABA UNIVERSITY

Copyright Elsevier 2024

Table 3 Performances of some d-block metal-based MOFs as photocatalysts for the photocatalytic degradation of organic pollutants in aqueous media—cont'd

MOFs	Organic pollutants	Light irradiation	Degradation (%)	Time (min)	Ref.
Cd $(btec)_{0.5}(bimb)_{0.5}$	X3B	Vis	90	540	Wen, Zhao, et al. (2012)
$Cd(npdyda)(H_2O)_2$	MO	UV	13.7	150	Gong, Jiang, Wang, Wu, & Lin (2013)
Cd(4-bpah)(1,3-bdc)(H_2O)	MB	UV	40	240	Wang, Luan, Lin, et al. (2013)
$Cd_2(4,4'\text{-bpy})_{2.5}(S_2O_3)_2$	MB	UV	76	60	Paul et al. (2009)
[Cd(2-ata)(4,4′-bpy)]	MB	Vis	82	90	Kaur et al. (2018)
Co-based MOFs					
$[Co_2(4,4'\text{-bpy})](4,4'\text{-obb})_2$	MB	UV	90	90	Mahata et al. (2006)
$[Co_2(4,4'\text{-bpy})](4,4'\text{-obb})_2$	RhB	UV	60	90	Mahata et al. (2006)
$[Co(3\text{-dpyh})_{0.5}(5\text{-aip})(H_2O)]\cdot 2H_2O$	MB	UV	47	240	Wang, Luan, Lin, Liu, and Le (2014)
$Co(btec)_{0.5}(4,4'\text{-bimb})$	X3B	Vis	80	540	Wen, Zhao, et al. (2012)
Co(4-bpah)(1,3-bdc)(H_2O)	MB	UV	25	240	Wang, Luan, Lin, et al. (2013)
$[Co(TPPA)(sdba)_2]_n$	RhB	UV	94	60	Xiao et al. (2019)
Ni-based MOFs					
$[Ni_2(4,4'\text{-bpy})_2](4,4'\text{-obb})_2\cdot H_2O$	MB	UV	80	90	Mahata et al. (2006)
$[Ni_2(4,4'\text{-bpy})_2](4,4'\text{-obb})_2\cdot H_2O$	RhB	UV	50	90	Mahata et al. (2006)
$Ni(btec)_{0.5}(bimb)$	X3B	Vis	80	540	Wen, Zhao, et al. (2012)
Ni(4-bpah)(1,3-bdc)(H_2O)	MB	UV	55	240	Wen, Zhao, et al. (2012)

Where 1,4-biyb = 1,4-bis(imidazol-1-ylmethyl)benzene; H_2adtz = 2,5-(s-acetic acid) dimercapto-1,3,4-thiadiazole; 4-bpah = N,N′-bis(4-pyridinecarboxamide)-1,2-cyclohexane; 3-bpah = N,N′-bis(3-pyridinecarboxamide)-1,2-cyclohexane; 1,3,5-H_3BTC = 1,3,5-benzenetricarboxylic acid; 1,2-H_2BDC = 1,2-benzenedicarboxylic acid; 1,3-H_2BDC = 1,3-benzenedicarboxylic acid; MOF-5: $[Zn_4O(1,4\text{-bdc})_3].(DMF)_8(C_6H_5Cl)$ (1,4-bdc, 1,4-benzenedicarboxylate, DMF, dimethylformamide, C6H5Cl, chlorobenzene); 4,4′-obb = 4,4′-oxybis(benzoate); 4,4′-bpy = 4,4′-bipyridine; (UTSA-38) = $Zn_4O(2,6\text{-NDC})_3.(DMF)_{1.5}(H_2O)_{0.5}\cdot 4DMF\cdot 7.5H_2O$; NDC = naphthalene dicarboxylate; dm-bim = 5,6-dimethylbenzimidazolate; dpsea = N,N′-di(3-pyridyl)sebacicdiamide; 3-dpyh = N,N′-di(3-pyridinecarboxamide)-1,6-hexane; 1,4-ndc = 1,4-naphthalenedicarboxylate; ptz = 5-(3-pyridyl)tetrazole; bhbdh = bis[2-hydroxybenzaldehyde]hydrazone; 3-dpyh = N,N′-di(3-pyridinecarboxamide)-1,6-hexane; 5-H_2aip = 5-aminoisophthalic acid; btec = 1,2,4,5-benzenetetracarboxylate; $H_2npdyda$ = naphthalene-1,5-diyldioxy-di-acetic acid; 4-bpah = N,N′-bis(4-pyridinecarboxamide)-1,2-cyclohexane; TPPA = tris(4-pyridin-4-ylphenyl)amine; H_2sdba = 4,4′-sulfonyldibenzoic acid; RBBR = Remazol Brilliant Blue R; X3B = reactive brilliant red; MO = methyl orange; MB = methylene blue; RhB = rhodamine B; and NR = neutral red.

This book belongs to Central Library BADJI Mokhtar-ANNABA UNIVERSITY
Copyright Elsevier 2024

formation of oxygen active species from the reaction of photogenerated electrons with oxygen or radical cation due to electron transfer from phenol to MOF-5 holes.

It was noticed that MOF-5 showed better photocatalytic efficiency than ZnO and TiO_2 due to its broad visible light absorption property. Furthermore, the shape-selective photocatalytic degradation efficiency of MOF-5 was also studied by Garcia et al. toward the different organic compounds. This study involves the competitive photodegradation of phenol (P) and 2,6-di-tert-butylphenol (DTBP), where phenol molecules were comparatively smaller than large-sized DTBP molecules. In this study, it was observed that the MOF-5 degraded the DTBP, which is larger in size at much faster rate than small-sized phenol as larger DTBP cannot diffuse into the micropores of MOF-5. Moreover, in the presence of UV light, the degradation rate of both DTBP and phenol was almost comparable at the initial rate. However, the degradation rate of DTBP was found to be 4.4-folds higher when a mixture of both the phenols and DTBP was irradiated in the presence of MOF-5, implying the selective photodegradation of DTBP with respect to phenol. This observation could be explained on the basis of smaller size of phenol molecules that can freely diffuse into the micropores of the MOF-5 and results in lower degradation rate. The reason may be envisaged that being a larger size of DTBP, which remained on the external surface of MOF, leads into higher degradation rate under UV light irradiation.

After the detailed research of MOF-5 as an efficient photocatalyst for the degradation of organic pollutants, a double-layered porous Zn-based MOF UTSA-38 with formula $[Zn_4O(2,6\text{-}ndc)_3(DMF)_{1.5}(H_2O)_{0.5}]\cdot 4(DMF)\cdot 7.5H_2O$ was reported by Chen and coworkers (Das et al., 2011). The bandgap of the MOF was found to be 2.85 eV and was explored for the photocatalytic degradation of aqueous solution of methyl orange (MO).The degradation study was performed both under visible and UV light, and it was found that the degradation rate was much faster under UV light irradiation. In this study, the authors were able to show the complete degradation of MO into a colorless small molecule within a time period of 120 min, indicating higher photocatalytic efficiency under UV light. The mechanism involved in the process of photocatalytic activity of UTSA-38 initiated with the generation of electron-hole pairs. The electrons from the valence band (VB) were excited to the conduction band (CB) leaving behind holes (h^+) in the VB, after absorbing energy equal to or greater than the bandgap energy of UTSA-38. The photogenerated electrons and holes then migrate to the surface of the photocatalyst (UTSA-38) and the photoinduced energy and then transferred to the adsorbed species: oxygen (O_2) was reduced by electrons to the oxygen radical ($O_2^{-\bullet}$) and finally transformed into hydroxyl radicals ($OH^\bullet$), whereas the holes oxidizes the hydroxyl to hydroxyl radicals ($OH^\bullet$). These hydroxyl radicals finally decomposed the MO dye into small molecules like CO_2 and H_2O. Furthermore, photocatalyst UTSA-38 was recovered after the photocatalytic reaction via simple filtration/centrifugation and was further used for the same purpose after the proper drying and washing process. It showed high photocatalytic efficiency without any obvious decay up to 7 cycles. Later on, a large number of novel Zn-based MOFs were synthesized and explored under UV and visible light irradiation for the photocatalytic degradation of organic pollutants. Some of these Zn-based MOFs have been listed here in Table 3.

3.4 Cd-based MOFs

A number of Cd-based MOFs are reported in literature, which includes $[Cd(4,4'\text{-bpy})(H_2O)_2(S_2O_3)]\cdot 2H_2O$, $Cd_2(4,4'\text{-bpy})_3(S_2O_3)_2$, $Cd(btec)_{0.5}(bimb)_{0.5}$, and $Cd(4\text{-bpah})(1,3\text{-bdc})(H_2O)$. These MOFs have been used extensively for the photocatalytic degradation of various organic pollutants including

This book belongs to Central Library BADJI Mokhtar-ANNABA UNIVERSITY Copyright Elsevier 2024

MB, MO, X3B, and RhB (Gong et al., 2013; Paul et al., 2009; Wen, Zhao, et al., 2012). The detailed catalytic efficiency along with the pollutant used has been listed in Table 3. Kaur et al. reported two cadmium-based MOFs for the photocatalytic degradation of organic pollutants. Firstly, they synthesized a Cd-MOF: $[Cd(2\text{-ATA})(4,4'\text{-bpy})]_n$ where 2-ATA = 2 aminoterephthalic acid and bpy = bipyridine, which was found to be visible light active (Kaur et al., 2018). This MOF was used for the photocatalytic degradation of MB under visible light irradiation and was able to degrade 82% of MB within 90 min. After this, another Cd-based MOF with different acidic linker was synthesized: $\{[Cd(PA)(4,4'\text{-bpy})_2](H_2O)\}n$ (where PA = pamoic acid and bpy = bipyridine) (Kaur et al., 2019). This MOF was used for the complete removal of different organic pollutants including MB, RhB, MO, and NR dyes. The MOF was used for the adsorption, separation, and photocatalytic degradation of less adsorbed dyes.

3.5 Other metal-based MOFs

Wang et al. synthesized a series of metal-organic coordination polymers using metals M = Cu, Co, Ni, Zn, and Cd, and the prepared MOFs are $\{[Cu_3(4\text{-bpah})_4(1,3,5\text{-BTC})_2]\cdot 8H_2O\}_n$ (1), $\{[Cu_3(4\text{-bpah})_3(1,2\text{-BDC})_3(H_2O)_2]\cdot 4H_2O\}_n$ (2), $\{[Cu(4\text{-bpah})(1,3\text{-BDC})(H_2O)]\}_n$ (3), $\{[Co(4\text{-bpah})(1,3\text{-BDC})(H_2O)]\}_n$ (4), $\{[Ni(4\text{-bpah})(1,3\text{-BDC})(H_2O)]\}_n$ (5), $\{[Zn(4\text{-bpah})(1,3\text{-BDC})(H_2O)]\}_n$ (6), $\{[Cd(4\text{-bpah})(1,3\text{-BDC})]\}_n$ (7), $\{[Cd(3\text{-bpah})(1,3\text{-BDC})]\cdot H_2O\}_n$ (8), and $\{[Cu_2(3\text{-bpah})(1,3\ BDC)_2]\cdot H_2O\}_n$ (9), where 1,3,5-H_3BTC = 1,3,5-benzenetricarboxylic acid, 4-bpah = *N*,*N*′-bis(4-pyridinecarboxamide)-1,2-cyclohexane, 3-bpah = *N*,*N*′-bis(3-pyridinecarboxamide)-1,2-cyclohexane, 1,2-H_2BDC = 1,2-benzenedicarboxylic acid, and 1,3-H_2BDC = 1,3-benzenedicarboxylic acid (Wang, Luan, Lin, et al., 2013). The structures of all these MOFs were determined using single-crystal X-ray diffraction analyses, and further characterization was done using powder X-ray diffraction (PXRD), infrared spectroscopy, elemental analyses, and thermogravimetric analyses (TGA). Complex 1 exhibits a 2D topological network; complex 2 shows a 2D topological framework that contains triflexural and left-hand helix chains. Complexes 3–6 also exhibit a similar 2D square lattice network, whereas complexes 7 and 8 show two different 2D double-layer structures. Complex 9 exhibits a new 3D trinodal topology. Complexes 1–9 imply that using semirigid bis-pyridyl-bis-amide ligands can result into various structural frameworks with small voids. The photocatalytic properties of complexes 1–9 have also been investigated. Controlled experiments were also performed to check the photodegradation of MB dye, but no significant changes were observed in the degradation of MB under the reaction conditions: in the dark and without catalyst. The complexes showed good photocatalytic activity as compared with controlled experiments that indicates that all of the catalysts 1–9 are photocatalytically active and decomposes MB dye in the presence of UV irradiation. The efficiency of catalyst 9 under ultraviolet light was found to be higher than all others complexes, which may attributed to the fact that the more extended network may supported the transport of excited holes to the surface and initiated the photocatalytic decomposition of MB dye.

As we know in the presence of UV light, electron transfer takes place from the highest occupied molecular orbital (HOMO) to the lowest unoccupied molecular orbital (LUMO). The HOMO consist of 2p bonding orbitals of nitrogen/oxygen (valence band), and the LUMO mainly corresponds to empty metal orbital (M = Zn/Co/Cu/Ni/Cd, conduction band). During photoexcitation, the charge transfer takes place from the O_2/N_2 of the ligand to the metal (Cu/Co/Ni/Zn/Cd). Additionally, there is need of one more electron by HOMO to return to its stable state, and that one electron was being captured

This book belongs to Central Library BADJI Mokhtar-ANNABA UNIVERSITY Copyright Elsevier 2024

from H_2O molecules and then oxygenated to form $^{\bullet}OH$-active species. These $^{\bullet}OH$ radicals finally attack MB and decompose it to complete the photocatalytic process.

Wang et al. reported three silver-based MOFs: $Ag_4(bpy)_4(ap)_2{\cdot}11H_2O$ (1), $Ag_2(bpe)_2(npdc){\cdot}2H_2O$ (2), and $[Ag_2(dpe)_{1.5}(sbdc)_{0.5}](sbdc)_{0.5}{\cdot}7H_2O$ (3) using $AgNO_3$ and ligands 5-aminoisophthalic acid (ap)/2,6-naphthalenedicarboxylic acid (npdc)/stilbenedicarboxylic acid (sbdc) and 1,2-di(4-pyridyl) ethylene (dpe)/4,4′-bipyridine (bpy) (Wang, Jing, & Wang, 2014). These complexes consist of infinite 1D silver-ligand cationic chains along with carboxylate anions providing charge compensation in the crystal frameworks. Complexes 1–3 displayed good photocatalytic activity for the degradation of MB under UV light and resulted into complete photodegradation of MB in just 3 h. In addition, a number of other metal-based MOFs including Cd, Pb, Gd, and Zr have been reported till date, which show high efficiency in photocatalytic degradation of organic pollutants. A few of them have been listed in Table 4.

4 Summary and perspectives

In the past two decades, a huge development has been made in the area of MOF synthesis, and it is still in progress. More efforts may be required in the design and synthesis of functional MOFs in which porosity plays an important role. In addition to experimental research, computational studies have also been proven to be more beneficial for the synthesis and utilization of sustainable MOFs for environmental remediation. To treat the wastewater, MOFs can be utilized for the various processes including adsorption and heterogeneous photocatalysis and enhancing the hydroxyl and sulfate radical generation. The photoactive MOFs have several advantages over the conventional semiconductors in the photocatalytic degradation of organic pollutants:

(i) Flexible synthesis strategies including solvothermal, slow diffusion, ultrasonication, and also postsynthetic modification yield into highly crystalline and different morphologies of MOFs
(ii) Defined crystalline and porous structures of MOFs proves to be beneficial in various characterizations and structure-property correlation studies of these solid photocatalysts.
(iii) High surface area and intrinsic porosity of MOFs can ease the diffusion of pollutant and product molecules to the active site through their open channels.
(iv) Tunable active sites and structural features including organic linkers and metal oxoclusters result into broad range of activity under different light irradiations.

Furthermore, the development of MOFs as photocatalysts may require a better and detailed understanding of the mechanism involved in the photochemical process and the other parameters for controlling the photocatalytic activity. Based on the optical properties and electrochemical/photochemical activities, some MOFs could be designated as semiconductors. MOFs should be treated as molecular catalyst instead of semiconductors in the process of photocatalysis. The HOMO-LUMO energy levels and bandgap terminology should be used to explain the distinct character of ligand-induced transitions. At last, we believe that, out of various photocatalytic materials, MOFs are the promising candidates for wastewater treatment and they could provide an ideal choice for the photocatalytic degradation of organic pollutants through light harvesting. For the next generation, MOFs as photocatalyst may include cost-effective synthesis and tandem catalysis. The structures of the MOFs may be designed in accordance to the stimulated enzymatic catalysis. In addition, new technologies may be investigated to

This book belongs to Central Library BADJI Mokhtar-ANNABA UNIVERSITY Copyright Elsevier 2024

Table 4 Performances of MOFs as photocatalysts for the photocatalytic degradation of organic pollutants in aqueous media.

MOFs	Organic pollutant	Light irradiation	Degradation (%)	Time (min)	Ref.
NTU-9	RhB (H_2O_2)	Vis	100	80	Gao et al. (2014)
MIL-53(Al)	MB	UV–vis	30	60	Du et al. (2011)
$[Pb_2(bpe)]_2(PF6)_4$	Sunset yellow	UV	100	60	Wang et al. (2015)
	MO	UV	95	300	Wang et al. (2015)
	Congo red	UV	18	100	Wang et al. (2015)
BiOBr/UiO-6	RhB	Vis	100	15	Sha and Wu (2015)
VNU-1 P	MB	UV–vis	100	180	Doan et al. (2015)
	MO	UV–vis	80	180	Doan et al. (2015)
$[Ag_2(pdbmb)_2(CF_3SO_3)_2]\cdot H_2O$	MB	UV–vis	90	540	Wałęsa-Chorab et al. (2012)
$[Ag_4(4,4'\text{-bpy})_4(ap)_2]\cdot 11H_2O$	MB	UV	98.2	180	Wang, Jing, and Wang (2014)
$[Ag_2(4,4'\text{-bpy})_2(npdc)]\cdot 2H_2O$	MB	UV	99.8	180	Wang, Jing, and Wang (2014)
$[Ag_2(dpe)_{1.5}(bdc)_{0.5}(sbdc)_{0.5}]\cdot 7H_2O$	MB	UV	99.9	180	Wang, Jing, and Wang (2014)
$Ag_2(phen)UO_2(btec)$	RhB	UV	99	120	Yu, Liao, Jiang, Li, and Chen (2005)
$(UO_2)_2(bta)(DMA)_2$	RhB	UV	100	130	Hou et al. (2014)
$[(UO_2)_2(bta)(\mu_3\text{-}OH_2)]\cdot 2(HN(CH_3)_2)\cdot H_2O$	RhB	UV	50	130	Hou et al. (2014)
$UO_2(1,4\text{-ndc})((CH_3)_2SO)_2$	RhB	UV–vis	100	70	Xia, Wang, and Chen (2010)
$UO_2(1,4\text{-ndc})((CH_3)_2SO)_2$	RhB	Vis	100	180	Xia et al. (2010)
$UO_2(1,4\text{-ndc})(CH_2OH)_2$	RhB	UV–vis	100	70	Xia et al. (2010)
$UO_2(1,4\text{-ndc})(CH_2OH)_2$	RhB	Vis	98	180	Xia et al. (2010)
$Gd(H_2O)_3Co(2,2\text{-pdc})_3$	RBBR	UV	90	90	Mahata, Sankar, Madras, and Natarajan (2005)
$[Sm(H_2O)_4(2,6\text{-pdc})]_3[Sm(H_2O)_3-(2,6\text{-pdc})](SiMo_{12}O_{40})\cdot 3H_2O$	RhB	UV	85	240	Chen et al. (2012)
$[La(H_2O)_4(2,6\text{-pdc})]_4(PMo_{12}O_{40})F$	RhB	UV	85	240	Chen et al. (2012)

Where NTU-9 = $Ti_2(dobdc)_3$; H_4dobdc = 2,5-dihydroxyterephthalic acid; TabH = 4-(trimethylammonio)benzenethiol; bpe = 1,2-bis(4-pyridyl)ethylene; VNU-1P = $Zr_6O_4(OH)_4(CO_2)_{12}$ with ligand CPEB = 1,4-bis(2-[4-carboxy phenyl] ethynyl)benzene; dpe = 1,2-di(4-pyridyl)ethylene; H_2ap = 5-aminophthalic acid; H_2npdc = 2,6-naphthalenedicarboxylic acid; H_2sbdc = 4,4′-stilbenedicarboxylic acid; H_4bta = 1,2,4,5-benzenetetracarboxylic acid; 2,3-pdc = pyridine-2,3-dicarboxylic acid; and 2,6-pdc = pyridine-2,6-dicarboxylic acid.

This book belongs to Central Library BADJI Mokhtar-ANNABA UNIVERSITY
Copyright Elsevier 2024

develop processes that include negligible metal loss and efficient removal of pollutants and mineralization via coupling with some other methods such as electrochemical or photochemical technologies.

Till now, it is difficult to carry out a high-throughput synthesis at a large scale of kilograms in hours at ambient conditions of temperature and pressure that seem to be an obstacle in the practical application of MOFs. The widely used solvothermal method using autoclave and other methods like slow diffusion one requires longer time period in terms of days/weeks for the completion of synthesis process of MOFs that makes it difficult at the industrial-scale preparation. Apart from this, the poor aqueous stability of MOFs adds to another disadvantage. A large number of MOFs are known to be unstable in aqueous media, and thus, it limits the practical application of MOFs for the intended application. However, MOFs based on soft metal ions like Zn^{2+} with imidazolate linkers, that is, ZIFs and hard metal ions including Zr^{4+}, Fe^{3+}, and Ti^{4+} linked by carboxylate-containing organic ligands (e.g., MIL-140, 101, 125 and UiOs), show high stability in the presence of water. The design and development of these types of MOFs is thus an immediate requirement for the practical applications like wastewater treatment through photocatalytic degradation of organic pollutants.

In addition to this, during the usage of MOFs as heterogeneous photocatalytic materials in wastewater treatment process, metal leaching emerges out to be an important problem to deal with. There are a limited number of reports focusing on the leaching of metal ions Cu, Pb, Cr, and Zn and surface modifier into aqueous media that causes detrimental effects (Kuila et al., 2017). These metal ions are linked with the organic moieties via weak interactions. A normal physical change in the aqueous region can disrupt the bonding and can result into leaching of toxic metal ions. A few MOF-based reports are there in which leaching of metal ions results in detrimental effects. However there is requirement of a detailed and thorough investigation to authenticate their detrimental effects. Additionally, the choice of the metal ion is also very important like choosing nontoxic metal ions including Fe, Ti, and Mn and suitable linkers that could minimize this uncertainty. Nonetheless, more detailed study is required in implementing them for commercial applications. Moreover, the rational design and development of near-IR potential MOFs could also benefit their sustainable application. However, most of the MOFs suffer from low electrical conductivity, poor process ability, and weak mechanical properties, which obstruct the incorporation of MOFs into functional solar devices. Thus, to get stable, cheap, and efficient MOFs for serving as photocatalyst for various practical applications is still a challenge. The viability of obtaining high yield products with high purity and accessibility of cheap starting materials must be taken into consideration while designing new MOFs. Concurrently, the development of synthetic methods to obtain low-cost MOFs should be considered. Simultaneously, the choice of the low-cost metal salts and ligands in synthesizing new MOFs for the photocatalysis is also significant. At last, MOFs can serve as highly efficient photocatalysts for the wastewater treatment through the photocatalytic process.

References

Abbasi, A., Geranmayeh, S., Skripkin, M. Y., & Eriksson, L. (2012). Potassium ion-mediated non-covalent bonded coordination polymers. *Dalton Transactions*, *41*, 850–859.

Ali, I., Asim, M., & Khan, T. A. (2012). Low cost adsorbents for the removal of organic pollutants from wastewater. *Journal of Environmental Management*, *113*, 170–183.

Alp, E., Mini, S., & Ramanathan, M. (1990). *X-ray absorption spectroscopy: EXAFS and XANES-A versatile tool to study the atomic and electronic structure of materials, ANL/APS/TM-7; 1990*.

This book belongs to Central Library BADJI Mokhtar-ANNABA UNIVERSITY

Copyright Elsevier 2024

Alvaro, M., Carbonell, E., Ferrer, B., Llabrés I Xamena, F. X., & Garcia, H. (2007). Semiconductor behavior of a metal-organic framework (MOF). *Chemistry—A European Journal*, *13*, 5106–5112.

Bang, J. H., & Suslick, K. S. (2010). Applications of ultrasound to the synthesis of nanostructured materials. *Advanced Materials*, *22*, 1039–1059.

Barrett, E. P., Joyner, L. G., & Halenda, P. P. (1951). The determination of pore volume and area distributions in porous substances. I. Computations from nitrogen isotherms. *Journal of the American Chemical Society*, *73*, 373–380.

Bedia, J., Muelas-Ramos, V., Peñas-Garzón, M., Gómez-Avilés, A., Rodríguez, J., & Belver, C. (2019). A review on the synthesis and characterization of metal organic frameworks for photocatalytic water purification. *Catalysts*, *9*, 52.

Bian, Y., Xiong, N., & Zhu, G. (2018). Technology for the remediation of water pollution: A review on the fabrication of metal organic frameworks. *Processes*, *6*, 122.

Brunauer, S., Emmett, P. H., & Teller, E. (1938). Adsorption of gases in multimolecular layers. *Journal of the American Chemical Society*, *60*, 309–319.

Butova, V. V. E., Soldatov, M. A., Guda, A. A., Lomachenko, K. A., & Lamberti, C. (2016). Metal-organic frameworks: Structure, properties, methods of synthesis and characterization. *Russian Chemical Reviews*, *85*, 280.

Chae, H. K., Siberio-Perez, D. Y., Kim, J., Go, Y., Eddaoudi, M., Matzger, A. J., et al. (2004). A route to high surface area, porosity and inclusion of large molecules in crystals. *Nature*, *427*, 523.

Chakma, S., Das, L., & Moholkar, V. S. (2015). Dye decolorization with hybrid advanced oxidation processes comprising sonolysis/Fenton-like/photo-ferrioxalate systems: A mechanistic investigation. *Separation and Purification Technology*, *156*, 596–607.

Chen, X.-Y., Chen, Y.-P., Xia, Z.-M., Hu, H.-B., Sun, Y.-Q., & Huang, W.-Y. (2012). Synthesis, crystal structure of α-Keggin heteropolymolybdates with pyridine-2, 6-dicarboxylate based frameworks, and associated RhB photocatalytic degradation and 2D-IR COS tests. *Dalton Transactions*, *41*, 10035–10042.

Chhabra, T., Kumar, A., Bahuguna, A., & Krishnan, V. (2019). Reduced graphene oxide supported MnO2 nanorods as recyclable and efficient adsorptive photocatalysts for pollutants removal. *Vacuum*, *160*, 333–346.

Chong, M. N., Jin, B., Chow, C. W., & Saint, C. (2010). Recent developments in photocatalytic water treatment technology: A review. *Water Research*, *44*, 2997–3027.

Comninellis, C., Kapalka, A., Malato, S., Parsons, S. A., Poulios, I., & Mantzavinos, D. (2008). Advanced oxidation processes for water treatment: Advances and trends for R&D. *Journal of Chemical Technology & Biotechnology: International Research in Process, Environmental & Clean Technology*, *83*, 769–776.

Das, M. C., Xu, H., Wang, Z., Srinivas, G., Zhou, W., Yue, Y.-F., et al. (2011). A Zn 4 O-containing doubly interpenetrated porous metal–organic framework for photocatalytic decomposition of methyl orange. *Chemical Communications*, *47*, 11715–11717.

Doan, T. L., Nguyen, H. L., Pham, H. Q., PHAM-Tran, N. N., Le, T. N., & Cordova, K. E. (2015). Tailoring the optical absorption of water-stable ZrIV-and HfIV-based metal–organic framework photocatalysts. *Chemistry—An Asian Journal*, *10*, 2660–2668.

Du, J.-J., Yuan, Y.-P., Sun, J.-X., Peng, F.-M., Jiang, X., Qiu, L.-G., et al. (2011). New photocatalysts based on MIL-53 metal–organic frameworks for the decolorization of methylene blue dye. *Journal of Hazardous Materials*, *190*, 945–951.

Eddaoudi, M., Kim, J., Rosi, N., Vodak, D., Wachter, J., O'Keeffe, M., et al. (2002). Systematic design of pore size and functionality in isoreticular MOFs and their application in methane storage. *Science*, *295*, 469–472.

Farha, O. K., Eryazici, I., Jeong, N. C., Hauser, B. G., Wilmer, C. E., Sarjeant, A. A., et al. (2012). Metal–organic framework materials with ultrahigh surface areas: Is the sky the limit? *Journal of the American Chemical Society*, *134*, 15016–15021.

Farha, O. K., & Hupp, J. T. (2010). Rational design, synthesis, purification, and activation of metal − organic framework materials. *Accounts of Chemical Research*, *43*, 1166–1175.

This book belongs to Central Library BADJI Mokhtar-ANNABA UNIVERSITY

Copyright Elsevier 2024

Farha, O. K., Yazaydın, A. Ö., Eryazici, I., Malliakas, C. D., Hauser, B. G., Kanatzidis, M. G., et al. (2010). De novo synthesis of a metal–organic framework material featuring ultrahigh surface area and gas storage capacities. *Nature Chemistry*, *2*, 944.

Gao, J., Miao, J., Li, P.-Z., Teng, W. Y., Yang, L., Zhao, Y., et al. (2014). A p-type Ti (IV)-based metal–organic framework with visible-light photo-response. *Chemical Communications*, *50*, 3786–3788.

Gao, G., Nie, L., Yang, S., Jin, P., Chen, R., Ding, D., et al. (2018). Well-defined strategy for development of adsorbent using metal organic frameworks (MOF) template for high performance removal of hexavalent chromium. *Applied Surface Science*, *457*, 1208–1217.

Garay, A. L., Pichon, A., & James, S. L. (2007). Solvent-free synthesis of metal complexes. *Chemical Society Reviews*, *36*, 846–855.

Gong, Y., Jiang, P.-G., Wang, Y.-X., Wu, T., & Lin, J.-H. (2013). Metal–organic frameworks based on 1, 3, 5-triazine-2, 4, 6-triyltrithio-triacetate: Structures, topologies, photoluminescence and photocatalytic properties. *Dalton Transactions*, *42*, 7196–7203.

Guillerm, V., Gross, S., Serre, C., Devic, T., Bauer, M., & Férey, G. (2010). A zirconium methacrylate oxocluster as precursor for the low-temperature synthesis of porous zirconium (IV) dicarboxylates. *Chemical Communications*, *46*, 767–769.

Hasan, Z., & Jhung, S. H. (2015). Removal of hazardous organics from water using metal-organic frameworks (MOFs): Plausible mechanisms for selective adsorptions. *Journal of Hazardous Materials*, *283*, 329–339.

Ho, Y., Show, K., Guo, X., Norli, I., Abbas, F. A., & Morad, N. (2012). Industrial discharge and their effect to the environment. In *Industrial Waste*. IntechOpen.

Holland, T., & Redfern, S. (1997). Unit cell refinement from powder diffraction data: The use of regression diagnostics. *Mineralogical Magazine*, *61*, 65–77.

Horiuchi, Y., Toyao, T., Saito, M., Mochizuki, K., Iwata, M., Higashimura, H., et al. (2012). Visible-light-promoted photocatalytic hydrogen production by using an amino-functionalized Ti (IV) metal–organic framework. *The Journal of Physical Chemistry C*, *116*, 20848–20853.

Hoskins, B., & Robson, R. (1990). Design and construction of a new class of scaffolding-like materials comprising infinite polymeric frameworks of 3D-linked molecular rods. A reappraisal of the zinc cyanide and cadmium cyanide structures and the synthesis and structure of the diamond-related frameworks [N (CH3) 4][CuIZnII (CN) 4] and CuI [4, 4′, 4″, 4″'-tetracyanotetraphenylmethane] BF4. xC6H5NO2. *Journal of the American Chemical Society*, *112*, 1546–1554.

Hoskins, B. F., & Robson, R. (1989). Infinite polymeric frameworks consisting of three dimensionally linked rod-like segments. *Journal of the American Chemical Society*, *111*, 5962–5964.

Hou, Y.-N., Xing, Y.-H., Bai, F.-Y., Guan, Q.-L., Wang, X., Zhang, R., et al. (2014). Synthesis, crystal structure, photoluminescence property and photoelectronic behavior of two uranyl-organic frameworks constructed from 1, 2, 4, 5-benzenetetracarboxylic acid as ligand. *Spectrochimica Acta Part A: Molecular and Biomolecular Spectroscopy*, *123*, 267–272.

Howarth, A. J., Peters, A. W., Vermeulen, N. A., Wang, T. C., Hupp, J. T., & Farha, O. K. (2016). Best practices for the synthesis, activation, and characterization of metal–organic frameworks. *Chemistry of Materials*, *29*, 26–39.

Jhung, S. H., Lee, J. H., & Chang, J. S. (2005). Microwave synthesis of a nanoporous hybrid material, chromium trimesate. *Bulletin of the Korean Chemical Society*, *26*, 880–881.

Jiang, J., Zhao, Y., & Yaghi, O. M. (2016). Covalent chemistry beyond molecules. *Journal of the American Chemical Society*, *138*, 3255–3265.

Juan-Alcañiz, J., Gielisse, R., Lago, A. B., Ramos-Fernandez, E. V., Serra-Crespo, P., Devic, T., et al. (2013). Towards acid MOFs–catalytic performance of sulfonic acid functionalized architectures. *Catalysis Science & Technology*, *3*, 2311–2318.

Kaupp, G. (2009). Mechanochemistry: The varied applications of mechanical bond-breaking. *CrystEngComm*, *11*, 388–403.

This book belongs to Central Library BADJI Mokhtar-ANNABA UNIVERSITY

Copyright Elsevier 2024

Kaur, H., Kumar, R., Kumar, A., Krishnan, V., & Koner, R. R. (2019). Trifunctional metal–organic platform for environmental remediation: Structural features with peripheral hydroxyl groups facilitate adsorption, degradation and reduction processes. *Dalton Transactions*, *48*, 915–927.

Kaur, H., Venkateswarulu, M., Kumar, S., Krishnan, V., & Koner, R. R. (2018). A metal–organic framework based multifunctional catalytic platform for organic transformation and environmental remediation. *Dalton Transactions*, *47*, 1488–1497.

Kettner, F., Worch, C., Moellmer, J., Gläser, R., Staudt, R., & Krautscheid, H. (2013). Synthesis, crystal structure and catalytic behavior of Homo-and heteronuclear coordination polymers [M (tdc)(bpy)](M2+= Fe2+, Co2+, Zn2+, Cd2+; tdc2–= 2, 5-thiophenedicarboxylate). *Inorganic Chemistry*, *52*, 8738–8742.

Khan, N. A., & Jhung, S. H. (2012). Low-temperature loading of cu+ species over porous metal-organic frameworks (MOFs) and adsorptive desulfurization with cu+−loaded MOFs. *Journal of Hazardous Materials*, *237*, 180–185.

Klimakow, M., Klobes, P., Thünemann, A. F., Rademann, K., & Emmerling, F. (2010). Mechanochemical synthesis of metal − organic frameworks: A fast and facile approach toward quantitative yields and high specific surface areas. *Chemistry of Materials*, *22*, 5216–5221.

Klinowski, J., Paz, F. A. A., Silva, P., & Rocha, J. (2011). Microwave-assisted synthesis of metal–organic frameworks. *Dalton Transactions*, *40*, 321–330.

Krishnakumar, B., & Swaminathan, M. (2011). Influence of operational parameters on photocatalytic degradation of a genotoxic azo dye acid violet 7 in aqueous ZnO suspensions. *Spectrochimica Acta Part A: Molecular and Biomolecular Spectroscopy*, *81*, 739–744.

Kuila, A., Surib, N. A., Mishra, N. S., Nawaz, A., Leong, K. H., Sim, L. C., et al. (2017). Metal organic frameworks: A new generation coordination polymers for visible light photocatalysis. *ChemistrySelect*, *2*, 6163–6177.

Kumar, A., Kumar, K., & Krishnan, V. (2019). Sunlight driven methanol oxidation by anisotropic Plasmonic au nanostructures supported on amorphous Titania: Influence of morphology on photocatalytic activity. *Materials Letters*, *245*, 45–48.

Kumar, S., Kumar, A., Kumar, A., Balaji, R., & Krishnan, V. (2018). Highly efficient visible light active 2D-2D nanocomposites of N-ZnO-g-C3N4 for photocatalytic degradation of diverse industrial pollutants. *ChemistrySelect*, *3*, 1919–1932.

Kumar, K. V., Porkodi, K., & Selvaganapathi, A. (2007). Constrain in solving Langmuir–Hinshelwood kinetic expression for the photocatalytic degradation of Auramine O aqueous solutions by ZnO catalyst. *Dyes and Pigments*, *75*, 246–249.

Kumar, A., Reddy, K. L., Kumar, S., Kumar, A., Sharma, V., & Krishnan, V. (2018). Rational design and development of lanthanide-doped NaYF4@ CdS–au–RGO as quaternary Plasmonic Photocatalysts for harnessing visible–near-infrared broadband Spectrum. *ACS Applied Materials & Interfaces*, *10*, 15565–15581.

Kumar, S., Sharma, R., Sharma, V., Harith, G., Sivakumar, V., & Krishnan, V. (2016). Role of RGO support and irradiation source on the photocatalytic activity of CdS–ZnO semiconductor nanostructures. *Beilstein Journal of Nanotechnology*, *7*, 1684–1697.

Kurihara, M., & Nishihara, H. (2002). Azo-and quinone-conjugated redox complexes—Photo-and proton-coupled intramolecular reactions based on d–π interaction. *Coordination Chemistry Reviews*, *226*, 125–135.

Lee, C. C., Chen, C. I., Liao, Y. T., Wu, K. C. W., Chueh, C. C., Lee, C. C., Chen, C. I., Liao, Y. T., Wu, K. C. W., & Chueh, C. C. (2019). Enhancing efficiency and stability of photovoltaic cells by using perovskite/Zr-MOF heterojunction including bilayer and hybrid structures. *Advanced Science*, *6*(5) 1801715.

Lee, P., Citrin, P., Eisenberger, P. T., & Kincaid, B. (1981). Extended X-ray absorption fine structure—Its strengths and limitations as a structural tool. *Reviews of Modern Physics*, *53*, 769.

Lee, J., Farha, O. K., Roberts, J., Scheidt, K. A., Nguyen, S. T., & Hupp, J. T. (2009). Metal–organic framework materials as catalysts. *Chemical Society Reviews*, *38*, 1450–1459.

This book belongs to Central Library BADJI Mokhtar-ANNABA UNIVERSITY

Copyright Elsevier 2024

Li, H., Eddaoudi, M., O'Keeffe, M., & Yaghi, O. M. (1999). Design and synthesis of an exceptionally stable and highly porous metal-organic framework. *Nature*, *402*, 276.

Li, X., Pi, Y., Wu, L., Xia, Q., Wu, J., Li, Z., et al. (2017). Facilitation of the visible light-induced Fenton-like excitation of H2O2 via heterojunction of g-C3N4/NH2-Iron terephthalate metal-organic framework for MB degradation. *Applied Catalysis B: Environmental*, *202*, 653–663.

Li, Y., Xu, H., Ouyang, S., & Ye, J. (2016). Metal–organic frameworks for photocatalysis. *Physical Chemistry Chemical Physics*, *18*, 7563–7572.

Liang, W., & D'Alessandro, D. M. (2013). Microwave-assisted solvothermal synthesis of zirconium oxide based metal–organic frameworks. *Chemical Communications*, *49*, 3706–3708.

Liang, R., Shen, L., Jing, F., Wu, W., Qin, N., Lin, R., et al. (2015). NH2-mediated indium metal–organic framework as a novel visible-light-driven photocatalyst for reduction of the aqueous Cr (VI). *Applied Catalysis B: Environmental*, *162*, 245–251.

Lin, K.-S., Adhikari, A. K., Ku, C.-N., Chiang, C.-L., & Kuo, H. (2012). Synthesis and characterization of porous HKUST-1 metal organic frameworks for hydrogen storage. *International Journal of Hydrogen Energy*, *37*, 13865–13871.

Lin, Y., Kong, C., & Chen, L. (2016). Amine-functionalized metal–organic frameworks: Structure, synthesis and applications. *RSC Advances*, *6*, 32598–32614.

Lin, D., Zhao, Q., Hu, L., & Xing, B. (2014). Synthesis and characterization of cubic mesoporous bridged polysilsesquioxane for removing organic pollutants from water. *Chemosphere*, *103*, 188–196.

Liu, H.-K., Tsao, T.-H., Zhang, Y.-T., & Lin, C.-H. (2009). Microwave synthesis and single-crystal-to-single-crystal transformation of magnesium coordination polymers exhibiting selective gas adsorption and luminescence properties. *CrystEngComm*, *11*, 1462–1468.

Liu, B., Zou, R.-Q., Zhong, R.-Q., Han, S., Shioyama, H., Yamada, T., et al. (2008). Microporous coordination polymers of cobalt (II) and manganese (II) 2, 6-naphthalenedicarboxylate: Preparations, structures and gas sorptive and magnetic properties. *Microporous and Mesoporous Materials*, *111*, 470–477.

Llabrés I Xamena, F. X., Corma, A., & Garcia, H. (2007). Applications for metal – organic frameworks (MOFs) as quantum dot semiconductors. *The Journal of Physical Chemistry C*, *111*, 80–85.

Mahata, P., Madras, G., & Natarajan, S. (2006). Novel photocatalysts for the decomposition of organic dyes based on metal-organic framework compounds. *The Journal of Physical Chemistry B*, *110*, 13759–13768.

Mahata, P., Sankar, G., Madras, G., & Natarajan, S. (2005). A novel sheet 4f–3d mixed-metal pyridine dicarboxylate: Synthesis, structure, photophysical properties and its transformation to a perovskite oxide. *Chemical Communications*, 5787–5789.

Martinez Joaristi, A., Juan-Alcañiz, J., Serra-Crespo, P., Kapteijn, F., & Gascon, J. (2012). Electrochemical synthesis of some archetypical Zn2+, Cu2+, and Al3+ metal organic frameworks. *Crystal Growth & Design*, *12*, 3489–3498.

Mason, T. J., & Peters, D. (2002). *Practical sonochemistry: Power ultrasound uses and applications.* Woodhead Publishing.

Mondloch, J. E., Bury, W., Fairen-Jimenez, D., Kwon, S., Demarco, E. J., Weston, M. H., et al. (2013). Vapor-phase metalation by atomic layer deposition in a metal–organic framework. *Journal of the American Chemical Society*, *135*, 10294–10297.

Mondloch, J. E., Katz, M. J., Planas, N., Semrouni, D., Gagliardi, L., Hupp, J. T., et al. (2014). Are Zr 6-based MOFs water stable? Linker hydrolysis vs. capillary-force-driven channel collapse. *Chemical Communications*, *50*, 8944–8946.

Mrowetz, M., & Selli, E. (2006). Photocatalytic degradation of formic and benzoic acids and hydrogen peroxide evolution in TiO2 and ZnO water suspensions. *Journal of Photochemistry and Photobiology A: Chemistry*, *180*, 15–22.

Mueller, U., Puetter, H., Hesse, M. & Wessel, H. 2007. WO 2005/049892, 2005. *BASF Aktiengesellschaft*.

This book belongs to Central Library BADJI Mokhtar-ANNABA UNIVERSITY

Copyright Elsevier 2024

Murray, L. J., Dincă, M., & Long, J. R. (2009). Hydrogen storage in metal–organic frameworks. *Chemical Society Reviews*, *38*, 1294–1314.

Nguyen, M.-T. H., & Nguyen, Q.-T. (2014). Efficient refinement of a metal–organic framework MIL-53 (Fe) by UV–vis irradiation in aqueous hydrogen peroxide solution. *Journal of Photochemistry and Photobiology A: Chemistry*, *288*, 55–59.

Ni, Z., & Masel, R. I. (2006). Rapid production of metal – organic frameworks via microwave-assisted solvothermal synthesis. *Journal of the American Chemical Society*, *128*, 12394–12395.

Olaopa, T. (2003). *Biological nutrient removal using the olaopa process; 2003*. Google Patents.

Parnham, E. R., & Morris, R. E. (2007). Ionothermal synthesis of zeolites, metal–organic frameworks, and inorganic–organic hybrids. *Accounts of Chemical Research*, *40*, 1005–1013.

Parsons, S. (2004). *Advanced oxidation processes for water and wastewater treatment*. IWA publishing.

Paul, A. K., Madras, G., & Natarajan, S. (2009). Adsorption–desorption and photocatalytic properties of inorganic–organic hybrid cadmium thiosulfate compounds. *Physical Chemistry Chemical Physics*, *11*, 11285–11296.

Pellegrino, F., Pellutiè, L., Sordello, F., Minero, C., Ortel, E., Hodoroaba, V.-D., et al. (2017). Influence of agglomeration and aggregation on the photocatalytic activity of TiO2 nanoparticles. *Applied Catalysis B: Environmental*, *216*, 80–87.

Pichon, A., Lazuen-Garay, A., & James, S. L. (2006). Solvent-free synthesis of a microporous metal–organic framework. *CrystEngComm*, *8*, 211–214.

Qin, J., Wang, S., & Wang, X. (2017). Visible-light reduction CO2 with dodecahedral zeolitic imidazolate framework ZIF-67 as an efficient CO-catalyst. *Applied Catalysis B: Environmental*, *209*, 476–482.

Ran, J.-W., Liu, S.-W., Wu, P., & Pei, J. (2013). Efficient photocatalytic properties of a dinuclear iron complex with bis [2-hydroxybenzaldehyde] hydrazonate ligand. *Chinese Chemical Letters*, *24*, 373–375.

Reddy, K. L., Kumar, S., Kumar, A., & Krishnan, V. (2019). Wide spectrum photocatalytic activity in lanthanide-doped upconversion nanophosphors coated with porous TiO2 and ag-cu bimetallic nanoparticles. *Journal of Hazardous Materials*, *367*, 694–705.

Reinsch, H. (2016). "Green" synthesis of metal-organic frameworks. *European Journal of Inorganic Chemistry*, *2016*, 4290–4299.

Rubio-Martinez, M., Avci-Camur, C., Thornton, A. W., Imaz, I., Maspoch, D., & Hill, M. R. (2017). New synthetic routes towards MOF production at scale. *Chemical Society Reviews*, *46*, 3453–3480.

Saien, J., & Khezrianjoo, S. (2008). Degradation of the fungicide carbendazim in aqueous solutions with UV/TiO2 process: Optimization, kinetics and toxicity studies. *Journal of Hazardous Materials*, *157*, 269–276.

Schlesinger, M., Schulze, S., Hietschold, M., & Mehring, M. (2010). Evaluation of synthetic methods for microporous metal–organic frameworks exemplified by the competitive formation of [Cu2 (btc) 3 (H2O) 3] and [Cu2 (btc)(OH)(H2O)]. *Microporous and Mesoporous Materials*, *132*, 121–127.

Sha, Z., & Wu, J. (2015). Enhanced visible-light photocatalytic performance of BiOBr/UiO-66 (Zr) composite for dye degradation with the assistance of UiO-66. *RSC Advances*, *5*, 39592–39600.

Sharmin, E., & Zafar, F. (2016). Introductory chapter: Metal organic frameworks (MOFs). In *Metal-Organic Frameworks*. IntechOpen.

Shearer, G. C., Chavan, S., Bordiga, S., Svelle, S., Olsbye, U., & Lillerud, K. P. (2016). Defect engineering: Tuning the porosity and composition of the metal–organic framework UiO-66 via modulated synthesis. *Chemistry of Materials*, *28*, 3749–3761.

Shiying, Y., Ping, W., Xin, Y., Guang, W., Zhang, W., & Liang, S. (2009). A novel advanced oxidation process to degrade organic pollutants in wastewater: Microwave-activated persulfate oxidation. *Journal of Environmental Sciences*, *21*, 1175–1180.

Sing, K. (2001). The use of nitrogen adsorption for the characterisation of porous materials. *Colloids and Surfaces A: Physicochemical and Engineering Aspects*, *187*, 3–9.

This book belongs to Central Library BADJI Mokhtar-ANNABA UNIVERSITY

Copyright Elsevier 2024

Sing, K. S. (1985). Reporting physisorption data for gas/solid systems with special reference to the determination of surface area and porosity (recommendations 1984). *Pure and Applied Chemistry*, *57*, 603–619.

Snyder, S. A., Westerhoff, P., Yoon, Y., & Sedlak, D. L. (2003). Pharmaceuticals, personal care products, and endocrine disruptors in water: Implications for the water industry. *Environmental Engineering Science*, *20*, 449–469.

Sofi, F. A., Majid, K., & Mehraj, O. (2018). The visible light driven copper based metal-organic-framework heterojunction: HKUST-1@ ag-Ag3PO4 for plasmon enhanced visible light photocatalysis. *Journal of Alloys and Compounds*, *737*, 798–808.

Son, W.-J., Kim, J., Kim, J., & Ahn, W.-S. (2008). Sonochemical synthesis of MOF-5. *Chemical Communications*, 6336–6338.

Sun, Y., & Zhou, H.-C. (2015). Recent progress in the synthesis of metal–organic frameworks. *Science and Technology of Advanced Materials*, *16*, 054202.

Tauc, J. (1970). Absorption edge and internal electric fields in amorphous semiconductors. *Materials Research Bulletin*, *5*, 721–729.

Thommes, M. (2010). Physical adsorption characterization of nanoporous materials. *Chemie Ingenieur Technik*, *82*, 1059–1073.

Tsai, W.-T., Hsu, H.-C., Su, T.-Y., Lin, K.-Y., Lin, C.-M., & Dai, T.-H. (2007). The adsorption of cationic dye from aqueous solution onto acid-activated andesite. *Journal of Hazardous Materials*, *147*, 1056–1062.

Unterlass, M. M. (2016). Green synthesis of inorganic–organic hybrid materials: State of the art and future perspectives. *European Journal of Inorganic Chemistry*, *2016*, 1135–1156.

Volkringer, C., Popov, D., Loiseau, T., Férey, G., Burghammer, M., Riekel, C., et al. (2009). Synthesis, single-crystal X-ray microdiffraction, and NMR characterizations of the giant pore metal-organic framework aluminum trimesate MIL-100. *Chemistry of Materials*, *21*, 5695–5697.

Wałęsa-Chorab, M., Patroniak, V., Kubicki, M., Kądziołka, G., Przepiórski, J., & Michalkiewicz, B. (2012). Synthesis, structure, and photocatalytic properties of new dinuclear helical complex of silver (I) ions. *Journal of Catalysis*, *291*, 1–8.

Wang, M., Cai, L., Wang, Y., Zhou, F., Xu, K., Tao, X., et al. (2017). Graphene-draped semiconductors for enhanced photocorrosion resistance and photocatalytic properties. *Journal of the American Chemical Society*, *139*, 4144–4151.

Wang, C.-C., Jing, H.-P., & Wang, P. (2014). Three silver-based complexes constructed from organic carboxylic acid and 4, 4′-bipyridine-like ligands: Syntheses, structures and photocatalytic properties. *Journal of Molecular Structure*, *1074*, 92–99.

Wang, C. J., & Li, H. X. (2019). Synthesis of iron-based metal organic framework and its visible light-driven photocatalytic degradation of dye pollutants. *Applied Organometallic Chemistry*, *33*, e4642.

Wang, C.-C., Li, H.-Y., Guo, G.-L., & Wang, P. (2013). Synthesis, characterization, and luminescent properties of a series of silver (I) complexes with organic carboxylic acid and 1, 3-bis (4-pyridyl) propane ligands. *Transition Metal Chemistry*, *38*, 275–282.

Wang, F., Li, F.-L., Xu, M.-M., Yu, H., Zhang, J.-G., Xia, H.-T., et al. (2015). Facile synthesis of a ag (i)-doped coordination polymer with enhanced catalytic performance in the photodegradation of azo dyes in water. *Journal of Materials Chemistry A*, *3*, 5908–5916.

Wang, X.-L., Luan, J., Lin, H.-Y., Liu, G.-C., & Le, M. (2014). Four cobalt (II) coordination polymers based on a flexible N, N′-bis (3-pyridinecarboxamide)-1, 6-hexane ligand: Modulation of crystal architectures through the substituent groups of isophthalates. *Polyhedron*, *71*, 111–118.

Wang, X.-L., Luan, J., Sui, F.-F., Lin, H.-Y., Liu, G.-C., & Xu, C. (2013). Structural diversities and fluorescent and photocatalytic properties of a series of CuII coordination polymers constructed from flexible bis-pyridyl-bis-amide ligands with different spacer lengths and different aromatic carboxylates. *Crystal Growth & Design*, *13*, 3561–3576.

This book belongs to Central Library BADJI Mokhtar-ANNABA UNIVERSITY

Copyright Elsevier 2024

Wang, X., Luan, J., Lin, H., Xu, C., Liu, G., Zhang, J., et al. (2013). The design and construction of a series of metal–organic coordination polymers based on two isomeric semi-rigid bis-pyridyl-bis-amide ligands and three aromatic polycarboxylates. *CrystEngComm*, *15*, 9995–10006.

Wang, X.-L., Qu, Y., Liu, G.-C., Luan, J., Lin, H.-Y., & Kan, X.-M. (2014). A series of flexible bis (imidazole)-based coordination polymers tuned by central metal ions and dicarboxylates: Diverse structures and properties. *Inorganica Chimica Acta*, *412*, 104–113.

Wang, S., & Wang, X. (2015). Multifunctional metal–organic frameworks for photocatalysis. *Small*, *11*, 3097–3112.

Wang, Q., Wang, G., Liang, X., Dong, X., & Zhang, X. (2019). Supporting carbon quantum dots on NH2-MIL-125 for enhanced photocatalytic degradation of organic pollutants under a broad spectrum irradiation. *Applied Surface Science*, *467*, 320–327.

Wang, X.-F., Zhang, Y.-B., Huang, H., Zhang, J.-P., & Chen, X.-M. (2008). Microwave-assisted solvothermal synthesis of a dynamic porous metal-carboxylate framework. *Crystal Growth & Design*, *8*, 4559–4563.

Wang, J.-L., Wang, C., & Lin, W. (2012). Metal–organic frameworks for light harvesting and photocatalysis. *ACS Catalysis*, *2*, 2630–2640.

Wen, T., Zhang, D.-X., Liu, J., Lin, R., & Zhang, J. (2013). A multifunctional helical cu (I) coordination polymer with mechanochromic, sensing and photocatalytic properties. *Chemical Communications*, *49*, 5660–5662.

Wen, T., Zhang, D.-X., & Zhang, J. (2012). Two-dimensional copper (I) coordination polymer materials as photocatalysts for the degradation of organic dyes. *Inorganic Chemistry*, *52*, 12–14.

Wen, L., Zhao, J., Lv, K., Wu, Y., Deng, K., Leng, X., et al. (2012). Visible-light-driven photocatalysts of metal–organic frameworks derived from multi-carboxylic acid and imidazole-based spacer. *Crystal Growth & Design*, *12*, 1603–1612.

West, A. R. (2014). *Solid state chemistry and its applications*. John Wiley & Sons.

Wu, Y., Luo, H., & Wang, H. (2014). Synthesis of iron (III)-based metal–organic framework/graphene oxide composites with increased photocatalytic performance for dye degradation. *RSC Advances*, *4*, 40435–40438.

Xia, Y., Wang, K.-X., & Chen, J.-S. (2010). Synthesis, structure characterization and photocatalytic properties of two new uranyl naphthalene-dicarboxylate coordination polymer compounds. *Inorganic Chemistry Communications*, *13*, 1542–1547.

Xiao, J., Xie, Y., & Cao, H. (2015). Organic pollutants removal in wastewater by heterogeneous photocatalytic ozonation. *Chemosphere*, *121*, 1–17.

Xiao, G.-B., Yao, X.-Q., Xie, H., Ma, H.-C., Yan, P.-J., & Qin, D.-D. (2019). Dinuclear cobalt-based pillar-layered-like MOF as an electrode material for supercapacitor and photocatalysis activity. *Polyhedron*, *162*, 39–44.

Yaghi, O. M., Li, G., & Li, H. (1995). Selective binding and removal of guests in a microporous metal–organic framework. *Nature*, *378*, 703.

Yam, V. W.-W., Ko, C.-C., & Zhu, N. (2004). Photochromic and luminescence switching properties of a versatile diarylethene-containing 1, 10-phenanthroline ligand and its rhenium (I) complex. *Journal of the American Chemical Society*, *126*, 12734–12735.

Yang, H., Orefuwa, S., & Goudy, A. (2011). Study of mechanochemical synthesis in the formation of the metal–organic framework Cu3 (BTC) 2 for hydrogen storage. *Microporous and Mesoporous Materials*, *143*, 37–45.

Yenisoy-Karakaş, S., Aygün, A., Güneş, M., & Tahtasakal, E. (2004). Physical and chemical characteristics of polymer-based spherical activated carbon and its ability to adsorb organics. *Carbon*, *42*, 477–484.

Yilmaz, B., Trukhan, N., & Mueller, U. (2012). Industrial outlook on zeolites and metal organic frameworks. *Chinese Journal of Catalysis*, *33*, 3–10.

Yoo, Y., Varela-Guerrero, V., & Jeong, H.-K. (2011). Isoreticular metal – organic frameworks and their membranes with enhanced crack resistance and moisture stability by surfactant-assisted drying. *Langmuir*, *27*, 2652–2657.

Yu, Z. T., Liao, Z. L., Jiang, Y. S., Li, G. H., & Chen, J. S. (2005). Water-insoluble ag–U–organic assemblies with photocatalytic activity. *Chemistry—A European Journal*, *11*, 2642–2650.

This book belongs to Central Library BADJI Mokhtar-ANNABA UNIVERSITY

Copyright Elsevier 2024

Zhang, M., Bosch, M., Gentle, T., III, & Zhou, H.-C. (2014). Rational design of metal–organic frameworks with anticipated porosities and functionalities. *CrystEngComm*, *16*, 4069–4083.

Zhang, T., & Lin, W. (2014). Metal–organic frameworks for artificial photosynthesis and photocatalysis. *Chemical Society Reviews*, *43*, 5982–5993.

Further reading

Olajire, A. A. (2018). Synthesis chemistry of metal-organic frameworks for CO 2 capture and conversion for sustainable energy future. *Renewable and Sustainable Energy Reviews*, *92*, 570–607.

This book belongs to Central Library BADJI Mokhtar-ANNABA UNIVERSITY

Copyright Elsevier 2024

CHAPTER

Photocatalytic degradation of petrochemical pollutants

7

Anupma Thakur[a,b], Praveen Kumar[c], Pardeep Singh[d], Pooja Devi[b]

Academy of Scientific and Innovative Research (AcSIR), Ghaziabad, India[a] CSIR-Central Scientific Instruments Organisation, Chandigarh, India[b] School of Material Science, Indian Association for the Cultivation of Science, Kolkata, India[c] Department of Environmental Studies, PGDAV College, University of Delhi, New Delhi, India[d]

1 Introduction: Petrochemical industry

Origin of "petroleum" attributes to "rock oil" and is a derivative of the two Latin words "petra" ascribing to rock and "oleum" to oil (Katz, 1995). In addition, petroleum is a blend of hydrocarbons and is produced from crude oil or natural gas, subjected to the state (either liquid or gaseous) of the mixture of hydrocarbons. It is a naturally occurring fluid formed by mounting up of decayed plants and animals, underneath the Earth's surface. It is in the late 1800s that petroleum became a key energy source for humankind as a substitute for "coal" for industrial revolution (Rogers, 1863). Since then the research groups, engineers, companies, and countries aided in developing the petrochemical industry revolution. In present civilization, petroleum means driving energy or power, and it is nowadays significant among humanities, including economic, political, and technological arenas. The petrochemical industry embraces the worldwide progressions and is usually organized in three main levels including (a) upstream, (b) midstream, and (c) downstream, as shown in Fig. 1. These level differs in the work distribution involving identification and production of petroleum sources, hydrocarbon processing (refineries and petrochemical plants), distribution, storage, transportation, retailing or wholesale marketing, etc. (Vassiliou, 2018).

For upstream, the activities of exploration deal with the finding of underground reservoirs, wells with detailed geological readings of liquid crude oil and gaseous fields. The practice of petroleum production employs the drilled wells, by means of which the reservoir's fluids including oil, gas, and water are fetched to the surface and classified (Gong, 2018). Further, under midstream, the events of hydrocarbon refining that include separation (by means of vacuum distillation or gas processing), petroleum-conversion methodologies (catalytic reforming, alkylation, and polymerization), and petrochemical handling (hydrotreating, hydrodesulfurization, acid gas removal, blending, storage, compressor engines, sulfur recovery plants, and wastewater treatment) (Simonsen, Strand, & Øye, 2018). Then the refined liquid petroleum products are stored aboveground chiefly in storage tanks, barrels, etc., while gaseous petroleum products majorly natural gas are stored underground in pressurized tanks, aquifers, salt domes, etc. For transportation of petrochemical products to end users largely, the use of pipelines, truck, rail, tankers, and other amenities is engaged (Albdiry & Almensory, 2016). Lastly, under downstream, petrochemical products such as gasoline, natural gas, and diesel are marketed in

Nano-Materials as Photocatalysts for Degradation of Environmental Pollutants. https://doi.org/10.1016/B978-0-12-818598-8.00007-9
© 2020 Elsevier Inc. All rights reserved.

This book belongs to Central Library BADJI Mokhtar-ANNABA UNIVERSITY

Copyright Elsevier 2024

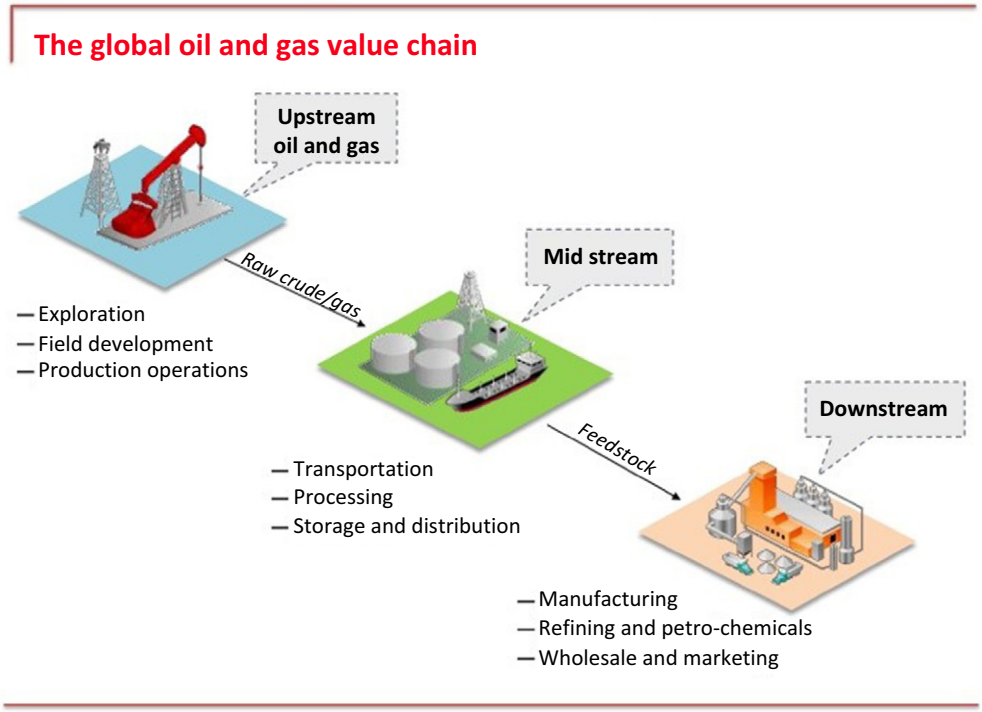

FIG. 1

Organizational levels of petrochemical industry (Themes, 2016).

retail or wholesale to end consumers. Furthermore, petroleum is a vibrant source to industrial conclave and accounts to a great fraction of the world's total energy consumption, which forms the epitome for the growth of petrochemical industry.

2 Petrochemical pollutants: Geological spread, toxicity, regulation, and environmental stress

The petrochemical industry results in the production of crude oil and natural gas by means of drilling, refining, polymerization, alkylation, distillation, and handling practices. Thereby, there are various environmental challenges imposed by the release of petrochemical pollutants, which include air emissions, wastewater, oil spills, and solid wastes from the petroleum industry as shown in Fig. 2. In the main the petroleum industry contributes to air emissions constituting of volatile organic compounds, oxides of nitrogen and sulfur, hydrogen sulfide, hydrocarbons, carbon dioxide, carbon monoxide, etc., generated from combustion and drilling activities associated with exploration and production of petroleum in petrochemical industry (Jones, 1973). Supplementary to air emissions the wastewater effluents are also produced like fluids by drilling activities, chemicals, drainage water,

This book belongs to Central Library BADJI Mokhtar-ANNABA UNIVERSITY Copyright Elsevier 2024

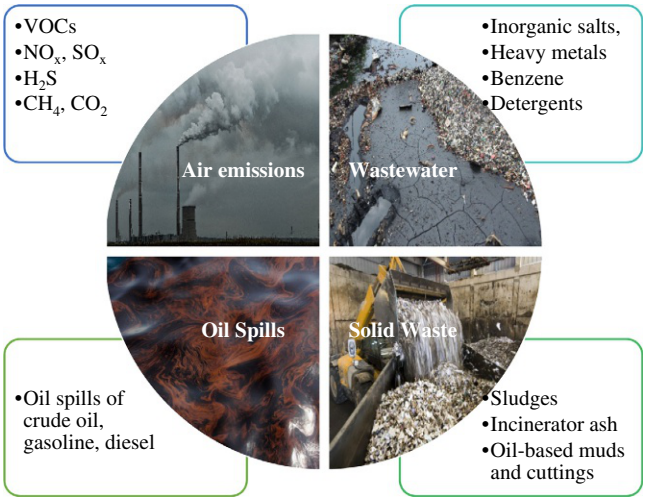

FIG. 2

Petrochemical pollutants causing environmental challenges.

leakage, and sewerage. Suitably, water is the prime aqueous resource used in petrochemical industry. In that way the wastewater is likely to be an industrial effluent and is released at the time of exploratory drilling and production operations carried out at petrochemical industry under upstream activities. Originating from the refineries, the wastewater also constitutes of crude oil, benzene, hydrocarbons, intermediates, toluene, ballast water tanks, utility service wastewater, cyanides, phenols, heavy metals, toluene, etc.(Connell, 2018).

Lying in the similar category are oil spills of gasoline, diesel, and other petrochemical products, which are largely released by the tankers, vessels of crude oil, wells, pipelines, drilling, and accidental oil spills (Fingas, 2016). Equally, the solid wastes are released to the environment by operations like piping, production activities that embrace solid wastes resembling sludge, tainted soils, semiliquid from refinery, ash, tar, oil-spilled mud and soil, etc. (Ahmed & Ahmaruzzaman, 2016). The geological spread of petrochemical pollutants is observed around the globe, but large petroleum reserves are located in middle east and northern countries, as shown in Fig. 3 (wikipedia, n.d.). The total world's energy consumption from petroleum as an energy carrier ranges from 32% for European and Asian regions and 53% for the Middle East (Cannizzaro & Weiner, 2015). Thus, dependence on petroleum reserves poses a severe threat to the environment and consequently leads its toxicity impacts causing water pollution, air pollution, soil pollution, greenhouse effect, acid rain, and climate change.

Toxicity spread of petrochemical pollutants is universally measured by standardized levels of risk exposure such as (1) acute toxicity referring to immediate effect to exposure and (2) chronic toxicity resulting by repeated, long-term exposure and health disorders like leukemia, lymphoma, and chromosomal breakage (Awasthi, Joshi, Swarup, Mandal, & Awasthi, 2016). The degree of toxicity is measured in terms of (1) lethal $dose_{50}$ (LD_{50}), dose of petrochemical pollutant with respect to tissue ($mg_{petrochemical\ pollutant}/g_{tissue}$) that roots to death; (2) lethal $concentration_{50}$ (LC_{50}), the concentration

This book belongs to Central Library BADJI Mokhtar-ANNABA UNIVERSITY
Copyright Elsevier 2024

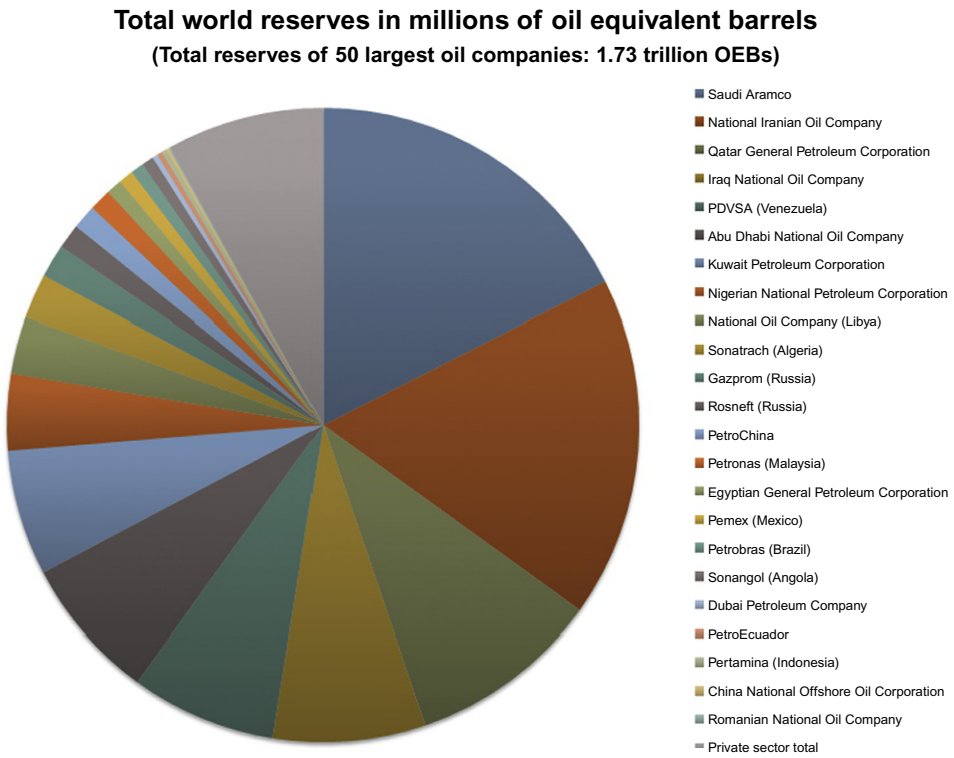

FIG. 3

World distribution of reserves of petroleum industry (wikipedia, n.d.).

(ppm) of petrochemical pollutant that eradicates the ecosystem completely; (3) lethal $dose_{LO}$ (LD_{LO}), minimal dose of a petrochemical pollutant that causes death; and (4) lethal concentration (LC_{LO}), minimal concentration of a petrochemical pollutant that causes death (Khan, Biswas, Smith, Naidu, & Megharaj, 2018). The corresponding environmental impact of toxicity spread due to petrochemical pollutants lead to greenhouse effect, smog release, climate change, acid rain, ozone depletion, heavy metal pollution in water and soil, and sludge contamination in soil and water, thus leading to devastation of ecology (Cole, 2018). The prominent greenhouse gases released by combustion operations, leaks, and vented emissions in petrochemical industry include methane, nitrous oxide, and carbon dioxide (Hentati, Lachhab, Ayadi, & Ksibi, 2013). Augmented release of greenhouse gases in the atmosphere causes escalation of greenhouse effect, which is the responsible for global warming of earth and climate change. Equally an acid rain consists of carbonic acid, sulfuric acid, and nitric acid in rainwater increasing acidity, which are due to carbon dioxide, sulfur dioxide, and nitrogen oxides dissolved in water (Kumar, 2017). As noted, the ecological impressions of petrochemical pollutants present a high risk to flora and fauna that necessitate extensive research efforts for the degradation of petrochemical effluents.

This book belongs to Central Library BADJI Mokhtar-ANNABA UNIVERSITY
Copyright Elsevier 2024

3 Methods of petrochemical pollutants degradation

Several research efforts have been made for the degradation/treatment of petrochemical pollutants and are categorized in (i) physical, (ii) chemical, and (iii) biological methods on the basis of their effectual and durable operation. The physical degradation/treatment methods, include adsorption (of organic compounds by employing activated carbon, clay, resins, etc.), coagulation, electrodialysis, microfiltration, evaporation, freezing, and air precipitation (Aljuboury, Palaniandy, Aziz, & Feroz, 2017). Largely the adsorption uses activated carbon, owing to the fact that it is substantial in porosity, structure (pellet, bead, rod, etc.), and its chemical nature, that is, acidic/basic or in terms of hydrophilicity or hydrophobicity, which makes it adaptive enough for the physical treatment of hazardous petrochemical wastes. Likewise, resins are principally investigated for the adsorption of aromatic and polymeric compounds. The chemical degradation/treatment opted is chemical oxidation by means of photocatalytic degradation under UV–vis irradiation and microwave-assisted catalytic wet air oxidation methodologies, demulsification, electrochemical process, Fenton process, ozonation, and chemical precipitation (Ding, Chu, & Wang, 2018). Amidst, the photocatalytic degradation is more effective as it employs the usage of an abundant light energy source, sun, for the degradation of pollutants. Also, chemical precipitation is adopted to precipitate out toxic wastes in the presence of the chemical that react to produce a soluble product. In the same way, biological degradation/treatment includes bioaugmentation, activated sludge, aerated filters, bioremediation, and chemostate reactors (Ghimire & Wang, 2018). The assorted metabolic, remedial, and enzymatic proficiencies of microbes/biological entities are employed for biological decontamination/mineralization of petrochemical pollutants. The fundamental principle of microbe-assisted detoxification of petrochemical pollutants is relied upon the utilization of the carbon functionalities of the petrochemical waste for their metabolic activities that, thus, degrade these pollutants. Of late, the photocatalytic degradation of petrochemical pollutants is recognized as an advanced oxidation process (AOP) and is viewed as an ecofriendly treatment practices that are efficient and cost effective in operation (Chan, Yeong Wu, Juan, & Teh, 2011).

4 Photocatalytic degradation of petrochemical pollutants: Principles and kinetic concepts of photo catalysis

Origin of "photocatalysis" is from two Greek words "phos" ascribing to photo/light and "katalyo" to catalysis or to break apart (Colmenares & Xu, 2016). Additionally, the IUPAC description of photocatalysis is stated as "a catalytic reaction involving light absorption by substrate" (Dionysiou, Puma, Ye, Schneider, & Bahnemann, 2016). So, the decisive elucidation of "photocatalysis," a process where photons are used as an excitation source for a photocatalyst and the generated charge carriers participate and accelerate the rate of chemical oxidation reaction. The fundamental principle of photocatalysis is grounded on the photoactivation of photocatalyst by the light irradiation of a suitable wavelength, followed by the absorption of photons by the photocatalyst nourishing enough energy to excite an electron from the valence band to the conduction of and generating holes in the valence band, which act as oxidizing sites for oxidation of pollutants as shown in Fig. 4.

It is witnessed that in the OH^- radicals produced after oxidation process react with the phenolic compound of petrochemical pollutants and convert them polyphenolic, aldehydes, and carboxylic acids

This book belongs to Central Library BADJI Mokhtar-ANNABA UNIVERSITY
Copyright Elsevier 2024

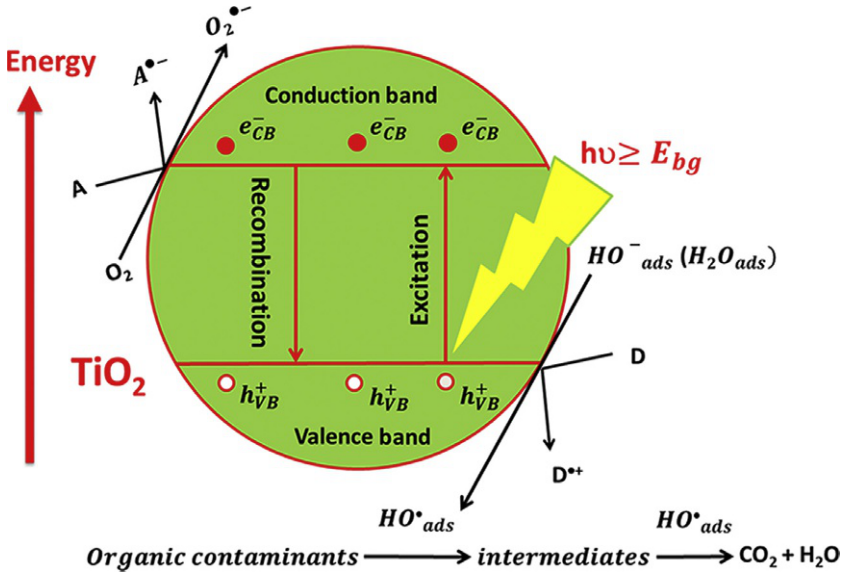

FIG. 4

Principle of photocatalytic degradation of petrochemical pollutants (Chowdhury, Nag, & Ray, 2017).

and lastly gets detoxified/mineralized to carbon dioxide and water as by-products. This chemical oxidation methodology has been widely explored for the photodegradation of numerous pollutants, namely, phenols, pesticides, alkanes, alkenes, etc. (Dionysiou et al., 2016). The reaction mechanistic of photocatalysis is experiential from the perspective of the fundamental principles of chemical kinetics, which can be a standpoint of change in color, concentration, or weight of any compound. The kinetics of the reaction predominantly is central on the law of mass action, which grounds to the increase in rate of reaction equivalently with concentration (Gaya, 2013). To understand this more clearly, let's assume photocatalytic transformation of a molecule:

$$X \xrightarrow{\text{Photocatalysis}} \text{Decomposed Products} \tag{1}$$

The decomposition of X and its rate of disappearance can be specified by a differential rate equation recognized globally as the differential rate law:

$$r = {}^{-d[X]}\!\big/_{dt} = k[\text{reactants}]^n \tag{2}$$

where k is the rate constant and n is the order, that is, 0, 1, 2, or 3, respectively; accordingly, k, the rate constant can be zero, first, second, or third order and r is expressed in mol dm^{-3} s^{-1} unit. Likewise, for the zero-order systems, the rate constant is specified as

$$r = k[X]^0 \tag{3}$$

This book belongs to Central Library BADJI Mokhtar-ANNABA UNIVERSITY
Copyright Elsevier 2024

and expressed in mol dm^{-3} s^{-1} for the time measured in seconds. Equally, for the first-order systems, the rate constant is specified as

$$k = {}^{r\left(\text{mol dm}^{-3}\text{s}^{-1}\right)} \Big/ {}_{[X]\left(\text{mol dm}^{-3}\right)} \tag{4}$$

and expressed in s^{-1}. Correspondingly, for the second-order systems, the rate constant is specified as

$$k = {}^{r\left(\text{mol dm}^{-3}\text{s}^{-1}\right)} \Big/ {}_{[X]^2\left(\text{mol dm}^{-3}\right)^2} \tag{5}$$

and expressed in mol^{-1} dm^{-3} s^{-1}. Compatibly, for the third-order systems, the rate constant is specified as

$$k = {}^{r\left(\text{mol dm}^{-3}\text{s}^{-1}\right)} \Big/ {}_{[X]^3\left(\text{mol dm}^{-3}\right)^3} \tag{6}$$

and expressed in mol^{-1} dm^{-6} s^{-1}. Typically, in literature, the research groups choose to specify rate constant with respect to min^{-1} and concentration in ppm. In the same way, in photocatalysis, the kinetic models referred to as decay models based upon the fading of the initial entities, namely, pseudo zero-order, first-order, and second-order models, are defined (Gaya, 2013). There are some foremost parametric factors that affect the photocatalytic degradation rate such as concentration and degradability of the reactant, temperature, light intensity, wavelength of light, irradiation time, and photocatalyst concentration, which require detailed studies for investigating the degradation efficiency (Bora & Mewada, 2017).

5 Perspectives and advances in photocatalysts for petrochemical degradation

Abundant photocatalysts have been investigated for the photodegradation of petrochemical compounds as tabulated in Table 1 (Abdullah et al., 2016; Basso et al., 2018; Chen et al., 2009; Hayati et al., 2018;

Table 1 Photocatalyst employed for photocatalytic petrochemical pollutant degradation

Catalyst	Pollutants degraded	Analytical metrics of degradation	Reference
Al/TiO_2	Benzene	60% in UV light	Lee, Park, Kang, Lee, and Choung (2003)
MWCNT/TiO_2	Phenol	Complete degradation in visible light	Wang, Serp, Kalck, and Faria (2005)
TiO_2/Sr_2CeO_4	Benzene	80% in UV light	Zhong et al. (2007)
CNT-doped TiO_2	Phenol	58% in UV light	Chen, Ho, Guo, Huang, and Pan (2009)
Pd/TiO_2	Benzene	60% in UV light	Zhong et al. (2009)
Zirconium-doped TiO_2/SiO_2	Toluene and xylene	Complete degradation in UV light	Kim, Shin, An, Jang, and Kim (2012)

Continued

This book belongs to Central Library BADJI Mokhtar-ANNABA UNIVERSITY

Copyright Elsevier 2024

Table 1 Photocatalyst employed for photocatalytic petrochemical pollutant degradation—cont'd

Catalyst	Pollutants degraded	Analytical metrics of degradation	Reference
Mg-ferrite/hematite/PANI nanospheres	Benzene	62% and 52% in visible light	Shen et al. (2012)
$Ca_2Nb_2O_7$ nanopolyhedra and TiO_2	Benzene	Complete degradation in UV light	Liang et al. (2013)
Nano-ZnO, TiO_2 and ZnO–TiO_2 composite	Phenol	80% in UV light	Prabha and Lathasree (2014)
$TiO_2/SiO_2/Bi_2O$	Benzene	96% in UV–visible light	Ren, Qiu, Zhang, He, and Chen (2015)
V_2O_5/TiO_2	1,3,5-Trichlorobenzene chlorinated benzenes	60% in UV light	Wang et al. (2015)
Carbon/nitrogen-doped TiO_2	Phenol	64% in UV light	Abdullah, Al-Thani, Tawbi, and Al-Kandari (2016)
ZnO/TiO_2 decorated rGO	Phenol and petrochemical wastewater	Complete degradation in visible light	Hayati, Isari, Fattahi, Anvaripour, and Jorfi (2018)
TiO_2-P25	Toluene	70% in UV light	Basso, Battisti, Moreira, and José (2018)
TiO_2-nanobelts	Toluene	60% in UV light	Wu, Jiang, Chen, and Xin (2018)
Gd-doped β-Bi_2O_3	4-Chlorophenol	92.3% in visible light	Lin, Du, Tong, Ji, and Jiao (2019)

Kim et al., 2012; Lee et al., 2003; Liang et al., 2013; Lin et al., 2019; Prabha & Lathasree, 2014; Ren et al., 2015; Shen et al., 2012; Wang et al., 2005; Wang et al., 2015; Wu et al., 2018; Zhong et al., 2007; Zhong et al., 2009) and are highlighted in this section. The research trend of photocatalytic degradation of petrochemical pollutants is portrayed in terms of number literature published and cited, as shown in Fig. 5.

5.1 UV/Visible light-driven photocatalysts

Quite a lot of semiconductor photocatalysts, namely, TiO_2, ZnO, CdS, etc., have been investigated for the photocatalytic degradation of petrochemical pollutants. TiO_2 is a naturally occurring metal oxide of transition metal family and is most frequently used for photocatalytic degradation in various industries, such as cosmetics, textiles, and pharmaceutics (Ohno, Sarukawa, Tokieda, & Matsumura, 2001). Owing to its chief properties like cost-effectiveness, chemical stability, biological inertness, and nontoxicity, it is widely opted photocatalyst. Several studies have been steered for photocatalytic degradation of petrochemical pollutants by employing the use of TiO_2, which are outlined here. Shahrezaei et al. reported the successful usage of TiO_2 photocatalyst for the photocatalytic degradation of phenol and its derivatives from polluted refinery wastewater of petrochemical industry under both circulating and

This book belongs to Central Library BADJI Mokhtar-ANNABA UNIVERSITY Copyright Elsevier 2024

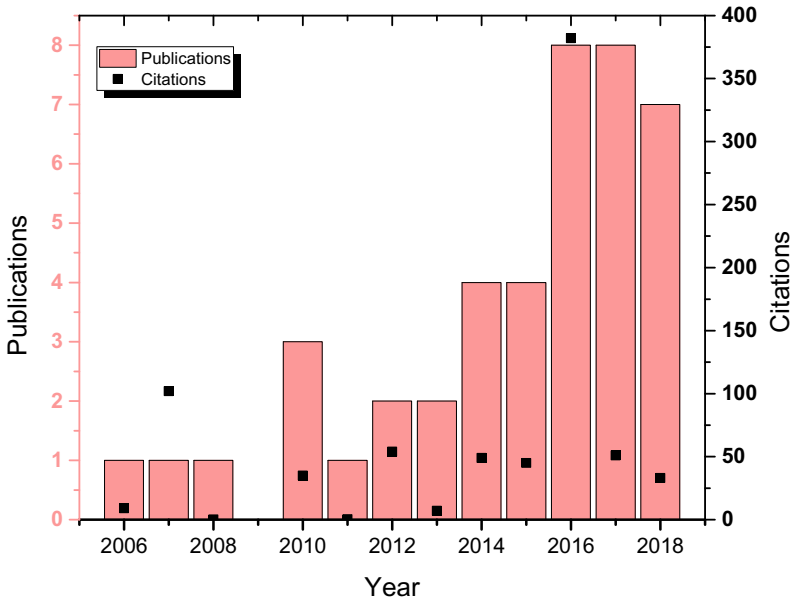

FIG. 5

Trends of published and cited literature on photocatalytic degradation of petrochemical pollutants (Web of Science, n.d.)

direct irradiation reactor. The tailed studies revealed about 90% of degradation of phenolic pollutants in 2 hours of irradiation time (Shahrezaei, Akhbari, & Rostami, 2012). Wang et al. deliberated the potential application of TiO_2 nanoparticles as an effectual photocatalyst for the photodegradation of gaseous benzene as compared with P25, owing to its high surface area and large charge carrier separation efficiency (Wang & Wu, 2015). Fard et al. studied the performance of photoreactor packed with titanium dioxide (TiO_2) toward the photodegradation of petroleum aromatic hydrocarbons. The presented results attribute to the successful degradation of aromatic hydrocarbons and obey the first-order kinetics (Alizadeh Fard, Aminzadeh, & Vahidi, 2013). Likewise, ZnO-based photocatalysts, having bandgap of 3.37 eV, thus, have capability to absorb in a wider spectrum of solar irradiation and is extensively used for degradation of a wide range of organic pollutants (Tian et al., 2012). There are studies available from literature for photocatalytic degradation of petrochemical pollutants by employing the use of ZnO, which are outlined here. Ashar et al. studied the potential application of ZnO nanoflowers for the photocatalytic degradation of nonylphenol ethoxylate-9 (NP9EO) and petrochemical pollutants in industrial wastewater under UV and solar irradiation successfully. The tailed studies revealed about complete degradation in 12 hours of irradiation (Ashar et al., 2016). In line, Abbad et al. reported the effectual use of commercial ZnO catalyst for the photocatalytic degradation of chlorophenols, a major pollutant found in petrochemical wastewater. The presented results showcase the successful degradation of these pollutants in 120 minutes, and this system follow the first-order kinetics, and the rate constant is inversely proportional to initial concentration of the chlorophenols (Ba-Abbad, Kadhum, Mohamad, Takriff, & Sopian, 2013).

This book belongs to Central Library BADJI Mokhtar-ANNABA UNIVERSITY Copyright Elsevier 2024

5.2 Heterogeneous photocatalysts (binary, ternary, etc.)

In comparison with individual UV/visible photocatalysts, the nanocomposites composed of two or more photocatalysts, that is, "heterophotocatalysts," are more effectual as they facilitate charge carrier separation and fast charge carrier transfer, resulting in remarkable photocatalytic efficiency. Few heterophotocatalysts have been investigated for the efficient photocatalytic degradation of petrochemical pollutants. Palaniandy et al. studied the effect TiO_2/ZnO photocatalyst to treat petroleum wastewater. This heterophotocatalyst was effective enough to treat petrochemical wastewater from 18% to 79% for total organic carbon (TOC) removal and from 24% to 51% for chemical oxygen demand (COD) removal (Palaniandy, Abdul Aziz, Feroz, Amr, & Salem, 2016). Similarly, Sharifnia et al. elucidated the TiO_2 nanoparticles immobilized on light expanded clay aggregate (LECA) as a new porous and light weight support for the photocatalytic degradation of ammonia from petrochemical wastewater under solar light irradiation. The presented experimental results showcase the maximum achieved ammonia (975 mg/L concentration) degradation of 96.5% with the proposed photocatalyst at pH 11 (Shavisi, Sharifnia, Zendehzaban, Mirghavami, & Kakehazar, 2014). Shokri et al. studied the effect of a novel boron–graphene oxide–TiO_2 (B–GO–TiO_2) photocatalyst to treat 4-nitrophenol. The photocatalytic degradation activity of 4-nitrophenol was examined by UV–vis absorption measurements in acidic pH. The presented results show the removal efficiency of 4-nitrophenol and chemical oxygen demand (COD) was about 100% and 85%, respectively, under visible light irradiation (Shokri, Mahanpoor, & Soodbar, 2016). Peng et al. reported zinc oxide thin films on aluminum foil synthesized by sol-gel approach to degrade phenol pollutants. The results presented the photocatalytic degradation of phenol (20 mg/L) under the visible light irradiation, with more than 40% degradation efficiency (Peng, Wang, Yu, & Chen, 2006). Wang et al. studied the nanosized multiwalled carbon nanotubes (MWCNTs)/TiO_2 composite toward the degradation of 2,4-dinitrophenol (DNP) under solar irradiation. The presented photocatalysts were synthesized by sol-gel method, further evaluated for their photocatalytic activity, and was found to be very effectual in the complete decolorization of DNP and COD reduction of real wastewater (Wang, Wang, Jiang, & Li, 2009). Similarly, McManamon et al. presented the photocatalytic degradation of phenol using zirconia-doped TiO_2 nanoparticles carried out using 40 W-UV bulb at 365 nm (McManamon, Holmes, & Morris, 2011). Jo et al. presented one-step synthesis of graphitic carbon–TiO_2 nanocomposites with different carbon loadings that were examined for the degradation of aqueous nitrobenzene (NB) under UV irradiation. Their results presented higher photocatalytic NB degradation yield (up to 96% in 4 hours) (Jo, Won, Hwang, & Tayade, 2014). Prince et al. investigated ZnAl and ZnGaAl layered double hydroxides for the photocatalytic degradation capability of these oxides toward phenol, a very recalcitrant compound, as a probe. The presented results portrayed about 80% degradation efficiency in 6 hours of the synthesized photocatalysts (Prince, Tzompantzi, Mendoza-Damián, Hernández-Beltrán, & Valente, 2015). He et al. studied Co-TiO_2/zeolite photocatalyst, which was synthesized by sol–gel method and was validated to possess a good efficiency toward degradation of petrochemical pollutants from petrochemical wastewater. The results presented 93.4% COD removal efficiency, and the Co-TiO_2/zeolite photocatalysts showed a good stability toward photocatalytic degradation of petrochemical wastewater (He et al., 2017). Hayati et al. investigated ZnO/TiO_2 anchored reduced graphene oxide (rGO), a ternary nanocomposite toward photocatalytic decontamination of phenol in aqueous solutions under visible light illumination. The results portrayed that the photocatalytic degradation process followed pseudo-first-order kinetic model (Hayati et al., 2018). Zhang et al. presented a bamboo-like architecture,

This book belongs to Central Library BADJI Mokhtar-ANNABA UNIVERSITY
Copyright Elsevier 2024

CuO nanosheets and Ag nanoparticles codecorated TiO_2 nanotube arrays ($Ag/CuO/TiO_2$), toward photocatalytic degradation of 2,4-dinitrophenol (DNP) under simulated solar light irradiation. The photocatalytic degradation rate of $Ag/CuO/TiO_2$ photocatalyst was about 2.0 times that over controls, which was ascribed to improved light absorption, reduced carrier recombination, and more exposed active sites (Zhang et al., 2016). Alalm et al. reported the photocatalytic degradation of phenol by TiO_2(P25) immobilized on powdered activated carbon (TiO_2/AC). The presented results portrayed the complete degradation of phenol at an illumination time of 120 minutes, which indicates that the studied photocatalyst is very effective for phenol degradation (Gar Alalm, Tawfik, & Ookawara, 2016). Lin et al. presented the photocatalytic degradation of 4-chlorophenol by Gd-doped β-Bi_2O_3 under visible light irradiation. The results showed the degradation rate of 4-chlorophenol reached 92.3%, and it was ventured that the mechanism of the degradation of 4-chlorophenol is based upon the oxidative photochemical process (Lin et al., 2019). Hamdi et al. reported the photodegradation of phenol with SnO_2 nanoparticles under UV light irradiation. Further, to augment more light absorption, SnO_2:Sb nanoparticles were synthesized, and the efficiency of 95% of phenol degradation in 2 h under solar light irradiation was achieved (Al-Hamdi, Sillanpää, Bora, & Dutta, 2016). Likewise, Anjum et al. reported a heterophotocatalyst, that is, $ZnO–ZnS/Ag_2O–Ag_2S$ nanocomposite for the photocatalytic degradation of 2-chlorophenol and phenolic pollutants in real sludge of petrochemical industrial wastewater. At the same time, this photocatalyst was operative enough in solubilization of sludge for biogas production. The results present nearly 43% of upsurge in the biogas production from the photocatalytically treated sludge (Anjum, Kumar, & Barakat, 2017). Equally, CdS-based photocatalysts, having narrow bandgap (2.4 eV), thus, aid in light-trapped greater photoactivity and better degradation potential of various environmental pollutants (Jing & Guo, 2006). There are studies available from literature for photocatalytic degradation of petrochemical pollutants by employing the use of CdS, which are outlined here. Additionally, CdS has been expansively studied for the photocatalytic degradation of petrochemical waste along with other semiconductors like TiO_2 and ZnO as heterogeneous photocatalytic nanocomposites. Lavand et al. reported the potential application of C/ZnO/CdS nanocomposite as an efficient photocatalyst for the photocatalytic degradation of 4-chlorophenol and phenolic compounds via Z-scheme mechanism. The CdS here plays a vital role as photosensitizers to extend the photon absorption of C-doped ZnO from UV to the visible solar spectrum (Lavand & Malghe, 2015).

6 Summary

This chapter has engaged its chief prominence on the essential features of solar energy–assisted photocatalytic degradation of petrochemical pollutants to benchmark the details of principles and kinetics of photocatalytic degradation methodologies. Further, a directed assessment of the photocatalysts investigated for the photocatalytic degradation of petrochemical pollutants is epitomized, concentrating onto the requisite of superior understanding and research efforts to realize more reckonable results with enhanced elucidation.

Acknowledgements

The authors acknowledge the consistent support received from Director, CSIR-CSIO, and Director, IACS, India. AT also acknowledges DST for the INSPIRE grant for her doctoral studies.

This book belongs to Central Library BADJI Mokhtar-ANNABA UNIVERSITY Copyright Elsevier 2024

References

Abdullah, A. M., Al-Thani, N. J., Tawbi, K., & Al-Kandari, H. (2016). Carbon/nitrogen-doped TiO2: New synthesis route, characterization and application for phenol degradation. *Arabian Journal of Chemistry*, *9*, 229–237.

Ahmed, M. J. K., & Ahmaruzzaman, M. (2016). A review on potential usage of industrial waste materials for binding heavy metal ions from aqueous solutions. *Journal of Water Process Engineering*, *10*, 39–47.

Albdiry, M., & Almensory, M. (2016). Failure analysis of drillstring in petroleum industry: A review. *Engineering Failure Analysis*, *65*, 74–85.

Al-Hamdi, A. M., Sillanpää, M., Bora, T., & Dutta, J. (2016). Efficient photocatalytic degradation of phenol in aqueous solution by SnO2: Sb nanoparticles. *Applied Surface Science*, *370*, 229–236.

Alizadeh Fard, M., Aminzadeh, B., & Vahidi, H. (2013). Degradation of petroleum aromatic hydrocarbons using TiO2 nanopowder film. *Environmental Technology*, *34*, 1183–1190.

Aljuboury, D., Palaniandy, P., Aziz, H. A., & Feroz, S. (2017). Treatment of petroleum wastewater by conventional and new technologies–A review. *Global NEST Journal*, *19*, 439–452.

Anjum, M., Kumar, R., & Barakat, M. (2017). Visible light driven photocatalytic degradation of organic pollutants in wastewater and real sludge using ZnO–ZnS/Ag2O–Ag2S nanocomposite. *Journal of the Taiwan Institute of Chemical Engineers*, *77*, 227–235.

Ashar, A., Iqbal, M., Bhatti, I. A., Ahmad, M. Z., Qureshi, K., Nisar, J., et al. (2016). Synthesis, characterization and photocatalytic activity of ZnO flower and pseudo-sphere: Nonylphenol ethoxylate degradation under UV and solar irradiation. *Journal of Alloys and Compounds*, *678*, 126–136.

Awasthi, G., Joshi, D., Swarup, A., Mandal, T., & Awasthi, D. (2016). Epidemiological studies on petroleum toxicity. *International Journal of Pharmaceutics & Drug Analysis*, *4*, 251–257.

Ba-Abbad, M. M., Kadhum, A. A. H., Mohamad, A. B., Takriff, M. S., & Sopian, K. (2013). Photocatalytic degradation of chlorophenols under direct solar radiation in the presence of ZnO catalyst. *Research on Chemical Intermediates*, *39*, 1981–1996.

Basso, A., Battisti, A. P., Moreira, R. d. F. P. M., & José, H. J. (2018). Photocatalytic effect of addition of TiO2 to acrylic-based paint for passive toluene degradation. *Environmental Technology*, 1–12.

Bora, L. V., & Mewada, R. K. (2017). Visible/solar light active photocatalysts for organic effluent treatment: Fundamentals, mechanisms and parametric review. *Renewable and Sustainable Energy Reviews*, *76*, 1393–1421.

Cannizzaro, A. P., & Weiner, R. J. (2015). Multinational investment and voluntary disclosure: Project-level evidence from the petroleum industry. *Accounting, organizations and society*, *42*, 32–47.

Chan, S. H. S., Yeong Wu, T., Juan, J. C., & Teh, C. Y. (2011). Recent developments of metal oxide semiconductors as photocatalysts in advanced oxidation processes (AOPs) for treatment of dye waste-water. *Journal of Chemical Technology & Biotechnology*, *86*, 1130–1158.

Chen, L. -C., Ho, Y. -C., Guo, W. -S., Huang, C. -M., & Pan, T. -C. (2009). Enhanced visible light-induced photoelectrocatalytic degradation of phenol by carbon nanotube-doped TiO2 electrodes. *Electrochimica Acta*, *54*, 3884–3891.

Chowdhury, P., Nag, S., & Ray, A. K. (2017). Degradation of phenolic compounds through UV and visible-light-driven photocatalysis: Technical and economic aspects. In *Phenolic Compounds-Natural Sources, Importance and Applications*. IntechOpen.

Cole, G. M. (2018). *Assessment and remediation of petroleum contaminated sites*. Routledge.

Colmenares, J. C., & Xu, Y. -J. (2016). Heterogeneous Photocatalysis. In *Green Chemistry and Sustainable Technology*.

Connell, D. W. (2018). *Pollution in tropical aquatic systems*. CRC Press.

Ding, P., Chu, L., & Wang, J. (2018). Advanced treatment of petrochemical wastewater by combined ozonation and biological aerated filter. *Environmental Science and Pollution Research*, 1–10.

This book belongs to Central Library BADJI Mokhtar-ANNABA UNIVERSITY

Copyright Elsevier 2024

Dionysiou, D. D., Puma, G. L., Ye, J., Schneider, J., & Bahnemann, D. (2016). *Photocatalysis: Applications*. Royal Society of Chemistry.

Fingas, M. (2016). *Oil spill science and technology*. Gulf Professional Publishing.

Gar Alalm, M., Tawfik, A., & Ookawara, S. (2016). Solar photocatalytic degradation of phenol by TiO2/AC prepared by temperature impregnation method. *Desalination and Water Treatment*, *57*, 835–844.

Gaya, U. I. (2013). *Heterogeneous photocatalysis using inorganic semiconductor solids*. Springer Science & Business Media.

Ghimire, N., & Wang, S. (2018). Biological treatment of petrochemical wastewater. In *Petroleum Chemicals*: IntechOpen.

Gong, B. (2018). Total-factor spillovers, similarities, and competitions in the petroleum industry. *Energy Economics*, *73*, 228–238.

Hayati, F., Isari, A. A., Fattahi, M., Anvaripour, B., & Jorfi, S. (2018). Photocatalytic decontamination of phenol and petrochemical wastewater through ZnO/TiO 2 decorated on reduced graphene oxide nanocomposite: influential operating factors, mechanism, and electrical energy consumption. *RSC Advances*, *8*, 40035–40053.

He, Q., Si, S., Song, L., Yan, H., Yao, Y., Zhao, D., et al. (2017). Refractory petrochemical wastewater treatment by K2S2O8 assisted photocatalysis. *Saudi Journal of Biological Sciences*.

Hentati, O., Lachhab, R., Ayadi, M., & Ksibi, M. (2013). Toxicity assessment for petroleum-contaminated soil using terrestrial invertebrates and plant bioassays. *Environmental Monitoring and Assessment*, *185*, 2989–2998.

Jing, D., & Guo, L. (2006). A novel method for the preparation of a highly stable and active CdS photocatalyst with a special surface nanostructure. *The Journal of Physical Chemistry B*, *110*, 11139–11145.

Jo, W. -K., Won, Y., Hwang, I., & Tayade, R. J. (2014). Enhanced photocatalytic degradation of aqueous nitrobenzene using graphitic carbon–TiO2 composites. *Industrial & Engineering Chemistry Research*, *53*, 3455–3461.

Jones, H. R. (1973). *Pollution control in the petroleum industry*. Noyes Data Corporation.

Katz, B. (1995). Petroleum source rocks—An introductory overview. In *Petroleum Source Rocks* (pp. 1–8). Springer.

Khan, M. A. I., Biswas, B., Smith, E., Naidu, R., & Megharaj, M. (2018). Toxicity assessment of fresh and weathered petroleum hydrocarbons in contaminated soil-a review. *Chemosphere*.

Kim, C. -S., Shin, J. -W., An, S. -H., Jang, H. -D., & Kim, T. -O. (2012). Photodegradation of volatile organic compounds using zirconium-doped TiO2/SiO2 visible light photocatalysts. *Chemical Engineering Journal*, *204*, 40–47.

Kumar, S. (2017). Acid rain—The major cause of pollution: Its causes, effects. *International Journal of Applied Chemistry*, *13*, 53–58.

Lavand, A. B., & Malghe, Y. S. (2015). Visible light photocatalytic degradation of 4-chlorophenol using C/ZnO/CdS nanocomposite. *Journal of Saudi Chemical Society*, *19*, 471–478.

Lee, B. -Y., Park, S. -H., Kang, M., Lee, S. -C., & Choung, S. -J. (2003). Preparation of Al/TiO2 nanometer photocatalyst film and the effect of H2O addition on photo-catalytic performance for benzene removal. *Applied Catalysis A: General*, *253*, 371–380.

Liang, S., Wen, L., Liu, G., Zhu, S., Yuan, R., & Wu, L. (2013). Comparative study of photocatalytic activities of Ca2Nb2O7 nanopolyhedra and TiO2: Degradations of benzene and methyl orange. *Catalysis Today*, *201*, 175–181.

Lin, S., Du, W., Tong, L., Ji, T., & Jiao, X. (2019). Photocatalytic Degradation of 4-Chlorophenol by Gd-Doped β-Bi 2 O 3 Under Visible Light Irradiation. *Chemical Research in Chinese Universities*, *35*, 120–124.

McManamon, C., Holmes, J. D., & Morris, M. A. (2011). Improved photocatalytic degradation rates of phenol achieved using novel porous ZrO2-doped TiO2 nanoparticulate powders. *Journal of Hazardous Materials*, *193*, 120–127.

This book belongs to Central Library BADJI Mokhtar-ANNABA UNIVERSITY

Copyright Elsevier 2024

Ohno, T., Sarukawa, K., Tokieda, K., & Matsumura, M. (2001). Morphology of a TiO2 photocatalyst (Degussa, P-25) consisting of anatase and rutile crystalline phases. *Journal of Catalysis*, *203*, 82–86.

Palaniandy, P., Abdul Aziz, H. B., Feroz, S., Amr, A., & Salem, S. (2016). Evaluating photo-degradation of COD and TOC in petroleum refinery wastewater by using TiO2/ZnO photo-catalyst. *Water Science and Technology*, *74*, 1312–1325.

Peng, F., Wang, H., Yu, H., & Chen, S. (2006). Preparation of aluminum foil-supported nano-sized ZnO thin films and its photocatalytic degradation to phenol under visible light irradiation. *Materials Research Bulletin*, *41*, 2123–2129.

Prabha, I., & Lathasree, S. (2014). Photodegradation of phenol by zinc oxide, titania and zinc oxide–titania composites: nanoparticle synthesis, characterization and comparative photocatalytic efficiencies. *Materials Science in Semiconductor Processing*, *26*, 603–613.

Prince, J., Tzompantzi, F., Mendoza-Damián, G., Hernández-Beltrán, F., & Valente, J. S. (2015). Photocatalytic degradation of phenol by semiconducting mixed oxides derived from Zn (Ga) Al layered double hydroxides. *Applied Catalysis B: Environmental*, *163*, 352–360.

Ren, C., Qiu, W., Zhang, H., He, Z., & Chen, Y. (2015). Degradation of benzene on TiO2/SiO2/Bi2O3 photocatalysts under UV and visible light. *Journal of Molecular Catalysis A: Chemical*, *398*, 215–222.

Rogers, H. D. (1863). Coal and petroleum. *Good Words*, *4*, 374–379.

Shahrezaei, F., Akhbari, A., & Rostami, A. (2012). Photodegradation and removal of phenol and phenolic derivatives from petroleum refinery wastewater using nanoparticles of TiO2. *IJEE*, *3*, 267–274.

Shavisi, Y., Sharifnia, S., Zendehzaban, M., Mirghavami, M. L., & Kakehazar, S. (2014). Application of solar light for degradation of ammonia in petrochemical wastewater by a floating TiO2/LECA photocatalyst. *Journal of Industrial and Engineering Chemistry*, *20*, 2806–2813.

Shen, Y., Zhao, Q., Li, X., Yuan, D., Hou, Y., & Liu, S. (2012). Enhanced visible-light induced degradation of benzene on Mg-ferrite/hematite/PANI nanospheres: In situ FTIR investigation. *Journal of Hazardous Materials*, *241*, 472–477.

Shokri, A., Mahanpoor, K., & Soodbar, D. (2016). Evaluation of a modified TiO2 (GO–B–TiO2) photo catalyst for degradation of 4-nitrophenol in petrochemical wastewater by response surface methodology based on the central composite design. *Journal of Environmental Chemical Engineering*, *4*, 585–598.

Simonsen, G., Strand, M., & Øye, G. (2018). Potential applications of magnetic nanoparticles within separation in the petroleum industry. *Journal of Petroleum Science and Engineering*, *165*, 488–495.

Themes, M. (2016). *Global energy trends and dynamics*. Available: https://energyroutes.eu/2016/05/23/porters-five-forces-model-for-oil-and-gas-industry/.

Tian, C., Zhang, Q., Wu, A., Jiang, M., Liang, Z., Jiang, B., et al. (2012). Cost-effective large-scale synthesis of ZnO photocatalyst with excellent performance for dye photodegradation. *Chemical Communications*, *48*, 2858–2860.

Vassiliou, M. S. (2018). *Historical dictionary of the petroleum industry*. Rowman & Littlefield.

Wang, W., Serp, P., Kalck, P., & Faria, J. L. (2005). Visible light photodegradation of phenol on MWNT-TiO2 composite catalysts prepared by a modified sol–gel method. *Journal of Molecular Catalysis A: Chemical*, *235*, 194–199.

Wang, H., Wang, H. -L., Jiang, W. -F., & Li, Z. -Q. (2009). Photocatalytic degradation of 2, 4-dinitrophenol (DNP) by multi-walled carbon nanotubes (MWCNTs)/TiO2 composite in aqueous solution under solar irradiation. *Water Research*, *43*, 204–210.

Wang, J., Wang, X., Liu, X., Zhu, T., Guo, Y., & Qi, H. (2015). Catalytic oxidation of chlorinated benzenes over V2O5/TiO2 catalysts: The effects of chlorine substituents. *Catalysis Today*, *241*, 92–99.

Wang, C., & Wu, T. (2015). TiO2 nanoparticles with efficient photocatalytic activity towards gaseous benzene degradation. *Ceramics International*, *41*, 2836–2839.

Web of Science, n.d. Available: https://www.webofknowledge.com/.

This book belongs to Central Library BADJI Mokhtar-ANNABA UNIVERSITY

Copyright Elsevier 2024

Wikipedia. n.d. Petroleum industry. Available: https://en.wikipedia.org/wiki/Petroleum_industry.

Wu, S., Jiang, Y., Chen, Q., & Xin, Y. (2018). Photocatalytic degradation of toluene by TiO_2 nanobelts: an experimental research. *Environmental Science & Technology*, 4.

Zhang, X., Wang, L., Liu, C., Ding, Y., Zhang, S., Zeng, Y., et al. (2016). A bamboo-inspired hierarchical nanoarchitecture of Ag/CuO/TiO2 nanotube array for highly photocatalytic degradation of 2, 4-dinitrophenol. *Journal of Hazardous Materials*, *313*, 244–252.

Zhong, J. B., Lu, Y., Jiang, W. D., Meng, Q. M., He, X. Y., Li, J. Z., et al. (2009). Characterization and photocatalytic property of Pd/TiO2 with the oxidation of gaseous benzene. *Journal of Hazardous Materials*, *168*, 1632–1635.

Zhong, J., Wang, J., Tao, L., Gong, M., Zhimin, L., & Chen, Y. (2007). Photocatalytic degradation of gaseous benzene over TiO2/Sr2CeO4: Preparation and photocatalytic behavior of TiO2/Sr2CeO4. *Journal of Hazardous Materials*, *140*, 200–204.

This book belongs to Central Library BADJI Mokhtar-ANNABA UNIVERSITY

Copyright Elsevier 2024

This page intentionally left blank

This book belongs to Central Library BADJI Mokhtar-ANNABA UNIVERSITY

Copyright Elsevier 2024

CHAPTER

Photodegradation of pharmaceutical waste by nano-materials as photocatalysts

8

Yong Chen

School of Environmental Science and Engineering, Huazhong University of Science and Technology, Wuhan, China

1 Introduction

In the recent years, the world has been well aware of the significance of the continuous improvement on the area of synthesis and production of various organic compounds for various industrial usages. Different chemical compounds were widely used as industrial products that are extensively used in various applications. Wastewater from these industries without proper disposal of the compounds may cause severe damage to the aquatic system (Czech & Buda, 2015; Deveci, Dizge, Yatmaz, & Tansel, 2016; Henneberg & Triebskorn, 2015). The occurrence of evolving organic compounds from some pharmaceutical industries was reported in treatment plant effluents. Usually, pharmaceutical compounds found in surface water, ground water, tap water, drinking water, ocean water, sediments, and soil. These compounds produced some physiological effects on human beings and also to the animals in minimum concentrations. The determination of these pharmaceuticals against biological degradation and its biological activity were the major advantages of the pollutants. They maintain their chemical form in the environment long enough to spread pollutions to the aquatic system. Both the low and high concentrations of the pharmaceutical pollutants are hazardous to the environment. Generally, antibiotics, painkillers, cytostatic drugs, anticonvulsants, and beta-blockers in the effluents were the possible pollutants in the water and create detrimental effects to the environment. Those pollutants persisted in the environment and then enter into the food chain to cause several effects to the humans. Therefore, degradation of pharmaceutical compounds in the environment has become a worldwide problem (Verma, Chhikara, & Dixit, 2014). However, it affects the environment; the usage of organic compounds is inevitable in the current scenario.

Several methods such as biological, chemical, physical, and electrochemical oxidation have been recognized particularly in effluent treatment in the wastewater system (Guo et al., 2016). Among these treatment methods, some of them use chemicals as catalyst or initiator to degrade the pollutants in the water. Retrieval of such compounds afterward the treatment process is an additional problem in the wastewater treatment. Conventional actions are sometimes ineffective, because some sort of pollutants found in the wastewater are recalcitrant to certain extent (Bergendahl & O'Shaughnessy, 2004). Therefore, an innovative treatment technique is required to degrade the contaminants in the wastewater system. In the recent past, investigation has been widely focused on the wastewater management

Nano-Materials as Photocatalysts for Degradation of Environmental Pollutants. https://doi.org/10.1016/B978-0-12-818598-8.00008-0
© 2020 Elsevier Inc. All rights reserved.

This book belongs to Central Library BADJI Mokhtar-ANNABA UNIVERSITY

Copyright Elsevier 2024

by advanced oxidation processes (AOPs). Among various AOPs, treatment of wastewater using nanoparticle has brought greater attention owing to its unique properties. Till now, several studies were found in the literature associated to the application of nanoparticles in AOPs. Because production of ˙OH radicals in the AOPs is usually high, these •OH radicals are accountable for the degradation of organic contaminants in the wastewater system. As associated with several conventional methods, AOPs are more effective and capable of degrading the pollutants with less toxic intermediate products. Various AOPs like ozonation, UV irradiation, UV with H_2O_2, ozone coupled with H_2O_2, ozone with both UV and H_2O_2, ozone with catalysts, Fenton, photo-Fenton (Fe^{2+}/H_2O_2 and Fe^{2+}/H_2O_2/UV), sonication, and photocatalysis were available for the treatment of wastewater pollutants (Bethi, Sonawane, Bhanvase, & Gumfekar, 2016). Yet, common wastewater handlings are usually expensive, and larger area is essential for the degradation process. Therefore, a simple low-cost method can be executed to degrade the effluents. One of the possible choices to change these downsides into better outcome is an application of photocatalysis using nanomaterials. Till date, various notable photocatalytic materials have shown promising photocatalytic activity. Moreover, the demand for exploring novel materials with improved reactivity in photocatalysis is also playing a key role in developing technologies. Henceforth, present research is mostly focused on the synthesis of visible light active photocatalyst for the degradation of organic compounds (Li et al., 2014; Rahman, Ahmad, Misra, & Lohani, 2013; Selvin et al., 2017). At present, semiconductor nanoparticles as a photocatalyst are widely used to treat the wastewater system. Several research investigation has been done in the field of water treatment by nanomaterials. It was proved that the use of nanomaterials are capable to degrade the pollutants effectively. Nanomaterials like nanomembrane, nanoparticles, nanopowder, and nanocomposites have been effectively used for the degradation of several pollutants such as chemical compounds and biological substances that contain heavy metals, algae, bacteria, viruses, organics, nutrients, and antibiotics (Bethi et al., 2016). For that reason, nanotechnology is the promising technology for creating new nanomaterials and devices that took advantage in the wastewater treatment due to their extreme small size with other unique properties. Normally, the high surface-area-to-volume/mass ratios of nanomaterials will significantly increase the adsorption capacity of corresponding materials (Qu, Alvarez, & Li, 2013; Rickerby & Morrison, 2007; Vaseashta et al., 2007). Recent literatures on wastewater treatment with nanotechnology have shown some promising outcome with several semiconductors such as nanocatalysts, nanoclusters, nanorods, nanoclays, and nanocomposites. The most reported semiconductor nanocatalysts are TiO_2 and ZnO (Klaine et al., 2008). Several other catalysts are also studied by various researchers. In this chapter, the various nanoparticles were classified according to the literature: (1) metal and metal oxide nanoparticles, (2) carbon-based nanomaterials, (3) zeolites, and (4) polymers. These are the types of nanomaterials usually used for the degradation of contaminants in the wastewater system (Pankaj, Tyagi, Smriti, Dharmendra, & Shruti, 2012).

2 Pharmaceuticals

Pharmaceuticals and personal care products have been widely used for the vast period of time in the history. Only in the past two decades the concerns have been raised due to their persistence in the environment over the long period of time. Those pollutants are usually bioactive species, which shows either long-term or short-term toxicity in the environment (Cizmas, Sharma, Gray, & McDonald, 2015; Hughes, Kay, & Brown, 2012; Luo et al., 2014). Pharmaceutical are used to treat human and animal

This book belongs to Central Library BADJI Mokhtar-ANNABA UNIVERSITY Copyright Elsevier 2024

illnesses, and personal care products are widely used in the cosmetics respectively. Even though the usage of those products is needed in the society, the excessive usage will cause harmful effects to the environment by letting the pollutants in the surrounding environment through wastewater treatment plants. These pharmaceutical compounds may appear in the aquatic system with a few $ng\,L^{-1}$ to $g\,L^{-1}$ to become a micropollutant in the environment. These ranges are usually very difficult to detect and degrade in the wastewater system. So an effective management method is needed for the treatment of pharmaceutical pollutants (Basile et al., 2011; Mottaleb, Meziani, Matin, Arafat, & Wahab, 2015).

3 Nanotechnology for pharmaceutical waste treatment

The conventional treatment methods are usually for the removal of the pollutants partially, but the non-conventional treatment methods like AOPs are generally for the degradation of the pollutants into eco-friendly products using reactive oxygen species such as H_2O_2, OH, O^{2-}, and O_3. AOPs with nanomaterials will improve the percentage degradation of the target pollutants. The most appropriate AOPs for pharmaceutical and personal care product removal are heterogeneous photocatalysis. Till now, many studies reported the existence of pharmaceutical pollutants in the raw drinking water or in the tap water. This chapter focuses on the treatment methods of pharmaceutical pollutants using nanomaterials (Compagnoni et al., 2017; Freyria et al., 2017).

4 Photodegradation of pharmaceuticals

Photodegradation of some compounds like cloxacillin, tetracycline, ampicillin, amoxicillin, sulfamethoxazole, atenolol, benzotriazole, clarithromycin, metformin, methylbenzotriazole, primidone, gabapentin, and metoprolol was studied by various researchers using photo-Fenton process and hydrogen peroxide (UV 254/H_2O_2) with UV light irradiation. Different types of AOPs were encountered for the degradation of pharmaceuticals in the wastewater system. TiO_2 photocatalytic oxidation process (TiO_2/UV), photo-Fenton process (Fe/H_2O_2/UV), and the combined ozone and hydrogen peroxide (O_3/H_2O_2) oxidation process were studied for the degradation of pollutants. Among these, semiconductor nanoparticle–assisted photocatalytic oxidation process shows promising efficacy for the degradation of pollutants not only via light scattering and scavenger effects but also by the adsorption of the active sites on the surface of the semiconductor nanoparticle photocatalyst (Bagheri, Termeh Yousefi, & Do, 2017).

5 Degradation pathways for pharmaceuticals and eco toxicity of photoproducts

The following major stages were involved in the photocatalytic degradation. That is, (1) light from higher energy than the corresponding bandgap of the photocatalyst is absorbed by the photocatalyst, thereby producing excited electrons and holes, which are responsible for the high reducing and oxidizing properties of the photocatalyst; (2) production of heat by the recombination of the electrons and holes in migration process; (3) movement of the electrons to the surface of the photocatalyst, a

This book belongs to Central Library BADJI Mokhtar-ANNABA UNIVERSITY Copyright Elsevier 2024

reductive pathway is commenced, where O_2 is reduced to $^{\bullet}O_2^-$; (4) on the other hand, an oxidative path initiate when the holes immigrate to the surface of the photocatalyst, and $^{\bullet}OH$ is produced upon oxidation of H_2O or the antibiotic compounds. The photocatalytic active species like $^{\bullet}O_2^-$ or $^{\bullet}OH$ processes effect the final rate and efficacy of the photocatalytic degradation of pollutants, hence lengthening the light absorption spectrum capability of the photocatalysts, which will enhance the charge separation and prevent the recombination. These could be overcome by choosing the semiconductor nanoparticles with suitable narrow bandgap that could absorb both visible and UV light respectively and suitable separating medium that is able to trapping the photoexcited electrons or holes to inhibit the recombination (Daghrir, Drogui, & Robert, 2013; Ibhadon & Fitzpatrick, 2013).

6 Nanophotocatalysts

Nanophotocatalysts are very small semiconductor particles with few nanometers in size. The attention in these small semiconductor particles initiates from their unique photophysical and photocatalytic properties that are different from those of bulk materials. The difference in the photoefficiencies of different forms of TiO_2 as being basically associated with its charge-carrier dynamics was studied by Martin, Herrmann, Choi, and Hoffmann (1995). The authors compared Q-TiO_2 (quantum) and Degussa P25 (made up of 20–35-nm primary particles) for charge-carrier dynamics. They found that the resultant interfacial electron transfer appeared to be faster for P25 than for Q-TiO_2. The slower electron-transfer rates observed for Q-TiO_2 were constant with the lower steady-state quantum yields (Beydoun, Amal, Low, & McEvoy, 1999). Zhang, Wang, Zakaria, and Ying (1998) supported this concept by giving some explanation for these observations. They proposed that, in large TiO_2 particles, volume recombination of the charge carriers is the main process and can be reduced by a reduction in particle size. This reduction also leads to an increase in the surface area, which can be translated as an increase in the existing surface active sites (Zhang et al., 1998). Therefore, decrease in particle size increases the interfacial charge-carrier transfer rates, which leads to higher photonic efficiencies. However, lower the particle size below certain limit should result in dominant surface recombination processes. Since, most of the electrons and holes are produced close to the surface. Since electrons and holes are closer to the surface, the recombination is faster compared with the interfacial charge-carrier transfer processes. So, an optimum particle size is needed for higher photocatalytic efficiency.

7 Metal/metal oxide nanoparticles

Gold, palladium, and silver metal nanoparticles have been generally studied for the wastewater management. For instance, silver nanoparticles have 10–200 nm size range, high surface area, and an effective antimicrobial activity. Silver nanomaterial acts as a better antimicrobial agent to deactivate the coliform microorganisms in the wastewater system. Further, gold nanoparticles with palladium have been used to degrade the trichloroethane from the groundwater (Jain & Pradeep, 2005; Tobiszewski & Namieśnik, 2012). Likewise, metal oxide nanoparticles such as ZnO, TiO_2, and CeO_2 have been extensively used as photocatalysts for the degradation of wastewater pollutants. The metal oxide nanoparticles were considered as better photocatalysts owing to its high surface area and good photolytic properties (Klaine et al., 2008).

This book belongs to Central Library BADJI Mokhtar-ANNABA UNIVERSITY Copyright Elsevier 2024

8 Carbon-based nanomaterials

Carbon-based nanomaterials are used as a potential sorbents for the organic pollutants in the wastewater owing to its selectivity, sorption capacity, and high surface area. Widely used carbon-based materials are carbon nanotubes, fullerenes, graphene oxide, etc.; further, they also display excellent properties like stable, thermal and electrical conductivity (Schierz & Zänker, 2009).

9 Zeolites

Zeolite nanoparticles have been prepared by introduction of pulsed laser on the zeolite LTA microparticles or using hydrothermal activation of fly ash. Laser-induced fragmentation of zeolite LTA microparticles produces the zeolite nanoparticles. It has a better ion exchange property. Further, it has been extensively used in water purification as an ion exchange media. Various work has been studied using zeolites for the removal of heavy metals like Cr(III), Zn(II), Cd(II), and Cu(II) from the acid mines and electroplating industries (Alvarez-Ayuso, Garcıa-Sánchez, & Querol, 2003).

10 Heterogeneous photocatalysis

Heterogeneous photocatalysis is a division that contains a huge variety of reactions, for instance, water splitting, organic synthesis, photoreduction, O_2^{18}–O_2^{16}, metal deposition, hydrogen transfer, disinfection, anticancer therapy, water detoxification, deuterium-alkane isotopic exchange, and gaseous pollutant removal. (Herrmann, 1999) Photocatalytic water splitting reaction comprises the formation of hydrogen and oxygen molecules while irradiated with light using semiconductor as electrode. In 1972, Fujishima and Honda use TiO_2 in electrochemical photolysis of water for the first time. Since then, there have been a lot of investigation and improvement made in heterogeneous photocatalysis (Fujishima & Honda, 1972). Most common heterogeneous photocatalysis is semiconductor-aided photodegradation of wastewater pollutants. It is one of the most promising methods for water purification. Several important features are accessible in heterogeneous photocatalysis that extended their extensive application in water treatment. The key benefits of the process is that it can be carried out in ambient temperature and pressure, it does not involve mass transfer, it is low cost, and it might lead to whole mineralization of organic compounds into CO_2 and H_2O (Konstantinou & Albanis, 2004). The basic principle of heterogeneous photocatalysis has been discussed as follows. Semiconductor nanoparticles have been extensively used as a better photocatalyst for getting a number of reduction and oxidation reactions on the surface of semiconductor photocatalyst. It can be understood by the electronic band structure of the semiconductor catalyst that has conduction band (cb) and valence band (vb). These two cb and vb are separated by the bandgap. When a photon energy equal to or higher to the band energy is irradiated on the surface of the semiconductor catalyst, it will excite the electron to cb and leave the hole in the vb within femtoseconds or it can be stuck in surface of the catalyst where it can react with the adsorbed species. From the excited and electron and hole reduction and oxidation can be commenced (Fig. 1) (Colmenares & Luque, 2014). The energy level of cb is in fact the reduction potential of photoelectrons, and the energy level of vb is oxidation potential of photoholes. Recombination between electron and hole pair occurs except oxygen is accessible to scavenge the electrons to

This book belongs to Central Library BADJI Mokhtar-ANNABA UNIVERSITY Copyright Elsevier 2024

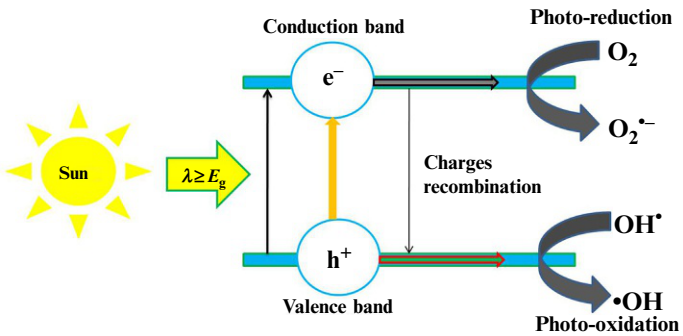

FIG. 1

Photoactivation of a semiconductor and primary reactions occurring on its surface.

form superoxides ($O_2^{\bullet-}$), its protonated form is the hydroperoxyl radicals ($HO_2^{\bullet}$) and subsequently production of H_2O_2 (Litter, 1999).

The series of reduction and oxidation reactions that happen at the surface were generally recommended as follows in Eqs. (1)–(6) (Philippopoulos & Nikolaki, 2010).

$$\text{Semiconductor photocatalyst} + h\nu \rightarrow e^- + h^+ \tag{1}$$

$$(O_2)_{ads} + e^- \rightarrow O_2^{\bullet-} \tag{2}$$

$$H_2O \rightarrow OH^- + H^+ \tag{3}$$

$$O_2^{\bullet-} + H^+ \rightarrow HOO\bullet \tag{4}$$

$$HOO^\bullet + e^- \rightarrow HO_2^- \tag{5}$$

$$HOO^- + H^+ \rightarrow H_2O_2 \tag{6}$$

11 Semiconductor nanophotocatalyst

Semiconductor nanoparticles have been of significant attention over the past years owing to its active light responsive nature. Semiconductor photocatalysis is generally focused on TiO_2 as an efficient photocatalyst in water and air purification. There are several other potential semiconducting nanomaterials that are existing for photodegradation of organic contaminants (Regulacio & Han, 2016). However, only certain semiconductor materials are to competently degrade the contaminants under light irradiation. The search for environmentally benign semiconductor nanomaterials with higher photocatalytic activity is of great attention worldwide. The redox potential of photoactivated vb hole should be sufficiently positive to produce hydroxyl radical, and the photoactivated cb electrons should be properly negative to reduce adsorbed oxygen to superoxide radical anion (Litter, 1999). There are several semiconductor nanomaterials that are generally used in the degradation of contaminants under light irradiation. For instance, titanium dioxide (TiO_2), zinc oxide (ZnO), vanadium (V) oxide (V_2O_5),

This book belongs to Central Library BADJI Mokhtar-ANNABA UNIVERSITY
Copyright Elsevier 2024

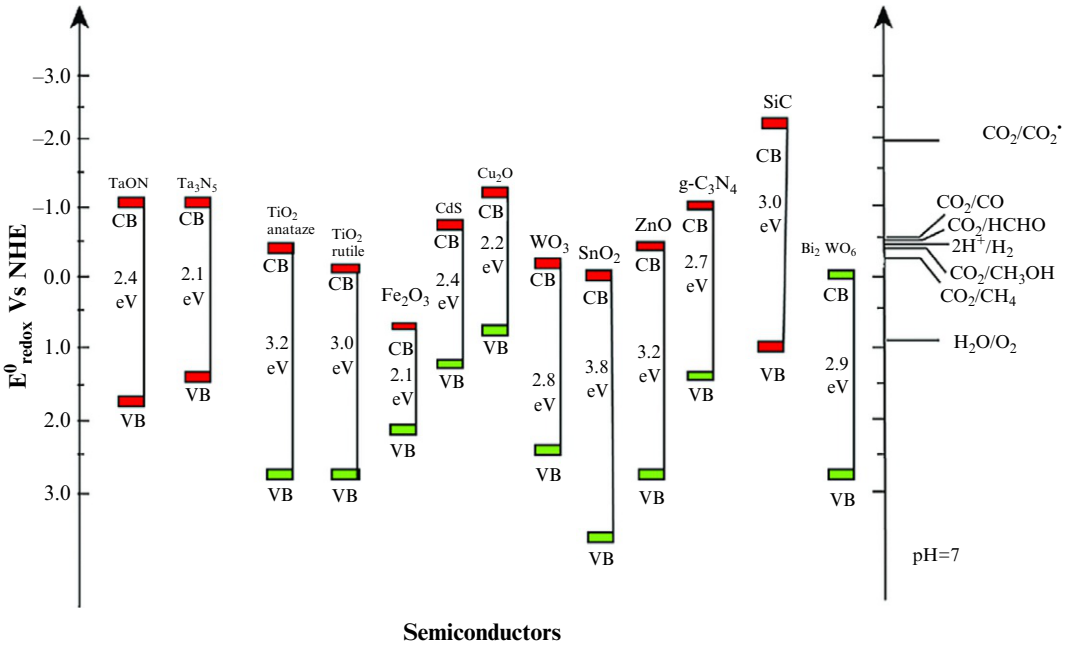

FIG. 2

Conduction band, valance band potentials, and bandgap energies of various semiconductor photocatalysts relative to the redox potentials at pH 7 of compounds involved in CO_2 reduction (Khan & Tahir, 2019).

zirconia (ZrO_2), niobium pentoxide (Nb_2O_5) iron (III) oxide (Fe_2O_3), and tungsten trioxide (WO_3) have been widely studied in wastewater treatment. Among these, TiO_2 is one of the favorable photocatalysts in the area of photocatalysis due to its great photocatalytic activity, nontoxicity, and stability. But, TiO_2 is uneconomic for large-scale management, so attention has been drawn in the way of suitable replacements to TiO_2 (Kansal, Singh, & Sud, 2008; Muhd Julkapli, Bagheri, & Bee Abd Hamid, 2014; Nakata & Fujishima, 2012).

The catalytic action of semiconductor strongly depends on the valence band and conduction band. Fig. 2 shows the bandgap energies and the band edge locations of common semiconductor photocatalysts.

12 Current scenario and future prospectus

Earlier, researches have been generally attentive on conventional techniques for wastewater treatment. But, nowadays, the researchers are focused on AOPs like ozonation and photocatalysis. Maximum research based on wastewater treatment was carried out using TiO_2 nanoparticles. Coupling of AOPs and nanotechnology was global interest in these days due to their excellent activity toward wastewater treatment. Even though many nanomaterial-based AOPs are reported, the feasibility of some nanomaterial with AOP combinations is still in the laboratory scale only. But, the promising future for

This book belongs to Central Library BADJI Mokhtar-ANNABA UNIVERSITY Copyright Elsevier 2024

wastewater treatment is nanomaterials with AOPs. More efforts are needed to overcome some key issues such as novel photocatalytic materials that could operate in visible region. Further research on nanomaterial-based AOPs will bring revolution on wastewater treatment in the future.

13 Conclusion

Safe water has become a challenge in many parts of the world owing to population, development, climate change, etc. This could be overcome by the treatment of wastewater using nanomaterials. It has unique characteristics like large surface area and small size, which will make these nanomaterials a promising catalyst for the treatment of wastewater. The chapter has shown that the wastewater treatment using nanomaterials with AOPs is a promising field for current and future research.

References

Alvarez-Ayuso, E., Garcıa-Sánchez, A., & Querol, X. (2003). Purification of metal electroplating waste waters using zeolites. *Water Research*, *37*(20), 4855–4862.

Bagheri, S., Termeh Yousefi, A., & Do, T. O. (2017). Photocatalytic pathway toward degradation of environmental pharmaceutical pollutants: Structure, kinetics and mechanism approach. *Catalysis Science & Technology*, *7*(20), 4548–4569.

Basile, T., Petrella, A., Petrella, M., Boghetich, G., Petruzzelli, V., Colasuonno, S., et al. (2011). Review of endocrine-disrupting-compound removal technologies in water and wastewater treatment plants: An EU perspective. *Industrial & Engineering Chemistry Research*, *50*(14), 8389–8401.

Bergendahl, J., & O'Shaughnessy, J. (2004). Applications of advanced oxidation for wastewater treatment. In: *Vol. 25. International Business and Education Conference "A Focus on Water Management"*, Worcester Polytechnic Institute.

Bethi, B., Sonawane, S. H., Bhanvase, B. A., & Gumfekar, S. P. (2016). Nanomaterials-based advanced oxidation processes for wastewater treatment: A review. *Chemical Engineering and Processing: Process Intensification*, *109*, 178–189.

Beydoun, D., Amal, R., Low, G., & McEvoy, S. (1999). Role of nanoparticles in photocatalysis. *Journal of Nanoparticle Research*, *1*(4), 439–458.

Cizmas, L., Sharma, V. K., Gray, C. M., & McDonald, T. J. (2015). Pharmaceuticals and personal care products in waters: Occurrence, toxicity, and risk. *Environmental Chemistry Letters*, *13*(4), 381–394.

Colmenares, J. C., & Luque, R. (2014). Heterogeneous photocatalytic nanomaterials: Prospects and challenges in selective transformations of biomass-derived compounds. *Chemical Society Reviews*, *43*(3), 765–778.

Compagnoni, M., Ramis, G., Freyria, F. S., Armandi, M., Bonelli, B., & Rossetti, I. (2017). Photocatalytic processes for the abatement of N-containing pollutants from waste water. Part 1: Inorganic pollutants. *Journal of Nanoscience and Nanotechnology*, *17*(6), 3632–3653.

Czech, B., & Buda, W. (2015). Photocatalytic treatment of pharmaceutical wastewater using new multiwall-carbon nanotubes/TiO2/SiO2 nanocomposites. *Environmental Research*, *137*, 176–184.

Daghrir, R., Drogui, P., & Robert, D. (2013). Modified TiO2 for environmental photocatalytic applications: A review. *Industrial & Engineering Chemistry Research*, *52*(10), 3581–3599.

Deveci, E. Ü., Dizge, N., Yatmaz, H. C., & Tansel, B. (2016). Degradation of recalcitrant textile dyes by coupling fungal and photocatalytic membrane reactors. *CLEAN—Soil, Air, Water*, *44*(10), 1345–1351.

This book belongs to Central Library BADJI Mokhtar-ANNABA UNIVERSITY

Copyright Elsevier 2024

Freyria, F. S., Armandi, M., Compagnoni, M., Ramis, G., Rossetti, I., & Bonelli, B. (2017). Catalytic and photocatalytic processes for the abatement of N-containing pollutants from wastewater. Part 2: Organic pollutants. *Journal of Nanoscience and Nanotechnology*, *17*(6), 3654–3672.

Fujishima, A., & Honda, K. (1972). Electrochemical photolysis of water at a semiconductor electrode. *Nature*, *238*(5358), 37.

Guo, J., Yuan, S., Jiang, W., Yue, H., Cui, Z., & Liang, B. (2016). Adsorption and photocatalytic degradation behaviors of rhodamine dyes on surface-fluorinated TiO2 under visible irradiation. *RSC Advances*, *6*(5), 4090–4100.

Henneberg, A., & Triebskorn, R. (2015). Efficiency of advanced wastewater treatment technologies for the reduction of hormonal activity in effluents and connected surface water bodies by means of vitellogenin analyses in rainbow trout (Oncorhynchus mykiss) and brown trout (Salmo trutta f. fario). *Environmental Sciences Europe*, *27*(1), 22.

Herrmann, J. M. (1999). Heterogeneous photocatalysis: Fundamentals and applications to the removal of various types of aqueous pollutants. *Catalysis Today*, *53*(1), 115–129.

Hughes, S. R., Kay, P., & Brown, L. E. (2012). Global synthesis and critical evaluation of pharmaceutical data sets collected from river systems. *Environmental Science & Technology*, *47*(2), 661–677.

Ibhadon, A., & Fitzpatrick, P. (2013). Heterogeneous photocatalysis: Recent advances and applications. *Catalysts*, *3*(1), 189–218.

Jain, P., & Pradeep, T. (2005). Potential of silver nanoparticle-coated polyurethane foam as an antibacterial water filter. *Biotechnology and Bioengineering*, *90*(1), 59–63.

Kansal, S. K., Singh, M., & Sud, D. (2008). Studies on TiO2/ZnO photocatalysed degradation of lignin. *Journal of Hazardous Materials*, *153*(1–2), 412–417.

Khan, A. A., & Tahir, M. (2019). Recent advancements in engineering approach towards design of photo-reactors for selective photocatalytic CO_2 reduction to renewable fuels. *Journal of CO_2 Utilization*, *29*, 205–239.

Klaine, S. J., Alvarez, P. J., Batley, G. E., Fernandes, T. F., Handy, R. D., Lyon, D. Y., et al. (2008). Nanomaterials in the environment: Behavior, fate, bioavailability, and effects. *Environmental Toxicology and Chemistry*, *27*(9), 1825–1851.

Konstantinou, I. K., & Albanis, T. A. (2004). TiO2-assisted photocatalytic degradation of azo dyes in aqueous solution: Kinetic and mechanistic investigations: A review. *Applied Catalysis B: Environmental*, *49*(1), 1–14.

Li, L., Zhang, X., Zhang, W., Wang, L., Chen, X., & Gao, Y. (2014). Microwave-assisted synthesis of nanocomposite ag/ZnO–TiO2 and photocatalytic degradation rhodamine B with different modes. *Colloids and Surfaces A: Physicochemical and Engineering Aspects*, *457*, 134–141.

Litter, M. I. (1999). Heterogeneous photocatalysis: Transition metal ions in photocatalytic systems. *Applied Catalysis B: Environmental*, *23*(2–3), 89–114.

Luo, Y., Guo, W., Ngo, H. H., Nghiem, L. D., Hai, F. I., Zhang, J., et al. (2014). A review on the occurrence of micropollutants in the aquatic environment and their fate and removal during wastewater treatment. *Science of the Total Environment*, *473*, 619–641.

Martin, S. T., Herrmann, H., Choi, W., & Hoffmann, M. R. (1995). *Photochemical destruction of chemical contaminants on quantum-sized semiconductor particles* [No. CONF-950336-]. New York, NY (United States): American Society of Mechanical Engineers.

Mottaleb, M. A., Meziani, M. J., Matin, M. A., Arafat, M. M., & Wahab, M. A. (2015). Emerging micro-pollutants pharmaceuticals and personal care products (PPCPs) contamination concerns in aquatic organisms-LC/MS and GC/MS analysis. In *Emerging micro-pollutants in the environment: occurrence, fate, and distribution* (pp. 43–74). Washington, DC, USA: American Chemical Society.

Muhd Julkapli, N., Bagheri, S., & Bee Abd Hamid, S. (2014). Recent advances in heterogeneous photocatalytic decolorization of synthetic dyes. *The Scientific World Journal*, *2014*.

This book belongs to Central Library BADJI Mokhtar-ANNABA UNIVERSITY

Copyright Elsevier 2024

Nakata, K., & Fujishima, A. (2012). TiO2 photocatalysis: Design and applications. *Journal of Photochemistry and Photobiology C: Photochemistry Reviews*, *13*(3), 169–189.

Pankaj, K., Tyagi, R., Smriti, V., Dharmendra, K., & Shruti, T. (2012). Nanomaterials use in wastewater treatment. In: *International Conference on Nanotechnology and Chemical Engineering (ICNCS'2012) Bangkok, Thailand*.

Philippopoulos, C. J., & Nikolaki, M. D. (2010). Photocatalytic processes on the oxidation of organic compounds in water. In *New trends in technologies*: IntechOpen.

Qu, X., Alvarez, P. J., & Li, Q. (2013). Applications of nanotechnology in water and wastewater treatment. *Water Research*, *47*(12), 3931–3946.

Rahman, Q. I., Ahmad, M., Misra, S. K., & Lohani, M. B. (2013). Hexagonal ZnO nanorods assembled flowers for photocatalytic dye degradation: Growth, structural and optical properties. *Superlattices and Microstructures*, *64*, 495–506.

Regulacio, M. D., & Han, M. Y. (2016). Multinary I-III-VI2 and I2-II-IV-VI4 semiconductor nanostructures for photocatalytic applications. *Accounts of Chemical Research*, *49*(3), 511–519.

Rickerby, D. G., & Morrison, M. (2007). Nanotechnology and the environment: A European perspective. *Science and Technology of Advanced Materials*, *8*(1–2), 19.

Schierz, A., & Zänker, H. (2009). Aqueous suspensions of carbon nanotubes: Surface oxidation, colloidal stability and uranium sorption. *Environmental Pollution*, *157*(4), 1088–1094.

Selvin, S. S. P., Lee, J., Kumar, S., Radhika, N., Merlin, J. P., & Lydia, I. S. (2017). Photocatalytic degradation of rhodamine B using cysteine capped ZnO/P (3HB-co-3HHx) fiber under UV and visible light irradiation. *Reaction Kinetics, Mechanisms and Catalysis*, *122*(1), 671–684.

Tobiszewski, M., & Namieśnik, J. (2012). Abiotic degradation of chlorinated ethanes and ethenes in water. *Environmental Science and Pollution Research*, *19*(6), 1994–2006.

Vaseashta, A., Vaclavikova, M., Vaseashta, S., Gallios, G., Roy, P., & Pummakarnchana, O. (2007). Nanostructures in environmental pollution detection, monitoring, and remediation. *Science and Technology of Advanced Materials*, *8*(1–2), 47.

Verma, A., Chhikara, I., & Dixit, D. (2014). Photocatalytic treatment of pharmaceutical industry wastewater over TiO2 using immersion well reactor: Synergistic effect coupling with ultrasound. *Desalination and Water Treatment*, *52*(34–36), 6591–6597.

Zhang, Z., Wang, C. C., Zakaria, R., & Ying, J. Y. (1998). Role of particle size in nanocrystalline TiO2-based photocatalysts. *The Journal of Physical Chemistry B*, *102*(52), 10871–10878.

This book belongs to Central Library BADJI Mokhtar-ANNABA UNIVERSITY

Copyright Elsevier 2024

CHAPTER

Photocatalytical degradation of pesticides

9

Deepak Pathania[a], Manita Thakur[b], Arush Sharma[c]

Department of Environmental Sciences, Central University of Jammu, Samba, India[a] Department of Chemistry, IEC University Baddi, Solan, India[b] School of Sciences, Baddi University of Emerging Sciences and Technology (BUEST), Solan, India[c]

1 Introduction

A variety of toxic organic and inorganic pollutants are generally released into the aquatic system, which pollute the aquatic system. These pollutants are of most toxicological concern because of their bioaccumulation and nonbiodegradability. The main sources of these pollutants into water system are mining, metallurgical, chemical manufacturing, tannery, battery manufacturing industries, fossil fuel, chemical industries, etc. The presence of organic pollutants in water is carcinogenic and nonbiodegradable and persists in the environment for long time and caused harmful effects in mammalian and aquatic life. A large number of herbicides are applied on the agricultural fields, which, apart from killing their respective weed, due to their chemical stability, resistance to biodegradation, and sufficient water solubility, either can penetrate deep into the groundwater aquifers or can be washed away to the surface water bodies (Hettige, Mani, & Wheeler, 2000).

These compounds, due to their toxicity, stability to natural decomposition, and persistence in the environment, have been of much concern to the societies and regulation authorities around the world (El-Geundi, 1997). 2,4-Dichlorophenoxy acetic is commonly known as 2,4-D. It is one of the most commonly used herbicides for controlling broadleaf weeds and other vegetation. 2,4-D is used to control broadleaf weeds in a variety of places such as home lawns, cereal and grain crops, commercial areas, commercial turf, rights-of-way, and forests. Because of the toxicity, conventional treatment methods are not suitable for wastewaters containing 2,4-D, as they can destroy the microbial population of the treatment plants. Therefore the development of an effective degradation process for this herbicide is very important (Khan, Zia, & Qasim, 2010; Li & Zhang, 1999; Malhat, Haggag, Loutfy, Osman, & Ahmed, 2015; Thuy, Van Geluwe, Nguyen, & Vander Bruggen, 2012).

The presence of pesticide contaminants in various water sources such as surface water and groundwater has increased manyfold in recent years due to their significant use in agricultural field for plant and crop protection. The contamination of water bodies may be due to direct applications of insecticides, rainwater runoff from agricultural fields, and disposal of outdated stocks and discharge of waste water from industries (Colabuono, Taniguchi, & Montone, 2010; Hu et al., 2011). To meet the global food demand, yearly, tonnes of pesticides have been used without apprehending their consequences (Karami-Mohajeri & Abdollahi, 2011). Currently, India involved in biggest producer of pesticides

Nano-Materials as Photocatalysts for Degradation of Environmental Pollutants. https://doi.org/10.1016/B978-0-12-818598-8.00009-2
© 2020 Elsevier Inc. All rights reserved.

This book belongs to Central Library BADJI Mokhtar-ANNABA UNIVERSITY

Copyright Elsevier 2024

in Asia, after China. India ranks as fourth largest pesticide-producing nation in the world after the United States, Japan, and China. Pesticides in Jammu with the highest consumption rates include monocrotophos, endosulfan, phorate, chlorpyriphos, methyl parathion, quinalphos, mancozeb, paraquat, butachlor, isoproturon, and phosphamidon. In India, due to intense agricultural activities, some organophosphates and organochlorine pesticides were detected abundantly in groundwater (Freire, Koifman, & Koifman, 2015).

Organophosphorus pesticides represent the most applied group of insecticides for the last two decades. OPs are composed of 10 most widely used pesticides all over the world. They have been used as an alternative to organochlorine compounds for pest control. However, they are considered as extremely toxic compounds. Organophosphorus pesticides like monocrotophos and chlorpyrifos are commonly used in India and noticed in various environmental segments, such as soil, water, and air due to their extensive use (Calle, Frumkin, Henley, Savitz, & Thun, 2002). Chlorpyrifos is another widely used organophosphorus pesticide in agriculture. This compound was first developed in 1965 and applied in over 100 countries across the world. Chlorpyrifos has become the largest organophosphate insecticide in world in both volume and value. It is used to control the populations of insects, soil grubs, rootworms, subterranean termites, foliage, and soil-born insects (Robinson et al., 2015). Chlorpyrifos is not readily soluble in water and easily comes out of solution. However, temperatures above 63 °C allow chlorpyrifos to dissolve at a faster rate into solution. Exposure to chlorpyrifos and its metabolites has resulted in a variety of nerve disorders in humans. Its acute poisoning causes headache, nausea, muscle twitching, and convulsions and in some extreme cases even death (Gasnier et al., 2009; Jaga & Dharmani, 2003; McKinlay, Plant, Bell, & Voulvoulis, 2008). Despite the major role of pesticides in increasing productivity, there is a concern about the progressive pesticide contamination of groundwater.

2 Entry of pesticides into animals

Insecticides are used to kill insects by getting inside their bodies where they then act as poison. There are three different ways of entry of pesticides into animals.

2.1 Dermal entry

The insecticides enter into the body of animals through the skin. In the case of insects, the skin is called the cuticle. Insecticides of this type are called as contact poisons. Dermal enter into the body of insect takes place when aerosol spray droplets hit the insect and insects walk over and in doing so come into contact with powder or granule forms of insecticide. In most work situations, absorption through the skin is the most common route of pesticide exposure. People can be exposed to a splash or mist when mixing, loading, or applying the pesticide. Pesticides can also be absorbed through eyes. In addition, pesticides can cause injuries to the eye itself.

2.2 Oral entry

When the insecticide enters the body through the mouth, then it is called oral entry. It occurs when the insect eats the insecticides. Insecticides of this type are called ingested poisons. The insecticides are ingested by the insect as poisonous bait and when it cleans itself after the poison comes into contact

This book belongs to Central Library BADJI Mokhtar-ANNABA UNIVERSITY
Copyright Elsevier 2024

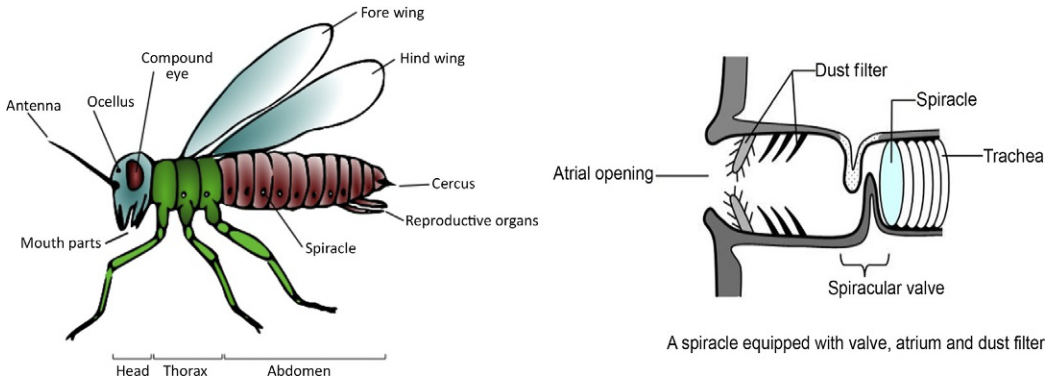

FIG. 1

Respiratory entry of pesticides.

with its body. There are numerous reports of people accidentally drinking a pesticide that has been put into an unlabeled bottle or beverage cup/container (including soft drink cans or bottles). Workers who handle pesticides may also inadvertently ingest when eating or smoking if they have not washed their hands first.

2.3 Respiratory entry

The insecticides are breathed in by the insect then it is called respiratory entry. These insecticides are called inhaled poisons. Insects do not breathe through the mouth as observed in most of animals. They breathe through spiracles. The pesticides with a high inhalation hazard will be labeled with directions to use a respirator. Fig. 1 shows the respiratory entry of pesticides.

3 Types of insecticides

3.1 Classification based on types of pests that they kill

The main groups of pesticides are categorized into the following six groups:

1. Insecticides—Killing insects
2. Herbicides—Killing plants
3. Rodenticides—Killing rodents, like mice and rats
4. Bactericides—Killing bacteria
5. Fungicides—Killing fungi
6. Larvicides—Killing larvae

3.2 Classification based on biodegradability

Pesticides can also be classified into two types based on biodegradability:

This book belongs to Central Library BADJI Mokhtar-ANNABA UNIVERSITY Copyright Elsevier 2024

3.2.1 Biodegradable

The biodegradable pesticides are those that can be broken down by microbes and other living beings into harmless compounds.

3.2.2 Persistent

The persistent pesticides are those that may take months or years to break down.

3.3 Chemically related pesticides

3.3.1 Organophosphate

Most organophosphates are insecticides; they affect the nervous system by disrupting the enzyme that regulates a neurotransmitter. Organophosphates, which were promoted as a more ecological alternative to organochlorines, include a great variety of pesticides, the most common of which is glyphosate. This class also includes other known pesticides, such as malathion, parathion, and dimethoate; some are known for their endocrine-disrupting potential. This class of pesticides has been associated with effects on the function of cholinesterase enzymes (Jaga & Dharmani, 2003; McKinlay et al., 2008); decrease in insulin secretion; disruption of normal cellular metabolism of proteins, carbohydrates, and fats; also genotoxic effects (Li et al., 2015); and effects on mitochondrial function, causing cellular oxidative stress and problems to the nervous and endocrine systems. Population-based studies have revealed possible relations between the exposure to organophosphorus pesticides and serious health effects including cardiovascular diseases, negative effects on the male reproductive system and on the nervous system, dementia, and also a possible increased risk for non-Hodgkin's lymphoma. Furthermore, prenatal exposure to organophosphates has been correlated with decreased gestational duration and neurological problems occurring in children (Jamal, Haque, Singh, & Rastogi, 2015).

3.3.2 Carbamate

Similar to the organophosphorus pesticides, the carbamate pesticides also affect the nervous system by disrupting an enzyme that regulates the neurotransmitter. However, the enzyme effects are usually reversible. Carbamate pesticides, such as aldicarb, carbofuran, and ziram, are another class of chemical pesticides that have been associated with endocrine-disrupting activity, possible reproductive disorders (Goad, Goad, Atieh, & Gupta, 2004), and effects on cellular metabolic mechanisms and mitochondrial function. Moreover, in vitro studies have revealed the ability of carbamate pesticides to cause cytotoxic and genotoxic effects in hamster ovarian cells and to induce apoptosis and necrosis in human immune cells and natural killer cells and also apoptosis in T lymphocytes (Li, Kobayashi, & Kawada, 2011; Soloneski, Kujawski, Scuto, & Larramendy, 2015).

Furthermore, it has been confirmed that carbaryl, which belongs to the category of carbamate pesticides, can act as a ligand for the hepatic aryl hydrocarbon receptor, a transcription factor involved in the mechanism of dioxin toxicity. There is also evidence for the ability of carbamate pesticides to cause neurobehavioral effects, increased risk for dementia, and non-Hodgkin's lymphoma (Denison, Phelan, Winter, & Ziccardi, 1998; Lifshitz, Shahak, Bolotin, & Sofer, 1997).

This book belongs to Central Library BADJI Mokhtar-ANNABA UNIVERSITY
Copyright Elsevier 2024

3.3.3 Organochlorine insecticides

They were commonly used earlier, but now, many countries have removed organochlorine insecticides from their market due to their health and environmental effects and their persistence (e.g., DDT, chlordane, and toxaphene). Exposure to organochlorines occurs through ingestion of contaminated food or water, inhalation of vapor, and absorption through the skin. Dietary exposure results in bioaccumulation of these chemicals in the human body. The accumulation of organochlorine compounds is a result of their chemical structure and their physical properties such as polarity and solubility. These fat-soluble compounds persist in both the body and the environment. Consequently, researchers and regulatory agencies have banned several organochlorines (Gomathi, Devi, & Kumar, 2009). The main symptoms of organochlorine intoxication are dizziness, headache, anorexia, nausea, vomiting, malaise, dermatitis, diarrhea, apprehension, excitement, irritability, gait disorders, excessive sweating, altered reflexes, muscle weakness, tremors, spasms, mental confusion, anxiety, seizures, coma, and death. The carcinogenicity of this class of compounds is assigned to polychlorocyclodiene compounds that form epoxides during their biotransformation. Because organochlorines have long half-life, these levels in the serum constitute a marker of exposure to these pesticides (Hossain, Fakhruddin, Chowdhury, & Alam, 2013).

3.3.4 Pyrethroid

These are a synthetic version of pyrethrin, a naturally occurring pesticide, found in chrysanthemums (flower). They were developed in such a way as to maximize their stability in the environment. They comprise active agents (pyrethrins I–VI), but pyrethrins I and II are the most active. These compounds decompose rapidly in the presence of light, but synthetic production of pyrethroids around 1950 overcame some disadvantages of natural pyrethrins (Hossain et al., 2013). After absorption, rapid pyrethroid distribution occurs in the organism. Therein, these compounds undergo biotransformation via two mechanisms: hydrolysis of the ester linkage by carboxylesterases and oxidation of the alcohol moiety by cytochromes P450. Pyrethroids exert the same mechanism of action in insects and mammals.

3.3.5 Sulfonylurea herbicides

The sulfonylureas herbicides have been commercialized for weed control such as pyrithiobac-sodium, cyclosulfamuron, bispyribac-sodium, terbacil, sulfometuron-methyl, sulfosulfuron, rimsulfuron, pyrazosulfuron-ethyl, imazosulfuron, nicosulfuron, oxasulfuron, flazasulfuron, primisulfuron-methyl, halosulfuron-methyl, flupyrsulfuron-methyl-sodium, ethoxysulfuron, chlorimuron-ethyl, bensulfuron-methyl, azimsulfuron, and amidosulfuron.

3.3.6 Biopesticide

The biopesticides are certain types of pesticides derived from such natural materials as animals, plants, bacteria, and certain minerals.

4 Usage of pesticides in India

The pesticide use has been started during the times of ancient Romans. The people burn the sulfur for destroying pests and employed the salt, ashes, and bitter for controlling weeds. A Roman naturalist insisted the use of arsenic as an insecticide (History of pesticide use 1998). Mixture of honey and

This book belongs to Central Library BADJI Mokhtar-ANNABA UNIVERSITY Copyright Elsevier 2024

arsenic has been employed for monitoring ants in 1600. During the 1800s, the US farmers used certain chemicals such as nicotine sulfate, calcium arsenate, and sulfur as pesticides (Wasse, Salmon, & Delaplane, 2000). In 1867, an impure form of copper, arsenic, has been utilized to check the potato beetle in the United States. The major burst through pesticide growth has been found in the era around and after the Second World War. The numerous operative and economical pesticides have been manufactured. This period is marked by the discovery of aldrin, dichlorodiphenyltrichloroethane (DDT) in 1939, dieldrin, β-benzene hexachloride (BHC), 2,4-dichlorophenoxyacetic acid (2,4-D), chlordane, and endrin. In 1962 an American scientist Rachel Carson emphasized in her book, *Silent Spring*, that DDT spray has found to cause the sudden death of nontarget creatures using direct or indirect noxiousness. (Delaplane, vander Steen, & Guzman-Novoa, 2013; Jabbar & Mallick, 1994).

The production of pesticides started in India in 1952 with the establishment of a plant for the production at Calcutta. Today, India is the second leading manufacturer of pesticides in Asia after China and ranks 12th globally (Mathur, 1999). There has been a steady increase in the production of pesticides in India, from 5000 metric tons in 1958 to 102,240 metric tons in 1998. The demand for pesticides in terms of value was estimated to be around Rs. 22 billion (USD 0.5 billion), which is about 2% of the total world market during 1996–97. The pattern of pesticide usage in India is different from has been shown Fig. 2. It was recorded that in India 76% of the pesticide used is insecticide, as against 44% globally (Mathur, 1999). The use of herbicides and fungicides usage is less compared with pesticides. The major use of pesticides in India has been recorded for cotton crops (45%), followed by paddy and wheat.

5 Harmful effects of pesticides

The harmful effects accompanying the pesticide usage have suppressed their positive effects. Pesticides have life-threatening effects on nontarget species including animal, plant biodiversity, and aquatic as well as terrestrial ecosystems. As per the data available, approximately 80%–90% of applied pesticides should volatilize after few days of applications (Majewski & Capel, 1996). The volatilized pesticides rapidly vaporize and consequently pose danger to nontarget creature. Abandoned uses of pesticides have threatened the existence of erratic species such as bald eagle, peregrine falcon,

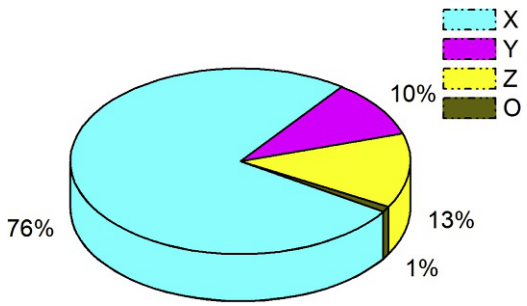

FIG. 2

Pattern of pesticides in India.

This book belongs to Central Library BADJI Mokhtar-ANNABA UNIVERSITY
Copyright Elsevier 2024

and osprey (Helfrich, Li, Sharp, & Sales, 2009). Furthermore, air, water, and soil have been polluted with these chemicals to the noxious level.

Depending upon the solubility of pesticides, they enter the ecosystem by two different methods. Water-soluble pesticides dissolved in water and arrive in the watercourse, rivers, and lake, therefore posing damage to the untargeted species. Secondly, fat-soluble pesticides enter into the animals using bioamplification process.

5.1 Effect on human

Pesticides have amended the standard of human well-being by monitoring vector-borne ailments, but long-term and random use has resulted in serious health issues. Human beings chiefly newborns and children are extremely prone to poisonous effects of pesticides due to nonspecific nature and inadequate usage of pesticides. The pesticide use has become augmented over past few decades. The exposure to these chemicals has also significantly increased. According to World Health Organization, approximate 3,000,000 cases of pesticide poisoning and 220,000 deaths have been reported in developing countries (Haakstad & Bø, 2011). Nearly about 2.2 million people in the developing countries are at threat to exposure of pesticides (Hicks et al., 2013).

Pesticides reach the human body by ingestion, inhalation, or the upper layer of the skin. Though, human bodies have mechanism for the removal of toxins. However, in some cases, it retains them through absorption in the circulatory system. Studies have revealed the close association of pesticides and the development of cancers in both children and adults. The close exposure with pesticide impart greater risk to various malignancies such as leukemia, Burkitt's lymphoma, neuroblastoma, Wilm's tumor, non-Hodgkin's lymphoma, soft tissue sarcoma, ovarian cancer, lung cancer, stomach cancer, colon cancer, bladder cancer, and rectal cancer (Bonner & Laskey, 1974). Many childhood cancers are found to be associated with pesticide exposure. Compared with other cancer types, more convincing evidence was presented in a population-based case-control study of acute myelocytic leukemia (AML). A comparison of 491 cases between an age group of 0–9 years was done for polymorphisms in CYP1A1, CYP2D6, GSTT1, and GSTM1 genes responsible to encode enzymes responsible to metabolize carcinogenic substances (Infante-Rivard, Labuda, Krajinovic, & Sinnett, 1999). Fig. 3 shows effect of pesticides on various cellular activities.

5.2 Effect on biodiversity

Pesticide-polluted water poses a hazard to aquatic life. It can affect aquatic plants. It declines the dissolved oxygen in the water system and causes physiological and behavioral change in the fish populations. Lawn care pesticides have been reported in the surface water and water bodies such as ponds, streams, and lakes. Pesticides applied to land drift to aquatic ecosystem are noxious to fish and non-target organism. These pesticides not only are poisonous themselves but also interact with stressors and include harmful algal blooms. However, excessive use of pesticides causes decrease in the populations of different fish species (Scholz, 2012). Roughly 80% of the dissolved oxygen has been supplied by aquatic plant. It is essential for the survival of aquatic life. The aquatic fauna have been killed by herbicides causing low O_2 level, hence finally leading to asphyxia and decreased fish productivity (Helfrich et al., 2009). Mostly, level of pesticides is too much higher in the surface water than groundwater. It was probably due to surface runoff from the farmland and contaminations using spray drift.

This book belongs to Central Library BADJI Mokhtar-ANNABA UNIVERSITY
Copyright Elsevier 2024

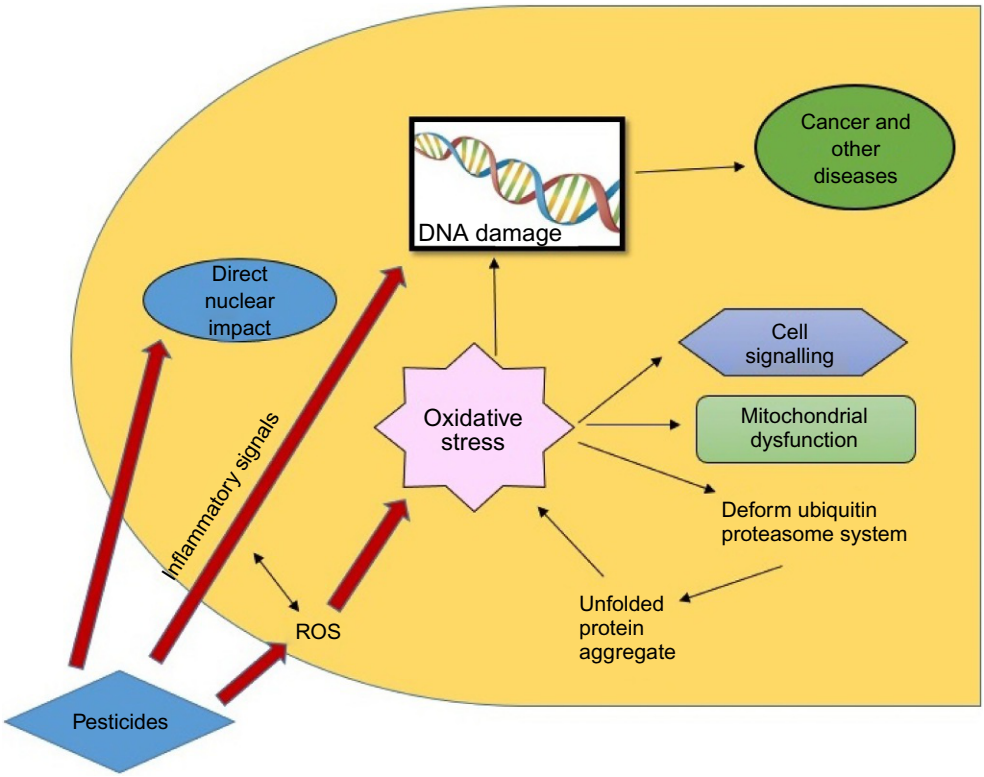

FIG. 3

Effect of pesticides on various cellular activities.

However, pesticides enter the underground by the seepage of polluted surface water, improper dumping, and accidental spill and leakage.

Pesticide exposure is also responsible for the lethal effect on the terrestrial plant apart from killing of nontarget plant. The volatilization of phenoxy herbicides caused harm to nearby trees and shrub. Herbicide such as glyphosate enhanced the susceptibility of plant to various noxious diseases (Brammall & Higgins, 1988), hence decreasing the quality of seed. However, low doses of herbicide, sulfonylureas, sulfonamides, imidazolinones, etc. have posed noxious effect onto the productivity of nontarget crop, natural plant, and wildlife (Fletcher, Pfleeger, & Ratsch, 1993).

5.3 Soil contamination

A large number of transformation products (TPs) from a widespread range of pesticides have been reported (Hutson & Roberts, 1999). Persistency and movement of these pesticides and their TPs have been measured using some parameters such as water solubility, soil-sorption constant, and half-life in soil (DT50). They can be moved from soil by runoff and leaching, thereby constituting a problem for the supply of drinking water to the population. The most researched pesticide TPs in soil are undoubtedly those from herbicides. Several metabolic pathways have been suggested, involving transformation

This book belongs to Central Library BADJI Mokhtar-ANNABA UNIVERSITY
Copyright Elsevier 2024

through hydrolysis, methylation, and ring cleavage that produce several toxic phenolic compounds. The pesticides and their TPs are retained by soils to different degrees, depending on the interactions between soil and pesticide properties. The most influential soil characteristic is the organic matter content. The larger the organic matter content, the greater the adsorption of pesticides and TPs. The capacity of the soil to hold positively charged ions in an exchangeable form is important with paraquat and other pesticides that are positively charged. Strong mineral acid is required for extracting these chemicals, without any analytical improvement or study reported in recent years. Soil pH is also of some importance. Adsorption increases with decreasing soil pH for ionizable pesticides (e.g., 2,4-D,2,4,5-T, picloram, and atrazine) (Andreu & Pico, 2004).

6 Different methods for the degradation of pesticides

Several attempts have been made for the treatment of pesticides and its residues from surroundings. The degradation of pesticides is the breakdown of toxic chemicals into nontoxic compounds. The process of breakdown can take a wide range of time, that is, from hours, to days, to years. It depends on the chemical properties of the pesticide and environmental conditions. Degradation of pesticide occurs by chemical and biological processes (Berg, Hagmeyer, & Gimbel, 1997; Gupta, Gupta, Rastogi, Agarwal, & Nayak, 2011). The pesticides that quickly breakdown do not persist in the environment and have short time control on crop. Due to adverse effects of using pesticides, researchers are encouraged to explore and design proficient techniques for the removal of different harmful pesticides. Several physical, chemical, and biological methods such as adsorption, catalytic degradation, membrane filtration, biological treatment, and advanced oxidation processes (AOP) have been investigated as shown in Fig. 4.

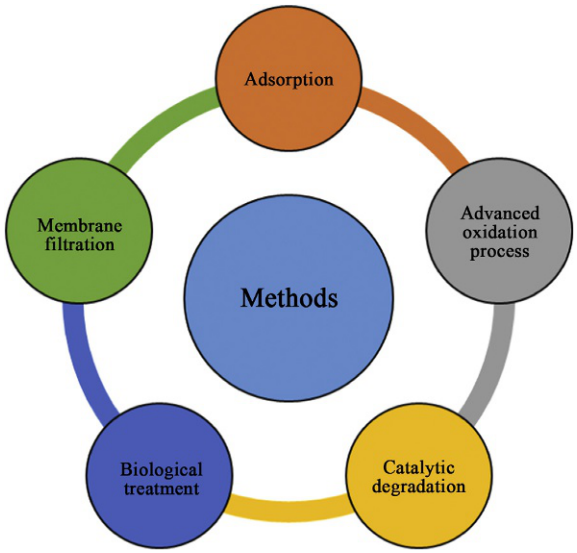

FIG. 4

Different methods for the degradation of pesticides.

This book belongs to Central Library BADJI Mokhtar-ANNABA UNIVERSITY Copyright Elsevier 2024

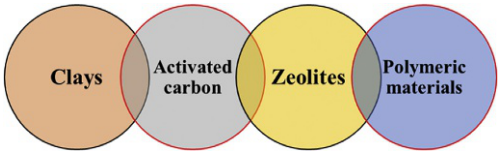

FIG. 5

Different physical methods for removal of pesticides.

6.1 Physical processes for remediation of pesticides

Various methods have been explored for the remediation of pesticides on large scale as shown in Fig. 5.

6.1.1 Clays

Natural clay particles are hydrophilic, negatively charged, and used for the retention of cationic pesticides because of their high surface area, low cost, and high availability. Natural clays have been modified to improve the retention of pesticides. Therefore, in recent years, much attention has been paid to the expansion of modified clays with enhanced sorption capacities for both polar and nonpolar pollutants (Haderlein, Weissmahr, & Schwarzenbach, 1996; Li, Sheng, Teppen, Johnston, & Boyd, 2003). Various parameters that effect the adsorption include initial pesticide concentrations, adsorbent mass, pH, contact time, ionic strength, and temperature. The efficiency of organoclays for the adsorption of different pesticides from water including prometron, butachlor, metsulfuron, and bensulfuron has been reported. But there is difficulty in the separation of clay minerals from water after treatment process and limits their use as adsorbent. Introduction of clay minerals as a coagulant aid made it easy for the separation of clay minerals after treatment because of improved sedimentation (Sanchez-Martin, Rodriguez-Cruz, Andrades, & Sanchez-Camazano, 2006). There are numerous benefits of using small amounts of clay minerals as a coagulant aid.

The pesticides get removed through flocculation process, and pesticides get adsorbed over the clay mineral, which improves the removal efficiency. In the presence of chemical coagulants, the low negatively charged organic clay may act as a sorbent for pesticides or nucleus for flocculation. Also, surfactant-modified nanomontmorillonites have been used to enhance the sorption capacity of the adsorbent as compared with commercial normal bentonites, which helps to remove the pesticides even at low concentration (Gerstl, Nasser, & Mingelgrin, 1998; Manisankar, Selvanathan, & Vedhi, 2006).

6.1.2 Activated carbon

Charcoal is porous, soft, black substance made by heating substances containing carbon such as material from hardwood trees and coconut shells. Activated charcoal has been used for many years to exclude organic contaminants from wastewaters and in water purification. Powdered activated charcoal is made up of very small carbon particles and has a high affinity for organic chemicals such as pesticides. Activated charcoal is used to adsorb and deactivate organic chemicals such as pesticides in soil. When pesticide has been adsorbed onto activated charcoal, it is biologically inactive and cannot cause injury to the turfgrass (Ayranci & Hoda, 2005; Hameed, Salman, & Ahmad, 2009). Due to its dark color, it has ability to absorb heat; therefore activated charcoal is also used to artificially warm the soil to minimize the effects of light frosts or to allow earlier seeding of an area.

Activated charcoal is an excellent adsorbent with large surface area and has high adsorption of pharmaceuticals and pesticides from water. The adsorption process of activated carbon depends on different

This book belongs to Central Library BADJI Mokhtar-ANNABA UNIVERSITY
Copyright Elsevier 2024

aspects like structure, surface chemistry, and nature of adsorbate and the properties of the adsorption solution (Salman, Njoku, & Hameed, 2011). Activated charcoal materials are of different types including granular active carbon, powder active carbon, black electrodes, fiber, and carbon. Powder active carbon is employed as an efficient approach to eliminate pesticide from drinking water treatment due to its cost-effectiveness and flexibility (Humbert, Gallard, Suty, & Croué, 2008; Zhang et al., 2017).

6.1.3 Zeolites and polymeric materials

Zeolites are widely used in pollution control, agriculture, and industry to remove pesticides and heavy metals. In recent years, zeolite has attracted much attention because of its excellent physicochemical properties, availability, and low cost. Zeolites are crystalline aluminosilicate materials and have extremely high adsorption capacity with interconnected micropores. They have superior catalytic properties and thermally stable and good resistance to most compounds (Kanan, Kanan, & Patterson, 2006).

Zeolites used as an adsorbent to treat water contaminated with pesticides are imidacloprid, bentazon, isoproturon, etc. The adsorption rate mainly depends on the mobility and polarity of pesticides. The high adsorption rate for carbamate pesticides has been detected by cetyltrimethyl ammonium bromide–modified zeolite (Kyriakopoulos & Doulia, 2006). The immobile pesticides like imidacloprid, isoproturon, and metalaxyl-m have been associated with zeolite, whereas more mobile pesticides like bentazon and clopyralid are partitioned in water. Isoproturon and metalaxyl-m are nonionic pesticides and show higher affinity for the zeolites on the basis of their polarity. Therefore the rate of trapping by zeolites mainly depends on the mobility and polarity of pesticide. Polymeric materials such as cyclodextrins, dendrimers, and hypercross-linked polymers have been employed for the elimination of pesticides. The most important advantages of polymeric materials in contrast to carbonaceous material are that they require lower energy and lower cost for the regeneration of adsorbents (Badawy, Ghaly, & Gad-Allah, 2006; Roy, Singh, Bajpai, & Bajpai, 2014).

6.2 Chemical treatment for removal of pesticides

Chemical treatment involves various processes including advanced oxidation process, adsorption, and biological treatment as shown in Fig. 6.

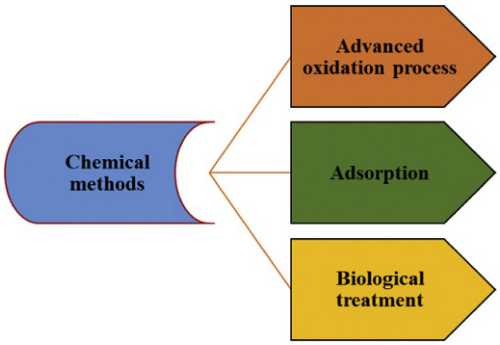

FIG. 6

Chemical processes for removal of pesticides.

This book belongs to Central Library BADJI Mokhtar-ANNABA UNIVERSITY Copyright Elsevier 2024

6.2.1 Advanced oxidation process (AOP's)

Advanced oxidation processes are the oxidation techniques in which hydroxyl radicals have been produced by different methods. These are used for the removal of pollutants that have high chemical stability and low biodegradability. The hydroxyl radicals are efficient enough to initiates a series of reactions and convert pollutants completely to carbon dioxide and water (Cheng et al., 2016; Ikehata & El-Din, 2006). These are environmental friendly because they do not transfer pollutants from one phase to another. AOP's mechanisms involved various processes such as the following:

Fenton process

Fenton reaction is one of the efficient tools used for the oxidation of organic pollutant. In this, oxidation of organic substrates by Fe (II) and hydrogen peroxide occurs. The reaction involves in situ generation of a strong oxidizing agent, hydroxyl radical from hydrogen peroxide. The chemical equation of Fenton reaction is

$$Fe^{2+} + H_2O_2 \rightarrow Fe^{3+} + OH^* + OH^- \tag{1}$$

Fe^{3+} forms further react with hydrogen peroxide, and catalyst is regenerated again.

$$Fe^{3+} + H_2O_2 \rightarrow Fe^{2+} + HO_2{}^* + H^+ \tag{2}$$

These OH* radicals will react with organics (RH) by the abstraction of proton and producing organic radicals (R*), and these are highly reactive and can be further oxidized (Malato et al., 2002). Two major drawbacks of this process are requirement of acidic pH and formation of iron sludge. H_2O_2 dosage, pH, and iron dosage are the main factors affecting the efficiency of the process. Fenton process has been extensively used for the removal of total organic carbon, dyes, pigments, phenolic compounds, etc. It is very difficult to oxidize highly colored effluents from textile industries at low concentration. Therefore Fenton oxidation was effectively used for the removal of such compounds (Hamby, 1996). This process was also explored for the degradation of specific compounds like cresols, phenols, EDTA, cyanides, and organics. Another main application is wastewater treatment from oil recovery industry wastewater, landfill leachate, and natural gas plant wastewater.

UV and UV/H2O2 process

In this method the compounds will absorb the radiation passing to excited state promoting reactions. Degradation may be by either direct photolysis or indirect photolysis. Effectiveness of UV treatment for the removal of pharmaceuticals was observed only for ketoprofen, diclofenac, and antipyrine. The applicability and productivity of UV process depend on the stability of the compound, pH, and the nature of light source (Galindo, Jacques, & Kalt, 2000; Yuan et al., 2011). When H_2O_2 is used in the presence of UV, there is the formation of hydroxyl radicals by the photolysis of H_2O_2.

In this the oxidation of compounds can occur by either direct photolysis or reaction with hydroxyl radicals. Different parameters including pH, intensity of UV light, and H_2O_2 dosage affect the performance of system. It has been observed that acidic condition favors UV/H_2O_2 process because the acidic pH favors the hydroxyl radical formation. The rate of photolysis of H_2O_2 is pH dependent and increases when more alkaline conditions are used. But at higher pH, H_2O_2 autodecomposes forming water and oxygen. Excessive dose of H_2O_2 will reduce the degradation of pollutant; therefore, sufficient dose of

This book belongs to Central Library BADJI Mokhtar-ANNABA UNIVERSITY Copyright Elsevier 2024

H_2O_2 is necessary to absorb UV to accelerate the generation of hydroxyl radicals (Gupta, Ali, & Saini, 2006).

6.3 Adsorption

Adsorption process by solid adsorbents is one of the most effective methods for dealing with the organic impurities from wastewater (Al-Qodah, Shawaqfeh, & Lafi, 2007). It is an excellent technique for the remediation of pesticides as compared with other traditional methods because of its simple design, high efficiency, low maintenance cost, highly economic benefits, and insensitivity for toxic substances. In recent years, the low-cost adsorbents with intensified pollutant removal capacities have been explored. Agricultural wastes, natural materials, and industrial wastes produced low-cost adsorbents like activated carbon that are used in wastewater treatment. Natural adsorbents have more advantages including technical feasibility, local availability, inexpensive, treatability, and their disposal (Kyriakopoulos, Doulia, & Anagnostopoulos, 2005; Lafi & Al-Qodah, 2006). There are some natural adsorbents that have excellent pesticide removal capacity as shown in Fig. 7. The role of various adsorbents for the removal of pesticide has been summarized in Table 1.

6.4 Biological treatment

Biological remediation involves complete transfer of organic compounds into less toxic end products like CO_2 and H_2O. This method is environmentally friendly and highly economic as compared with other tools for eliminating pollutants (Shawaqfeh, 2010).

There are three types of bioremediation with micro scale organism:

- Remediation through improved natural attenuation
- Bioaugmentation
- Biostimulation

The microorganisms capable of degrading organic pollutants can be isolated from surroundings including contaminated site or marine sediment. In recent decades, fungi have been used for biodegradation and bioremediation of pesticides. It has been observed that fungal isolates have found to be effective bioresource to degrade different pesticides such as lindane, methamidophos, atrazine, cypermethrin, endosulfan, chlorpyrifos, dieldrin, methyl parathion, and heptachlor. (Gerhardson, 2002). The main disadvantage is the speed of fungal degradation of pesticides, which depends on temperature, pH,

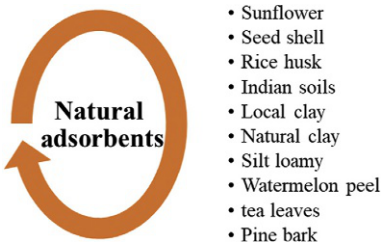

FIG. 7

Natural adsorbents used for the removal of pesticides.

This book belongs to Central Library BADJI Mokhtar-ANNABA UNIVERSITY Copyright Elsevier 2024

Table 1 List of adsorbents used for the remediation of pesticides from aqueous system.

Adsorbent	Pesticides	Q_{max} (mg/g)	Reference
Activated carbon	Bromopropylate	18.9×10^{-2}	Ioannidou, Zabaniotou, Stavropoulos, Islam, and Albanis (2010)
Activated carbon	Bromopropylate	11.6×10^{-2}	Ioannidou et al. (2010)
Activated carbon	Bromopropylate	12.3×10^{-2}	Ioannidou et al. (2010)
Commercial activated carbon	4,4 DDT	163	Boussahel, Irinislimane, Harik, and Moussaoui (2009)
Cork wastes	4,4 DDT	2.03–19.08	Boussahel et al. (2009)
Wood saw dust	4,4 DDT	4.25–69.44	Boussahel et al. (2009)
Bagasse fly ash	9DDD	7.69×10^{-3}	Zolgharnein, Shahmoradi, and Ghasemi (2011)
Bagasse fly ash	DDE	6.67×10^{-3}	Zolgharnein et al. (2011)
Bagasse fly ash	Lindane	2.51×10^{-3}	Zolgharnein et al. (2011)
Bagasse fly as	Endrin	43.71	Zolgharnein et al. (2011)
Bagasse fly as	Aldrin	19.54×10^{-3}	Zolgharnein et al. (2011)
Tea leaves	Quinalphos	196.07×10^{-3}	Islam, Sakkas, and Albanis (2009)
Cork	α-Cypermethrin	303×10^{-3}	Ahmad et al. (2010)
Activated carbon	2(3H)-one	4.32	Arvand et al. (2009)
Commercial activated carbon	2,4D	8.13–10.48	Chingombe, Saha, and Wakeman (2006)
Vegetable activated carbon	Prometon	23.51	Moreno, López, Galvín, Cordón, and Mellado (2010)
Coconut activated carbon	Prometon	26.02	Moreno et al. (2010)
Vegetable activated carbon	Propazine	25.62	Moreno et al. (2010)
Coconut activated carbon	Propazine	27.15	Moreno et al. (2010)
Lignocellulosic material	Terbumeton	11.2	Boudesocque, Guillon, Aplincourt, Martel, and Noël (2008)
Lignocellulosic material	Isoproturon	61.8	Boudesocque et al. (2008)
Ayous saw dust	Praquat	9.47	Nanseu-Njiki, Dedzo, and Ngameni (2010)

nutrient availability, oxygen level, and soil moisture content. Different enzymes such as peroxidase, hydrolase, lactase, esterase, dehydrogenase, manganese peroxidase, lignin peroxidase mediate the biodegradation of a wide range of pesticides. Different biochemistry processes such as hydroxylation, dechlorination, demethylation, dioxygenation, dehydrochlorination, esterification, and oxidation have been employed on the fungal strains during the biodegradation of pesticides (Reddy & Kim, 2015). Biological processes for the elimination of pesticides may be affected by various environmental factors such as nutrients, pH, temperature, inoculum density, pesticide concentration, and chemical and physical characteristics of substrate (Chishti, Hussain, Arshad, Khalid, & Arshad, 2013).

This book belongs to Central Library BADJI Mokhtar-ANNABA UNIVERSITY
Copyright Elsevier 2024

6.5 Photocatalysis

Photocatalysis is one of the effective and competent advanced oxidation processes (AOPs) used to detoxify the contaminants emitted from the various industrial processes with negligible waste. Photocatalysis typically ensues with the illumination of solar light and photon generated catalytically species. The process of photodegradation involves the following steps: Initially, solar irradiation of certain wavelength is incident onto semiconductor. If the energy of incident radiation is equal to band energy or band gap of the photocatalyst, then electrons are excited from the valence band (VB) to the conduction band (CB) of photocatalyst and holes (h^+) left in the valence shell.

The electrons (e^-) and holes (h^+) endure the successive oxidation and reduction reactions with active compounds adsorbed onto the semiconductor surface to produce the degraded products. The photocatalytic processes involve the highly reactive hydroxyl radicals (OH*). These radicals are capable of degrading the organic pollutants into innocuous product from aqueous system. It has high capacity to mineralize nearly all organic pollutants into harmless substance such as CO_2 and H_2O under ambient conditions. The schematic representation of photocatalytic process under visible region is shown in Fig. 8.

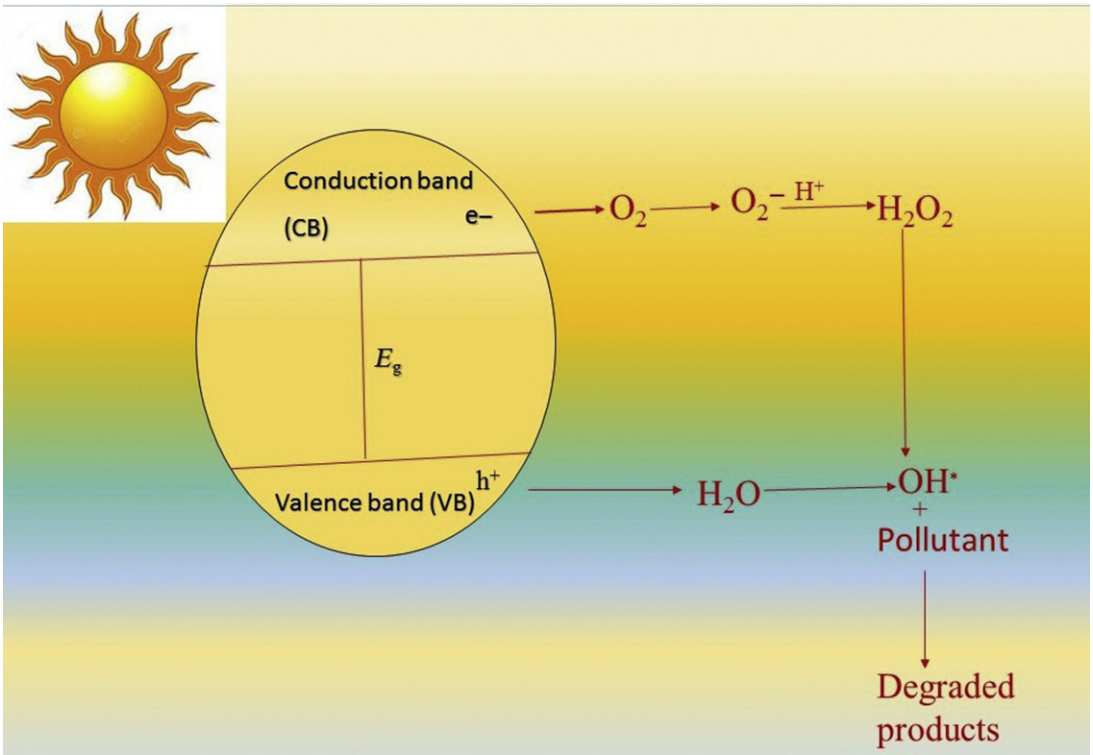

FIG. 8

Photocatalytic mechanism.

This book belongs to Central Library BADJI Mokhtar-ANNABA UNIVERSITY
Copyright Elsevier 2024

Since the revolutionary work in the 1970s, semiconductor-based nanocomposites have revealed the higher degradation rate for various pollutants (Liu, Chen, Hu, Wu, & Wang, 2011). Semiconductor-based composites were used as excellent photocatalytsts due to their potential applications for environmental decontamination. Photocatalysis using heterogeneous semiconductor appeared as most agreeable mean of degradation due to economical, nontoxic, higher–surface area, broad absorption spectra with greater absorption and capability for multi–electron transfer, etc.

Higher adsorption increased the catalytic degradation of organic and inorganic pollutants. Therefore nanoparticles are incorporated into some organic moieties and provide the enhanced surface area for the photodegradation of pollutants. Some of the advantages of carbon supported nanoparticles are as follows:

- They are innocuous in nature.
- Carbon suppresses the electron–hole pair recombination by acting as an electron acceptor.
- Organic moieties keep the metal nanoparticles in dispersed phase, hence preventing the agglomeration of nanoparticles.

7 Conclusions

Aquatic pollution is the biggest and most alarming problem that requires effective solutions. However, various initiatives have been taken to tackle this problem. Further, research dedicated to this problem is still needed. Recently, bionanocomposites have been widely explored for the removal of various pesticides from water system. Photodegradation is an abiotic method for the removal of pesticide. In this method, molecular excitation occurred by the absorption of solar energy. This results in the generation of various highly reactive species such as oxide and peroxide radicals. This specifically or nonspecifically oxidize the functional group present in a pesticide. However, extensive research has been conducted for the degradation of pesticide. However, additional research is required to evaluate the environmental impact of these ubiquitous pesticides.

References

Ahmad, T., Rafatullah, M., Ghazali, A., Sulaiman, O., Hashim, R., & Ahmad, A. (2010). Removal of pesticides from water and wastewater by different adsorbents: A review. *Journal of Environmental Science and Health. Part C*, *28*(4), 231–271.

Al-Qodah, Z., Shawaqfeh, A. T., & Lafi, W. K. (2007). Adsorption of pesticides from aqueous solutions using oil shale ash. *Desalination*, *208*, 294–305.

Andreu, V., & Pico, Y. (2004). Determination of pesticides and their degradation products in soil: Critical review and comparison of methods. *Trends in Analytical Chemistry*, *23*, 772–789.

Arvand, M., Latify, L., Tajmehri, H., Yagubov, A. I., Nuriyev, A. N., & Pourhabib, A. (2009). Comparative study for the removal of oxadiazon from aqueous solutions by adsorption on chitosan and activated carbon. *Analytical Letters*, *42*(6), 856–869.

Ayranci, E., & Hoda, N. (2005). Adsorption kinetics and isotherms of pesticides onto activated carbon-cloth. *Chemosphere*, *60*, 1600–1607.

Badawy, M. I., Ghaly, M. Y., & Gad-Allah, T. A. (2006). Advanced oxidation processes for the removal of organophosphorus pesticides from wastewater. *Desalination*, *194*, 166–175.

This book belongs to Central Library BADJI Mokhtar-ANNABA UNIVERSITY Copyright Elsevier 2024

Berg, P., Hagmeyer, G., & Gimbel, R. (1997). Removal of pesticides and other micropollutants by nanofiltration. *Desalination*, *30*, 205–208.

Bonner, W. M., & Laskey, R. A. (1974). A film detection method for tritium-labelled proteins and nucleic acids in polyacrylamide gels. *European Journal of Biochemistry*, *46*, 83–88.

Boudesocque, S., Guillon, E., Aplincourt, M., Martel, F., & Noël, S. (2008). Use of a low-cost biosorbent to remove pesticides from wastewater. *Journal of Environmental Quality*, *37*(2), 631–638.

Boussahel, R., Irinislimane, H., Harik, D., & Moussaoui, K. M. (2009). Adsorption, kinetics, and equilibrium studies on removal of 4, 4-DDT from aqueous solutions using low-cost adsorbents. *Chemical Engineering Communications*, *196*(12), 1547–1558.

Brammall, R. A., & Higgins, V. J. (1988). The effect of glyphosate on resistance of tomato to Fusarium crown and root rot disease and on the formation of host structural defensive barriers. *Canadian Journal of Botany*, *66*, 1547–1555.

Calle, E. E., Frumkin, H., Henley, S. J., Savitz, D. A., & Thun, M. J. (2002). Organochlorines and breast cancer risk. *CA: A Cancer Journal for Clinicians*, *52*, 301–309.

Cheng, M., Zeng, G., Huang, D., Lai, C., Xu, P., Zhang, C., et al. (2016). Hydroxyl radicals based advanced oxidation processes (AOPs) for remediation of soils contaminated with organic compounds: A review. *Chemical Engineering Journal*, *284*, 582–598.

Chingombe, P., Saha, B., & Wakeman, R. J. (2006). Effect of surface modification of an engineered activated carbon on the sorption of 2, 4-dichlorophenoxy acetic acid and benazolin from water. *Journal of Colloid and Interface Science*, *297*(2), 434–442.

Chishti, Z., Hussain, S., Arshad, K. R., Khalid, A., & Arshad, M. (2013). Microbial degradation of chlorpyrifos in liquid media and soil. *Journal of Environmental Management*, *114*, 372–380.

Colabuono, F. I., Taniguchi, S., & Montone, R. C. (2010). Polychlorinated biphenyls and organochlorine pesticides in plastics ingested by seabirds. *Marine Pollution Bulletin*, *60*, 630–634.

Delaplane, K. S., vander Steen, J., & Guzman-Novoa, E. (2013). Standard methods for estimating strength parameters of Apis mellifera colonies. *Journal of Apicultural Research*, *52*, 1–2.

Denison, M. S., Phelan, D., Winter, G. M., & Ziccardi, M. H. (1998). Carbaryl, a carbamate insecticide, is a ligand for the hepatic ah (dioxin) receptor. *Toxicology and Applied Pharmacology*, *152*, 406–14.10.

El-Geundi, M. S. (1997). Adsorbents for industrial pollution control. *Adsorption Science and Technology*, *15*, 777–787.

Fletcher, J. S., Pfleeger, T. G., & Ratsch, H. C. (1993). Potential environmental risks associated with the new sulfonylurea herbicides. *Environmental Science & Technology*, *27*, 2250–2252.

Freire, C., Koifman, R. J., & Koifman, S. (2015). Hematological and hepatic alterations in brazilian population heavily exposed to organochlorine pesticides. *Journal of Toxicology and Environmental Health. Part A*, *78*, 534–548.

Galindo, C., Jacques, P., & Kalt, A. (2000). Photodegradation of the aminoazobenzene acid orange 52 by three advanced oxidation processes: UV/H_2O_2, UV/TiO_2 and VIS/TiO_2: Comparative mechanistic and kinetic investigations. *Journal of Photochemistry and Photobiology A: Chemistry*, *130*, 35–47.

Gasnier, C., Dumont, C., Benachour, N., Clair, E., Chagnon, M. C., & Séralini, G. E. (2009). Glyphosate-based herbicides are toxic and endocrine disruptors in human cell lines. *Toxicology*, *262*, 184–191.

Gerhardson, B. (2002). Biological substitutes for pesticides. *Trends in Biotechnology*, *20*, 338–343.

Gerstl, Z., Nasser, A., & Mingelgrin, U. (1998). Controlled release of pesticides into soils from clay – polymer formulations. *Journal of Agricultural and Food Chemistry*, *46*, 3797–3802.

Goad, E. R., Goad, J. T., Atieh, B. H., & Gupta, R. C. (2004). Carbofuran-induced endocrine disruption in adult male rats. *Toxicology Mechanisms and Methods*, *14*, 233–239.

Gomathi, L., Devi, B., & Kumar, G. (2009). Photocatalytic activity of V^{5+}, Mo^{6+} and Th^{4+} doped polycrystalline TiO_2 for the degradation of chlorpyrifos under UV/solar light. *Journal of Molecular Catalysis A: Chemical*, *308*, 174–181.

This book belongs to Central Library BADJI Mokhtar-ANNABA UNIVERSITY

Copyright Elsevier 2024

Gupta, V. K., Ali, I., & Saini, V. K. (2006). Adsorption of 2, 4-D and carbofuran pesticides using fertilizer and steel industry wastes. *Journal of Colloid and Interface Science*, *299*(2), 556–563.

Gupta, V. K., Gupta, B., Rastogi, A., Agarwal, S., & Nayak, A. (2011). Pesticides removal from waste water by activated carbon prepared from waste rubber tire. *Water Research*, *45*, 4047–4055.

Haakstad, L. A., & Bø, K. (2011). Exercise in pregnant women and birth weight: A randomized controlled trial. *BMC Pregnancy and Childbirth*, *11*, 66.

Haderlein, S. B., Weissmahr, K. W., & Schwarzenbach, R. P. (1996). Specific adsorption of nitroaromatic explosives and pesticides to clay minerals. *Environmental Science & Technology*, *30*, 612–622.

Hamby, D. M. (1996). Site remediation techniques supporting environmental restoration activities—A review. *The Science of the Total Environment*, *191*, 203–224.

Hameed, B. H., Salman, J. M., & Ahmad, A. L. (2009). Adsorption isotherm and kinetic modeling of 2, 4-D pesticide on activated carbon derived from date stones. *Journal of Hazardous Materials*, *163*, 121–126.

Helfrich, C. D., Li, Y. F., Sharp, N. D., & Sales, A. E. (2009). Organizational readiness to change assessment (ORCA): Development of an instrument based on the promoting action on research in health services (PARIHS) framework. *Implementation Science*, *4*, 38.

Hettige, H., Mani, M., & Wheeler, D. (2000). Industrial pollution in economic development: The environmental Kuznets curve revisited. *Journal of Development Economics*, *62*, 445–476.

Hicks, J. K., Swen, J. J., Thorn, C. F., Sangkuhl, K., Kharasch, E. D., Ellingrod, V. L., et al. (2013). Clinical Pharmacogenetics implementation consortium guideline for CYP2D6 and CYP2C19 genotypes and dosing of tricyclic antidepressants. *Journal of Clinical Pharmacy and Therapeutics*, *93*, 402–408.

Hossain, M. S., Fakhruddin, A. N., Chowdhury, M. A., & Alam, M. K. (2013). Degradation of chlorpyrifos, an organophosphorus insecticide in aqueous solution with gamma irradiation and natural sunlight. *Journal of Environmental Chemical Engineering*, *1*, 270–274.

Hu, Y., Qi, S., Zhang, J., Tan, L., Zhang, J., Wang, Y., et al. (2011). Assessment of organochlorine pesticides contamination in underground rivers in Chongqing, Southwest China. *Journal of Geochemical Exploration*, *111*, 47–55.

Humbert, H., Gallard, H., Suty, H., & Croué, J. P. (2008). Natural organic matter (NOM) and pesticides removal using a combination of ion exchange resin and powdered activated carbon (PAC). *Water Research*, *42*, 1635–1643.

Hutson, D. H., & Roberts, T. R. (1999). *Metabolic pathways of agrochemicals:-insecticides and fungicides.* RSC Publishing.

Ikehata, K., & El-Din, M. G. (2006). Aqueous pesticide degradation by hydrogen peroxide/ultraviolet irradiation and Fenton-type advanced oxidation processes: A review. *Applied Journal of Environmental Engineering Science*, *5*, 81–135.

Infante-Rivard, C., Labuda, D., Krajinovic, M., & Sinnett, D. (1999). Risk of childhood leukemia associated with exposure to pesticides and with gene polymorphisms. *Epidemiology*, 481–487.

Ioannidou, O. A., Zabaniotou, A. A., Stavropoulos, G. G., Islam, M. A., & Albanis, T. A. (2010). Preparation of activated carbons from agricultural residues for pesticide adsorption. *Chemosphere*, *80*(11), 1328–1336.

Islam, M. A., Sakkas, V., & Albanis, T. A. (2009). Application of statistical design of experiment with desirability function for the removal of organophosphorus pesticide from aqueous solution by low-cost material. *Journal of Hazardous Materials*, *170*(1), 230–238.

Jabbar, A., & Mallick, S. (1994). *Pesticides and environment situation in Pakistan.* Islamabad: Sustainable Development Policy Institute.

Jaga, K., & Dharmani, C. (2003). Sources of exposure to and public health implications of organophosphate pesticides. *Revista Panamericana de Salud Pública*, *14*, 171–185.

Jamal, F., Haque, Q. S., Singh, S., & Rastogi, S. (2015). The influence of organophosphate and carbamate on sperm chromatin and reproductive hormones among pesticide sprayers. *Toxicology and Industrial Health*, 1–10.

This book belongs to Central Library BADJI Mokhtar-ANNABA UNIVERSITY

Copyright Elsevier 2024

Kanan, S. M., Kanan, M. C., & Patterson, H. H. (2006). Silver nanoclusters doped in X and mordenite zeolites as heterogeneous catalysts for the decomposition of carbamate pesticides in solution. *Research on Chemical Intermediates*, *32*, 871–885.

Karami-Mohajeri, S., & Abdollahi, M. (2011). Toxic influence of organophosphate, carbamate, and organochlorine pesticides on cellular metabolism of lipids, proteins, and carbohydrates: A systematic review. *Human & Experimental Toxicology*, *30*, 1119–1140.

Khan, M. J., Zia, M. S., & Qasim, M. (2010). Use of pesticides and their role in environmental pollution. *World Academy of Science, Engineering and Technology*, *72*, 122–128.

Kyriakopoulos, G., & Doulia, D. (2006). Adsorption of pesticides on carbonaceous and polymeric materials from aqueous solutions: A review. *Separation and Purification Reviews*, *35*, 97–191.

Kyriakopoulos, G., Doulia, D., & Anagnostopoulos, E. (2005). Adsorption of pesticides on porous polymeric adsorbents. *Chemical Engineering Science*, *60*, 1177–1186.

Lafi, W. K., & Al-Qodah, Z. (2006). Combined advanced oxidation and biological treatment processes for the removal of pesticides from aqueous solutions. *Journal of Hazardous Materials*, *137*, 489–497.

Li, D., Huang, Q., Lu, M., Zhang, L., Yang, Z., Zong, M., et al. (2015). The organophosphate insecticide chlorpyrifos confers its genotoxic effects by inducing DNA damage and cell apoptosis. *Chemosphere*, *135*, 387–393.

Li, H., Sheng, G., Teppen, B. J., Johnston, C. T., & Boyd, S. A. (2003). Sorption and desorption of pesticides by clay minerals and humic acid-clay complexes. *Soil Science Society of America Journal*, *67*, 122–131.

Li, Q., Kobayashi, M., & Kawada, T. (2011). Ziram induces apoptosis and necrosis in human immune cells. *Archives of Toxicology*, *85*, 55–61.

Li, Y., & Zhang, J. (1999). Agricultural diffuse pollution from fertilisers and pesticides in China. *Water Science and Technology*, *39*, 25–32.

Lifshitz, M., Shahak, E., Bolotin, A., & Sofer, S. (1997). Carbamate poisoning in early childhood and in adults. *Journal of Toxicology. Clinical Toxicology*, *35*, 25–27.

Liu, M., Chen, C., Hu, J., Wu, X., & Wang, X. (2011). Synthesis of magnetite/graphene oxide composite and application for cobalt (II) removal. *Journal of Physical Chemistry C*, *115*(51), 25234–25240.

Majewski, M. S., & Capel, P. D. (1996). *Pesticides in the atmosphere: Distribution, trends, and governing factors*. CRC Press.

Malato, S., Blanco, J., Cáceres, J., Fernández-Alba, A. R., Agüera, A., & Rodrıguez, A. (2002). Photocatalytic treatment of water-soluble pesticides by photo-Fenton and TiO_2 using solar energy. *Catalysis Today*, *76*, 209–220.

Malhat, F. M., Haggag, M. N., Loutfy, N. M., Osman, M. A., & Ahmed, M. T. (2015). Residues of organochlorine and synthetic pyrethroid pesticides in honey, an indicator of ambient environment, a pilot study. *Chemosphere*, *120*, 457–461.

Manisankar, P., Selvanathan, G., & Vedhi, C. (2006). Determination of pesticides using heteropolyacid montmorillonite clay-modified electrode with surfactant. *Talanta*, *68*, 686–692.

Mathur, V. K. (1999). Human capital-based strategy for regional economic development. *Economic Development Quarterly*, *13*, 203–216.

McKinlay, R., Plant, J. A., Bell, J. N. B., & Voulvoulis, N. (2008). Endocrine disrupting pesticides: Implications for risk assessment. *Environment International*, *34*, 168–183.

Moreno, R. F., López, C. J., Galvín, M. R., Cordón, M. M., & Mellado, R. J. (2010). On the removal of s-triazine herbicides from waters using commercial low-cost granular carbons. *Journal of the Serbian Chemical Society*, *75*(3), 405–412.

Nanseu-Njiki, C. P., Dedzo, G. K., & Ngameni, E. (2010). Study of the removal of paraquat from aqueous solution by biosorption onto Ayous (Triplochiton schleroxylon) sawdust. *Journal of Hazardous Materials*, *179*(1), 63–71.

This book belongs to Central Library BADJI Mokhtar-ANNABA UNIVERSITY

Copyright Elsevier 2024

Reddy, P. V., & Kim, K. H. (2015). A review of photochemical approaches for the treatment of a wide range of pesticides. *Journal of Hazardous Materials*, *285*, 325–335.

Robinson, T., Ali, U., Mahmood, A., Chaudhry, M. J., Li, J., Zhang, G., et al. (2015). Concentrations and patterns of organochlorines (OCs) in various fish species from the Indus River, Pakistan: A human health risk assessment. *The Science of the Total Environment*, *541*, 1232–1242.

Roy, A., Singh, S. K., Bajpai, J., & Bajpai, A. K. (2014). Controlled pesticide release from biodegradable polymers. *Central European Journal of Chemistry*, *12*, 453–469.

Salman, J. M., Njoku, V. O., & Hameed, B. H. (2011). Adsorption of pesticides from aqueous solution onto banana stalk activated carbon. *Chemical Engineering Journal*, *174*, 41–48.

Sanchez-Martin, M. J., Rodriguez-Cruz, M. S., Andrades, M. S., & Sanchez-Camazano, M. (2006). Efficiency of different clay minerals modified with a cationic surfactant in the adsorption of pesticides: Influence of clay type and pesticide hydrophobicity. *Applied Clay Science*, *31*, 216–228.

Scholz, E. (2012). *Karl Fischer titration: Determination of water*. Springer Science & Business Media.

Shawaqfeh, A. T. (2010). Removal of pesticides from water using anaerobic-aerobic biological treatment. *Chinese Journal of Chemical Engineering*, *18*, 672–680.

Soloneski, S., Kujawski, M., Scuto, A., & Larramendy, M. L. (2015). Carbamates: A study on genotoxic, cytotoxic, and apoptotic effects induced in Chinese hamster ovary (CHO-K1) cells. *Toxicology In Vitro*, *29*, 834–844.

Thuy, P. T., Van Geluwe, S., Nguyen, V. A., & Vander Bruggen, B. (2012). Current pesticide practices and environmental issues in Vietnam: Management challenges for sustainable use of pesticides for tropical crops in (south-east) Asia to avoid environmental pollution. *Journal of Material Cycles and Waste Management*, *14*, 379–387.

Wasse, J. C., Salmon, P. S., & Delaplane, R. G. (2000). Structure of molten holmium and erbium trichlorides and tribromides. *Physica B: Condensed Matter*, *276*, 433–434.

Yuan, F., Hu, C., Hu, X., Wei, D., Chen, Y., & Qu, J. (2011). Photodegradation and toxicity changes of antibiotics in UV and UV/H_2O_2 process. *Journal of Hazardous Materials*, *185*, 1256–1263.

Zhang, S., Yang, Q., Yang, X., Wang, W., Li, Z., Zhang, L., et al. (2017). A zeolitic imidazolate framework based nanoporous carbon as a novel fiber coating for solid-phase microextraction of pyrethroid pesticides. *Talanta*, *166*, 46–53.

Zolgharnein, J., Shahmoradi, A., & Ghasemi, J. (2011). Pesticides removal using conventional and low-cost adsorbents: A review. *Clean—Soil, Air, Water*, *39*(12), 1105–1119.

This book belongs to Central Library BADJI Mokhtar-ANNABA UNIVERSITY

Copyright Elsevier 2024

CHAPTER

Imidazole framework based metal oxide nanoparticles photocatalysts: An approach towards amputation of organic pollutants from water

10

Benjamin Raj[a], Arun Kumar Padhy[a], Gajendra Prasad Singh[b], Ratan Kumar Dey[a], Ramesh Oraon[b]

Department of Chemistry, Central University of Jharkhand, Ranchi, Jharkhand, India[a] Department of Nanoscience and Technology, Central University of Jharkhand, Ranchi, Jharkhand, India[b]

1 Introduction

Presently, rapid developments of industry and human population are putting an incredible strain on environment more likely as an environmental, water, and soil pollution leads to severe ecological and economical concern (Rajeshwar et al., 2008). Among all the preceding text, water pollution has become a major look out for the life standard of human being and animals. The pollutants or waste by-product released directly or indirectly from industry, agricultural, and domestic activities are the main sources of water pollution (Chaousis, Leusch, & van de Merwe, 2018). Previously, it has been reported that the major organic pollutants are responsible for the environmental threat coming from industrial and textile dyes, respectively. These dyes are very toxic and highly carcinogenic even at trace level (used in food and textile industries) and considered to be first contaminants in industrial waste water. Thus these dyes pose a serious hazard to human and to marine ecosystem at large. As per the report, each year, approximately ~0.7 million ton of organic synthetic dyes are manufactured for utilization in the paper industries, leather goods, industrial painting, food, cosmetics, plastics, and other consumer service sectors (Rajeshwar et al., 2008). These dyes are basically derived from the two main sources, that is coal tar and petroleum intermediates. About, 10%–20% (~1000 tons) of these nonbiodegradable textile dyes are directly discharged as effluents into the green environment (natural streams and to the water bodies) (Ajmal, Majeed, Malik, Idriss, & Nadeem, 2014; Houas et al., 2001; Pagga & Brown, 1986). As a result, worldwide 3.2 million people die every year because of polluted water, poor sanitation, and inadequate hygiene (Hisatomi, Kubota, & Domen, 2014). Thus it is of prime necessity to understand the fundamental aspects of dye in order to overcome their associated problems on the environment.

Nano-Materials as Photocatalysts for Degradation of Environmental Pollutants. https://doi.org/10.1016/B978-0-12-818598-8.00010-9
© 2020 Elsevier Inc. All rights reserved.

This book belongs to Central Library BADJI Mokhtar-ANNABA UNIVERSITY

Copyright Elsevier 2024

1.1 Classification of dye

Dyes (also termed as colorant) are complex organic material, which shows an affinity toward the substrate to which it is being applied inherently or through the action of additives (Barnett, 2007). Most often the term colorant is also used for pigments; however, the major difference between them is their particle size. Dyes are much finer than pigments and can effortlessly penetrate deeper into the surface. Therefore dyes are not UV stable, whereas pigments are usually UV stable. Classification of dye is difficult on the basis of only one parameter due to their many structural varieties theoretically and practically (Camarero, Peche, Merino, & Rodríguez, 2003; Khan, Khan, & Cho, 2018; Wang et al., 2010). However, apart from solubility and chemical properties and based on their sources and general structure, they are divided into different groups and class as shown in Fig. 1.

Natural dyes are biodegradable under natural condition without the use of any oxidant or reluctant. The major source of natural dyes is plants (viz., madder, indigo, and saffron) and animals (Tyrian purple, crimson kermes, etc.). On the other hand, synthetic or artificial dyes are (manmade from petrochemicals) mostly nonbiodegradable and quite stable to redox process as per designing and thus difficult to remove from industry effluents. Synthetic dyes further divided into nonazo or azo group depending on their chemical structure (Borthakur, Boruah, Hussain, Silla, & Das, 2017; Salleh, Mahmoud, Karim, & Idris, 2011). Azo dye has the largest group of colorants containing double bond nitrogen (—N═N—), where one of the nitrogen atom is directly attached with the aromatic ring (He, Freeman, Lu, & Zhang, 2011). It is further classified into the acidic (anionic), basic (cationic), reactive, sulfuric, and vat dyes, respectively (Zaharia, Suteu, & Muresan, 2012). Because of the presence of

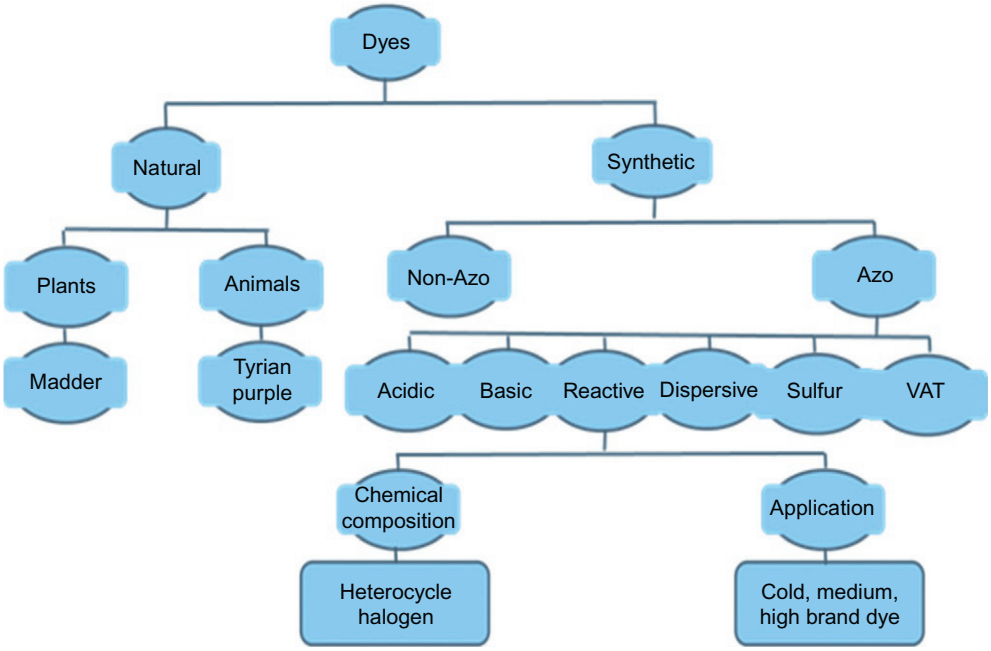

FIG. 1

Classification of dyes.

This book belongs to Central Library BADJI Mokhtar-ANNABA UNIVERSITY
Copyright Elsevier 2024

additional functional groups (like carbonyl, hydroxyl, amino, and sulfonyl group), it shows amphoteric behavior (acidic or basic). Acidic dyes are normally applied for the nitrogenous fiber or fabrics in inorganic or organic acid solution, whereas basic dyes are used in acrylic or modacrylic fiber. Disperse dyes (due to low solubility in water) can be applied to polyester chain by forming dispersed particles. Primarily, reactive dyes are utilized in the cellulosic fiber and occasionally on protein fibers, nylon. Sulfur dyes are used in cellulosic fibers to produce dull shades like black, brown, and navy. Lastly, vat dyes are used in the chlorination and bleach. Examples of various natural and synthetic dyes are listed in Fig. 2A and B.

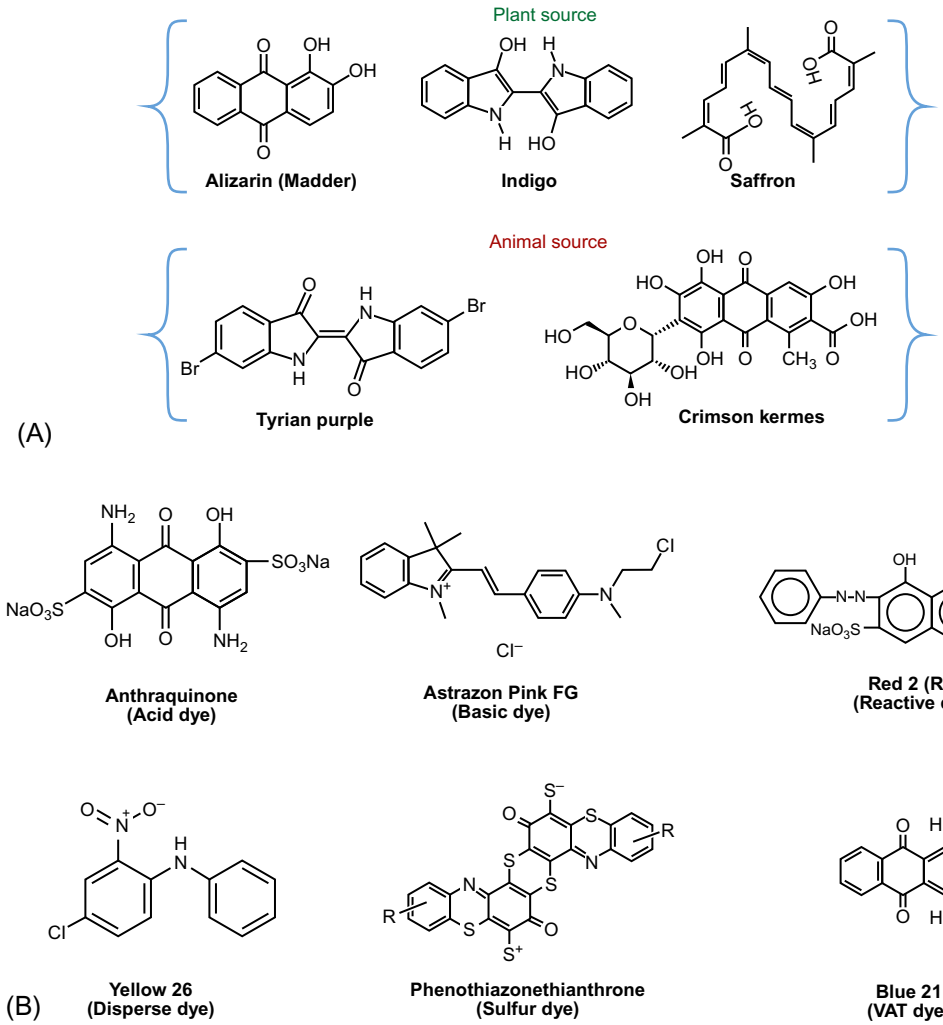

FIG. 2

(A) Dyes from natural sources. (B) Dyes from synthetic or manmade sources.

This book belongs to Central Library BADJI Mokhtar-ANNABA UNIVERSITY

Copyright Elsevier 2024

Since most of the dyes are of synthetic origin and complex molecular structure, they are very difficult to degrade and thus often cause unfavorable environmental pollution during their making process. Hence, it has become an urgent task to carry out essential and convenient environmental-economic strategies, technologies for waste water disposal without affecting ecosystems at large. A large number of consecutive physicochemical treatment processes (like coagulation (Alderman & Clifton-Hadley, 1993), adsorption (Ashour, 2010; Panizza, Barbucci, Ricotti, & Cerisola, 2007), biological treatments (Habib, Ismail, Mahmood, & Ullah, 2012), liquid-liquid extraction (Gajbhiye, 2012), and ultrasonic decomposition (Thanh, Thien, Du, Hung, & Khieu, 2018)) have been employed to conquer the effects of dye from the contaminated water. In addition to this, advanced technologies (like catalytic and photocatalytic oxidation method) are also required to eliminate water pollution and to increase the pollutants destruction with the separation process. During concomitant efforts, dye degradation is the process by which large molecules are broken into the simpler one in the form of water, CO_2, and several mineral by-products (Rathore, Ameta, & Sharma, 2015). Photocatalysis has witnessed intense scientific attention as a green environmental remediation process of dyes from contaminant water. Photocatalysis is the degradation process in which chemical are employed for speeding up rate of chemical reaction in the presence of light. It is highly efficient on the oxidation of the organic compounds even at low concentration.

1.2 Definition of photocatalysis

The term photocatalysis is an amalgamation of photochemistry and catalysis. Photocatalysis (a Greek word) comprises two parts:

- Photo means light.
- Catalysis is the process of modifying a chemical reaction with the use of catalyst. Catalyst is the substance, which increases rate of chemical reaction by reducing the activation energy of reactant.

In general, photocatalysis is the process where catalyst and light concurrently speed up the rate of chemical reaction. A photocatalyst is defined as the substance, which is capable of absorbing light and creating electron-hole pairs that help in the chemical transformation of the reaction and regenerate the composition after each cycle of such interaction (Djurišić, Leung, & Ng, 2014; Hisatomi et al., 2014; Hoffmann, Martin, Choi, & Bahnemann, 1995; Khan, Adil, & Al-Mayouf, 2015). They are classified into two categories as follows (Fujishima, Rao, & Tryk, 2000; Rajeshwar et al., 2008):

- *Homogeneous photocatalysis*: This process is carried out involving transition metal complexes as catalyst (like iron, copper, and chromium). During this process, under thermal condition and photon, the higher oxidation state of metal ion complexes generated hydroxyl radicals, which further react with organic matter leading to destruction of toxic matters. Since reactant, catalyst, and products are present in same phase, hence, it offers several advantages like high selectivity, cost-effective, no requirement of harsh condition (high temperature and pressure), no waste disposal problem, more susceptible to decomposition, and complete mineralization (Hisatomi et al., 2014). However, common problems like poor mechanistic insight and large-scale handling of products and their isolation from liquid media still remain challenging for practical applicability in commercialization.

This book belongs to Central Library BADJI Mokhtar-ANNABA UNIVERSITY Copyright Elsevier 2024

- *Heterogeneous photocatalysis*: This process utilizes semiconducting materials (like TiO_2, ZnO, SnO_2, and CeO_2), as a heterogeneous photocatalyst. Because of favorable electronic structure combination, charge transport characteristic, and high biocompatibility and stability in various condition when stimulated in light, these materials are considered as a potential photocatalyst (Chen, Nanayakkara, & Grassian, 2012; Wang, Zhang, et al., 2014). Heterogeneous photocatalyst can decompose the pollutants into the biodegradable compound and eventually mineralizing them into the harmless carbon dioxide and water. Despite such intriguing properties, heterogeneous catalysis is not comprehensively studied.

Under such fundamental assessment, photocatalyst- and catalysis-driven acceleration of light-induced reaction (called photocatalysis) is found to be phenomenal method that could be an elegant way to waste water treatment. In this process, photocatalyst symbolizes noteworthy features where photon generates catalytically active species in the presence of sunlight as a source of irradiation.

2 Photocatalysis for pollutant degradation

Pollutant degradation through photocatalysis process is being considered as one of the vibrant and eco-friendly processes among other available purification/degradation processes because it uses renewal resource of energy. Photocatalysis process is most commonly carried out in the presence of metal oxides or semiconductors because they enable the photocatalysis on its surface through the photoinduced production of reactive species. Fig. 3 describes the schematic of the general process of photocatalysis.

Here, the electrons are migrated in the conduction band (e_c) upon the absorption of the sufficient photon energy and leaving high energy holes in the valence band (h_v). These high energy holes can then undergo surface reactions with electron donors (D) or acceptors (A), thus finishing the cycle and returning the semiconductor to its original state. But the recombination of electron and hole is a major obstacle in photocatalysis, which needs to be overcome, where the charges do not reach the surface to

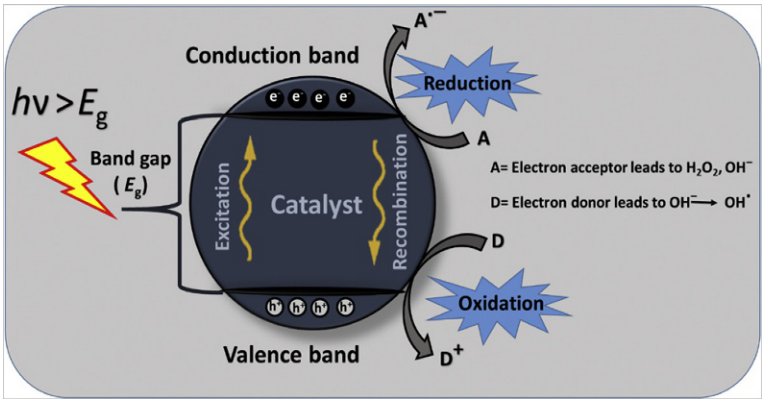

FIG. 3

Schematic representation of the reactive oxygen species (ROS) on a metal oxide or semiconductor photocatalyst under solar irradiation.

This book belongs to Central Library BADJI Mokhtar-ANNABA UNIVERSITY Copyright Elsevier 2024

react and conduction band electrons simply combine to holes in the valence band (Hoffmann et al., 1995). In order to cover come this problem, attention on materials designing is required in such a way that the short routes and quick transport of charges to the particle surface is suppressed or mechanisms by which the lifetime of charges are increased by separation across multiple materials (Wang et al., 2013; Wang et al., 2018). Further, the requirement of the production of the reactive oxygen species (ROS), which carry out the degradation of organic or bacteriological contaminants, is also needed to be considered (Karaolia et al., 2018; Nosaka & Nosaka, 2017). The energy required for the redox processes, which allow ROS to form at semiconductors surfaces, is given in Table 1.

It is valuable to consider the upper and lower extremes of these processes and keep them in mind when designing a new photocatalytic material. For instance the reduction of oxygen is an important step in scavenging photogenerated electrons from the excited semiconductor, which may occur at potentials more negative than the conduction band minima of some semiconductors. In such cases, either adjusting the pH can be used to promote the reduction of oxygen to the hydroperoxyl radical or loading a noble metal cocatalyst that allow the two electron reduction of oxygen to hydrogen peroxide (Abe, Takami, Murakami, & Ohtani, 2008). In case of energetic valence band holes, hydroxyl radicals can be generated from surface hydroxide groups. For complete mineralization of organic material, hydroxyl radicals are generally required due to their high oxidizing power, but producing hydroxyl radicals adsorbed onto the surface requires only a moderately oxidizing hole, whereas generating free hydroxyl radicals desorbed from the surface requires a significantly deeper valence band, with implications for the degradation of adsorbing versus nonadsorbing pollutant kill (Khaki, Shafeeyan, Raman, & Daud, 2017; Kim, Tachikawa, Moon, Majima, & Choi, 2014; Nagarajan et al., 2017; Schneider et al., 2014). This highlights an important factor, which should be considered when designing new photocatalytic materials. Materials, which use visible light sources and/or solar irradiation, are attractive but may be unable to form the more oxidizing ROS species effectively. Accessing such highly oxidizing ROS has been noted as a viable route to degrade persistent micropollutants, toxic organic contaminants, which are not removed by current water treatment strategies. Hence, at the nanoscale, the process can be understood relatively/simply; however, to apply these processes in practice implementation, barriers must be overcome.

Undoubtedly, there has been growing importance in the investigation of photocatalysts to alleviate the problem of water pollution. Several photocatalysts such as ZnO, ZnS, semiconductor-graphene composites, perovskites, MoS_2, WO_3, and Fe_2O_3 were developed and were tested in different environments. In addition to these, composites of two different photocatalysts has also recently gained interest

Table 1 Photocatalytic energetic redox process on the semiconductor surface

S. no.	Reactive oxygen species (ROS) generating redox reaction	Redox potential (V) vs NHE
1.	$O_2 + e_c^- \rightarrow O_2^-$	−0.33
2.	$O_2 + H^+ + e_c^- \rightarrow HO_2^\bullet$	−0.05
3.	$HO_2^\bullet + H^+ + e_c^- \rightarrow H_2O_2$	1.44
4.	$O_2 + 2H^+ + 2e_c^- \rightarrow H_2O_2$	0.695
5.	$H_2O_2 + 2H^+ + 2e_c^- \rightarrow OH^\bullet + H_2O$	1.14
6.	$OH_{adsorbed}^- + h_v^+ \rightarrow OH_{adsorbed}^\bullet$	1.6
7.	$OH_{free}^- + h_v^+ \rightarrow OH_{free}^\bullet$	2.72

This book belongs to Central Library BADJI Mokhtar-ANNABA UNIVERSITY
Copyright Elsevier 2024

because it forms heterojunctions between the photocatalysts (Shaham-Waldmann & Paz, 2016). The energy adsorbed by the first photocatalyst is transferred to the second photocatalyst and leads the increment in charge separation period, thus significantly influencing on the rate of degradation (Koppenol & Liebman, 1984).

Since several decades, metal oxides like TiO_2, ZnO, SnO_2, and CeO_2 as an individual or in the form of composite remains most popular photocatalyst due to their low cost, nontoxicity, and high oxidizing ability (Chen et al., 2012; Wang, Zhang, et al., 2014). As per literature, they can be easily immobilized on various surfaces and can be scaled up for large-scale water treatment. They are the most viable option for reclamation of agricultural/irrigational waste water is being considered as standard materials to destroy a variety of pollutants under UV irradiation. Alvarez-Corena, Bergendahl, and Hart (2016) reported on the evaluation of concurrent degradation of different contaminants such as 1,4-dioxane, N-nitrosodimethylamine (NDMA), tris(2-chloroethyl) phosphate (TCEP), gemfibrozil, and 17β estradiol. It was found that 77% for 1,4-dioxane, 92% for NDMA, 45% for TCEP, 95% for gemfibrozil, and 93% for 17β estradiol were degraded within 30 min. Under optimized conditions like pH 5.0 and TiO_2 dosage of $1.5\,gL^{-1}$. Interestingly, almost water-insoluble compounds (gemfibrozil and 17β estradiol) were also degraded quicker than the other contaminants examined (Alvarez-Corena et al., 2016). Quite different from the usual studies that employ single contaminant to evaluate TiO_2 photocatalysis, Pino and Encinas (2012) studied the concurrent degradation of two phenolic pollutants 4-CP and 2,6-DCP to understand TiO_2 catalysis in competitive conditions. Additionally, TiO_2 immobilized on glass substrate was also successfully applied for the solar photocatalytic degradation of 15 emerging contaminants (viz., acetaminophen, antipyrine, atrazine, carbamazepine, diclofenac, flumequine, hydroxybiphenyl, ibuprofen, isoproturon, ketorolac, ofloxacin, progesterone, sulfamethoxazole, and triclosan) (Arlos et al., 2016). Significantly (∼85%), removal of these contaminants was achieved within 120 min, revealing its potential application of this technology for wastewater treatment plant effluents displaying good efficiencies owing to their charge separation across the anatase/rutile phase interface. Similarly, Paramarta, Taufik, Munisa, and Saleh (2017) reported the catalytic activity of SnO_2 (synthesized by sol-gel technique) against degradation of methylene blue and Congo red dye under UV light. The maximum degradation of photocatlytic activity was measured to be 32.5% and 64.1% for Congo red and methylene blue, respectively. Aisah, Gustiono, Fauzia, Sugihartono, and Nuryadi (2017) highlighted photocatalytic activity of Ce-doped zinc oxide nanorods synthesized by low-temperature hydrothermal process. He demonstrated the improved photocatalytic reaction of Ce-doped ZnO in the degradation of methylene blue. The improved performance was attributed to decreased bandgap from 3.23 to 3.18 eV due to increased number of electron hole pair within ZnO lattice and better surface morphology. Table 2 summarizes the degradation of the various pollutants using different photocatalysts.

Typically, it is evident that photocatalytic performance of these metal oxides primarily depends on intriguing physicochemical properties (typically size, shape, morphology, and composition) (Khan, Adil, et al., 2015). Till the date, various synthetic procedures were utilized to control their physicochemical properties toward the development of photoactive materials to harness the overall catalytic performance. In this cocontinuous search, metal oxide photocatalyst derived from imidazole framework-based organic precursor is recognized as new and exciting material for the amputation of organic pollutant due to its high surface area, mesoporous structure, crystallinity, and thermal chemical stabilities (Thanh et al., 2018; Zhang & Jiang, 2013; Zhu, Srinivas, Bhogeswararao, Ratnasamy, & Carreon, 2013). Because of enhanced surface-enriched property (controlled mesoporosity, uniform

This book belongs to Central Library BADJI Mokhtar-ANNABA UNIVERSITY Copyright Elsevier 2024

Table 2 The photocatalytic degradation performance of various photocatalysts

No.	Photocatalysts	Pollutants	Photocatalytic degradation performance	References
1.	WO_3-vanadium phosphate	Rhodamine B	100% removal in 10 min	Behera, Biswal, and Parida (2017)
2.	$SrTiO_3$-Ag-AgCl	Bisphenol A	83% removal in 4 h	Yang et al. (2017)
3.	Boron nitride-TiO_2	Rhodamine B	99% removal in 6 h	Arlos et al. (2016)
4.	Boron nitride-BiOI	Methylene blue and rhodamine B	90% removal in 100 min	Liu et al. (2016)
5.	C_3N_4-TiO_2	Sulfamethoxazole	69% removal in 30 h	Yu, Wang, Sun, Wang, and Zhou (2018)
6.	C_3N_4	Rhodamine B	18% to 92% removal	Shen et al. (2017)
7.	ZnO	Compost leachate	61% COD removal in 4 h	Ranjbari and Mokhtarani (2018)
8.	Bi_2O_3-TiO_2	Acid orange II	45% removal in 2 h	Yuan et al. (2017)
9.	ZnO/AgBr/Fe_3O_4/Ag_3VO_4	Rhodamine B	0.029 min^{-1}	Shekofteh-Gohari and Habibi-Yangjeh (2016)
10.	NiAl layered double hydroxide/Fe_3O_4 reduced	Ciprofloxacin	0.0235 min^{-1}	Ni et al. (2018)
11.	Fe_3O_4-TiO_2	Reactive brilliant red 3	0.03–0.035 min^{-1}	Sun, Hong, Liu, and Dong (2018)
12.	Bi_2MoO_6/$ZnFe_2O$	Rhodamine B	0.0034 min^{-1}	Zhao et al. (2018)
13.	$CoFe_2O_4$-PANI	Methyl orange	85% degradation in 2 h	Kim, Jung, and Lee (2016)
14.	C_3N_4@$MnFe_2O_4$-graphene	Various antibiotics	0.017–0.042 min^{-1}	Wang, Wang, and Ma (2017)
15.	Au-graphene	Methylene blue	65% in 7 h	Khan, Khan, and Cho (2015b)
16.	Ag-graphene	Methylene blue and Congo red	65% and 90% in 6 and 5 h	Khan, Khan, and Cho (2015a)
17.	Pt-Graphene/TiO_2	Methylene blue	93% in 150 min	Ye and Oh (2017)
18.	Graphene-gold	Methylene blue, rhodamine B, and orange II	88.6%, 27.6% and 8.5%	Xiong, Zhang, Ma, and Zhao (2010)
19.	Au@TiO_2-graphene	Acid blue 92	72% and 43% in 120 min	Ghasemi, Hashemian, Alamolhoda, Gocheva, and Setayesh (2017)
20.	Au@TiO_2/graphene	2,4-Dichlorophenol (2,4-DCP)	78% in 150 min	Dang et al. (2014)
21.	Ag-Au-rGO nanocomposite	4-Nitrophenol	100% in 360 s	Hareesh, Joshi, Sunitha, Bhoraskar, and Dhole (2016)
22.	Graphene-Bi_2WO_6 nanosheets	Rhodamine B	90% in 120 min	Low, Yu, Li, and Cheng (2014)

This book belongs to Central Library BADJI Mokhtar-ANNABA UNIVERSITY
Copyright Elsevier 2024

Table 2 The photocatalytic degradation performance of various photocatalysts—cont'd

No.	Photocatalysts	Pollutants	Photocatalytic degradation performance	References
23.	Ag/reduced graphene oxide	Congo red and brilliant blue	25.74% for BB and 20.98% for CR in 120 min	Borthakur et al. (2017)
24.	Pt/graphene	Rhodamine B and methylene blue	70% and 82% in 180 min	Ullah et al. (2014)
25.	Pt-Pd-graphene	Basic fuchsin and indigo carmine dyes	70% and 65% in 50 min	Kurt, Durmus, and Durmus (2016)

pore size distribution, and pore volume), metal oxide maximizes the possibility of the formation of a huge number of electron-hole pair in generation of hydroxyl ion. These hydroxyl ions can actively react with organic pollutant and favor the facile decomposition of dye into nonhazardous carbon dioxide and water. These metal oxides can be effectively used as both complementary and supplementary for organic pollutant in wastewater treatment through complete mineralization. Hence, it is important to have a fundamental insight of imidazole, their derivative, and process making of metal oxide through the imidazole framework. The MOF-based metal oxide is listed in the Table 3.

Table 3 MOF-based metal oxide

Sl. no.	Materials (derived from zeolite imidazole framework) family of MOFs	Pollutants	Percentage degradation of dye	References
1.	Ag^+ doped ZIF-8	Methylene blue	100% in 40 min	Yurtsever, Akgunlu, Kurt, Yurttaş, and Topuz (2016)
2.	Zn/Fe (Fe-ZIF-8)	Rhodamine B	90% in 300 min	Thanh et al. (2018)
3.	PTA/ZIF-8	Methylene blue	Almost disappear at 20 min	Guo, Yang, Guo, Yang, and Chen (2017)
4.	ZIF-8	Methylene Blue	82.3% in 120 min	Jing, Wang, Zhang, Wang, and Li (2014)
5.	MOF/$BiFeO_3$	Methylene blue	98% in 150 min	Ramezanalizadeha and Manteghia (2016)
6.	MIL-88(Fe)@GO	Methylene blue and rhodamine B	Almost disappear in 30 min	Wu, Luo, and Wang (2014)
7.	Zr-based MOFs	Acid dyes	Disappear in 90 min	Lin, Yang, and Hsu (2018)
8.	MIL-100(Fe)/GO	Methyl orange	Disappear in 240 min	Tang and Wang (2017)
9.	MIL-125(Ti)@TiO_2	Rhodamine B	83.1%	Zhu and Yan (2018)
10.	Cu-based MOF	Methyl orange	90% in 180 min	Lin, Wan, et al. (2018)

This book belongs to Central Library BADJI Mokhtar-ANNABA UNIVERSITY
Copyright Elsevier 2024

3 Imidazole and imidazole-derived metal oxide photocatalyst

Imidazole is an organic compound with the formula C_3H_4N. It is a five-membered heterocyclic aromatic compound, which contains two annular nitrogen atoms, one in pyrrole and another in pyridine ring, respectively. This ring system is present in important biological building blocks, namely, histidine and histamine, which have been efficiently utilized in biological activities and pharmaceutical applications. Fig. 4 shows the different imidazole derivatives.

3.1 Structure, reactivity, and properties

Due to five-member planar ring, imidazole can behave like a monoacidic base with the ability to form crystalline salts with an acid. It is highly polar compound (dipole moment ~3.61 D) and hence easily soluble in water and other polar solvents. It has two tautomeric forms, namely, 1H-imidazole and 3H-imidazole, because hydrogen atom can be located in either of the position. Because of its unique chemical structure, unshared electron pair on N-3 is more susceptible toward electrophilic attack rather on annular carbon. It is much less likely to become involved in nucleophilic substitution reaction unless there is strong electron withdrawing groups. The overall reactivity of imidazole is referred from sets of resonance structure and tautomerism (shown in Fig. 5).

3.2 Literature review on imidazole-based metal complexes and metal oxides

Abuskhuna, McCann, Briody, Devereux, and McKee (2004) reported on the successful synthesis of metal complexes with bis-(imidazole-2-yl) methane (abbreviated as 2-BIM) using Mn (II), Cu (II), and Zn (II) transition metal. Common structural feature of this imidazole derivative lies in its single spacer tetrahedral carbon, which are able to form a stable six-membered chelate ring to metallic center. X-crystal structure augments its successful formation of these metal complexes (shown in Fig. 6).

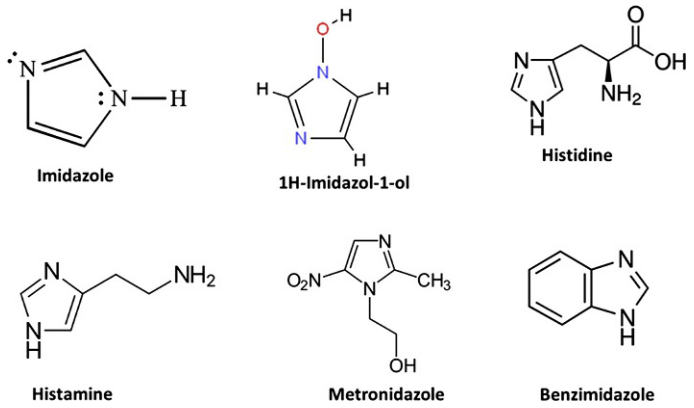

FIG. 4

Imidazole derivatives.

This book belongs to Central Library BADJI Mokhtar-ANNABA UNIVERSITY
Copyright Elsevier 2024

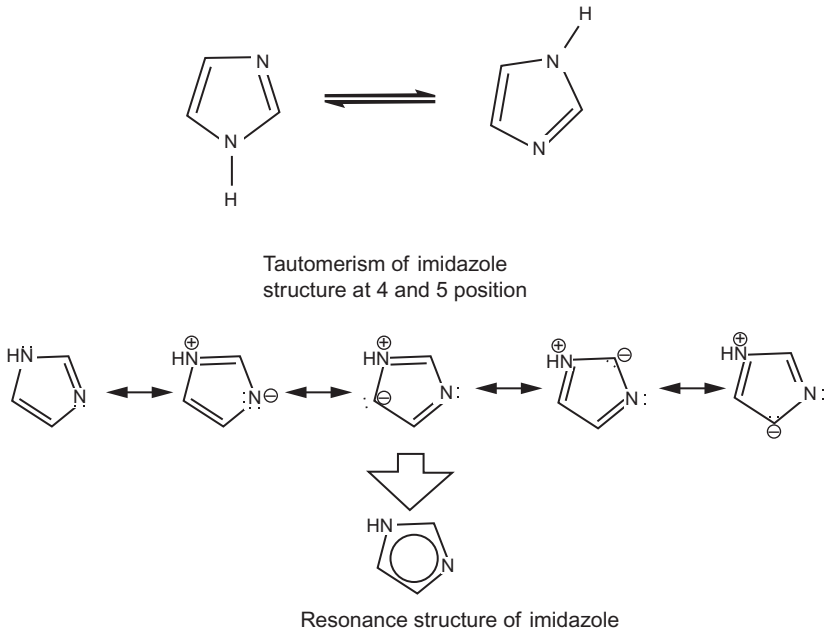

FIG. 5

Tautomerism and resonance structure of imidazole.

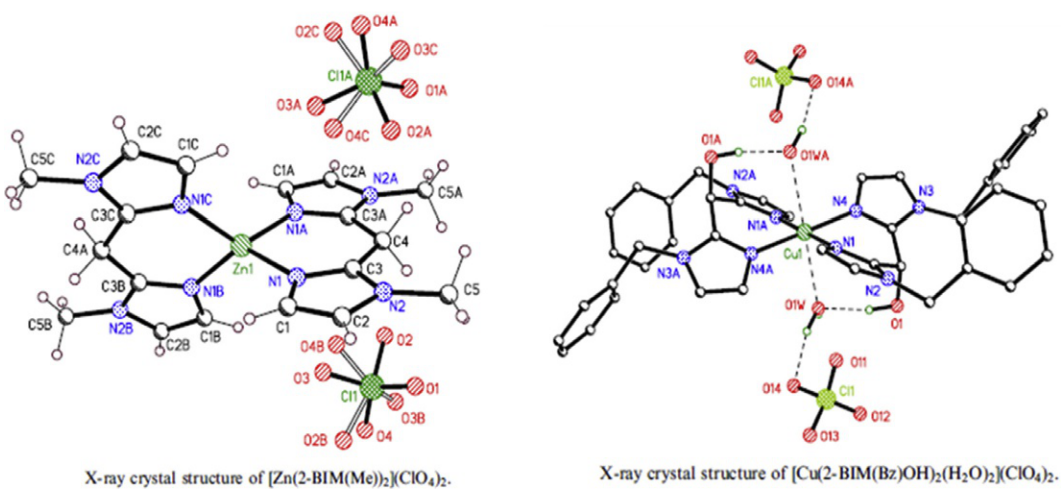

	R	R'
2-BIM	H	H
2-BIM(Me)	Me	H
2-BIM(Bz)OH	$PhCH_2$	OH
2-BIM(CN)	$NC(CH_2)_2$	H
2-BIM(ClBz)	Cl_2PhCH_2	H

Ligand symbols and structures.

X-ray crystal structure of $[Zn(2\text{-}BIM(Me))_2](ClO_4)_2$.

X-ray crystal structure of $[Cu(2\text{-}BIM(Bz)OH)_2(H_2O)_2](ClO_4)_2$.

FIG. 6

X-ray crystal structure of metal complexes from imidazole derivative (Abuskhuna et al., 2004).

This book belongs to Central Library BADJI Mokhtar-ANNABA UNIVERSITY

Copyright Elsevier 2024

In continuation, Padhy et al. reported on the successful preparation of ZnO nanoparticle using imidazole derivative as the organic precursor (Padhy, Chetia, Mishra, Pati, & Iyer, 2010). For the synthesis of ZnO, N-hydroxy 2,4,5-trisubstituted imidazoles were used as a imidazole derivative (organic precursor) starting from 1,2-diketones and demonstrated their complexation with unusual intermolecular hydrogen bonding through association of water molecules (in water bridging) followed by metalation process to give zeolitic imidazole framework belonging to the family of metal organic frameworks (MOFs) (shown schematically in Fig. 7). A zeolitic imidazole framework (ZIF) is a well-known subfamily of MOFs formed through the coordination interaction between the metal ion and imidazole derivatives. Such observations are well complemented with metalation reactions of 1,2-dimethylimidazole reported by Iddon and Lim (1983).

Successful preparation of ZnO nanoparticles and their involved complexation through intermolecular hydrogen bonding were characterized via single crystal structure and TEM analysis, which revealed hydrogen bonding to protonated amine, oxime O-atom, and perchlorate O-atom along with nanostructured formation of ZnO (in Fig. 8).

Similarly, ***Yamauchi groups*** also reported the crucial role of imidazole toward core-shell structured formation and designing of ZIFs (like ZIF-8 and ZIF-67) by seed-mediated growth method (in Fig. 9) (Tang et al., 2015) by varying the feeding molar ratio of Co^{+2}/Zn^{+2} for supercapacitor application. It was found that ZIF-8@ZIF-67 and their composite with nitrogen-doped carbon and graphitic carbon, respectively, after direct carbonization process give extremely high surface area ($\sim$1276 m^2/g) with superior graphitic structures. Hasan and Jhung (2015) very nicely demonstrated the potential interaction mechanism (through electrostatic, hydrogen bonding, acid base, π-π interactions/stacking, pore/size-selective adsorption, and hydrophobic interactions) between ZIFs and hazardous organic pollutants in water. They also explored the effect of framework metal on the binding energy with water and

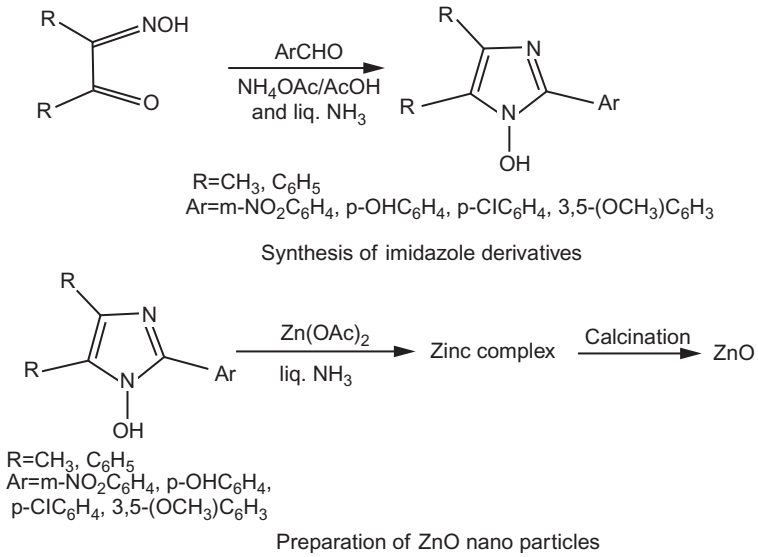

FIG. 7

Synthesis of imidazole derivative and preparation of ZnO nanoparticle (Padhy et al., 2010).

This book belongs to Central Library BADJI Mokhtar-ANNABA UNIVERSITY
Copyright Elsevier 2024

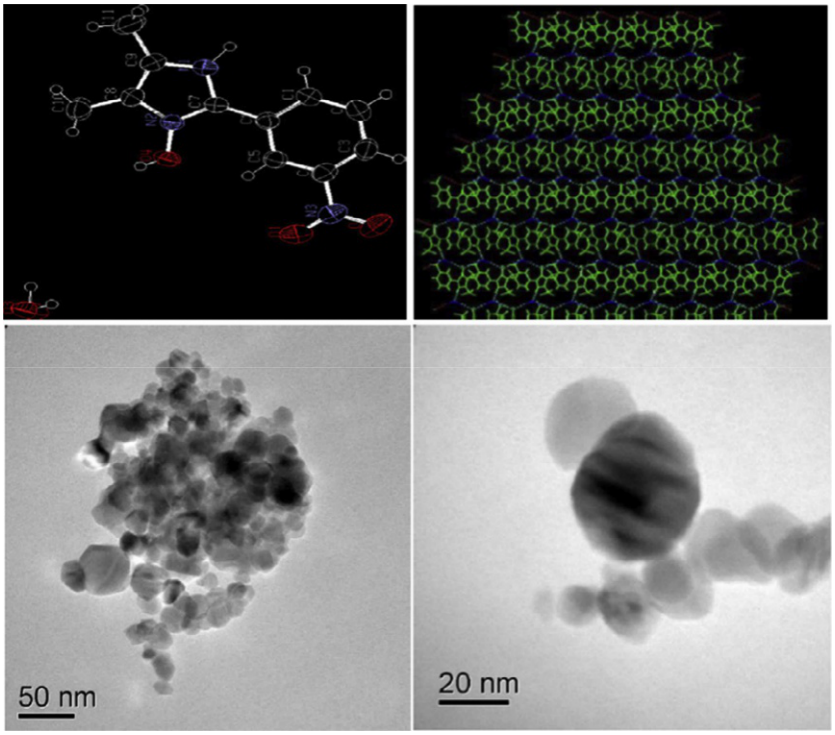

FIG. 8

Crystal structure and TEM image of imidazole-derived ZnO nanoparticle (Padhy et al., 2010).

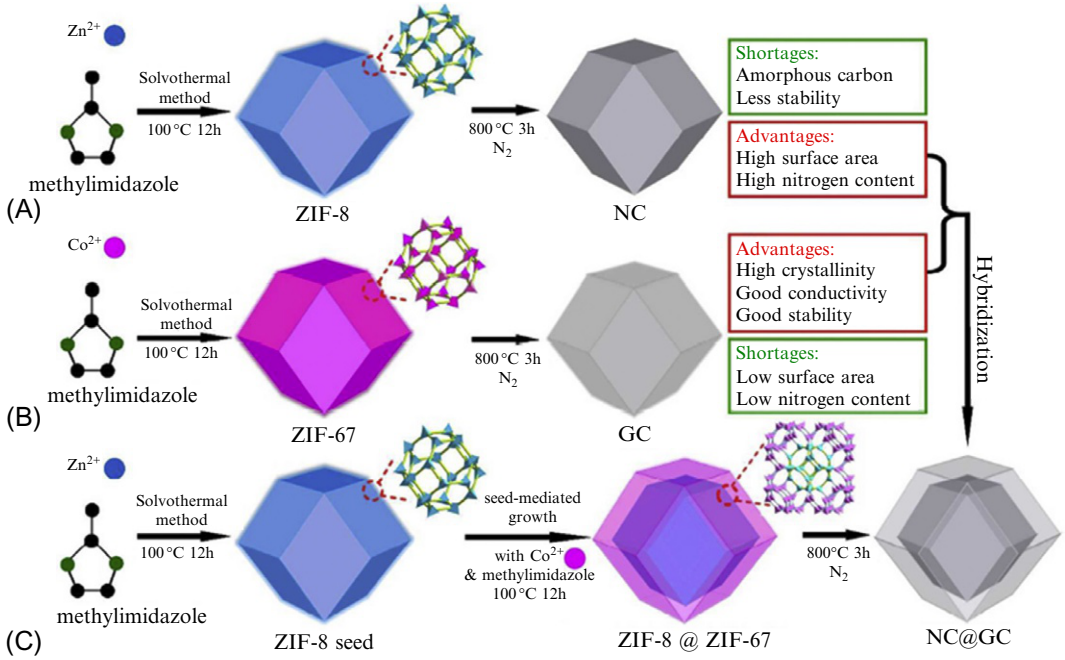

FIG. 9

Preparation of ZIF-based metal oxide.

This book belongs to Central Library BADJI Mokhtar-ANNABA UNIVERSITY

Copyright Elsevier 2024

pore size accessibility of organic pollutant. Laurier et al. (2013) prepared Fe (III)-based metal organic framework containing Fe_3-μ_3-oxo clusters for visible light (350 up to 850 nm) photocatalysis of rhodamine 6G in aqueous solution.

4 Prospects and challenges of imidazole framework-based metal oxide photocatalyst

It is evident that such synthetic route can provide uniform nanosized metal oxide particles with very high surface-enriched property (like high surface area, uniform pore size, and pore volume), which can be further utilized for several potential applications (shown in Fig.10).

Over the past few decades, synthesis of nanostructured metal oxide photocatalyst with controlled size, shape, and moderate bandgap (1.1–3.8 eV) between valence-conduction band and composition with overall morphological utilization has received tremendous research attention (Saravanan, Gracia, & Stephen, 2017). Metal oxide with such property is expected to provide a high ratio of surface atoms, which are potentially active or can be tuned for catalysis. Owing to its large surface area/well-ordered porous structure and tunable organic linkers/metal clusters, ZIF-based metal oxides can endow promising photophysical/photochemical properties by providing extra pathways to facilitate the

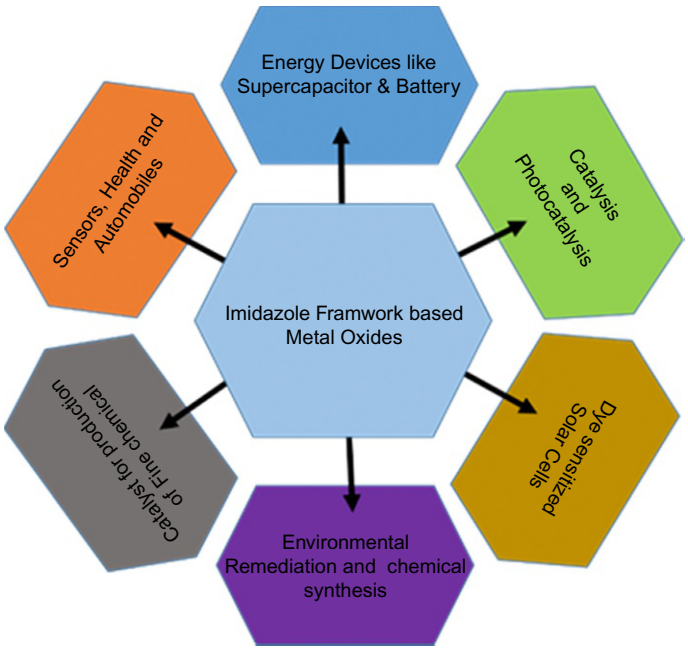

FIG. 10

Imidazole framework-based metal oxide and their promising application.

This book belongs to Central Library BADJI Mokhtar-ANNABA UNIVERSITY
Copyright Elsevier 2024

electron-holes separation as a result of the existence of structural defect, which leads to longer lifetime of e^-/h^+ and photocatalytic performance.

The most efficient photocatalytic materials reported earlier are metal oxides (like TiO_2, ZnO, SnO_2, and CeO_2), metal sulfides (MoS_2, ZnS, etc.), and metal selenides (Ag_2Se, CuSe, CdSe, etc.) that are not stable, photoanodic corrosive, and also toxic in nature. Hence, in this context synthesis of metal oxide photocatalyst via imidazole framework, a family of metal organic frameworks (MOFs) can be explored to overcome problems associated with conventional methods like adsorption, coagulation, sedimentation, filtration, chemical, and membrane technology. Additionally, these conventional methods do not completely eliminate wastewater, involving high operating costs, and can further generate toxic secondary pollutants. Contrarily, large porosity and tunability of imidazole-based framework are likely to be highly desirable to adsorption, catalytic nature, and then beneficial for degradation. The proposed photocatalytic reaction mechanism of as prepared metal oxides can be represented by following equation based on earlier reports:

$$\text{Semiconductor} + \text{Light Energy} \rightarrow \text{Semiconductor}(e_{cb}{}^- + h_{vb}{}^+) \tag{1}$$

$$\text{Organic Pollutant} + \text{Semiconductor}(h_{vb}{}^+) \rightarrow \text{Oxidation Process} \tag{2}$$

$$\text{Semiconductor}(h_{vb}{}^+) + H_2O \rightarrow \text{Semiconductor} + H^+ + OH \tag{3}$$

$$\text{Semiconductor}(h_{vb}{}^+) + OH^- \rightarrow \text{Semiconductor} + OH \tag{4}$$

$$\text{Organic Pollutant} + \text{Semiconductor}(e_{cb}{}^-) \rightarrow \text{Reduction Process} \tag{5}$$

$$\text{Semiconductor}(e_{cb}{}^-) + O_2 \rightarrow \text{Semiconductor} + O_2{}^- \tag{6}$$

$$O_2{}^- + H^+ \rightarrow HO_2 \tag{7}$$

$$HO_2 + HO_2 \rightarrow H_2O_2 + O_2 \tag{8}$$

$$H_2O_2 + O_2{}^- \rightarrow OH + OH^- + O_2 \tag{9}$$

$$\text{Pollutant} + OH \rightarrow \text{Degradation Product} \tag{10}$$

Because of many fascinating properties of ZIFs (in bridging organic linker) such as ultrahigh surface area, tunable compositions, and diverse structural topologies, the use of imidazole-derived metal oxide was further extended by Panchariya, Rai, Anil Kumar, and Singh (2018) to explore its possibility in improved CO_2 capture and H_2 storage due controlled structural feature endorsed by rationally designed porous material (method of synthesis shown in Fig. 11). Due to the involvement of advanced oxidation process, ZIFs can generate highly reactive radicals to partially oxidize organic molecules into less toxic ones or fully degrade them to CO_2 and water via facile in situ approach. By the use of these ZIFs, amputation of organic pollutants can be seen as another dimension of energy generation in the form of chemical energy, H_2 storage to treatment process.

Despite such intense significance, challenges like modest hydrolytic and undesirable stabilities often limit ZIFs overall performance (Wang, Li, Lv, Zhang, and Guo, 2014). Additionally, performance of ZIF-based metal oxides is not comparable with that of inorganic semiconductors owing to relatively low solar energy conversion and charge separation efficiency.

This book belongs to Central Library BADJI Mokhtar-ANNABA UNIVERSITY
Copyright Elsevier 2024

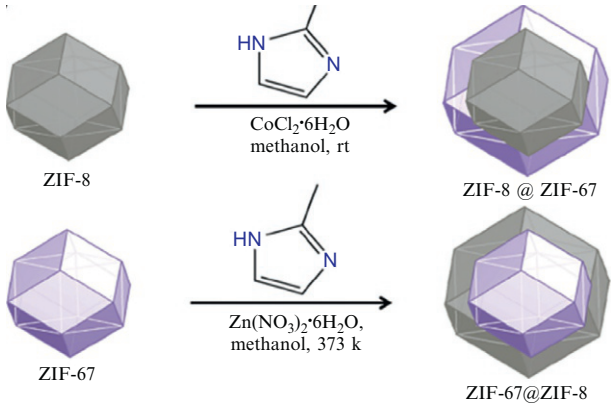

FIG. 11

Schematic of synthesis of ZIF-based photocatalyst.

5 Summary

In present chapter, efforts are devoted to the basic fundamental insight of different organic pollutant (called dye), photocatalysis with their plausible mechanism, and formation of imidazole-derived metal oxide-based photocatalyst. These ZIF-based metal oxides were further explored for their potential application in amputation of organic pollutant along with prospects to energy generation via CO_2 capture and H_2 gas. Unlike conventional methods, large porosity, tunability of ZIFs can endow promising photocatalytic property by providing extra pathways to facilitate electron-holes separation as a result of existence of structural defect, which leads to longer lifetime of e^-/h^+, which is highly desirable for adsorption, catalytic nature, and amputation of organic pollutant.

References

Abe, R., Takami, H., Murakami, N., & Ohtani, B. (2008). Pristine simple oxides as visible light driven photocatalysts: highly efficient decomposition of organic compounds over platinum-loaded tungsten oxide. *Journal of the American Chemical Society*, *130*, 7780–7781.

Abuskhuna, S., McCann, M., Briody, J., Devereux, M., & McKee, V. (2004). Synthesis and structure of Mn (II), Cu (II) and Zn (II) complexes containing bis-imidazole ligands. *Polyhedron*, *23*, 1731–1737.

Aisah, N., Gustiono, D., Fauzia, V., Sugihartono, I., & Nuryadi, R. (2017). Synthesis and Enhanced Photocatalytic Activity of Ce-Doped Zinc Oxide Nanorods by Hydrothermal Method. In *IOP Conference Series: Materials Science and Engineering, IOP Publishing* (p. 012037). .

Ajmal, A., Majeed, I., Malik, R. N., Idriss, H., & Nadeem, M. A. (2014). Principles and mechanisms of photocatalytic dye degradation on TiO2 based photocatalysts: a comparative overview. *RSC Advances*, *4*, 37003–37026.

Alderman, D., & Clifton-Hadley, R. (1993). Malachite green: a pharmacokinetic study in rainbow trout, Oncorhynchus mykiss (Walbaum). *Journal of Fish Diseases*, *16*, 297–311.

This book belongs to Central Library BADJI Mokhtar-ANNABA UNIVERSITY

Copyright Elsevier 2024

Alvarez-Corena, J. R., Bergendahl, J. A., & Hart, F. L. (2016). Advanced oxidation of five contaminants in water by UV/TiO2: reaction kinetics and byproducts identification. *Journal of Environmental Management*, *181*, 544–551.

Arlos, M. J., Hatat-Fraile, M. M., Liang, R., Bragg, L. M., Zhou, N. Y., Andrews, S. A., et al. (2016). Photocatalytic decomposition of organic micropollutants using immobilized TiO2 having different isoelectric points. *Water Research*, *101*, 351–361.

Ashour, S. S. (2010). Kinetic and equilibrium adsorption of methylene blue and remazol dyes onto steam-activated carbons developed from date pits. *Journal of Saudi Chemical Society*, *14*, 47–53.

Barnett, J. C. (2007). Synthetic organic dyes, 1856–1901: an introductory literature review of their use and related issues in textile conservation. *Studies in Conservation*, *52*, 67–77.

Behera, G. C., Biswal, N., & Parida, K. (2017). Unexpected rapid photo-catalytic decolourisation/degradation of organic pollutants over highly active hetero junction based vanadium phosphate catalyst. *Catalysis Today*, *284*, 84–91.

Borthakur, P., Boruah, P. K., Hussain, N., Silla, Y., & Das, M. R. (2017). Specific ion effect on the surface properties of Ag/reduced graphene oxide nanocomposite and its influence on photocatalytic efficiency towards azo dye degradation. *Applied Surface Science*, *423*, 752–761.

Camarero, L., Peche, R., Merino, J. M., & Rodríguez, E. (2003). Photo-assisted oxidation of indigocarmine in an acid medium. *Environmental Engineering Science*, *20*, 281–287.

Chaousis, S., Leusch, F. D., & van de Merwe, J. P. (2018). Charting a path towards non-destructive biomarkers in threatened wildlife: A systematic quantitative literature review. *Environmental Pollution*, *234*, 59–70.

Chen, H., Nanayakkara, C. E., & Grassian, V. H. (2012). Titanium dioxide photocatalysis in atmospheric chemistry. *Chemical Reviews*, *112*, 5919–5948.

Dang, X., Zhang, X., Lu, Z., Yang, Z., Dong, X., Zhang, X., et al. (2014). Construction of Au@ TiO_2/graphene nanocomposites with plasmonic effect and super adsorption ability for enhanced visible-light-driven photocatalytic organic pollutant degradation. *Journal of Nanoparticle Research*, *16*, 2215.

Djurišić, A. B., Leung, Y. H., & Ng, A. M. C. (2014). Strategies for improving the efficiency of semiconductor metal oxide photocatalysis. *Materials Horizons*, *1*, 400–410.

Fujishima, A., Rao, T. N., & Tryk, D. A. (2000). Titanium dioxide photocatalysis. *Journal of Photochemistry and Photobiology C: Photochemistry Reviews*, *1*, 1–21.

Gajbhiye, S. B. (2012). Photocatalytic degradation study of methylene blue solutions and its application to dye industry effluent. *International Journal of Modern Engineering Research*, *2*, 1204–1208.

Ghasemi, S., Hashemian, S., Alamolhoda, A., Gocheva, I., & Setayesh, S. R. (2017). Plasmon enhanced photocatalytic activity of Au@ TiO_2-graphene nanocomposite under visible light for degradation of pollutants. *Materials Research Bulletin*, *87*, 40–47.

Guo, J., Yang, L., Guo, R., Yang, S., & Chen, J. (2017). Enhanced photocatalytic activity of zeolitic imidazolate framework-8 by modification with phosphor tungstic acid. In *IOP Conference Series: Earth and Environmental Science*, IOP Publishing. pp. 012048.

Habib, M. A., Ismail, I. M. I., Mahmood, A. J., & Ullah, M. R. (2012). Photocatalytic decolorization of brilliant golden yellow in TiO2 and ZnO suspensions. *Journal of Saudi Chemical Society*, *16*, 423–429.

Hareesh, K., Joshi, R., Sunitha, D., Bhoraskar, V., & Dhole, S. (2016). Anchoring of Ag-Au alloy nanoparticles on reduced graphene oxide sheets for the reduction of 4-nitrophenol. *Applied Surface Science*, *389*, 1050–1055.

Hasan, Z., & Jhung, S. H. (2015). Removal of hazardous organics from water using metal-organic frameworks (MOFs): plausible mechanisms for selective adsorptions. *Journal of Hazardous Materials*, *283*, 329–339.

He, L., Freeman, H. S., Lu, L., & Zhang, S. (2011). Spectroscopic study of anthraquinone dye/amphiphile systems in binary aqueous/organic solvent mixtures. *Dyes and Pigments*, *91*, 389–395.

Hisatomi, T., Kubota, J., & Domen, K. (2014). Recent advances in semiconductors for photocatalytic and photoelectrochemical water splitting. *Chemical Society Reviews*, *43*, 7520–7535.

This book belongs to Central Library BADJI Mokhtar-ANNABA UNIVERSITY

Copyright Elsevier 2024

Hoffmann, M. R., Martin, S. T., Choi, W., & Bahnemann, D. W. (1995). Environmental applications of semiconductor photocatalysis. *Chemical Reviews*, *95*, 69–96.

Houas, A., Lachheb, H., Ksibi, M., Elaloui, E., Guillard, C., & Herrmann, J.-M. (2001). Photocatalytic degradation pathway of methylene blue in water. *Applied Catalysis B: Environmental*, *31*, 145–157.

Iddon, B., & Lim, B. L. (1983). Reactions of 1, 2-dimethylimidazole, particularly its metallation. *Journal of the Chemical Society, Perkin Transactions 1*, 271–277.

Jing, H.-P., Wang, C.-C., Zhang, Y.-W., Wang, P., & Li, R. (2014). Photocatalytic degradation of methylene blue in ZIF-8. *RSC Advances*, *4*, 54454–54462.

Karaolia, P., Michael-Kordatou, I., Hapeshi, E., Drosou, C., Bertakis, Y., Christofilos, D., et al. (2018). Removal of antibiotics, antibiotic-resistant bacteria and their associated genes by graphene-based TiO2 composite photocatalysts under solar radiation in urban wastewaters. *Applied Catalysis B: Environmental*, *224*, 810–824.

Khaki, M. R. D., Shafeeyan, M. S., Raman, A. A. A., & Daud, W. M. A. W. (2017). Application of doped photocatalysts for organic pollutant degradation—A review. *Journal of Environmental Management*, *198*, 78–94.

Khan, M. M., Adil, S. F., & Al-Mayouf, A. (2015). Metal oxides as photocatalysts. *Journal of Saudi Chemical Society*, *19*, 462–464.

Khan, M. E., Khan, M. M., & Cho, M. H. (2015a). Biogenic synthesis of a Ag–graphene nanocomposite with efficient photocatalytic degradation, electrical conductivity and photoelectrochemical performance. *New Journal of Chemistry*, *39*, 8121–8129.

Khan, M. E., Khan, M. M., & Cho, M. H. (2015b). Green synthesis, photocatalytic and photoelectrochemical performance of an Au–Graphene nanocomposite. *RSC Advances*, *5*, 26897–26904.

Khan, M. E., Khan, M. M., & Cho, M. H. (2018). Recent progress of metal-graphene nanostructures in photocatalysis. *Nanoscale*, *10*, 9427–9440.

Kim, K. N., Jung, H.-R., & Lee, W.-J. (2016). Hollow cobalt ferrite–polyaniline nanofibers as magnetically separable visible-light photocatalyst for photodegradation of methyl orange. *Journal of Photochemistry and Photobiology A: Chemistry*, *321*, 257–265.

Kim, W., Tachikawa, T., Moon, G.-h., Majima, T., & Choi, W. (2014). Molecular-level understanding of the photocatalytic activity difference between anatase and rutile nanoparticles. *Angewandte Chemie International Edition*, *126*, 14260–14265.

Koppenol, W., & Liebman, J. F. (1984). The oxidizing nature of the hydroxyl radical. A comparison with the ferryl ion (FeO2+). *The Journal of Physical Chemistry*, *88*, 99–101.

Kurt, B. Z., Durmus, Z., & Durmus, A. (2016). Preparation and characterization of platinum (Pt) and palladium (Pd) nanoparticle decorated graphene sheets and their utilization for the elimination of basic fuchsin and indigo carmine dyes. *Solid State Sciences*, *51*, 51–58.

Laurier, K. G., Vermoortele, F., Ameloot, R., De Vos, D. E., Hofkens, J., & Roeffaers, M. B. J. (2013). Iron (III)-based metal–organic frameworks as visible light photocatalysts. *Journal of the American Chemical Society*, *135*, 14488–14491.

Lin, Y., Wan, H., Chen, F., Liu, X., Ma, R., & Sasaki, T. (2018). Two-dimensional porous cuprous oxide nanoplatelets derived from metal–organic frameworks (MOFs) for efficient photocatalytic dye degradation under visible light. *Dalton Transactions*, *47*, 7694–7700.

Lin, K. A., Yang, H., & Hsu, F.-K. (2018). Zr-metal organic framework and derivatives for adsorptive and photocatalytic removal of acid dyes. *Water Environment Research*, *90*, 144–154.

Liu, D., Jiang, Z., Zhu, C., Qian, K., Wu, Z., & Xie, J. (2016). Graphene-analogue BN-modified microspherical BiOI photocatalysts driven by visible light. *Dalton Transactions*, *45*, 2505–2516.

Low, J., Yu, J., Li, Q., & Cheng, B. (2014). Enhanced visible-light photocatalytic activity of plasmonic Ag and graphene co-modified Bi_2WO_6 nanosheets. *Physical Chemistry Chemical Physics*, *16*, 1111–1120.

This book belongs to Central Library BADJI Mokhtar-ANNABA UNIVERSITY

Copyright Elsevier 2024

Nagarajan, S., Skillen, N. C., Fina, F., Zhang, G., Randorn, C., Lawton, L. A., et al. (2017). Comparative assessment of visible light and UV active photocatalysts by hydroxyl radical quantification. *Journal of Photochemistry and Photobiology A: Chemistry*, *334*, 13–19.

Ni, J., Xue, J., Xie, L., Shen, J., He, G., & Chen, H. (2018). Construction of magnetically separable NiAl LDH/Fe 3 O 4–RGO nanocomposites with enhanced photocatalytic performance under visible light. *Physical Chemistry Chemical Physics*, *20*, 414–421.

Nosaka, Y., & Nosaka, A. Y. (2017). Generation and detection of reactive oxygen species in photocatalysis. *Chemical Reviews*, *117*, 11302–11336.

Padhy, A. K., Chetia, B., Mishra, S., Pati, A., & Iyer, P. K. (2010). Imidazole derivatives as the organic precursor of ZnO nano particle. *Tetrahedron Letters*, *51*, 2751–2753.

Pagga, U., & Brown, D. (1986). The degradation of dyestuffs: Part II Behaviour of dyestuffs in aerobic biodegradation tests. *Chemosphere*, *15*, 479–491.

Panchariya, D. K., Rai, R. K., Anil Kumar, E., & Singh, S. K. (2018). Core–shell zeolitic imidazolate frameworks for enhanced hydrogen storage. *ACS Omega*, *3*, 167–175.

Panizza, M., Barbucci, A., Ricotti, R., & Cerisola, G. (2007). Electrochemical degradation of methylene blue. *Separation and Purification Technology*, *54*, 382–387.

Paramarta, V., Taufik, A., Munisa, L., & Saleh, R. (2017). Sono-and photocatalytic activities of SnO2 nanoparticles for degradation of cationic and anionic dyes. In *AIP Conference Proceedings*: AIP Publishing. pp. 030125.

Pino, E., & Encinas, M. V. (2012). Photocatalytic degradation of chlorophenols on TiO2-325mesh and TiO2-P25. An extended kinetic study of photodegradation under competitive conditions. *Journal of Photochemistry and Photobiology A: Chemistry*, *242*, 20–27.

Rajeshwar, K., Osugi, M., Chanmanee, W., Chenthamarakshan, C., Zanoni, M. V. B., Kajitvichyanukul, P., et al. (2008). Heterogeneous photocatalytic treatment of organic dyes in air and aqueous media. *Journal of Photochemistry and Photobiology C: Photochemistry Reviews*, *9*, 171–192.

Ramezanalizadeha, H., & Manteghia, F. (2016). Photocatalytic degradation of MB as an organic dye over a novel MOF/BiFeO3 composite. In: *The 20th International Electronic Conference on Synthetic Organic Chemistry (ECSOC)*.

Ranjbari, A., & Mokhtarani, N. (2018). Post treatment of composting leachate using ZnO nanoparticles immobilized on moving media. *Applied Catalysis B: Environmental*, *220*, 211–221.

Rathore, P., Ameta, R., & Sharma, S. (2015). Photocatalytic degradation of Azure A using N-doped zinc oxide. *Journal of Textile Science and Technology*, *1*, 118.

Salleh, M. A. M., Mahmoud, D. K., Karim, W. A. W. A., & Idris, A. (2011). Cationic and anionic dye adsorption by agricultural solid wastes: A comprehensive review. *Desalination*, *280*, 1–13.

Saravanan, R., Gracia, F., & Stephen, A. (2017). Basic principles, mechanism, and challenges of photocatalysis. In *Nanocomposites for visible light-induced photocatalysis* (pp. 19–40): Springer.

Schneider, J., Matsuoka, M., Takeuchi, M., Zhang, J., Horiuchi, Y., Anpo, M., et al. (2014). Understanding TiO2 photocatalysis: mechanisms and materials. *Chemical Reviews*, *114*, 9919–9986.

Shaham-Waldmann, N., & Paz, Y. (2016). Away from TiO_2: A critical minireview on the developing of new photocatalysts for degradation of contaminants in water. *Materials Science in Semiconductor Processing*, *42*, 72–80.

Shekofteh-Gohari, M., & Habibi-Yangjeh, A. (2016). Novel magnetically separable ZnO/AgBr/Fe 3 O 4/Ag 3 VO 4 nanocomposites with tandem n–n heterojunctions as highly efficient visible-light-driven photocatalysts. *RSC Advances*, *6*, 2402–2413.

Shen, X., Zhang, T., Xu, P., Zhang, L., Liu, J., & Chen, Z. (2017). Growth of C_3N_4 nanosheets on carbon-fiber cloth as flexible and macroscale filter-membrane-shaped photocatalyst for degrading the flowing wastewater. *Applied Catalysis B: Environmental*, *219*, 425–431.

This book belongs to Central Library BADJI Mokhtar-ANNABA UNIVERSITY

Copyright Elsevier 2024

Sun, Q., Hong, Y., Liu, Q., & Dong, L. (2018). Synergistic operation of photocatalytic degradation and Fenton process by magnetic Fe3O4 loaded TiO2. *Applied Surface Science*, *430*, 399–406.

Tang, J., Salunkhe, R. R., Liu, J., Torad, N. L., Imura, M., Furukawa, S., et al. (2015). Thermal conversion of core–shell metal–organic frameworks: A new method for selectively functionalized nanoporous hybrid carbon. *Journal of the American Chemical Society*, *137*, 1572–1580.

Tang, J., & Wang, J. (2017). Fe-based metal organic framework/graphene oxide composite as an efficient catalyst for Fenton-like degradation of methyl orange. *RSC Advances*, *7*, 50829–50837.

Thanh, M. T., Thien, T. V., Du, P. D., Hung, N. P., & Khieu, D. Q. (2018). Iron doped zeolitic imidazolate framework (Fe-ZIF-8): synthesis and photocatalytic degradation of RDB dye in Fe-ZIF-8. *Journal of Porous Materials*, *25*, 1–13.

Ullah, K., Ye, S., Zhu, L., Meng, Z.-D., Sarkar, S., & Oh, W.-C. (2014). Microwave assisted synthesis of a noble metal-graphene hybrid photocatalyst for high efficient decomposition of organic dyes under visible light. *Materials Science and Engineering: B*, *180*, 20–26.

Wang, X., Bai, L., Liu, H., Yu, X., Yin, Y., & Gao, C. (2018). A unique disintegration–Reassembly route to mesoporous titania nanocrystalline hollow spheres with enhanced photocatalytic activity. *Advanced Functional Materials*, *28*, 1704208.

Wang, M., Chamberland, N., Breau, L., Moser, J.-E., Humphry-Baker, R., Marsan, B., et al. (2010). An organic redox electrolyte to rival triiodide/iodide in dye-sensitized solar cells. *Nature Chemistry*, *2*, 385.

Wang, C.-C., Li, J.-R., Lv, X.-L., Zhang, Y.-Q., & Guo, G. (2014). Photocatalytic organic pollutants degradation in metal–organic frameworks. *Energy & Environmental Science*, *7*, 2831–2867.

Wang, X., Wang, A., & Ma, J. (2017). Visible-light-driven photocatalytic removal of antibiotics by newly designed C_3N_4@ $MnFe_2O_4$-graphene nanocomposites. *Journal of Hazardous Materials*, *336*, 81–92.

Wang, Y., Wang, Q., Zhan, X., Wang, F., Safdar, M., & He, J. (2013). Visible light driven type II heterostructures and their enhanced photocatalysis properties: A review. *Nanoscale*, *5*, 8326–8339.

Wang, H., Zhang, L., Chen, Z., Hu, J., Li, S., Wang, Z., et al. (2014). Semiconductor heterojunction photocatalysts: Design, construction, and photocatalytic performances. *Chemical Society Reviews*, *43*, 5234–5244.

Wu, Y., Luo, H., & Wang, H. (2014). Synthesis of iron (III)-based metal–organic framework/graphene oxide composites with increased photocatalytic performance for dye degradation. *RSC Advances*, *4*, 40435–40438.

Xiong, Z., Zhang, L. L., Ma, J., & Zhao, X. (2010). Photocatalytic degradation of dyes over graphene–gold nanocomposites under visible light irradiation. *Chemical Communications*, *46*, 6099–6101.

Yang, S.-F., Niu, C.-G., Huang, D.-W., Zhang, H., Liang, C., & Zeng, G.-M. (2017). SrTiO 3 nanocubes decorated with Ag/AgCl nanoparticles as photocatalysts with enhanced visible-light photocatalytic activity towards the degradation of dyes, phenol and bisphenol A. *Environmental Science: Nano*, *4*, 585–595.

Ye, S., & Oh, W.-C. (2017). Novel synthesis and characterization of Pt-graphene/TiO_2 composite designed for high photonic effect and photocatalytic activity under visible light. *Journal of the Korean Ceramic Society*, *54*, 28–32.

Yu, S., Wang, Y., Sun, F., Wang, R., & Zhou, Y. (2018). Novel mpg-C_3N_4/TiO_2 nanocomposite photocatalytic membrane reactor for sulfamethoxazole photodegradation. *Chemical Engineering Journal*, *337*, 183–192.

Yuan, X., Yi, J., Wang, H., Yu, H., Zhang, S., & Peng, F. (2017). New route of fabricating BiOI and Bi_2O_3 supported TiO_2 nanotube arrays via the electrodeposition of bismuth nanoparticles for photocatalytic degradation of acid orange II. *Materials Chemistry and Physics*, *196*, 237–244.

Yurtsever, H. A., Akgunlu, M. Y., Kurt, T., Yurttaş, A. S., & Topuz, B. (2016). Photocatalytic activities of Ag+ doped ZIF-8 and ZIF-L crystals. *Journal of the Turkish Chemical Society Section A: Chemistry*, *3*, 265–280.

This book belongs to Central Library BADJI Mokhtar-ANNABA UNIVERSITY

Copyright Elsevier 2024

Zaharia, C., Suteu, D., & Muresan, A. (2012). Options and solutions for textile effluent decolorization using some specific physico-chemical treatment steps. *Environmental Engineering and Management Journal*, *11*, 493–509.

Zhang, X., & Jiang, J. (2013). Thermal conductivity of zeolitic imidazolate framework-8: A molecular simulation study. *The Journal of Physical Chemistry C*, *117*, 18441–18447.

Zhao, C., Shao, C., Li, X., Li, X., Tao, R., & Liu, Y. (2018). Magnetically separable $Bi_2MoO_6/ZnFe_2O_4$ heterostructure nanofibers: Controllable synthesis and enhanced visible light photocatalytic activity. *Journal of Alloys and Compounds*, *747*, 916–925.

Zhu, M., Srinivas, D., Bhogeswararao, S., Ratnasamy, P., & Carreon, M. A. (2013). Catalytic activity of ZIF-8 in the synthesis of styrene carbonate from CO2 and styrene oxide. *Catalysis Communications*, *32*, 36–40.

Zhu, S.-Y., & Yan, B. (2018). Photofunctional hybrids of TiO_2 and titanium metal–organic frameworks for dye degradation and lanthanide ion-tuned multi-color luminescence. *New Journal of Chemistry*, *42*, 4394–4401.

This book belongs to Central Library BADJI Mokhtar-ANNABA UNIVERSITY

Copyright Elsevier 2024

This page intentionally left blank

This book belongs to Central Library BADJI Mokhtar-ANNABA UNIVERSITY

Copyright Elsevier 2024

CHAPTER

11

Exploitation of antibiotics: Mechanism of resistance, consequences, challenges of conventional remediation, and promise of nanomaterials in mitigation

Niloy Sarkar[a,b], Radhey Shyam Sharma[b], Mahima Kaushik[a]
Cluster Innovation Centre, University of Delhi, Delhi, India[a] Department of Environmental Studies, University of Delhi, Delhi, India[b]

1 Introduction

The term "antibiotic" in Latin means "opposing life." They are chemotherapeutic agents, which are used to treat microbial infections, and their discoveries have revolutionized human healthcare, animal husbandry, apiculture, and aquaculture. Antibiotics are actually a class of agents, which are able to retard or end bacterial growth by interfering in cytological pathways through various mechanisms. Antibiotics and their resistance are not novel human creations or effects but have been present in the microbiome for millions of years, as a means of evolutionary survival. However, overuse and mismanagement of these drugs have led to the excessive proliferation of antibiotic-resistant genes (ARGs) and antibiotic-resistant bacteria (ARB), which pose a grave danger to human health. It is perhaps ironic that wastewater treatment plants (WWTPs), which are designed to remove pollutants from wastewater, are aggravating the situation by acting as sinks and exposing more bacteria to antibiotic pollutants, thereby increasing chances of resistance. Therefore a novel solution must be found for the emerging problem at hand. Engineered nanomaterials offer one such possible solution, which can use their unique properties for the detection of antibiotics and photocatalytic destruction of dissolved antibiotics, ARGs, and ARB in situ.

Nano-Materials as Photocatalysts for Degradation of Environmental Pollutants. https://doi.org/10.1016/B978-0-12-818598-8.00011-0
© 2020 Elsevier Inc. All rights reserved.

This book belongs to Central Library BADJI Mokhtar-ANNABA UNIVERSITY
Copyright Elsevier 2024

2 Classes of antibiotics and their mechanism of action

Antibiotics can be classified on the basis of their mechanism of action, chemical structure, and route of administration (Gothwal & Sashidhar, 2015), to better understand the scope and environmental impact of antibiotics. Table 1 discusses the classes of antibiotics, based on their target, site of action, and brief physiology (Kapoor, Saigal, & Elongavan, 2017) and (Le-Minh, Khan, Drewes, & Stuetz, 2010).

3 Sources of antibiotic pollutants

Antibiotics are present in nature as natural defense mechanism against bacterial infections; however, antibiotics started entering the environment as effluents only after their discovery and production (Gothwal & Sashidhar, 2015). If one uses the principle of "what goes in must come out," then it's not difficult to understand that usage of all these antibiotics will eventually cause them and their metabolites to end up in the environment as micropollutants (Farre, Perez, Kantiani, & Barcelo, 2008).

3.1 Pharmaceutical

Pharmaceutical antibiotic consumption is globally increasing, which is driven by similar increase in income, insurance, and large burden of diseases (Laxminarayan & Chaudhury, 2016). Globally between 2000 and 2010, there had been a 36% increase in antibiotic consumption in 71 countries with Brazil, Russia, India, China, and South Africa (BRICS) nations accounting for two-thirds of that increase (Laxminarayan & Chaudhury, 2016). In 2010 India had been ranked first globally in the use of antibiotics, where consumption was estimated as 10.7 units per capita (Laxminarayan & Chaudhury, 2016). There are several reasons behind the misuse of antibiotics ranging from healthcare infrastructure not keeping pace with rise of income, poor enforcement of drug laws, widespread availability of antibiotics over the counter, and doctors receiving kickbacks from pharmaceutical companies to overprescribe antibiotics of their brand (Laxminarayan & Chaudhury, 2016).

Table 1 Brief mechanism of action of important classes of antibiotics.

Class	Site and mechanism of action	Chemical/environmental fate
Cell wall synthesis		
β-Lactams Glycopeptides	β-Lactams and glycopeptides bind to penicillin-binding proteins (PBP) and D-alanyl-al-alanine, respectively, and interfere in PBP-D-alanyl-al-alanine interaction and prevent peptidoglycan cross-linking, which is crucial in bacterial cell wall synthesis	• Four-membered β-lactam ring is strained and highly susceptible to enzymatic hydrolysis, as such they are not found to persist in wastewater
Protein synthesis		
Aminoglycosides	Bind to 16S rRNA and 30S ribosomal unit, near the A-site, and cause premature termination of the mRNA	• Mostly nonmetabolized and hence secreted as parent compounds • Highly susceptible to sorption

This book belongs to Central Library BADJI Mokhtar-ANNABA UNIVERSITY
Copyright Elsevier 2024

Table 1 Brief mechanism of action of important classes of antibiotics—cont'd

Class	Site and mechanism of action	Chemical/environmental fate
Cell wall synthesis		
Tetracyclines	Bind to 16S rRNA and 30S ribosomal unit, near the A-site, and prevents binding of tRNA to A-site of 30S ribosomal unit	• Some tetracyclines are quite susceptible to being adsorbed on biomass, while others such as oxytetracycline are quite soluble and poorly adsorbed • Nonhydrophobic interactions play an important role in the adsorption of tetracyclines
Chloramphenicol	The drug acts on the peptidyl transferase cavity of 23S rRNA of the 50S ribosomal subunit, which prevents binding of tRNA to A-site of 50S ribosomal unit	
Macrolides	The drug acts on the peptidyl transferase cavity of 23S rRNA of the 50S ribosomal subunit, which causes premature detachment of peptide chains	• Excreted largely in their unchanged parent form with excretion rate around 60%. This means that wastewater plants would contain high amounts of macrolides • Sorption onto biomass largely due to hydrophobic reactions
Oxazolidinones	The drug acts on peptidyl transferase cavity of 23s rRNA of the 50s ribosomal subunit and interferes tRNA and ribosomal attachment	
DNA replication		
Quinolones	Binds to a subunit of DNA gyrase and DNA topoisomerase IV and inhibits DNA replication	• Fluoroquinolones appeared not to be readily biodegradable in controlled batch tests • Sorption is a better method of removal than biodegradation
Folic acid synthesis		
Sulfonamides	Both the drugs inhibit the enzyme dihydropteroate synthase, which inhibits folic acid synthesis, which is necessary for the biosynthesis of purines and pyrimidines. Therefore inhibition of folic acid synthesis results in inability of bacterial cell to synthesize nucleic acids	• Sulfonamides aren't completely metabolized and released into the environment as parent compound metabolites • Major metabolites are biologically inert; however, reverse transition into active forms has been recorded in water treatment plants
Trimethoprim		• Presence correlated with that of the sulfonamide and sulfamethoxazole, as they are often administered in the ratio of 1:5 • Sorption to biomass appears to be minimal, and only minor removal in primary and secondary treatment has been reported

This book belongs to Central Library BADJI Mokhtar-ANNABA UNIVERSITY
Copyright Elsevier 2024

3.2 Animal husbandry

Antibiotics are also used in low concentrations as a substitute for good animal husbandry practices such as cleanliness and animal crowding. Globally the antibiotic usage for animal husbandry is estimated to rise by two-thirds between 2010 and 2030 (Laxminarayan & Chaudhury, 2016). India also has the world's largest cattle and poultry population with a sizable aquaculture industry, which consumes vast quantities of antibiotics to maximize yield. The use of prophylactic antibiotics in animal husbandry and aquaculture is increasing antibiotic-resistant pathogens, which remains a grave concern (Ghosh & Mandal, 2010). In one example, some shrimp farmers in the coast of Bengal (India) use as much as 65 different types of drugs to maximize yield (Ghosh & Mandal, 2010). Multiple ARB have been isolated from fish guts off the coast of Digha, Bengal. The *Escherichia coli* species were found to be resistant to ampicillin and chloramphenicol (Ghosh & Mandal, 2010). This threat will increase because the demand for meat and animal products are increasing from 30 kg/km^2 to an estimated increase by 312% by 2030 (Laxminarayan & Chaudhury, 2016). At present, India has no regulations or limits on the amount of permissible antibiotics used in animal husbandry, poultry, aquaculture, and discharge limits in wastewater (Laxminarayan & Chaudhury, 2016).

4 Percolation of antibiotics into the environment

One way to analyze the environmental course and fate of antibiotics is studying its percolation from the source (pharmaceutical effluents) and wastewater (containing human wastes) into surface water and eventually into marine water. Direct discharge from formulation or production facilities can lead to very high concentration in the industrial effluents. Several times, concentration of over 1 mg/L has been detected downstream (Larsson, 2014). For many antibiotics, urine and feces from consumers consist of considerable amount of active residues in wastewater, where microbes in treatment plants are exposed to concentrations up to μg/L (Larsson, 2014). This is because about 10%–90% of antibiotics administered will be excreted out of the body as urine, feces, and perspiration as the parent compound or metabolites (Sulfikar, Honda, Noguchi, Yamamoto-Ikemoto, & Watanabe, 2018). In surface waters, the concentration of antibiotics remains in the ng/L level, and antibiotics have also been detected in marine environments (Larsson, 2014).

When it comes to agriculture and animal husbandry, except for aquaculture (Larsson, 2014), the sludge from wastewater treatment plants and manure is applied on the fields as fertilizers, and hence the soil acts as a recipient of the antibiotic residue. Unused antibiotics, which are discarded in garbage, also end up in landfills and finally into the soil (Larsson, 2014). High microbial activity in the soil can translate to rapid degradation of antibiotics; however, some antibiotics are more resistant than others and can remain in the soil for years (Larsson, 2014).

Antibiotics are often classed as emerging contaminants or pollutants because they are not commonly monitored in the environment. However, what they lack in sheer volume, they can more than make up for by the detrimental effects they have on human health via emergence of new and untreatable diseases. This becomes even more relevant, when one considers the fact that wastewater treatment plants (WWTPs) aren't specifically designed or constructed to address this problem. Rather, they act as sinks for antibiotic pollutants and bacteria, thereby increasing the chances of antibiotic-resistant proliferation. The challenges for the remediation of antibiotic pollution in conventional wastewater treatment methods will be discussed in the following section.

This book belongs to Central Library BADJI Mokhtar-ANNABA UNIVERSITY
Copyright Elsevier 2024

5 Environmental consequences of antibiotic pollution

Antibiotics are a specific type of pharmaceutically active compounds (PhAC) (Watkinson, Murby, & Costanzo, 2007), which have emerged as a concerning and persistent environmental pollutant due to their undue use and the potential risks posed by them onto the organisms present in the environment (Ambrosetti, Campanella, & Palmisano, 2015). The first detriment of antibiotics in the environment can be thought in terms of ecosystem services offered by microflora and microfauna. Microbes are essential for nutrient cycles, for example, nitrogen cycle, and there is potential for antibiotics to disrupt such processes (Larsson, 2014). The phenomenon of stresses on microbial communities, either in soil or water due to antibiotic pollution, has not been studied satisfactorily as of now. Microbial communities show a remarkable level of resilience and adaptability via means of rapid mutation and horizontal gene transfer; however, it is this very same phenomenon that poses the most risk to human health and well-being. One good way of quantifying the amount of antibiotics in the environment is by using liquid chromatography coupled with a spectroscopic technique and its comparison with a standard of that antibiotic sample. Table 2 discusses the ecological impact of antibiotic wastes (Grenni, Ancona, & Caracciolo, 2018).

Table 2 briefly describes some of the consequences of antibiotic pollution on the soil microbial fauna and geological cycles. Soil is a vast reservoir for microorganisms, in which the rhizosphere (top 10-cm fertile layer of soil) may contain as much as 2 tons of microorganisms per acre (Nwosu, 2001). Soil microorganisms are vital in maintaining normal soil mineralization and decomposition profiles (Nwosu, 2001). It can be seen from Table 2 that the chemical fate, interaction with surrounding geology, and ecological effects of antibiotic pollutants are varied and are not completely understood. However, unabated discharge of antibiotics into the ecosystem can cause a change in community structures and in turn influence geochemical cycles.

6 Development of antibiotic-resistant genes (ARGs) and bacteria (ARB)

The main concern behind the environmental release of antibiotics is the development of ARGs and ARB (Ambrosetti et al., 2015), which poses a serious and direct risk to human health. As a result, the World Health Organization (WHO) has classified antibiotic pollution as one of the three most serious threats to public health in the 21st century (Rizzo et al., 2013). In fact resistosome, a new term, has been coined by eminent antibiotic biochemist, Dr. G.D. Wright, to denote antibiotic-resistant genes and their precursors. However, it must be noted that ARGs are an integral part of microbial evolutionary strategy. The primary ecological and evolutionary role of antibiotics produced by microbes is to limit the growth of competitors (Martinez, 2008). Therefore microbes parallelly evolved antibiotic resistance via ARGs to counter antibiotics produced by their competitors. It can be thus summed up that bacterial microhabitats act as a natural reservoir of ARGs, which act to modulate microbial community interactions (Martinez, 2008). Development of antibiotic resistance in microbes can be divided into intrinsic (developed by the bacterium itself) and acquired (by virtue of foreign genetic elements). Acquired resistance can itself be subdivided into transformation (uptake and incorporation of exogenous material), transduction (transfer of ARGs via bacteriophage infection), and conjugation (mutual exchange of exogenous material between microbes). Fig. 1 shows the evolutionary response by bacteria to directional pressure of antibiotics by ARG formation.

This book belongs to Central Library BADJI Mokhtar-ANNABA UNIVERSITY
Copyright Elsevier 2024

Table 2 Environmental consequences of antibiotic pollution.

Experimental concentrations	Indicator	Result	Environmental impact
Hou et al. (2014)			
Sulfonamide: (0.005–50 μM) in sediment slurry incubation	Denitrification gene quantification using real-time PCR	Decrease in denitrifying bacterial biomass in soil	Greater risk of eutrophication
Awad et al. (2016)			
Sulfonamide: (20–100 mg/L) in poultry manure applied to soil	Soil microbial quantification and qualification done via unique surface fatty acid analysis and C—N mineralization measure via titration	Initial decrease in microbial biomass, followed by gradual recovery due to drug degradation or adsorption	Soil carbon and nitrogen mineralization and bacteria: fungal ratio in microfauna altered
Hammesfahr, Bierl, and Thiele-Bruhn (2011)			
Sulfonamide: (0–100 mg/kg) in pig manure liquid applied to soil	Soil microbial biomass determined by fumigation-extraction method	Soil microbes increased with the addition of liquid manure but remained unchanged with addition of antibiotic	Due to biostatic nature of sulfonamide, inhibiting folic acid pathway, a supplementary nutrient source is needed to detect its effects
Laverman et al. (2015)			
Vancomycin: (1000 μg/L)—river sediments 10 m up and down wastewater treatment plant	Soil microbial species richness quantified by (16s rDNA) real-time PCR and denaturing gradient gel electrophoresis	Bacterial community structure showed a slight shift at drug concentration of 200 μg/L and highest changed at 1000 μg/L	Antibiotic dosing, even in small amounts, can alter the microbial community structure of river sediment
Demoling and Baath (2008)			
Tylocin (tetracyclines): (50–1500 mg/kg) in agricultural sandy loam soil	Bacterial biomass was estimated using the leucine incorporation technique	Pollution-induced community tolerance (PICT) study indicated initial increase post drug exposure, decrease after 25 days, and adjustment to near control level after 95 days of exposure	Post exposure sensitive species are eliminated, and therefore the gradient of exposure to antibiotics causes change in soil microbial community

6.1 Intrinsic

Intrinsic mechanisms of ARG formation can be summarized under three basic processes: preventing antibiotic access, modifying antibiotic target, and modifying the antibiotic itself (Blair, Webber, Baylay, Ogbolu, & Piddock, 2015). The first strategy involves the limiting of access of antibiotic agent to intracellular targets. This is achieved in two ways: Firstly, by reducing the membrane permeability

This book belongs to Central Library BADJI Mokhtar-ANNABA UNIVERSITY
Copyright Elsevier 2024

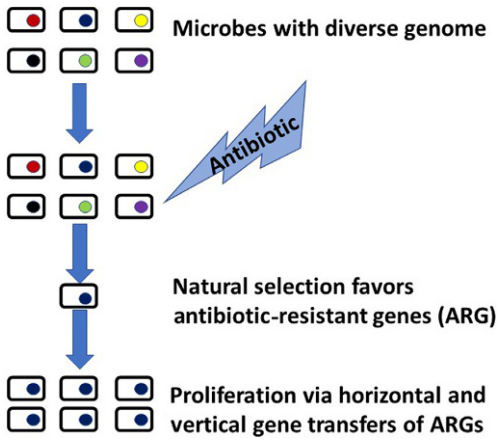

FIG. 1

Directional evolutionary effect of antibiotic pollution.

toward these antibiotics, mainly by downregulation of porins (transmembrane β-barrel proteins, which facilitate the diffusion of molecules inside the cell) or with their replacement with more selective channels (Blair et al., 2015). The second mechanism involves the overexpression of efflux pumps, which can be of either narrow specificity or multidrug resistance (MDR); this causes an efflux or "flushing out" of the antibiotics outside the microbe (Blair et al., 2015). The second strategy involves the alteration of the antibiotic targets themselves as antibiotics bind to their targets in a very specific manner with high affinity; any structural change in their targets would reduce their affinity and effectiveness. Microbes can respond to antibiotic exposure by the formation of mosaic genes, which are essentially alternating polymorphs of the microbial DNA or integrated foreign DNA and confer phenotypic variations to target proteins, reducing their binding affinity with antibiotics (Blair et al., 2015). The final method of antibiotic resistance is by directly modifying the antibiotic to reduce or negate the affinity of thousands of enzymes that have been identified, which is also accomplished by various methods such as hydrolysis or transfer of a chemical group on the antibiotic molecule (Blair et al., 2015). As a consequence of growing antibiotic resistance in microbes from a pharmacological view, either the dosage must be increased, or the number of antibiotics in a formulation (combination therapy) must be used, which presents its own set of environmental challenges.

6.2 Acquired

The second method of antibiotic resistance in microbes is via a process called natural transformation, which involves the interesting phenomenon of horizontal or lateral gene transfer. The importance of horizontal gene transfer can be imagined from the role it played in microbial primitive evolution, where, according to eminent microbiologist Carl R. Woese, the universal ancestor of life were communities of closely knit primordial cells evolving together (Nwosu, 2001). It can be thought of as a primitive precursor to sexual reproduction, whereby the microbes could rapidly incorporate genetic variations and avoid directional purging evolutionary pressures. However, to be susceptible to transformation, a microbe must be in a state of competence, which is characterized by uptake of DNA across

This book belongs to Central Library BADJI Mokhtar-ANNABA UNIVERSITY Copyright Elsevier 2024

the cell membrane and incorporation into the native genome using DNA repair enzymes. Competence may have triggered by conditions of starvation and increased cell density and therefore appears to be primarily a stress response (Johnston, Martin, Fichant, Polard, & Claverys, 2014). The mechanism of horizontal gene transfer can involve either uptake of naked DNA (transformation) or mobile genetic elements such as plasmids, transposons, integrons, gene cassettes, and bacteriophages (Sharma, Johnson, Cizmas, McDonald, & Kim, 2016).

7 Consequences on human health

The overall burden of disease due to antibiotic-resistant microbes are hard to assess due to complexity of data; however, it is estimated globally annually that 214,000 neonatal sepsis deaths can be attributed to antibiotic-resistant pathogens (Laxminarayan et al., 2013). A multicountry analysis estimated that prevalence of methicillin-resistant *Staphylococcus aureus* (MRSA) in Asian hospitals is up to 67.4%, whereas community-acquired MRSA averaged 25.5% (Laxminarayan et al., 2013). Multiresistant *Enterobacteriaceae* have become very common in India (Kumar et al., 2013). Reduced susceptibility to vancomycin was observed in about 12% of *Enterococcus faecalis* sample isolates (Kumar et al., 2013). Methicillin-resistant *Staphylococci* (MRS) constituted about 4.16% of *S. aureus* strains in a sample of children in an urban community of Nagpur (Maharashtra, India). There is also a high degree of correlation between veterinary antimicrobial use and antimicrobial resistance in food products (Chantziaras, Boyen, Callens, & Dewulf, 2014).

Many eukaryotic chromosomes contain DNA of bacterial origin incorporated via horizontal gene transfer, and there are 10 times more bacterial cells inside the human body than human cells (Robinson, Sieber, & Hotopp, 2013). Therefore genes acquired from such horizontal transfers may be mutagenic in nature and play a role in nongenetic-bacteria-associated diseases such as cancer and autoimmune disorders (Robinson et al., 2013). The role played by antibiotics and subsequent ARGs and ARB in this phenomenon is barely understood.

8 Challenges in conventional wastewater treatment methods in remediation of antibiotic pollutants

Antibiotics are classified under emerging pollutants, and thus vast majority of wastewater treatment plants are not specifically designed to remove them. The effectiveness of conventional water in preventing disseminating antibiotic resistance is questionable because of the amount of antibiotics, which is being found in both effluents and solid waste (Oncu & Balcioglu, 2013). It must be noted that inactivation of microbes doesn't necessarily mean inactivation of intracellular ARGs (Dodd, 2012). Treatment of ARB can be done in three steps: inactivating the antibiotic molecule in the wastewater solution, killing the ARB to prevent replication, and destroying the ARGs to prevent horizontal gene transfer. Nanomaterials can be used in several ways to mitigate the risks of ARB and associated diseases. They can be used as nucleic acid nanobiosensors for the detection of ARGs in the wastewater or even processed soil samples. Nanomaterials could also be used as a bactericide and/or DNA-destabilizing agent either in vivo or in vitro.

It can be seen via Table 3 that conventional methods of wastewater and potable water treatment are not adequate to address the antibiotic pollution problem. Most of them focus only on the adsorption of

This book belongs to Central Library BADJI Mokhtar-ANNABA UNIVERSITY Copyright Elsevier 2024

Table 3 Conventional methods of waste and potable water treatment and effectiveness in antibiotic pollution.

Physical separation **Li, Li, and Wang (2004)**		
Membrane	Mechanism of action	Size or electrostatic exclusion across a membrane
	Example	Oxytetracycline conc. Reduced from 1000 to 80 mg/L (92% removal)
	Remarks	Removal depends on multitude of interactions from size, steric hindrance, electrostatic, etc.
Choi, Kim, and Kim (2008)		
Powdered activated carbon (PAC)	Mechanism of action	Size or electrostatic exclusion across a membrane
	Example	Sulfonamide and tetracycline removed up to 99% (low conc. 1 mg/L) after 1 day of exposure
	Remarks	Method used to purify antibiotics
Le-Minh et al. (2010)		
Ion exchange	Mechanism of action	Size or electrostatic exclusion across a membrane
	Example	Effective for the removal of 14 antibiotics from the sulfonamide and tetracycline class
	Remarks	Effective way of removing negatively charged antibiotics
Chemical **Dodd (2012), Gou, Yuan, and Yang (2015), Le-Minh et al. (2010)**		
Chlorination	Mechanism of action	Cl_2 dissociates into HOCl and OCL^- in solution, the former being more active. HOCl reacts mostly with the surface membrane and DNA of the cell
	Example	• Dosage of up to 40 mg/L can increase frequency of transfers by a factor of 2–5 times due to increase of membrane permeability, while decrease in bacterial population is not significant • Dosage of over 80 mg/L greatly reduced the frequency of transfers and decreased the bacterial concentration from 10^7 CFU/mL to 10^4 CFU/mL
	Remarks	• Chlorination of water generated chloramine, which promoted membrane permeability in *E. coli* via pore formation, which may lead to ARG escaping into the environment • At higher conc. (upper limit of wastewater treatment plants), Cl_2 derivatives can bind to and deactivate DNA including ARGs • Reaction of chlorine with antibiotics may produce by-products, which are more harmful than the parent compounds
Dodd (2012), Sharma et al. (2016), Oncu and Balcioglu (2013)		
Ozonation	Mechanism of action	• Ozone is a very strong oxidant • Ozone is highly reactive toward cell wall constituents and hence not expected to penetrate well initially • Ozone in high conc. Penetrates the cell, binds with, and degrades DNA, much like chlorine

Continued

This book belongs to Central Library BADJI Mokhtar-ANNABA UNIVERSITY
Copyright Elsevier 2024

Table 3 Conventional methods of waste and potable water treatment and effectiveness in antibiotic pollution—cont'd

	Example Remarks	• Complete inhibition of plasmids at a dose of 4 mg/mL • Reaction with dsDNA is lower than expected, because of hydrogen bonding, which shields the base pairs • Increasing cell wall permeability may increase ARG release into the environment, much like chlorine • Dissolved solids decrease effectiveness
Radiation **Gou et al. (2015)**		
UV irradiation	Mechanism of action Example Remarks	UV radiation inactivates DNA via pyrimidine dimerization and had no significant impact on membrane permeability • Low doses up to 10 mJ/sq cm. caused marginal change in spread of ARGs but decreased bacterial load from 10^7 CFU/mL to 10^4 CFU/mL • High doses of over 10 mJ/sq cm. caused transfer of ARGs to be largely suppressed and kept bacterial load below 10^4 CFU/mL • Both reduce the bacterial concentration and ARG proliferative ability • Better option than chlorination because lower conc. Doesn't lead to increased ARG proliferation due to increased membrane permeability
Biological **Le-Minh et al. (2010), Gothwal and Sashidhar (2015)**		
Activated sludge	Mechanism of action Example Remarks	Antibiotics are adsorbed onto the growing biomass In activated sludge process, cephalexin, sulfamethoxazole, and sulfadiazine are the only antibiotics reported to have been removed predominantly from fresh and saline water sewage systems • Antibiotics removed from the aqueous phase can end up in primary or secondary sludge • Increasing the solid retention time and exposing the antibiotic pollutants to greater number and diversity of microbes have been said to increase its chances of removal via exposure to different enzymes • Activated sludge contains high density of microbes, which may increase competence and therefore uptake in ARGs • Sludge from WWTPs are often applied in agricultural fields as fertilizers

antibiotics onto solid medium or killing of harmful microbes but do not deal explicitly with the inactivation of the ARGs. Most of the time the ARGs and subsequent bacteria are only changing phases from wastewater medium to sludge, which is later applied onto soil as fertilizer. The microbes present in the activated sludge treatment process are contributing to the problem by acting as a reservoir for development of ARGs and ARB.

This book belongs to Central Library BADJI Mokhtar-ANNABA UNIVERSITY
Copyright Elsevier 2024

9 Nanomaterials in antibiotic pollution mitigation

As discussed previously, conventional wastewater treatment plants do not directly address the issue of antibiotic pollutants. They do not specifically remove antibiotics or ARGs in the wastewater; hence, new ways have to be searched for the remediation of antibiotic pollution. Nanomaterials have emerged as a possible solution by utilizing the unique properties of nanoparticles as being an intermediate between the molecular and bulk phases. Nanomaterials can be used in a multitude of ways to address this growing problem. They can be used in situ and ex situ to detect, adsorb, and degrade antibiotics or ARGs and ARB from wastewater.

9.1 Detection

Nanomaterials have found popular use as biosensors due to their ability to greatly increase the surface area. Nanobiosensors have two components: a nucleic acid receptor, which can be a genoprobe complimentary to a known stretch of antibiotic-resistant gene, or it may assume a secondary structure, in which case it would be called an aptamer and be specifically chosen to noncovalently conjugate with an antibiotic pollutant of interest. The nucleic acid receptor is attached with a nanoparticle transducer, which converts the physical conjugation into an electrical signal, which can be detected using techniques such as cyclic voltammetry (CV). Such genoprobing nucleic acid biosensors have been developed as a diagnostic to detect several pathogens such as *Leishmania donovani*, using a genoprobe conjugated onto nickel oxide nanoparticles, using indium tin oxide-coated glass as transducer (Mohan, Srivastava, Maheshwari, Sundar, & Prakash, 2011). There have been extensive research on ARGs, their isolation, and sequencing, and many of them have been catalogued and published. Several of these ARGs have been isolated from commensal bacteria in animal husbandry operations and exposed to antibiotics such as ampC, tetA, and ermA genes, sequences of which can be used in nanobiosensors as genoprobes to detect these genes in solution. Likewise, aptamers for commonly used antibiotics such as ampicillin and penicillin have also been isolated, which can be used on similar nanobiosensors to detect the same in wastewater. Fig. 2 demonstrates an assembly of a nanobiosensor, which can be used to detect ARGs and antibiotics in wastewater.

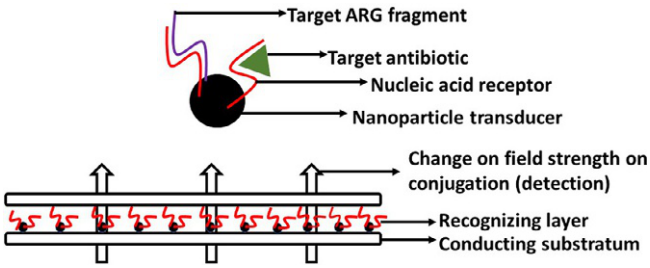

FIG. 2

Schematic representation of nanobiosensors capable of detecting either antibiotics or antibiotic-resistant genes (ARGs) in situ.

This book belongs to Central Library BADJI Mokhtar-ANNABA UNIVERSITY Copyright Elsevier 2024

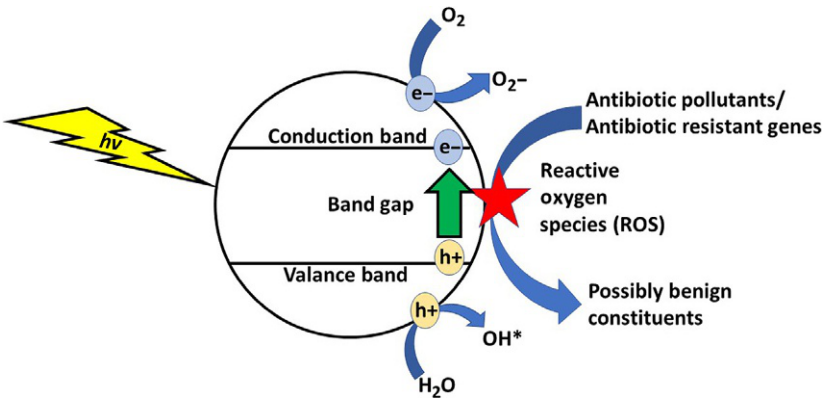

FIG. 3

Phenomenon of photocatalytic degradation used to degrade either antibiotic pollutants or antibiotic-resistant genes (ARGs) in situ.

9.2 Degradation

It would be of little concern, if these microbes were to remain confined in the wastewater only; however, they "leak" into the environment and can infect humans and animals. It is therefore important to neutralize them in their native antibiotic-rich habitat using physiochemical means, which destroy them physically. Engineered nanomaterials achieve this in many ways; from encouraging oxidative stress and release of reactive oxygen species (ROS), to genotoxicity, to oxidation of proteins, to release of metal ions intercellularly, or even through rupture of the cell membrane (Simeonidis, Mourdikoudis, Kaprara, Mitrakas, & Polavarapu, 2016; Hegde, Brar, Verma, & Surampalli, 2016; Mondal & Sharma, 2016). In a study, sulfur-doped titanium oxide nanoparticles have been used to neutralize gram-positive bacteria, *Micrococcus lylae*, where they rupture the cell membrane and cause death by uncontrolled influx of potassium ions (Mondal & Sharma 2016). As mentioned previously, killing microbes is only part of the solution, as antibiotic gene released into the environment can be still taken up by other microbes. Nanomaterials can also be used to neutralize these genes by photocatalytic degradation. Studies have been conducted using TiO nanoparticles and its ability to degrade plasmid DNA under UVA light irradiation (Ashikaga et al., 2000). Some nanoparticles such as TiO are especially useful because they don't induce mutations in mammalian or bacterial cells (Ashikaga et al., 2000). The exact method of DNA damage is via ROS formation as illustrated in Fig. 3, which is directly proportional to the irradiation time. Using TiO nanocatalyst in concentration 0.5 μg/μL, plasmid DNA at 0.13 μg/μL, and using a 2.0 W/m^2 UV source, it can be seen that DNA damage starts as early as 5 s, and at 2 min of exposure, 37% of the DNA had already been damaged (Yang & Wang, 2008).

10 Conclusions

Antibiotics are a class of bactericidal and bacteriostatic agents that have evolved within microbiota for millions of years as a means of evolutionary survival and have recently been isolated, modified, and used by humans to greatly improve their survival and quality of life. However, maleficent and

This book belongs to Central Library BADJI Mokhtar-ANNABA UNIVERSITY Copyright Elsevier 2024

excessive use of these revolutionary drugs has forced their increase in microhabitats, putting the same microbiota under evolutionary pressure, increasing proliferation of antibiotic resistance. This increase in antibiotic resistance is potentially very harmful to human health and well-being, as it can lead to pathologies, which become untreatable by available antibiotics. Contemporary conventional wastewater treatment technologies and infrastructure seem to add to this problem by acting as sinks for antibiotic pollutants, bacteria, and other microfauna, thereby increasing the chance for antibiotic resistance proliferation. Engineered nanomaterials have emerged as a novel solution, as they address multiple fronts of the detection of such antibiotics, antibiotic-resistant genes, and their photocatalytic degradation at the same time. A large number of options may even be explored for the possible remediation of antibiotic pollution using novel nanomaterials.

Acknowledgments

Authors are thankful to DU-DST purse grant from Department of Science and Technology (Gov. of India) to University of Delhi. Also, Niloy Sarkar is thankful to UGC for providing JRF scholarship, certificate no. F.16-6(DEC. 2016)/2017(NET).

References

Ambrosetti, B., Campanella, L., & Palmisano, R. (2015). Degradation of antibiotics in aqueous solution by photocatalytic process: Comparing the efficiency in the use of ZnO or TiO2. *Journal of Environmental Science and Engineering A*, *4*, 273–281.

Ashikaga, T., Wada, M., Kobayashi, H., Mori, M., Katsumura, Y., Fukui, H., et al. (2000). Effects of the photocatalytic activity of TiO_2 on plasmid DNA. *Mutation Research*, *466*(1), 1–7.

Awad, Y. M., Ok, Y. S., Igalavithana, A. D., Lee, Y. H., Sonn, Y. K., Usman, A. R. A., et al. (2016). Sulphamethazine in poultry manure changes carbon and nitrogen mineralization in soils. *Chemistry and Ecology*, *32*(10), 899–918.

Blair, J. M. A., Webber, M. A., Baylay, A. J., Ogbolu, D. O., & Piddock, L. J. V. (2015). Molecular mechanisms of antibiotic resistance. *Nature Reviews Microbiology*, *13*(1), 42–51.

Chantziaras, I., Boyen, F., Callens, B., & Dewulf, J. (2014). Correlation between veterinary antimicrobial use and antimicrobial resistance in food-producing animals: A report on seven countries. *Journal of Antimicrobial Chemotherapy*, *69*, 287–834.

Choi, K. J., Kim, S. G., & Kim, S. H. (2008). Removal of tetracycline and sulfonamide classes of antibiotic compound by powdered activated carbon. *Environmental Technology*, *29*, 333–342.

Demoling, L. A., & Baath, E. (2008). No long-term persistence of bacterial pollution-induced community tolerance intylosin-polluted soil. *Environmental Science and Technology*, *42*, 6917–6921.

Dodd, M. C. (2012). Potential impacts of disinfection processes on elimination and deactivation of antibiotic resistance genes during water and wastewater treatment. *Journal of Environmental Monitoring*, *14*(7), 1754–1771.

Farre, M. L., Perez, S., Kantiani, L., & Barcelo, D. (2008). Fate and toxicity of emerging pollutants, their metabolites and transformations products in the aquatic environment. *Trends in Analytical Chemistry*, *27*(11), 991–1007.

Ghosh, K., & Mandal, S. (2010). Antibiotic resistant bacteria in consumable fishes from Digha coast, West Bengal, India. *Proceedings of the Zoological Society*, *63*(1), 13–20.

This book belongs to Central Library BADJI Mokhtar-ANNABA UNIVERSITY

Copyright Elsevier 2024

Gothwal, R., & Sashidhar, T. (2015). Antibiotic pollution in the environment: A review. *Clean—Soil, Air, Water*, *43*(4), 479–489.

Gou, M. T., Yuan, Q. B., & Yang, J. (2015). Distinguishing effects of ultraviolet exposure and chlorination on the horizontal transfer of antibiotic resistant genes in municipal wastewater. *Environmental Science and Technology*, *49*(9), 5771–5778.

Grenni, P., Ancona, V., & Caracciolo, A. B. (2018). Ecological effects of antibiotics on natural ecosystems: A review. *Microchemical Journal*, *136*, 25–39.

Hammesfahr, U., Bierl, R., & Thiele-Bruhn, S. (2011). Combined effects of the antibiotic sulfadiazine and liquid manure on the soil microbial-community structure and functions. *Journal of Plant Nutrition and Soil Science*, *174*(4), 614–623.

Hegde, K., Brar, S. K., Verma, M., & Surampalli, R. Y. (2016). Current understandings of toxicity, risks and regulations of engineered nanoparticles with respect to environmental microorganisms. *Nanotechnology for Environmental Engineering*, *1*(5), 1–12.

Hou, L., Yin, G., Liu, M., Zhou, J., Zheng, Y., Gao, J., et al. (2014). Effects of sulfamethazine on denitrification and the associated N2O release in estuarine and coastal sediments. *Environmental Science and Technology*, *49*(1), 326–333.

Johnston, C., Martin, B., Fichant, G., Polard, P., & Claverys, J. P. (2014). Bacterial transformation, distribution, shared mechanisms, and divergent control. *Nature Reviews Microbiology*, *12*(2), 181–196.

Kapoor, G., Saigal, S., & Elongavan, A. (2017). Action and resistance mechanisms of antibiotics: A guide for clinicians. *Journal of Anesthesiology Clinical Pharmacology*, *33*, 300–305.

Kumar, S. G., Adithan, C., Harish, B. N., Sujatha, S., Roy, G., & Malini, A. (2013). Antimicrobial resistance in India: A review. *Journal of Natural Science, Biology and Medicine*, *4*(2), 286–291.

Larsson, D. G. J. (2014). Antibiotics in the environment. *Upsala Journal of Medical Sciences*, *119*, 108–112.

Laverman, A. M., Cazier, T., Yan, C., Roose-Amsaleg, C., Petit, F., Garnier, J., et al. (2015). Exposure to vancomycin causes a shift in the microbial community structure without affecting nitrate reduction rates in river sediments. *Microbial Ecology of the Continental and Coastal Environments*, *22*(18), 13,702–13,709.

Laxminarayan, R., & Chaudhury, R. R. (2016). Antibiotic resistance in India: Drivers and opportunities for action. *PLoS Medicine*, *13*(2), 1–7.

Laxminarayan, R., Matsoso, P., Pant, S., Brower, C., Røttingen, J. A., Klugman, K., et al. (2013). Access to effective antimicrobials: A worldwide challenge. *Lancet*, *387*(10014), 168–175.

Le-Minh, N., Khan, S. J., Drewes, J. E., & Stuetz, R. M. (2010). Fate of antibiotics during municipal water recycling treatment processes. *Water Research*, *44*, 4295–4323.

Li, S., Li, X., & Wang, D. (2004). Membrane (RO-UF) filtration for antibiotic wastewater treatment and recovery of antibiotics. *Seperation and Purification Technology*, *34*, 109–114.

Martinez, J. L. (2008). Antibiotics and antibiotic resistant genes in natural environments. *Science*, *321*(5887), 365–367.

Mohan, S., Srivastava, P., Maheshwari, S. N., Sundar, S., & Prakash, R. (2011). Nanostructured nickel oxide based DNA biosensor for detection of visceral leishmaniasis (Kala-Azar). *The Analyst*, *136*(13), 2845–2851.

Mondal, K., & Sharma, A. (2016). Recent advances in the synthesis and application of photocatalytic metal–metal oxide core–shell nanoparticles for environmental remediation and their recycling processes. *RSC Advances*, *6*(87), 83589–83612.

Nwosu, V. C. (2001). Antibiotic resistance with particular reference to soil microorganisms. *Research in Microbiology*, *152*(5), 421–430.

Oncu, N. B., & Balcioglu, I. A. (2013). Antimicrobial contamination removal from environmentally relevant matrices: A literature review and a comparison of three process for drinking water treatment. *Ozone: Science & Engineering*, *35*, 73–85.

This book belongs to Central Library BADJI Mokhtar-ANNABA UNIVERSITY

Copyright Elsevier 2024

Rizzo, L., Manaia, C., Merlin, C., Schwartz, T., Dagot, C., Ploy, M. C., et al. (2013). Urban wastewater treatment plants as hotspots for antibiotic resistant bacteria and genes spread into the environment: A review. *Science of the Total Environment*, *447*, 345–360.

Robinson, K. M., Sieber, K. B., & Hotopp, J. C. D. (2013). A review of bacteria-animal lateral gene transfer may inform our understanding of diseases like cancer. *PLoS Genetics*, *9*(10) e1003877.

Sharma, V. K., Johnson, N., Cizmas, L., McDonald, T. J., & Kim, H. (2016). A review of the influence of treatment strategies on antibiotic resistant bacteria and antibiotic resistant genes. *Chemosphere*, *150*, 702–714.

Simeonidis, K., Mourdikoudis, S., Kaprara, E., Mitrakas, M., & Polavarapu, L. (2016). Inorganic engineered nanoparticles in drinking water treatment: A critical review. *Environmental Science: Water Research & Technology*, *2*, 43–70.

Sulfikar., Honda, R., Noguchi, M., Yamamoto-Ikemoto, R., & Watanabe, T. (2018). Effect of sedimentation and aeration on antibiotic resistance induction in the activated sludge process. *Journal of Water and Environment Technology*, *16*(2), 94–105.

Watkinson, A. J., Murby, E. J., & Costanzo, S. D. (2007). Removal of antibiotics in conventional and advanced wastewater: Implications for environmental discharge and wastewater recycling. *Water Research*, *41*, 4164–4176.

Yang, X., & Wang, Y. (2008). Photocatalytic effect on plasmid DNA damage under different UV irradiation time. *Building and Environment*, *43*, 253–257.

This book belongs to Central Library BADJI Mokhtar-ANNABA UNIVERSITY

Copyright Elsevier 2024

This page intentionally left blank

This book belongs to Central Library BADJI Mokhtar-ANNABA UNIVERSITY

Copyright Elsevier 2024

CHAPTER

Photochemical and photocatalytical degradation of antibiotics in water promoted by solar irradiation

12

Ricardo A. Torres-Palma[a], Efraím A. Serna-Galvis[a], Yenny P. Ávila-Torres[b]

Grupo de Investigación en Remediación Ambiental y Biocatálisis (GIRAB), Instituto de Química, Facultad de Ciencias Exactas y Naturales, Universidad de Antioquia UdeA, Medellin, Colombia[a] Grupo de Investigación Química y Biotecnología (QUIBIO), Facultad de Ciencias Básicas, Universidad Santiago de Cali, Santiago de Cali, Colombia[b]

1 Introduction

1.1 Environmental concern of antibiotics

Pharmaceuticals have been created to stimulate a physiological response of organisms for preventing and treating human and animal diseases (Kümmerer, 2003). They are categorized according to their action: analgesics, antibiotics, antipyretic, antihypertensives, antidiabetics, corticosteroids, diagnostic agents, diuretics, estrogens, immunosuppressants, psychiatrics, sweeteners, etc. Many researches have evidenced that after passing through municipal wastewater treatment plants, the most of pharmaceuticals are not completely degraded. Subsequently, these substances are released into the environment (Gothwal & Shashidhar, 2015).

The environmental concerns of pharmaceutical have been extensively reported, and a serious current problem is the selection and development of antibiotic resistant bacteria, which is derived from the overuse of antibiotics (Homem & Santos, 2011; Martinez, 2009; Michael et al., 2013; Rizzo et al., 2013; Rodriguez-Mozaz et al., 2015). Nowadays, antibiotics are ubiquitous in waters from hospital, domestic, livestock, veterinary, and pharmaceutical industry activities (Botero-Coy et al., 2018; Rizzo et al., 2013). Also, in natural media, antibiotics show low degradation rates by hydrolysis and biological action.

Due to the continuous input, persistence and negative impact in the aquatic ecosystems, antibiotics are considered contaminants of emerging concern (CEC) (Homem & Santos, 2011), which require the application of efficient processes to limit the input of the variety type of antibiotics into the environment.

1.2 Antibiotics classification and their presence in waters

Antibiotics are defined as chemical compounds able to eradicate or inhibit the growth of microorganisms (mainly bacteria). Most of antibiotics have a microbial origin, but they are also hemi-synthetic or entirely synthetic. Antibiotics can be divided into several classes: aminoglycosides, anthracyclines,

Nano-Materials as Photocatalysts for Degradation of Environmental Pollutants. https://doi.org/10.1016/B978-0-12-818598-8.00012-2
© 2020 Elsevier Inc. All rights reserved.

This book belongs to Central Library BADJI Mokhtar-ANNABA UNIVERSITY

Copyright Elsevier 2024

β-lactams, phenicols, glycopeptides, imidazoles, lincosamides, lipopeptides, macrolides, (fluoro)quinolones, sulfonamides, and tetracyclines (Homem & Santos, 2011).

Antibiotic consumption worldwide is very high (Klein et al., 2018). It is reported that most prescribed/utilized antibiotics are β-lactams (which comprise penicillins, cephalosporins, carbapenems, clavulanates, and monobactams), (fluoro)quinolones, lincosamides, macrolides, sulfonamides, and tetracyclines (Fig. 1) (Euro-CDC, 2017; Homem & Santos, 2011; WHO, 2018). As a consequence of the elevated consumption and inability of conventional treatments to eliminate them, antibiotics belonging to such classes are frequently found in diverse wastewaters and aqueous media (Botero-Coy et al., 2018; Gothwal & Shashidhar, 2015; Hernández et al., 2015, 2019; Oliveira, Al Aukidy, & Verlicchi, 2018; Rodriguez-Mozaz et al., 2015; Verlicchi, Al Aukidy, & Zambello, 2012). Hence, to face the water pollution problem associated to antibiotics, light-based processes can be used. Considering that one of the most common possibilities to activate photocatalysts for the treatment of antibiotics involves solar light and such irradiation has itself a degrading action, this chapter initially deals with photochemical degradations by using the sole sunlight action. Afterwards, TiO_2-photocatalysis and photocatalytic process based on nano-sized materials for antibiotics degradation are presented and discussed.

2 Photochemical degradation of antibiotics by solar light

2.1 Sunlight action on antibiotics

The sunlight that reaches the earth surface has visible (400–700 nm), UVA (320–400 nm), and a portion of UVB (290–320 nm) component. This radiation is able to promote direct and/or indirect (mediated) transformations of organic pollutants such as antibiotics. Direct route (direct photolysis) is initiated by absorption of sunlight radiation, whereas indirect photolysis (also named sensitization) occurs throughout interaction of antibiotics with transient reactive intermediates such as singlet oxygen, hydroxyl radicals, or other reactive species formed from other substances present in the water matrix (Periša, Babić, Irena, Frömel, & Knepper, 2013).

Direct photodegradation firstly requires sunlight absorption. For example, ciprofloxacin, cephalexin, and sulfamethoxazole antibiotics are able to absorb some of sunlight components (which is evidenced from its UV-vis absorption spectrum, Fig. 2); then, their photo-transformations by solar irradiation are plausible. However, it must be mentioned that photodegradation also depends on light intensity as well as on the ability of photons to effectively promote antibiotic modifications (this last factor is determined by the molecular/electronic structure of the substance and it is reflected by the quantum yield "Φ," Eq. 1) (Albini & Monti, 2003; Boreen, Arnold, & McNeill, 2003; Yan & Song, 2014).

$$\Phi = \text{moles of antibiotic transformed/mol of photons absorbed} \quad (1)$$

In the direct route, after an effective light absorption by an antibiotic (A), a singlet excited electronic state can be generated (Eq. 2), which may experiment an intersystem crossing toward a triplet state (Eq. 3). The triplet state can led to photoproducts (Eq. 4) or interact with dissolved oxygen to form reactive oxygen species (ROS) such as singlet oxygen (Eq. 5) or superoxide anion (Eq. 6) (Derosa & Crutchley, 2002). Because ROS are oxidizing agents, they can degrade antibiotics (Eq. 7).

This book belongs to Central Library BADJI Mokhtar-ANNABA UNIVERSITY Copyright Elsevier 2024

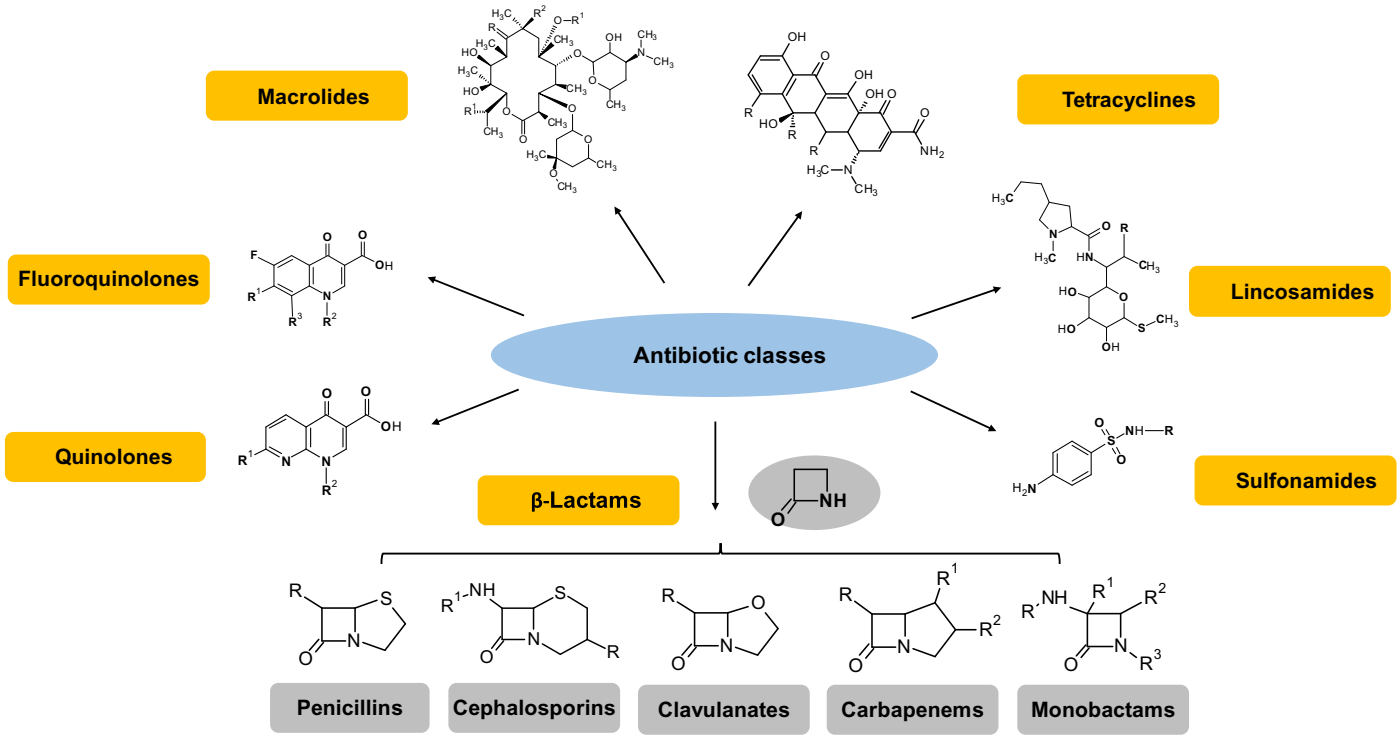

FIG. 1

Base chemical structure of highly consumed antibiotics classes.

This book belongs to Central Library BADJI Mokhtar-ANNABA UNIVERSITY

Copyright Elsevier 2024

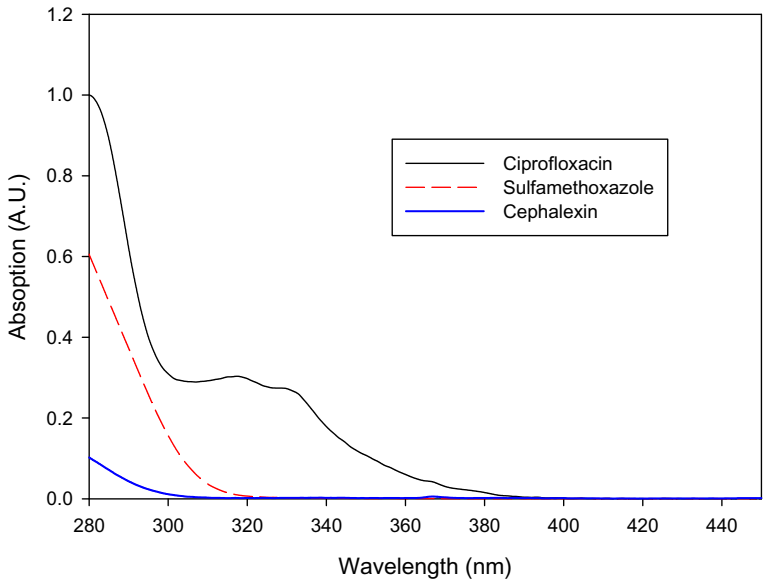

FIG. 2

UV-vis spectra for ciprofloxacin, sulfamethoxazole, and cephalexin.

Eqs. (2), (3), (5)–(7) represent the commonly called the self-sensitization route (Challis, Hanson, Friesen, & Wong, 2014).

$$^{1}A + h\nu \rightarrow {}^{1}A^{*} \tag{2}$$

$$^{1}A^{*} \rightarrow {}^{3}A^{*} \tag{3}$$

$$^{3}A^{*} \rightarrow \text{products} \tag{4}$$

$$^{3}A^{*} + {}^{3}O_2 \rightarrow {}^{1}A + {}^{1}O_2 \tag{5}$$

$$^{3}A^{*} + {}^{3}O_2 \rightarrow A^{+}\bullet + O_2\bullet^{-} \tag{6}$$

$$A + \text{ROS} \rightarrow \text{products} \tag{7}$$

The mediated degradation route is very common in sunlit natural waters, where dissolved organic matter (DOM) and nitrate anions (NO_3^-) are present. Irradiated DOM can promote both antibiotics transformation and formation of ROS (Eq. 8–12). Additionally, the interaction of UVB component with NO_3^- produces hydroxyl radicals (HO•, Eq. 13) (Serna-Galvis et al., 2018; Wang & Yu-Chen Lin, 2012).

$$^{1}\text{DOM} + h\nu \rightarrow {}^{1}\text{DOM}^{*} \tag{8}$$

$$^{1}\text{DOM}^{*} \rightarrow {}^{3}\text{DOM}^{*} \tag{9}$$

This book belongs to Central Library BADJI Mokhtar-ANNABA UNIVERSITY

Copyright Elsevier 2024

$$^{3}DOM^{*} + A \rightarrow \text{products} \tag{10}$$

$$^{3}DOM^{*} + {}^{3}O_2 \rightarrow {}^{1}DOM + {}^{1}O_2 \tag{11}$$

$$^{3}DOM^{*} + {}^{3}O_2 \rightarrow DOM^{+}\bullet + O_2\bullet^{-} \tag{12}$$

$$NO_3^{-} + H_2O + hv\,(UVB) \rightarrow \bullet NO_2 + HO\bullet + HO^{-} \tag{13}$$

Photodegradation process can take place in illuminated surface water, but it may not occur when the compounds are in turbid water, if rivers or lakes are shadowed by trees, or if the compounds are in sewage and sewage pipes because they have low light exposure (Periša et al., 2013). Antibiotics from different classes (i.e., β-lactams, fluoroquinolones, sulfonamides, macrolides, tetracyclines, lincosamides, and phenicols) have been submitted to actual or simulated sunlight in pure and natural waters (Table 1). The antibiotics photodegradation by sunlight fits well to a pseudo-first-order kinetics (i.e., during treatment, degradation rate of pollutant is proportional to its concentration). Also, it can be indicated that in pure water, antibiotic molecules undergo fragmentations, substitutions, isomerizations, and oxidations (Fig. 3).

In natural waters, besides to these photo-transformations, other degradation pathways (e.g., chlorination) are possible (Li et al., 2016; Porras et al., 2016). Although matrix composition depends on location, a common factor in natural waters is the presence of DOM (e.g., humic and fulvic acids), nitrate, carbonate/bicarbonate, and halide ions, in some cases ferric ions are also available in aqueous media; thus, many photochemical responses are determined by these substances. ROS such as hydroxyl radical are also produced from photoreduction of ferric ion (Eq. 14). HO• is able to react with carbonate/bicarbonate (CO_3^{2-}/HCO_3^{-}) leading to carbonate radicals (Eqs. 15 and 16), while $^{3}A^{*}$ (triplet excited state of antibiotics), HO•, and $^{3}DOM^{*}$ can react with halide ions (X^{-}: F^{-}, Cl^{-}, and Br^{-}) to form halide radicals (Eqs. 17–19). Both, carbonate and halide radicals, are able to degrade antibiotics (Li et al., 2016; Mcneill & Canonica, 2016).

$$Fe^{3+} + H_2O + hv \rightarrow Fe^{2+} + HO\bullet + H^{+} \tag{14}$$

$$HO\bullet + CO_3^{2-} \rightarrow HO^{-} + CO_3\bullet^{-} \tag{15}$$

$$HO\bullet + HCO_3^{-} \rightarrow HO^{-} + H^{+} + CO_3\bullet^{-} \tag{16}$$

$$HO\bullet + 2X^{-} \rightarrow HO^{-} + X_2\bullet^{-} \tag{17}$$

$$^{3}DOM^{*} + 2X^{-} \rightarrow A^{+} + X_2\bullet^{-} \tag{18}$$

$$^{3}A^{*} + 2X^{-} \rightarrow A^{+} + X_2\bullet^{-} \tag{19}$$

In contrast to photolysis in pure water, in natural water, the components of the matrix can undergo competitive phenomena such as absorption and scattering of light. For example, some penicillins (see amoxicillin in Fig. 4) showed lower degradation rates in surface waters compared to photolysis in pure water because of turbidity and absorbance of UV-light by organic matter in the natural matrix (Timm et al., 2019). Interestingly, for many antibiotics, the competitive phenomena are superpassed by photosensitization (mediated route). Fig. 4 presents the matrix effect (accelerating or inhibiting) for some antibiotics. This effect can be denoted by *Rk* (the ratio between rate constants in natural water

This book belongs to Central Library BADJI Mokhtar-ANNABA UNIVERSITY Copyright Elsevier 2024

Table 1 Degradation of diverse antibiotics by sunlight

Antibiotics	Conditions of photodegradation	Remarkable aspects
Amoxicillin, ampicillin, penicillin V and piperacillin (penicillins, ***β-lactams***) ***Reference:*** Timm et al. (2019)	***Light:*** simulated sunlight (300–1400 nm, 1000 W m^{-2} provided by a Xe lamp) ***Antibiotics concentration:*** a mixture of antibiotics at the concentration of 1 μg L^{-1} each one was treated. ***Water matrices:*** pure water and two surface river water.	***Kinetics:*** all antibiotics followed a pseudo-first-order kinetics. Amoxicillin and ampicillin were degraded faster than penicillin V and piperacillin. ***Transformations:*** the four antibiotics showed hydrolytic opening of the β-lactam ring; ampicillin, penicillin V and piperacillin experimented decarboxylation; penicillin V also exhibited epimerization, whereas piperacillin showed a cleavage of the molecule at the piperazinedione ring. ***Treatment extent:*** 5%–7% of mineralization coming from decarboxylation. ***Matrix effects:*** Degradation in river waters was associated to adsorption, microbial degradation and photosensitization via excited organic matter. Turbidity and absorbance of UV-light by organic matter were related to the lower degradation rates compared to the photolysis in ultrapure water.
Cephalexin (CFX), cephradine (CFD), cefotaxime (CTX), cefazolin (CFZ), and cephapirin (CFP) (cephalosporins, ***β-lactams***) ***Reference:*** Wang & Yu-Chen Lin (2012)	***Light:*** simulated sunlight (>300 nm, provided by a Xe lamp). ***Antibiotics concentration:*** Individual standards of cephalosporins in deionized water (20 μg L^{-1}) were individually treated. ***Water matrices:*** pure water river water (natural surface water) and simulated natural water.	***Kinetics:*** all antibiotics followed a pseudo-first-order kinetics; Φ values were ranged from 0.001 to 0.091. Cefazolin and cephapirin had faster degradation than cephalexin, cephradine, and cefotaxime. ***Transformations:*** sunlight led to decarboxylation of cephradine, cephalexin, and cephapirin; fragmentations of all antibiotics were also promoted. ***Treatment extent:*** no significant mineralization after 42 h of irradiation was observed. Parent cephalosporins have no acute toxicity against *Vibrio fischeri*. However, in irradiated samples, the by-products exhibit significantly increasing of toxicity.

This book belongs to Central Library BADJI Mokhtar-ANNABA UNIVERSITY

Copyright Elsevier 2024

		***Matrix effects*:** degradation of cephalexin, cephradine, and cefotaxime (antibiotics with low photodegradation in deionized water) was strongly accelerated in simulated and real surface natural water. In contrast, elimination of cefazolin and cephapirin in such matrices were inhibited.
Ciprofloxacin, danofloxacin, levofloxacin, sarafloxacin, difloxacin, enrofloxacin, gatifloxacin, and balofloxacin (***fluoroquinolones***) ***References:*** Ge et al. (2015, 2010)	***Light:*** simulated sunlight (290–420 nm, 0.83 mW cm^{-2} at the reaction solutions, light provided by a Xe lamp). ***Antibiotics concentration:*** 5–100 μmol L^{-1} and 1–30 μmol L^{-1} ***Water matrices:*** pure water, seawater and freshwater.	***Kinetics:*** the fluoroquinolones photodegradation followed a pseudo-first-order kinetics. Φ values were ranged from 0.005 to 0.069. Enrofloxacin, danofloxacin, and ciprofloxacin presented the fastest photodegradation. ***Transformations*:** defluorination, decarboxylation, and piperazyl-dealkylation were the main photodegradation pathways. In some cases (e.g., ciprofloxacin) oxidation and fragmentation of the piperazine ring were also found. ***Treatment extent*:** during the photodegradation, toxicities (against *Vibrio fischeri*) first decreased; then, increased, and finally decreased, implying the generation of some more toxic intermediates than the parent compound. Additionally, the antibacterial activity of levofloxacin, danofloxacin enrofloxacin, and difloxacin did not decrease significantly in the initial photodegradation period, indicating the notable antimicrobial activity of their primary degradation intermediates. Meanwhile, treatment of ciprofloxacin and sarafloxacin led to a decreasing of antimicrobial activity (against *Escherichia coli*). ***Matrix effects:*** the photodegradation in natural waters was slower than in pure water in most cases. Experimental results indicated that the inhibiting effects caused by competitive absorption or ROS scavenging were stronger than the sensitization effects.

Continued

This book belongs to Central Library BADJI Mokhtar-ANNABA UNIVERSITY

Copyright Elsevier 2024

Table 1 Degradation of diverse antibiotics by sunlight—cont'd

Antibiotics	Conditions of photodegradation	Remarkable aspects
Ciprofloxacin (CIP), danofloxacin (DAN), levofloxacin (LEV) and moxifloxacin (MOX) (***fluoroquinolones***) ***Reference:*** Sturini et al. (2012)	***Light:*** real sunlight (outdoor Irradiation 10:00 am–4:00 pm in July). The sunlight power was ranged from 290 to 470 $W\,m^{-2}$ (in visible range) and from 20 to 30 $W\,m^{-2}$ (in UV range). ***Antibiotics concentration:*** 20–50 $\mu g\,L^{-1}$. ***Water matrix:*** river water.	***Kinetics:*** the decomposition followed a first-order kinetics for all fluoroquinolones. Ciprofloxacin and danofloxacin were decomposed faster than levofloxacin and moxifloxacin. ***Transformations*:** Three general pathways occurred depending on the structure of the considered fluoroquinolones, viz. (i) degradation of the electron rich amine side-chain leading to oxidized products, (ii) photosubstitution of the fluorine on carbon 6 by a hydroxyl group, or (iii) by a hydrogen. Photosubstitution (ii) prevails for ciprofloxacin and danofloxacin. ***Treatment extent*:** antimicrobial activity decreased upon irradiation, due to the photodegradation of the parent compound. However, the active nucleus required for the biological effect is not affected during the first steps of the photolytic process and a number of byproducts active against both gram-negative and gram-positive bacteria are formed.
Roxithromycin, erythromycin (***macrolides***) ***Reference:*** Batchu, Panditi, O'Shea, et al. (2014)	***Light:*** Simulated sunlight (300–800 nm, 750 $W\,m^{-2}$ provided by a Xe lamp). ***Antibiotics concentration:*** waters were spiked with antibiotics at 100 $\mu g\,L^{-1}$. ***Water matrices:*** pure water, canal fresh water (rich in DOC) and salt water (high ionic strength).	***Kinetics:*** antibiotics degradation fitted well to a pseudo-first-order kinetics. Φ value at 350 nm (UV irradiation of 350 nm is comparable to the range of UVA region of sunlight and typically used to predict the UV initiated photodegradation of pharmaceuticals in environment) was 0.0002 for both macrolides. ***Transformations*:** hydrolysis of imine nitrogen on C-9 substituent of roxithromycin, which results in the formation of erythromycin. Other observed pathway was the loss/rupture of cladinose sugar from erythromycin. ***Treatment extent*:** primary products from the photodegradation of macrolides retain lactone

This book belongs to Central Library BADJI Mokhtar-ANNABA UNIVERSITY

Copyright Elsevier 2024

		ring and desosamine sugar functionalities critical to biological activity. ***Matrix effects:*** photodegradation of roxithromycin in natural waters revealed significant enhancement in the rates in natural waters relative to pure water. On contrary, erythromycin degradation in natural waters was slower than in pure water.
Tetracycline (***tetracycline***) ***Reference:*** Chen, Hu, Qu, & Yang (2008)	***Light:*** Simulated sunlight (>300 nm, 150 W provided by a Xe lamp). ***Antibiotic concentrations:*** 10 and 200 μmol L^{-1} ***Water matrices:*** pure water, water containing HCO_3-, NO_3-, Fe^{3+} or humic acid.	***Kinetics:*** the tetracycline antibiotic degradation followed a pseudo-first-order kinetics. Φ value increased as pH was higher. ***Degradation routes:*** direct and mediated (self-sensitization, by ROS: singlet oxygen and radical species). ***Matrix effects***: degradation of tetracycline in presence of HCO_3-, NO_3-, Fe^{3+} or humic acid was examined. The photolysis was unaffected in the natural pH by the presence of nitrate, bicarbonate, and humic acid. The ferric ions enhanced photodegradation over the pH range of 6.0–8.0, but an inhibition was observed at pH 9.0
Tetracycline (***tetracycline***) ***Reference:*** Niu, Li, & Wang (2013)	***Light:*** solar light in Peking (116°17′N, 39°56′E, March, 11:00 am–1:00 pm, 2012). ***Antibiotic concentrations:*** 10–40 mg L^{-1}. ***Water matrices:*** pure water, water containing nitrate or humic acid.	***Kinetics:*** photodegradation of the antibiotic in pure water followed pseudo-first-order kinetics. ***Degradation routes:*** direct and mediated by ROS. ***Transformations***: hydroxylation and loss of some groups (such as *N*-methyl, hydroxyl, and amino groups) from the ring of tetracycline. It was noted that its aromatic ring was not opened and the naphthol ring remained intact during process. ***Treatment extent***: toxicity against *P. phosphoreum* was evaluated, indicating that more toxic intermediates than parent tetracycline were generated. ***Matrix effects***: photodegradation was enhanced by humic acid when its concentration was

Continued

This book belongs to Central Library BADJI Mokhtar-ANNABA UNIVERSITY

Copyright Elsevier 2024

Table 1 Degradation of diverse antibiotics by sunlight—cont'd

Antibiotics	Conditions of photodegradation	Remarkable aspects
		$<6.0\,mg\,L^{-1}$. Also, degradation rate was elevated markedly by nitrate ions (rate proportionally increased with nitrate concentration from 5.0 to $20.0\,mg\,L^{-1}$ but decreased from 20.0 to $50.0\,mg\,L^{-1}$.
Thiamphenicol and florfenicol (***phenicols***) ***Reference:*** Ge, Chen, Qiao, Lin, & Cai (2009)	***Light:*** actual sunlight ($\lambda > 290\,nm$, $7.37\,mW\,cm^{-2}$, 38°53′N, 121°31′E, July 2007) and simulated sunlight ($\lambda > 290\,nm$, $0.83\,mW\,cm^{-2}$ provided Xe lamp) ***Antibiotics concentration:*** $10–400\,mg\,L^{-1}$. ***Water matrices:*** pure water, freshwater and seawater.	***Kinetics:*** these antibiotics in pure water were no photolyzed under actual or simulated sunlight irradiation ($\lambda > 290\,nm$), since they do not absorb light at $\lambda > 290\,nm$. ***Transformations***: dissolved organic matter (e.g., humic acids) in the freshwater produced singlet oxygen, which promoted dechlorination-oxidation of both phenicols. ***Matrix effects***: photodegradation of both phenicols in freshwater was efficiently promoted following pseudo-first-order kinetics. Meanwhile, in the seawater, degradation of the antibiotics was no observed.
Sulfamethazine, sulfamerazine, sulfadiazine, sulfachloropyridazine, and sulfadimethoxine (***sulfonamides*** containing six-membered heterocyclic substituents) Boreen, Arnold, & McNeill (2005)	***Light:*** experiments were performed under natural sunlight in Minneapolis, MN (45° latitude). ***Antibiotics concentration:*** $10\,\mu mol\,L^{-1}$. ***Water matrices:*** pure water and natural lake water.	***Kinetics:*** all antibiotics followed pseudo-first-order kinetics; Φ values were ranged from 0.01×10^{-3} to 5×10^{-3}. ***Degradation routes:*** direct photolysis involving self-triplet excited states of sulfonamides. ***Transformations***: SO_2 extrusion, generating a p-aminobenzene group linked to the six-membered heterocycle through an NH bond. ***Matrix effects***: photodegradation of the antibiotics in the lake water revealed a significant enhancement relative to that observed in pure water.
Sulfamethazine, sulfadiazine, and sulfamethoxazole and their N^4-acetylated metabolites (N^4-acetylsulfadiazine, N^4-acetylsulfamethazine and N^4-acetylsulfamethoxazole) (***sulfonamides***)	***Light:*** Simulated sunlight (>290 nm, $250\,W\,m^{-2}$ provided by a Xe lamp). ***Antibiotics concentration:*** $10\,mg\,L^{-1}$ ***Water matrix:*** Milli-Q water was spiked with individual pharmaceuticals.	***Kinetics:*** antibiotics and their N^4-acetylated metabolites followed pseudo-first-order kinetics. ***Transformations***: SO_2 extrusion was observed for sulfamethazine, sulfadiazine (sulfonamides containing six-membered heterocyclic

This book belongs to Central Library BADJI Mokhtar-ANNABA UNIVERSITY

Copyright Elsevier 2024

Reference: Periša et al. (2013)		substituents), whereas sulfamethoxazole showed a different behavior. In addition to desulfonated products, other products from direct cleavage of the sulfonamide (S—N) bond were also detected. For the metabolites, photodegradation products were also formed via cleavage of S—N bond and SO_2 extrusion.
Sulfamethoxazole (***sulfonamide***) ***Reference:*** Trovó, Nogueira, Aguera, Sirtori, & Fernández-Alba (2009)	***Light:*** Simulated sunlight (300–800 nm, 500 W m^{-2} provided by a Xe lamp). ***Antibiotic concentration:*** 10 mg L^{-1} ***Water matrices:*** pure water, pure water with nitrate ions and seawater.	***Transformations***: cleavage of the sulfonamide bond and the photoisomerization by rearrangement of the isoxazole ring represent the main pathways. ***Treatment extent***: phototransformation products had higher toxicity against *Vibrio fischeri* and *Daphnia magna* bioassays than parent antibiotic. ***Matrix effects***: differences in the degradation rates were observed between pure water and seawater, being slower in the seawater. Presence of nitrate in pure water did not affect sulfamethoxazole photodegradation rate.
Lincomycin (lincosamide) ***Reference:*** Andreozzi et al. (2006)	***Light:*** actual sunlight. Sunlight irradiation runs were performed in Naples (40°N–14°E). ***Antibiotic concentrations:*** 25 μmol L^{-1}. ***Water matrices:*** pure water and pure water containing nitrate or humic acid.	***Kinetics:*** Lincomycin presented Φ value of 1.3×10^{-4} at pH 7.5. Seasons having higher solar light intensity (i.e., spring and summer) favored lincomycin photodegradation. ***Matrix effects***: solar experiments in the presence of photosensitizers (nitrate and humic acids) were compared with the direct photolysis. Both nitrates and humic acids markedly increased the rate of lincomycin photolysis with respect to the case in which no photosensitizers were added.

This book belongs to Central Library BADJI Mokhtar-ANNABA UNIVERSITY

Copyright Elsevier 2024

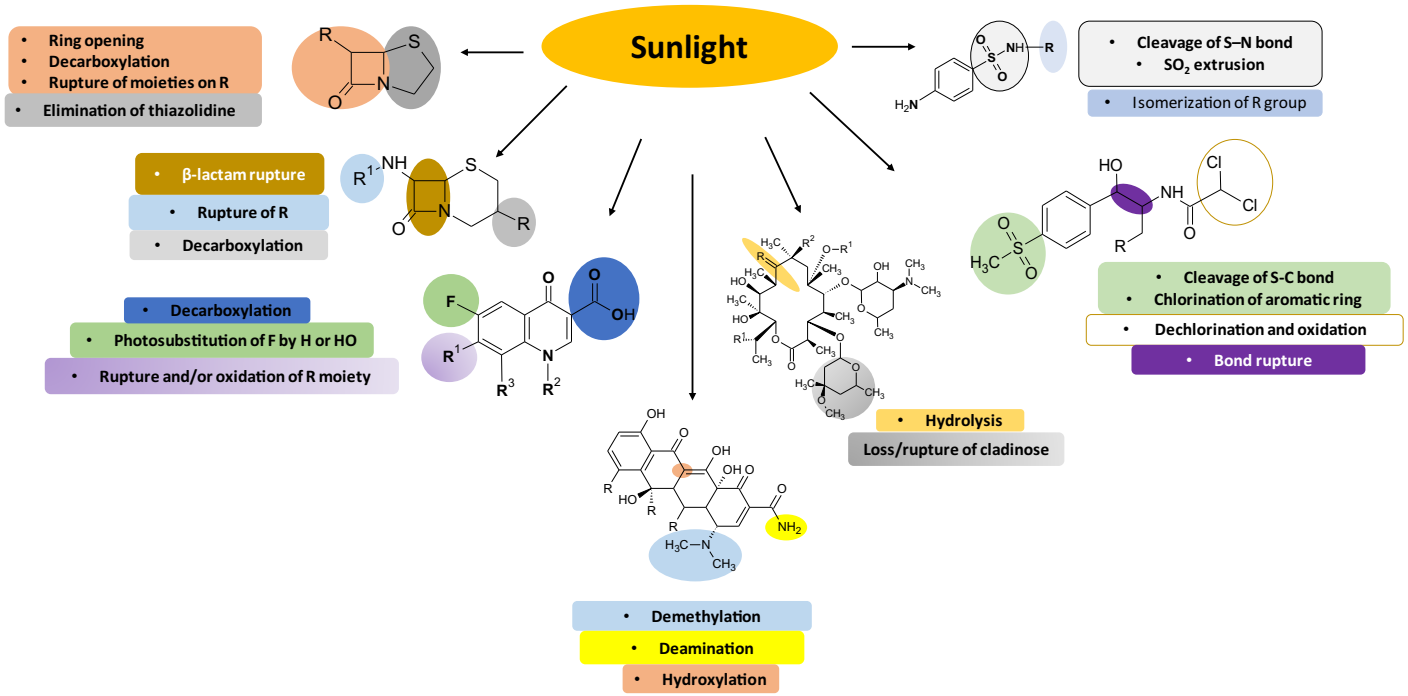

FIG. 3

Scheme of diverse transformations induced by sunlight to antibiotics in pure water.

This book belongs to Central Library BADJI Mokhtar-ANNABA UNIVERSITY

Copyright Elsevier 2024

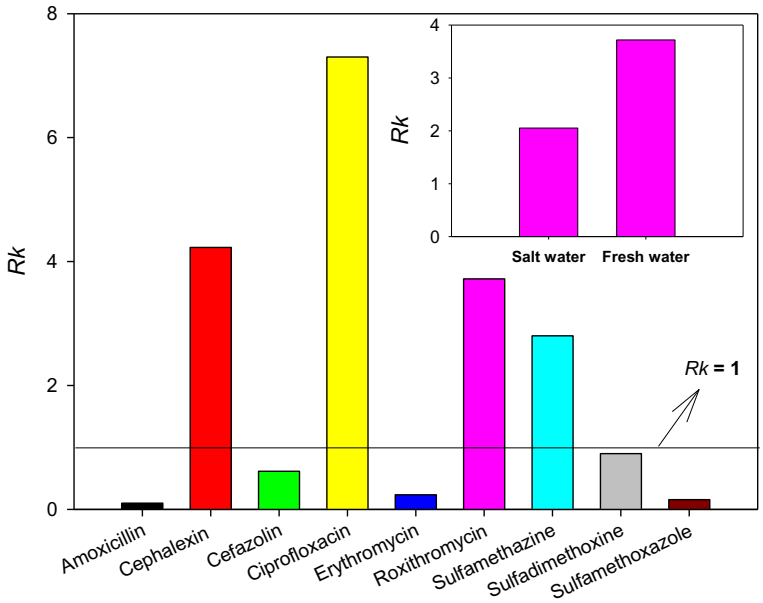

FIG. 4

Accelerating and inhibiting effects of natural water matrix on photodegradation of some antibiotics. Inset: *Rk* values for roxithromycin photodegradation in two natural waters. *Rk* is the ratio between rate constants in natural water and pure water; that is, $Rk = k_{\text{in matrix}}/k_{\text{in pure water}}$. It should be indicated that for DOM in the range 2–6 mg L^{-1} accelerating effects were observed. Also, nitrate ions in the range 5–20 mg L^{-1} induced significant improvements of antibiotics photodegradation. The calculation of *Rk* was based on data from Batchu, Panditi, O'Shea, et al. (2014), Boreen et al. (2005), Timm et al. (2019), and Wang and Yu-Chen Lin (2012).

and pure water; that is, $Rk = k_{\text{in matrix}}/k_{\text{in pure water}}$). A value of $Rk > 1$ means that matrix accelerates antibiotic degradation, $Rk < 1$ indicates inhibiting effect and $Rk = 1$ represents noneffect of matrix components.

As observed in Fig. 4, natural water components can have contrary effects on antibiotics belonging to the same class, if we compare the photodegradation of cephalexin and cefazolin (two cephalosporins), which were submitted to sunlight at the same conditions, a big difference between them can be evidenced. Cephalexin has low photolysis in pure water, but in the real matrix this is enhanced and the indirect photolysis (promoted by fulvic acid and nitrate) is the primary degradation process. In contrast, cefazolin presents high photolysis in pure water and its elimination is strongly inhibited in the river water, implying that the matrix components compete hindering the light transmission, and consequently reducing the photolysis rate (Wang & Yu-Chen Lin, 2012).

On the other hand, differential interaction with photosensitizers leads to unlike results, as reported for sulfamethazine and sulfadimethoxine. The former antibiotic is able to interact with ^{3}DOM*, whereas the latter is unable to interact with such species; in fact, it is proposed that sulfadimethoxine has a more energetic or different character of triplet excited state than sulfamethazine (Boreen et al., 2005). Besides, the degradation of the same antibiotic in different natural matrices (e.g., roxithromycin,

This book belongs to Central Library BADJI Mokhtar-ANNABA UNIVERSITY Copyright Elsevier 2024

inset in Fig. 4) indicates that dissimilar water composition has different enhancing (or inhibiting) effects (Batchu, Panditi, & Gardinali, 2014; Batchu, Panditi, O'Shea, et al., 2014). Furthermore, it is recognized that the increasing of photosensitizes (as DOM or nitrate) amount leads to higher degradation rates of antibiotics; however, an excess of photosensitizer amount has negative effects associated to competition by photons and self-scavenging of ROS (Ge et al., 2009; Porras et al., 2016). At this point, it is clear that photodegradation in natural water is highly dependent on both the matrix composition and the nature of antibiotic.

Other important factor in the antibiotics photodegradation by sunlight is the pH. For example, kinetics data for the photolysis of sulfamethoxazole under sunlight irradiation have shown that this antibiotic is more stable at natural water pH, when it is in its anionic form (Batchu, Panditi, O'Shea, et al., 2014). Similarly, the direct photolysis of tetracycline increases with increasing of pH at the range of 6.0–9.0. At low pH, tetracycline is fully protonated and as pH is augmented predominates its anion, which is relevant at the environmental pH (i.e., 6–8); accordingly, photodegradation of tetracycline correlates well with the fraction of anionic form (Chen et al., 2008; Jiao, Zheng, Yin, Wang, & Chen, 2008). Unlike to sulfamethoxazole and tetracycline, the zwitterionic forms of sarafloxacin and gatifloxacin (fluoroquinolones) may have higher sunlight absorption and quantum yield. Consequently, the zwitterionic forms of sarafloxacin and gatifloxacin are photodegraded faster than their acidic or basic forms (Albini & Monti, 2003; Ge et al., 2010). Therefore, it can be indicated that photolysis rate is also dependent on antibiotic speciation in the given pH of the water sample, and the response to sunlight of each species is generally different.

All previous information was been focused on degradation promoted by sunlight; however, it should be mentioned that UV irradiation of 254 nm (light belonging to UVC range) is commonly used to induce photodegradation of several organic compounds. In fact, such radiation has been widely applied to eliminate antibiotics from different classes (Batchu, Panditi, O'Shea, et al., 2014; Serna-Galvis, Ferraro, Silva-Agredo, & Torres-Palma, 2017; Serna-Galvis, Giraldo-Aguirre, Silva-Agredo, Florez-Acosta, & Torres-Palma, 2017). Although the topic is out of the scope of this chapter, relevant information about it can be found in the next references: Batchu, Panditi, O'Shea, et al. (2014), De la Cruz et al. (2013, 2012), He, Mezyk, Michael, Fatta-Kassinos, and Dionysiou (2014), Hokanson, Li, and Trussell (2015), Jung et al. (2012), Keen and Linden (2013), Niu et al. (2013), Prados-Joya, Sánchez-Polo, Rivera-Utrilla, and Ferro-garcía (2011), Serna-Galvis, Ferraro, et al. (2017), Serna-Galvis, Giraldo-Aguirre, et al. (2017), and Wols and Hofman-caris (2012).

2.2 Environmental implications of photodegradation using sunlight

When antibiotics are degraded by sunlight, low mineralization (i.e., complete transformation of organic pollutants into carbon dioxide, water, and inorganic ions) is observed (Timm et al., 2019; Wang & Yu-Chen Lin, 2012). This indicates that the process results in formation of photodegradation products, which demands environmental risk assessment. Hence, during the treatment of antibiotics with sunlight, evolution of both toxicity and antimicrobial activity must be determined.

In some cases, the transformations induced by sunlight lead to a decreasing in the antimicrobial activity of antibiotics. Such transformations imply strong modifications of the compound on important moieties or on the nucleus active against bacteria. Nevertheless, the photodegradation process of other antibiotics may form stable products, which could maintain biological activity and/or increase the

This book belongs to Central Library BADJI Mokhtar-ANNABA UNIVERSITY
Copyright Elsevier 2024

sensitivity of bacterial strains (Batchu, Panditi, O'Shea, et al., 2014; Ge et al., 2015; Niu, Glady-Croué, & Croué, 2017; Porras et al., 2016; Sturini et al., 2012).

Regarding toxicity, in most of cases, upon photodegradation by sunlight, this parameter is increased (as indicated in Table 1), even if antimicrobial activity is removed (Trovó et al., 2014; Wammer, Slattery, Stemig, & Ditty, 2011). From an environmental point of view, this is not good news, because such fact is reflecting the actual situation of natural waters, where solar light may induce photodegradation (through both direct and mediated routes) of antibiotics, producing substances retaining the antimicrobial activity and/or more hazardous than the parent compounds. Then, an alternative to face this concern is the application of photocatalytical systems, which can generate environmentally friendly substances from antibiotics and limit the input of these pollutants into the environment. It should be mentioned that photocatalytical processes can also utilize solar irradiation to degrade both antibiotics sensitive to light action and antibiotics that have no direct photodegradation (see next section).

3 Heterogeneous photocatalysis for antibiotics degradation

3.1 Photocatalytic process based on TiO_2

Classical heterogenous photocatalysis is based on the utilization of TiO_2 semiconductor. In the TiO_2-photocatalysis process, when light with wavelength ≤ 387 nm illuminates the semiconductor, a promotion of electrons from the valence band to the conduction band occurs, generating electron-hole pairs (Eq. 20) (Ohtani, 2014). The photogenerated holes are able to oxidize water molecules or the hydroxide anion (Eqs. 21 and 22) to produce hydroxyl radicals ($E^\circ = 2.8$ V). In turn, the excited electrons may react with dissolved oxygen in water to form superoxide anion radicals, which can evolve to produce more radicals and hydrogen peroxide (Eq. 23) (Chen, Yang, Wang, & Lou, 2005). TiO_2-photocatalysis takes advantage of the generated ROS (i.e., HO•, HOO•, $O_2\bullet^-$, and H_2O_2) for degrading antibiotics (A) (Eq. 24). Additionally, the hole can also react directly with A and degrade it (Eq. 25).

$$TiO_2 + h\nu_{(\lambda<387\,\mathrm{nm})} \rightarrow TiO_2\,(e^- - h^+) \tag{20}$$

$$h^+ + H_2O \rightarrow H^+ + HO\bullet \tag{21}$$

$$h^+ + HO^- \rightarrow HO\bullet \tag{22}$$

$$e^- + O_2 \rightarrow O_2\bullet^- \rightarrow\rightarrow\rightarrow HO\bullet, HOO\bullet, H_2O_2 \tag{23}$$

$$HO\bullet, HOO\bullet, H_2O_2 + A \rightarrow \text{products} \tag{24}$$

$$h^+ + A \rightarrow \text{products} \tag{25}$$

A lot of researches have been addressed in the application of TiO_2-photocatalysis process to eliminate antibiotics from waters (Homem & Santos, 2011; Kanakaraju, Glass, & Oelgemöller, 2014; Miklos, Remy, Jekel, Linden, & Hübner, 2018). Table 2 summarizes remarkable aspects for some illustrative cases. TiO_2-photocatalytical degradation of antibiotics evidences that in many cases, this process can be fitted to a Langmuir-Hinshelwood kinetic model (which describes a correlation between degradation rate constants and the initial concentration of antibiotic). Besides, pH effect on degradation by TiO_2-photocatalysis depends on both the ionized forms of the antibiotic and the point of zero charge

This book belongs to Central Library BADJI Mokhtar-ANNABA UNIVERSITY Copyright Elsevier 2024

Table 2 Illustrative cases of antibiotics degradation by TiO_2-photocatalysis

Antibiotics	Conditions of photodegradation	Remarkable aspects
Amoxicillin (penicillin, ***β-lactam***) ***Reference:*** Dimitrakopoulou et al. (2012)	***Light:*** UV-A (350–400 nm, provided by a lamp) ***Antibiotic concentrations:*** 2.5–30 mg L^{-1}. ***TiO_2 concentration:*** 0.10 and 0.75 g L^{-1}. ***Water matrices:*** pure water and municipal secondary effluent.	***Kinetics:*** initial degradation rates can be approached by a Langmuir-Hinshelwood kinetic model. ***Treatment extent:*** 93% of mineralization and complete removal of antibiotic activity against *Escherichia coli* and *K. pneumoniae*. ***Matrix effects:*** degradation in ultrapure water is considerably faster than in secondary effluent, which contains about 8 mg L^{-1} of organic matter that compete with the antibiotic for hydroxyl radicals and other oxidizing species. Furthermore, radical scavenging induced by the presence of about 180 mg L^{-1} of bicarbonate and 220 mg L^{-1} of chloride in the actual matrix are also responsible for decreasing in degradation efficiency.
Oxacillin, cloxacillin and dicloxacillin (penicillin, ***β-lactams***) ***References:*** Giraldo-Aguirre, Erazo-Erazo, Flórez-Acosta, Serna-Galvis, & Torres-Palma (2015), Serna-Galvis, Ferraro, et al. (2017), Serna-Galvis, Giraldo-Aguirre, et al. (2017), Serna-Galvis, Silva-Agredo, Giraldo, Flórez, & Torres-Palma (2016), Villegas-Guzman et al. (2017, 2015)	***Light:*** UVA and visible light (provided by actinic lamps). ***Antibiotics concentration:*** 25 μmol L^{-1}–438 μmol L^{-1}. ***TiO_2 concentration:*** 0.05–2.0 g L^{-1}. ***Water matrices:*** pure water and synthetic wastewaters	***Kinetics:*** photocatalytical process for oxacillin and dicloxacillin fitted well to Langmuir-Hinshelwood kinetics. ***Degradation route:*** these penicillins were mainly degraded by hydroxyl radical and holes. ***Transformations:*** for oxacillin and cloxacillin were found pathways of aromatic ring hydroxylation, opening of β-lactam moiety, decarboxylation and breakdown of central amide. ***Treatment extent:*** mineralization higher than 50%, complete elimination of antimicrobial activity against *S. aureus*. In the case of dicloxacillin, water biodegradability increased with the photocatalytic treatment. ***Matrix effects*:** in presence of organic component (e.g., glucose) and inorganic anions (e.g., bicarbonate, sulfate, chloride) antibiotics degradations were inhibited. In contrast, small amounts of ferrous or ferric cations enhanced the photocatalytical process.

This book belongs to Central Library BADJI Mokhtar-ANNABA UNIVERSITY

Copyright Elsevier 2024

Ofloxacin, norfloxacin, ciprofloxacin and enrofloxacin (***fluoroquinolones***) ***References:*** Li, Guo, Su, and Xu (2012)	***Light:*** Simulated solar irradiation provided by a xenon lamp (800 W) ***Antibiotics concentration:*** ~0.03 mmol L^{-1}. ***TiO_2 concentration:*** 0.1–1.5 g L^{-1}. ***Water matrix:*** pure water	***Kinetics:*** photocatalytic degradation kinetics of these fluoroquinolones were successfully fitted to the Langmuir-Hinshelwood model. ***Treatment extent***: mineralization from 25 to 75% and complete elimination of antimicrobial activity against *Bacillus subtilis*. ***Matrix effects:*** the addition of H_2O_2 to pure water improved the antibiotics degradation.
Moxifloxacin (***fluoroquinolone***) ***Reference:*** Van Doorslaer et al. (2012)	***Light:*** UV-A (485 μW m^{-2} provided by a lamp with main peak at 365 nm) ***Antibiotic concentrations:*** 12.5–124.6 μmol L^{-1}. ***TiO_2 concentration:*** 0.25–8.00 g L^{-1}. ***Water matrix:*** pure water	***Kinetics:*** the process followed a Langmuir-Hinshelwood kinetics. ***Degradation route:*** the holes are the dominant reactive species, contributing up to 63%, and hydroxyl radicals participate for about 24% in the photocatalytic degradation of moxifloxacin. Reactive oxygen species created by conduction band electrons had lower importance (<13%).
Oxolinic acid (**quinolone**) ***Reference:*** Giraldo et al. (2010)	***Light:*** UV-A (14 W m^{-2}, emission maximum at 365 nm) ***Antibiotic concentration:*** 20 mg L^{-1}. ***TiO_2 concentration:*** 0.2–1.5 g L^{-1}. ***Water matrix:*** pure water	***Kinetics:*** oxolinic acid degradation can follow the Langmuir-Hinshelwood (LH) model. ***Degradation route:*** for oxolinic acid, in photocatalytical treatment, the hydroxyl radical presented a minor role in the photocatalytic oxidation and the hole mechanism was the prevailing route. ***Transformations:*** the process induced decarboxylation (via photo-Kolbe), hydroxylation, and hydrogen abstraction as primary transformations of the quinolone antibiotic. ***Treatment extent***: 50% of mineralization, complete elimination of antimicrobial activity against *Escherichia coli*, in addition to significant reduction toxicity toward *Vibrio Fischeri* was achieved by the process.
Sulfacetamide, sulfathiazole, sulfamethoxazole and sulfadiazine (***sulfonamides***) ***Reference:*** Baran, Sochacka, and Wardas (2006)	***Light:*** UV-A radiation (366 nm) ***Antibiotics concentration*** 0.1 mmol L^{-1}. ***TiO_2 concentration:*** **2.5 g L^{-1}**. ***Water matrix:*** pure water	***Kinetics:*** the order of antibiotics degradation rate was sulfamethoxazole > sulfathiazole > sulfacetamide ~ sulfadiazine. ***Treatment extent***: for all treated sulfonamides the biodegradability of water increased and the toxicity of degradation products was significantly lower than toxicity of their parent antibiotics

Continued

This book belongs to Central Library BADJI Mokhtar-ANNABA UNIVERSITY

Copyright Elsevier 2024

Table 2 Illustrative cases of antibiotics degradation by TiO_2-photocatalysis—cont'd

Antibiotics	Conditions of photodegradation	Remarkable aspects
Sulfamethoxazole and trimethoprim ***Reference:*** Cai and Hu (2017)	***Light:*** UVA LED (4.32×10^3 mW cm^{-2}) ***Antibiotics concentration:*** 0.2–1.0 mg L^{-1}. ***TiO_2 concentration:*** 0.05 g L^{-1}. ***Water matrix:*** pure water	***Transformations:*** for sulfamethoxazole, hydroxylation of aromatic and isoxazole ring, opening of isoxazole ring and cleavage within molecules thorough the S—N bond were reported. In turn, for trimethoprim, hydroxylation/oxidation of its bridging methylene group, hydroxylation on the trimethoxybenzyl moiety, demethylation and cleavage of the molecule were found. ***Treatment extent***: There was a decreasing residual antibacterial activity (against *Escherichia coli*) by action of the photocatalytical process. Also, toxicity studies conducted with *Vibrio fischeri* suggested no acute toxicity generated during the UV/TiO_2 photocatalysis of these antibiotics. ***Matrix effects:*** the addition of H_2O_2 to pure water improved the antibiotics degradation.
Tetracycline (***tetracycline***) ***Reference:*** Zhu, Wang, Sun, and Zhou (2013)	***Light:*** UV-A (365 nm, 525 μW cm^{-2}) ***Antibiotics concentration:*** 40 mg L^{-1}. ***TiO_2 concentration:*** 1.0 g L^{-1}. ***Water matrix:*** pure water	***Degradation route:*** both holes and hydroxyl radicals contributed to degradation of tetracycline. ***Transformations:*** elimination of the antibiotic involved the loss of *N*-methyl group and hydroxyl group. The successive attack by degrading agents led to destruction of tetra-cycle (rings opening), producing small organic molecules such as organic acids and alcohols. ***Treatment extent***: 90% of mineralization was achieved by the process. Moreover, toxicity increased in the first stage of the process, but it was decreased at long treatment times.

This book belongs to Central Library BADJI Mokhtar-ANNABA UNIVERSITY

Copyright Elsevier 2024

(PZC) of the catalyst. If at experimental pH, TiO_2 and the pollutant have opposed charges, an electrostatic attraction occurs, and then, the catalyst-antibiotic interaction is favored. As a consequence, the antibiotic degradation is also favored (Villegas-Guzman et al., 2015). On the contrary, when TiO_2 and the pollutant have similar charges, the electrostatic repulsion between the antibiotic and the catalyst disfavors the degradation process (Dimitrakopoulou et al., 2012; Giraldo et al., 2010). Furthermore, for some antibiotics, at basic pH an acceleration of their degradation may be observed, due to a higher production of hydroxyl radicals coming from hydroxyl anions reaction at the holes (Eq. 22) (Li et al., 2012; Zhu et al., 2013).

It is recognized that the TiO_2-photocatalysis process has a high mineralizing ability (see Table 2). Moreover, this system is able to generate degradation products without antimicrobial activity and less toxic than the parent antibiotic. Also, it should be pointed out that the antibiotics degradation by action of TiO_2-photocatalysis can be rationalized as a sequence of three stages (Fig. 5), which consists in formation of primary intermediates from parent compounds (stage 1), generation of short-chain molecules from primary intermediates (stage 2) and transformation of these small substances into CO_2, H_2O and inorganic ions (stage 3).

On the other hand, in TiO_2-photocatalysis, many matrix components (e.g., organic acids, alcohols, sugars, carbonate/bicarbonate, phosphate, nitrate, chloride, and sulfate anions) have interfering effects which decrease the antibiotic elimination. These matrix components are able to diminish light penetration and/or limit antibiotics adsorption on catalyst surface, and they also compete by the ROS and the holes photocatalytically generated (Dimitrakopoulou et al., 2012; Giraldo-Aguirre et al., 2015; Prieto-Rodríguez et al., 2013; Villegas-Guzman et al., 2015). However, an alternative to enhance pollutants degradation is the addition of moderate amounts of an electron acceptor as hydrogen peroxide or ferric ions. Such additions lead to extra production of radicals (Eqs.14, 26–29) usable for organic compounds removal (Giraldo-Aguirre et al., 2015; Homem & Santos, 2011; Li et al., 2012; Torres, Nieto, Combet, Pétrier, & Pulgarin, 2008).

$$e^{-}{}_{\text{conduction band}} + H_2O_2 \rightarrow HO\bullet + HO^{-} \tag{26}$$

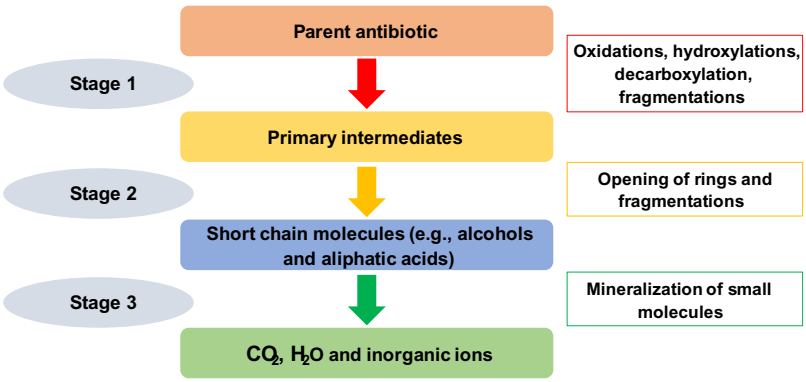

FIG. 5

Stages of antibiotics transformation by TiO_2 photocatalysis.

This book belongs to Central Library BADJI Mokhtar-ANNABA UNIVERSITY
Copyright Elsevier 2024

$$e^{-}{}_{\text{conduction band}} + Fe^{3+} \rightarrow Fe^{2+} \tag{27}$$

$$Fe^{2+} + O_2 \rightarrow Fe^{3+} + O_2 \bullet^{-} \tag{28}$$

$$Fe^{2+} + H_2O_2 \rightarrow HO \bullet + HO^{-} \tag{29}$$

Despite TiO_2-photocatalysis is one of the first photochemical processes applied for water treatment and the very high volume of information about degradation of antibiotics by this system, there is a restriction for heterogeneous photocatalysis utilization at full scale, which is mainly associated to factors such as: (1) poor sunlight absorption (~3%), (2) complications on separation of catalyst from the water suspension after treatment, and (3) mass transfer limitations to the surface of the immobilized catalyst on a substrate (Miklos et al., 2018). However, this process has opened the door for the investigation on the development of new materials (e.g., photocatalytic nanomaterials), which could offer other applicative opportunities, maintaining interest on the transformation of pollutants via heterogeneous photocatalysis.

3.2 Photocatalytic process using nanomaterials for antibiotics degradation

Nanomaterials have emerged as an interesting option to enhance the photochemical degradation of antibiotics. Nanomaterials (nanoparticles, nanoplates, nanocubes, nanowires, nanotubes, nanobars, etc.) can be prepared in two ways: organic-based nanomaterials, such as fullerenes and carbon nanotubes or inorganic as metal oxides (zinc oxide, iron oxide, dioxide titanium, etc.), single metals (gold, silver, or iron) and quantum dots molecules or compounds confined (cadmium sulfide, cadmium selenide, among others) (Darwish, Mohammadi, & Assi, 2016; Kaur et al., 2018; Kaur, Mehta, & Kansal, 2018).

Nanomaterials (in order of 10–100 nm) can be used in photocatalysis due to the following advantages: extremely small size; greater surface area in relation to volume, which favors the mechanisms of mass transfer; enhanced and controllable optical properties; and quantum effects that govern the movement of electrons and holes, changing the catalytic, electrical, mechanical, and reactivity properties of systems. The quantic effect is related to the transformation of bands at discrete energy levels, resulting in an increase in bandwidth of the semiconductor, which increase the redox potential of the species photogenerated (Peng et al., 2019).

For the conventional preparation of nanophotocatalysts high temperatures need to be used to favor the nucleation. However, alternative methods for the synthesis of property-tailored nanomaterials have been developed, which include coprecipitation, sol-gel, ultrasonic impregnation, ionic liquid-assisted photochemical synthesis, electrochemical synthesis, facile chemical impregnation, microwave-assisted synthesis, and so on (Jeyaraman et al., 2019; Jorge de Souza, Rosa Souza, & Franchi, 2019; Kulkarni, Mhaisalkar, Mathews, & Boix, 2019; Stevanović et al., 2019).

TiO_2-based nanomaterials are among the most used photocatalysts. Remarkably, the small size of nanomaterials introduces significant differences respect to their properties in bulk. For instance, at environmental conditions, rutile constitutes the most thermodynamically stable phase of TiO_2; but when the particle size is 10–20 nm, the most stable and photo-sensible phase is anatase. In addition, the surface area of nanomaterials can grow in a quasiexponential way at sizes lower than 10 nm (Chen, Wang, Lin, & Lin, 1997). Under these conditions, it is possible to decrease the crystalline defects of nanomaterials and consequently reduce the recombination tendency of the excited electrons. One illustrative case is the ternary heterostructure synthesized for degrading tetracyclines by coanchoring the graphitic

This book belongs to Central Library BADJI Mokhtar-ANNABA UNIVERSITY
Copyright Elsevier 2024

carbon nitride quantum dots (CNQDs) and nitrogen-doped carbon quantum dots (NCDs) on the surface of BiVO4 microsphere ($BiVO_4$/CNQDs/NCDs). This nanostructure increased the efficient separation and transport of photogenerated charge carriers, enhanced the photocatalytic efficiency related to the enhanced visible light harvesting capacity, and presented an enlarged BET surface area (Lin et al., 2019).

Interestingly, physical or structural properties of nanomaterials may be beneficial in some cases, but not in all. A disadvantage is the aggregation of the nanoparticles during the photocatalytical process and therefore a reduction of the active surface area takes place. Furthermore, due to its small size, removing the catalyst from the solution becomes a complex task. In order to solve this problem, the nanomaterial can be imbibed or immobilized on surfaces or separated from the solution by conventional methods such as centrifugation and filtration. However, the cost and the energy consumption during the separation step increase significantly. An alternative strategy to favor the removal of the nanocatalysts from the solution is by using magnetic surfaces or microparticles, which can be easily removed using an external magnetic field. Thus, Fe_3O_4, γFe_2O_3, $NiFe_2O_4$, $CoFe_2O_4$, FeCo, and Co_3O_4 have been used as magnetic core, being Fe_3O_4 of particular interest due to its magnetic properties, low toxicity, and biocompatibility. Unfortunately, iron photodissolution may occur when iron nanoparticles are used. For example, during the degradation of ampicillin, it was reported a decreasing in the photocatalytic efficiency of Fe_3O_4@TiO_2 hybrid nanostructures caused by iron dissolution. This phenomenon can be partially counteracted by incorporating the nanoparticles in silica membranes (Zhao et al., 2016).

Other disadvantage of several nanomaterials is their transparency under visible light. To face that problem, heterostructures (semiconductor-metal) have been prepared to favor the absorption of visible light. These semiconductor-metal hybrids often exhibit different properties that the individual components, thereby providing a powerful strategy for altering the properties of nanoparticles. The charges generated from the optical excitation of the semiconductor can be transferred efficiently to the metal part, shifting the plasmon frequency and/or promoting redox reactions. For example, CdS-Au hybrids exhibit absorption in the visible and near-UV regions, which comes from contributions of both the metal (plasmon resonance peak) and the semiconductor (exciton band edge absorption peak). Under such conditions, additional ROS can be generated from the interaction between oxygen and the fermi level (E_f) of the metal (Kaur, Mehta, & Kansal, 2018; Tong et al., 2012) (Fig. 6). As a result, the electron-hole recombination also decreases and the degradation of pollutants occurs in a higher extent.

Another mechanism of avoiding the recombination is the use of photoelectrocatalytical systems based on heterogeneous nanomaterials. In these systems the application of a voltage creates a current that ensures separation between holes and electrons; the electrons can move to other atoms throughout the heterogeneous structure, generating internal current that well separate hole-electron pairs (Wang, Zhang, Li, Li, & Wu, 2017). In turn, immobilization of the nanostructured particles combined with membrane-photocatalytic treatments arises as a promissory alternative treatment to deal with antibiotics and other water pollutants. The nanoparticle can improve permeability, selectivity, and antifouling properties of membrane during filtration processes. In terms of integration of these nanostructured photocatalytic films on membrane, research is still in its beginning and much more remains to be done.

On the other hand, several nanophotocatalysts have been used to promote the elimination of organic pollutants from aqueous media. Table 3 summarizes the most significant reports in relation to the degradation of antibiotics mainly using solar photocatalysis with nanomaterials. As seen, β-lactams, aminoglycosides, fluoroquinolones, tetracyclines, imidazoles, lincosamides, and sulfonamide antibiotics have been eliminated using a variety of nanomaterials. The reports highlight the particular advantages

This book belongs to Central Library BADJI Mokhtar-ANNABA UNIVERSITY Copyright Elsevier 2024

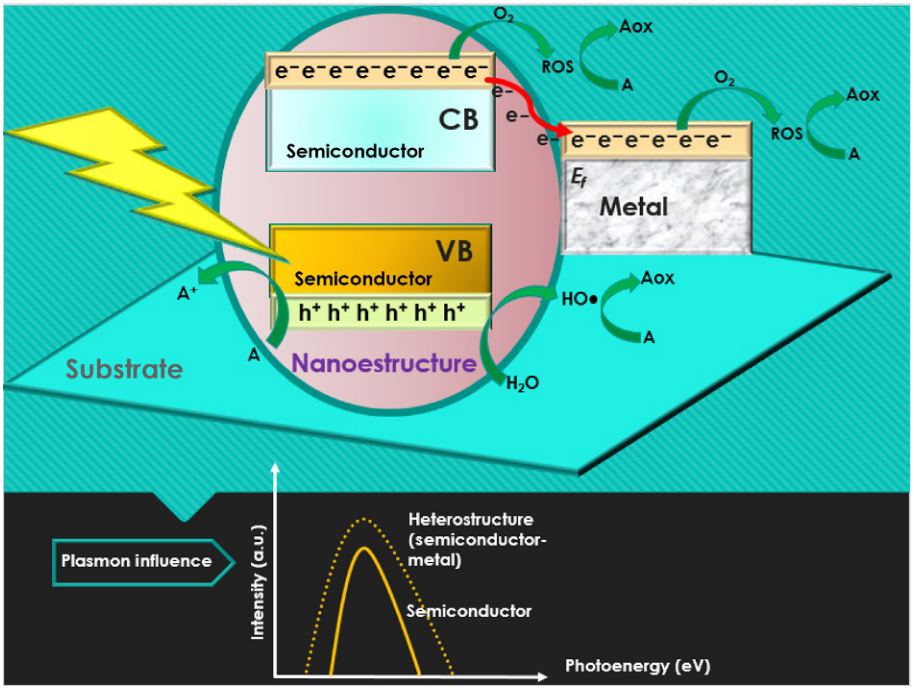

FIG. 6

Description of energy levels in a heterostructure (semiconductor-metal) and the influence on plasmon in the electronic spectrum. A: antibiotic, A^+ and Aox: oxidized forms of antibiotics, CB: conduction band, CV: valence band, and ROS: reactive oxygen species (e.g., anion superoxide).

Table 3 Illustrative cases of antibiotics degradation by (solar)photocatalysis with nanomaterials

Reference	Antibiotic	Some experimental conditions	Nanomaterial	ROS involved in degradation
β-lactams antibiotics				
Penicillins				
Sharma et al. (2018)	Ampicillin	Transparent glass photo-reactor chamber jacketed with water circulation and magnetic stirrer for controlled agitation. The remediation of antibiotic was investigated under two different conditions,	La/Cu/Zr TNPs	–

This book belongs to Central Library BADJI Mokhtar-ANNABA UNIVERSITY
Copyright Elsevier 2024

Table 3 Illustrative cases of antibiotics degradation by (solar)photocatalysis with nanomaterials—cont'd

Reference	Antibiotic	Some experimental conditions	Nanomaterial	ROS involved in degradation
β-lactams antibiotics				
		i.e., equilibrium Adsorption followed by photocatalysis and synergistic adsorption/ photocatalysis six reuse cycles of catalyst.		
Zhao et al. (2016)	Ampicillin	Ultraviolet (365 nm) and visible irradiation. The catalyst (0.02 g) was dispersed within a 20 mL of ampicillin (20 mg L^{-1}), which was stirred in the dark or light at 25°C. In the process, the lamps were placed 10 cm away from the reaction vessel.	$TiO_2/Fe_3O_4/Ag$ heterojunction	–
Tetracycline antibiotics				
Liu, Zhou, and Hu (2019)	Doxycycline	Photocatalyst was combined with H_2O_2.	Nano-sized g-C_3N_4 thin layer @ CeO_2 sphere	O_2•-, HO• and h^+
Lin et al. (2019)	Tetracycline	Visible-light (420 nm) illumination.	$BiVO_4$/CNQDs/NCD ternary heterostructure	. O_2•- and HO•
Li, Yu, et al. (2018)	Tetracycline	A Xenon lamp (500 W) with 420 nm cutoff filter as light source.	Sn_3O_4 nanoclusters on g-C_3N_4 nanosheets	O_2•-, HO• and h^+
Li et al. (2018a)	Tetracycline	The irradiation ($\lambda > 400$ nm) was provided by a xenon lamp (300 W).	Nanoparticles of CeO_2 / Bi_2MoO_6 heterojunctions	O_2•- and h^+
Li, Yu, et al. (2018)	Tetracycline	A Xe lamp (300 W) was used as light source.	Nanoparticles $Bi_4Ti_3O_{12}$/BiOCl	HO•
Li et al. (2018b)	Tetracycline	Degradation performed under visible light irradiation xenon lamp (300 W, $\lambda > 400$ nm).	Bi_2MoO_6 nanosheets/ $NiTiO_3$ nanofibers	O_2•- and h^+
Chen, Wu, and Xin (2016)	Oxytetracycline	Photocatalytic activity of nanobelts was tested under simulated solar light by using a 35 W Xenon lamp. Antibiotic concentration: 5 mg L^{-1} (volume: 35 mL).	Au-CuS-TiO_2 NBs	H_2O_2 and O_2•− are the dominant active species and h+ and HO• give the secondary contribution.

Continued

This book belongs to Central Library BADJI Mokhtar-ANNABA UNIVERSITY

Copyright Elsevier 2024

Table 3 Illustrative cases of antibiotics degradation by (solar)photocatalysis with nanomaterials—cont'd

Reference	Antibiotic	Some experimental conditions	Nanomaterial	ROS involved in degradation
β-lactams antibiotics				
Wang et al. (2016)	Tetracycline	The photocatalytic activity of the photocatalysts was evaluated under visible light irradiation. Experimental details: of the catalyst (40 mg) was dispersed into 40 mL of antibiotic solution (35 mg L^{-1}) in a Pyrex glass reactor. The light source was a Xe lamp (300 W) with a UV cutoff filter (<420 nm). The suspension was magnetically stirred in the dark for 30 min to achieve absorption-desorption equilibrium between the catalyst and pollutant.	AgI/WO_3 nanocomposite	O_2•− is crucial part in the photodegradation process.
Fluoroquinolone antibiotics				
Zhang et al. (2019)	Levofloxacin	Simulated sunlight irradiation	RGO/In_2TiO_5 Nanobelts RGO: reduced grapheme oxide	HO•
Hernández-Uresti, Alanis-Moreno, and Sanchez-Martinez (2019)	Ciprofloxacin	UV-vis light irradiation	Fe-impregnated BiVO4	HO•
Karuppaiah et al. (2019)	Ciprofloxacin	Visible light.	Gd_2WO_6 /ZnO/ bentonite nanocomposite GWZB	.O_2•−
Zheng et al. (2018)	Ciprofloxacin	A UVC lamp (14 W, 254 nm) as light source in a cylindrical Pyrex	Mesoporous carbon (GMC)-TiO_2 nanocomposites	HO•
Wang et al. (2017)	Ciprofloxacin	The photocatalytic activities of Bi_3TaO_7QDs/ g-C_3N_4NSs composites were evaluated by the degradation under visible light irradiation, using a blue LED lamp	0D/2D *Z*-Scheme Heterojunctions of Bismuth Tantalate Quantum Dots/ Ultrathin g-C_3N_4 Nanosheets	. O_2•- and HO•

This book belongs to Central Library BADJI Mokhtar-ANNABA UNIVERSITY
Copyright Elsevier 2024

Table 3 Illustrative cases of antibiotics degradation by (solar)photocatalysis with nanomaterials—cont'd

Reference	Antibiotic	Some experimental conditions	Nanomaterial	ROS involved in degradation
β-lactams antibiotics				
		($\lambda = 420$ nm, 86 W) as the light source. In a typical test, the catalyst (0.05 g) was placed in 100 mL antibiotic solution (10 mg L^{-1}).		
Kaur, Gupta, et al. (2018)	Ofloxacin	For degradation experiments, 0.025 g of silver modified ZnO was dispersed in a 100 mL ofloxacin solution (10 mg L^{-1}) and the reaction was performed in a cylindrical vessel under solar irradiation	Ag modified ZnO nanoplates	HO•
Kaur, Mehta, and Kansal (2018)	Ofloxacin	Under visible light (85 W, $\lambda = 450$–650 nm).	Nanoparticles CdS	HO•
Aminoglycoside antibiotics				
Fakhri et al. (2018)	Neomycin	UVC lamp (11 W, 254 nm) was used as a source light irradiation for photocatalytic study	WS2 decorated and immobilized on chitosan and polycaprolactone as biodegradable polymers nanofibers	O_2•-, HO• and h^+
Imidazole antibiotics				
Malakootian, Olama, Malakootian, and Nasiri (2018)	Metronidazole	UVC light and antibiotic at 80 mg L^{-1}. Parameters tested in the removal process were pH = 3, 7, and 11; contact times of 30, 60, 90, and 120 min; and nano-photocatalyst concentrations of 30, 60, 90, 250, 500, 750, and 1000 mg L^{-1}.	TiO_2-doped Fe^{3+} nano-photocatalyst	HO•
Cephalosporin antibiotics				
Dao et al. (2018)	Cefixime	Novel reactor configurations with a volume of 100 mL containing the sample and a magnetic stirrer in the presence UV-C light	TiO_2 nanoparticles	–

Continued

This book belongs to Central Library BADJI Mokhtar-ANNABA UNIVERSITY

Copyright Elsevier 2024

Table 3 Illustrative cases of antibiotics degradation by (solar)photocatalysis with nanomaterials—cont'd

Reference	Antibiotic	Some experimental conditions	Nanomaterial	ROS involved in degradation
β-lactams antibiotics				
		(280 nm). Parameters such as contact time, pH of solution, initial concentration of antibiotic and dosage of TiO_2-NPs were systematically studied for removal of antibiotic.		
Darwish et al. (2016)	Cephalexin	The light source was a 650 W halogen lamp ($\lambda_{max} = 465$ nm, 14.7 mW cm^{-2}).	G-NiCdS	HO• and h^+
Chen et al. (2016)	Cefradine	Irradiation of a UV lamp ($\lambda_{max} = 365$ nm, 8 W).	TiO_2 nanocomposite CQDs/TiO_2	H_2O_2 and HO•
Sulfonamide antibiotics				
Darwish et al. (2016)	Sulfamethoxazole	Concentrations of SMX in the range 5–20 mg L^{-1}. The light source was a 650 W halogen lamp (λmax = 465 nm, 14.7 mWcm^{-2}).	G-NiCdS	O_2•-

above indicated owing of the use of nanomaterials for the removal of antibiotics, such as their extremely small size; greater surface area, favored mass transfer, and quantum effects favoring the catalytic, electrical, mechanical, and reactivity properties of systems. In spite of that, in future works, additional efforts need to be carried out concerning the evaluation of mineralization extent, biodegradability, and toxicity of resultant waters during antibiotics treatment using nanophotocatalysts. Furthermore, special attention must be paid to the risk associated to both the toxicity of nanoparticles and the possibility of nonbiocompatible substances lixiviation (e.g., heavy metals) from the nanomaterials (Peng et al., 2019). Extra information about other opportunities and challenges of nanophotocatalytic materials can be found in Tong et al. (2012).

4 Concluding remarks

Action of sunlight is strongly determined by both chemical structure of pollutants and matrix composition of water. These aspects should be taken into account to understanding the photochemical performance of the antibiotics submitted to solar irradiation. Indeed, the matrix components can have a

This book belongs to Central Library BADJI Mokhtar-ANNABA UNIVERSITY Copyright Elsevier 2024

dual role (i.e., accelerating or inhibiting) on the degradation of antibiotics by light alone. Although direct and mediated routes can effectively degrade antibiotics, the transformations may have negative environmental impacts (e.g., generation of substances more toxic than parent antibiotics and/or byproducts with high antimicrobial activity), which can be faced through the application of photocatalytical process.

The application of TiO_2 photocatalysis for treatment of water polluted with antibiotics lead to environmental benefits (e.g., high degree of mineralization, transformation of parent compounds into innocuous or biocompatible substances with no antimicrobial activity). Nevertheless, the process has two main operational limitations: separation of catalyst from the water after treatment and nonefficient mass transfer to the surface in the case of the immobilized catalyst. Such limitations of the heterogeneous photocatalysis could be overcome by the development of new photocatalytic materials (nanomaterials) having special properties (such as magnetism or higher superficial area and enhanced optical properties). In spite of that, special concern arise from the recent debate about toxicity and biocompatibility of nanoparticles.

Finally, it can be indicated that the future outlooks in photocatalysis should not be the treatment of municipal wastewaters at high scale; the efforts may be focused on niche applications such as the treatment of low and moderate aqueous volumes using new materials (e.g., nano-catalysts) to deal with primary sources of antibiotics or mixtures of antibiotics (e.g., in human urine or washing water and wastewater from pharmaceutical industry).

References

Albini, A., & Monti, S. (2003). Photophysics and photochemistry of fluoroquinolones. *Chemical Society Reviews*, *32*, 238–250. https://doi.org/10.1039/b209220b.

Andreozzi, R., Canterino, M., Giudice, R. L., Marotta, R., Pinto, G., & Pollio, A. (2006). Lincomycin solar photodegradation, algal toxicity and removal from wastewaters by means of ozonation. *Water Research*, *40*, 630–638. https://doi.org/10.1016/j.watres.2005.11.023.

Baran, W., Sochacka, J., & Wardas, W. (2006). Toxicity and biodegradability of sulfonamides and products of their photocatalytic degradation in aqueous solutions. *Chemosphere*, *65*, 1295–1299. https://doi.org/10.1016/j.chemosphere.2006.04.040.

Batchu, S. R., Panditi, V. R., & Gardinali, P. R. (2014). Photodegradation of sulfonamide antibiotics in simulated and natural sunlight: Implications for their environmental fate. *Journal of Environmental Science and Health, Part B Pesticides, Food Contaminants, and Agricultural Wastes*, *49*, 200–211. https://doi.org/10.1080/03601234.2014.858574.

Batchu, S. R., Panditi, V. R., O'Shea, K. E., & Gardinali, P. R. (2014). Photodegradation of antibiotics under simulated solar radiation: Implications for their environmental fate. *Science of the Total Environment*, *470–471*, 299–310. https://doi.org/10.1016/j.scitotenv.2013.09.057.

Boreen, A. L., Arnold, W. A., & McNeill, K. (2003). Photodegradation of pharmaceuticals in the aquatic environment: A review. *Aquatic Sciences*, *65*, 320–341. https://doi.org/10.1007/s00027-003-0672-7.

Boreen, A. L., Arnold, W. A., & McNeill, K. (2005). Triplet-sensitized photodegradation of sulfa drugs containing six-membered heterocyclic groups: Identification of an SO2 extrusion photoproduct. *Environmental Science & Technology*, *39*, 3630–3638. https://doi.org/10.1021/es048331p.

Botero-Coy, A. M., Martínez-Pachón, D., Boix, C., Rincón, J. R., Castillo, N., Arias-Marín, L. P., et al. (2018). An investigation into the occurrence and removal of pharmaceuticals in colombian wastewater. *Science of the Total Environment*, *62*, 842–853.

This book belongs to Central Library BADJI Mokhtar-ANNABA UNIVERSITY

Copyright Elsevier 2024

Cai, Q., & Hu, J. (2017). Decomposition of sulfamethoxazole and trimethoprim by continuous UVA/LED/TiO2 photocatalysis: decomposition pathways, residual antibacterial activity and toxicity. *Journal of Hazardous Materials*, *323*, 527–536. https://doi.org/10.1016/j.jhazmat.2016.06.006.

Challis, J. K., Hanson, M. L., Friesen, K. J., & Wong, C. S. (2014). A critical assessment of the photodegradation of pharmaceuticals in aquatic environments: defining our current understanding and identifying knowledge gaps. *Environmental Science: Processes and Impacts*, *16*, 672–696. https://doi.org/10.1039/c3em00615h.

Chen, Y., Hu, C., Qu, J., & Yang, M. (2008). Photodegradation of tetracycline and formation of reactive oxygen species in aqueous tetracycline solution under simulated sunlight irradiation. *Journal of Photochemistry and Photobiology A: Chemistry*, *197*, 81–87. https://doi.org/10.1016/j.jphotochem.2007.12.007.

Chen, J., Shu, J., Anqi, Z., Juyuan, H., Yan, Z., & Chen, J. (2016). Synthesis of carbon quantum dots/TiO_2 nanocomposite for photo-degradation of Rhodamine B and cefradine. *Diamond and Related Materials*, *70*, 137–144. https://doi.org/10.1016/j.diamond.2016.10.023.

Chen, W., Wang, Z., Lin, Z., & Lin, L. (1997). Thermoluminescence of ZnS nanoparticles. *Applied Physics Letters*, *70*, 1465–1467. https://doi.org/10.1063/1.118563.

Chen, Q., Wu, S., & Xin, Y. (2016). Synthesis of Au–CuS–TiO2 nanobelts photocatalyst for efficient photocatalytic degradation of antibiotic oxytetracycline. *Chemical Engineering Journal*, *302*, 377–387. https://doi.org/10.1016/j.cej.2016.05.076.

Chen, Y., Yang, S., Wang, K., & Lou, L. (2005). Role of primary active species and TiO2 surface characteristic in UV-illuminated photodegradation of Acid Orange 7. *Journal of Photochemistry and Photobiology A: Chemistry*, *172*, 47–54. https://doi.org/10.1016/j.jphotochem.2004.11.006.

Dao, T. H., Tran, T. T., Nguyen, V. R., Pham, T. N. M., Vu, C. M., & Pham, T. D. (2018). Removal of antibiotic from aqueous solution using synthesized TiO2 nanoparticles: characteristics and mechanisms. *Environment and Earth Science*. *77*, https://doi.org/10.1007/s12665-018-7550-z.

Darwish, M., Mohammadi, A., & Assi, N. (2016). Integration of nickel doping with loading on graphene for enhanced adsorptive and catalytic properties of CdS nanoparticles towards visible light degradation of some antibiotics. *Journal of Hazardous Materials*, *320*, 304–314. https://doi.org/10.1016/j.jhazmat.2016.08.043.

De la Cruz, N., Esquius, L., Grandjean, D., Magnet, a., Tungler, a., de Alencastro, L. F., et al. (2013). Degradation of emergent contaminants by UV, UV/H_2O_2 and neutral photo-Fenton at pilot scale in a domestic wastewater treatment plant. *Water Research*, *47*, 5836–5845. https://doi.org/10.1016/j.watres.2013.07.005.

De la Cruz, N., Giménez, J., Esplugas, S., Grandjean, D., De Alencastro, L. F., & Pulgarín, C. (2012). Degradation of 32 emergent contaminants by UV and neutral photo-fenton in domestic wastewater effluent previously treated by activated sludge. *Water Research*, *46*, 1947–1957. https://doi.org/10.1016/j.watres.2012.01.014.

Derosa, M. C., & Crutchley, R. J. (2002). Photosensitized singlet oxygen and its applications. *Coordination Chemistry Reviews*, *233–234*, 351–371.

Dimitrakopoulou, D., Rethemiotaki, I., Frontistis, Z., Xekoukoulotakis, N. P., Venieri, D., & Mantzavinos, D. (2012). Degradation, mineralization and antibiotic inactivation of amoxicillin by UV-A/TiO2 photocatalysis. *Journal of Environmental Management*, *98*, 168–174. https://doi.org/10.1016/j.jenvman. 2012.01.010.

Euro-CDC. (2017). *Summary of the latest data on antibiotic consumption in the European Union, ESAC-Net surveillance data. http://ecdc.europa.eu/en/eaad/Documents/EARS-Net-summary-antibiotic-resistance.pdf.*

Fakhri, A., Gupta, V. K., Rabizadeh, H., Agarwal, S., Sadeghi, N., & Tahami, S. (2018). Preparation and characterization of WS2 decorated and immobilized on chitosan and polycaprolactone as biodegradable polymers nanofibers: Photocatalysis study and antibiotic-conjugated for antibacterial evaluation. *International Journal of Biological Macromolecules*, *120*, 1789–1793. https://doi.org/10.1016/j.ijbiomac.2018.09.207.

Ge, L., Chen, J., Qiao, X., Lin, J., & Cai, X. (2009). Light-source-dependent effects of main water constituents on photodegradation of phenicol antibiotics: Mechanism and kinetics. *Environmental Science & Technology*, *43*, 3101–3107. https://doi.org/10.1021/es8031727.

Ge, L., Chen, J., Wei, X., Zhang, S., Qiao, X., Cai, X., et al. (2010). Aquatic photochemistry of fluoroquinolone antibiotics: Kinetics, pathways, and multivariate effects of main water constituents. *Environmental Science & Technology*, *44*, 2400–2405. https://doi.org/10.1021/es902852v.

This book belongs to Central Library BADJI Mokhtar-ANNABA UNIVERSITY Copyright Elsevier 2024

Ge, L., Na, G., Zhang, S., Li, K., Zhang, P., Ren, H., et al. (2015). New insights into the aquatic photochemistry of fluoroquinolone antibiotics: Direct photodegradation, hydroxyl-radical oxidation, and antibacterial activity changes. *Science of the Total Environment*, *527–528*, 12–17. https://doi.org/10.1016/j.scitotenv.2015.04.099.

Giraldo, A. L., Peñuela, G. A., Torres-Palma, R. A., Pino, N. J., Palominos, R. A., & Mansilla, H. D. (2010). Degradation of the antibiotic oxolinic acid by photocatalysis with TiO2 in suspension. *Water Research*, *44*, 5158–5167.

Giraldo-Aguirre, A. L., Erazo-Erazo, E. D., Flórez-Acosta, O. A., Serna-Galvis, E. A., & Torres-Palma, R. A. (2015). TiO2 photocatalysis applied to the degradation and antimicrobial activity removal of oxacillin: Evaluation of matrix components, experimental parameters, degradation pathways and identification of organics by-products. *Journal of Photochemistry and Photobiology A: Chemistry*, *311*, 95–103. https://doi.org/10.1016/j.jphotochem.2015.06.021.

Gothwal, R., & Shashidhar, T. (2015). Antibiotic pollution in the environment: A review. *Clean: Soil, Air, Water*, *43*, 479–489. https://doi.org/10.1002/clen.201300989.

He, X., Mezyk, S. P., Michael, I., Fatta-Kassinos, D., & Dionysiou, D. D. (2014). Degradation kinetics and mechanism of β-lactam antibiotics by the activation of H_2O_2 and $Na_2S_2O_8$ under UV-254nm irradiation. *Journal of Hazardous Materials*, *279*, 375–383.

Hernández, F., Calısto-Ulloa, N., Gómez-Fuentes, C., Gómez, M., Ferrer, J., González-Rocha, G., et al. (2019). Occurrence of antibiotics and bacterial resistance in wastewater and sea water from the Antarctic. *Journal of Hazardous Materials*, *363*, 447–456. https://doi.org/10.1016/j.jhazmat.2018.07.027.

Hernández, F., Ibáñez, M., Botero-Coy, A. -M., Bade, R., Bustos-López, M. C., Rincón, J., et al. (2015). LC-QTOF MS screening of more than 1,000 licit and illicit drugs and their metabolites in wastewater and surface waters from the area of Bogotá, Colombia. *Analytical and Bioanalytical Chemistry*, *407*, 6405–6416. https://doi.org/10.1007/s00216-015-8796-x.

Hernández-Uresti, D. B., Alanis-Moreno, C., & Sanchez-Martinez, D. (2019). Novel and stable Fe-BiVO4 nanocatalyst by efficient dual process in the ciprofloxacin degradation. *Materials Science in Semiconductor Processing*, *102*, 104585. https://doi.org/10.1016/j.mssp.2019.104585.

Hokanson, D. R., Li, K., & Trussell, R. R. (2015). A photolysis coefficient for characterizing the response of aqueous constituents to photolysis. *Frontiers of Environmental Science & Engineering*, 1–10. https://doi.org/10.1007/s11783-015-0780-3.

Homem, V., & Santos, L. (2011). Degradation and removal methods of antibiotics from aqueous matrices—A review. *Journal of Environmental Management*, *92*, 2304–2347. https://doi.org/10.1016/j.jenvman.2011.05.023.

Jeyaraman, A. R., Balasingam, S. K., Lee, C., Lee, H., Balakrishnan, B., Manickam, S., et al. (2019). Enhanced solar to electrical energy conversion of titania nanoparticles and nanotubes-based combined photoanodes for dye-sensitized solar cells. *Materials Letters*, *243*, 180–182. https://doi.org/10.1016/j.matlet.2019.02.006.

Jiao, S., Zheng, S., Yin, D., Wang, L., & Chen, L. (2008). Aqueous photolysis of tetracycline and toxicity of photolytic products to luminescent bacteria. *Chemosphere*, *73*, 377–382. https://doi.org/10.1016/j.chemosphere.2008.05.042.

Jorge de Souza, T. A., Rosa Souza, L. R., & Franchi, L. P. (2019). Silver nanoparticles: An integrated view of green synthesis methods, transformation in the environment, and toxicity. *Ecotoxicology and Environmental Safety*, *171*, 691–700. https://doi.org/10.1016/j.ecoenv.2018.12.095.

Jung, Y., Gi, W., Yoon, Y., Kang, J., Min, Y., & Wook, H. (2012). Removal of amoxicillin by UV and UV/H2O2 processes. *Science of the Total Environment*, *420*, 160–167. https://doi.org/10.1016/j.scitotenv.2011.12.011.

Kanakaraju, D., Glass, B. D., & Oelgemöller, M. (2014). Titanium dioxide photocatalysis for pharmaceutical wastewater treatment. *Environmental Chemistry Letters*, *12*, 27–47. https://doi.org/10.1007/s10311-013-0428-0.

Karuppaiah, S., Annamalai, R., Muthuraj, A., Kesavan, S., Palani, R., Ponnusamy, S., et al. (2019). Efficient photocatalytic degradation of ciprofloxacin and bisphenol A under visible light using Gd 2 WO 6 loaded ZnO/bentonite nanocomposite. *Applied Surface Science*, *481*, 1109–1119. https://doi.org/10.1016/j.apsusc.2019.03.178.

This book belongs to Central Library BADJI Mokhtar-ANNABA UNIVERSITY

Copyright Elsevier 2024

Kaur, A., Gupta, G., Ibhadon, A. O., Salunke, D. B., Sinha, A. S. K., & Kansal, S. K. (2018). A Facile synthesis of silver modified ZnO nanoplates for efficient removal of ofloxacin drug in aqueous phase under solar irradiation. *Journal of Environmental Chemical Engineering*, *6*, 3621–3630. https://doi.org/10.1016/j.jece.2017.05.032.

Kaur, M., Mehta, S. K., & Kansal, S. K. (2018). Visible light driven photocatalytic degradation of ofloxacin and malachite green dye using cadmium sulphide nanoparticles. *Journal of Environmental Chemical Engineering*, *6*, 3631–3639. https://doi.org/10.1016/j.jece.2017.04.006.

Keen, O. S., & Linden, K. G. (2013). Degradation of antibiotic activity during UV/H2O2 advanced oxidation and photolysis in wastewater effluent. *Environmental Science & Technology*, *47*, 13020–13030. https://doi.org/10.1021/es402472x.

Klein, E. Y., Van Boeckel, T. P., Martinez, E. M., Pant, S., Gandra, S., & Levin, S. A. (2018). Global increase and geographic convergence in antibiotic consumption between 2000 and 2015. *PNAS*, *115*, 3463–3470. https://doi.org/10.1073/pnas.1717295115.

Kulkarni, S. A., Mhaisalkar, S. G., Mathews, N., & Boix, P. P. (2019). Perovskite Nanoparticles: Synthesis, Properties, and Novel Applications in Photovoltaics and LEDs. *Small Methods*, *3*, 1800231. https://doi.org/10.1002/smtd.201800231.

Kümmerer, K. (2003). Significance of antibiotics in the environment. *The Journal of Antimicrobial Chemotherapy*, *52*, 5–7. https://doi.org/10.1093/jac/dkg293.

Li, W., Guo, C., Su, B., & Xu, J. (2012). Photodegradation of four fluoroquinolone compounds by titanium dioxide under simulated solar light irradiation. *Journal of Chemical Technology and Biotechnology*, *87*, 643–650. https://doi.org/10.1002/jctb.2759.

Li, S., Hu, S., Jiang, W., Liu, Y., Zhou, Y., Liu, Y., et al. (2018a). Hierarchical architectures of bismuth molybdate nanosheets onto nickel titanate nanofibers: Facile synthesis and efficient photocatalytic removal of tetracycline hydrochloride. *Journal of Colloid and Interface Science*, *521*, 42–49. https://doi.org/10.1016/j.jcis.2018.03.033.

Li, S., Hu, S., Jiang, W., Liu, Y., Zhou, Y., Liu, J., et al. (2018b). Facile synthesis of cerium oxide nanoparticles decorated flower-like bismuth molybdate for enhanced photocatalytic activity toward organic pollutant degradation. *Journal of Colloid and Interface Science*, *530*, 171–178. https://doi.org/10.1016/j.jcis.2018.06.084.

Li, Y., Qiao, X., Zhang, Y., Zhou, C., Xie, H., & Chen, J. (2016). Effects of halide ions on photodegradation of sulfonamide antibiotics: Formation of halogenated intermediates. *Water Research*, *102*, 405–412. https://doi.org/10.1016/j.watres.2016.06.054.

Li, C., Yu, S., Dong, H., Liu, C., Wu, H., Che, H., et al. (2018). Z-scheme mesoporous photocatalyst constructed by modification of Sn3O4 nanoclusters on g-C3N4 nanosheets with improved photocatalytic performance and mechanism insight. *Applied Catalysis B: Environmental*, *238*, 284–293. https://doi.org/10.1016/j.apcatb.2018.07.049.

Lin, X., Liu, C., Wang, J., Yang, S., Shi, J., & Hong, Y. (2019). Graphitic carbon nitride quantum dots and nitrogen-doped carbon quantum dots co-decorated with BiVO4 microspheres: A ternary heterostructure photocatalyst for water purification. *Separation and Purification Technology*, *226*, 117–127. https://doi.org/10.1016/j.seppur.2019.05.093.

Liu, W., Zhou, J., & Hu, Z. (2019). Nano-sized g-C3N4 thin layer @ CeO2 sphere core-shell photocatalyst combined with H2O2 to degrade doxycycline in water under visible light irradiation. *Separation and Purification Technology*, *227*, 115665. https://doi.org/10.1016/j.seppur.2019.06.003.

Malakootian, M., Olama, N., Malakootian, M., & Nasiri, A. (2018). Photocatalytic degradation of metronidazole from aquatic solution by TiO2-doped Fe3+ nano-photocatalyst. *International Journal of Environmental Science and Technology*, *2*, 1–10. https://doi.org/10.1007/s13762-018-1836-2.

Martinez, J. L. (2009). Environmental pollution by antibiotics and by antibiotic resistance determinants. *Environmental Pollution*, *157*, 2893–2902. https://doi.org/10.1016/j.envpol.2009.05.051.

This book belongs to Central Library BADJI Mokhtar-ANNABA UNIVERSITY

Copyright Elsevier 2024

Mcneill, K., & Canonica, S. (2016). Triplet state dissolved organic matter in aquatic photochemistry: reaction mechanisms, substrate scope, and photophysical properties. *Environmental Science: Processes and Impacts*, *18*, 1381–1399. https://doi.org/10.1039/c6em00408c.

Michael, I., Rizzo, L., McArdell, C. S., Manaia, C. M., Merlin, C., Schwartz, T., et al. (2013). Urban wastewater treatment plants as hotspots for the release of antibiotics in the environment: A review. *Water Research*, *47*, 957–995. https://doi.org/10.1016/j.watres.2012.11.027.

Miklos, D. B., Remy, C., Jekel, M., Linden, K. G., & Hübner, U. (2018). Evaluation of advanced oxidation processes for water and wastewater treatment—A critical review. *Water Research*, *139*, 118–131. https://doi.org/10.1016/j.watres.2018.03.042.

Niu, X. -Z., Glady-Croué, J., & Croué, J. -P. (2017). Photodegradation of sulfathiazole under simulated sunlight: Kinetics, photo-induced structural rearrangement, and antimicrobial activities of photoproducts. *Water Research*, *124*, 576–583. https://doi.org/10.1016/j.watres.2017.08.019.

Niu, J., Li, Y., & Wang, W. (2013). Light-source-dependent role of nitrate and humic acid in tetracycline photolysis: Kinetics and mechanism. *Chemosphere*, *92*, 1423–1429. https://doi.org/10.1016/j.chemosphere.2013.03.049.

Ohtani, B. (2014). Revisiting the fundamental physical chemistry in heterogeneous photocatalysis: its thermodynamics and kinetics. *Physical Chemistry Chemical Physics*, *16*, 1788–1797. https://doi.org/10.1039/c3cp53653j.

Oliveira, T. S., Al Aukidy, M., & Verlicchi, P. (2018). Occurrence of common pollutants and pharmaceuticals in Hospital Effluents. In P. Verlicchi (Ed.), *Hospital wastewaters—Characteristics, management, treatment and environmental risks* (pp. 17–32). Springer International Publishing.

Peng, F., Setyawati, M. I., Tee, J. K., Ding, X., Wang, J., Nga, M. E., et al. (2019). Nanoparticles promote in vivo breast cancer cell intravasation and extravasation by inducing endothelial leakiness. *Nature Nanotechnology*, *14*, 279–286. https://doi.org/10.1038/s41565-018-0356-z.

Periša, M., Babić, S., Irena, Š., Frömel, T., & Knepper, T. P. (2013). Photodegradation of sulfonamides and their N4-acetylated metabolites in water by simulated sunlight irradiation: kinetics and identification of photoproducts. *Environmental Science and Pollution Research*, *20*, 8934–8946. https://doi.org/10.1007/s11356-013-1836-1.

Porras, J., Bedoya, C., Silva-Agredo, J., Santamaría, A., Fernández, J. J., & Torres-Palma, R. A. (2016). Role of humic substances in the degradation pathways and residual antibacterial activity during the photodecomposition of the antibiotic ciprofloxacin in water. *Water Research*, *94*, 1–9. https://doi.org/10.1016/j.watres.2016.02.024.

Prados-Joya, G., Sánchez-Polo, M., Rivera-Utrilla, J., & Ferro-garcía, M. (2011). Photodegradation of the antibiotics nitroimidazoles in aqueous solution by ultraviolet radiation. *Water Research*, *45*, 393–403. https://doi.org/10.1016/j.watres.2010.08.015.

Prieto-Rodríguez, L., Oller, I., Klamerth, N., Agüera, A., Rodríguez, E. M., & Malato, S. (2013). Application of solar AOPs and ozonation for elimination of micropollutants in municipal wastewater treatment plant effluents. *Water Research*, *47*, 1521–1528. https://doi.org/10.1016/j.watres.2012.11.002.

Rizzo, L., Manaia, C., Merlin, C., Schwartz, T., Dagot, C., Ploy, M. C., et al. (2013). Urban wastewater treatment plants as hotspots for antibiotic resistant bacteria and genes spread into the environment: A review. *Science of the Total Environment*, *447*, 345–360. https://doi.org/10.1016/j.scitotenv.2013.01.032.

Rodriguez-Mozaz, S., Chamorro, S., Marti, E., Huerta, B., Gros, M., Sànchez-Melsió, A., et al. (2015). Occurrence of antibiotics and antibiotic resistance genes in hospital and urban wastewaters and their impact on the receiving river. *Water Research*, *69*, 234–242. https://doi.org/10.1016/j.watres.2014.11.021.

Serna-Galvis, E. A., Ferraro, F., Silva-Agredo, J., & Torres-Palma, R. A. (2017). Degradation of highly consumed fluoroquinolones, penicillins and cephalosporins in distilled water and simulated hospital wastewater by UV254 and UV254/persulfate processes. *Water Research*, *122*, 128–138. https://doi.org/10.1016/j.watres.2017.05.065.

Serna-Galvis, E. A., Giraldo-Aguirre, A. L., Silva-Agredo, J., Florez-Acosta, O. A., & Torres-Palma, R. A. (2017). Removal of antibiotic cloxacillin by means of electrochemical oxidation, TiO2 photocatalysis, and photo-

This book belongs to Central Library BADJI Mokhtar-ANNABA UNIVERSITY

Copyright Elsevier 2024

Fenton processes: analysis of degradation pathways and effect of the water matrix on the elimination of antimicrobial activity. *Environmental Science and Pollution Research*, *24*, 6339–6352. https://doi.org/10.1007/s11356-016-6257-5.

Serna-Galvis, E. A., Silva-Agredo, J., Giraldo, A. L., Flórez, O. A., & Torres-Palma, R. A. (2016). Comparison of route, mechanism and extent of treatment for the degradation of a β-lactam antibiotic by TiO2 photocatalysis, sonochemistry, electrochemistry and the photo-Fenton system. *Chemical Engineering Journal*, *284*, 953–962. https://doi.org/10.1016/j.cej.2015.08.154.

Serna-Galvis, E. A., Troyon, J. A., Giannakis, S., Torres-Palma, R. A., Minero, C., Vione, D., et al. (2018). Photoinduced disinfection in sunlit natural waters : Measurement of the second order inactivation rate constants between E. coli and photogenerated transient species. *Water Research*, *147*, 242–253. https://doi.org/10.1016/j.watres.2018.10.011.

Sharma, G., Gupta, V. K., Agarwal, S., Bhogal, S., Naushad, M., Kumar, A., et al. (2018). Fabrication and characterization of trimetallic nano-photocatalyst for remediation of ampicillin antibiotic. *Journal of Molecular Liquids*, *260*, 342–350. https://doi.org/10.1016/j.molliq.2018.03.059.

Stevanović, M., Miodrag, L., Stanković, A., Filipović, N., Kuzmanović, N., & Anićijević, Z. (2019). Biomedical inorganic nanoparticles: preparation, properties, and perspectives. In *Materials for biomedical engineering, inorganic micro and nanostructures* (pp. 1–46). . https://doi.org/10.1016/B978-0-08-102814-8.00001-9.

Sturini, M., Speltini, A., Maraschi, F., Pretali, L., Profumo, A., Fasani, E., et al. (2012). Photodegradation of fluoroquinolones in surface water and antimicrobial activity of the photoproducts. *Water Research*, *46*, 5575–5582. https://doi.org/10.1016/j.watres.2012.07.043.

Timm, A., Borowska, E., Majewsky, M., Merel, S., Zwiener, C., Bräse, S., et al. (2019). Photolysis of four β-lactam antibiotics under simulated environmental conditions: Degradation, transformation products and antibacterial activity. *Science of the Total Environment*, *651*, 1605–1612. https://doi.org/10.1016/j.scitotenv.2018.09.248.

Tong, H., Ouyang, S., Bi, Y., Umezawa, N., Oshikiri, M., & Ye, J. (2012). Nano-photocatalytic materials: Possibilities and challenges. *Advanced Materials*, *24*, 229–251. https://doi.org/10.1002/adma.201102752.

Torres, R. A., Nieto, J. I., Combet, E., Pétrier, C., & Pulgarin, C. (2008). Influence of TiO_2 concentration on the synergistic effect between photocatalysis and high-frequency ultrasound for organic pollutant mineralization in water. *Applied Catalysis B: Environmental*, *80*, 168–175. https://doi.org/10.1016/j.apcatb.2007.11.013.

Trovó, A. G., Nogueira, R. F. P., Aguera, A., Sirtori, C., & Fernández-Alba, A. R. (2009). Photodegradation of sulfamethoxazole in various aqueous media: Persistence, toxicity and photoproducts assessment. *Chemosphere*, *77*, 1292–1298. https://doi.org/10.1016/j.chemosphere.2009.09.065.

Trovó, A. G., Paiva, V. A. B., Filho, B. M. C., Machado, A. E. H., Oliveira, C. A., Santos, R. O., et al. (2014). Photolytic degradation of chloramphenicol in different aqueous matrices using artificial and solar radiation: Reaction kinetics and initial transformation products. *Journal of the Brazilian Chemical Society*, *25*, 2007–2015. https://doi.org/10.5935/0103-5053.20140185.

Van Doorslaer, X., Heynderickx, P. M., Demeestere, K., Debevere, K., Van Langenhove, H., & Dewulf, J. (2012). TiO2 mediated heterogeneous photocatalytic degradation of moxifloxacin: Operational variables and scavenger study. *Applied Catalysis B: Environmental*, *111–112*, 150–156. https://doi.org/10.1016/j.apcatb.2011.09.029.

Verlicchi, P., Al Aukidy, M., & Zambello, E. (2012). Occurrence of pharmaceutical compounds in urban wastewater: Removal, mass load and environmental risk after a secondary treatment—A review. *Science of the Total Environment*, *429*, 123–155. https://doi.org/10.1016/j.scitotenv.2012.04.028.

Villegas-Guzman, P., Silva-Agredo, J., Florez, O., Giraldo-Aguirre, A. L., Pulgarin, C., & Torres-Palma, R. A. (2017). Selecting the best AOP for isoxazolyl penicillins degradation as a function of water characteristics: Effects of pH, chemical nature of additives and pollutant concentration. *Journal of Environmental Management*, *190*, 72–79. https://doi.org/10.1016/j.jenvman.2016.12.056.

This book belongs to Central Library BADJI Mokhtar-ANNABA UNIVERSITY Copyright Elsevier 2024

Villegas-Guzman, P., Silva-Agredo, J., González-Gómez, D., Giraldo-Aguirre, A. L., Flórez-Acosta, O., & Torres-Palma, R. A. (2015). Evaluation of water matrix effects, experimental parameters, and the degradation pathway during the TiO 2 photocatalytical treatment of the antibiotic dicloxacillin. *Journal of Environmental Science and Health, Part A: Toxic/Hazardous Substances and Environmental Engineering*, *50*, 40–48. https://doi.org/10.1080/10934529.2015.964606.

Wammer, K. H., Slattery, M. T., Stemig, A. M., & Ditty, J. L. (2011). Tetracycline photolysis in natural waters: Loss of antibacterial activity. *Chemosphere*, *85*, 1505–1510. https://doi.org/10.1016/j.chemosphere.2011.08.051.

Wang, T., Quan, W., Jiang, D., Chen, L., Li, D., Meng, S., et al. (2016). Synthesis of redox-mediator-free direct Z-scheme AgI/WO3 nanocomposite photocatalysts for the degradation of tetracycline with enhanced photocatalytic activity. *Chemical Engineering Journal*, *300*, 280–290. https://doi.org/10.1016/j.cej.2016.04.128.

Wang, X. -H., & Yu-Chen Lin, A. (2012). Phototransformation of cephalosporin antibiotics in an aqueous environment results in higher toxicity. *Environmental Science & Technology*, *46*, 12417–12426. https://doi.org/10.1021/es301929e.

Wang, K., Zhang, G., Li, J., Li, Y., & Wu, X. (2017). 0D/2D Z-Scheme heterojunctions of bismuth tantalate quantum dots/ultrathin g-C 3 N 4 nanosheets for highly efficient visible light photocatalytic degradation of antibiotics. *ACS Applied Materials & Interfaces*, *9*, 43704–43715. https://doi.org/10.1021/acsami.7b14275.

WHO. (2018). *WHO Report on Surveillance of Antibiotic Consumption 2016–2018; 2018*. Geneva.

Wols, B. A., & Hofman-caris, C. H. M. (2012). Review of photochemical reaction constants of organic micropollutants required for UV advanced oxidation processes in water. *Water Research*, *46*, 2815–2827. https://doi.org/10.1016/j.watres.2012.03.036.

Yan, S., & Song, W. (2014). Photo-transformation of pharmaceutically active compounds in the aqueous environment: A review. *Environmental Science: Processes and Impacts*, *16*, 697–720. https://doi.org/10.1039/c3em00502j.

Zhang, Q., Han, F., Yan, Y., Dai, Q., Proctor, G., Cheah, P., et al. (2019). Preparation and properties of visible light responsive RGO/In2TiO5 nanobelts for photocatalytic degradation of organic pollutants. *Applied Surface Science*, *485*, 547–553. https://doi.org/10.1016/j.apsusc.2019.04.185.

Zhao, Y., Tao, C., Xiao, G., Wei, G., Li, L., Liu, C., et al. (2016). Controlled synthesis and photocatalysis of Sea Urchin-Like Fe3O4@TiO2@Ag nanocomposite. *Nanoscale*, *8*, 5313–5326.

Zheng, X., Xu, S., Wang, Y., Sun, X., Gao, Y., & Gao, B. (2018). Enhanced degradation of ciprofloxacin by graphitized mesoporous carbon (GMC)-TiO2 nanocomposite: Strong synergy of adsorption-photocatalysis and antibiotics degradation mechanism. *Journal of Colloid and Interface Science*, *527*, 202–213. https://doi.org/10.1016/j.jcis.2018.05.054.

Zhu, X. D., Wang, Y. J., Sun, R. J., & Zhou, D. M. (2013). Photocatalytic degradation of tetracycline in aqueous solution by nanosized TiO2. *Chemosphere*, *92*, 925–932. https://doi.org/10.1016/j.chemosphere.2013.02.066.

Further reading

Aghdasi, S., & Shokri, M. (2016). Photocatalytic degradation of ciprofloxacin in the presence of synthesized ZnO nanocatalyst: The effect of operational parameters. *Iranian Journal of Catalysis*, *6*(5), 481–487.

Liu, W., Dai, Z., Liu, Y., Zhu, A., Zhong, D., Wang, J., et al. (2018). Intimate contacted two-dimensional/zero-dimensional composite of bismuth titanate nanosheets supported ultrafine bismuth oxychloride nanoparticles for enhanced antibiotic residue degradation. *Journal of Colloid and Interface Science*, *529*, 23–33. https://doi.org/10.1016/j.jcis.2018.05.112.

This book belongs to Central Library BADJI Mokhtar-ANNABA UNIVERSITY

Copyright Elsevier 2024

This page intentionally left blank

This book belongs to Central Library BADJI Mokhtar-ANNABA UNIVERSITY

Copyright Elsevier 2024

CHAPTER

Carbon-supported semiconductor nanoparticles as effective photocatalysts for water and wastewater treatment

13

Jaimy Scaria[a], Ansaf V. Karim[b], G. Divyapriya[c], P.V. Nidheesh[d], M. Suresh Kumar[a,d]

Academy of Scientific and Innovative Research (AcSIR), Ghaziabad, India[a] Center for Environmental Science and Engineering, Indian Institute of Technology Bombay, Mumbai, India[b] Environmental Water Resources Engineering Division, Department of Civil Engineering, Indian Institute of Technology Madras, Chennai, India[c] Environmental Impact and Sustainability Division, CSIR-National Environmental Engineering Research Institute, Nagpur, India[d]

1 Introduction

Photocatalysis is a light-mediated advanced oxidation process, where reactive oxygen species (ROS) are generated normally on a semiconductor surface through the photoexcitation of electron on electromagnetic irradiation of suitable energy (Carp, Huisman, & Reller, 2004). Even though semiconductor materials such as TiO_2 (Fujishima, Rao, & Tryk, 2000; Schneider et al., 2014), ZnO (Kumar, Muralidhara, & Nayaka, 2013; Mirzaei et al., 2016), ZnS (Hu et al., 2005), and CdS (Chen et al., 2013) were found to be good candidates for pollutant abatement in water medium, some constraints are still remaining. Poor adsorption of pollutant molecules in semiconductor surface lowers the removal rate; wide energy gap between valence band and conduction band leads to poor quantum efficiency and ineffective harvesting of sunlight especially in the visible spectrum (Carp et al., 2004); the lower photostability due to leaching (e.g., CdS) and the dispersion of the powder photocatalyst in water medium restricts its stability, recovery and reuse. Another important fact to obtain the lesser performance of photocatalyst is the faster recombination of the photogenerated electron-hole pair, which happens at the rate of 10^{-9} s, while the reaction time between the TiO_2 and the adsorbed chemical species is about 10^{-8} to 10^{-3} s (Khalid et al., 2017; Woan, Pyrgiotakis, & Sigmund, 2009; Zhou et al., 2011). To overcome these basic limitations, many modifications are under research. When choosing a supporting material for the catalysts, certain properties should be considered. The immobilization of photocatalytic material onto good support, which is possessing ideal characteristics such as strong entrapping ability, stability against hydroxyl radical attack, provider of improved pollutant adsorption capacity from high surface area and cost-effectiveness, could enhance the photocatalytic pollutant degradation ability to many folds (Puma et al., 2008). Among the studied materials, carbon modification is having high popularity. The micro- and nanosized carbon forms such as activated carbon, mesoporous

Nano-Materials as Photocatalysts for Degradation of Environmental Pollutants. https://doi.org/10.1016/B978-0-12-818598-8.00013-4
© 2020 Elsevier Inc. All rights reserved.

This book belongs to Central Library BADJI Mokhtar-ANNABA UNIVERSITY

Copyright Elsevier 2024

carbon, carbon allotropes like buckminsterfullerenes C_{60}, carbon nanotubes (CNTs), graphitic materials (carbon quantum dots, graphene nanorods, and graphene carbon nanofibers), carbon black, and graphitic nitride (g-C_3N_4) are extensively studied (Khalid et al., 2017; Leary & Westwood, 2010). Carbon materials are getting special attention among different supports in heterogeneous catalysis due to their chemical inertness, stability toward acidic/alkaline conditions, possibility to control porosity and surface properties to some extent, and possible metal recovery (Morales-Torres et al., 2012; Serp, Corrias, & Kalck, 2003). Especially, carbon nanoparticles (fullerenes, carbon nanotubes, and graphene) are under intensive research due to the extraordinary structural, electronic, and supportive properties (Wang & Zhang, 2012). Those carbonaceous nanomaterials can function as support and a dopant. Thus immobilization, adsorption, and photocatalysis properties can be significantly enhanced by their incorporation into semiconductor materials.

2 Various carbonaceous materials as support for semiconductor photocatalysts

The carbonaceous materials normally used as supportive material for semiconductor photocatalysts are either macro-/micromaterials or nanomaterials. Among bulk materials, activated carbon with porosity, as the defining characteristic, provides the fundamental benefits of higher surface area (typically 900–1200 $m^2\ g^{-1}$) available for the anchorage of nanoparticles and the adsorption of pollutant molecules (Serp et al., 2003; Velasco, Parra, & Ania, 2010). The nanomaterials used for photocatalytic improvement promise effective nanoscale interaction in composite material, thus enhancement arising not only from increased adsorption but also improved chemical, physical, and structural characteristics of the composite. Fig. 1 shows the various carbon materials in usage as support for heterogeneous photocatalysis. The macro-/microsized supportive materials are activated charcoal and mesoporous carbon. The nanoscale carbon particles, namely, 0D fullerenes, 1D carbon nanotubes (single-walled carbon

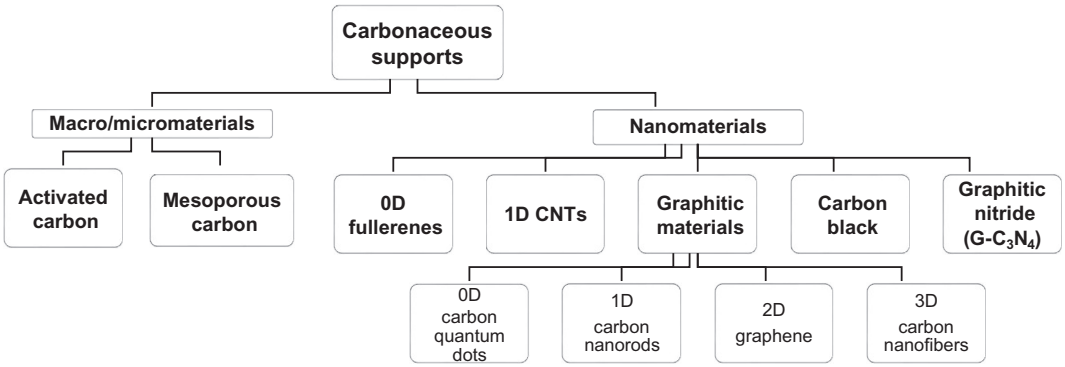

FIG. 1

The different supportive carbon materials in heterogeneous photocatalysis.

This book belongs to Central Library BADJI Mokhtar-ANNABA UNIVERSITY
Copyright Elsevier 2024

nanotubes [SWCNT], and multiwalled carbon nanotubes [MWCNT]), graphitic materials (carbon quantum dots, graphene nanorods, and graphene carbon nanofibers) and other carbon materials such as graphitic nitride and carbon black, are widely under research for evaluating their cocatalyst property in heterogeneous photocatalysis.

2.1 Activated carbon

Activated carbon (AC) material, possessing higher specific surface area and extensive porous structure, is the most ordinarily used adsorbent for water treatment (Melian et al., 2009). AC composites increase the surface area for adsorption, hinder electron-hole recombination, facilitate charge transfer to catalytic reaction sites, and thus exhibit a synergistic effect on adsorption and photodegradation of organic compounds (Gamage McEvoy, Cui, & Zhang, 2014; Li et al., 2017; Melian et al., 2009). A synergistic effect is hypothesized when a photocatalyst is supported on materials such as activated carbon that possess large specific surface areas and good absorbent properties (Puma et al., 2008; Velasco et al., 2010).

Li et al. (2006) prepared TiO_2-coated activated carbon (TiO_2/AC) by hydrolytic precipitation of TiO_2 from tetrabutyl orthotitanate and followed by heat treatment from 300°C to 700°C for 2 h in a flow of high-purity nitrogen using an electric oven. They observed an enhanced photodegradation of methyl orange dye in the presence of TiO_2/AC, which followed a pseudo-first-order kinetics. The lower photocatalytic activity of TiO_2, either due to contamination or due to the smaller quantity of active catalyst after immobilization, can be overcome by doping with metals or nonmetals (Zhang, Zhou, & Lei, 2005). Nitrogen-doped TiO_2 particles supported on AC synthesized by Yap et al. (2010) using sol-gel method for the adsorption-photocatalytic degradation of bisphenol A using solar light. The synthesized catalyst was found photoactive under visible light irradiation, and maximum photocatalytic performance was observed at acidic pH and decreased at alkaline pH due to the net electrostatic repulsion.

The effect of adsorption during the photocatalytic dye degradation using nano-ZnO supported on AC prepared by simple coprecipitation method was studied by Raizada et al. (2014), and they observed that the composite particles exhibited simultaneous photocatalytic activity and adsorption resulting in higher degradation of dyes. A similar kind of study where ZnO supported on AC was prepared by simple mixing resulted in less photodegradation of 2,4-dichlorophenol (Melian et al., 2009). The higher adsorption affinity of the compound to AC resulted in lower diffusion to the catalyst surface and resulted in reducing the photocatalytic degradation rate.

The easy recovery of catalysts after photocatalytic studies can be facilitated by functionalizing AC to make magnetic AC, and thus convenient recovery is possible under an external magnetic field (Ma et al., 2017). F-N-codoped TiO_2 particles supported on magnetic activated carbon were synthesized by coprecipitation for the degradation of salicylic acid. The catalyst remained stable for four repeated degradation cycles and the removal rate to 62.3% degradation from 76.3% after the fourth cycle.

Apart from TiO_2 and ZnO, several other photocatalysts supported on AC were used for photocatalytic degradation of organic compounds. Wang, Fan, and Chang (2009) prepared a $ZnFe_2O_4/TiO_2$ composite photocatalyst supported on AC by combining sol-gel process and dipping impregnation method for the degradation of an acid dye inside a recycle fluidized bed reactor. The degradation followed pseudo-first-order kinetics with increase in degradation rate with increasing $ZnFe_2O_4/TiO_2$-AC loading amount. A similar visible light active photocatalyst, Ag/AgCl-AC composite, was prepared

This book belongs to Central Library BADJI Mokhtar-ANNABA UNIVERSITY Copyright Elsevier 2024

using an impregnation-precipitation-photoreduction method by Gamage McEvoy et al. (2014) for the abatement of methyl orange and phenol. A synergistic adsorption-photocatalysis mechanism was observed due to the combined action of Ag (electron/hole generator), AgCl (electron charge separation by the polarization of photoinduced charges), and AC (adsorption site), which facilitated the compound degradation. Similarly, several catalysts such as zirconium oxide, tungsten-doped TiO_2, Ag-TiO_2, and Er^{3+}/$YFeO_3$-doped TiO_2 supported on AC were successfully used for photocatalytic studies (Hou et al., 2012b; Qin et al., 2012; Suresh, Vijaya, & Kennedy, 2014; Zhang et al., 2005).

Activated carbon fibers (ACF) having higher adsorption capacity were used by Shi (2009) for supporting Fe(III)- and Ho(III)-codoped TiO_2 films loaded for the photocatalytic removal of methyl orange. These materials are a kind of microporous carbon material possessing greater adsorption and desorption rates than granulated activated carbon (GAC) that had efficiently decontaminated methyl orange in water. They are produced in the form of cloth or felt with a higher specific area and micropore volume having larger adsorption ability (Zhao et al., 2010). In another study, Yao et al. (2014) synthesized ACF-supported Ce-doped TiO_2 for the photocatalytic degradation of methylene orange. They were able to reuse the composite catalyst for four cycles of experiments with a slight reduction in photocatalytic activity.

2.2 Mesoporous carbon

Porous carbon materials with controlled pore size, thermal and chemical stability, and interconnected pore structure can be effectively used a catalyst supports for photocatalysis (Bo et al., 2013; Chen et al., 2012; Yi et al., 2008). Supporting the photocatalyst on a porous material with higher specific surface area and small crystal size will improve the photocatalytic activity by preventing the agglomeration of particles (Chen et al., 2012). Owing to excellent conductivity, chemical stability, and corrosion resistance, mesoporous carbon remains as an excellent component of photocatalyst (Wang et al., 2017). Yi et al. (2008) observed an enhanced photocatalytic degradation of rhodamine B for TiO_2 supported on mesoporous graphite carbon due to the smaller size of the composite, higher surface area, and improved conductivity of the support all of which facilitate easy transfer of electrons and holes. Similarly a highly efficient visible light photocatalyst Bi_2WO_6 powder supported on mesoporous carbon synthesized via a simple hydrothermal process was used for the decoloration of rhodamine B under visible light (Chen et al., 2012). The presence of mesoporous carbon (MC) support significantly improved the photon absorption property and crystallization of Bi_2WO_6 species and enhanced the oxidative decomposition of rhodamine B. A synergistic effect of adsorption and photocatalytic degradation of methyl orange was observed by Bo et al. (2013) for TiO_2/MC composites due to its excellent electron conductivity and reduced recombination rates. The higher surface area of the composites resulted in more adsorption of the compound to its surface and improved the photocatalytic reaction rates.

2.3 Fullerene

Fullerene (C_{60}) is receiving great consideration due to its extraordinary physical, chemical, and structural properties along with their unique electronic properties owing to its delocalized conjugated assembly (Khalid et al., 2017). Moreover, carbon nanotubes are considered to be the cylindrical version of fullerene. Fullerene consists of closed shell structure having 30 bonding molecular orbits with 60 π-electrons that makes it as an excellent electron acceptor and can accept as many as six

This book belongs to Central Library BADJI Mokhtar-ANNABA UNIVERSITY Copyright Elsevier 2024

electrons (Apostolopoulou et al., 2009; Hasobe et al., 2006; Kratschmer, Lamb, Fostiropoulos, & Huffman, 1990). It is a well suitable material for electron transfer reactions since the structural change during the reaction is negligible. Thus C_{60} has the property of efficiently retarding the recombination of charge carriers. Moreover, fullerene not only absorbs the UV light range strongly but also responses to the visible region reasonably (Guldi, Prato, & Farmaceutiche, 2000; Khalid et al., 2017). Hence it also can act as the good sensitizer to give electrons when combined with the photocatalyst semiconductor during the illumination of the visible light source. However, fullerene lacks the active sites on the cages for the direct catalytic applications. Importantly, fullerene cages are highly hydrophobic in nature; also, it is insoluble in water and other polar solvents. Many researchers had reported the surface modification of fullerene by hydroxyl functional groups to introduce the fullerene in a polar environment. The surface functionalization of fullerene with hydroxyl groups produces polyhydroxylated fullerene (PHF), which is also called as fullerenols. Also the functionalization of fullerene could also enhance the electron donor-acceptor property of fullerene-TiO_2 photocatalyst (Khalid et al., 2017; Krishna et al., 2006, 2008).

Krishna et al. (2006) studied the enhancement in the photocatalytic activity of TiO_2 along with water-soluble PHF while treating the organic dye procion red. At low pH, high amount of PHF was adsorbed to the surface of TiO_2 through electrostatic interactions. The optimum surface coverage of TiO_2 by PHF was determined through dosage optimizing experiments along with the dye degradation studies. The optimum dosage ratio of PHF to TiO_2 was found to be 0.001 (wt/wt), which exhibited the maximum degradation efficiency. Long et al. (2009) performed the degradation studies of rhodamine B using C_{60}-incorporated TiO_2 nanorods under visible light. C_{60}-incorporated TiO_2 nanorods were synthesized through the hydrothermal process. The enhancement in the visible light was about 3.3 times higher than the bare TiO_2 nanorods and 2.7 times higher than the Degussa P25. The improvement in the removal efficiency at the visible range is ascribed to the efficient separation of charge carrier species due to the incorporation of fullerene C_{60}. Zhang et al. (2010b) studied the performance of TiO_2 photocatalyst along with the surface hybridization of fullerene C_{60} at visible light. C_{60}-hybridized TiO_2 exhibited about four times higher performance than Degussa P25. The enhancement in the performance of photocatalysis is mainly due to the increased migration efficiency of the photogenerated electrons at the interface between TiO_2 and fullerene C_{60}. Surface hybridization increased the conjugation between TiO_2 and fullerene C_{60}, thus increasing the migration efficiency of photogenerated electrons. The enhancement in the performance was mainly depending on the surface coverage of the TiO_2 photocatalyst by fullerene C_{60}. The optimum loading ratio between C_{60} and TiO_2 is estimated to be 2.5%.

Da Meng et al. (2012) developed the metal-fullerene/TiO_2 composites such as Pt-fullerene/TiO_2, Pd-fullerene/TiO_2, and Y-fullerene/TiO_2 by sol-gel method for the removal of methylene blue. The quantum efficiency of the metal-fullerene/TiO_2 composites is as follows: Pd-fullerene/TiO_2 > Pt-fullerene/TiO_2 > Y-fullerene/TiO_2. Among all the composites, Pd-fullerene/TiO_2 showed very good performance mainly because of the reduced charge transference potential and increased photoabsorption effect resulted due to the synergistic effects exerted by fullerene and the metal dopant. Bai et al. (2012) examined the thin and transparent photocatalytic layer for the rapid microbial disinfection. The coating contains PHF as the photocatalytic enhancer for the TiO_2 semiconductor photocatalyst. Nanocomposites of PHF/TiO_2 were synthesized through physical mixing in aqueous suspension. The optimum ratio of PHF/TiO_2 was found as 0.01 through the photocatalytic degradation of procion red MX-5B under UV irradiation. The dye degradation rate was two times higher than the bare TiO_2. Later the PHF/TiO_2 composite was used to inactivate the spores of common household fungus *Aspergillus niger*. The inactivation rate was three times higher than the bare TiO_2.

This book belongs to Central Library BADJI Mokhtar-ANNABA UNIVERSITY Copyright Elsevier 2024

Cho et al. (2015) studied the fullerene C_{60}- and C_{70}-decorated TiO_2 nanowires for the enhancement in the photocatalysis under visible light. Fullerene-modified TiO_2 nanowire was synthesized through interfacial chemical bonding. The results revealed that the fullerene derivatives improve photoactivity by acting as the electron sink. Significant enhancement in the removal of methylene blue was observed at the visible light. The study also suggested that the C_{60}- and C_{70}-modified TiO_2 nanowire can also be used in the solar photocatalysis processes where fullerene derivatives act as the sensitizer for expanding the solar light utilization range to the visible range. Hamandi et al. (2017) studied the enhancement in the photocatalytic properties of PHF incorporation on calcined hydrogenotitanate nanotubes (HNT). The synthesized PHF/HNT composite was used for the formic acid degradation. Incorporation of PHF on TiO_2 nanotubes was studied before and after calcination of TiO_2 nanotubes. Incorporation of PHF on the already calcined TiO_2 nanotubes helped in maintaining the surface oxygen vacancies, which resulted in maintaining the anatase crystallinity of TiO_2 nanotubes and increased faradic current across the interfaces. Hence, significant enhancement in the photocatalytic activity was observed.

2.4 Carbon nanotubes

Carbon nanotubes (CNTs) are considered to be the promising material in various fields of application due to its excellent structural, thermal, electrical, and mechanical properties associated to its one-dimensional structures (Khalid et al., 2017; Leary & Westwood, 2010; Serp et al., 2003). CNTs exhibit enhancement in the photocatalytic performance of TiO_2 due to high surface area and high-quality surface active sites, by increasing the lifetime of the photogenerated electron-hole pair (Akhavan et al., 2009; Serp et al., 2003). Moreover, CNTs participate in greater control over surface morphology in different forms of the CNTs-TiO_2 photocatalysts (Li et al., 2011; Yu et al., 2007). For providing the high-quality surface active sites, CNTs are categorized into (i) single-walled CNTs (SWCNTs) that contain a cylindrical shaped single-atom carbon sheets with the total surface area of 400–900 $m^2\ g^{-1}$ and (ii) multiwalled CNTs (MWCNTs) that consist multiple concentric nanotubes with the total surface area of 200–400 $m^2\ g^{-1}$ (Gao et al., 2008; Gao, Chen, & Li, 2009; Leary & Westwood, 2010; Serp et al., 2003). The surface chemistry involving in the CNTs-TiO_2 can be modified to enhance the selective adsorption toward the specific contaminants. Moreover, CNTs have the huge electron storage capacity within the structure, which is about one electron for every 32 carbon atoms (Kongkanand & Kamat, 2007). Hence it has the excellent charge transfer capability, which could facilitate the fast transfer of electrons between TiO_2 and CNTs. The surface modifications of CNTs are made through the formation of surface alcohol, keto, and acid groups. The surface functionalization of CNT can be done to attain strong surface interaction with the TiO_2 (Bandosz, 2009).

The widely reported synergistic photocatalysis enhancement mechanism in CNT composite is through retarding the recombination rate of photogenerated electron-hole pair. One of the mechanisms of photocatalytic enhancement elucidated based on the capability of CNTs to form Schottky barrier at the interface of CNTs-TiO_2, which comprises the space charge region (Chen et al., 2005; Leary & Westwood, 2010). During the irradiation the photogenerated electrons freely move toward the surface of CNT, which lower the Fermi level. Hence CNT can act as the electron sink that creates the hole in the valence band of TiO_2 (Chen et al., 2005; Kongkanand & Kamat, 2007; Leary & Westwood, 2010). These holes can move toward the surface of TiO_2 and participate in the contaminant degradation reactions. In this case, TiO_2 acts as the p-type semiconductor, whereas TiO_2 is the n-type semiconductor in general (Chen et al., 2005). Secondly, CNTs can act as the photosensitizer, which enhances the

This book belongs to Central Library BADJI Mokhtar-ANNABA UNIVERSITY
Copyright Elsevier 2024

photocatalytic activity by transferring electrons to TiO_2. This behavior may be the reason for extending the photocatalytic activity in the visible region (Wang et al., 2005, 2009). In this process, photogeneration of electrons happens at the surface of CNTs. These photogenerated electrons transferred to the conduction band of TiO_2 and then form the superoxide radicals in reaction with the adsorbed molecular oxygen at the surface of TiO_2 (Leary & Westwood, 2010; Oh, Jung, & Ko, 2009). As a result the positively charged CNTs take the electrons away from the valence band of TiO_2, leaving the holes. These holes generated at TiO_2 further participate in the oxidation of contaminants.

Wang et al. (2009) studied the photocatalytic degradation of 2,4-dinitrophenol using MWCNTs/TiO_2 photocatalyst under solar irradiation. MWCNTs/TiO_2 photocatalyst was synthesized using sol-gel technique. The results reported that the addition of MWCNTs had significantly enhanced the photocatalytic activity due to the increased electron transfer ability between TiO_2 and MWCNTs, which could possibly retard the recombination rate of the photogenerated electron-hole pair. The maximum degradation rate was attained at the optimal MWCNT-to-TiO_2 ratio of 0.05% (wt/wt%). Similarly, Wang et al. (2010) reported the solar photocatalytic degradation of mordant black 7 and reactive light yellow azo dyes using MWCNT/TiO_2 photocatalyst. The optimum ratio between MWCNTs and TiO_2 was found to be 0.07% (wt/wt%), and the complete removal of dyes was observed within 240 min of solar irradiation. Zhou et al. (2010) elucidated the bonding TiO_2/SWCNTs through a facile sol-solvothermal technique. The characterization results confirmed that TiO_2 and SWCNTs were linked entirely through ester bonds, which could help in enhancing the interface electron transfer activities. Thus the recombination between the photogenerated electron and hole was reduced, and the enhancement in the degradation of rhodamine B and nitrobenzene was observed. Moreover, the higher surface area of SWCNTs provided huge active sites for the photocatalytic reaction. A higher photocatalytic activity was observed with bonding in TiO_2/SWCNT photocatalyst than the Degussa P25 (~91%). Peining et al. (2011) reported the synthesis of rice grain-shaped TiO_2-MWCNT nanocomposites by electrospinning method. The complete integration of MWCNTs along with the TiO_2 was observed mainly through the Ti-O-C chemical bonding. The enhancement in the photocatalytic activity was studied through the degradation of alizarin red dye in comparison with the Degussa P25. The enhancement in the photocatalytic activity is attributed to increased charge separation due to the single crystalline nature, enhanced surface area, pore size, and pore volume.

Li et al. (2013b) demonstrated the phosphate-functionalized MWCNT-TiO_2 composites for the enhanced oxygen adsorption on MWCNT. The composite was synthesized through one-pot phase-separated hydrolysis-solvothermal technique. In general the photocatalysis process is reported to be much efficient when the photoexcited electrons are captured efficiently. In most cases, oxygen is used as the electron acceptor. The phosphate present in the phosphate-functionalized MWCNT-TiO_2 composite enhanced the oxygen adsorption on the surface of TiO_2 and thus prevents the development of negative charge on the composite. This phenomenon helps in charge separation and enhances degradation significantly. They have also observed the variation in the degradation of colored and noncolored contaminants significantly. MWCNT-TiO_2 composite exhibited a higher rate for the removal of colored contaminants, whereas the rate was low for the noncolored contaminants. This variation was significantly controlled through the use of phosphate-functionalized MWCNT-TiO_2 composite by enhancing the electron capture ability via increased oxygen adsorption on TiO_2. Natarajan et al. (2016) studied the rhodamine 6G dye degradation using MWCNT-loaded TiO_2 nanotube (TNT) composite synthesized through hydrothermal method. Experimental results revealed that about 10% w/w loading of MWCNT on TNT exhibited higher removal efficiency (89%) than the bare TNT (78%) and Degussa

This book belongs to Central Library BADJI Mokhtar-ANNABA UNIVERSITY Copyright Elsevier 2024

P-25 (60%). The 10% w/w MWCNT-TNT exhibited higher removal efficiency mainly because of the unique tubular structure and high electronic conductance property that attributed to the higher active sites, and fast transfer of the electrons to tubular structure of MWCNTs resulted in the retardation of the recombination effect. The study also elucidated the correlation of photoluminescence with the recombination rate. Lesser photoluminescence intensity indicates lower recombination rate.

Chaudhary, Khare, and Vankar (2016) studied the degradation of methylene blue using Ag nanoparticle-loaded TiO_2/MWCNT composite under UV and visible light irradiation. About nine times higher the degradation rate was observed with Ag/TiO_2/MWCNTs than the TiO_2/MWCNTs when irradiated with visible light. The enhancement in the degradation efficiency is resulted mainly due to the synergistic interaction between the Ag and MWCNT. The charge transfer efficiency is enhanced mainly due to the formation of the Schottky barrier at Ag/TiO_2 interface where MWCNT act as the electron sink. About 98.5% of removal efficiency was observed in 80 min under visible light irradiation, whereas about 97% of removal efficiency was observed in 35 min of UV light irradiation.

2.5 Graphene

Graphene, the wonder kid among the carbon allotropes, is the two-dimensional honeycomb spatial arrangement of sp^2 carbon atoms. It can be considered as the basic building block of all other graphitic materials with different dimensionalities such as 0D fullerenes, 1D nanotubes, and 3D graphite (Geim & Novoselov, 2007). Graphene can be chemically or physically exfoliated from graphite through chemical vapor deposition, thermal exfoliation, mechanical cleavage, and chemical functionalization (Green & Hersam, 2010; Hummers & Offeman, 1958; Juang et al., 2010; Novoselov, Jiang, et al., 2005; Park & Ruoff, 2009; Schniepp et al., 2006; Wei et al., 2009).

Long-range π-electron conjugation provides extraordinary properties to graphene, including exceptional thermal; mechanical; and electrical properties (Allen, Tung, & Kaner, 2010) such as high thermal conductivity ($5000\,Wm^{-1}\,K^{-1}$) (Balandin et al., 2008), high charge carrier mobility of $>200{,}000\,cm^2\,V^{-1}\,s^{-1}$ at electron densities of $\sim 2\times 10^{11}\,cm^{-2}$ (Bolotin et al., 2008), and high specific surface area up to $2630\,m^2\,g^{-1}$ (Steurer et al., 2009). The charge carriers in graphene resemble two-dimensional Dirac fermions, and thus it is able to give a minimum value of conductivity, even when the charge carrier concentration is zero (Novoselov, Geim, et al., 2005).

Graphene can also act as good supporting material, allowing semiconductor particles such as TiO_2 to anchor on its surface and can form efficient heterojunction that can facilitate better charge transfer through intimate contact (Yamashita & Li, 2016). In the two-dimensional structure of graphene, both outer and inner surfaces are available for interaction. So, efficient adsorption of pollutant molecules, anchoring of photocatalyst particles, and diffusion of charge carriers are possible (Xie, Kretschmer, & Wang, 2013). Such utilization of inner surfaces is not possible in other carbonaceous graphitic materials such as 0D fullerenes and 1D nanotubes. The ease of preparation from graphite and the low-cost availability of graphite as compared with SWNTs make it more attractive among other carbonaceous nanomaterials (Stankovich et al., 2006). All these characteristics make graphene a promising material for energy and environmental applications ever since the discovery by Novoselov et al. in 2004 by physical exfoliation (Novoselov et al., 2004).

Pristine graphene is a zero bandgap semimetallic material consisting of solely sp^2-hybridized carbon atoms (Li & Kaner, 2012) where its bonding π-orbitals and antibonding π^* orbitals degenerate and its valence and conduction bands touch in the Brillouin zone (Putri et al., 2015; Xie et al., 2013). Thus it

This book belongs to Central Library BADJI Mokhtar-ANNABA UNIVERSITY Copyright Elsevier 2024

is a hydrophobic, inert material. While the formation of graphene oxide (GO), considerable disruption of graphene electronic properties by breaking the Π conjugation of graphene and forms sp^3 hybridized carbon atoms by covalently bonded to oxygen groups along with sp^2 hybridized carbons, makes it an insulator (Lu et al., 2012a; Xie et al., 2013; Zhang et al., 2015). Thus GO, the highly oxidized form of graphene that is abundant with oxygen containing functional groups like hydroxyl, carbonyl, and epoxy groups, shows excellent reactant interaction and easy dispersion in polar solvents like water due to improved hydrophilicity (Shahriary & Athawale, 2014; Zaaba et al., 2017). Despite all these benefits the presence of polar functional groups lowers the conductivity and carrier mobility (Bagri et al., 2010) and, in turn, diminishes the photoactivity as compared with pristine graphene (Liang et al., 2011). Thus GO is a good tool for adsorptive removal of pollutants but a poor performer in photocatalysis.

The sp^3/sp^2 carbon fraction of GO can be appropriately tuned by oxidizing/reducing GO, which in turn can make GO into semimetallic, semiconducting, or insulating material (Putri et al., 2015). To retain the conductive properties to an extent, the polar oxygen functional groups in GO can be removed by various reduction conditions. Graphene-like properties can be regained through the chemical or thermal reduction of GO to form reduced GO (rGO) (Yang et al., 2008). This rGO is otherwise called chemically modified graphene. The reduced graphene oxide, formed by the reduction of GO, is almost devoid of GO basal functional groups and resembles graphene with less conductive and more defective sites than mechanically exfoliated graphene. Pristine graphene is a zero bandgap semimetal, while rGO is a semiconductor with tunable bandgap (Trapalis, Todorova, & Giannakopoulou, 2016). Along with providing enhanced photoactivity, rGO is found to be a strong material and provides mechanical properties to the composite (Eigler, Dotzer, & Hirsch, 2012).

The relatively easy synthesis methods and flexibility to modifications through doping and the hydrophilic nature as compared with pristine graphene make GO/rGO research in water purification more interesting (Avouris & Dimitrakopoulos, 2012; Gandhi, Vasudevan, & Shibayama, 2016; Song et al., 2012; Zhang et al., 2010a).

Two different strategies, namely, the top-down process and bottom-up process, are in usage for developing graphene. Of these, solvent-based, Hummer's method and its modifications, a top-down process where the graphite flakes are oxidized to GO by strong oxidizing agents is the extensively used method (Hummers & Offeman, 1958). Thus, through oxidation, oxygen functional groups such as carboxyl, hydroxyl, and epoxides are introduced between the layers that make them partially separated which then exfoliated using ultrasonication or stirring. Later, rGO can be synthesized from GO by chemical or thermal reduction (Fig. 2).

2.5.1 Synthesis of graphene-based photocatalyst composites

The synthesis strategies adopted for fabricating graphene-based semiconductor photocatalysts can be broadly categorized into in situ method and ex situ method. In in situ procedure the nucleation and growth of semiconductor nanoparticles take place on the surface of the graphene sheet. Normally the metal precursors (e.g., metal salts) and the precursors of graphene (e.g., solvent-exfoliated graphene, GO) are dispersed in a suitable solvent. Then an appropriate treatment is provided in terms of chemical, thermal, optical, or ultrasonic means so that the metal salts get converted into nanoparticles and get anchored on the graphene surface. Based on the experimental conditions, a variety of nanostructures such as nanowires (Cao et al., 2014; Dai et al., 2014; Lu et al., 2012b), nanoparticles (Jiang et al., 2011), nanospheres (Liang et al., 2012), nanotubes (Perera et al., 2012), and microstructures such as microspheres (Liu et al., 2016) can be yielded with a morphology different than its

This book belongs to Central Library BADJI Mokhtar-ANNABA UNIVERSITY Copyright Elsevier 2024

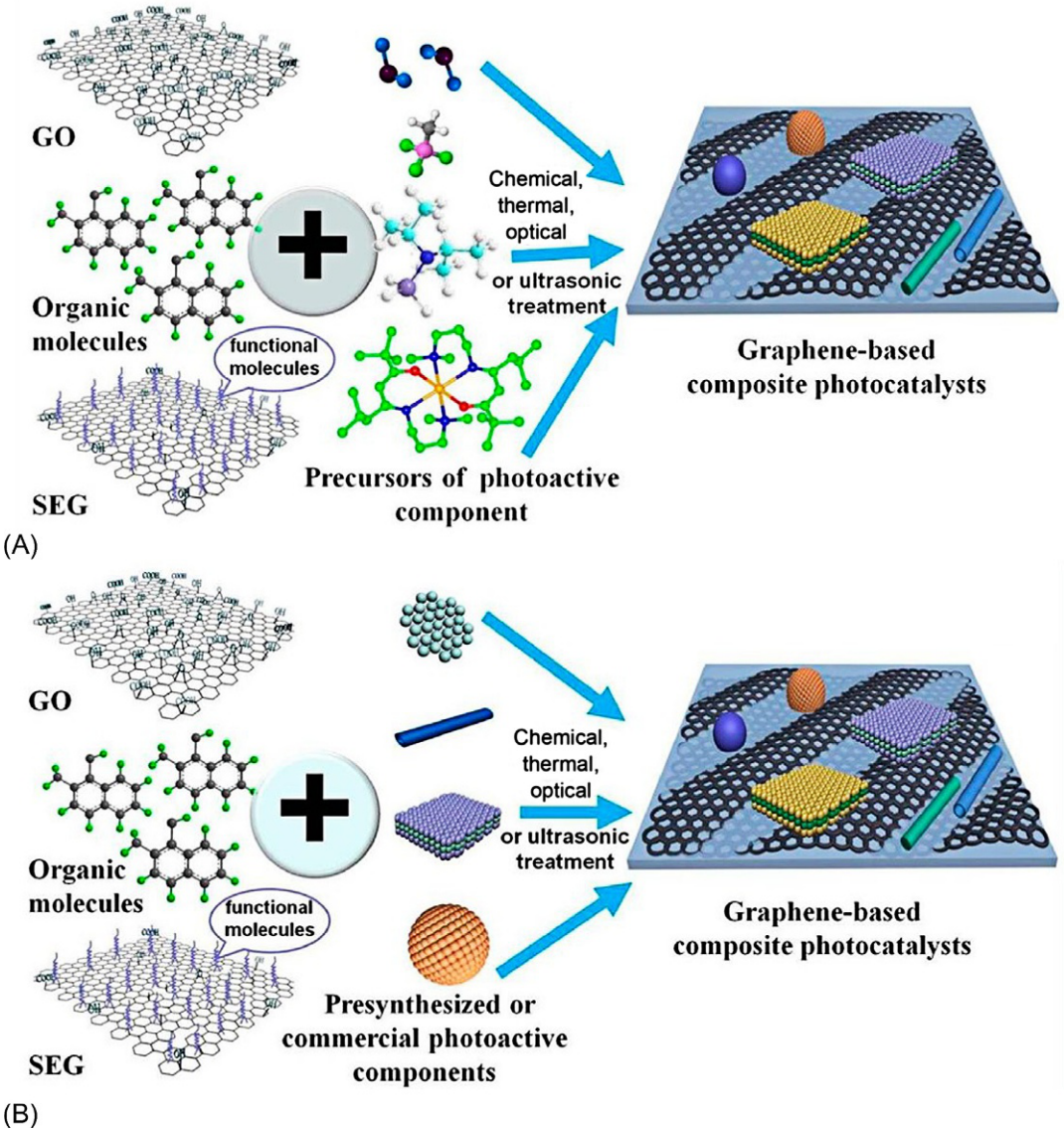

FIG. 2

The different synthesis strategies for semiconductor/graphene composite formation. (A) In situ procedure and (B) ex situ procedure.

Reproduced with permission from *Zhang, N. et al. (2015). Waltzing with the versatile platform of graphene to synthesize composite photocatalysts.* Chemical Reviews. *doi:10.1021/acs.chemrev.5b00267. Copyright © 2015, American Chemical Society.*

This book belongs to Central Library BADJI Mokhtar-ANNABA UNIVERSITY Copyright Elsevier 2024

precursors. The oxygen functional groups in modified graphene, GO, can act as nucleation and growth sites for the nanoparticles and, in turn, can be reduced to rGO during treatment. In situ growth strategies prevent agglomeration of semiconductor nanoparticles (Song et al., 2011; Xiang, Yu, & Jaroniec, 2012). In situ strategy improves charge carrier separation and thus overall photocatalytic activity through providing uniform coverage of nanostructures on graphene sheets and good interfacial contact, which helps (Zhang et al., 2015; Zhang, Zhang, & Xu, 2012). In situ synthesis can be done by adopting solution mixing, hydrothermal/solvothermal process, sol-gel method, combustion method, microwave-assisted deposition, electrochemical deposition, photoassisted reduction, etc. (Chowdhury & Balasubramanian, 2014a).

In ex situ strategies the predeveloped semiconductor nanoparticles mixed with graphene precursors, followed by an appropriate treatment for anchoring nanoparticles on the surface of graphene. Simultaneously, GO gets reduced to rGO. Here the nanoparticle morphology and nanostructure are not altered by the composite formation (Weng et al., 2014a, 2014b). Thus, for the preselection of nanostructures having desired functionalities or for the precise control of size, shape, and morphology of nanostructures even after the composite formation, ex situ methods are preferable (Chowdhury & Balasubramanian, 2014a). Surface modification can be carried out for both precursors, prior to mixing for improving nanoparticle deposition (Weng et al., 2014a, 2014b). This synthesis route is especially preferable for comparison studies between bare nanoparticles and hybridized nanoparticles. But the limitations of this strategy include the less efficiency in terms of interfacial contact, carrier mobility, and photocatalytic activity as compared with in situ procedures (Zhang et al., 2015), poor utilization of extraordinary structural benefits of graphene, and nonuniform dispersion and poor coverage of nanoparticles over graphene sheet (Zhang, Zhang, & Xu, 2012).

2.5.2 Benefits of graphene/semiconductor composite

Photoelectron mediator and acceptor

When a heterojunction is developed, electrons tend to flow from the material having higher Fermi level to the material having lower Fermi level, till the Fermi energy levels become in line (Woan et al., 2009). Due to the high work function of graphene (4.42 eV) and the more positive Fermi level (−0.08 V vs NHE), than most semiconductors (Gao et al., 2011; Han et al., 2014a), there is an instantaneous transfer of photogenerated electrons from the conduction band of semiconductors to graphene sheets when they are in contact (Fig. 3A and B) (Jianwei et al., 2013). Further, due to the high charge carrier mobility of graphene at room temperature, the transferred electrons can move through the graphene sheets with ease. Consequently the recombination rate can be considerably reduced. In graphene, these photogenerated electrons can then be captured by electron acceptors, which increase the photocatalytic performances toward different applications (Xie et al., 2013). On the one hand, electrons transferred to graphene matrix can react with surface-adsorbed O_2 to form superoxide radical species or H_2O_2 (Weng et al., 2014a, 2014b), which can be further utilized for oxidative removal of pollutants (Zhang et al., 2013). On the other hand, those transferred electrons can directly reduce the nitrocompounds adsorbed on graphene (Xiao, Miao, & Liu, 2014).

The major steps involved in the electron transfer mechanism between TiO_2 and graphene for the degradation of pollutant under UV light irradiation are as per the following Eqs. (1)–(5) (Xiang et al., 2012):

$$TiO_2 + h\nu \rightarrow TiO_2\,(e^- + h^+) \tag{1}$$

$$TiO_2\,(e^-) + \text{Graphene} \rightarrow TiO_2 + \text{Graphene}\,(e^-) \tag{2}$$

This book belongs to Central Library BADJI Mokhtar-ANNABA UNIVERSITY
Copyright Elsevier 2024

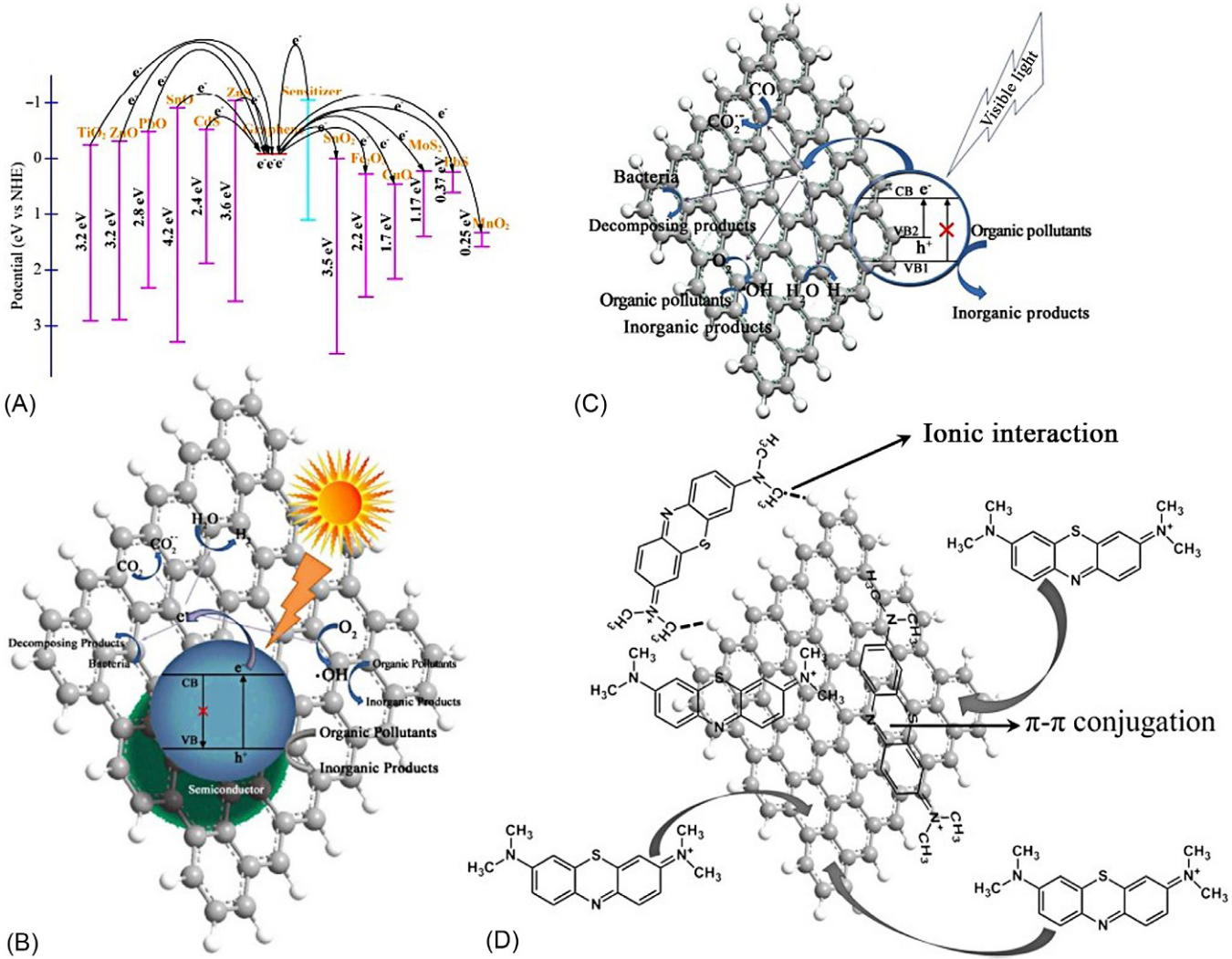

FIG. 3

Photocatalytic enhancement mechanism by graphene. (A) Bandgap comparison of graphene with common semiconductor materials, (B) photoelectron mediator and acceptor, (C) bandgap narrowing, and (D) enhanced adsorption of reactants.

Reproduced with permission from *Jianwei, C., et al. (2013). Recent progress in the preparation and application of semiconductor/graphene composite photocatalysts.* Chinese Journal of Catalysis, 34*(4), pp. 621–640. doi:10.1016/S1872-2067(12)60530-0. Copyright © 2013 Dalian Institute of Chemical Physics, the Chinese Academy of Sciences. Published by Elsevier B·V. All rights reserved.*

This book belongs to Central Library BADJI Mokhtar-ANNABA UNIVERSITY

Copyright Elsevier 2024

$$\text{Graphene}\,(e^-) + O_2 \rightarrow \text{Graphene} + O_2^- \tag{3}$$

$$TiO_2\,(h^+) + OH^- \rightarrow TiO_2 + {}^{\bullet}OH \tag{4}$$

$${}^{\bullet}OH + \text{Pollutants} \rightarrow \text{Degradation products} \tag{5}$$

Unlike other dopants such as noble metals, which are trapping electrons, graphene can store and shuttle electrons. The ability of graphene to act as a pathway for photoexcited electrons is revealed by the work of Liu et al. (2016). According to their observations, rGO transmits the photoexcited electron from the conduction band of {1 0 1} facets to the valence band of {0 0 1} facet-exposed TiO_2 nanocrystals, thus facilitating the redox reactions, especially reduction of Cr(VI) and oxidation of rhodamine B simultaneously (Liu et al., 2016).

Extended light absorption range

An efficient photocatalyst composite should be able to harvest the visible light, which accounts for 43% of the whole solar spectrum (Grabstanowicz et al., 2013; Schultz et al., 2014). Instead, most of the widely studied semiconductor photocatalysts (e.g., TiO_2 and ZnO) depend primarily on UV radiation, which is only 4% of the total spectrum (Addamo et al., 2006). Doping semiconductor material with graphene is a promising strategy to overcome this limitation. Surface carbon doping with graphene results in covalent bonding between semiconductor and graphene. For example, in TiO_2/graphene composite, the presence of π electrons on graphene can bond with the surface titanium atoms of TiO_2 to form interfacial Ti-O-C or C—Ti bonds (Liu et al., 2013; Zhang et al., 2010a). The energy that favored hybridization between O2p and C2p atomic orbitals can create few midgap states closer to TiO_2 valence band (Li et al., 2013a) and thus lead to bandgap narrowing and in turn a red-shift in the absorption range (Fig. 3C) (Zhang et al., 2010a).

P25-rGO has shown a bandgap of ca. 3.06 eV instead of the 3.22 eV of P25, thus extending absorption to visible spectrum (Hou et al., 2012a). Zhang et al. (2010a) found photoactivity of P25-G in violet-blue region in electromagnetic spectrum range of ca. 430–440 nm, absorption edge red-shifted of ca. 30–40 nm compared with bare P25. Thus significant visible light photodegradation of pollutants is possible. Several works have shown the visible light activity of UV active metal oxide/metal sulfide nanoparticles, when hybridized with graphene (Guo et al., 2011; Hou et al., 2012a; Jiang et al., 2011; Li & Cao, 2011; Liu et al., 2013; Perera et al., 2012; Qianqian, Tang, & Guoxin, 2011; Stengl et al., 2013; Weng et al., 2014a, 2014b; Zhang et al., 2010a, 2012b).

Graphene as an adsorptivity enhancer

Surface adsorption is a mandatory step in photocatalysis. If the reactants (pollutants, H_2O, O_2, etc.) are efficiently preadsorbed on to the surface of the photocatalyst, the surface reaction probability can be significantly improved by effective utilization of photogenerated electrons and holes (Fox & Dulay, 1993; Liu et al., 2015a). The semiconductor nanoparticles itself are showing poor sorption property (Li, Zhao, & Ray, 2007; Xu, Gao, & Liu, 2002). Thus photocatalyst supported on to graphene, possessing extraordinary adsorption properties, is a good choice. In general the adsorbent-adsorbate interactions include π–π binding, electrostatic interaction, hydrophobic association, van der Waals interaction, and hydrogen bonds (Chagovets et al., 2012; Wang et al., 2015b; Xiao et al., 2016). The rGO/GO can interact to reactants through physical adsorption (π–π stacking interaction), chemical interaction (surface complexation), or electrostatic attraction through the available oxygen functional groups and/or defect sites (Li et al., 2016). The possible interactions in pollutant adsorption on

This book belongs to Central Library BADJI Mokhtar-ANNABA UNIVERSITY Copyright Elsevier 2024

graphene-based semiconductor composite are given in Fig. 3D. The increased adsorption of both target species (pollutant) and reactive species (electrons, holes, superoxide radicals, and hydroxyl radicals) on to the graphene matrix can significantly improve their contacts and thus total photoredox activity (Li et al., 2016).

The high theoretical surface area and surface-to-volume ratio of graphene contribute to the good adsorption ability (Williams, Seger, & Kamt, 2008; Zhang et al., 2011b). GO are decorated with the epoxy (C—O—C) and hydroxyl (—OH) functional groups on the basal plane and with carboxyl (—COOH) and carbonyl (—C═O) groups at the edges (Chowdhury & Balasubramanian, 2014b; Kim et al., 2010b; Stankovich et al., 2006). The oxygen functionalities and the corresponding sp^3 bonding are the reasons for the defects in GO (Hu, Song, & Lopez-valdivieso, 2015), when on getting reduced, epoxy/hydroxyl groups are considerably removed, while most of the carboxyl groups are retained (Xiao et al., 2016). Thus rGO possesses additional surface defects due to the vacancies by the functional group removal and residual oxygen impurities (Bagri et al., 2010; Eigler et al., 2012). Thus GO and rGO are ready to undergo covalent or noncovalent interactions with inorganic and organic compounds through these functional groups and/or defect sites (Chowdhury & Balasubramanian, 2014b). Moreover, both GO and rGO possess higher dispersion property in water medium as compared with graphene and graphite, due to the weakened interplanar π–π interactions or increased interplanar distance (Minitha et al., 2017). In addition, as rGO regains graphene-conjugated structure to an extent, it can act as good organic dye adsorbent particularly the aromatic complex dyes (Han et al., 2014b; Ramesha et al., 2011). A combined effect of noncovalent interactions probably initiated by the π–π conjugated structures, vacancy sites, and oxygen functional groups is proposed to be the reason behind the adsorption property of rGO (Minitha et al., 2017). Besides, it can bind to heavy metal ions through surface complexation (Zhao et al., 2011). Graphene nanomaterials and their derivatives are found to be benign adsorbents for ionic pollutants (heavy metal ions and nonmetal ions), hazardous organic dyes (methylene blue, methyl orange, orange G, rhodamine B, etc.), and other organic pollutants from aqueous solutions (Apul et al., 2012; Fakhri, 2013; Kemp et al., 2013; Liu et al., 2012; Minitha et al., 2017; Ramesha et al., 2011; Shen, Fang, & Chen, 2014; Wang et al., 2015a; Yang et al., 2011).

Selective adsorption of reactants

Selective photocatalysis is of special interest because it can develop specific practically feasible catalysts based on the application. The nonspecific oxidizing property of the strong oxidizing agent, hydroxyl radical, is a drawback of semiconductor photocatalysis (Xiang & Jaroniec, 2011). This limitation can be overcome by using surface tunable graphene-based materials. The graphene, GO, and rGO, through the ability to tune the chemical property by the presence of oxygen functionalities and through other surface modifications, can selectively adsorb pollutants, and thus specific degradation becomes possible (Upadhyay & Sinha, 2014). Lightcap, Kosel, and Kamat (2010) successfully anchored semiconductor (TiO_2) and metal (silver ions) nanoparticles into distinct sites on rGO, thus showing the possibility of selective adsorption in graphene-based materials.

In the case of graphene, the enhanced adsorptivity is not directly linked with specific surface area. Zhang et al. (2010a) have shown valid evidence toward the enhanced adsorptive property of graphene composite than other carbonaceous composites. They compared three catalysts (1) P25, (2) P25-CNTs, and (3) P25-graphene photocatalysts toward methylene blue (MB) dye degradation. In spite of the comparable BET specific area (47.572, 54.226, and 51.034 $m^2\,g^{-1}$ for P25, P25-CNTs, and P25-graphene, respectively), P25-graphene showed the best adsorption strength among them. Thus physical,

This book belongs to Central Library BADJI Mokhtar-ANNABA UNIVERSITY
Copyright Elsevier 2024

nonspecific adsorption emerging from the increased surface area is not the primary adsorption mechanism involved. The selective adsorption of aromatic dyes on to the graphene composite surface through the π-conjugation system is the reason behind the improved pollutant adsorption and degradation in graphene composites. Hou et al. (2012a) also given proof for the aforementioned mechanism by comparing adsorption and specific area of bare TiO_2, TiO_2-CNT, and TiO_2-graphene. Even though the specific surface area are comparable in three catalysts, about 96% of the initial dyes was decomposed by P25-graphene within 1 h under UV irradiation, the removal rate of pure P25 and P25-MWCNTs goes behind at nearly 68% and 73% after the same experimental conditions.

GO, as acidic in nature, can readily adsorb basic and cationic pollutants (Upadhyay & Sinha, 2014), compared with that of anionic pollutants. Because the interaction of cationic pollutants in GO composites predominantly through the electrostatic interaction with negatively charged GO surface provided by the oxygen functional groups (Minitha et al., 2017; Xiao et al., 2016). On the other hand, rGO can permit other interactions such as π–π interaction, hydrophobic association, and structural conjugation in addition to electrostatic interaction, which can give applicability to a wide variety of pollutants (Minitha et al., 2017). The large negative charge density in GO helps in the effective adsorption of cationic dyes on GO, with insignificant adsorption for anionic dyes. On the other hand, rGO as it does not possess a high negative charge is found to be a very good adsorbent for anionic dyes as well (Ramesha et al., 2011). Minitha et al. (2017) have proved the preferable adsorption possibility in GO as it provides higher adsorption of the cationic dye, methylene blue, as compared with an anionic dye, methyl orange, while rGO shows fast and efficient adsorption of both the cationic and anionic dyes.

Selective adsorption onto graphene sheets provides additional benefits such as uniform dispersion of nanoparticles over graphene sheet, size-controlled growth of nanoparticles, and efficient electron storing and shuttling (Lightcap et al., 2010).

Photosensitizer/photon absorber

Recent studies are revealing the ability of graphene to function as a visible light photosensitizer for photocatalysts (Du et al., 2011; Long, English, & Prezhdo, 2012). The semiconductor characteristics of rGO with a narrow bandgap make it a good candidate for visible light sensitizer for semiconductor nanoparticles (Li et al., 2016). When irradiated with visible light, photoexcited electrons of graphene can be directly injected to the conduction band of the semiconductor, from there to the active sites of the photocatalytic composite to generate oxidizing and/or reducing agents (Du et al., 2011; Xiang, Cheng, & Yu, 2015). Du et al. (2011) suggested the possibility of photosensitization property of graphene based on their work on TiO_2/graphene. But the robust experimental evidence confirming the photosensitizer role of graphene for the visible light activity in semiconductor-graphene composite is given by Zhang et al. (2012b). They have shown the macromolecular organic dye-like photosensitizer role of G to ZnS to make it visible light photoactive. Even though the bandgap narrowing is also accompanied in the composite, it is still insufficient for electron excitation under visible light irradiation. Thus the photosensitizer role of graphene is proved without doubt in the visible light photoactivity of ZnS-graphene nanocomposites toward the selective oxidation of alkenes and alcohols under ambient conditions. Yang and Xu (2013) also give an experimental proof for the same through the photocatalytic reduction of hexavalent chromium by ZnO-rGO under visible light irradiation.

Thus, for analyzing photosensitizer role of graphene in the corresponding graphene nanocomposite, three basic principles should be followed: (1) The semiconductor in the rGO-semiconductor

This book belongs to Central Library BADJI Mokhtar-ANNABA UNIVERSITY Copyright Elsevier 2024

composites should be visible light inactive, in spite of bandgap narrowing effect (Yang & Xu, 2013; Zhang et al., 2012b); (2) intimate interfacial interaction between metal oxide and graphene is essential (Yang & Xu, 2013; Zhang et al., 2012b); (3) the reacting substrate should be devoid of any other photosensitizing materials such as dyes (Yang & Xu, 2013).

Photothermal effect in graphene

Along with the widely studied mechanisms involved in the better photocatalytic pollutant degradation through graphene incorporation, such as electron trapping and shuttling, increasing light absorption range, and enhancing adsorption of pollutants, the photothermal effect of graphene in near IR illumination is also playing a significant role, which was underestimated in the past. Gan et al. (2014) have revealed for the first time the indirect contribution of photothermal effect of graphene for improved pollutant abatement. In the effective degradation of methylene blue by P25/rGO, >38% of the contribution is through photothermal effect. Even though NIR radiation itself is not able to generate electron-hole pairs, it can vary the temperature of graphene sheets through photothermal effect. Thus the excited electrons generated through UV/visible light when transferred to rGO matrix are moving through hot rGO sheet. The rise in temperature of graphene through photothermal effect can improve the electron mobility and thus the overall photocatalytic degradation efficiency. Neelgund and Oki (2018) are also providing evidence for the importance of photothermal effect in complete degradation of methyl orange by their studies on ZnO-graphene. They found the photothermal conversion efficiency of ZnO-graphene as 48.6%.

Other functions of graphene

Graphene is a good cocatalyst for semiconductor nanoparticles. Along with its role in improving photoactivity, it can support semiconductor nanoparticles by acting as nucleation site, can suppress its agglomeration, provides mechanical strength (Singh et al., 2018), and provides structural stability (Liang et al., 2012) and photostability by preventing leaching and inhibiting photocorrosion originating from the irreversible hole-driven oxidation reactions (Li et al., 2015a; Xian et al., 2014). Besides, the use of graphene composite film as photocatalyst helps to overcome the recovery and reuse issues in powder photocatalysts (Xiao et al., 2014) and promotes recyclability (Neelgund & Oki, 2018; Weng et al., 2014a, 2014b). The addition of graphene to TiO_2-CdS can lower the CdS leaching by ~8 times as compared with TiO_2-CdS (Xian et al., 2014). All of these features enhance the practical application of graphene composite photocatalysts.

2.5.3 Further modifications for improving results

In graphene-supported semiconductor photocatalysts, further enhancement in photoactivity can be achieved by (1) improving the quality of the constituents (graphene and semiconductor nanoparticles), (2) improving the interfacial interaction between the constituents, and (3) optimizing the system as a whole. Physiochemical properties of graphene can be improved by reducing the defect density and by chemical modifications.

Reducing defect density

The rGO derived from GO followed by Hummer's method contains oxygen functional groups and defect sites, through the disruption of sp^2 cloud. Although these imperfections and oxygen functionalities are beneficial for the interaction with reactants and for hydrophilic nature, the charge carrier mobility

This book belongs to Central Library BADJI Mokhtar-ANNABA UNIVERSITY
Copyright Elsevier 2024

and electrical conductivity and thus photoactivity of rGO are lower than pristine graphene composites. Despite these limitations, this chemical oxidation-reduction strategy is widely used due to the structure-directing role of GO in a solution phase and the easy processability for bulk synthesis (Yang et al., 2014). Thus advancing the synthesis strategies to reduce the defects in graphene is necessary. The another solution-based technique uses neither oxidation nor reduction step; instead, graphite is exfoliated into sheets through ultrasonication in an appropriate solvent medium to form solvent-exfoliated graphene (SEG) with lower defect sites and higher carrier mobility than chemically modified graphene (rGO), thus showing good photocatalytic activity (Green & Hersam, 2010; Liang et al., 2011). Even though SEG is replacing rGO in recent studies, low yield and low solution processability are restricting its application in photocatalysis (Yang et al., 2014). Thus no single synthesis strategy is currently available for wide application range. Based on the requirement the available techniques need to be tailored for emphasizing benefits and lowering the limitations.

Tuning the size, shape, and morphology of graphene and semiconductor nanoparticles could improve the quality of the constituents in composite. For example, the development of peculiar dimensionality structures for semiconductor-graphene composite such as 1D semiconductor-2D graphene and 2D semiconductor-2D graphene has integratively influence the overall performance of photocatalysts (Yang et al., 2014). Besides the typical 2D graphene sheets, other dimensionalities of graphene such as 0D graphene quantum dots, 1D graphene nanoribbons, and 3D nanostructures were also developed. These can be utilized as per the nanostructure of semiconductor material for ensuring effective contact through increasing the contact area and reducing the diffusion distance for charge carriers (Zhang et al., 2015). Three-dimensional nanostructures are more preferable in this aspect as it possesses accessibility to large surface area, resistance to aggregation, fast mass kinetics, development of distinctive microenvironment, and interconnected conductive framework (Hou et al., 2012a; Yang et al., 2014).

Increasing catalytically active sites on graphene/chemical modifications

As photocatalysis is a surface-mediated reaction, the active site availability is as much important as the carrier mobility. If there will be more active sites, the rate of pollutant degradation will be more. Active sites can be improved either by creating active sites, by substitutional doping, or by loading more co-catalysts with new active sites on to graphene sheets (Singh et al., 2018). The heteroatom doping to graphene by boron, nitrogen, phosphorus, and sulfur is effective for creating active sites (Duan et al., 2015; Putri et al., 2015). The presence of foreign atoms and the creation of defect sites on graphene sheets through doping can alter its electrical properties and thus can enhance the photocatalytic performance by choosing proper modifications based on the application. Chemical doping can be done as either surface transfer doping, where additional functional groups are being introduced, or substitutional doping, where carbon atoms of graphene lattice are substituted by foreign atoms. In surface transfer doping, based on whether the introduced functional groups tend to donate or draw electrons from graphene sheets, n-type or p-type conductivity is developing, respectively. As in the case of GO, the oxygen functional groups tend to draw electrons away from graphene sheet; thus GO is a p-type semiconductor. In substitutional doping, if carbon atom is replaced by an atom with more valence electrons, then n-type will result, but if replacement is with lesser valence electrons, it leads to p-type conductivity (Li et al., 2018; Putri et al., 2015). Chemical modifications in graphene can open a bandgap and can convert its semimetallic character to the semiconductor to either p-type or n-type depending on

This book belongs to Central Library BADJI Mokhtar-ANNABA UNIVERSITY Copyright Elsevier 2024

the dopant. The bandgap and thus the semiconductor properties can be tuned through optimizing dopant concentration (Li et al., 2018; Putri et al., 2015; Xie et al., 2013).

Improving heterojunction interaction

The electron transfer across the composite strongly depends on the interaction of semiconductor and graphene at the interface. Increasing the contact area and bonding at the heterojunction will lead to enhanced photoactivity, as it directly influences the electron transfer and thus charge carrier separation. Heterojunction interaction improvement can be done by doping, adopting in situ synthesis strategy, and developing electrostatic attraction between the constituents through surface charge modifications (e.g., p-n junction by cationic semiconductor N-doped rGO).

Optimization of the entire system

For achieving excellent photoactivity the entire system should be thoroughly considered and engineered. The benefits of graphene incorporation can be fully utilized by properly engineering the system by taking into consideration all the aspects of heteroatom interaction. Through this way the dimensionalities of the semiconductor nanoparticles should be suitable for maximizing the contact. The doping concentration of graphene is also a deciding factor as, if it exceeded than optimum concentration, the same graphene sheets can lower photoactivity through shielding effect by acting as recombination sites (Li et al., 2013a, 2015a; Zhang et al., 2010c, 2014).

The electron transfer pathway can be optimized by the introduction of some mediators such as metal ions (Ca^{2+}, Cr^{3+}, Fe^{2+}, Zn^{2+}, Ni^{2+}, Mn^{2+}, Co^{2+}, and Cu^{2+}) (Zhang et al., 2014) or noble metals, such as Pd (Han & Xu, 2014), in to the interfacial matrix. This can improve the photoelectron transfer and thus hinders the charge carrier recombination effectively. This strategy can in addition offset the shielding effect on over addition of graphene (Zhang et al., 2014).

2.6 Carbon quantum dots

Recently, carbon quantum dots (CQDs), a new class of carbon nanoparticles, have attracted much attention as a prospective competitor to conventional semiconductor quantum dots owing to its excellent optical absorptivity, chemical stability, nontoxicity, and facile synthesis. CQDs are the potential replacement for the toxic metal-based quantum dots. CQDs are being used in various fields of applications such as bioimaging, medical diagnosis, biosensing, chemical sensing, photocatalysis, and photovoltaic devices (Lim, Shen, & Gao, 2014). CQDs are characteristically quasispherical carbon nanoparticles composed of amorphous to crystalline carbon base. It is primarily made up of sp^2-graphitic carbon (or) graphene and graphene oxide sheets combined through the insertion of sp^3-hybridized carbon that exhibits fluorescence properties. Physicochemical properties of CQDs can be easily controlled through surface functionalization and surface passivation. Based on the route of synthesis, the oxygen functional groups present on CQDs can be varied in between 5% and 50% by weight (Baker & Baker, 2010). The solubility of CQDs in water and surface functionalization mainly depends on the presence of surface carboxylic groups, which is controlled by the synthesis route (Zhu et al., 2012). In general, CQDs are being synthesized in two routes, namely, the top-down and the bottom-up routes such as arc-discharge methods, ablation of a carbon target, chemical oxidation of soots, electrochemical oxidation of graphite rod, thermal route, microwave route, and supported synthesis (Baker & Baker, 2010; Cao et al., 2007; Li et al., 2010).

This book belongs to Central Library BADJI Mokhtar-ANNABA UNIVERSITY Copyright Elsevier 2024

Li et al. (2010) demonstrated the synthesis of TiO_2/CQDs and its photocatalytic application for the oxidative removal of methylene blue under visible light irradiation. The composite removed methylene blue completely within 25 min of treatment, whereas pure TiO_2 photocatalyst removed only <5% within the same duration. In the TiO_2/CQDs, CQDs not only help in harvesting the visible light but also facilitate in the transfer of photoexcited electrons and thus retard the recombination of electron-hole pairs. Yu et al. (2013) synthesized the CQD/TiO_2 nanosheet (TNS) composites by low thermal process in which TNS were dispersed in the CQD solution and then the dispersion was dried at 60°C. The characterization results revealed that the CQDs and TiO_2 nanosheets were well merged through the linkage between surface carbon-oxygen functional groups. The enhancement in the photocatalytic performance under visible light was investigated through the degradation of dye rhodamine B. CQD/TiO_2 nanosheets exhibited higher removal efficiency than the TNS and pure TiO_2. Enhancement in the photocatalytic activity was attributed mainly due to the unique upconversion photoluminescence property of CQDs and the presence highly reactive {0 0 1} facets of TNS (68%), which combined with CQDs through surface carbon-oxygen functional groups. Sun et al. (2014) fabricated the nanocomposite of CQDs and TiO_2 nanotube arrays, and the performance was evaluated through degradation of methylene blue. CQDs were synthesized through the electrochemical etching graphite electrodes, and anodization technique was used to prepare the TiO_2 nanotube. It was stated that about 14% improvement in the degradation efficiency in the presence of CQDs than the pure TiO_2.

Zhang et al. (2011a) reported the facile synthesis of Fe_2O_3/CQD nanocomposites by hydrothermal method in CQD aqueous solution, and the performance of the nanocomposite was investigated through the photooxidation of toxic gases, namely, benzene and methanol, under visible light irradiation. The enhancement in the degradation was mainly due to the following combined effects: (i) CDQs act as the electron reservoir that trap the electrons effectively, thereby retarding the recombination of charge carriers; (ii) CDQs exhibit the unique upconverted photoluminescence behavior in which it absorbs the visible light with longer wavelength and emits shorter wavelength light, which subsequently excites the electrons and creates holes in Fe_2O_3; (iii) π–π interaction between the benzene and the CDQs benefits for the increasing interaction between the molecules, thus enhancing the removal rate. Similarly, Yu and Kwak (2012) studied the photocatalytic performance of CQDs and mesoporous hematite α-Fe_2O_3 complex synthesized via a facile solvothermal process. Characterization studies revealed that the CQD/α-Fe_2O_3 hybrid clusters were uniform in size (~700 nm), possessing 3D spherical structure and having high internal surface area (~187 $m^2\ g^{-1}$) and worm hole-like mesoporous structure, which is important for the effective adsorption of photons and enhancing the photocatalytic ability under visible light.

Zhang et al. (2012a) reported the facile synthesis of CQDs/Ag_3PO_4 and related complexes and studied their photocatalytic performance under visible light for the degradation of methyl orange. Photocatalytic performance of CQDs/Ag/Ag_3PO_4 and CQDs/Ag_3PO_4 complexes was 5.5 and 2.2 times higher than the Ag_3PO_4, respectively. It was stated that the stability of the photocatalyst complex was protected by the insoluble coating of CQDs on Ag/Ag_3PO_4 and Ag_3PO_4, which prevented their dissolution in the aqueous solution. CQDs act as both electron acceptors and donors that effectively transfer the electrons between CQDs and Ag/Ag_3PO_4 (or) Ag_3PO_4 and thus prevent the photocorrosion due to the redundant electrons.

This book belongs to Central Library BADJI Mokhtar-ANNABA UNIVERSITY Copyright Elsevier 2024

2.7 Carbon nanofibers

Carbon nanofibers (CNFs) are three-dimensional cylindrical shaped graphene nanostructure constructed in cone or cylindrical shapes. The average diameter values are in the range of 70–200 nm, and the average length is in the range of 50–200 μm (Kim, Kim, & Yang, 2011; Yazdani & Mohanam, 2014). CNFs are characterized to be the flexible filaments with the large aspect ratio of >100 (Kim et al., 2011). Carbon nanofibers are discontinuous, sp^2 carbon-based linear filaments with the diameter in the range of nanometer, whereas carbon fibers are having the diameter in the range of micrometers (Kim et al., 2011). The integrated characteristic features such as high surface area, porosity, flexibility, and the higher mechanical strength allow CNFs to be used in the various fields of applications. In general, CNFs are produced through the catalytic chemical vapor deposition, combined processes of electrospinning with organic polymers and thermal method (Kim et al., 2011; Yazdani & Mohanam, 2014). Due to the shallow micropores and uniform pore structure, CNFs show improved adsorption properties compared with the conventional activated carbon adsorbent. The direct accessibility of micropores due to open external surface and the shallow nature exhibits the larger adsorption capacity and faster adsorption of contaminants (Kim et al., 2010a). When CNFs are used as the supporting matrix for photocatalytic semiconductors, these unique properties of the CNFs help in enhancing the photocatalytic behaviors of semiconductors.

Kim et al. (2010a) studied the photocatalytic activity of TiO_2/SiO_2-supported CNFs for the treatment of methylene blue under UV irradiation. TiO_2/SiO_2-supported CNFs were synthesized through the sol-gel method and followed by dip-coating process and thermal treatment up to 900°C. The results revealed that TiO_2/SiO_2-supported CNFs exhibited a higher removal rate than the TiO_2-supported CNFs. It is mainly due to the phase transformation that happens to TiO_2 crystals from anatase to rutile during the thermal treatment. Presence of SiO_2 suppressed the phase transformation; hence the TiO_2/SiO_2-supported CNFs exhibited higher removal efficiency. Kim et al. (2011) reported the photocatalytic activity of Ag-containing TiO_2/CNFs on the degradation of methylene blue under visible light irradiation. Ag-containing TiO_2/CNFs showed 17 times higher removal rate compared with the TiO_2/CNFs in 3 h visible light irradiation. When the photogenerated electrons are produced, the Ag particles acted as the electron acceptor, which helped in the retardation of charge carrier recombination. Moreover, high surface area CNFs provide large adsorption sites for the physical adsorption of methylene blue. Thus Ag-containing TiO_2/CNFs exhibited the combined photocatalytic ability and adsorption by CNFs on removing methylene blue under visible light irradiation.

The same group (Kim, Kim, & Yang, 2012) studied the photocatalytic activity of TiO_2-loaded graphene/carbon composite nanofibers (CCNFs), synthesized through electrospinning for the degradation of methylene blue. TiO_2/CCNFs exhibited higher removal rate than other TiO_2/CNFs. Graphene embedded in the composite prevented the agglomeration of TiO_2 particles resulting in small nanoparticles and helped the uniform distribution of the TiO_2 particles on the surface of CNFs. Also, graphene acts as the electron sink, which prevents the recombination of photoinduced holes and electron pair. Thus the enhanced photocatalytic activity achieved in visible light was mainly due to the high migration efficiency of the photoinduced electrons. CNFs enhanced the physical adsorption of methylene blue owing to the larger surface area. Ouzzine, Lillo-Ródenas, and Linares-Solano (2012) studied the influence of carbon nanofiber crystallinity on the TiO_2 deposition quality. The low-to-moderate level CNF crystallinities were suitable for the dense and uniform deposition of TiO_2 with remarkable characteristics such as high surface area ($\sim 400\,m^2\,g^{-1}$) and anatase phase, whereas high crystallinity did not exhibit these

This book belongs to Central Library BADJI Mokhtar-ANNABA UNIVERSITY
Copyright Elsevier 2024

favorable characteristics. TiO_2/CNF hybrid materials were used for the oxidation of propene under UV irradiation. The amorphous nature in low-to-moderate level crystallinities of CNFs contains higher defective carbon than the more crystalline ones. Defects present in the amorphous CNFs act as the nucleation point for the deposition of TiO_2. At low-to-moderate level crystallinities of CNFs, a large number of nucleation points were observed, which resulted in the production of a dense and uniform layer of TiO_2. In the case of high crystalline CNFs, TiO_2 was deposited on the defective points that were presented in the minimal numbers and subsequent deposition leading to the coverage of the previously deposited TiO_2.

Pant et al. (2014) synthesized CdS/TiO_2 nanoparticle-decorated CNFs through electrospinning method and studied the photocatalytic activities under visible light irradiation through the decomposition of methylene blue (MB), reactive orange 16, and reactive black 5. The degradation strategy depends on the combined removal through adsorption onto CNFs and photocatalysis by CdS and TiO_2. Li et al. (2015b) fabricated TiO_2/CNFs where CNFs were synthesized through electrospinning technique. The photocatalytic activity of the TiO_2/CNFs was studied under visible light irradiation through the degradation of methylene blue. Different loading of TiO_2 to CNFs was studied on the removal efficiency. All the composites exhibited enhanced methylene blue removal efficiency due to improved visible light absorption and high separation efficiency of charge carriers.

2.8 Carbon black

Carbon black (CB) can be used as a reactive template and suitable support for photocatalyst because of its unique structure and morphology (Cong et al., 2014). Also the ready availability, lower cost, higher surface area, and good conductivity made it a feasible and promising material for photocatalyst support in environment pollution treatment (Darvishi et al., 2013; Rincón et al., 2006). Mao and Weng (2009) prepared TiO_2 supported on CB through sol-gel method and pointed out the advantages of composites, which enhanced the photocatalytic removal of methyl orange. Increase in adsorption capability of the composite, easy separation of the catalyst, and suppressing the phase change from anatase to rutile helped in overcoming the transport of pollutant molecules toward the photocatalyst surface. CB promoted the efficient transfer of electron-hole pairs that reduced the recombination due to its higher electrical conductivity (Liu et al., 2018). Even if photocatalytic enhancement is observed, the molar ratio of CB and photocatalyst plays a crucial role in the structure and composition of the composites (Rincón et al., 2006). At lower dosages of CB, the composite could not reach its maximum performance, while at higher dosages the CB partially covers the catalyst surface leading to recombination of charge carries and weakens the photocatalytic activity (Liu et al., 2018). Cheshmeh et al. (2014) prepared CB/ZnO nanoparticle composite for the photodegradation of methyl orange and observed a maximum of 80% decolorization at 0.05 CB/ZnO ratio. A similar conclusion was reached by Takeda et al. (1998) on the relative placement of TiO_2 on CB beyond an optimum value, which resulted in decreasing the photocatalytic degradation of propyzamide.

2.9 Graphitic carbon nitride

Graphitic carbon nitride (GCN), low-cost metal-free polymeric semiconductor with high thermal and chemical stability has emerged as a promising support for photocatalysts for the degradation of organic compounds (Ran et al., 2015; Zhang et al., 2018). These materials are synthesized by treating high

This book belongs to Central Library BADJI Mokhtar-ANNABA UNIVERSITY Copyright Elsevier 2024

nitrogen-rich organic precursors at higher temperatures to form a unique structure with good textual and morphological property (Gong et al., 2015). GCN itself can be used as visible light catalyst, but the rapid recombination rate of electron-hole pairs and low quantum yield limits its potential application for pollutant degradation (Zhu et al., 2014). Using GCN as a substrate to support photocatalyst for the degradation of organic compounds has a number of inherent advantages, including extending the light absorption into the visible region and minimizing the recombination of photogenerated electron-hole pairs in the electron transfer process and good visible light harvesting capacity (Liu et al., 2015b). Carbon-doped ZnO supported on GCN composites was synthesized through simple one-step calcination of an evaporation-dried mixture of dicyandiamide and zinc nitrate for the photocatalytic degradation of methylene blue (Zhu et al., 2014). An enhanced photocatalytic activity of the composite was achieved due to the well-established heterojunction between GCN and ZnO, which initiated effective separation of the photoinduced electrons and holes. In another study, carbon-doped TiO_2 supported on mesoporous GCN was prepared by a facile heating method for the visible light photocatalytic degradation of methylene blue (Wu et al., 2016). The higher stability of the composite material together with enhanced visible light absorption and adsorption of dye on the photocatalyst resulted in four times higher degradation than that of carbon-doped TiO_2. The heterojunction structures formed by the composites can facilitate the photocatalytic activity by retarding the recombination rate, enabling a larger amount of reactive sites with high surface-to-volume ratio and convenient mass transfer (Chang et al., 2014; Wei et al., 2017).

3 Conclusion and future perspectives

Carbon-supported semiconductor photocatalysis is a promising strategy not only for overcoming the limitations of semiconductor photocatalyst but also for developing new and enhanced properties through their synergy. The combination of photocatalyst and the carbonaceous nanomaterial gives the opportunity to enhance the reaction efficiency through the following mechanisms: (i) enhances the adsorption of organic contaminants, (ii) enhances the adsorption of light in visible range, and (iii) reduces the recombination rate of the photogenerated electron-hole pair and facilitates the transportation of photoexcited electrons (Khalid et al., 2017; Leary & Westwood, 2010;Park et al., 2016 ; Shi, 2013). Primarily, it is the obvious factor that the combination of carbonaceous nanomaterial into semiconductor photocatalyst can improve the pollutant degradation efficiency significantly through the excellent adsorption properties of the carbon nanomaterials (Khalid et al., 2017; Leary & Westwood, 2010). Secondly, many studies stated that the carbonaceous materials can improve the adsorption of light in visible range than the pure TiO_2 due to the chemical bonding (Ti-O-C) between the TiO_2 and the carbon molecules (Khalid et al., 2017; Leary & Westwood, 2010; Woan et al., 2009). Most significantly, carbon materials play a key role as the electron reservoir by spontaneously transporting away the photogenerated electrons during the irradiation of light, thus reducing the recombination rate of photogenerated electron-hole pair, thereby increasing the treatment efficiency of the photocatalytic process (Park et al., 2016; Shi, 2013). As ideal support, carbonaceous composites can reduce the nanoparticle aggregation, improve mechanical strength, and increase the stability by inhibiting leaching and corrosion and immobilizing photocatalyst nanoparticles. Along with these the practical feasibility due to low cost, easy availability, and processing and innocuous nature are additional boon.

This book belongs to Central Library BADJI Mokhtar-ANNABA UNIVERSITY
Copyright Elsevier 2024

Although carbonaceous materials including activated carbon, carbon nanotubes, graphene and its derivatives, and fullerenes are widely investigated in recent past, still various synthetic carbon allotropes are yet to discover. So the world of carbonaceous materials will continue to expand in the near future. The macroscale particles enhance photocatalytic activity mainly through improving the adsorption capacity with very minimal chances of intimate heterojunction interactions. Nanocarbon materials, on the other hand, can build a heterojunction with semiconductor particles in molecular level. This leads to the direct involvement of the nanocarbon materials in photocatalysis, that is, in electron transfer mechanism. In essence the mechanism of enhancement by nanocarbon materials remains the same (Zhang, Zhang, & Xu, 2012). The difference lies mainly in the effectiveness of interaction, which is tunable to an extent. Thus optimization of the system as a whole with the target of achieving intimate contact between heteroatoms can give excellent photoactivity in carbonaceous nanomaterial-supported photocatalysts. Optimizing each nanocarbon-based semiconductor system can further help for comparison studies to determine better nanocarbon for photocatalytic applications. Even though nanocarbons are found to be having lesser toxicity (Bianco, 2013; Bradley, 2012; Guo & Mei, 2014; Miyawaki et al., 2008; Wang et al., 2014), extensive and in-detail studies are demanded before implementing in large-scale water treatment processes. When it comes to application scale, effective techniques for recovery and disposal of composite photocatalysts become mandatory. Therefore enough research is required to focus on promoting reusability such as through the development of magnetic property to the composite photocatalyst.

References

Addamo, M., et al. (2006). Preparation and photoactivity of nanostructured anatase, rutile and brookite TiO_2 thin films. *Chemical Communications*, (47), 4943–4945. https://doi.org/10.1039/b612172a.

Akhavan, O., et al. (2009). Synthesis of titania/carbon nanotube heterojunction arrays for photoinactivation of *E. coli* in visible light irradiation. *Carbon*, *47*(14), 3280–3287. https://doi.org/10.1016/j.carbon.2009.07.046.

Allen, M. J., Tung, V. C., & Kaner, R. B. (2010). Honeycomb carbon: A review of graphene. *Chemical Reviews*, *110*(1), 132–145. https://doi.org/10.1021/cr900070d.

Apostolopoulou, V., et al. (2009). Preparation and characterization of [60] fullerene nanoparticles supported on titania used as a photocatalyst. *Colloids and Surfaces A: Physicochemical and Engineering Aspects*, *349*, 189–194. https://doi.org/10.1016/j.colsurfa.2009.08.016.

Apul, O. G., et al. (2012). Adsorption of aromatic organic contaminants by graphene nanosheets: Comparison with carbon nanotubes and activated carbon. *Water Research*, *47*(4), 1648–1654. https://doi.org/10.1016/j.watres.2012.12.031.

Avouris, P., & Dimitrakopoulos, C. (2012). Graphene: Synthesis and applications. *Materials Today*, *15*(3), 86–97. https://doi.org/10.1016/S1369-7021(12)70044-5.

Bagri, A., et al. (2010). Structural evolution during the reduction of chemically derived graphene oxide. *Nature Chemistry*, *2*(7), 581–587. https://doi.org/10.1038/nchem.686.

Bai, W., et al. (2012). Enhancement of nano titanium dioxide photocatalysis in transparent coatings by polyhydroxy fullerene. *Applied Catalysis B: Environmental*, *125*, 128–135. https://doi.org/10.1016/j.apcatb.2012.05.026.

Baker, S. N., & Baker, G. A. (2010). Luminescent carbon nanodots: Emergent nanolights. *Angewandte Chemie International Edition*, 6726–6744. https://doi.org/10.1002/anie.200906623.

Balandin, A. A., et al. (2008). Superior thermal conductivity of single-layer graphene. *Nano Letters*, *8*, 902–907. https://doi.org/10.1021/nl0731872.

This book belongs to Central Library BADJI Mokhtar-ANNABA UNIVERSITY Copyright Elsevier 2024

Bandosz, T. (2009). Surface chemistry of carbon materials. In *Carbon materials for catalysis*. USA: John Wiley & Sons.

Bianco, A. (2013). Graphene: Safe or toxic? The two faces of the medal. *Angewandte Chemie International Edition*, *52*, 2–14. https://doi.org/10.1002/anie.201209099.

Bo, Y. I. N., et al. (2013). Preparation of TiO_2/mesoporous carbon composites and their photocatalytic performance for methyl orange degradation. *New Carbon Materials*, *28*(1), 47–54. https://doi.org/10.1016/S1872-5805(13)60064-5.

Bolotin, K. I., et al. (2008). Ultrahigh electron mobility in suspended graphene. *Solid State Communications*, *146* (9–10), 351–355. https://doi.org/10.1016/j.ssc.2008.02.024.

Bradley, D. (2012). Is graphene safe? concerns. *Materials Today*, *15*(6), 230. https://doi.org/10.1016/S1369-7021(12)70101-3.

Cao, L., et al. (2007). Carbon dots for multiphoton bioimaging. *Journal of the American Chemical Society*, *129*, 11318–11319. https://doi.org/10.1021/ja073527l.

Cao, X. R., et al. (2014). Hierarchical composites of TiO_2 nanowire arrays on reduced graphene oxide nanosheets with enhanced photocatalytic hydrogen evolution performance. *Journal of Materials Chemistry A*, *2*(12), 4366–4374. https://doi.org/10.1039/c3ta14272h.

Carp, O., Huisman, C. L., & Reller, A. (2004). Photoinduced reactivity of titanium dioxide. *Progress in Solid State Chemistry*, *32*, 33–177. https://doi.org/10.1016/j.progsolidstchem.2004.08.001.

Chagovets, V. V., et al. (2012). Noncovalent interaction of methylene blue with carbon nanotubes: Theoretical and mass spectrometry characterization noncovalent interaction of methylene blue with carbon nanotubes: Theoretical and mass spectrometry characterization. *The Journal of Physical Chemistry C*, 1–37. https://doi.org/10.1021/jp306333c.

Chang, C., et al. (2014). Novel mesoporous graphite carbon nitride/BiOI heterojunction for enhancing photocatalytic performance under visible-light irradiation. *Applied Materials and Interfaces*, *6*, 5083–5093. https://doi.org/10.1021/am5002597.

Chaudhary, D., Khare, N., & Vankar, V. D. (2016). Ag nanoparticles loaded TiO_2/MWCNT ternary nanocomposite: A visible-light-driven photocatalyst with enhanced photocatalytic performance and stability. *Ceramics International*. https://doi.org/10.1016/j.ceramint.2016.07.056.

Chen, Y., et al. (2005). Preparation of a novel TiO_2-based p-n junction nanotube photocatalyst. *Environmental Science & Technology*, *39*(5), 1201–1208.

Chen, S., et al. (2012). Photoreactive mesoporous carbon/bi 2 WO 6 composites: Synthesis and reactivity. *Applied Surface Science*, *259*, 7–12.

Chen, F., et al. (2013). Facile synthesis of CdS nanoparticles photocatalyst with high performance. *Ceramics International*, *39*(2), 1511–1517. https://doi.org/10.1016/j.ceramint.2012.07.098.

Cheshmeh, R. D., et al. (2014). Photocatalytic process by immobilized carbon black/ZnO nanocomposite for dye removal from aqueous medium: Optimization by response surface methodology. *Journal of Industrial and Engineering Chemistry*, *20*, 1861–1868.

Cho, E.-C., et al. (2015). Fullerene C70 decorated TiO2 nanowires for visible-light-responsive photocatalyst. *Applied Surface Science*, *355*, 536–546. https://doi.org/10.1016/j.apsusc.2015.07.062.

Chowdhury, S., & Balasubramanian, R. (2014a). Graphene/semiconductor nanocomposites (GSNs) for heterogeneous photocatalytic decolorization of wastewaters contaminated with synthetic dyes: A review. *Applied Catalysis B: Environmental*, *160–161*, 307–324. https://doi.org/10.1016/j.apcatb.2014.05.035.

Chowdhury, S., & Balasubramanian, R. (2014b). Recent advances in the use of graphene-family nanoadsorbents for removal of toxic pollutants from wastewater. *Advances in Colloid and Interface Science*, *204*, 35–56. https://doi.org/10.1016/j.cis.2013.12.005.

Cong, Y., et al. (2014). Core–shell structured carbon black@TiO2 microsphere with enhanced visible light photocatalytic activity. *Materials Letters*, *138*, 200–203. https://doi.org/10.1016/j.matlet.2014.09.061.

This book belongs to Central Library BADJI Mokhtar-ANNABA UNIVERSITY

Copyright Elsevier 2024

Da Meng, Z., et al. (2012). Synthesis and characterization of M-fullerene/TiO_2 photocatalysts designed for degradation azo dye. *Materials Science and Engineering C*, *32*(8), 2175–2182. https://doi.org/10.1016/j.msec.2012.05.048.

Dai, K., et al. (2014). In situ assembly of MnO_2 nanowires/graphene oxide nanosheets composite with high specific capacitance. *Electrochimica Acta*, *116*, 111–117. https://doi.org/10.1016/j.electacta.2013.11.036.

Darvishi, R., et al. (2013). Combination of carbon black-ZnO/ UV process with an electrochemical process equipped with a carbon black-PTFE-coated gas-diffusion cathode for removal of a textile dye combination of carbon black-ZnO/UV process with an electrochemical process equipped. *Industrial & Engineering Chemistry Research*, *52*(39), 14133–14142. https://doi.org/10.1021/ie402478p.

Du, A., et al. (2011). Hybrid graphene/titania nanocomposite: Interface charge transfer, hole doping, and sensitization for visible light response. *Journal of Physical Chemistry Letters*, *2*, 894–899. https://doi.org/10.1021/jz2002698.

Duan, J., et al. (2015). Heteroatom-doped graphene-based materials for energy-relevant electrocatalytic processes. *ACS Catalysis*, *5*(9), 5207–5234. https://doi.org/10.1021/acscatal.5b00991.

Eigler, S., Dotzer, C., & Hirsch, A. (2012). Visualization of defect densities in reduced graphene oxide. *Carbon*, *50*(10), 3666–3673. https://doi.org/10.1016/j.carbon.2012.03.039.

Fakhri, A. (2013). Adsorption characteristics of graphene oxide as a solid adsorbent for aniline removal from aqueous solutions: Kinetics, thermodynamics and mechanism studies. *Journal of Saudi Chemical Society*, *21*(Suppl 1), S52–S57. https://doi.org/10.1016/j.jscs.2013.10.002.

Fox, M. A., & Dulay, M. T. (1993). Heterogeneous photocatalysis. *Chemical Reviews*, *93*, 341–357. https://doi.org/10.1021/cr00017a016.

Fujishima, A., Rao, T. N., & Tryk, D. A. (2000). Titanium dioxide photocatalysis. *Journal of Photochemistry and Photobiology C: Photochemistry Reviews*, *1*(1), 1–21. https://doi.org/10.1016/S1389-5567(00)00002-2.

Gamage McEvoy, J., Cui, W., & Zhang, Z. (2014). Synthesis and characterization of Ag/AgCl-activated carbon composites for enhanced visible light photocatalysis. *Applied Catalysis B: Environmental*, *144*, 702–712. https://doi.org/10.1016/j.apcatb.2013.07.062.

Gan, Z., et al. (2014). Photothermal contribution to enhanced photocatalytic performance of graphene-based nanocomposites. *ACS Catalysis*, (9), 9304–9310.

Gandhi, M. R., Vasudevan, S., & Shibayama, A. (2016). Graphene and graphene-based composites: A rising star in water purification—A comprehensive overview. *Chemistry Select Reviews*, 4358–4385. https://doi.org/10.1002/slct.201600693.

Gao, B., Chen, G. Z., & Li, G. (2009). Carbon nanotubes/titanium dioxide (CNTs/TiO 2) nanocomposites prepared by conventional and novel surfactant wrapping sol–gel methods exhibiting enhanced photocatalytic activity. *Applied Catalysis B: Environmental*, *89*, 503–509. https://doi.org/10.1016/j.apcatb.2009.01.009.

Gao, B., et al. (2008). Photo-electro-catalysis enhancement on carbon nanotubes/titanium dioxide (CNTs/TiO_2) composite prepared by a novel surfactant wrapping sol–gel method. *Applied Catalysis B: Environmental*, *85*, 17–23. https://doi.org/10.1016/j.apcatb.2008.06.027.

Gao, E., et al. (2011). Synthesis and enhanced photocatalytic performance of graphene-Bi 2 WO 6 composite. *Physical Chemistry Chemical Physics*, *13*, 2887–2893. https://doi.org/10.1039/c0cp01749c.

Geim, A. K., & Novoselov, K. S. (2007). The rise of graphene. *Nature Materials*, *6*(3), 183–191. https://doi.org/10.1038/nmat1849.

Gong, Y., et al. (2015). Graphitic carbon nitride polymers: Promising oxidation and hydrogenation. *Green Chemistry*, *17*, 715–736. https://doi.org/10.1039/c4gc01847h.

Grabstanowicz, L. R., et al. (2013). Facile oxidative conversion of TiH_2 to high-concentration Ti 3+-self-doped rutile TiO_2 with visible-light photoactivity. *Inorganic Chemistry*, *527*, 3884–3890.

Green, A. A., & Hersam, M. C. (2010). Emerging methods for producing monodisperse graphene. *Journal of Physical Chemistry Letters*, 544–549. https://doi.org/10.1021/jz900235f.

This book belongs to Central Library BADJI Mokhtar-ANNABA UNIVERSITY

Copyright Elsevier 2024

Guldi, D. M., Prato, M., & Farmaceutiche, S. (2000). Excited-state properties of C 60 fullerene derivatives. *Accounts of Chemical Research*, *33*(10), 695–703.

Guo, X., & Mei, N. (2014). Assessment of the toxic potential of graphene. *Journal of Food and Drug Analysis*, *22* (1), 105–115. https://doi.org/10.1016/j.jfda.2014.01.009.

Guo, J., et al. (2011). Sonochemical synthesis of TiO_2 nanoparticles on graphene for use as photocatalyst. *Ultrasonics Sonochemistry*, *18*(5), 1082–1090. https://doi.org/10.1016/j.ultsonch.2011.03.021.

Hamandi, M., et al. (2017). Titanium dioxide nanotubes/polyhydroxyfullerene composites for formic acid photodegradation. *Applied Surface Science*, *412*, 306–318. https://doi.org/10.1016/j.apsusc.2017.03.261.

Han, C., & Xu, Y. (2014). Enhancing the visible light photocatalytic performance of ternary CdS–(graphene–Pd) nanocomposites via a facile interfacial mediator and co-catalyst strategy. *Journal of Materials Chemistry A: Materials for Energy and Sustainability*, *2*(45), 19156–19166. https://doi.org/10.1039/C4TA04151H.

Han, C., et al. (2014a). Hierarchically CdS decorated 1D ZnO Nanorods-2D graphene hybrids: Low temperature synthesis and enhanced photocatalytic performance. *Advanced Functional Materials*, 1–9. https://doi.org/10.1002/adfm.201402443.

Han, Q., et al. (2014b). Adsorption isotherms and kinetics of cationic and anionic dyes on three-dimensional reduced graphene oxide macrostructure. *Journal of Industrial and Engineering Chemistry*, 1–6. https://doi.org/10.1016/j.jiec.2014.05.033.

Hasobe, T., et al. (2006). Supramolecular nanostructured assemblies of different types of porphyrins with fullerene using TiO_2 nanoparticles for light energy conversion. *Tetrahedron*, *62*(9), 1937–1946. https://doi.org/10.1016/j.tet.2005.05.113.

Yamashita, H, & Li, H (Eds.), (2016). *Nanostructured photocatalysts. Nanostructure science and technology*. Cham: Springer.

Hou, C., et al. (2012a). P25—Graphene hydrogels: Room-temperature synthesis and application for removal of methylene blue from aqueous solution. *Journal of Hazardous Materials*, *205–206*, 229–235. https://doi.org/10.1016/j.jhazmat.2011.12.071.

Hou, D., et al. (2012b). Preparation, characterization and performance of a novel visible light responsive spherical activated carbon-supported and Er 3+:YFeO 3-doped TiO_2 photocatalyst. *Journal of Hazardous Materials*, *199–200*, 301–308. https://doi.org/10.1016/j.jhazmat.2011.11.011.

Hu, Y., Song, S., & Lopez-valdivieso, A. (2015). Effects of oxidation on the defect of reduced graphene oxides in graphene preparation. *Journal of Colloid and Interface Science*, *450*, 68–73. https://doi.org/10.1016/j.jcis.2015.02.059.

Hu, J.-S., et al. (2005). Mass production and high photocatalytic activity of ZnS nanoporous nanoparticles. *Angewandte Chemie International Edition*, *44*, 1269–1273. https://doi.org/10.1002/anie.200462057.

Hummers, W. S., & Offeman, R. E. (1958). Preparation of graphitic oxide. *Journal of American Chemical Society*, *80*(6), 1339. https://doi.org/10.1021/ja01539a017.

Jianwei, C., et al. (2013). Recent progress in the preparation and application of semiconductor/graphene composite photocatalysts. *Chinese Journal of Catalysis*, *34*(4), 621–640. https://doi.org/10.1016/S1872-2067(12)60530-0.

Jiang, G., et al. (2011). TiO_2 nanoparticles assembled on graphene oxide nanosheets with high photocatalytic activity for removal of pollutants. *Carbon*, *49*(8), 2693–2701. https://doi.org/10.1016/j.carbon.2011.02.059.

Juang, Z., et al. (2010). Graphene synthesis by chemical vapor deposition and transfer by a roll-to-roll process. *Carbon*, *48*(11), 3169–3174. https://doi.org/10.1016/j.carbon.2010.05.001.

Kemp, K. C., et al. (2013). Environmental applications using graphene composites: Water remediation and gas adsorption. *Nanoscale*, *5*, 3149–3171. https://doi.org/10.1039/c3nr33708a.

Khalid, N. R., et al. (2017). Carbonaceous-TiO_2 nanomaterials for photocatalytic degradation of pollutants: A review. *Ceramics International*, *47*(1), 14552–14571. https://doi.org/10.1016/j.ceramint.2017.08.143.

This book belongs to Central Library BADJI Mokhtar-ANNABA UNIVERSITY

Copyright Elsevier 2024

Kim, C. H., Kim, B. H., & Yang, K. S. (2011). Visible light-induced photocatalytic activity of Ag-containing TiO_2/carbon nanofibers composites. *Synthetic Metals*, *161*(11 – 12), 1068–1072. https://doi.org/10.1016/j.synthmet.2011.03.017.

Kim, C. H., Kim, B. H., & Yang, K. S. (2012). TiO_2 nanoparticles loaded on graphene/carbon composite nanofibers by electrospinning for increased photocatalysis. *Carbon*, *50*(7), 2472–2481. https://doi.org/10.1016/j.carbon.2012.01.069.

Kim, B.-H., et al. (2010a). Synthesis, characterization, and photocatalytic activity of TiO_2/SiO_2 nanoparticles loaded on carbon nanofiber web. *Journal of Nanoscience and Nanotechnology*, *10*(5), 3331–3335. https://doi.org/10.1166/jnn.2010.2289.

Kim, J., et al. (2010b). Graphene oxide sheets at interfaces. *Journal of the American Chemical Society*, *132*(23), 8180–8186. https://doi.org/10.1021/ja102777p.

Kongkanand, A., & Kamat, P. V. (2007). Electron storage in single wall carbon semiconductor—SWCNT suspensions. *ACS Nano*, *1*(1), 13–21.

Kratschmer, W., Lamb, L. D., Fostiropoulos, K., & Huffman, D. R. (1990). Solid C60: A new form of carbon. *Nature*, *347*(1990), 354–358.

Krishna, V., et al. (2006). Enhancement of titanium dioxide photocatalysis by water-soluble fullerenes. *Journal of Colloid and Interface Science*, *304*(1), 166–171. https://doi.org/10.1016/j.jcis.2006.08.041.

Krishna, V., et al. (2008). Mechanism of enhanced photocatalysis with polyhydroxy fullerenes. *Applied Catalysis B: Environmental*, *79*(4), 376–381. https://doi.org/10.1016/j.apcatb.2007.10.020.

Kumar, K. Y., Muralidhara, H. B., & Nayaka, Y. A. (2013). Hierarchically assembled mesoporous ZnO nanorods for the removal of lead and cadmium by using differential pulse anodic stripping voltammetric method. *Power Technology*, *239*, 208–216.

Leary, R., & Westwood, A. (2010). Carbonaceous nanomaterials for the enhancement of TiO_2 photocatalysis. *Carbon*. *9*, https://doi.org/10.1016/j.carbon.2010.10.010.

Li, B., & Cao, H. (2011). ZnO @ graphene composite with enhanced performance for the removal of dye from water. *Journal of Materials Chemistry*, *21*, 3346–3349. https://doi.org/10.1039/c0jm03253k.

Li, D., & Kaner, R. B. (2012). Graphene-based materials. *Science*. *1170*(2008)https://doi.org/10.1126/science.1158180.

Li, G., Zhao, X. S., & Ray, M. B. (2007). Advanced oxidation of orange II using TiO_2 supported on porous adsorbents: The role of pH, H_2O_2 and O_3. *Separation and Purification Technology*, *55*, 91–97. https://doi.org/10.1016/j.seppur.2006.11.003.

Li, Y., et al. (2006). Photocatalytic degradation of methyl orange by TiO2-coated activated carbon and kinetic study. *Water Research*, *40*(6), 1119–1126. https://doi.org/10.1016/j.watres.2005.12.042.

Li, H., et al. (2010). Water-soluble fluorescent carbon quantum dots and photocatalyst design. *Angewandte Chemie International Edition*, *49*(26), 4430–4434. https://doi.org/10.1002/anie.200906154.

Li, Z., et al. (2011). Carbon nanotube/titanium dioxide (CNT/TiO_2) core-shell nanocomposites with tailored shell thickness, CNT content and photocatalytic/photoelectrocatalytic properties. *Applied Catalysis B: Environmental*, *110*, 50–57. https://doi.org/10.1016/j.apcatb.2011.08.023.

Li, K., et al. (2013a). Design of graphene and silica co-doped titania composites with ordered mesostructure and their simulated sunlight photocatalytic performance towards atrazine degradation. *Colloids and Surfaces A: Physicochemical and Engineering Aspects*, *422*, 90–99. https://doi.org/10.1016/j.colsurfa.2013.01.039.

Li, Z., et al. (2013b). Facile synthesis of phosphate-functionalized MWCNT-TiO_2 nanocomposites as efficient photocatalysts and insights into the roles of nanostructured carbon. *ChemPlusChem*, *78*(7), 670–676. https://doi.org/10.1002/cplu.201300083.

Li, Q., et al. (2015a). CdS/graphene nanocomposite photocatalysts. *Advanced Energy Materials*, 1500010. https://doi.org/10.1002/aenm.201500010.

This book belongs to Central Library BADJI Mokhtar-ANNABA UNIVERSITY

Copyright Elsevier 2024

Li, X., et al. (2015b). Fabrication of TiO_2/porous carbon nanofibers with superior visible photocatalytic activity. *New Journal of Chemistry*, *39*(10), 7863–7872. https://doi.org/10.1039/c5nj01189b.

Li, X., et al. (2016). Graphene in photocatalysis: A review. *Small*, *12*(48), 1–57. https://doi.org/10.1002/smll.201600382.

Li, M., et al. (2017). Synergetic effect between adsorption and photodegradation on nanostructured TiO_2/activated carbon fiber felt porous composites for toluene removal. *Journal of Hazardous Materials*, *333*, 88–98. https://doi.org/10.1016/j.jhazmat.2017.03.019.

Li, X., et al. (2018). Graphene-based heterojunction photocatalysts. *Applied Surface Science*, *430*, 53–107. https://doi.org/10.1016/j.apsusc.2017b.08.194.

Liang, Y. T., et al. (2011). Minimizing graphene defects enhances titania nanocomposite-based photocatalytic reduction of CO_2 for improved solar fuel production. *Nano Letters*, 2865–2870.

Liang, Q., et al. (2012). Enhanced photocatalytic activity and structural stability by hybridizing Ag_3PO_4 nanospheres with graphene oxide sheets. *Physical Chemistry Chemical Physics*, 15657–15665. https://doi.org/10.1039/c2cp42465g.

Lightcap, I. V., Kosel, T. H., & Kamat, P. V. (2010). Anchoring semiconductor and metal nanoparticles on a two-dimensional catalyst mat. storing and shuttling electrons with reduced graphene oxide. *Nano Letters*, *10*(2), 577–583. https://doi.org/10.1021/nl9035109.

Lim, S. Y., Shen, W., & Gao, Z. (2014). Carbon quantum dots and their applications. *Chemical Society Reviews*. https://doi.org/10.1039/C4CS00269E.

Liu, T., et al. (2012). Adsorption of methylene blue from aqueous solution by graphene. *Colloids and Surfaces B: Biointerfaces*, *90*, 197–203. https://doi.org/10.1016/j.colsurfb.2011.10.019.

Liu, S., et al. (2013). Graphene facilitated visible light photodegradation of methylene blue over titanium dioxide photocatalysts. *Chemical Engineering Journal*, *214*, 298–303. https://doi.org/10.1016/j.cej.2012.10.058.

Liu, S., et al. (2015a). One-dimension-based spatially ordered architectures for solar energy conversion. *Chemical Society Reviews*. https://doi.org/10.1039/C4CS00408F.

Liu, Y., et al. (2015b). Enhanced visible - light photocatalytic activity of Z - scheme graphitic carbon nitride/oxygen vacancy - rich zinc oxide hybrid photocatalysts. *Chinese Journal of Catalysis*, *36*(12), 2135–2143. https://doi.org/10.1016/S1872.

Liu, H., et al. (2016). Hydrothermal etching fabrication of TiO_2@graphene hollow structures: Mutually independent exposed {001} and {101} facets nanocrystals and its synergistic photocaltalytic effects. *Scientific Reports*, *6*(August), 33839. https://doi.org/10.1038/srep33839.

Liu, D., et al. (2018). Synthesis, performance and action mechanism of carbon black/Ag_3PO_4 photocatalysts. *Ceramics International*, *44*(12), 13712–13719. https://doi.org/10.1016/j.ceramint.2018.04.212.

Long, R., English, N. J., & Prezhdo, O. V. (2012). Photo-induced charge separation across the graphene – TiO_2 interface is faster than energy losses: A time-domain ab initio analysis. *Journal of the American Chemical Society*.

Long, Y., et al. (2009). Effect of C60 on the photocatalytic activity of TiO_2 nanorods. *Journal of Physical Chemistry C*, *113*(31), 13899–13905. https://doi.org/10.1021/jp902417j.

Lu, G., et al. (2012a). Semiconducting graphene: Converting graphene from semimetal to semiconductor. *Nanoscale*, *5*, 1358–1363. https://doi.org/10.1039/b000000x.

Lu, Z., et al. (2012b). In situ growth of Si nanowires on graphene sheets for Li-ion storage. *Electrochimica Acta*, *74*, 176–181. https://doi.org/10.1016/j.electacta.2012.04.046.

Ma, R., et al. (2017). Photocatalytic degradation of salicylic acid with magnetic activated carbon-supported F-N codoped TiO_2 under visible light. *Vacuum*, *141*, 157–165. https://doi.org/10.1016/j.vacuum.2017.04.003.

Mao, C. C., & Weng, H. S. (2009). Promoting effect of adding carbon black to TiO_2 for aqueous photocatalytic degradation of methyl orange. *Chemical Engineering Journal*, *155*(3), 744–749. https://doi.org/10.1016/j.cej.2009.09.016.

This book belongs to Central Library BADJI Mokhtar-ANNABA UNIVERSITY

Copyright Elsevier 2024

Melian, P. E., et al. (2009). ZnO activation by using activated carbon as a support: Characterisation and photoreactivity. *Applied Catalysis A: General*, *364*, 174–181. https://doi.org/10.1016/j.apcata.2009.05.042.

Minitha, C. R., et al. (2017). Adsorption behaviour of reduced graphene oxide towards cationic and anionic dyes: Co-action of electrostatic and π–π interactions. *Materials Chemistry and Physics*. https://doi.org/10.1016/j.matchemphys.2017.03.048.

Mirzaei, A., et al. (2016). Removal of pharmaceuticals and endocrine disrupting compounds from water by zinc oxide-based photocatalytic degradation: A review. *Sustainable Cities and Society*, *27*, 407–418. https://doi.org/10.1016/j.scs.2016.08.004.

Miyawaki, J., et al. (2008). Toxicity of single-walled carbon nanohorns. *ACS Nano*, *2*(2), 213–226.

Morales-Torres, S., et al. (2012). Design of graphene-based TiO_2 photocatalysts—A review. *Environmental Science and Pollution Research*, *19*, 3676–3687. https://doi.org/10.1007/s11356-012-0939-4.

Natarajan, T. S., et al. (2016). Synthesis of multiwall carbon nanotubes/TiO_2 nanotube composites with enhanced photocatalytic decomposition efficiency. *Catalysis Today*, *282*, 13–23. https://doi.org/10.1016/j.cattod.2016.03.018.

Neelgund, G. m., & Oki, A. (2018). Photothermal effect: An important aspect for enhancement of photocatalytic activity under illumination to NIR radiations. *Materials Chemistry Frontiers*, *2*, 64–75. https://doi.org/10.1039/C7QM00337D.

Novoselov, K. S., Geim, A. K., et al. (2005). Two-dimensional gas of massless Dirac fermions in graphene. *Nature*, *438*(7065), 197–200. https://doi.org/10.1038/nature04233.

Novoselov, K. S., Jiang, D., et al. (2005). Two-dimensional atomic crystals. *Proceedings of the National Academy of Sciences of the United States of America*, *102*(30), 10451–10453.

Novoselov, K. S., et al. (2004). Electric field effect in atomically thin carbon films. *Science*, *306*(October), 666–670.

Oh, W. C., Jung, A. R., & Ko, W. B. (2009). Characterization and relative photonic efficiencies of a new nanocarbon/TiO_2 composite photocatalyst designed for organic dye decomposition and bactericidal activity. *Materials Science and Engineering C*, *29*(4), 1338–1347. https://doi.org/10.1016/j.msec.2008.10.034.

Ouzzine, M., Lillo-Ródenas, M. A., & Linares-Solano, A. (2012). Carbon nanofibres as substrates for the preparation of TiO_2 nanostructured photocatalysts. *Applied Catalysis B: Environmental*, *127*, 291–299. https://doi.org/10.1016/j.apcatb.2012.08.029.

Pant, B., et al. (2014). Electrospun CdS-TiO2 doped carbon nanofibers for visible-light-induced photocatalytic hydrolysis of ammonia borane. *Catalysis Communications*, *50*, 63–68. https://doi.org/10.1016/j.catcom.2014.03.002.

Park, S., & Ruoff, R. S. (2009). Chemical methods for the production of graphenes. *Nature Nanotechnology*, *4*(4), 217–224. https://doi.org/10.1038/nnano.2009.58.

Park, H., et al. (2016). Photoinduced charge transfer processes in solar photocatalysis based on modified TiO_2. *Energy & Environmental Science*, *9*(2), 411–433. https://doi.org/10.1039/C5EE02575C.

Peining, Z., et al. (2011). TiO_2-MWCNT rice grain-shaped nanocomposites—Synthesis, characterization and photocatalysis. *Materials Research Bulletin*, *46*(4), 588–595. https://doi.org/10.1016/j.materresbull.2010.12.025.

Perera, S. D., et al. (2012). Hydrothermal synthesis of graphene-TiO 2 nanotube composites with enhanced photocatalytic activity. *ACS Catalysis*, *2*(6), 949–956. https://doi.org/10.1021/cs200621c.

Puma, G. L., et al. (2008). Preparation of titanium dioxide photocatalyst loaded onto activated carbon support using chemical vapor deposition: A review paper. *Journal of Hazardous Materials*, *157*, 209–219. https://doi.org/10.1016/j.jhazmat.2008.01.040.

Putri, L. K., et al. (2015). Heteroatom doped graphene in photocatalysis: A review. *Applied Surface Science*, *358*, 2–14. https://doi.org/10.1016/j.apsusc.2015.08.177.

This book belongs to Central Library BADJI Mokhtar-ANNABA UNIVERSITY

Copyright Elsevier 2024

Qianqian, Z., Tang, B., & Guoxin, H. (2011). High photoactive and visible-light responsive graphene/titanate nanotubes photocatalysts: Preparation and characterization. *Journal of Hazardous Materials*, *198*, 78–86. https://doi.org/10.1016/j.jhazmat.2011.10.012.

Qin, S., et al. (2012). Photodecolorization of Rhodamine B on tungsten-doped TiO_2/activated carbon under visible-light irradiation. *Journal of Hazardous Materials*, *227–228*, 25–33. https://doi.org/10.1016/j.jhazmat.2012.04.071.

Raizada, P., et al. (2014). Solar photocatalytic activity of nano-ZnO supported on activated carbon or brick grain particles: Role of adsorption in dye degradation. *Applied Catalysis A: General*, *486*, 159–169. https://doi.org/10.1016/j.apcata.2014.08.043.

Ramesha, G. K., et al. (2011). Graphene and graphene oxide as effective adsorbents toward anionic and cationic dyes. *Journal of Colloid and Interface Science*, *361*(1), 270–277. https://doi.org/10.1016/j.jcis.2011.05.050.

Ran, J., et al. (2015). Porous P-doped graphitic carbon nitride nanosheets for synergistically enhanced. *Energy & Environmental Science*, *8*, 44–46. https://doi.org/10.1039/c5ee02650d.

Rincón, M. E., et al. (2006). Surface characterization of nanostructured TiO_2 and carbon blacks composites by dye adsorption and photoelectrochemical studies. *Applied Catalysis B: Environmental*, *69*(1–2), 65–74. https://doi.org/10.1016/j.apcatb.2006.05.018.

Schneider, J., et al. (2014). Understanding TiO_2 photocatalysis: Mechanisms and materials. *Chemical Reviews*, *114*, 9919–9986. https://doi.org/10.1021/cr5001892.

Schniepp, H. C., et al. (2006). Functionalized single graphene sheets derived from splitting graphite oxide. *The Journal of Physical Chemistry*, *110*, 8535–8539.

Schultz, D. M., et al. (2014). Solar synthesis: Prospects in visible light photocatalysis. *Science*. https://doi.org/10.1126/science.1239176.

Serp, P., Corrias, M., & Kalck, P. (2003). Carbon nanotubes and nanofibers in catalysis. *Applied Catalysis A: General*, *253*, 337–358. https://doi.org/10.1016/S0926-860X(03)00549-0.

Shahriary, L., & Athawale, A. A. (2014). Graphene oxide synthesized by using modified Hummers approach. *International Journal of Renewable Energy and Environmental Engineering*, *02*(01), 58–63.

Shen, Y., Fang, Q., & Chen, B. (2014). Environmental applications of three-dimensional graphene-based macrostructures: Adsorption, Transformation, and Detection. *Environmental Science & Technology*. https://doi.org/10.1021/es504421y.

Shi, J. W. (2009). Preparation of Fe(III) and Ho(III) co-doped TiO_2 films loaded on activated carbon fibers and their photocatalytic activities. *Chemical Engineering Journal*, *151*(1–3), 241–246. https://doi.org/10.1016/j.cej.2009b.02.034.

Shi, J. (2013). On the synergetic catalytic effect in heterogeneous nanocomposite catalysts. *Chemical Reviews*, *113*(3), 2139–2181. https://doi.org/10.1021/cr3002752.

Singh, P., et al. (2018). Review on various strategies for enhancing photocatalytic activity of graphene based nanocomposites for water purification. *Arabian Journal of Chemistry*. https://doi.org/10.1016/j.arabjc.2018.12.001.

Song, H., et al. (2011). Graphene sheets decorated with SnO_2 nanoparticles: In situ synthesis and highly efficient materials for cataluminescence gas sensors. *Journal of Materials Chemistry*, *21*, 5972–5977. https://doi.org/10.1039/c0jm04331a.

Song, H., et al. (2012). Stable and water-dispersible graphene nanosheets: Sustainable preparation, functionalization, and high-performance adsorbents for Pb 2+. *ChemPlusChem*, *610064*, 379–386. https://doi.org/10.1002/cplu.201200012.

Stankovich, S., et al. (2006). Graphene-based composite materials. *Nature*, *442*(7100), 282–286. https://doi.org/10.1038/nature04969.

Stengl, V., et al. (2013). TiO2-graphene oxide nanocomposite as advanced photocatalytic materials. *Chemistry Central Journal*, *7*(1), 41. https://doi.org/10.1186/1752-153X-7-41.

This book belongs to Central Library BADJI Mokhtar-ANNABA UNIVERSITY

Copyright Elsevier 2024

Steurer, P., et al. (2009). Functionalized graphenes and thermoplastic nanocomposites based upon expanded graphite oxide. *Macromolecular Rapid Communications*, *30*(4–5), 316–327. https://doi.org/10.1002/marc.200800754.

Sun, M., et al. (2014). A nanocomposite of carbon quantum dots and TiO2 nanotube arrays: Enhancing photoelectrochemical and photocatalytic properties. *RSC Advances*, *4*(3), 1120–1127. https://doi.org/10.1039/c3ra45474f.

Suresh, P., Vijaya, J. J., & Kennedy, L. J. (2014). Photocatalytic degradation of textile-dyeing wastewater by using a microwave combustion-synthesized zirconium oxide supported activated carbon. *Materials Science in Semiconductor Processing*, *27*, 482–493. https://doi.org/10.1016/j.mssp.2014.06.050.

Takeda, N., et al. (1998). Influence of carbon black as an adsorbent used in TiO_2 photocatalyst films on photodegradation behaviors of propyzamide. *Journal of Catalysis*, *177*(2), 240–246. https://doi.org/10.1006/jcat.1998.2117.

Trapalis, A., Todorova, N., & Giannakopoulou, T. (2016). TiO_2/graphene composite photocatalysts for NOx removal: A comparison of surfactant-stabilized graphene and reduced graphene oxide. *Applied Catalysis B: Environmental*, *180*, 637–647.

Upadhyay, R. K., & Sinha, S. (2014). Role of graphene/metal oxide composites as photocatalysts, adsorbents and disinfectants in water treatment: A review. *RSC Advances*, *4*, 3823–3851. https://doi.org/10.1039/c3ra45013a.

Velasco, L. F., Parra, J. B., & Ania, C. O. (2010). Role of activated carbon features on the photocatalytic degradation of phenol. *Applied Surface Science*, *256*(17), 5254–5258.

Wang, F., & Zhang, K. (2012). Physicochemical and photocatalytic activities of self-assembling TiO_2 nanoparticles on nanocarbons surface. *Current Applied Physics*, *12*(1), 346–352. https://doi.org/10.1016/j.cap.2011.07.030.

Wang, W., et al. (2005). Visible light photodegradation of phenol on MWNT-TiO2 composite catalysts prepared by a modified sol-gel method. *Journal of Molecular Catalysis A: Chemical*, *235*(1–2), 194–199. https://doi.org/10.1016/j.molcata.2005.02.027.

Wang, H., et al. (2009). Photocatalytic degradation of 2,4-dinitrophenol (DNP) by multi-walled carbon nanotubes (MWCNTs)/TiO_2 composite in aqueous solution under solar irradiation. *Water Research*, *43*(1), 204–210. https://doi.org/10.1016/j.watres.2008.10.003.

Wang, R. C., Fan, K. S., & Chang, J. S. (2009). Removal of acid dye by ZnFe2O4/TiO2-immobilized granular activated carbon under visible light irradiation in a recycle liquid-solid fluidized bed. *Journal of the Taiwan Institute of Chemical Engineers*, *40*(5), 533–540. https://doi.org/10.1016/j.jtice.2009.02.001.

Wang, H., et al. (2010). Solar photocatalytic decomposition of two azo dyes on multi-walled carbon nanotubes (MWCNTs)/TiO2 composites. *Frontiers of Environmental Science and Engineering in China*, *4*(3), 311–320. https://doi.org/10.1007/s11783-010-0237-7.

Wang, J., et al. (2014). Therapeutic applications of low-toxicity spherical nanocarbon materials. *Nature*, *6*(2), e84. https://doi.org/10.1038/am.2013.79.

Wang, H., et al. (2015a). Microwave-assisted synthesis of reduced graphene oxide/titania nanocomposites as an adsorbent for methylene blue adsorption. *Applied Surface Science*. https://doi.org/10.1016/j.apsusc.2015.11.075.

Wang, H., et al. (2015b). Three dimensional graphene based materials: Synthesis and applications from energy storage and conversion to electrochemical sensor and environmental remediation. *Advances in Colloid and Interface Science*. https://doi.org/10.1016/j.cis.2015.04.005.

Wang, Z., et al. (2017). Photocatalytic active mesoporous carbon/ZnO hybrid materials from block copolymer tethered ZnO nanocrystals. *Langmuir*, *33*(43), 12276–12284. https://doi.org/10.1021/acs.langmuir.7b02492.

Wei, D., et al. (2009). *Synthesis of N-doped graphene by chemical vapor deposition and its electrical properties 2009; 2009*.

This book belongs to Central Library BADJI Mokhtar-ANNABA UNIVERSITY

Copyright Elsevier 2024

Wei, X.-N., et al. (2017). Facile fabrication of mesoporous g-C_3 N_4/TiO_2 photocatalyst for efficient degradation of DNBP under visible light irradiation. *Applied Surface Science*. https://doi.org/10.1016/j.apsusc.2017.08.181.

Weng, B., et al. (2014a). Observing the role of graphene in boosting the two-electron reduction of oxygen in graphene—WO3 nanorod photocatalysts. *Langmuir*, *30*, 5574–5584.

Weng, B., et al. (2014b). Toward the enhanced photoactivity and photostability of ZnO nanospheres via intimate surface coating with reduced graphene oxide. *Journal of Materials Chemistry A*, *2*(24), 9380–9389. https://doi.org/10.1039/C4ta01077a.

Williams, G., Seger, B., & Kamt, P. V. (2008). TiO2-graphene nanocomposites. UV-assisted photocatalytic reduction of graphene oxide. *ACS Nano*, *2*(7), 1487–1491. https://doi.org/10.1021/nn800251f.

Woan, K., Pyrgiotakis, G., & Sigmund, W. (2009). Photocatalytic carbon-nanotube-TiO_2 composites. *Advanced Materials*, *21*(21), 2233–2239. https://doi.org/10.1002/adma.200802738.

Wu, Y., et al. (2016). Mesoporous graphitic carbon nitride and carbon-TiO2 hybrid composite photocatalysts with enhanced photocatalytic activity under visible light irradiation. *Journal of Environmental Chemical Engineering*, *4*(1), 797–807. https://doi.org/10.1016/j.jece.2015.10.023.

Xian, J., et al. (2014). TiO_2 nanotube array-graphene-CdS quantum dots composite film in Z-Scheme with enhanced photoactivity and photostability. *ACS Applied Materials & Interfaces*, *6*(15).

Xiang, Q., Cheng, B., & Yu, J. (2015). Graphene-based photocatalysts for solar-fuel generation. *Angewandte Chemie International Edition*, 11350–11366. https://doi.org/10.1002/anie.201411096.

Xiang, Q., & Jaroniec, M. (2011). Tunable photocatalytic selectivity of TiO 2 films consisted of flower-like. *Chemical Communications*, 4532–4534. https://doi.org/10.1039/c1cc10501a.

Xiang, Q., Yu, J., & Jaroniec, M. (2012). Graphene-based semiconductor photocatalysts. *Chemical Society Reviews*, *41*(2), 782–796. https://doi.org/10.1039/c1cs15172j.

Xiao, F., Miao, J., & Liu, B. (2014). Layer-by-layer self-assembly of CdS quantum dots/graphene Nanosheets hybrid films for Photoelectrochemical and photocatalytic applications. *Journal of the American Chemical Society*, *136*, 1559–1569.

Xiao, J., et al. (2016). Environment-friendly reduced graphene oxide as a broad-spectrum adsorbent for anionic and cationic dyes via π-π interaction. *Journal of Materials Chemistry A*, 1–29. https://doi.org/10.1039/C6TA04119A.

Xie, X., Kretschmer, K., & Wang, G. W. (2013). Advances in graphene-based semiconductor photocatalysts for solar energy conversion: Fundamentals and materials engineering. *Nanoscale*. https://doi.org/10.1039/C5NR03338A.

Xie, G., et al. (2013). Graphene-based materials for hydrogen generation from light-driven water splitting. *Advanced Materials*. https://doi.org/10.1002/adma.201301207.

Xu, A., Gao, Y., & Liu, H. (2002). The preparation , characterization , and their photocatalytic activities of rare-earth-doped TiO 2 nanoparticles. *Journal of Catalysis*, *207*, 151–157. https://doi.org/10.1006/jcat.2002.3539.

Yang, M., & Xu, Y. (2013). Basic principles for observing the photosensitizer role of graphene in the graphene—semiconductor composite photocatalyst from a case study on graphene—ZnO. *Journal of Physical Chemistry C*.

Yang, D., et al. (2008). Chemical analysis of graphene oxide films after heat and chemical treatments by X-ray photoelectron and micro-Raman spectroscopy. *Carbon*, *7*, 1–8. https://doi.org/10.1016/j.carbon.2008.09.045.

Yang, S., et al. (2011). Removal of methylene blue from aqueous solution by graphene oxide. *Journal of Colloid and Interface Science*, *359*(1), 24–29. https://doi.org/10.1016/j.jcis.2011.02.064.

Yang, M., et al. (2014). Artificial photosynthesis over graphene-semiconductor composites. Are we getting better? *Chemical Society Reviews*. https://doi.org/10.1039/C4CS00213J.

Yao, S., et al. (2014). Preparation, characterization and photocatalytic activity of cerium-doped titanium dioxide supported on activated carbon fiber composite. *Indian Journal of Chemistry*, *53*(June), 665–671.

This book belongs to Central Library BADJI Mokhtar-ANNABA UNIVERSITY

Copyright Elsevier 2024

Yap, P., et al. (2010). Synthesis and characterization of nitrogen-doped TiO 2/AC composite for the adsorption – photocatalytic degradation of aqueous bisphenol-A using solar light. *Catalysis Today*, *151*(1–2), 8–13. https://doi.org/10.1016/j.cattod.2010.01.012.

Yazdani, N., & Mohanam, V. (2014). Carbon nano-tube and nano-fiber in cement mortar: Effect of dosage rate and water-cement ratio. *International Journal of Material Sciences*, *4*(2), 45. https://doi.org/10.14355/ijmsci.2014.0402.01.

Yi, X., et al. (2008). Photocatalytic degradation of rhodamine B and phenol by TiO_2 loaded on mesoporous graphitic carbon. *Chinese Journal of Catalysis*, *29*(1), 31–36.

Yu, B. Y., & Kwak, S. Y. (2012). Carbon quantum dots embedded with mesoporous hematite nanospheres as efficient visible light-active photocatalysts. *Journal of Materials Chemistry*, *22*(17), 8345–8353. https://doi.org/10.1039/c2jm16931b.

Yu, H., et al. (2007). TiO2-multiwalled carbon nanotube heterojunction arrays and their charge separation capability. *Journal of Physical Chemistry C*, *111*(35), 12987–12991. https://doi.org/10.1021/jp0728454.

Yu, Y., et al. (2013). Preparation and visible light photocatalytic activity of carbon quantum dots/TiO_2 nanosheet composites. *Carbon*, *68*, 718–724. https://doi.org/10.1016/j.carbon.2013.11.053.

Zaaba, N. I., et al. (2017). Synthesis of graphene oxide using modified Hummers method: Solvent influence. *Procedia Engineering*, *184*, 469–477. https://doi.org/10.1016/j.proeng.2017.04.118.

Zhang, N., Zhang, Y., & Xu, Y. (2012). Recent progress on graphene-based photocatalysts: Current status and future perspectives. *Nanoscale*. https://doi.org/10.1039/c2nr31480k.

Zhang, X., Zhou, M., & Lei, L. (2005). Preparation of an Ag-TiO_2 photocatalyst coated on activated carbon by MOCVD. *Materials Chemistry and Physics*, *91*(1), 73–79. https://doi.org/10.1016/j.matchemphys.2004.10.058.

Zhang, H., et al. (2010a). P25--graphene composite as a high performance photocatalyst. *ACS Nano*, *4*(1), 380–386. https://doi.org/10.1021/nn901221k.

Zhang, L., et al. (2010b). Surface hybridization effect of C60 molecules on TiO2 and enhancement of the photocatalytic activity. *Journal of Molecular Catalysis A: Chemical*, *331*(1–2), 7–14. https://doi.org/10.1016/j.molcata.2010.07.015.

Zhang, Y., et al. (2010c). TiO 2/graphene nanocomposites for gas-phase photocatalytic degradation of volatile aromatic pollutant: Is TiO_2-graphene truly different from other TiO_2-carbon composite materials? *ACS Nano*, *4*(12), 7303–7314.

Zhang, H., et al. (2011a). Fe_2O_3/carbon quantum dots complex photocatalysts and their enhanced photocatalytic activity under visible light. *Dalton Transactions*. *40*(41)10822https://doi.org/10.1039/c1dt11147g.

Zhang, L., et al. (2011b). SiO2/graphene composite for highly selective adsorption of Pb (II) ion. *Journal of Colloid and Interface Science*, *369*(1), 381–387. https://doi.org/10.1016/j.jcis.2011.12.023.

Zhang, H., et al. (2012a). Carbon quantum dots/Ag_3PO_4 complex photocatalysts with enhanced photocatalytic activity and stability under visible light. *Journal of Materials Chemistry*. *22*(21)10501https://doi.org/10.1039/c2jm30703k.

Zhang, Y., et al. (2012b). Graphene transforms wide band gap ZnS to a visible light photocatalyst. The new role of graphene as a macromolecular photosensitizer. *ACS Nano*, (11), 9777–9789.

Zhang, N., et al. (2013). Progress on graphene-based composite photocatalysts for selective organic synthesis. *Current Organic Chemistry*, *17*, 2503–2515. https://doi.org/10.2174/13852728113179990062.

Zhang, N., et al. (2014). Toward improving the graphene-semiconductor composite photoactivity via the addition of metal ions as generic interfacial mediator. *ACS Catalysis*, (1), 623–633.

Zhang, N., et al. (2015). Waltzing with the versatile platform of graphene to synthesize composite photocatalysts. *Chemical Reviews*. https://doi.org/10.1021/acs.chemrev.5b00267.

Zhang, T., et al. (2018). Mesoporous graphitic carbon nitrides decorated with Cu nanoparticles: Efficient Photocatalysts for degradation of Tartrazine yellow dye. *Nanomaterials*, 636. https://doi.org/10.3390/nano8090636.

This book belongs to Central Library BADJI Mokhtar-ANNABA UNIVERSITY

Copyright Elsevier 2024

Zhao, W., et al. (2010). Sunlight photocatalytic activity of CdS modified TiO_2 loaded on activated carbon fibers. *Applied Surface Science*, *256*(11), 3492–3497. https://doi.org/10.1016/j.apsusc.2009.12.062.

Zhao, G., et al. (2011). Few-layered graphene oxide nanosheets as superior sorbents for heavy metal ion pollution management. *Environmental Science and Technology*, *45*(24), 10454–10462. https://doi.org/10.1021/es203439v.

Zhou, W., et al. (2010). Photodegradation of organic contamination in wastewaters by bonding TiO2/single-walled carbon nanotube composites with enhanced photocatalytic activity'. *Chemosphere*, *81*(5), 555–561. https://doi.org/10.1016/j.chemosphere.2010.08.059.

Zhou, K., et al. (2011). Preparation of graphene-TiO_2 composites with enhanced photocatalytic activity. *New Journal of Chemistry*, *35*(2), 353–359. https://doi.org/10.1039/c0nj00623h.

Zhu, S., et al. (2012). Graphene quantum dots with controllable surface oxidation, tunable fluorescence and up-conversion emission. *RSC Advances*, *2*(7), 2717–2720. https://doi.org/10.1039/c2ra20182h.

Zhu, Y., et al. (2014). Carbon-doped ZnO hybridized homogeneously with graphitic carbon nitride nanocomposites for photocatalysis. *The Journal of Physical Chemisty C*, *118*, 10963–10971. https://doi.org/10.1021/jp502677h.

This book belongs to Central Library BADJI Mokhtar-ANNABA UNIVERSITY

Copyright Elsevier 2024

CHAPTER

Synthesis of graphitic carbon nitride—Nanostructured photocatalyst

14

Bin Xue[a,b,c]

Department of Chemistry, College of Food Science and Technology, Shanghai Ocean University, Shanghai, China[a] *Quality Supervision, Inspection and Testing Center for Cold Storage and Refrigeration Equipment (Shanghai), Ministry of Agriculture, Shanghai, China*[b] *National Experimental Teaching Demonstration Center for Food Science and Engineering (Shanghai Ocean University), Shanghai, China*[c]

1 Introduction

Energy and environment are the two major themes of current matter science. Photocatalytic technology combines perfectly of them and is committed to the use of solar energy as a sustainable energy source for environmental remediation, clean energy, and high-quality chemical manufacturing, including degradation of organic pollutants, reduction of heavy metal ions, reduction of carbon dioxide, reduction of nitrogen oxides, decomposition of water to produce hydrogen, and nitrogen fixation (Yang & Wang, 2018; Zhu & Wang, 2017). The development of photocatalytic active materials is the core issue of photocatalytic technology. Since 1972, Fujishima and Honda (1972) discovered that TiO_2 can be used as a photoelectrode to decompose water. A wide variety of semiconductor materials including TiO_2, ZnO, ZnS, CdS, Fe_2O_3, AgX (X = Cl, Br, I), Ag_2S, Ag_3PO_4, $BiPO_4$, and BiOX (X = Cl, Br, I) have been extensively studied as photocatalysts. In 2009, Wang et al. (2009) discovered the photocatalytic hydrogen production activity of graphitic carbon nitride (abbreviated as g-C_3N_4, also known as polymeric carbon nitride). Since then a new wave of research on photocatalytic materials has been set off (Iqbal et al., 2018; Naseri, Samadi, Pourjavadi, Moshfegh, & Ramakrishna, 2017; Zheng, Shen, & Shuai, 2017). The result of querying the *Web of Science* with the theme of "(graphitic carbon nitride AND photocatalyst) OR (g-C_3N_4 AND photocatalysts) OR (polymeric carbon nitride AND photocatalyst)" is shown in Fig. 1. It can be found that the research papers in this field have shown a spurt growth during the decade, which largely reflects the importance of g-C_3N_4 materials in the field of photocatalysis.

G-C_3N_4 is an inorganic metal-free polymer composed of abundant elements of carbon and nitrogen that is environmentally friendly, stable in physicochemical properties, and biocompatible (Wang et al., 2009). G-C_3N_4 is usually obtained by thermal polycondensation with nitrogen-rich organic compounds as the precursors, which has the characteristics of facile and low cost in material synthesis. More importantly the bandgap of g-C_3N_4 is moderate, at 2.7 eV, with visible light-induced photocatalytic activity. Compared with wide-bandgap semiconductors (typical as TiO_2 and ZnO), g-C_3N_4 has visible-light absorption, and it has no photoetching phenomenon compared with narrow-bandgap

Nano-Materials as Photocatalysts for Degradation of Environmental Pollutants. https://doi.org/10.1016/B978-0-12-818598-8.00014-6
© 2020 Elsevier Inc. All rights reserved.

This book belongs to Central Library BADJI Mokhtar-ANNABA UNIVERSITY

Copyright Elsevier 2024

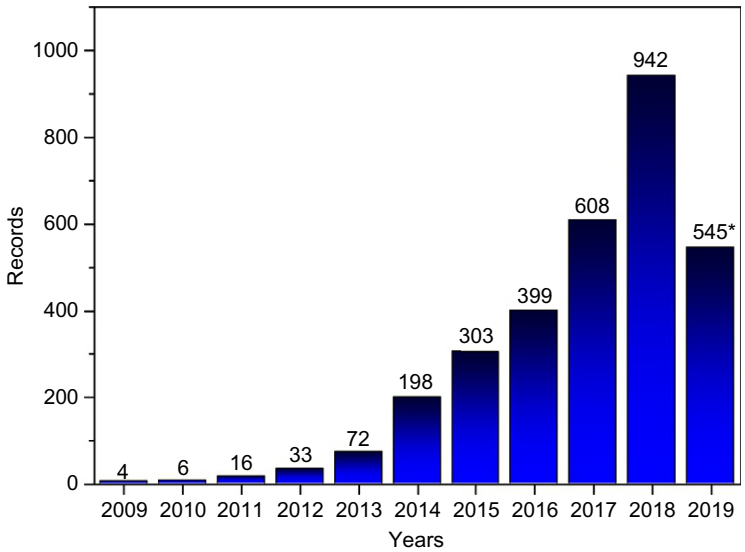

FIG. 1

The relationship between the literature records related on carbon nitride photocatalyst and the years. (*Data ended at 23:20 GMT on June 18, 2019.)

semiconductors (typical as CdS and Fe_2O_3). Therefore g-C_3N_4 is considered to be a very promising visible-light photocatalyst. However, it also has some serious shortcomings. For example, the specific surface area is low, usually only a few $m^2\ g^{-1}$, and the visible-light response range is still narrow, up to 460 nm; the separation efficiency of photogenerated electrons and holes is still low. As a result, its low visible-light photocatalytic activity is far from meeting actual demand.

In view of this, modification of g-C_3N_4 has become a necessary way to improve its photocatalytic activity and promote practical applications. There are a variety of strategies for the modification of g-C_3N_4, including size and shape control (Zhang, Chen, & Wang, 2015); pore creating (primarily mesopores) (Lakhi et al., 2017); doping of metal (alkali metal and transition metal) and nonmetal (boron, carbon, nitrogen, oxygen, sulfur, phosphorus, and halide) (Jiang et al., 2017); constructing heterojunction (type II heterojunction, p-n heterojunction, Schottky heterojunction, and *Z*-scheme heterojunction) (Fu, Yu, Jiang, & Cheng, 2018); combining with carbon materials including carbon quantum dots (Qu et al., 2018), carbon nanotubes (Guo et al., 2018), graphene (Tong et al., 2015), and carbon spheres (Li, Xie, & Zhang, 2016); and defect engineering (nitrogen vacancies and carbon vacancies) (Xiong, Di, Xia, Zhu, & Li, 2018). These efforts explore the possibility of improving the surface/interface properties, photoresponse characteristics, and photogenerated carrier separation efficiency of g-C_3N_4 from different angles and made many exciting developments.

For a new material the primary issue is its size and shape control synthesis, which is essential for understanding the intrinsic properties of the material and exploiting its application potential. However, as an inorganic polymer semiconductor, g-C_3N_4 is quite different in chemical structure and crystallographic properties from inorganic semiconductors, which are well known in the past, and thus has great challenges in morphology controllability. In this chapter the latest advances in the size and shape control synthesis of g-C_3N_4 nanostructured materials are focused from different dimensions, including

This book belongs to Central Library BADJI Mokhtar-ANNABA UNIVERSITY Copyright Elsevier 2024

zero-dimensional (0D) quantum dots (QDs), one-dimensional (1D) nanorods/nanotubes, two-dimensional (2D) nanosheets, and three-dimensional (3D) hollow spheres/nanospheres/microspheres/irregular shapes.

2 Synthesis of bulk g-C_3N_4

Compared with nanostructured g-C_3N_4 materials, the so-called bulk g-C_3N_4 is a product that does not deliberately control the size and shape in the synthesis, which is usually an irregular agglomerate with a micron-scale and dense texture. It itself has visible-light response photocatalytic activity, which is limited. As mentioned in the Introduction, the synthesis of bulk g-C_3N_4 is relatively simple. Usually, organic molecules rich in amino groups, such as melamine, dicyandiamide, cyanamide, urea, or thiourea, are used as the precursors, and the bulk g-C_3N_4 is obtained by thermal polycondensation under heating. The reaction temperature is usually between 500°C and 600°C, and the reaction atmosphere may be air or an inert gas such as nitrogen or argon. During the synthesis process a large amount of irritating gas containing ammonia as a main component is released due to volatilization and decomposition of the precursor. With this method the physicochemical properties of bulk g-C_3N_4 may vary slightly depending on the parameters of the synthesis conditions. On the whole, however, in addition to urea as a precursor, other precursor-derived materials have larger sizes and smaller specific surface areas (usually below $20\,m^2\,g^{-1}$). The materials obtained from urea as a precursor tend to be loose in texture and have a large specific surface area (usually above $50\,m^2\,g^{-1}$). In terms of yield, when thiourea and urea are used as precursors, the yields are often below 10%, and the yields of other precursor-derived materials are up to about 50%. In addition, factors such as heating rate, constant temperature and time, and inert gas flow rate all have an effect on the properties of bulk g-C_3N_4.

3 Synthesis of g-C_3N_4 QDs

Like other semiconductor QDs, 0D g-C_3N_4 has unique physicochemical properties such as large surface area/volume ratio, rich surface functional groups, better solubility, and high quantum yield. More importantly, g-C_3N_4 QDs expose more active sites due to the presence of a large number of nitrogen species, which is critical for tuning surface/interface properties and increasing photocatalytic activity (Wang, Li, Huang, Qian, & Feng, 2016). In addition, the enhanced photoluminescence properties caused by quantum size effects also make g-C_3N_4 QDs have potential application value in chemical and biosensor applications such as ion and molecular detection and cell imaging (Dong et al., 2016; Wang, Sun, Li, & Chen, 2016).

The synthesis approaches of g-C_3N_4 QDs can be divided into two categories: top-down and bottom-up. The top-down method is to cut the bulk g-C_3N_4 into a small-sized 0D QDs by physical or chemical treatment such as acidification, oxidation, hydrothermal, or ultrasonic. Some typical examples are as follows: Zhang, Wang, et al. (2014) prepared the single-layered g-C_3N_4 QDs with stable and strong two-photon fluorescence by modified liquid exfoliation strategies, which involved three steps of concentrated sulfuric acid-nitric acid oxidation treatment, concentrated ammonia water-assisted hydrothermal reaction, and ultrasonic exfoliation (Fig. 2). Wang, Yu, Shen, Chan, and Gu (2014) prepared g-C_3N_4 QDs by a thermal-chemical etching process (Fig. 3). First the bulk g-C_3N_4 directly was heat-treated in air to obtain nanosheets, after which nanosheets were etched in concentrated sulfuric

This book belongs to Central Library BADJI Mokhtar-ANNABA UNIVERSITY
Copyright Elsevier 2024

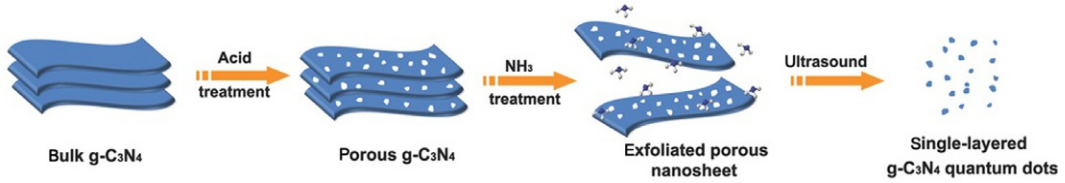

FIG. 2

Schematic illustration of the strategy for the preparation of g-C_3N_4 single-layered QDs (Zhang, Zhang, Yang, & Wang, 2014).

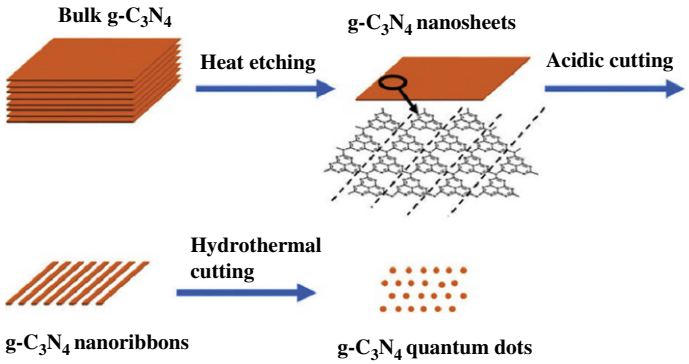

FIG. 3

Schematic illustration of the controllable synthesis of g-C_3N_4 nanosheets, nanoribbons, and quantum dots (Wang, Yu, et al., 2014).

acid-nitric acid to obtain nanoribbons, and the hydrothermal treatment was continued to obtain QDs. The g-C_3N_4 QDs showed strong blue emission and upconversion behavior and were promising for visible-near infrared light photocatalytic systems. Xie et al. (2019) prepared QDs with a high fluorescence quantum yield of 21% and good hydrophilicity by a more convenient one-step hydrothermal cutting process using ethylenediamine as an alkaline corrosive agent. In an easier way, Zhou et al. (2015) obtained g-C_3N_4 QDs with a photoluminescence quantum yield up to 46%. Their approach was to first dissolve the bulk g-C_3N_4 in concentrated sulfuric acid and then added protic solvents to break the hydrogen bond and induce partial hydrolysis of g-C_3N_4. Interestingly, g-C_3N_4 QDs and nanoleaves were obtained in water during the hydrolysis, whereas g-C_3N_4 nanorods were obtained in methanol. That is the morphology of g-C_3N_4 can be adjusted by different hydrolysis conditions. He et al. (2018) first self-assembled 2-, 4-, and 6-triaminopyrimidine, melamine, and cyanuric acid into a supramolecular precursor, which was calcined to produce the bulk g-C_3N_4. Subsequently the electron-rich heterocycle-embedded g-C_3N_4 QDs were prepared by acid treatment and ultrasonication of the modified bulk g-C_3N_4. The presence of 2-, 4-, and 6-triaminopyrimidine as electron donor increased the conjugation effect on triazine ring, which endowed tunable fluorescence properties to g-C_3N_4 QDs. Dai, Han, Fan, and Ai (2018) prepared sulfur-doped g-C_3N_4 QDs by ultrasonic treatment of bulk S-doped g-C_3N_4. The fluorescence intensity of this sulfur-doped g-C_3N_4 QDs was significantly enhanced compared with its bulk counterpart.

This book belongs to Central Library BADJI Mokhtar-ANNABA UNIVERSITY Copyright Elsevier 2024

Bottom-up method converts small molecule organic amine precursors into g-C_3N_4 QDs under heated condition or solid-phase reaction or thermal polycondensation. This method is similar to the synthesis of bulk g-C_3N_4, but the size of the material is limited significantly due to changes in polymerization conditions or adjustment of the composition of the precursors. Examples of using the bottom-up method include the following: for the first time, Liu et al. (2011) reported that photoluminescent g-C_3N_4 QDs were prepared by polymerization of CCl_4 and 1- and 2-ethylenediamine under simple reflux, microwave, or solvothermal heating. Barman and Sadhukhan (2012) synthesized highly blue fluorescent QDs by a simple microwave heating with formamide as precursor. Under solvent-free condition, Zhou, Yang, and Zhang (2013) synthesized g-C_3N_4 QDs with a fluorescent quantum yield of 42% by solid-phase method with urea and sodium citrate as precursors in an autoclave at 180°C. The fluorescent emission properties of g-C_3N_4 QDs can be modulated by varying the ratio of the two reactants. Using human urine as a green and low-cost precursor, Zhuang et al. (2018) achieved the synthesis of luminescent g-C_3N_4 QDs by hydrothermal approach at 200°C for 2 h. This report skillfully used human urine, a urea-rich biowaste, as a raw material to prepare g-C_3N_4 QDs, which was in line with the concept of green chemistry. Precursors containing heteroatoms can be conveniently used to prepare doped QDs. Patir and Gogoi (2018) synthesized sulfur and oxygen doped with a quantum yield of about 13.4% by a facile one-pot thermal method using thiourea and ethylenediaminetetraacetic acid disodium salt as raw materials.

Precursors, synthesis approaches, sizes, and applications of aforementioned g-C_3N_4 QDs are listed in Table 1.

In the aforementioned examples, most g-C_3N_4 QDs are having difficulty to achieve an improvement in photocatalytic activity under visible-light irradiation due to the quantum confinement effect but more apparently promoted in photoluminescence properties. However, g-C_3N_4 QDs modifying itself or other semiconductors to form heterojunctions may be more effective in improving

Table 1 Synthesis conditions, sizes, and applications of g-C_3N_4 QDs.

Nanostructures	Precursors	Synthesis approaches	Sizes	Applications	References
Single-layered QDs	Melamine-derived bulk g-C_3N_4	Acid treatment-hydrothermal treatment-ultrasonication	Diameter ranging from 2 to 6 nm and mainly located at ~4 nm. Thickness of ~0.35 nm	Fluorescence imaging of cellular nucleus	Zhang, Zhang, et al. (2014)
QDs	Thiourea-derived bulk g-C_3N_4	Heat etching-acidic cutting-hydrothermal cutting	Diameters in the range of 5–9 nm (average 6.7 nm)	Photocatalytic H_2 production	Wang, Yu, et al. (2014)
QDs	Melamine-derived bulk g-C_3N_4	Hydrothermal cutting	Diameters in the range of 2–4 nm (average 3.7 nm)	Label-free detection of ascorbic acid	Xie et al. (2019)

Continued

This book belongs to Central Library BADJI Mokhtar-ANNABA UNIVERSITY

Copyright Elsevier 2024

Table 1 Synthesis conditions, sizes, and applications of g-C_3N_4 QDs—cont'd

Nanostructures	Precursors	Synthesis approaches	Sizes	Applications	References
QDs	Dicyandiamide-derived bulk g-C_3N_4	Acid dissolution-hydrolysis	Diameter ranging from 2 to 4 nm and centered at ~3 nm	Photoluminescence probe for rapid detection of Fe^{3+} and a photoconductor in an all-solid state device	Zhou et al. (2015)
Heterocycle-embedded QDs	2, 4, 6-Triaminopyrimidine-melamine-cyanuric acid self-assembled precursor-derived bulk g-C_3N_4	Acid treatment-ultrasonication	Size distribution between 2.5 and 4.0 nm	Cellular fluorescence imaging	He et al. (2018)
S-doped QDs	Dicyandiamide- and thiourea-derived bulk g-C_3N_4	Ultrasonication	Average size of 2.0 nm	Cell imaging	Dai et al. (2018)
QDs	CCl_4 and 1,2-ethylenediamine	Reflux, microwave, or solvothermal heating	Diameters ranging from 1 to 5 nm	Photoluminescence	Liu et al. (2011)
QDs	Formamide	Microwave	Diameter ranging from 2 to 15 nm (average 7 nm). Thickness ranging from 0.3 to 2.1 nm (average ~1.1 nm)	Fluorescence probe for detection of mercuric ions and iodide ions	Barman and Sadhukhan (2012)
QDs	Urea and sodium citrate	Solid-phase reaction	Diameter range of 2.6–5.5 nm (average 4.3 nm). Thickness ranging from 1.5 to 2.5 nm	Cellular fluorescence imaging	Zhou et al. (2013)
QDs	Human urine	Hydrothermal reaction	Size distribution of 2.34 ± 0.57 nm	Cellular fluorescence imaging	Zhuang et al. (2018)
S, O-doped QDs	Thiourea and ethylenediaminetetraacetic acid disodium salt	Thermal treatment	Size in the range of 3–13 nm (average ~6 nm)	Filter paper-based mercury (II) fluorescence sensor	Patir and Gogoi (2018)

This book belongs to Central Library BADJI Mokhtar-ANNABA UNIVERSITY
Copyright Elsevier 2024

photocatalytic activity. For example, Zhou et al. (2018) prepared a composite of g-C_3N_4 QDs and bulk g-C_3N_4 by solvothermal treatment. The QDs self-modifying g-C_3N_4 exhibited a significantly promoted activity in photodegradation of rhodamine B (RhB) due to efficient interfacial charge separation and transport. Wang et al. (2019) fabricated a type II heterojunction by hydrothermal reaction of hydroxyl-modified 0D g-C_3N_4 nanoparticles with a size of less than 20 nm and ZnS. For ZnS the presence of g-C_3N_4 nanoparticles improved hydrophilicity, passivated surface defects, and expanded absorption band edges. As a result, this heterojunction has significant photocatalytic hydrogen production activity, even without any cocatalysts.

4 Synthesis of 1D g-C_3N_4

One-dimensional semiconductor nanostructures including nanorods and nanotubes can be significantly improved in photocatalytic activity due to the fact that photogenerated electrons can be transported in the axial direction. In particular the cavity structure of the nanotube can be used as a nanoreactor to confine the reactants therein, increase its contact with the reactive site, and improve the catalytic efficiency (Wang, Ioccozia, Sun, Lin, & Lin, 2014). Due to the intrinsic properties of lamellar structure, 1D g-C_3N_4 nanostructures are not easy to be formed, but g-C_3N_4 nanorods or nanotubes can still be obtained by taking advantage of the crimpability of 2D lamellar structure under control conditions. For instance, Bai, Wang, Zong, and Zhu (2013) reported a facile reflux method of achieving transformation of g-C_3N_4 from bulk nanoplates to nanorods in methanol solution. The intensity of the photocurrent response and photocatalytic activity of the g-C_3N_4 nanorods was significantly enhanced. They proved the formation mechanism of g-C_3N_4 nanorods involved in the exfoliation and rolling process of g-C_3N_4 nanoplates. The process effectively reduced surface defects and increased active lattice face for g-C_3N_4. By a so-called confined reaction strategy, Liu, Pang, He, and Ge (2017) synthesized mesoporous g-C_3N_4 nanorods. The thermal polycondensation process of cyanamide as a precursor was confined in the prefabricated SiO_2 nanotubes, and the layer of SiO_2 was removed to obtain g-C_3N_4 nanorods. The mesoporous g-C_3N_4 nanorods exhibited high photocatalytic activity and perfect stability in degradation of RhB and H_2 production. Wang et al. (2014) synthesized g-C_3N_4 nanotubes by simply heating an appropriate compact melamine with an NH_3 template-assisted rolling-up mechanism (Fig. 4). They found that the degree of compaction of the precursor melamine was critical for the formation of g-C_3N_4 nanotubes. This can be attributed to the appropriate compact construction that allows the ammonia gas generated by the pyrolysis of melamine to flow in the vertical direction, thereby inducing curling of melamine layers to form nanotubes. In addition, the tendency to reduce surface energy also contributed to the curling of the g-C_3N_4 nanosheets. Liu, Chen, Li, Peng, and Xiong (2017) prepared holey g-C_3N_4 nanotubes by thermal polycondensation of nitric acid-assisted melamine self-assembly products. The adsorption edge of the g-C_3N_4 nanotubes was blue shifted from ~450 to 400 nm compared with bulk g-C_3N_4 due to quantum confinement effects. Furthermore, strong absorption tail of the g-C_3N_4 nanotubes existed simultaneously in visible-light range of 450–800 nm, which was attributed to abundant surface defects. More importantly the photocatalytic activity of the g-C_3N_4 nanotubes was further enhanced after loading the transparent zeolitic imidazo-late framework-8 (ZIF-8) nanoclusters. Bai, Han, Cheng, and Qu (2018) fabricated the wall mesoporous g-C_3N_4 nanotubes by thermal polycondensation of urea microtube arrays produced by vertical gradient freeze growth (VGFG) method (Fig. 5). Because of the benefit from these merits of abundant surface bonding sites, improved

This book belongs to Central Library BADJI Mokhtar-ANNABA UNIVERSITY
Copyright Elsevier 2024

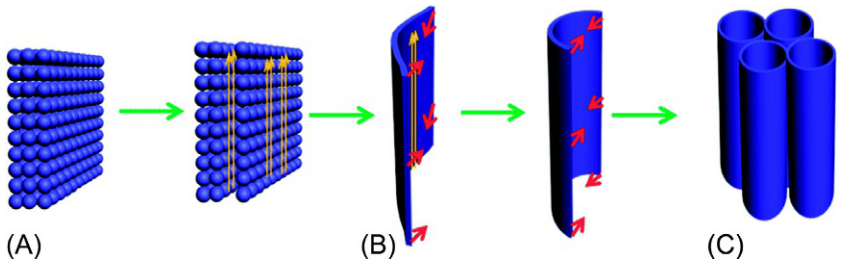

FIG. 4

A proposed formation process of g-C_3N_4 nanotubes: (A) melamine powder packed in an appropriate compact mode, (B) the formation of melamine layers with the assistance of flowing NH_3, and (C) the formation of g-C_3N_4 nanotubes (Wang, Ioccozia, et al., 2014).

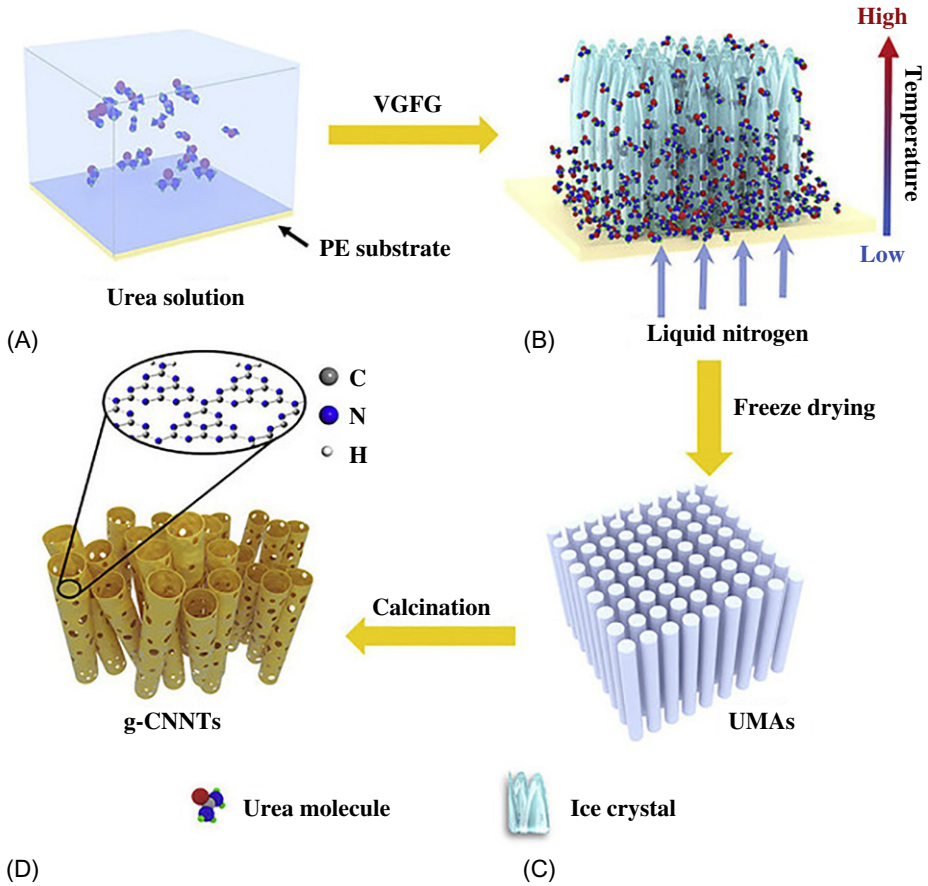

FIG. 5

Schematic of the experimental procedure for fabrication of g-C_3N_4 nanotubes. (A) Urea solution, (B) frozen urea that was synthesized under temperature gradient by unidirectional freezing of the urea solution on top of liquid nitrogen with a VGFG method, (C) parallel urea microrod arrays, and (D) g-C_3N_4 nanotubes (Bai et al., 2018).

This book belongs to Central Library BADJI Mokhtar-ANNABA UNIVERSITY Copyright Elsevier 2024

Table 2 Synthesis conditions, sizes, specific surface areas, and photocatalytic applications of 1D g-C_3N_4 nanostructures.

Nanostructures	Precursors	Synthesis approaches	Sizes	specific surface areas ($m^2\ g^{-1}$)	Photocatalytic applications	References
Nanorods	Dicyandiamide-derived bulk g-C_3N_4	Reflux	0.5–3 μm in length and 100–150 nm in diameter	15.3	Photocatalytic decomposition of methylene blue (MB)	Bai et al. (2013)
Nanorods	Cyanamide	Nanoconfined thermal condensation	Diameter of ~100 nm	135.1	Photodegradation of RhB and photocatalytic H_2 production	Liu, Chen, et al. (2017)
Nanotubes	Melamine	Thermal polycondensation	Wall thickness of about 15 ± 2 nm, inner diameter of about 18 ± 2 nm	~10	Photocatalytic decomposition of MB	Wang, Ioccozia, et al. (2014)
Nanotubes	Melamine	Self-assembly thermal polycondensation	Diameters of 0.5–3 μm and lengths of several tens to hundreds micrometers	11	Photocatalytic CO_2 reduction	Liu, Pang, et al. (2017)
Nanotubes	Urea	Vertical gradient freeze growth-freezing drying-calcination	Diameter of hundreds of nanometers. Wall thickness of 3.3 nm	248	Photocatalytic hydrogen evolution	Bai et al. (2018)

electron-transfer ability, and multielectron transport channels, the nanotubes exhibited a high photocatalytic H_2 production rate and long-term cycling stability under visible-light irradiation.

Precursors, synthesis approaches, sizes, specific surface area, and photocatalytic applications of the aforementioned g-C_3N_4 nanorods or nanotubes are summarized in Table 2.

5 Synthesis of g-C_3N_4 nanosheets

As just mentioned the layered structure is the intrinsic property of bulk g-C_3N_4. In the tendency to minimize the surface energy, however, the bulk g-C_3N_4 obtained under the thermal polycondensation conditions is usually stacked by tens of layers, hundreds of layers, or even more. A small number of layers (or ultrathin) g-C_3N_4 nanosheet materials have a larger surface area-to-volume ratio, more exposed active sites, and more abundant edge defects than bulk counterparts (Zhang et al., 2015).

This book belongs to Central Library BADJI Mokhtar-ANNABA UNIVERSITY
Copyright Elsevier 2024

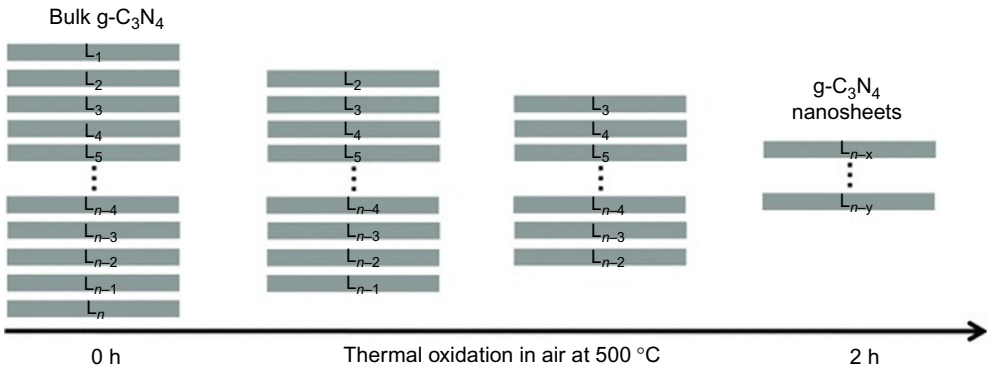

FIG. 6

Schematic of the formation process of the g-C_3N_4 nanosheets by thermal oxidation etching of bulk g-C_3N_4 at 500°C in air (Niu et al., 2012).

Therefore, the intrinsic properties and nanosize effects of g-C_3N_4 are more clearly exhibited. This provides an opportunity for photocatalysis, chemical sensor, and biosensor applications of g-C_3N_4 nanosheets. A large number of reports on the synthesis of g-C_3N_4 nanosheets have recently emerged. Similar to the synthesis methods of QDs, the synthesis of nanosheets generally includes two categories: top-down and bottom-up. For top-down the bulk materials are peeled off into nanosheets, and for bottom-up the modified precursors are thermally polycondensed to nanosheets with a limited stacking.

Top-down examples include the following: in 2012, Niu, Zhang, Liu, and Cheng (2012) first reported the synthesis of g-C_3N_4 nanosheets by thermal oxidative etching (Fig. 6). They calcined the previously prepared bulk g-C_3N_4 in air to obtain nanosheets having a thickness of about 2 nm, a high specific surface area (306 $m^2\ g^{-1}$), and a larger bandgap (2.97 eV). The ultrathin sheetlike nanostructured improved electron transport along the in-plane direction and increased lifetime of photogenerated carriers. The photocatalytic activities of the g-C_3N_4 nanosheets had been remarkably enhanced for •OH radical generation and hydrogen evolution. In the aforementioned method, most of g-C_3N_4 was burned off by the oxidation of air under the secondary calcination, leaving ultrathin nanosheets. Although the yield was only about 6%, the method was very simple, thus becoming a classic synthesis method of g-C_3N_4 nanosheets. Thereafter the details of this method were further studied. Dong, Li, Wang, and Ho (2015) explored the effect of temperature on the synthesis of g-C_3N_4 nanosheets by the thermal oxidation etching. They found that increasing the thermal oxidation etching temperature can increase the specific surface area of the nanosheets and reduce their particle size. Li, Jin, et al. (2016) demonstrated that prolonging the thermal oxidation etching time resulted in macroscopic foamlike holey ultrathin g-C_3N_4 nanosheets with high activity of photocatalytic hydrogen generation and photodegradation of pollutant. In addition, a variety of modified thermal oxidation etching methods was used for the synthesis of the g-C_3N_4 nanosheets. Che et al. (2019) combined NO_3^- insertion with thermal oxidation etching to obtain g-C_3N_4 nanosheets with super large specific surface area and nitrogen vacancy rich. After the bulk g-C_3N_4 was contacted with nitric acid, NO_3^- was intercalated between the layers. Also, hydrogen bond was formed from O in NO_3^- and NH_2 in g-C_3N_4. The bulk g-C_3N_4 was stripped into nanosheets along with the cleavage of hydrogen bonds and the decomposition of NO_3^- during subsequent calcination. Gao et al. (2018) prepared wrinkled ultrathin g-C_3N_4 nanosheets by adding a rapid

This book belongs to Central Library BADJI Mokhtar-ANNABA UNIVERSITY
Copyright Elsevier 2024

cooling treatment in liquid nitrogen after thermal oxidation etching. The layer contraction forces caused by rapid cooling broke the van der Waals forces between layers, which was the main reason for the exfoliating of the bulk g-C_3N_4.

In addition to thermal oxidation etching, ultrasonic liquid exfoliation is also a common method of synthesis of g-C_3N_4 nanosheets. In 2013, for the first time, Zhang et al. (2013) applied ultrasonic-assisted liquid-phase exfoliation to the synthesis of g-C_3N_4 nanosheets. They obtained ultrathin g-C_3N_4 nanosheets with quantum yields up to 19% by sonicating the bulk g-C_3N_4 in water for 16 h. The ultrathin nanosheets exhibited enhanced photoabsorption, photoresponse, and good biocompatibility that could be used in biological imaging. Xu, Zhang, Shi, and Zhu (2013) used sulfuric acid-assisted ultrasonic exfoliation to obtain single atomic layer g-C_3N_4 nanosheets for the first time and applied it in photocatalysis. Sulfuric acid molecules were inserted between the layers to promote the effect of ultrasonic peeling. The single layer g-C_3N_4 nanosheets showed much higher photocatalytic hydrogen production and pollutant decomposition activity than the bulk g-C_3N_4. Cheng, Wang, and Dong (2015) also obtained g-C_3N_4 nanosheets using a similar sulfuric acid-assisted ultrasonic exfoliation method. Moreover, they found that the surface of the g-C_3N_4 nanosheets contained a carboxyl group due to the oxidation of sulfuric acid, and the coexistence of this carboxyl group and the intrinsic amino group of g-C_3N_4 made the nanosheets have amphiphilic properties. Therefore, the g-C_3N_4 nanosheets can be assembled with various charged guests into composite semiconductors with high photocatalytic activity.

Soon after Wang et al. reported the photocatalysis of g-C_3N_4, Zhang, Thomas, Antonietti, and Wang (2009) found that the protonation of hydrochloric acid can cause g-C_3N_4 to be delamination. Therefore, the combination of protonation and ultrasound is more conducive to the exfoliation of g-C_3N_4 nanosheets. Ma, Tang, Dai, and Qiao (2014) prepared 6–12 atomic monolayers of g-C_3N_4 nanosheets by ultrasonically stripping protonated bulk g-C_3N_4. The protonation treatment of hydrochloric acid can shorten the ultrasonic exfoliation time and change the surface charge properties of g-C_3N_4 to cause electrostatic interaction with heparin. The intrinsic fluorescence properties of the as-prepared g-C_3N_4 nanosheets can be used as a chemical sensor for the detection of heparin. Cao, Chen, Jiang, Hu, and Wang (2018) prepared acetaldehyde-modified ultrathin g-C_3N_4 nanosheets through an ethylene glycol-assisted liquid exfoliation route. Ethylene glycol-derived acetaldehyde regulated the surface energy of g-C_3N_4 to better match with that of water, which improved the ultrasonication exfoliation efficiency. The modification of the acetaldehyde group also changed the fluorescent emission of g-C_3N_4 to give it a selective fluorescence response to Ag^+ in both aqueous solution and living HeLa cells.

Intercalation-exfoliation is also a widely used method for the synthesis of g-C_3N_4 nanosheets. Different from the aforementioned intercalation or protonation-assisted ultrasonic exfoliation, Zhou, Wang, et al. (2015) found that bulk g-C_3N_4 can be dissolved in concentrated sulfuric acid at 100°C and form a liquid crystal phase without ultrasonic. This means that the bulk g-C_3N_4 could also be peeled off by simply intercalating with sulfuric acid without ultrasound. This discovery brings a dawn to the efficient liquid-phase exfoliation preparation of g-C_3N_4 nanosheets. Sure enough, almost at the same time, the report of large-scale synthesis of ultrathin g-C_3N_4 nanosheets by dissolution-recrystallization route in concentrated sulfuric acid has emerged. Du, Zou, Wang, and Wang (2015) increased the temperature of the intercalation treatment in concentrated sulfuric acid to 140–170°C to dissolve bulk g-C_3N_4 and then introduced chloride ions to form a well-dissolved poly-ammonium salt by ion exchange, which was convenient for separation and purification. Finally a white ultrathin g-C_3N_4 nanosheet solid was

This book belongs to Central Library BADJI Mokhtar-ANNABA UNIVERSITY Copyright Elsevier 2024

precipitated by recrystallization at a low temperature. In addition to concentrated sulfuric acid, phosphoric acid can also act as an intercalant. Shi et al. (2016) found that, during synthesis of porous g-C_3N_4 nanosheets, phosphoric acid not only played the role of intercalation to help exfoliation but also removed carbon species impurities by protonation to improve charge separation efficiency. The as-prepared porous g-C_3N_4 nanosheets exhibited excellent photocatalytic activities for hydrogen evolution and CO_2 conversion. Interestingly, not only that but also the alkali can dissolve and exfoliate g-C_3N_4. Li et al. (2017) placed bulk g-C_3N_4 in a KOH solution and stirred at 80°C for 24 h to obtain a transparent nanosheet colloid with relatively high concentration (12 g L^{-1}). They proved by theoretical calculation that the interaction of OH^- with terminal -NH_2 or bridged -NH group of the triazine units within bulk g-C_3N_4 promoted the delamination due to decreased bonding energy between layers. Besides, Fang, Dong, Wei, and Ho (2017) reported the exfoliation of g-C_3N_4 nanosheets using anhydrous ethylenediamine as an alkaline assistance reagent. The nanosheets prepared by this method had a thickness of about 3–4 nm and a lateral dimension of more than 15 μm, and this aspect ratio was larger than that of a conventional g-C_3N_4 nanosheets. Salts with good water solubility are also good candidates for intercalators. Ma et al. (2016) calcined melamine and lithium chloride to insert lithium chloride in situ into the layer of bulk g-C_3N_4, and then the obtained bulk g-C_3N_4 was stirred in water, and the lithium chloride was dissolved while peeling off the layer. At the same time the presence of lithium chloride also contributed to the porosity of the g-C_3N_4 nanosheets. Song, Feng, Deng, Xie, and Zheng (2017) used metal lithium to reduce g-C_3N_4 in anhydrous tetrahydrofuran with the presence of naphthalene and added 1-bromododecane as an alkylating agent to obtain surface-functionalized nanosheets. During this process, strong coulombic repulsions between reductive g-C_3N_4 layers and intercalation of Li^+(THF)x complex ions together contributed to exfoliation of g-C_3N_4 sheets. Surface alkylation of the g-C_3N_4 nanosheets also reduced the bandgap and thus increased visible-light harvesting ability. Cui et al. (2018) combined the intercalation and oxidation strategies to hydrothermally heat bulk g-C_3N_4 in a NaClO solution to obtain ultrathin holey nanosheets. NaClO was essential in this route, with sodium ions acting as intercalants and hypochlorite as oxidants. They claimed that this green and clean process could readily expand the production of nanosheets to the kilogram level. In addition to the aforementioned chemical substances, even water molecules can be used as a green intercalator for the exfoliation of g-C_3N_4. Yang, Ou, Fang, and Wang (2017) introduced the water vapor into the system of calcining the bulk g-C_3N_4 at 500°C to obtain exfoliated nanosheets. During the process, water molecules that were inserted between the layers of g-C_3N_4 at a high temperature undergo a steam-reforming reaction with the carbon and nitrogen atoms to release CO, NO, and H_2 gas, thereby cracking the layers. Inspired by this work, Zhou et al. (2019) used the gas bubbles generated by the electrolyzed water to achieve flaking of the layer of g-C_3N_4 under mild conditions. Interestingly, even bacteria can act as intercalations to peeling the nanosheets. Inspired by the ability of bacteria to degrade polymers, Kang et al. (2018) attempted to etch bulk g-C_3N_4 with *Escherichia coli* bacteria to obtain exfoliated nanosheets. It turns out that bacteria can indeed peel off the layers of g-C_3N_4 by breaking weak interlayer van der Waals force and interlayer covalent C—N bond. Furthermore the corrosion action of bacteria created the porous structure of g-C_3N_4 nanosheets. This report provides a new idea to the synthesis of g-C_3N_4 nanosheets by bioengineering.

Ball milling is also an attractive green strategy for preparing g-C_3N_4 nanosheets. Peeling is achieved by mechanical shearing forces to weaken the van der Waals interaction forces between the layers during the ball milling. Zhu et al. (2015) first reported the mechanical peeling of bulk g-C_3N_4 to prepare thin nanosheets by ball milling at large scales. Bu, Chen, Xie, Li, and Ao (2016)

This book belongs to Central Library BADJI Mokhtar-ANNABA UNIVERSITY Copyright Elsevier 2024

obtained ultrathin g-C_3N_4 nanosheets with a yield of about 90% in a similar manner. Ji et al. (2017) ball milled the bulk g-C_3N_4 together with 1-pyrenebutyrate to obtain noncovalently modified nanosheets. The g-C_3N_4 nanosheets had a friendly interface that can covalently interact with DNA to construct electrochemiluminescent biosensor for DNA detection.

The details including precursors, synthesis approaches, thickness, bandgaps, specific surface areas, and applications of the top-down synthesis of g-C_3N_4 nanosheets are shown in Table 3.

As mentioned in the synthesis of bulk g-C_3N_4, the g-C_3N_4 obtained by thermal polycondensation of different precursors is different in size, shape, and specific surface area. Therefore, the rational choice of new precursors or modulation of the structure of precursors will result in a structure-controlled g-C_3N_4. This is the main idea for preparing g-C_3N_4 nanosheets from the bottom-up strategy. The typical examples of this include the following: following the idea of finding a novel precursor, Huang, Li, Chen, and Yuan (2015) chose guanidinium cyanurate as a precursor for one-step thermal polycondensation in air to obtain nanoporous g-C_3N_4 nanosheets. Modifying precursors is one of the easier ways to achieve, and hydrothermal treatment is an effective modification method. For the first time, Hong, Li, Fang, Luo, and Shi (2017) prepared g-C_3N_4 nanosheets using hydrothermally treated melamine as a thermal polycondensation precursor. They found that the hydrothermal treatment temperature of the precursor strongly influenced the morphologies, microstructures, and physicochemical properties of as- prepared g-C_3N_4 nanosheets. Then the same group found that the thickness of g-C_3N_4 nanosheets can be precisely regulated by changing hydrochloric acid-induced hydrothermal assembly of melamine as a precursor (Hong et al., 2017). This was because the concentration of hydrochloric acid during hydrothermal treatment of melamine strongly affected the morphology and crystal structure of the assembly, which were closely related to the thickness of the g-C_3N_4 nanosheets formed by subsequent thermal polycondensation. Huang et al. (2017) introduced thiourea into the hydrothermal pretreatment melamine system to obtain the etched precursor, which was then thermally polycondensed to prepare porous and thin g-C_3N_4 nanosheets. Yan et al. (2019) hydrothermally pretreated melamine in a solution containing Pluronic P123 in hydrochloric acid. It was found that the introduction and removal of P123 changed the structure of g-C_3N_4, and the nanosheets containing a large number of irregular pores were obtained after thermal polycondensation. Xiao et al. (2019) first prepared phosphoric acid-assisted hydrothermally treated melamine and then intercalated glycerol and ethanol into the precursor sheets to obtain finally porous and few-layer g-C_3N_4 nanosheets by thermal polycondensation. Sun et al. (2019) combined the two strategies of doping and shape control. The hydrothermally pretreated melamine in KOH solution was used as a precursor to prepare K-doped g-C_3N_4 nanosheets by thermal polycondensation.

In addition, there have recently been some novel synthesis examples that can be attributed to bottom-up strategies. Iqbal et al. (2017) reported a method for preparing thin g-C_3N_4 nanosheets using gaseous bubble as a template. In the preparation process, melamine and ammonium sulfate were used as precursors, and while melamine was thermally polycondensed, ammonium sulfate was thermally decomposed to release NH_3 and SO_2 gases, which promoted the exfoliation of the nanosheets. Shi et al. (2017) found that melamine and polyacrylamide can undergo self-assembly through hydrogen bonding and electrostatic interaction. The resulting composite was subjected to thermal polycondensation to obtain a single layer of g-C_3N_4 nanosheets. Hydrogen bonding was critical to increasing layer spacing and reducing layer stacking. Zhang et al. (2018) prepared ultrathin g-C_3N_4 nanosheets by thermal polycondensation of urea coated with melamine sponge on the surface. This interesting phenomenon can be explained as follows: a large amount of ammonia gas and cyanic acid produced by the

This book belongs to Central Library BADJI Mokhtar-ANNABA UNIVERSITY Copyright Elsevier 2024

Table 3 Synthesis conditions, thickness, bandgaps, specific surface areas, and applications of g-C_3N_4 nanosheets by top-down method.

Nanostructures	Precursors	Synthesis approaches	Thickness (nm)	Bandgaps (eV)	Specific surface areas ($m^2\ g^{-1}$)	Applications	References
Nanosheets	Dicyandiamide-derived bulk g-C_3N_4	Thermal oxidation etching	Around 2	2.97	306	Photocatalytic hydrogen evolution	Niu et al. (2012)
Nanosheets	Thiourea-derived bulk g-C_3N_4	Thermal oxidation etching	16	2.86	151	Photocatalytic removal of gaseous NO	Dong et al. (2015)
Macroscopic foamlike holey ultrathin nanosheets	Melamine-derived bulk g-C_3N_4	Thermal oxidation etching	About 9.2	2.81	277.98	Photocatalytic H_2 generation	Li, Jin, et al. (2016)
Nanosheets	Urea-derived bulk g-C_3N_4	NO_3^--assisted thermal oxidation etching	4	2.78	421.588	Photocatalytic H_2 evolution and 2-Mercaptobenzothiazole (MBT) decomposition	Che et al. (2019)
Wrinkled ultrathin nanosheets	Dicyandiamide-derived bulk g-C_3N_4	Thermal oxidation etching and rapid cooling	4–5	2.57	142.836	Photodegradations for MB and methyl orange (MO)	Gao et al. (2018)
Nanosheets	Melamine-derived bulk g-C_3N_4	Ultrasonication	~2.5	2.70	–	Bioimaging of the HeLa cells	Zhang et al. (2013)
Nanosheets	Dicyandiamide-derived bulk g-C_3N_4	H_2SO_4 assisted-ultrasonication	0.4	2.92	205.8	Photodegradation of phenol and MB, photocatalytic hydrogen evolution	Xu et al. (2013)
Nanosheets	Melamine-derived bulk g-C_3N_4	H_2SO_4-assisted exfoliation	~9.0	3.42	–	Photodegradation of MO and 4-aminobenzoic acid (ABA)	Cheng et al. (2015)
Nanosheets	Dicyandiamide-derived bulk g-C_3N_4	HCl protonation-assisted ultrasonication	2–4	2.75	305	Heparin sensing	Ma et al. (2014)
Acetaldehyde-modified nanosheets	Urea-derived bulk g-C_3N_4	Ethylene glycol-assisted ultrasonication	2.5	3.01	–	Fluorescence sensing of Ag^+	Cao et al. (2018)

This book belongs to Central Library BADJI Mokhtar-ANNABA UNIVERSITY

Copyright Elsevier 2024

Nanosheets	Dicyandiamide-derived bulk g-C_3N_4	H_2SO_4 intercalation	–	–	–	–	Zhou, Wang, et al. (2015)
Nanosheets	Dicyandiamide-derived bulk g-C_3N_4	H_2SO_4 intercalation	1.0–1.5	3.78	42	–	Du et al. (2015)
Porous nanosheets	Dicyandiamide-derived bulk g-C_3N_4	H_3PO_4 intercalation	~1	2.74	55.4	Photocatalytic H_2 production and CO_2 reduction	Shi et al. (2016)
Nanosheets	Melamine-derived bulk g-C_3N_4	KOH intercalation	0.40 ± 0.16	3.93	–	–	Li et al. (2017)
Nanosheets	Dicyandiamide-derived bulk g-C_3N_4	Ethylenediamine intercalation	Around 3–4	2.76	31.1	Photocatalytic hydrogen evolution	Fang, Dong, et al. (2017), Fang, Li, et al. (2017)
Porous nanosheets	Melamine and lithium chloride	LiCl intercalation	2–3	2.82	186.3	Photocatalytic H_2 production	Ma et al. (2016)
Surface-modified nanosheets	Dicyandiamide-derived bulk g-C_3N_4	Li^+(THF)x complex ion intercalation	1.5	2.38	50	Photodegradation of RhB, photocatalytic hydrogen evolution	Song et al. (2017)
Nanosheets	Melamine-derived bulk g-C_3N_4	Na^+ intercalation and ClO^- oxidation	~4 nm	2.55	170.7	Photocatalytic H_2 evolution	Cui et al. (2018)
Nanosheets	Urea-derived bulk g-C_3N_4	H_2O intercalation	~1.2 nm	2.82	210	Photocatalytic H_2 production	Yang et al. (2017)
Nanosheets	Melamine-derived bulk g-C_3N_4	H_2O intercalation and electrolysis	3–5 nm	2.77	161.2	Degradation of MB	Zhou et al. (2019)
Nanosheets	Melamine-derived bulk g-C_3N_4	Bacterial etching	15.4	2.11	82.61	Photocatalytic disinfection of *Escherichia coli* bacteria photocatalytic degradation humic acid	Kang et al. (2018)
Nanosheets	Melamine-derived bulk g-C_3N_4	Ball milling	0.5–5	2.98	–	Photodegradation of RhB	Zhu et al. (2015)
Nanosheets	Dicyandiamide-derived bulk g-C_3N_4	Ball milling	~2	2.78	–	Photocatalysis water splitting and photodegradation of RhB	Bu et al. (2016)
Noncovalent-modified nanosheets	Dicyandiamide-derived bulk g-C_3N_4 and 1-pyrenebutyrate	Ball milling	~2	–	63.62	Electrochemiluminescent biosensor for the target DNA	Ji et al. (2017)

This book belongs to Central Library BADJI Mokhtar-ANNABA UNIVERSITY
Copyright Elsevier 2024

pyrolysis of urea eliminate the air and prevent the combustion of melamine sponge from carbonizing it. In turn the carbonization product of this sponge acts as a plugging function, creating a nitrogen-rich environment for the thermal condensation of urea and preventing the stacking of nanosheets. Song, Zhang, Wang, Ali, and Zeng (2019) prepared g-C_3N_4 nanosheets using a unique device for placing small crucible inside large crucible. The melamine in the large crucible was sublimated and deposited in the empty small crucible, and finally, carbon-rich holey few-layer g-C_3N_4 nanosheets with large domain size were obtained under the oxygen in situ regulation.

Precursors, synthesis approaches, thickness, bandgaps, specific surface areas, and applications of the bottom-up synthesis of g-C_3N_4 nanosheets are summarized in Table 4.

6 Synthesis of 3D g-C_3N_4

Three-dimensional nanostructures are better candidates for efficient photocatalysts because of their large specific surface areas and interconnected network that facilitate transport of photogenerated carriers (Fang, Li, et al., 2017). Various hierarchical 3D nanostructures have emerged. The hollow sphere is a type of 3D nanostructured photocatalyst that is widely concerned because light can be repeatedly refracted in the inner cavity to improve light utilization efficiency (Nguyen, Vu, & Do, 2015). For g-C_3N_4 the hollow spherical nanostructure is also highly anticipated. The silica sphere hard template method is a more general strategy for preparing hollow spherical structures. To fully fuse the precursor molecules with the silica sphere template, water-soluble cyanamide is often the best choice when preparing g-C_3N_4. As early as 2012, Sun et al. (2012) used this method to prepare hollow g-C_3N_4 nanospheres. They first prepared a silica core-shell structure with a porous nature of the shell. The cyanamide was loaded as a precursor into the pores of the silica shell, and after thermal polycondensation a composite of g-C_3N_4 and silica was obtained. The silica template was etched away with NH_4HF_2 to finally obtain hollow g-C_3N_4 nanospheres. Also the wall thickness of the nanosphere can be adjusted by changing the thickness of the shell of the silica template. Yang et al. (2019) used a similar method to prepare hollow g-C_3N_4 nanospheres with more abundant nanopores and found that the nanospheres showed significant activity in photodegradation of antibiotics. Although silica spheres are used as sacrificial templates, g-C_3N_4 structures obtained from silica spheres of different structures are also different. Zhang, Wang, et al. (2014) prepared a highly open-up g-C_3N_4 nanosphere assembled from interconnected 2D nanosheets using a KCC-1 silica sphere composed of a 2D fiber structure as a template. The nanospheres had sharp edges that facilitate rapid collection and separation of charge, thereby increasing photocatalytic activity. Si et al. (2018) prepared hierarchical macromesoporous g-C_3N_4 microspheres with a bandgap as low as 1.88 eV using silica spheres with hierarchical pores as sacrificial templates. In addition to the hard template method described earlier, the templateless method can also be used to prepare g-C_3N_4 microspheres. Gu et al. (2015) obtained hierarchical g-C_3N_4 microspheres with nanopores on the surface by a templateless solvothermal method and subsequent calcination, which provided a new idea for the synthesis of microspheres. Under solvothermal conditions, cyanuric chloride and melamine in acetonitrile solvent self-assembled to produce polycondensation and after Ostwald ripening to form a microsphere structure. Moreover, postcalcination plays a role in enhancing the degree of polycondensation and increasing the specific surface area.

In addition to the spherical structure, some other 3D structures are also prepared. For instance, Ou, Yang, Lin, Anpo, and Wang (2017) prepared 3D aerogels through g-C_3N_4 nanoparticle self-assembly

This book belongs to Central Library BADJI Mokhtar-ANNABA UNIVERSITY
Copyright Elsevier 2024

This book belongs to Central Library BADJI Mokhtar-ANNABA UNIVERSITY

Table 4 Synthesis conditions, thickness, bandgaps, specific surface areas, and applications of g-C_3N_4 nanosheets by bottom-up method.

Nanostructures	Precursors	Synthesis approaches	Thickness (nm)	Bandgaps (eV)	Specific surface areas ($m^2 g^{-1}$)	Applications	References
Nanoporous nanosheets	Guanidinium cyanurate	Thermal polycondensation	0.6–1.5	2.83	194.7	Photodegradation of RhB	Huang et al. (2015)
Nanosheets	Hydrothermally pretreated melamine	Thermal polycondensation	Around 3	2.63	44.4	Photocatalytic hydrogen evolution	Hong, Li, Fang, et al. (2017)
Nanosheets	HCl-induced hydrothermal assembled melamine	Thermal polycondensation	Approximately 4	2.75	170	Photocatalytic hydrogen evolution	Hong, Li, Li, et al. (2017)
Porous nanosheets	Hydrothermally treated mixture of melamine and thiourea	Thermal polycondensation	3–5	2.63	44.2	Hydrogen evolution and removal of NO	Huang et al. (2017)
Nanosheets with irregular holes	Hydrothermal treatment of melamine with Pluronic P123 as template	Thermal polycondensation	–	2.75	73.29	Photocatalytic degradation of RhB and photocatalytic H_2 evaluation	Yan et al. (2019)
Porous nanosheets	Hydrothermal treatment of melamine and phosphoric acid	Glycerol and ethanol intercalation and thermal polycondensation	~1	2.75	164.2	Photocatalytic hydrogen evolution photocatalytic amine oxidation	Xiao et al. (2019)
K-doped nanosheets	KOH-assisted hydrothermal-reformed melamine	Thermal polycondensation	Around 2	2.60	46.0	Photocatalytic hydrogen evolution	Sun et al. (2019)
Nanosheets	Melamine and ammonium sulfate	Thermal polycondensation	–	2.82	75	Photocatalytic hydrogen production, photodegradation of RhB and phenol	Iqbal et al. (2017)

Continued

Copyright Elsevier 2024

Table 4 Synthesis conditions, thickness, bandgaps, specific surface areas, and applications of g-C_3N_4 nanosheets by bottom-up method—cont'd

Nanostructures	Precursors	Synthesis approaches	Thickness (nm)	Bandgaps (eV)	Specific surface areas ($m^2 g^{-1}$)	Applications	References
Nanosheets	Melamine and polyacrylamide	Thermal polycondensation	c. 0.46–0.93	2.89	31.46	Degradation of MB, MO, and RhB, photocatalytic H_2 evolution	Shi et al. (2017)
Nanosheets	Urea covered with kitchen-available melamine foam	Thermal polycondensation	~4.5	2.4	150.3	Photocatalytic hydrogen evolution	Zhang et al. (2018)
Carbon-rich holey few-layer nanosheets	Melamine	Vapor-polymerization	0.64	2.58	328.6	Photocatalytic H_2 evolution	Song et al. (2019)

This book belongs to Central Library BADJI Mokhtar-ANNABA UNIVERSITY

Copyright Elsevier 2024

FIG. 7

Formation mechanism of hierarchical sea urchin-structure g-C_3N_4 using sealed condensation approach (Zeng et al., 2019).

and gelation strategies. First the g-C_3N_4 nanoparticles were obtained by temperature-induced condensation of melamine in combination with a salt-molten method in which potassium thiocyanate was used as a solvent. The g-C_3N_4 nanoparticles then formed a hydrogel in water, which was converted to an aerogel after freeze-drying. No inorganic or organic cross-linkers were used throughout the process. This 3D aerogel was macroscopic and self-supporting; had a large specific surface area, low density, and good electron conductivity; and had higher photocatalytic activity than the powder counterpart. Luo, Song, Geng, Jing, and Zhang (2018) first protonated bulk g-C_3N_4 and then calcined it in air to obtain a porous, irregular 3D structure. Although the latter process was the same as the synthesis of g-C_3N_4 nanosheets by thermal oxidation etching, the protonation process was added, which greatly improved the yield and the photocatalytic activity. Zeng et al. (2019) prepared a sea urchin-like 3D g-C_3N_4 structure with narrow bandgap ($\sim$2.0 eV) by a combination of sealed condensation and hydrothermal treatment (Fig. 7). During the sealed condensation in a crucible sealed with aluminum foil, porous g-C_3N_4 with nitrogen vacancies was formed under the etching of ammonia gas. After further hydrothermal treatment the porous structure can be transformed into sea urchin-like 3D structure. And due to the presence of nitrogen defects, the bandgap of sea urchin-like 3D structure was significantly reduced.

Precursors, synthesis approaches, sizes, bandgaps, specific surface areas, and photocatalytic applications of 3D g-C_3N_4 nanostructures are summarized in Table 5.

7 Conclusion and outlook

In summary, g-C_3N_4-based materials are new stars in the field of photocatalysis research. The advantages of metal-free, visible-light absorption and stability in g-C_3N_4 provide an opportunity for its application of visible light-induced photocatalysis. The rapid development of synthesis chemistry of g-C_3N_4 materials has opened an avenue for fabricating highly efficient visible-light photocatalyst and exploring structure-activity relationship of photocatalyst. In this chapter the recent advances in the synthesis of g-C_3N_4 nanostructures including QDs, nanorods/nanotubes, nanosheets, and nanospheres/microspheres/irregular 3D structures were summarized. Although exciting results have been achieved in this area, it still faces many challenges. The following three aspects may need to be focused in the future.

This book belongs to Central Library BADJI Mokhtar-ANNABA UNIVERSITY Copyright Elsevier 2024

Table 5 Synthesis conditions, sizes, bandgaps, specific surface areas, and photocatalytic applications of 3D g-C_3N_4 nanostructures.

Nanostructures	Precursors	Synthesis approaches	Sizes	Bandgap (eV)	Specific surface areas ($m^2 g^{-1}$)	Photocatalytic applications	References
Hollow nanosphere	Cyanamide	Core/shell silica templates	Shell thickness of approached 85 nm	–	35	Photocatalytic H_2 production	Sun et al. (2012)
Hollow nanospheres	Cyanamide	Core-shell-structured silica templates	A smaller particle size of 200 nm and a thinner shell thickness of 40 nm	2.89	122	Degradation of levofloxacin (LEVO) and trimethoprim (TMP)	Yang et al. (2019)
Nanospheres	Cyanamide	KCC-1 silica templates	–	2.86	160	Photocatalytic H_2 production	Zhang, Zhang, et al. (2014)
Microspheres	Cyanamide	Hierarchical porous silica templates	Diameter of around 387 nm	1.88	69.1	Photocatalytic hydrogen production	Si et al. (2018)
Microspheres	Cyanuric chloride and melamine	Solvothermal reaction and calcination	Diameter of ~2 μm	2.42	8.5	Photocatalytic H_2 production	Gu et al. (2015)
Aerogels	Melamine	Self-assembly	Diameter of ~2.5 cm	2.77	133	Photocatalytic hydrogen evolution and H_2O_2 production	Ou et al. (2017)
Porous 3D	Melamine-derived bulk g-C_3N_4	Protonation and thermal oxidation	–	–	75.65	Photocatalytic hydrogen production	Luo et al. (2018)
Sea urchin structure	Melamine	Sealed condensation and hydrothermal reaction	–	~2.0	65.6	Photocatalytic hydrogen evolution	Zeng et al. (2019)

This book belongs to Central Library BADJI Mokhtar-ANNABA UNIVERSITY

Copyright Elsevier 2024

Firstly, the synthesis of g-C_3N_4 is relatively simple, and there are not many parameters that can be changed, but the g-C_3N_4 obtained so far is mostly amorphous and nonstoichiometric. Therefore, our understanding of the formation process and crystallization characteristics of g-C_3N_4 nanostructures is still ambiguous. To a certain extent, it is far from being able to precisely manipulate the composition, size, and shape of g-C_3N_4 nanostructures like organic synthesis. As a result, we need to continue to strengthen the research on the synthesis methodology of g-C_3N_4 nanostructures, observe the polymerization process of g-C_3N_4 nanostructures in situ, explore synthetic methods that can precisely control the molecular structure of g-C_3N_4 nanostructures, and develop new synthesis that conforms to atomic economics and green chemistry.

Secondly, defect chemistry is closely related to photocatalytic activity. At present, extensive research has been carried out on defect engineering. However, the defect chemistry involved in g-C_3N_4 nanostructures has not been studied in depth. Are defects generated during the synthesis of g-C_3N_4 nanostructures? How to rationally control defects in g-C_3N_4 nanostructures? How to achieve simultaneous tuning of size, shape, and defect concentration in g-C_3N_4 nanostructures? These are all worthy of further discussion.

Thirdly, when g-C_3N_4 is control synthesized into nanostructures, it is generally possible to increase the specific surface area and improve the separation and migration of photogenerated carriers to improve the photocatalytic activity. However, due to the limitations of intrinsic semiconductor properties, the improvement of photocatalytic activity still needs to be further extended for g-C_3N_4. Building a heterojunction is an effective way to deal with this problem. Coupling heterogeneous semiconductors with g-C_3N_4 can enhance the surface/interface effect of photocatalysis and provide more opportunities for improving photocatalytic activity of g-C_3N_4. Combining the size and shape effects of nanostructured g-C_3N_4 with the surface/interface characteristics of the heterojunction can further provide the effectiveness and stability of the composite photocatalyst. In the future, many new discoveries are worth looking forward to in the development of g-C_3N_4 nanostructure-based heterojunction photocatalyst.

In conclusion the research on g-C_3N_4 materials is on the rise. The application potential of this emerging photocatalytic material is still far from being tapped. The in-depth exploration of g-C_3N_4 brings a new look to the field of photocatalysis.

Acknowledgments

B. X. acknowledges the financial support from Shanghai Ocean University Science and Technology Development Fund (2018).

References

Bai, J. X., Han, Q., Cheng, Z. H., & Qu, L. T. (2018). Wall-mesoporous graphitic carbon nitride nanotubes for efficient photocatalytic hydrogen evolution. *Chemistry—An Asian Journal*, *13*(21), 3160–3164.

Bai, X. J., Wang, L., Zong, R. L., & Zhu, Y. F. (2013). Photocatalytic activity enhanced via g-C_3N_4 nanoplates to nanorods. *Journal of Physical Chemistry C*, *117*(19), 9952–9961.

Barman, S., & Sadhukhan, M. (2012). Facile bulk production of highly blue fluorescent graphitic carbon nitride quantum dots and their application as highly selective and sensitive sensors for the detection of mercuric and iodide ions in aqueous media. *Journal of Materials Chemistry*, *22*(41), 21832–21837.

This book belongs to Central Library BADJI Mokhtar-ANNABA UNIVERSITY

Copyright Elsevier 2024

Bu, Y. Y., Chen, Z. W., Xie, T., Li, W. B., & Ao, J. P. (2016). Fabrication of C_3N_4 ultrathin flakes by mechanical grind method with enhanced photocatalysis and photoelectrochemical performance. *RSC Advances*, *6*(53), 47813–47819.

Cao, S. H., Chen, H., Jiang, F., Hu, Z. X., & Wang, X. (2018). Construction of acetaldehyde-modified g-C_3N_4 ultrathin nanosheets via ethylene glycol-assisted liquid exfoliation for selective fluorescence sensing of Ag^+. *ACS Applied Materials & Interfaces*, *10*(51), 44624–44633.

Che, H. N., Liu, L. H., Che, G. B., Dong, H. J., Liu, C. B., & Li, C. M. (2019). Control of energy band, layer structure and vacancy defect of graphitic carbon nitride by intercalated hydrogen bond effect of NO_3^- toward improving photocatalytic performance. *Chemical Engineering Journal*, *357*, 209–219.

Cheng, F. X., Wang, H. N., & Dong, X. P. (2015). The amphoteric properties of g-C_3N_4 nanosheets and fabrication of their relevant heterostructure photocatalysts by an electrostatic re-assembly route. *Chemical Communications*, *51*(33), 7176–7179.

Cui, L., Liu, Y. F., Fang, X. Y., Yin, C. C., Li, S. S., Sun, D., et al. (2018). Scalable and clean exfoliation of graphitic carbon nitride in NaClO solution: Enriched surface active sites for enhanced photocatalytic H_2 evolution. *Green Chemistry*, *20*(6), 1354–1361.

Dai, X. H., Han, Z. W., Fan, H., & Ai, S. Y. (2018). Sulfur doped carbon nitride quantum dots with efficient fluorescent property and their application for bioimaging. *Journal of Nanoparticle Research*, *20*(12), 315.

Dong, F., Li, Y. H., Wang, Z. Y., & Ho, W. K. (2015). Enhanced visible light photocatalytic activity and oxidation ability of porous graphene-like g-C_3N_4 nanosheets via thermal exfoliation. *Applied Surface Science*, *358*, 393–403.

Dong, Y. Q., Wang, Q., Wu, H. S., Chen, Y. M., Lu, C. H., Chi, Y. W., et al. (2016). Graphitic carbon nitride materials: Sensing, imaging and therapy. *Small*, *12*(39), 5376–5393.

Du, X. R., Zou, G. J., Wang, Z. H., & Wang, X. L. (2015). A scalable chemical route to soluble acidified graphitic carbon nitride: An ideal precursor for isolated ultrathin g-C_3N_4 nanosheets. *Nanoscale*, *7*(19), 8701–8706.

Fang, M., Dong, G. F., Wei, R. J., & Ho, J. C. (2017). Hierarchical nanostructures: Design for sustainable water splitting. *Advanced Energy Materials*, *7*(23).

Fang, L. J., Li, Y. H., Liu, P. F., Wang, D. P., Zeng, H. D., Wang, X. L., et al. (2017). Facile fabrication of large-aspect-ratio g-C_3N_4 nanosheets for enhanced photocatalytic hydrogen evolution. *ACS Sustainable Chemistry & Engineering*, *5*(3), 2039–2043.

Fu, J. W., Yu, J. G., Jiang, C. J., & Cheng, B. (2018). G-C_3N_4-based heterostructured photocatalysts. *Advanced Energy Materials*, *8*(3).

Fujishima, A., & Honda, K. (1972). Electrochemical photolysis of water at a semiconductor electrode. *Nature*, *238*(5358), 37.

Gao, M., Feng, J., Zhang, Z., Gu, M., Wang, J., Zeng, W., et al. (2018). Wrinkled ultrathin graphitic C_3N_4 nanosheets for photocatalytic degradation of organic wastewater. *ACS Applied Nano Materials*, *1*(12), 6733–6741.

Gu, Q., Liao, Y. S., Yin, L. S., Long, J. L., Wang, X. X., & Xue, C. (2015). Template-free synthesis of porous graphitic carbon nitride microspheres for enhanced photocatalytic hydrogen generation with high stability. *Applied Catalysis B: Environmental*, *165*, 503–510.

Guo, Z., Cao, H. B., Wang, Y. X., Xie, Y. B., Xiao, J. D., Yang, J., et al. (2018). High activity of g-C_3N_4/multiwall carbon nanotube in catalytic ozonation promotes electro-peroxone process. *Chemosphere*, *201*, 206–213.

He, X. C., Gu, Y. X., Ai, S. C., Xie, M. M., Lu, Q., Wang, Y. Q., et al. (2018). Electron-rich heterocycle induced tunable emitting fluorescence of graphitic carbon nitride quantum dots. *Applied Surface Science*, *462*, 303–309.

Hong, Y. Z., Li, C. S., Fang, Z. Y., Luo, B. F., & Shi, W. D. (2017). Rational synthesis of ultrathin graphitic carbon nitride nanosheets for efficient photocatalytic hydrogen evolution. *Carbon*, *121*, 463–471.

Hong, Y. Z., Li, C. S., Li, D., Fang, Z. Y., Luo, B. F., Yan, X., et al. (2017). Precisely tunable thickness of graphitic carbon nitride nanosheets for visible-light-driven photocatalytic hydrogen evolution. *Nanoscale*, *9*(37), 14103–14110.

This book belongs to Central Library BADJI Mokhtar-ANNABA UNIVERSITY

Copyright Elsevier 2024

Huang, Z. J., Li, F. B., Chen, B. F., & Yuan, G. Q. (2015). Nanoporous photocatalysts developed through heat-driven stacking of graphitic carbon nitride nanosheets. *RSC Advances*, *5*(18), 14027–14033.

Huang, H. W., Xiao, K., Tian, N., Dong, F., Zhang, T. R., Du, X., et al. (2017). Template-free precursor-surface-etching route to porous, thin g-C_3N_4 nanosheets for enhancing photocatalytic reduction and oxidation activity. *Journal of Materials Chemistry A*, *5*(33), 17452–17463.

Iqbal, W., Qiu, B. C., Lei, J. Y., Wang, L. Z., Zhang, J. L., & Anpo, M. (2017). One-step large-scale highly active g-C_3N_4 nanosheets for efficient sunlight-driven photocatalytic hydrogen production. *Dalton Transactions*, *46*(32), 10678–10684.

Iqbal, W., Yang, B., Zhao, X., Rauf, M., Waqas, M., Gong, Y., et al. (2018). Controllable synthesis of graphitic carbon nitride nanomaterials for solar energy conversion and environmental remediation: The road travelled and the way forward. *Catalysis Science & Technology*, *8*(18), 4576–4599.

Ji, J. J., Wen, J., Shen, Y. F., Lv, Y. Q., Chen, Y. L., Liu, S. Q., et al. (2017). Simultaneous noncovalent modification and exfoliation of 2D carbon nitride for enhanced Electrochemiluminescent biosensing. *Journal of the American Chemical Society*, *139*(34), 11698–11701.

Jiang, L. B., Yuan, X. Z., Pan, Y., Liang, J., Zeng, G. M., Wu, Z. B., et al. (2017). Doping of graphitic carbon nitride for photocatalysis: A reveiw. *Applied Catalysis B: Environmental*, *217*, 388–406.

Kang, S. F., Huang, W., Zhang, L., He, M. F., Xu, S. Y., Sun, D., et al. (2018). Moderate bacterial etching allows scalable and clean delamination of g-C_3N_4 with enriched unpaired electrons for highly improved photocatalytic water disinfection. *ACS Applied Materials & Interfaces*, *10*(16), 13796–13804.

Lakhi, K. S., Park, D. H., Al-Bahily, K., Cha, W., Viswanathan, B., Choy, J. H., et al. (2017). Mesoporous carbon nitrides: Synthesis, functionalization, and applications. *Chemical Society Reviews*, *46*(1), 72–101.

Li, Y. F., Jin, R. X., Xing, Y., Li, J. Q., Song, S. Y., Liu, X. C., et al. (2016). Macroscopic foam-like holey ultrathin g-C_3N_4 nanosheets for drastic improvement of visible-light photocatalytic activity. *Advanced Energy Materials*, *6*(24).

Li, G. N., Li, L., Yuan, H. Y., Wang, H. F., Zeng, H. R., & Shi, J. L. (2017). Alkali-assisted mild aqueous exfoliation for single-layered and structure-preserved graphitic carbon nitride nanosheets. *Journal of Colloid and Interface Science*, *495*, 19–26.

Li, K., Xie, X., & Zhang, W. D. (2016). Photocatalysts based on g-C_3N_4-encapsulating carbon spheres with high visible light activity for photocatalytic hydrogen evolution. *Carbon*, *110*, 356–366.

Liu, S. W., Chen, F., Li, S. T., Peng, X. X., & Xiong, Y. (2017). Enhanced photocatalytic conversion of greenhouse gas CO_2 into solar fuels over g-C_3N_4 nanotubes with decorated transparent ZIF-8 nanoclusters. *Applied Catalysis B: Environmental*, *211*, 1–10.

Liu, X. T., Pang, F., He, M. Y., & Ge, J. P. (2017). Confined reaction inside nanotubes: New approach to mesoporous g-C_3N_4 photocatalysts. *Nano Research*, *10*(11), 3638–3647.

Liu, S., Tian, J. Q., Wang, L., Luo, Y. L., Zhai, J. F., & Sun, X. P. (2011). Preparation of photoluminescent carbon nitride dots from CCl_4 and 1,2-ethylenediamine: A heat-treatment-based strategy. *Journal of Materials Chemistry*, *21*(32), 11726–11729.

Luo, B., Song, R., Geng, J. F., Jing, D. W., & Zhang, Y. Z. (2018). Facile preparation with high yield of a 3D porous graphitic carbon nitride for dramatically enhanced photocatalytic H_2 evolution under visible light. *Applied Catalysis B: Environmental*, *238*, 294–301.

Ma, L. T., Fan, H. Q., Wang, J., Zhao, Y. W., Tian, H. L., & Dong, G. Z. (2016). Water-assisted ions in situ intercalation for porous polymeric graphitic carbon nitride nanosheets with superior photocatalytic hydrogen evolution performance. *Applied Catalysis B: Environmental*, *190*, 93–102.

Ma, T. Y., Tang, Y. H., Dai, S., & Qiao, S. Z. (2014). Proton-functionalized two-dimensional graphitic carbon nitride nanosheet: An excellent metal-/label-free biosensing platform. *Small*, *10*(12), 2382–2389.

Naseri, A., Samadi, M., Pourjavadi, A., Moshfegh, A. Z., & Ramakrishna, S. (2017). Graphitic carbon nitride (g-C_3N_4)-based photocatalysts for solar hydrogen generation: Recent advances and future development directions. *Journal of Materials Chemistry A*, *5*(45), 23406–23433.

This book belongs to Central Library BADJI Mokhtar-ANNABA UNIVERSITY

Copyright Elsevier 2024

Nguyen, C. C., Vu, N. N., & Do, T. O. (2015). Recent advances in the development of sunlight-driven hollow structure photocatalysts and their applications. *Journal of Materials Chemistry A*, *3*(36), 18345–18359.

Niu, P., Zhang, L. L., Liu, G., & Cheng, H. M. (2012). Graphene-like carbon nitride nanosheets for improved photocatalytic activities. *Advanced Functional Materials*, *22*(22), 4763–4770.

Ou, H. H., Yang, P. J., Lin, L. H., Anpo, M., & Wang, X. C. (2017). Carbon nitride aerogels for the photoredox conversion of water. *Angewandte Chemie International Edition*, *56*(36), 10905–10910.

Patir, K., & Gogoi, S. K. (2018). Facile synthesis of photoluminescent graphitic carbon nitride quantum dots for Hg^{2+} detection and room temperature phosphorescence. *ACS Sustainable Chemistry & Engineering*, *6*(2), 1732–1743.

Qu, D., Liu, J., Miao, X., Han, M. M., Zhang, H. C., Cui, Z., et al. (2018). Peering into water splitting mechanism of g-C_3N_4-carbon dots metal-free photocatalyst. *Applied Catalysis B: Environmental*, *227*, 418–424.

Shi, L., Chang, K., Zhang, H. B., Hai, X., Yang, L. Q., Wang, T., et al. (2016). Drastic enhancement of photocatalytic activities over phosphoric acid protonated porous g-C_3N_4 nanosheets under visible light. *Small*, *12*(32), 4431–4439.

Shi, A. Y., Li, H. H., Yin, S., Liu, B., Zhang, J. C., & Wang, Y. H. (2017). Effect of conjugation degree and delocalized 7-system on the photocatalytic activity of single layer g-C_3N_4. *Applied Catalysis B: Environmental*, *218*, 137–146.

Si, Y. S., Huang, T. Q., Li, Q. J., Huang, Y. T., Gao, S. P., Chen, M., et al. (2018). Hierarchical macro-mesoporous polymeric carbon nitride microspheres with narrow bandgap for enhanced photocatalytic hydrogen production. *Advanced Materials Interfaces*, *5*(22).

Song, X. H., Feng, L., Deng, S. L., Xie, S. Y., & Zheng, L. S. (2017). Simultaneous exfoliation and modification of graphitic carbon nitride nanosheets. *Advanced Materials Interfaces*, *4*(15) 1700339.

Song, T., Zhang, P. Y., Wang, T. T., Ali, A., & Zeng, H. P. (2019). Vopor-polymerization strategy to carbon-rich holey few-layer carbon nitride nanosheets with large domain size for superior photocatalytic hydrogen evolution. *Applied Surface Science*, *464*, 195–204.

Sun, S. D., Li, J., Cui, J., Gou, X. F., Yang, Q., Jiang, Y. H., et al. (2019). Simultaneously engineering K-doping and exfoliation into graphitic carbon nitride (g-C3N4) for enhanced photocatalytic hydrogen production. *International Journal of Hydrogen Energy*, *44*(2), 778–787.

Sun, J. H., Zhang, J. S., Zhang, M. W., Antonietti, M., Fu, X. Z., & Wang, X. C. (2012). Bioinspired hollow semiconductor nanospheres as photosynthetic nanoparticles. *Nature Communications*, *3*.

Tong, Z. W., Yang, D., Shi, J. F., Nan, Y. H., Sun, Y. Y., & Jiang, Z. Y. (2015). Three-dimensional porous aerogel constructed by g-C_3N_4 and graphene oxide nanosheets with excellent visible-light photocatalytic performance. *ACS Applied Materials & Interfaces*, *7*(46), 25693–25701.

Wang, M. Y., Ioccozia, J., Sun, L., Lin, C. J., & Lin, Z. Q. (2014). Inorganic-modified semiconductor TiO_2 nanotube arrays for photocatalysis. *Energy & Environmental Science*, *7*(7), 2182–2202.

Wang, A. J., Li, H., Huang, H., Qian, Z. S., & Feng, J. J. (2016). Fluorescent graphene-like carbon nitrides: Synthesis, properties and applications. *Journal of Materials Chemistry C*, *4*(35), 8146–8160.

Wang, S. P., Li, C. J., Wang, T., Zhang, P., Li, A., & Gong, J. L. (2014). Controllable synthesis of nanotube-type graphitic C_3N_4 and their visible-light photocatalytic and fluorescent properties. *Journal of Materials Chemistry A*, *2*(9), 2885–2890.

Wang, X. C., Maeda, K., Thomas, A., Takanabe, K., Xin, G., Carlsson, J. M., et al. (2009). A metal-free polymeric photocatalyst for hydrogen production from water under visible light. *Nature Materials*, *8*(1), 76–80.

Wang, X. W., Sun, G. Z., Li, N., & Chen, P. (2016). Quantum dots derived from two-dimensional materials and their applications for catalysis and energy. *Chemical Society Reviews*, *45*(8), 2239–2262.

Wang, W. J., Yu, J. C., Shen, Z. R., Chan, D. K. L., & Gu, T. (2014). G-C_3N_4 quantum dots: Direct synthesis, upconversion properties and photocatalytic application. *Chemical Communications*, *50*(70), 10148–10150.

This book belongs to Central Library BADJI Mokhtar-ANNABA UNIVERSITY

Copyright Elsevier 2024

Wang, L. J., Zhou, G., Tian, Y., Yan, L. K., Deng, M. X., Yang, B., et al. (2019). Hydroxyl decorated g-C_3N_4 nanoparticles with narrowed bandgap for high efficient photocatalyst design. *Applied Catalysis B: Environmental*, *244*, 262–271.

Xiao, Y. T., Tian, G. H., Li, W., Xie, Y., Jiang, B. J., Tian, C. G., et al. (2019). Molecule self-assembly synthesis of porous few-layer carbon nitride for highly efficient photoredox catalysis. *Journal of the American Chemical Society*, *141*(6), 2508–2515.

Xie, H. Q., Fu, Y., Zhang, Q. Z., Yan, K., Yang, R., Mao, K. H., et al. (2019). Selective and high-sensitive label-free detection of ascorbic acid by carbon nitride quantum dots with intense fluorescence from lone pair states. *Talanta*, *196*, 530–536.

Xiong, J., Di, J., Xia, J. X., Zhu, W. S., & Li, H. M. (2018). Surface defect engineering in 2D nanomaterials for Photocatalysis. *Advanced Functional Materials*, *28*(39).

Xu, J., Zhang, L. W., Shi, R., & Zhu, Y. F. (2013). Chemical exfoliation of graphitic carbon nitride for efficient heterogeneous photocatalysis. *Journal of Materials Chemistry A*, *1*(46), 14766–14772.

Yan, Q. Y., Zhao, C. C., Zhang, L., Hou, Y. L., Wang, S. J., Dong, P., et al. (2019). Facile two-step synthesis of porous carbon nitride with enhanced photocatalytic activity using a soft template. *ACS Sustainable Chemistry & Engineering*, *7*(4), 3866–3874.

Yang, Y. X., Hu, A., Wang, X. Y., Meng, J. Q., Guo, Y. H., Huo, M. X., et al. (2019). Nanopore enriched hollow carbon nitride nanospheres with extremely high visible-light photocatalytic activity in the degradation of aqueous contaminants of emerging concern. *Catalysis Science & Technology*, *9*(2), 355–365.

Yang, P. J., Ou, H. H., Fang, Y. X., & Wang, X. C. (2017). A facile steam reforming strategy to delaminate layered carbon nitride semiconductors for Photoredox catalysis. *Angewandte Chemie International Edition*, *56*(14), 3992–3996.

Yang, X., & Wang, D. (2018). Photocatalysis: From fundamental principles to materials and applications. *ACS Applied Energy Materials*, *1*(12), 6657–6693.

Zeng, Y. X., Li, H., Luo, J. M., Yuan, J. L., Wang, L. L., Liu, C. B., et al. (2019). Sea-urchin-structure g-C_3N_4 with narrow bandgap (~2.0 eV) for efficient overall water splitting under visible light irradiation. *Applied Catalysis B: Environmental*, *249*, 275–281.

Zhang, J. S., Chen, Y., & Wang, X. C. (2015). Two-dimensional covalent carbon nitride nanosheets: Synthesis, functionalization, and applications. *Energy & Environmental Science*, *8*(11), 3092–3108.

Zhang, J. H., Hou, Y. J., Wang, S. J., Zhu, X. J., Zhu, C. Y., Wang, Z., et al. (2018). A facile method for scalable synthesis of ultrathin g-C_3N_4 nanosheets for efficient hydrogen production. *Journal of Materials Chemistry A*, *6*(37), 18252–18257.

Zhang, Y. J., Thomas, A., Antonietti, M., & Wang, X. C. (2009). Activation of carbon nitride solids by protonation: Morphology changes, enhanced ionic conductivity, and photoconduction experiments. *Journal of the American Chemical Society*, *131*(1), 50.

Zhang, X. D., Wang, H. X., Wang, H., Zhang, Q., Xie, J. F., Tian, Y. P., et al. (2014). Single-layered graphitic-C_3N_4 quantum dots for two-photon fluorescence imaging of cellular nucleus. *Advanced Materials*, *26*(26), 4438–4443.

Zhang, X. D., Xie, X., Wang, H., Zhang, J. J., Pan, B. C., & Xie, Y. (2013). Enhanced photoresponsive ultrathin graphitic-phase C_3N_4 nanosheets for bioimaging. *Journal of the American Chemical Society*, *135*(1), 18–21.

Zhang, J. S., Zhang, M. W., Yang, C., & Wang, X. C. (2014). Nanospherical carbon nitride frameworks with sharp edges accelerating charge collection and separation at a soft photocatalytic Interface. *Advanced Materials*, *26*(24), 4121–4126.

Zheng, Q. M., Shen, H. C., & Shuai, D. M. (2017). Emerging investigators series: Advances and challenges of graphitic carbon nitride as a visible-light-responsive photocatalyst for sustainable water purification. *Environmental Science: Water Research & Technology*, *3*(6), 982–1001.

This book belongs to Central Library BADJI Mokhtar-ANNABA UNIVERSITY

Copyright Elsevier 2024

Zhou, Z. X., Shen, Y. F., Li, Y., Liu, A. R., Liu, S. Q., & Zhang, Y. J. (2015). Chemical cleavage of layered carbon nitride with enhanced photoluminescent performances and photoconduction. *ACS Nano*, *9*(12), 12480–12487.

Zhou, L., Tian, Y. H., Lei, J. Y., Wang, L. Z., Liu, Y. D., & Zhang, J. L. (2018). Self-modification of g-C_3N_4 with its quantum dots for enhanced photocatatytic activity. *Catalysis Science & Technology*, *8*(10), 2617–2623.

Zhou, Z. X., Wang, J. H., Yu, J. C., Shen, Y. F., Li, Y., Liu, A. R., et al. (2015). Dissolution and liquid crystals phase of 2D polymeric carbon nitride. *Journal of the American Chemical Society*, *137*(6), 2179–2182.

Zhou, J. X., Xue, J. B., Pan, Q. L., Yang, X. F., Shen, Q. Q., Ma, T., et al. (2019). A gas bubble exfoliation method to prepare g-C_3N_4 nanosheets with enhanced photocatalytic activities. *Journal of Photochemistry and Photobiology A-Chemistry*, *372*, 147–155.

Zhou, J., Yang, Y., & Zhang, C. Y. (2013). A low-temperature solid-phase method to synthesize highly fluorescent carbon nitride dots with tunable emission. *Chemical Communications*, *49*(77), 8605–8607.

Zhu, S. S., & Wang, D. W. (2017). Photocatalysis: Basic principles, diverse forms of implementations and emerging scientific opportunities. *Advanced Energy Materials*, *7*(23) 1700841.

Zhu, K. X., Wang, W. J., Meng, A., Zhao, M., Wang, J. H., Zhang, D. L., et al. (2015). Mechanically exfoliated g-C_3N_4 thin nanosheets by ball milling as high performance photocatalysts. *RSC Advances*, *5*(69), 56239–56243.

Zhuang, Q. F., Guo, P., Zheng, S., Lin, Q., Lin, Y. Y., Wang, Y., et al. (2018). Green synthesis of luminescent graphitic carbon nitride quantum dots from human urine and its bioimaging application. *Talanta*, *188*, 35–40.

This book belongs to Central Library BADJI Mokhtar-ANNABA UNIVERSITY

Copyright Elsevier 2024

CHAPTER

Advancement and modification in photoreactor used for degradation processes

15

Gyanendra Tripathi[a], Dhirendra Kumar Srivastava[b], Jyoti Singh[c], Vishal Mishra[c]

Department of Bioengineering, Integral University, Lucknow, India[a] Council of Science and Technology, Lucknow, India[b] School of Biochemical Engineering, IIT (BHU) Varanasi, Varanasi, India[c]

1 Introduction

Environmental contamination is considered to be one of the major problems worldwide. All classes of living beings are affected by this. New technologies are regularly explored in a way to develop remediation for contaminants of water, soil, and air (Masciangioli & Zhang, 2003). The tremendous increase in the use of particulate matter, pesticides, fertilizers, heavy matter, toxic gases, sewage, oil spills, industrial effluents, and organic compounds over past few decades has inescapably resulted in an increased influx of such pollutants in the environment (Khan & Ghoshal, 2000; Vaseashta et al., 2007).

The increased concentration of such pollutants has severe toxicological effects on living beings (Norton, Baskaran, & Mckenzie, 2004). For this reason, it is essential to remove such pollutants before transport and to cycle into the natural environment. Various materials can be utilized in trademark remediation. A prompt delayed in entrapment and debasements can be attempted because of low reactivity and high instability. To defeat this, nanotechnology has appeared all the more simple way for the advancement of new natural remediation's advances (Tratnyek & Johnson, 2006).

Nanotechnology has pulled several looks in the earlier decades because of its novel physical properties of nanoscale material. Its evolution in the past few years has shown an ever-improving discovery, design, and creation and unique utilization of natural and artificial nanoscale material. Nanomaterial shows better reactivity, that is, better viability when contrasted with their bulkier partners because of their higher surface-to-volume proportion. Nanomaterial can be joined or functionalized with utilitarian gatherings that can target toxins for viable remediation. Also, the purposeful changes in physical properties of the nanomaterial (like shape, measure, porosity, morphology, and concoction creation) give additional beneficial properties that influence the viability of the material for tainting remediation (Guerra, Campbell, Whitehead, & Alexis, 2017). Several methods have been developed in a way to make a composite of two different nanomaterials (composites) having specific desired properties. These composites are more efficient, stable, and selective than those of the single nanoplatforms. Sometimes, appending nanoparticles to a platform has expanded the solidness of the material with correlation with the utilization of nanoparticles alone (Ojea-Jiménez, López, Arbiol, & Puntes, 2012). The explicitness and productivity of the material can likewise be expanded by doping the material with

Nano-Materials as Photocatalysts for Degradation of Environmental Pollutants. https://doi.org/10.1016/B978-0-12-818598-8.00015-8
© 2020 Elsevier Inc. All rights reserved.

This book belongs to Central Library BADJI Mokhtar-ANNABA UNIVERSITY

Copyright Elsevier 2024

explicit synthetic in charge of the focusing on contaminant atoms of intrigue (Campbell, Guerra, Dhulekar, Alexis, & Whitehead, 2015; Shah & Imae, 2016).

The biodegradable materials have been broadly utilized for the aforementioned methodologies as it is essential that the material used for the remediation of contamination is not another toxin themselves; there must not have a shelf life of a waste material to be arranged after its treatment. This will finally result in the more secure and greener alternative for the biological remediation of a toxic substance (Pandey & Fulekar, 2012). Presently, various examinations have been done on utilizing the standard of nanotechnology joining with the physical and substantial alteration of the material to get a built material that can beat a considerable lot of the issues engaged with the remediation of a toxin (Kamat & Meisel, 2003).

2 Remediation

It is an exploration of the degradation of toxins from the earth utilizing complex or natural methods. Late works have made ways for the control and perversion of pollutants in water, air, and soil—the major ecological issue. The traditional procedures of remediation produce troublesome side effects. Likewise, pollutants like chlorinated hydrocarbon have polluted water bodies and now have achieved the base region creating it incredibly hard to remediate water level with present methodology. These confinements can be successfully overwhelmed with the utilization of the nanotechnology (Masciangioli & Zhang, 2003). As nanoparticles can be carried with a stream of water, this characteristic can be utilized for the treatment of underground water contaminants without scooping. The development of nanoparticles is to a great extent constrained by sedimentation.

What's more utilized naturally, they can likewise be a dock on a secure network and can be used for wastewater or vaporous stream treatment (Mueller et al., 2012; Karn, Kuiken, & Otto, 2009). The most typically utilized nanoparticle is iron, which is used as a remediation tool (Mehndiratta, Jain, Srivastava, & Gupta, 2013). It is a pioneering reductant to be employed as remediation of any pollutant that can be degraded by the procedure. The iron nanoparticle is used to remediate surface and subsurface contaminants like conventional solvents, composts, pesticides, petrochemical blends, and overpowering metals.

The proximity of antibiotics agents in the oceanic condition has additionally raised a significant issue. The conventional techniques like the utilization of nonpermeable graphite and nonpermeable enacted carbon are used as remediation. Conversely, with these procedures, the single- and the multiwalled carbon nanotubes give a better usage as adsorbent as the course of action allocation coefficient and adsorption tendency for antibiotics (Lead et al., 2018).

3 Photoremediation

Photoremediation by semiconductor nanoparticles relies upon the oxidation and diminishing of adsorbed pollutant upon bandgap stimulation of the nanoparticles. The photocatalytic properties of specific material have been utilized to change over sun-powered vitality into compound vitality to oxidize or decrease material. This is done to acquire valuable material hydrogen and hydrocarbon and to clear

This book belongs to Central Library BADJI Mokhtar-ANNABA UNIVERSITY
Copyright Elsevier 2024

contaminations and microscopic organisms present in soil air and water (Fujishima & Honda, 1972; Fujishima, Zhang, & Tryk, 2008). Of many photocatalysts, TiO_2 is most generally contemplated and utilized for some applications on account of its solid oxidizing abilities (Hoffmann, Martin, Choi, & Bahnemann, 1995). The nanoparticles of TiO_2 are energized by UV-emission presentation provoking the entry of OH/OH^-. Radicals may decline or oxidize the contaminant after experiencing oxidative degradation. The adsorbed electron upon excitation by bright light shifted to the nanoscale particle. In this technique at the time of photocurrent, TiO_2 nanoparticles can be used. In this technique at the time of photocurrent, TiO_2 nanoparticles can be used (Kamat & Meisel, 2003). For example, by semiconductor nanoparticles, on doping with transitional metal parts extends the photoresponse of TiO_2 nanoparticles to indisputable luminous (Anpo et al., 1998). The semiconductor nanocluster of ZnO plays an active role in the biological applications as it originates solidly in a perceptible zone. Like this, nanoparticle of ZnO can be effectively used for the degradation of particular contaminants, for example, PCBs adsorbed to its surface (Kamat & Meisel, 2003).

4 Semiconductor nanoparticles as a photocatalyst

Semiconductor nanoparticles in a photocatalysis process participate in either direct or indirect manner. The bandgap excitation of semiconductor particles results in the charge separation. The retained substrates are reduced or oxidized by the photogenerated electrons and gaps (Fig. 1). Then again, the charge exchange between two assimilated particles additionally happens as a result of the photocatalytic response by the semiconductor nanocluster. This procedure is called photosensitization, which is broadly utilized in photochemistry and picture science (Vinodgopal, Wynkoop, & Kamat, 1996). Photograph-initiated charge move forms in semiconductor nanoclusters are completed in two different ways: under bandgap excitation and sharpened charge infusion by energizing adsorbed color particle. Primarily in the case of band excitation of semiconductor particles, they are trailed by the charge trade at semiconductor interface.

Nonetheless, on the other hand, some nanoparticles tolerating an electron quenches the energized state and after that charge exchange to another molecule or makes photocurrent. The pollutant color exclusively goes about as a sensitizer and encounters degradation by oxidation. This step is considered to be valuable in the staining of TiO_2 nanoparticle color (Nasr et al., 1996).

There are numerous components that can apply critical impact on photocatalytic execution, including specific surface zone, crystalline stage, shape, estimate, pore structure, and the uncovered surface features. Thus adjustment in these properties at last improves the photocatalytic execution. For instance, a sphere has zero dimensionality and also with a high unequivocal surface region, and as a result, there is an increment in the rate of photocatalytic decay of natural contamination (Liu et al., 2011). One-dimensional cylinders have points of interest concerning less recombination on account of the least separation for charge transporter dispersion, light-dissipating properties. Zero-dimensional and one-dimensional structures have been examined and created. Two-dimensional nanosheet has shiny surfaces and grip.Three-dimensional stone landmarks may have higher transporter flexibility because of interconnecting structure and fitting dimensionalities that enable to take the full ideal position of remarkable properties provided by nanomaterials.

This book belongs to Central Library BADJI Mokhtar-ANNABA UNIVERSITY Copyright Elsevier 2024

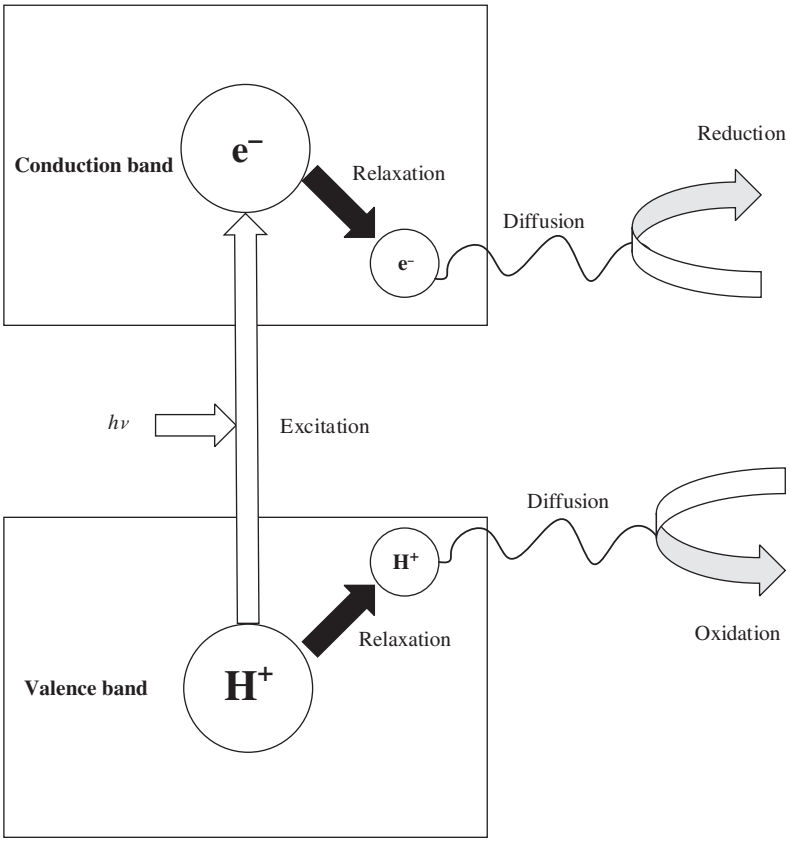

FIG. 1

Schematic diagram of an improvement of photogenerated charge transporters (gap and electrons) upon an endless supply of bright (UV) light.

5 Advancement of photocatalyst/auxiliary structure and properties of photocatalysts

5.1 Zero-dimensional

Micro- or nanostructured spheres are considered to be widely studied and helpful when used. The TiO_2 nanostructured domains that contain a higher specific surface area, as well as higher pore size and volume, provide a high available surface area and rate of mass transfer. It results in better photocatalytic execution as photocatalytic response gives synthetic reactions on the outside of photocatalyst.

Moreover, these essential highlights increment the light-gathering capacities of materials because it improves light use by permitting much light more than expected to get inside. Their light-collecting ability makes them the excellent possibility for utilizing in photocatalysis, yet additionally in DSSCs (Kondo et al., 2008; Liu, Yu, & Jaroniec, 2010). Domains of this sort are ordinarily arranged from a

This book belongs to Central Library BADJI Mokhtar-ANNABA UNIVERSITY
Copyright Elsevier 2024

titanium alkoxide, for example, titanium tetraisopropoxide or titanium tetrabutoxide, within the polymer sight to furnish a porous structure with/without the expansion of a corrosive to quicken the response. TiO_2 domains got further treated as indicated by aqueous techniques to deliver permeably or various leveled structures (Liu et al., 2011). TiO_2 at higher toughening temperatures displayed prevalent photocatalytic exercises and framed after a strengthening procedure at 400°C specifically. It demonstrates the most astounding photocatalytic action for the deterioration of natural particles on account of their high explicit surface territory and an exceptionally crystalline structure (Li et al., 2007). The possibility of the development of empty structures for getting high photocatalytic execution is because of a vacant structure that possesses not only an upper explicit surface zone but also empowers various diffractions and impressions of light (Li, Xiong, Li, & Xie, 2006).

TiO_2 gems with uncovered high-vitality (001) features have high photocatalytic action. Considering this, TiO_2 spheres containing such features would show incredibly upgraded dimensions of photocatalytic movement (Nosaka, Komori, Yawata, Hirakawa, & Nosaka, 2003). Hierarchical and empty structures with (001) aspects were commonly arranged by the hydro- or solvothermal techniques utilizing titanium alkoxides. Both the presentation of the progressive structure and high-vitality (001) aspects can provide higher photocatalytic action (Chen et al., 2010; Delaiásun, 2010; Liu et al., 2010; Xiang, Yu, & Jaroniec, 2011). Liu et al. revealed the formation of core-shell (mesoporous) circles made out of little TiO_2 nanocrystals with uncovered advanced features using a blend of electrospray and fluid treatment strategies (Liu et al., 2011). The electrospray technique uses electric field of high voltage to get scale or can say nanosized circles, and TiO_2 (core-shell) domains were conveyed by electrospray with the help of polyvinylpyrrolidone (PVP) and titanium alkoxide. Ensuring watery treatment gave a dynamic structure with tunable pore measure, specific surface domain, pore volume, and dimension of decided valuable stone highlights. In the light that the PVP encircled a sort out, the indistinct particles (TiO_2) can fill the pores inside the framework after electrospray of TiO_2 (core-shell) circles. In this way the PVP was expelled from the TiO_2 circles. Also the subsequent TiO_2 was solidified amid the aqueous process. The *gem* morphology relied upon a few conditions counting the measure of PVP utilized and the states of the aqueous strategy.

5.2 One-dimensional

A material having one-dimensional structures, for example, filaments and tubes, has exceptional properties and focal points for the photocatalytic responses. In filaments and cylinders, greater surface-to-volume extent enables a decline in recombination of hole-electron rate. The high interfacial charge transporter conversion scale is useful for the photocatalytic responses (Almquist & Biswas, 2002). TiO_2 fibers are now utilized in a broad scope of utilization, including photocatalysis, gas detecting, and batteries (Fujishima & Zhang, 2006; Moon, Park, Lee, Zyung, & Kim, 2010; Park et al., 2010). There are a few techniques accessible for planning TiO_2 strands as a useful tool in the creation of TiO_2 filaments is electrospinning, that is, an essential technique for conveying nanofibers. Along with this method, an electric field of high voltage with the setup being applied on a fundamental level that was equivalent to the methodology known as electrospray (Ramakrishna, 2005) (Fig. 2).

Morphologies of the filament can be fitted extraordinarily by changing the methodology parameters, consisting of the game-plan fixation, a subatomic load of the polymer, decision of dissolvable, related electric-field quality, and promise free. Nonwoven carpets cumulative from filaments have

This book belongs to Central Library BADJI Mokhtar-ANNABA UNIVERSITY
Copyright Elsevier 2024

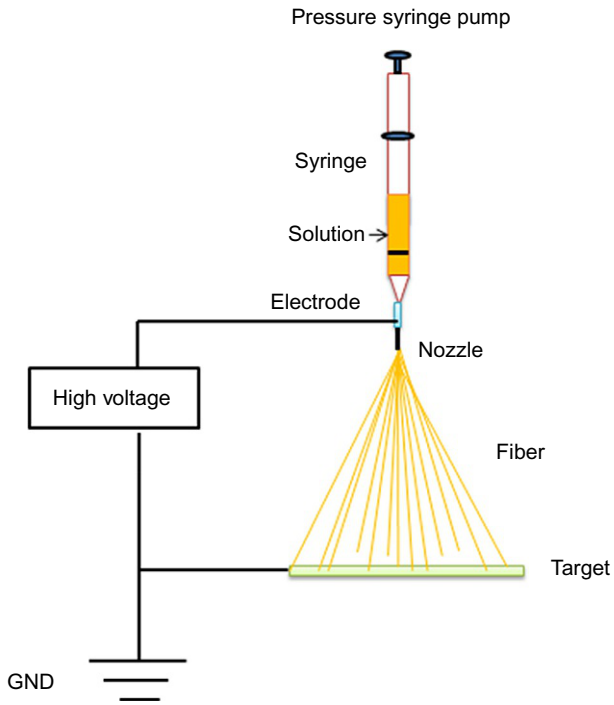

FIG. 2

Diagrammatic representation of setup for electrospinning.

properties, for example, low protection from mass transports also and a vast volumetric surface region in context on their open model with a gap between the strands.

From electrospinning blend of polymer, the titanium alkoxide has engineered TiO_2 strands, for example, PVP, with a resulting step termed as the calcination step can be further used to clear the polymer and must also solidify TiO_2 (Li & Xia, 2003). The standard extensiveness of TiO_2 filaments can be constrained by changing various arranging parameters, for instance, the nature of the electric field, the degree of polymer to that of titanium tetraisopropoxide, and then the rate of envoy in the electrospinning strategy. Electrospun TiO_2 filament, for the most part, has large surface-zone-to-volume degrees and is in this manner expected to give productive photocatalytic shows to the corruption of ordinary particles, for example, methylene blue and methyl orange (Alves, Berutti, Clemens, Graule, & Bergmann, 2009). We should need to bring up that stringy photocatalysts are connecting with the likelihood for reasonable applications in the environmental cleanup. In a photocatalytic methodology, the division of atom-type photocatalysts from the course of action following the response can be troublesome. Also the propensity of the particles to agglomerate into more prominent particles adequately reduces the photocatalytic advancement amid the cycled use. On the other hand the strands can be utilized as a tangle, getting out the issues related to the division.

Anodization is seemed to be a remarkable asset for the generation of tubes made up of TiO_2. The term anodization usually is used in an electrolyte containing HF-based watery course of action. A foil

This book belongs to Central Library BADJI Mokhtar-ANNABA UNIVERSITY Copyright Elsevier 2024

of titanium terminal and counter anode are ingested in the electrolyte, with the two being connected with a power supply to apply an anticipated voltage (Zhang et al., 2007; Liu et al., 2008). Following the anodization strategy, TiO_2 nanotube had a straight channel against the foil and restricted on the foil surface. This associate trademark gives unavoidable photocatalytic spoil of common toxic substances since it empowers the clear dispersing of basic contaminations into the TiO_2 nanotubes. In a photocatalytic system the division of molecule-type photocatalysts from the course of action following the response can be troublesome. In addition to this, the propensity of particles to agglomerate into more noteworthy particles successfully diminishes the photocatalytic advancement amid the cycled use.

On the other hand the strands can be utilized as a tangle, getting out issues related to division Mor, Varghese, Paulose, Shankar, & Grimes, 2006; Liu et al., 2008; Mor, Varghese, Paulose, & Grimes, 2005; Prakasam, Shankar, Paulose, Varghese, & Grimes, 2007; Paulose et al., 2006; Albu, Ghicov, Macak, Hahn, & Schmuki, 2007; Quan, Yang, Ruan, & Zhao, 2005). The morphology, as well as particularly the stretch of the nanotubes, impacts the photocatalytic execution of nanotube (TiO_2) shows. Developing the length of the TiO_2 nanotubes in this manner redesigns the photocatalytic implementation due to the extensive definite surface area. Liu et al. engineered 17-m TiO_2 nanotube shows by a mix of broadening the anodization time and the utilization of blended electrolyte comprising formamide, ammonium fluoride, and water (Liu et al., 2008). An overhaul in the photocatalytic execution for the spoil of trademark particles (acetaldehyde for this situation) was seen, which was credited to the more noteworthy surface zone. They show that the high-TiO_2 nanotubes demonstrated a more recognizable photocatalytic execution than that nanoparticulate P25 film of about a similar thickness. The altogether requested TiO_2 nanotube bundle has longitudinally straight canals with open mouths against the substrates that enabled essential passage of the acetaldehyde to that of the surface of TiO_2. Then again, the film of P25 TiO_2 nanoparticles consists of a disordered structure in light of unpredictably stuffed particles of TiO_2 that secures the dissipating of typical iotas.

5.3 Two-dimensional

A nanosized drop-framed material (nanosheet) possesses a dimension surface of a large perspective extent. Also, nanosheets have 1–10 nm of unimaginably small thickness and a flat side of the range from the submicrometric level to few micrometers. The resulting shape has low turbidity, high smoothness, and a splendid connection to substrates (Wen, Itoh, Tang, & Feng, 2007). Nanosheets display photocatalytic qualities including the superhydrophilicity and the photocatalytic devastating of ordinary particles, under UV light (Xiang et al., 2011). The blend of their significantly smooth surface and photocatalytic properties has incited the significant use as self-cleaning coating nanosheet film (Wen et al., 2007). TiO_2 nanosheets are generally organized by a fundamental watery technique using TiO_2 powder from protonictitanate hydrates, trailed by either a hydro-/solvothermal responses or calcination procedure (Wen et al., 2007; Xiang et al., 2011).

The photocatalytic breakdown of standard particles by nanosheets of TiO_2 was researched a lot. Shibata et al. revealed that the collection of nanostructured (TiO_2) films from that of TiO_2 nanosheets furthermore kept on defining their photocatalytic execution for the crumbling of 2-propanol and the methylene blue color (Xiang et al., 2011). Moderate photocatalytic breaking down of 2-propanol has been recognized under UV light, with the delivery of CO_2. It was found that the valence band edge of TiO_2 nanosheet is 0.5 eV, which was more significant than that of mass anatase. It was found that there is enough ability of TiO_2 nanosheet to break down 2-propanol (Sakai, Ebina, Takada, & Sasaki,

This book belongs to Central Library BADJI Mokhtar-ANNABA UNIVERSITY Copyright Elsevier 2024

2004). Electron opening sets are created in photocatalysts under the enlightenment of light with a photon imperativeness identifying along with the bandgap, and along these lines, they diffuse from the inside mass to that of the surface. It was found that each of the TiO_2 nanosheets is electronically ensured, regardless, not a lot of the electron-opening sets made inside a party of TiO_2 nanosheets and these nanosheets can diffuse on the surface and the (nanosheet) TiO_2 along these lines merely gives moderate breaking down of 2-propanol.

TiO_2 nanosheets can also show the photo impelled hydrophilicity under the UV brightening.As communicated more than, merely a nanosheet of TiO_2 not only contains photocatalytic properties but can also provide lower turbidity and astounding security, that provides higher smoothness, and contain one potential utilization of the nanosheets of TiO_2 accordingly in self-cleaning surfaces. Shichi et al. uncovered the formation of a self-cleaning glass with the help of TiO_2 nanosheets (Wen et al., 2007). The production system ordinarily incorporated the use of a thick blocking layer, for instance, SiO_2 onto soft drink lime glass to keep up a vital separation from scattering of Na^+ particles from the glass in the midst of the warming strategy, in light of the way that the closeness of Na^+ particles altogether diminished the photocatalytic development. The TiO_2 nanosheet was used to secure glass followed by a calcination methodology. The TiO_2 nanosheet had stable attachment to glass, low turbidity, and exceptional rigidity, which is for the most part assessed by a film hardness analyzer utilizing pencils in a pencil test (Katsumata et al., 2010). Also, following the dive covering of one self-cleaning glass in an answer consisting of methylene blue, hardly any of the methylene blue was affixed to one self-cleaning glass, showing higher antifouling properties. Instead of this result, the glass secured with the nanoparticles (TiO_2) experiences a critical association of methylene blue. Differences between the results can be credited to that of the smooth surface of oneself cleaning glass arranged via nanosheets of TiO_2 that reduces the association of methylene blue iotas, while the glass masterminded using particles (TiO_2) has a considerable upsetting surface, which propels the association of the molecules of methylene blue. Materials with this blend of low hold and the photocatalytic properties (oxidative crumbling of characteristic particles and the photo-induced hydrophilicity) are incredible plausibility for the applications as of new coatings/self-cleaning coating.

5.4 Three-dimensional

For making another class of materials with novel applications, the three-dimensional interconnected structures possess great potential. Arrangements of this sort are fundamental for sober utilizations in light of the way that the three-dimensional distinctive leveled structure-containing pores have perhaps gigantic surface-to-volume degrees that give a giant favored perspective as valuable dispersal pathways for visitor species, for example, trademark dangerous substances, into the system lastly help fruitful purifying, division, and farthest point. An interconnected structure is considered to be a potentially unrivaled for transporter flexibility, anyway additionally from a practical perspective. For instance, virtually all photocatalytic purifiers utilize particles of TiO_2 verified onto vulnerable stoneware. The TiO_2 particles might be taken from the ceramics, regardless, urging the passage of little development particles and the degradation of photocatalytic properties. To keep up a primary partition from this stripping philosophy, an interlayer, for example, SiO_2, is consistently put between a substrate and TiO_2 particles, which is utilized to tie the TiO_2 particles.

This book belongs to Central Library BADJI Mokhtar-ANNABA UNIVERSITY
Copyright Elsevier 2024

6 Advancement of photoreactor in terms of applications for the degradation of the following contaminants

6.1 Dye

A rotating disk reactor that essentially builds proficiency has been planned and assessed for the use of photocatalytic disintegration of color (dye) contaminations in liquid solutions. Under this technique, a multilayer turning circle reactor (MLRDR) was introduced having a speed of 600 rpm (Fig. 3). The disk has a diameter of 12 cm and photocatalyst (TiO_2) particles immobilized on the surfaces of rings.

Inside each layer of the reactor, methyl orange fluid arrangement is permitted to spill out of the focal point of the circle in a spiral heading along the outside of the plate (inlet at a speed of 4×10^{-5} M MO), which is turning at fast and is illuminated with eight UV-light lamps (4 W). The emanating is then co-ordinated to the focal point of another layer that lies at the bottom. Four irregular layers have been tried in this examination, and the impacts because of the volumetric stream rate and quantity of the sheets on response transformation are explored. The productivity of this photocatalytic reactor shows complexity for these parameters. Under selected working conditions, productivity >95% can be accomplished at 5 mL min^{-1} (Lin, Chang, Huang, Tsai, & Wu, 2012).

(a) In a way to research cheap adsorbents to evacuate methylene blue (MB) from watery arrangements, volcanic fiery remains (VAs) with Ti-changed volcanic cinders (TVA) are used. TVA showed higher and quicker adsorption of methyl blue than flaming volcanic remains. Adsorption was done in a batch framework at room temperature. High-weight Na vapor light (Philips, model400-W G/92/2) was kept 50 cm away from the reactor (Fig. 4). A fixed-bed photocatalytic reactor was used.

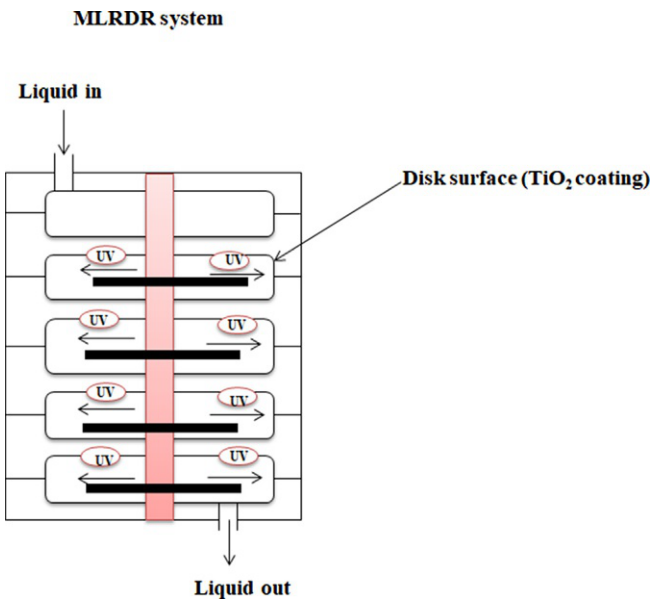

FIG. 3

Diagrammatic representation of the MLRDR system.

This book belongs to Central Library BADJI Mokhtar-ANNABA UNIVERSITY
Copyright Elsevier 2024

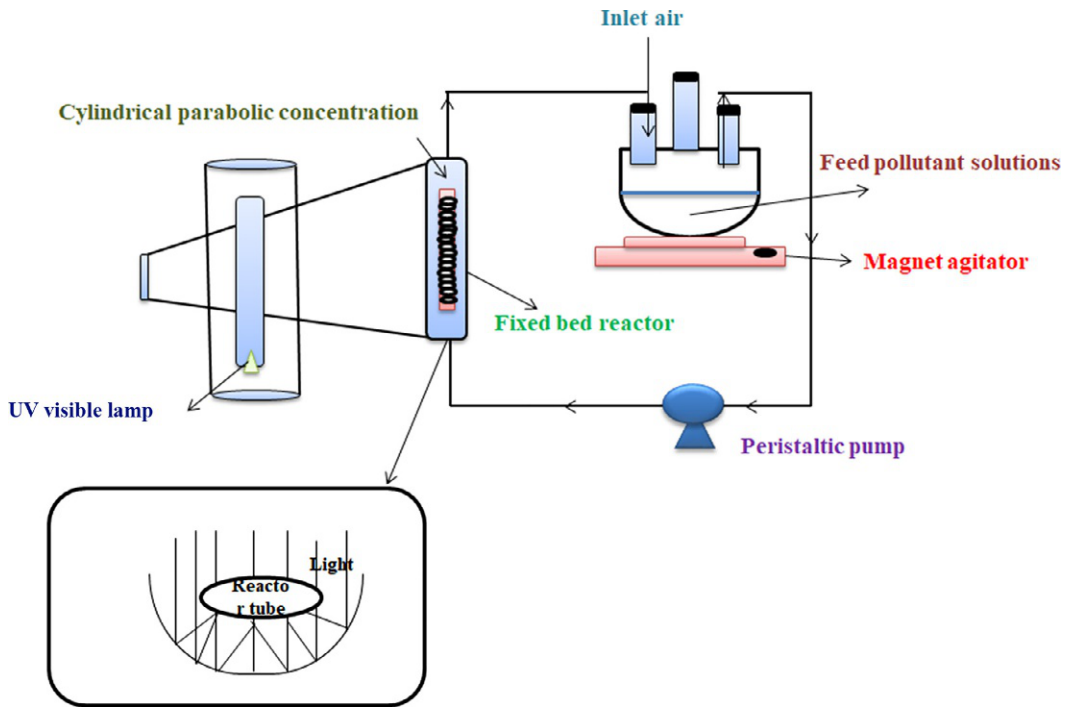

FIG. 4

Representation of the experimental setup.

(b) It is an easy and effective technique to make photocatalytic responses without requiring postprocessing of water filtration. In this work, a few factors were considered: pH, adsorbent dose, initial MB fixation, and contact time. The harmony information of methyl blue adsorption was examined by the adsorption isotherm models (Langmuir and Freundlich). Ideal execution for the adsorption of Ti-changed volcanic cinder (TVA) particles, arranged utilizing an aqueous strategy, was getting at $3\,g\,L^{-1}$ adsorbent portion and pH 10. Transformation if there should be an occurrence of TVA, autonomous of stream rate was seems to be 90.3% for about 3 h of response time (Esparza, Borges, Díaz, Alvarez-Galván, & Fierro, 2011).

(c) Azo colors present in material wastewater require evacuation because of their negative environmental and well-being impacts. Even though there are a few different ways to treat such sewage, this examination concentrated on photocatalytic degradation on a titanium dioxide (TiO_2) paper substrate. The colors contemplated were Direct Yellow 27 and 50; Direct Red 23, 80, and 81; and Direct Violet 51. Arrangements of each color were set up at a grouping of $25\,mg\,L^{-1}$ in water equalized for 30 min, run for 24 h, and go through a photocatalytic reactor. Shading evacuation in the arrangement was observed utilizing UV-vis spectroduplicate. Toward the finish of the test, the last method was tried for harmfulness, total natural carbon, and the nearness of smelling salts and nitrate particles. Complete shading expulsion was watched for each color.

This book belongs to Central Library BADJI Mokhtar-ANNABA UNIVERSITY Copyright Elsevier 2024

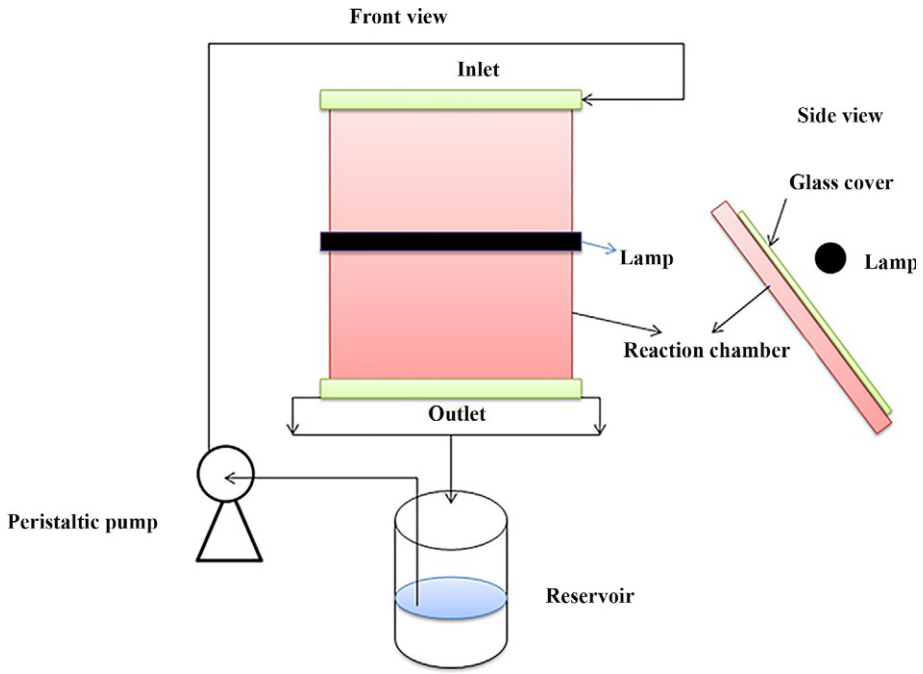

FIG. 5

Diagrammatic representation of a reactor used at ENSIC.

The outcomes were demonstrated dependent on a pseudo-first-order reaction. It was discovered that the degradation rate of the azo colors was related to the essential highlights. This rate expanded with the nearness of sulfate gatherings and diminished with particles containing multiple azo gatherings—extra sweet-smelling rings. Complete oxidation of the color particles was not accomplished, which brought about numerous by-items framed (Fig. 5). Nitrogen molecules in the structure of every single tried color changed over to alkali and nitrate. In any case the outcomes demonstrate that a significant part of the nitrogen was changed over to N_2 gas. Most arrangements had a diminished complete natural substance of at any rate of 80% with the least decrease being 60%.

The color arrangement expanded in poisonous quality after the presentation to the reactor due to the nearness of sweet-smelling amines. To diminish toxicity an optional natural treatment would be necessary as it would additionally corrupt the toxic sweet-smelling amines.

(d) Dye degradation in light and dark from the synergetic nanocomposite

Typical hazard caused because of the section of hues in discharge is a worry worldwide. To battle this issue the advanced oxidation process, where semiconductor photocatalysts have been utilized, is the best one among all the researched systems. The reactive oxygen species (ROS) discharge from these metals, for example, superoxide and hydroxyl radical in suspension that ruins it into nonterrible minerals. This strategy requires UV light for inception. From this time forward, there is a need to make materials that discharge ROS, both in the nonattendance and inside observing light, so the ability of

This book belongs to Central Library BADJI Mokhtar-ANNABA UNIVERSITY Copyright Elsevier 2024

shading takeoff is improved. Toward this goal, an analyst has sorted out and facilitated another nanocomposite of ZnO_2 and polypyrrole, which even in uncertain quality discharges ROS. With standard frameworks, the ROS released in the absence of transparency and light were studied. The point to be seen is that ZnO_2 ruins the shading just under UV light yet not under reduce or inside observing clear light zone. The nanocomposite synergically coupled of ZnO_2/polypyrrole is the essential model that degenerate hues in the lack of clarity, through improvement oxidation process without utilizing extra reagents (Rajagopalan, 2016).

6.2 Drugs

In recent work the proficiency of another TiO_2 impetus (ECT), combined by methods for an upgraded sol-gel technique, is examined for corruption of a critical water poison from pharmaceutical industries, diphenhydramine (DP). Its movement is contrasted with P25, the standard impetus, delivered by Evonik Degussa Corporation, within various impetus loadings up to $2\,g\,L^{-1}$ and starting arrangement pH at 3.0–11.0. As a result, it was clear that the DP is truly steady beneath nonsynergist conditions; however, total corruption and significant mineralization with 60%–70% calcium under UV to clear light at $\sim 50\,mW\,cm^{-2}$ can be accomplished in 1 h by choosing the fitting TiO_2 stacking. Emerging contaminate technology (ECT) is altogether more dynamic than the standard impetus for loadings $>1.00\,g\,L^{-1}$, while the pseudo-first-request rate constants expanded with the underlying arrangement from pH 3.0 to 11.0. The most elevated rate constant was gotten with ECT at pH 11 ($173 \times 10^{-3}\,min^{-1}$ against $116 \times 10^{-3}\,min^{-1}$ for P25). Scrounger operators were utilized as an indicative device for the investigation of the photocatalytic instrument. It was conceivable to demonstrate that gaps were critical dynamic species taking an interest in the photocatalytic system just as that ECT has a vast accessibility than P25 to produce receptive radicals, for example, hydroperoxyl ($HOO^{\bullet}$) and hydroxyl ($HO^{\bullet}$) radicals (Morales-Torres, Pastrana-Martínez, Figueiredo, Faria, & Silva, 2013). Fluid arrangements of four pharmaceutical mixes, having a place with the gathering of the rising pollutant of water, ofloxacin (OFX), atenolol (ATL), hydrochlorothiazide (HCT), and trimethoprim (TMP), are designed to be treated with various oxidation frameworks, principally, ozonation, photocatalytic ozonation, and photocatalytic oxidation. For photocatalytic responses both within sight of air, ozone-oxygen gas or oxygen blends, TiO_2 has been utilized as a semiconductor. The most part of dark light transmitted at 365-nm wavelength was the wellspring of radiation. In most cases the impact of a few factors like convergences of semiconductor, ozone gas and ionic strength (pH) on the evacuation of medicines, all-out polyphenol content (total phenolic concentration), and all-out natural carbon (total organic carbon) was examined. A dialogue on the conceivable courses of pharmaceutical and the intermediate (TPC and TOC) disposal has been created. In this manner the OFX TiO_2/UVA corruption system appears to generate through the interest of nonhydroxyl free extreme species.

Moreover, in the photocatalytic procedure, the nearness of OFX represses the development of hydroxyl radicals. The best method was the inclusion of ozone that resulted in finishing the disposal of parent mixes under half an hour for starting pharmaceutical fixations lower than 2.5 $mg\,L^{-1}$. In ozonation frameworks, paying little heed to the nearness of TiO_2 and pH, pharmaceuticals are debased through their immediate response with ozone. Photocatalytic ozonation emerged as the most effective procedure for TOC and TPC evacuations ($\geq$60% and $\geq$80% end after treatment for 2 h, individually) just as regarding the ozone utilization effectiveness at 1 mol, 4 mol, and 5.5 mol of ozone devoured per mol of TOC mineralized, at pH 4, pH 7, and pH 9, respectively. Unfortunately, corrosive conditions at

This book belongs to Central Library BADJI Mokhtar-ANNABA UNIVERSITY
Copyright Elsevier 2024

pH 4 were the most advantageous ones for TOC and TPC expulsion by ozonation of photocatalyst. This was because of the arrangement of OH radicals by the ozonide created at these reactions (Rodriguez et al., 2013).

6.3 Organic and microorganism

(a) Purification of household gray water

The purification of household gray water that is overloaded with several hair colorants by solar photocatalysis follows flocculation with chitosan using TiO_2-coated textile by implementing TiO_2-chitosan paste diffusion on the wool or polyester blend textile (Fig. 6). The waste materials were used to assemble the reactor that result in a significant decline of organic content up to 50.8%, chemical oxygen demand, and toxicity throughout 4 h. The complete degradation of color particles and an aromatic compound. Floscan is observed just after the treatment, and a complete sedimentation 12 h in dark can take place.

(b) Solar photocatalyst reactor for wastewater treatment

Another solar-based photocatalytic reactor (photoreactor) utilizing TiO_2 nanoparticles covered onto plastic granule has been planned. Impetus granules are set into the pit of a reactor board made of glass. A syphon is used to course wastewater in the photoreactor. Methylene blue (MB) broke up in water was picked as the wastewater show. The execution of the photoreactor was assessed dependent on changes in MB focus with admiration to time. The photoreactor demonstrated a decent implementation by debasing 10 L of MB arrangement up to 96.54% after 48 h of sun-oriented illumination. The photoreactor was scaled up by expanding the board territory to twice its unique size. The expansion in the surface territory of the reactor board and this manner of the mass of impetus granules and reactor volume prompted a three-crease increment of the photodegradation rate.

Moreover, MB degradation energy was contemplated. Information examination affirmed the pertinence of the pseudo-first-request Langmuir-Hinshelwood. The proposed photoreactor has incredible potential for use in substantial-scale wastewater treatment (Rokhmat, Wibowo, Murniati, & Abdullah, 2017).

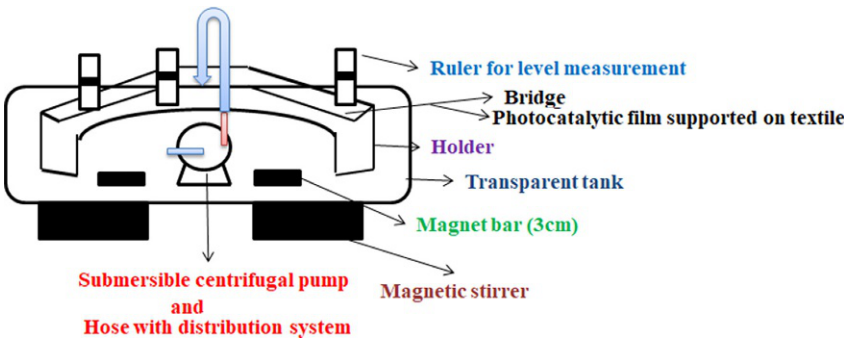

FIG. 6

Diagrammatic representation (front view) of the reactor used for solar photocatalysis.

This book belongs to Central Library BADJI Mokhtar-ANNABA UNIVERSITY
Copyright Elsevier 2024

(c) Adaptable recirculating (bench-scale) flow CPC photoreactor that is used in the solar photocatalytic degradation of methylene blue using removable TiO_2 immobilized on PET sheets

TiO_2 can be immobilized on polyethylene (PET) nonwoven sheets that were utilized in sunlight-based photocatalytic debasement of a methylene blue (MB). The TiO_2 Evonik peroxide P25 has been used in this investigation. The measure of stacked TiO_2 on PET was around 24%. The immobilization of TiO_2 on PET was directed by the phenomenon termed as plunge covering pursued by presenting to mellow warmth and weight. PET sheets or can say TiO_2 was wrapped on a removable Teflon poles inside a homemade seat scale recycling stream compound parabolic concentrator (CPC) photoreactor model ($0.7 \times 0.2 \times 0.4\,m^3$ stage). Compound parabolic concentrator photoreactor is composed of seven borosilicate glass tubes associated in the arrangement. Compound parabolic concentrator reflectors are made up of hardened steel 304. This model was firmly fitted on a stage tilted at 30°N neighborhood scope in Cairo. Different syphon was utilized to course water containing methylene blue (MB) color inside the glass tubes. Proficient photocatalytic corruption of MB utilizing PET/TiO_2 was accomplished upon the presentation to coordinate daylight. Concoction oxygen request (COD) examinations uncover the total mineralization of MB. The sturdiness of PET/TiO_2 composite was likewise tried under daylight illumination. Results show just 6% decrease in the measure of TiO_2 after seven cycles. No noteworthy change has been observed for the physicochemical qualities of PET/TiO_2 after progressive illumination forms (El-Mekkawi, Nady, Abdelwahab, Mohamed, & Abdel-Mottaleb, 2016).

7 Conclusion

Research on the advancement and modification of the photoreactor used for the degradation of the pollutants is a field of continued expansion in the last few decades. There are different strategies to modify the photoreactor and increase its efficiency. The photocatalyst plays a significant role in the photoreactor for the degradation processes. Various approaches have been invented in a way to improve its effectiveness: morphological modification, composites of multiple semiconductors, and combination with other functional groups.

Photocatalysis has a bright future in coming years, but more focus must be on the development of solar light-activated photocatalysts with the higher surface area so that they can be useful in conversion of the solar energy into chemical or electrical energy.

References

Almquist, C. B., & Biswas, P. (2002). Role of synthesis method and particle size of nanostructured TiO2 on its photoactivity. *Journal of Catalysis*, *212*, 145–156.

Anpo, M., Yamashita, H., Ikeue, K., Fujii, Y., Zhang, S. G., Ichihashi, Y., et al. (1998). Photocatalytic reduction of CO_2 with H_2O on Ti-MCM-41 and Ti-MCM-48 mesoporous zeolite catalysts. *Catalysis Today*, *44*, 327–332.

Campbell, M. L., Guerra, F. D., Dhulekar, J., Alexis, F., & Whitehead, D. C. (2015). Target-specific capture of environmentally relevant gaseous aldehydes and carboxylic acids with functional nanoparticles. *Chemistry—A European Journal*, *21*, 14834–14842.

Albu, S. P., Ghicov, A., Macak, J. M., Hahn, R., & Schmuki, P. (2007). Self-organized, free-standing TiO_2 nanotube membrane for flow-through photocatalytic applications. *Nano Letters*, *7*, 1286–1289.

This book belongs to Central Library BADJI Mokhtar-ANNABA UNIVERSITY Copyright Elsevier 2024

Alves, A., Berutti, F., Clemens, F., Graule, T., & Bergmann, C. (2009). Photocatalytic activity of titania fibers obtained by electrospinning. *Materials Research Bulletin*, *44*, 312–317.

Chen, J. S., Tan, Y. L., Li, C. M., Cheah, Y. L., Luan, D., Madhavi, S., et al. (2010). Constructing hierarchical spheres from large ultrathin anatase TiO2 nanosheets with nearly 100% exposed (001) facets for fast reversible lithium storage. *Journal of the American Chemical Society*, *132*, 6124–6130.

Delaiásun, D. (2010). Hierarchically multifunctional TiO_2 nano-thorn membrane for water purification. *Chemical Communications*, *46*, 6542–6544.

El-Mekkawi, D. M., Nady, N., Abdelwahab, N. A., Mohamed, W. A., & Abdel-Mottaleb, M. (2016). Flexible bench-scale recirculating flow CPC photoreactor for solar photocatalytic degradation of methylene blue using removable TiO_2 immobilized on PET sheets. *International Journal of Photoenergy*, *2016*, 1–9.

Esparza, P., Borges, M. E., Díaz, L., Alvarez-Galván, M. C., & Fierro, J. L. G. (2011). Equilibrium and kinetics of adsorption of methylene blue on Ti-modified volcanic ashes. *AIChE Journal*, *57*, 819–825.

Fujishima, A., & Honda, K. (1972). Electrochemical photolysis of water at a semiconductor electrode. *Nature*, *238*(5358), 37–38.

Fujishima, A., & Zhang, X. (2006). Titanium dioxide photocatalysis: Present situation and future approaches. *Comptes Rendus Chimie*, *9*, 750–760.

Fujishima, A., Zhang, X., & Tryk, D. A. (2008). TiO_2 photocatalysis and related surface phenomena. *Surface Science Reports*, *63*, 515–582.

Guerra, F. D., Campbell, M. L., Whitehead, D. C., & Alexis, F. (2017). Cover picture: Tunable properties of functional nanoparticles for efficient capture of VOCs (chemistry select 31/2017). *ChemistrySelect*, *2*, 9888.

Hoffmann, M. R., Martin, S. T., Choi, W., & Bahnemann, D. W. (1995). Environmental applications of semiconductor photocatalysis. *Chemical Reviews*, *95*, 69–96.

Kamat, P. V., & Meisel, D. (2003). Nanoscience opportunities in environmental remediation. *Comptes Rendus Chimie*, *6*, 999–1007.

Karn, B., Kuiken, T., & Otto, M. (2009). Nanotechnology and in situ remediation: a review of the benefits and potential risks. *Environmental Health Perspectives*, *117*, 1813–1831.

Khan, F. I., & Ghoshal, A. K. (2000). Removal of volatile organic compounds from polluted air. *Journal of Loss Prevention in the Process Industries*, *13*, 527–545.

Katsumata, K. -I., Okazaki, S., Cordonier, C. E., Shichi, T., Sasaki, T., & Fujishima, A. (2010). Preparation and characterization of self-cleaning glass for vehicle with niobia nanosheets. *ACS Applied Materials & Interfaces*, *2*, 1236–1241.

Kondo, Y., Yoshikawa, H., Awaga, K., Murayama, M., Mori, T., Sunada, K., et al. (2008). Preparation, photocatalytic activities, and dye-sensitized solar-cell performance of submicron-scale TiO2 hollow spheres. *Langmuir*, *24*, 547–550.

Lead, J. R., Batley, G. E., Alvarez, P. J. J., Croteau, M. -N., Handy, R. D., Mclaughlin, M. J., et al. (2018). Nanomaterials in the environment: Behavior, fate, bioavailability, and effects—An updated review. *Environmental Toxicology and Chemistry*, *37*, 2029–2063.

Li, H., Bian, Z., Zhu, J., Zhang, D., Li, G., Huo, Y., et al. (2007). Mesoporous titania spheres with tunable chamber stucture and enhanced photocatalytic activity. *Journal of the American Chemical Society*, *129*, 8406–8407.

Li, D., & Xia, Y. (2003). Fabrication of titania nanofibers by electrospinning. *Nano Letters*, *3*, 555–560.

Li, X., Xiong, Y., Li, Z., & Xie, Y. (2006). Large-scale fabrication of TiO2 hierarchical hollow spheres. *Inorganic Chemistry*, *45*, 3493–3495.

Lin, C. N., Chang, C. Y., Huang, H. J., Tsai, D. P., & Wu, N. L. (2012). Photocatalytic degradation of methyl orange by a multi-layer rotating disk reactor. *Environmental Science and Pollution Research International*, *19*, 3743–3750.

Liu, B., Nakata, K., Sakai, M., Saito, H., Ochiai, T., Murakami, T., et al. (2011). Mesoporous TiO2 core–shell spheres composed of nanocrystals with exposed high-energy facets: Facile synthesis and formation mechanism. *Langmuir*, *27*, 8500–8508.

This book belongs to Central Library BADJI Mokhtar-ANNABA UNIVERSITY

Copyright Elsevier 2024

Liu, M., Piao, L., Lu, W., Ju, S., Zhao, L., Zhou, C., et al. (2010). Flower-like TiO_2 nanostructures with exposed {001} facets: Facile synthesis and enhanced photocatalysis. *Nanoscale*, *2*, 1115–1117.

Liu, S., Yu, J., & Jaroniec, M. (2010). Tunable photocatalytic selectivity of hollow TiO_2 microspheres composed of anatase polyhedra with exposed {001} facets. *Journal of the American Chemical Society*, *132*, 11914–11916.

Liu, Z., Zhang, X., Nishimoto, S., Jin, M., Tryk, D. A., Murakami, T., et al. (2008). Highly ordered TiO_2 nanotube arrays with controllable length for photoelectrocatalytic degradation of phenol. *The Journal of Physical Chemistry C*, 112, 253–259.

Masciangioli, T., & Zhang, W. X. (2003). Environmental technologies at the nanoscale. *Environmental Science & Technology*, *37*, 102a–108a.

Mehndiratta, P., Jain, A., Srivastava, S., & Gupta, N. (2013). Environmental pollution and nanotechnology. *Environment and Pollution*, *2*, 49.

Moon, J., Park, J. -A., Lee, S. -J., Zyung, T., & Kim, I. -D. (2010). Pd-doped TiO_2 nanofiber networks for gas sensor applications. *Sensors and Actuators B: Chemical*, *149*, 301–305.

Mor, G. K., Varghese, O. K., Paulose, M., & Grimes, C. A. (2005). Transparent highly ordered TiO_2 nanotube arrays via anodization of titanium thin films. *Advanced Functional Materials*, *15*, 1291–1296.

Mor, G. K., Varghese, O. K., Paulose, M., Shankar, K., & Grimes, C. A. (2006). A review on highly ordered, vertically oriented TiO_2 nanotube arrays: Fabrication, material properties, and solar energy applications. *Solar Energy Materials and Solar Cells*, *90*, 2011–2075.

Morales-Torres, S., Pastrana-Martínez, L. M., Figueiredo, J. L., Faria, J. L., & Silva, A. M. T. (2013). Graphene oxide-P25 photocatalysts for degradation of diphenhydramine pharmaceutical and methyl orange dye. *Applied Surface Science*, *275*, 361–368.

Mueller, N. C., Braun, J., Bruns, J., Černík, M., Rissing, P., Rickerby, D., & Nowack, B. (2012). Application of nanoscale zero valent iron (NZVI) for groundwater remediation in Europe. *Environmental Science and Pollution Research*, 19, 550–558.

Norton, L., Baskaran, K., & Mckenzie, T. (2004). Biosorption of zinc from aqueous solutions using biosolids. *Advances in Environmental Research*, *8*, 629–635.

Nasr, C., Vinodgopal, K., Fisher, L., Hotchandani, S., Chattopadhyay, A., & Kamat, P. V. (1996). Environmental photochemistry on semiconductor surfaces. Visible light induced degradation of a textile diazo dye, naphthol blue black, on TiO_2 nanoparticles. *The Journal of Physical Chemistry*, *100*, 8436–8442.

Nosaka, Y., Komori, S., Yawata, K., Hirakawa, T., & Nosaka, A. Y. (2003). Photocatalytic OH radical formation in TiO 2 aqueous suspension studied by several detection methods. *Physical Chemistry Chemical Physics*, *5*, 4731–4735.

Ojea-Jiménez, I., López, X. N., Arbiol, J., & Puntes, V. (2012). Citrate-coated gold nanoparticles as smart scavengers for mercury (II) removal from polluted waters. *ACS Nano*, *6*, 2253–2260.

Pandey, B., & Fulekar, M. H. (2012). Nanotechnology: Remediation technologies to clean up the environmental pollutants. *Research Journal of Chemical Sciences*, *2*(2), 90–96.

Park, J. -A., Moon, J., Lee, S. -J., Kim, S. H., Zyung, T., & Chu, H. Y. (2010). Structure and CO gas sensing properties of electrospun TiO_2 nanofibers. *Materials Letters*, *64*, 255–257.

Prakasam, H. E., Shankar, K., Paulose, M., Varghese, O. K., & Grimes, C. A. (2007). A new benchmark for TiO_2 nanotube array growth by anodization. *The Journal of Physical Chemistry C*, 111, 7235–7241.

Paulose, M., Shankar, K., Yoriya, S., Prakasam, H. E., Varghese, O. K., Mor, G. K., et al. (2006). Anodic growth of highly ordered TiO_2 nanotube arrays to 134 microm in length. *The Journal of Physical Chemistry B*, *110*, 16179–16184.

Quan, X., Yang, S., Ruan, X., & Zhao, H. (2005). Preparation of titania nanotubes and their environmental applications as electrode. *Environmental Science & Technology*, *39*, 3770–3775.

Rajagopalan, V. (2016). A new synergetic nanocomposite for dye degradation in dark and light. *Scientific Reports*, *6*, 38606.

This book belongs to Central Library BADJI Mokhtar-ANNABA UNIVERSITY

Copyright Elsevier 2024

Ramakrishna, S. (2005). *An introduction to electrospinning and nanofibers*. World Scientific. New Jersey, London, Singapore, Beijing, Shanghai, Hong Kong, Taipei, Chennai: World Scientific Publishing Co. Pte. Ltd.

Rodriguez, E. M., Marquez, G., Leon, E. A., Alvarez, P. M., amat, A. M., & Beltran, F. J. (2013). Mechanism considerations for photocatalytic oxidation, ozonation and photocatalytic ozonation of some pharmaceutical compounds in water. *Journal of Environmental Management*, *127*, 114–124.

Rokhmat, M., Wibowo, E., Murniati, R., & Abdullah, M. (2017). Novel solar Photocatalytic reactor for wastewater treatment. In: *IOP conference series: Materials science and engineering*, IOP Publishing 012010.

Sakai, N., Ebina, Y., Takada, K., & Sasaki, T. (2004). Electronic band structure of titania semiconductor nanosheets revealed by electrochemical and photoelectrochemical studies. *Journal of the American Chemical Society*, *126*, 5851–5858.

Shah, K. J., & Imae, T. (2016). Selective gas capture ability of gas-adsorbent-incorporated cellulose nanofiber films. *Biomacromolecules*, *17*, 1653–1661.

Tratnyek, P. G., & Johnson, R. L. (2006). Nanotechnologies for environmental cleanup. *Nano Today*, *1*, 44–48.

Vaseashta, A., Vaclavikova, M., Vaseashta, S., Gallios, G., Roy, P., & Pummakarnchana, O. (2007). Nanostructures in environmental pollution detection, monitoring, and remediation. *Science and Technology of Advanced Materials*, *8*, 47–59.

Vinodgopal, K., Wynkoop, D. E., & Kamat, P. V. (1996). Environmental photochemistry on semiconductor surfaces: Photosensitized degradation of a textile azo dye, acid orange 7, on TiO_2 particles using visible light. *Environmental Science & Technology*, *30*, 1660–1666.

Wen, P., Itoh, H., Tang, W., & Feng, Q. (2007). Single nanocrystals of anatase-type TiO_2 prepared from layered titanate nanosheets: Formation mechanism and characterization of surface properties. *Langmuir*, *23*, 11782–11790.

Xiang, Q., Yu, J., & Jaroniec, M. (2011). Tunable photocatalytic selectivity of TiO_2 films consisted of flower-like microspheres with exposed {001} facets. *Chemical Communications*, *47*, 4532–4534.

Zhang, Z., Yuan, Y., Shi, G., Fang, Y., Liang, L., Ding, H., & Jin, L. (2007). Photoelectrocatalytic activity of highly ordered TiO_2 nanotube arrays electrode for azo dye degradation. *Environmental Science & Technology*, *41*, 6259–6263.

This book belongs to Central Library BADJI Mokhtar-ANNABA UNIVERSITY

Copyright Elsevier 2024

This page intentionally left blank

This book belongs to Central Library BADJI Mokhtar-ANNABA UNIVERSITY

Copyright Elsevier 2024

CHAPTER

Nanocatalyst types and their potential impacts in agroecosystems: An overview

16

Rahul Bhadouria[a], Disha Mishra[b], Vipin Kumar Singh[c], Pardeep Singh[d], Pratap Srivastava[e], Sachchidanand Tripathi[f], Rishikesh Singh[g]

Department of Botany, University of Delhi, New Delhi, India[a] Central Institute of Medicinal and Aromatic Plants (CIMAP), Lucknow, India[b] Department of Botany, Centre of Advanced Study (CAS), Institute of Science, Banaras Hindu University, Varanasi, India[c] Department of Environmental Studies, PGDAV College, University of Delhi, New Delhi, India[d] Department of Botany, Shyama Prasad Mukherjee Post-graduate College, University of Allahabad, Prayagraj, India[e] Department of Botany, Deen Dayal Upadhyaya College, University of Delhi, New Delhi, India[f] Institute of Environment & Sustainable Development (IESD), Banaras Hindu University, Varanasi, India[g]

1 Introduction

Nanotechnology has its application in observing, measuring, manipulating, and manufacturing objects at the nanometer (nm) scale. The term "nanomaterials" is generally used for materials with a size ranging between 1 and 100 nm (Rai & Ingle, 2012). Nanotechnology is an emerging area of science that has applicability in various fields. These materials produced at nanoscale have unique physical, chemical, and biological properties that arise from their small size, shape, surface area, conductivity, or surface chemistry and have been applied in numerous ways in different fields such as textiles, electronics, engineering, medicine, and agriculture (Rai & Ingle, 2012; Smith, Shaw, & Handy, 2007). Nanosized materials have bridged the gap between the tiny atoms and bulk-sized particles and have come up with the innovative solutions for many chemical transformations in biomedical, environmental, agricultural, and pharmaceutical fields. Unique properties of NPs include very large specific surface area, high surface energy, and quantum confinement (Nel, Xia, Mädler, & Li, 2006). Interestingly the characteristic feature of NPs may result in different environmental fate and behaviors as compared with their bulk counterparts.

Owing to extraordinary physicochemistry, optoelectronics, high surface area, enhanced reactivity, and stability, nanomaterials play a central role in catalytic reactions by adapting green and sustainable nanocatalyst technology, thereby providing convenient reaction and low temperature requirement for transformation together with the minimal generation of unwanted reagent wastes. The nanosize of catalysts affects the reaction rate due to more contact in both homogeneous and heterogeneous system with lesser aggregation, high reaction yield, and easy catalyst separation. Many metals and their oxides, polymers, carbon-based materials, and silica have been opted for the fabrication of nanocatalysts.

Nano-Materials as Photocatalysts for Degradation of Environmental Pollutants. https://doi.org/10.1016/B978-0-12-818598-8.00016-X
© 2020 Elsevier Inc. All rights reserved.

This book belongs to Central Library BADJI Mokhtar-ANNABA UNIVERSITY

Copyright Elsevier 2024

Appropriate understanding of these points would be able to generate an efficient, industrially viable, and economical catalyst. The intrinsic properties of nanomaterials such as mean lattice constant, self-organization growth, atomic density, critical temperature for phase transitions, binding energy, thermal stability, mechanical strength, core-level energy, photoabsorption, photoemission, activation energy for atomic dislocation, diffusion, and chemical reactions are the key parameters in deciding their application in catalytic transformations. Additionally the use of biodegradable materials with desired properties would offer greener and consumer-acceptable technology for the development of newer catalytic systems. Therefore, to understand the practical applications of nanomaterials, their types, fabrication process, and performance optimization are highly desirable (Chaturvedi, Dave, & Shah, 2012). Some of the inorganic-, carbon-, and polymer-based materials employed for catalytic applications are briefly described in the next subsections.

2 Metal-based nanocatalysts

Over the past few decades, simple and efficient methods have largely been adopted for the synthesis of metal nanoparticle-based catalyst. Due to the selective activity, stability, and porous structures, these metal nanoparticle-based catalysts can perform specific reactions. Their growth and chemical composition can be controlled by optimizing experimental conditions to construct different shapes and structures. Metal-based/metal oxide-based nanomaterials exhibiting good stability, controlled shape, and well dispersibility have been synthesized for in situ and ex situ applications. Synthesis of these types of catalysts is often achieved through thermal decomposition, chemical reduction, and hydrothermal or coprecipitation routes. Further, nanoparticles with highly reactive surfaces can be achieved through the introduction of diatomites and ligands or capping agents. These nanoparticles are mainly investigated as supported/nonsupported metal catalyst, metal oxide catalyst, core-shell structures, layered oxides, ceramic nanocatalyst, etc. In addition, transition metal-based catalysts have also been largely exploited for their active catalytic applications due to partially filled *d*-orbital. For instance, the sensitive monitoring of chloramphenicol residues in environmental matrices based on immunosensing gold nanoparticles catalyzing the reduction of 4-nitrophenol followed by analysis through ultraviolet-visible (UV-vis) spectrometry has been reported (Que, Tang, Xia, Lu, & Tang, 2014). A multipurpose recyclable catalyst comprising polydopamine/Ag/polystyrene films have been constructed to facilitate the catalytic degradation of pendimethalin, and it has potential applications in the fields of environmental protection, remediation of soil contamination, and sewage treatment (Xu, Sun, Bai, Wang, & Suo, 2019). Bimetallic silver/copper (Ag/Cu) nanoparticles synthesized through the application of herbal extract for the efficient removal of chlorpyrifos are recently described (Rosbero & Camacho, 2017). Cheaper and easily available metals like Fe-, Pd-, Co-, and Ni-based catalyst have also been used for catalytic reactions. For instance, silver nanoparticles, titanium oxides, doped titania, iron oxide nanoparticles, manganese oxides, aluminum oxides, titanium oxides, magnesium oxides, and cerium oxides have been utilized for the construction of nanocatalyst due to short intraparticle diffusion, high reactive surface area, faster kinetics, and high adsorption with active reaction sites. In contrast to pure titania, the doping of nonmetal into nanotitania-based catalyst was able to photochemically degrade aldicarb (Manoharan & Sankaran, 2018). Similarly, tungsten doping into titanium oxides catalyzed faster degradation of paraquat (Kaur, Verma, Setia, & Toor, 2019). So far, different bimetallic

This book belongs to Central Library BADJI Mokhtar-ANNABA UNIVERSITY
Copyright Elsevier 2024

nanomaterials with enhanced activity, selectivity, and stability have been described. The newly synthesized catalyst may possess more active surface structures, exhibit improved electronic properties, and act synergistically due to the presence of more than one metal. Contaminant degradation strategies with particular reference to synthesized catalysts have been presented by Rani, Shanker, and Jassal (2017). Many researchers have demonstrated the importance of bimetallic catalyst for the degradation and removal of various organophosphorus and organochlorine pesticides (Marcelo et al., 2016; Nguyen et al., 2018; Ortiz & Velasco, 2019). In this series of development, multimetallic nanocatalysts have also been introduced as a smart catalyst for utilization in several catalytic reactions for synthesis and oxidation and in pollution control. The heterometallic nanostructures with proper composition, structure, size, and morphology have been proved as more efficient tool for catalytic activity. For instance, a visible light-responsive photocatalyst BiOBr/UiO-66 was synthesized for successful degradation of atrazine in acidic pH (Xue, Wang, Wang, & Ao, 2018). To date, various types of metal oxides have been investigated as a support for enhancing the catalytic features of nanometal catalysts via metal-support interaction.

2.1 Core-shell nanocatalyst

This type of nanostructures consists of two metals designed in a core-shell manner. Currently, research has been focused on the core-shell-type materials due to their extraordinary optical, magnetic, and synergetic properties. The core-shell-type catalyst with multimetallic nanocatalysts of different atomic distribution obtained through encapsulation of an active metal, metal oxide, or other porous materials is able to deliver diversified catalytic applications. Core-shell of many metal nanoparticles has been developed with core of zerovalent metal and mixed-valent metal for catalytic activity (Trujillo-Reyes, Majumdar, Botez, Peralta-Videa, & Gardea-Torresdey, 2014). Parallel to this, yolk-shell structures with heterogeneous metal core while maintaining a homogeneous environment for heterogeneous catalytic reactions are also developed. Noteworthy, they are able to prevent aggregation, with sufficient catalytic activity located at the center and act as nanoreactor framework.

2.2 Silica nanomaterials

Nanosilica and mesoporous silica materials are proven as versatile catalytic agent due to high surface area, porous structure, and facile surface chemistry with multifaceted applications in the environment. The hydroxyl groups of silica materials play an important role in adsorption, wetting, catalytic cracking, or degradation of pollutants. They usually occur with pore diameter of 1.5–50 nm. Mesoporous silica shell nanospheres are important for hydrogenation catalysis, magnetic catalysis, nano-noble-metal-based catalysis, etc. Silica nanoparticles have also been used for targeted delivery of DNA, proteins, nutrients, and chemicals to plants. Rastogi et al. (2019) have briefly discussed the importance of silicon nanoparticles for the plant growth, development, and productivity. The controlled release of herbicide diquat (Shan et al., 2019), pesticide abamectin (Gao et al., 2019), intracellular protein (Deodhar, Adams, & Trewyn, 2017), pesticide chlorpyrifos (Chen et al., 2016), and fungicide pyraclostrobin (Cao et al., 2016) was attempted through the modification or single mesoporous silica nanomaterials.

This book belongs to Central Library BADJI Mokhtar-ANNABA UNIVERSITY Copyright Elsevier 2024

2.3 Layered double hydroxides

Layered double hydroxides or hydrotalcite compounds are primarily composed of two or more metallic elements of hydroxide-like crystal structure. They are highly compatible for organic and biological materials due to interlayer anion exchange ability. Recently, research has been directed toward the preparation, self-assembly, intercalation kinetics, and supramolecular structure of layered double hydroxides. The catalytic reactions can take place inside the layers; therefore maximum reaction yield can be obtained. Owing to their unique structure, stability, recyclability, compositional variation, and simple preparation methods, they have been frequently utilized for designing novel catalyst. Layered oxide with photocatalytic activity can be developed by changing the properties with composite oxide, intercalation oxide, and laminated doping. They can be easily synthesized through coprecipitation, sol-gel, hydrothermal, ion-exchange, and salt-oxide methods. Their application as slow release of nutrients, agrochemicals, and adsorbent has been previously reported for soils and plants. The eradication of phenylurea-based pesticides from the soil was achieved through the application of heterogeneous Fe-based layered double hydroxide materials, and it was suggested as an efficient chemical oxidant for the remediation of toxic pollutant from contaminated soil (Liu et al., 2018). The application of layered double hydroxides is gaining attention nowadays. In this regard, Benício et al. (2015) have reviewed the application of such types of nanomaterials in agricultural practices. Also, various studies have been conducted to explore the role of these nanomaterials in agricultural applications like storage and release of agrochemical and nutrient availability for plants (Bernardo, Moreira, & Ribeiro, 2017; de Castro et al., 2018; Imran, López-Rayo, Magid, & Hansen, 2016).

2.4 Nanocarbon catalysts

Nanostructured carbon materials are also widely applied for catalytic purposes due to unique physical, chemical, and electronic properties. Different hybridization state of carbon generates different configurations like fullerene C_{60}, fullerene C_{540}, single-walled nanotubes, multiwalled nanotubes, nanoonions, nanocones, nanohorns, carbon dots, nanobeads, nanofibers, nanodiamonds, and graphene. Application of single-walled and multiwalled carbon nanotubes for the catalytic applications has opened the new possibilities due to the reactions inside the tubes. Due to the stability of resonance structures, quantum effects, and tunable characteristics of C—C bonds, they were frequently utilized for adsorption and degradation of various contaminants present in environmental matrices. The tubular structures are certainly fascinating in catalysis because of the possibility of chemical reactions occurring inside the nanodimensions of the tube. Furthermore, fullerene C_{60} is likely to have its entire surface easily available for catalysis. However, mainly because of its higher cost and lower density, nanocarbon catalysts are not extensively employed. Recently, studies have been conducted to explore the doping of carbonaceous materials with other metals to attain more stability. The concept of nanocarbon for the benefit of agricultural production is explored by several researchers (Mohamed, Hashim, Alghuthaymi, & Abd-Elsalam, 2018; Singh, Bhati, Tripathi, & Sonkar, 2018; Vithanage, Seneviratne, Ahmad, Sarkar, & Ok, 2017). The hydrophobic property of nanocarbon and their derivatization was successfully utilized for plant growth, agricultural production, growth regulation, disease control, and establishment of young saplings.

This book belongs to Central Library BADJI Mokhtar-ANNABA UNIVERSITY
Copyright Elsevier 2024

2.5 Quantum dots

The water-soluble, atomically thin, and semiconductor nanocatalysts are the new class of zero-dimensional nanomaterials. Prominently the CdS, CdSe, CdTe, and ZnS quantum dots have been used for optoelectronics and biological labeling process due to their highly visible luminescent properties. They are very much helpful in the detection of residual agriculture products, chemicals, and pesticides in the soil. The catalytic application of the nanoquantum dots is increasing rapidly for optical sensing, single-electron transitions, drug delivery, catalysis, etc. (Liu et al., 2019; Nsibande & Forbes, 2016; She et al., 2019; Srivastava, Dev, & Karmakar, 2018).

2.6 Polymeric nanomaterials

To overcome the aggregation, nonspecificity, and low stability of the existing nanocatalysts, host matrices for catalytic reactions have been developed. In this context, polymer-supported nanocomposites have been fabricated as catalysts that are consisted of a polymer as a host material on which various nanoparticles can be anchored. This system delivers extraordinary mechanical strength, thermal activity, higher reactivity, and stability in the medium of reaction. They can be fabricated through different strategies such as sol-gel processes, self-assembly techniques, assembling of nanobuilding blocks, and chemical grafting. Currently the application of biodegradable polymers such as starch, chitosan, cellulose, lignin, hemicellulose, polylactic acid, and polyglycolic acid is in the process for the development of biodegradable nanocatalyst for industrial application (Campos et al., 2015; Fukamachi, Konishi, & Nomura, 2019; Ihegwuagu et al., 2016; Kumaraswamy et al., 2018; Méndez et al., 2019; Tang, Li, Pun, Osman, & Tam, 2019).

3 Nanocatalysts in agriculture

Economy of most of the developing countries is based on agriculture. The explosive growth of ever-increasing world population requires higher agricultural productivity to survive. It is now essential to use the advanced technologies in agricultural practices to raise the crop productivity (Batsmanova, Gonchar, Taran, & Okanenko, 2013; Scott & Chen, 2012). Nanotechnology and nanobiotechnology are the emerging fields that have tremendous potentials to boost the productivity of agriculture and allied fields in different ways along with their renovation. Nanotechnology relying on nanoparticles (NPs) with specific unique properties has the potential to (i) increase food quality, (ii) improve crop and livestock production, (iii) increase global food production, (iv) enhance seed germination and seedling growth, (v) control pest effectively, (vi) monitor plant growth, (vii) protect plants, (viii) detect plant and animal diseases, (ix) monitor plant growth and reduction in agricultural waste, (x) be used as fertilizer and pesticide, and (xi) be used as sensors in monitoring soil quality for sustainable agriculture (Fig. 1) (Scott & Chen, 2012; Zaytseva & Neumann, 2016). Fertilizers play a very important role in seed germination, plant growth, and development. However, very large fraction of the used agrochemicals remains unavailable to crops due to several processes such as volatilization, percolation, surface runoff, degradation by hydrolysis, and decomposition. The most important drawback of heavy application of chemical fertilizers like herbicides, pesticides and insectides is the longer residence period because of slow decomposition. In addition, the application of conventional fertilizers at a high

This book belongs to Central Library BADJI Mokhtar-ANNABA UNIVERSITY
Copyright Elsevier 2024

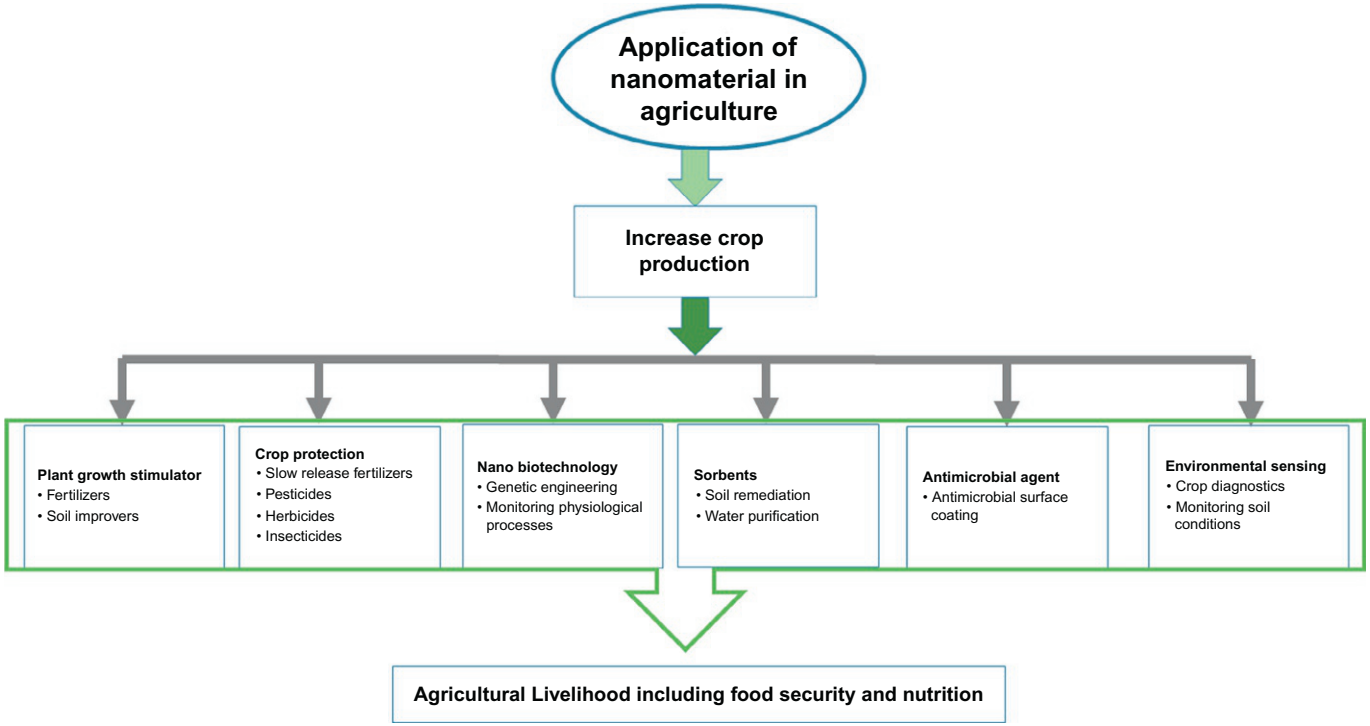

FIG. 1

Potential benefits of nanomaterials in agriculture and environment.

This book belongs to Central Library BADJI Mokhtar-ANNABA UNIVERSITY

Copyright Elsevier 2024

rate and for a longer period in agricultural field could have major environmental issues worldwide. Intensive utilization of N- and P-based agrochemicals is the important man-made factor resulting in worldwide nutrient enrichment in freshwater bodies and marine environments. Thus it is imperative to develop the mechanisms to minimize nutrient loss in agriculture fertilization and reduction in environmental issues along with the increase in crop yield and productivity through the exploitation of emergent applications of nanomaterials and nanotechnology. Further, nanotechnology is considered as the most important approach for sustainable agriculture with enhanced productivity (Lal, 2008). It is considered that nanotechnology could have the potential to transform the agriculture and food sector (Norman & Hongda, 2013). Nanoparticles having the potential features like high reactivity, better bioavailability, bioactivity, and surface effects may be employed to increase crop productivity. Nanofertilizers or nanoencapsulated nutrients have properties to effectively release nutrients and chemical fertilizers on demand that may effectively regulate plant growth and enhance target activity (Gutiérrez, Mussons, Gatón, & Rojo, 2011).

In the area of agriculture, the use of nanotechnology is comparatively new and rapidly evolving area of research with the potential to foster positive impacts under resource stressed conditions and needs further exploration (Huang, Wang, Liu, Hou, & Li, 2015). With numerous historical examples that have demonstrated the ineffectiveness and potential to introduce adverse environmental and human health outcomes of the current approaches (Hristozov & Ertel, 2009), it is evident that an alternative holistic path toward the development of nanotechnology-enabled agriculture is necessary. The engineered nanoparticles (ENPs) have various applications as they have potential to enter into plants, cells, and leaves and are able to transport DNA and chemicals into plant cells (Galbraith, 2007). This provides a way to targeted gene manipulation and expression in the specific cells of the plants. Further, studies in the area of nanotechnology are desired to discover the novel applications for target specific delivery of chemicals, proteins, and nucleotides for genetic transformation of crops, thereby increasing the crop productivity (Scrinis & Lyons, 2007). There are various methods for the synthesis of NPs; however, much attention has been given to the green synthesis of NPs where mostly plant extract is used to synthesize NPs. It has been claimed that green synthesized NPs from its corresponding metal ions is environment-friendly, free from chemical contamination and toxicity, cost-effective, and safe for biological application (Ankamwar, Chaudhary, & Sastry, 2005; Gopinath et al., 2014).

In the field of agriculture, the use of NMs is comparatively new and needs further exploration. At present the agriculture sector is and will continue to face challenges emanating from global food demand, strain on natural resources, and the changing seasonal and climate patterns (Bodirsky et al., 2015; Tilman, Balzer, Hill, & Befort, 2011). Further, increased demand for food is inevitable given the current and predicted trend in population growth (9.7 billion by 2050, a 32% increase from 2015, according to the UN medium-variant projection (UN DESA, 2015)), thereby requiring an increased means and desire for resource-intensive foods. Given the current inefficient farming practices, an increased stress on food supply systems is directly related to the depletion of natural resources, including energy, water, and nonrenewable feedstocks (e.g., fertile soils and sources of primary crop nutrients such as phosphorus) (Mueller et al., 2012; Tilman, Cassman, Matson, Naylor, & Polasky, 2002). Moreover an erratic seasonal behavior of temperature and precipitation is leading to unpredictability and increased frequency of extreme climate events (e.g., severe drought and flood conditions), which has significant impact on agricultural yield and productivity (Dall'Erba & Domínguez, 2016; Piao et al., 2010; Rosenzweig, Iglesias, Yang, Epstein, & Chivian, 2001). Also, shifts in political, geopolitical, consumer preference, and consumer behavior further exert pressure on food supply chain.

This book belongs to Central Library BADJI Mokhtar-ANNABA UNIVERSITY Copyright Elsevier 2024

Therefore, under this scenario, there is a significant need to design and implement lasting sustainable solutions.

The utilization of engineered nanomaterials (ENMs) and application of nanotechnology are considered as a sustainable path toward the development of these solutions (Baruah & Dutta, 2009; Bülbül, Hayat, & Andreescu, 2015; Khot, Sankaran, Maja, Ehsani, & Schuster, 2012; Nuruzzaman, Rahman, Liu, & Naidu, 2016; Rodrigues et al., 2017). The nanomaterials have their application in large-scale precision monitoring of soil and weather conditions, detection of lower limits, detection of previously undetectable analytes, development of multifunctional materials and systems for treatment of waste streams, recovery of finite resources, and efficient delivery of antibiotics, pesticides, and essential nutrients. However, the application of nanomaterial has certain undesired potential consequences ranging from increased embedded resource intensity necessary to produce the ENMs to phytotoxicity to important crops. Environmental and human health impacts are particularly relevant considering the direct release and exposure pathways through their application in agriculture. Since there is an intimate connection between food systems, the environment, and humans, design, development, and implementation of any novel technique warrant serious cautiousness (Scrinis & Lyons, 2007; Torney, Trewyn, Lin, & Wang, 2007). Therefore it is evident that an alternative holistic path toward the development of nanotechnology-enabled agriculture is necessary.

4 Fate and transport of nanocatalysts in agroecosystems

Fate and transport of nanocatalysts in the environment along with their behavior in various abiotic and biotic components such as air, water, soil, sediments, plants, human, and animal are considered as one of the important issues in agroecosystems. Translocation of nanocatalysts in agroecosystems has both positive (good seed germination, improved plant growth and development, nanofertilizers, nanoremediation, nanoencapsulated pesticides, nanostructured soil sensors, nanoreclamants, etc.) and deleterious (induction of cellular stress, toxicity, carcinogenesis, etc.) consequences (Fig. 2). Various studies have been conducted to explore the fate, mobility, and toxicological assessment of synthesized nanoparticles existing in natural ecosystem (Maurer-Jones, Gunsolus, Murphy, & Haynes, 2013; Tolaymat, Genaidy, Abdelraheem, Dionysiou, & Andersen, 2017); however, uncertainty still prevails regarding the fate and transport of various nanocatalysts in different environments. In nature, nanoparticles contribute substantially to the transport and cycling of C, N, S, and P. Thus nanotechnology suggests some novel approaches to enhance the crop productivity and amelioration of polluted agricultural soils (Prasad, Bhattacharyya, & Nguyen, 2017; Sekhon, 2014; Theng & Yuan, 2008; Wang et al., 2017). Majority of nanoparticles are consisted of C, Si, metals, or their oxides and thereby affect environment and eventually human health. An increasing concern toward the use of nanomaterial is the release of nanoparticles during their use into soil and water, thereby increasing their presence in various environmental matrices (El Hadri, Louie, & Hackley, 2018; Theng & Yuan, 2008). By different transport mechanisms, nanoparticles may get entry into the cells or may be transferred into organisms of different trophic levels from similar or dissimilar natural conditions (Bouldin et al., 2008; Bundschuh et al., 2018; Lin et al., 2009). Further, nanoparticles possess the ability to adsorb potentially toxic materials (e.g., lipophilic pollutants and heavy metals) because of increased surfaces and are very much reactive under natural environment (De Jong & Borm, 2008; Khan, Saeed, & Khan, 2017). Some types of nanoparticles have the tendency to penetrate the plants through the root cell walls having small apertures with size 5–20 nm and permitting the mobilization of

This book belongs to Central Library BADJI Mokhtar-ANNABA UNIVERSITY
Copyright Elsevier 2024

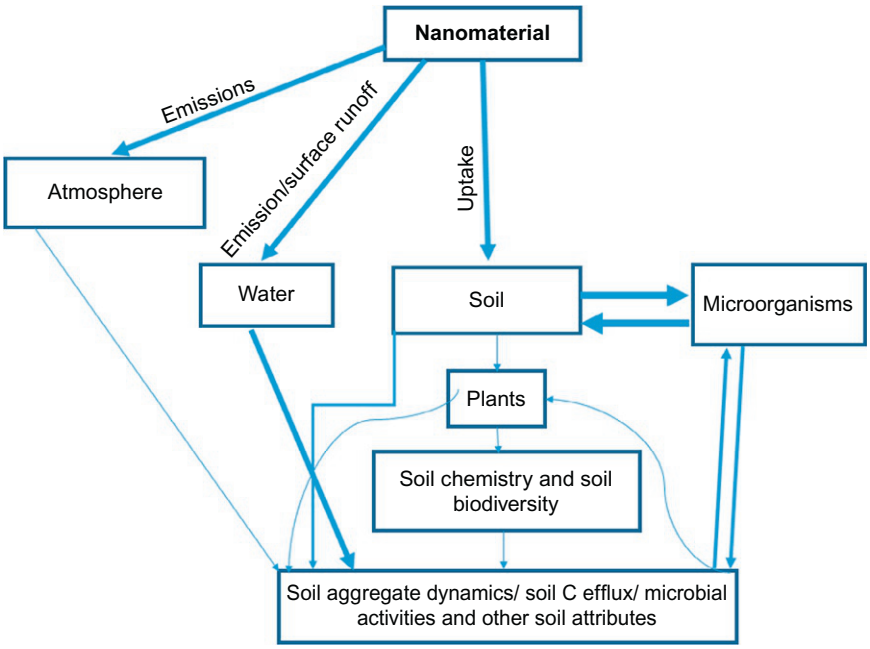

FIG. 2

Fate and transport of nanomaterials in agroecosystems.

smaller particles (Cifuentes et al., 2010; Khan et al., 2017; Tripathi et al., 2017). Therefore nanoparticles having diameter lower than that of the pores may traverse and get access to plasmalemma. Further, studies have indicated that nanoparticles may get access to cellular systems via ion channels and may be intercalated into different proteins responsible for mobilization, eventually resulting into considerable interference in normal metabolic processes, perhaps via generation of reactive oxygen species (Tripathi et al., 2017). Studies have been conducted to assess the current utilizations of applications of nanotechnology in agroecosystems like mobilization, behavior, and future of these NMs, apart from benefits of their application. Further the interface occurring among nanoparticles in a given soil-plant system is considered as one of the fascinating research area in agroecosystems. A number of studies have been conducted to understand the relations existing among nanoparticles in a given soil-plant environment (Soni, Naoghare, Saravanadevi, & Pandey, 2015; Wu, Xie, Fang, Cheng, & Tsang, 2016; Yan et al., 2013; Yang, Cao, & Rui, 2017), the effect of introduced nanoparticles on soil microbiological features (Frenk, Ben-Moshe, Dror, Berkowitz, & Minz, 2013; Grün et al., 2019; Rajput et al., 2018; Simonin & Richaume, 2015), the use of nanoparticles for contaminant removal from terrestrial and aquatic environments (Bueno, Gillerman, Gehr, & Oron, 2017; Kuppusamy et al., 2017), the application of nanoformulated fertilizers and pesticides for enhancing the plant growth and its defense (Omara et al., 2019; Petosa, Rajput, Selvam, Öhl, & Tufenkji, 2017), the application of soil nanoreclamants and nanoconditioners for sustainable agricultural productivity (Fernandes et al., 2017; Omara et al., 2019), and the application of NMs in enhancement of crop yield under environmental stresses (Rizwan et al., 2017; Tassi et al., 2017).

This book belongs to Central Library BADJI Mokhtar-ANNABA UNIVERSITY Copyright Elsevier 2024

5 Multifaceted benefits of nanocatalysts application on soil, plant, and microorganisms

As discussed earlier, nanotechnology is a potential tool to enhance the overall food productivity, food characteristics, plant defense, identification of diseases affecting plant and animals, assessment of plant development, and reduction of unwanted substances for enhanced agricultural production (Ditta, Arshad, & Ibrahim, 2015; Mishra, Pandey, Dutta, & Giri, 2017; Servin et al., 2017). The ultimate goal of using nanoparticles in agroecosystem is to increase the effectiveness and sustainability of crop yield and production with minimal input and less amount of waste generation. Globally, intensive application of nitrogen and phosphorus fertilizers to increase crop productivity has led to nutrient enrichment of freshwater and marine environments (Ansari, Singh, Lanza, & Rast, 2010; Carpenter, 2005; Chislock, Doster, Zitomer, & Wilson, 2013; Wang et al., 2017). Hence the use of nanotechnology in agricultural practices is assumed as a vital tool for enhancing agricultural productivity and ensuring global food security by minimizing nutrient deficiency occurring through leaching at the time of fertilizer application (Lal, 2008; Prasad et al., 2017). To understand the effect of nanoparticles and its contribution in raising agricultural yield, it is essential to investigate the interaction of nanoparticles with plants, that is, from the primary events of seedling emergence to the harvesting of the crop (Khan et al., 2017). Nanoparticles are able to induce considerable alteration in physiology and biochemistry of the cultivated crops depending on their properties and concentrations; however, the responses vary from plant to plant according to soil attributes (Ditta et al., 2015; Tripathi et al., 2017). Recently, a number of studies have reported various effects of nanoparticles on seed germination, photosynthetic activities, and other plant processes to support their application in agriculture (Chhipa & Joshi, 2016; Mani & Mondal, 2016; Singh & Kumar, 2016). Some studies have reported effects of nanoparticle application on the entire phases of plant's life cycle (Milewska-Hendel, Gawecki, Zubko, Stróz, & Kurczynska, 2016). There are various factors known to affect the crop yield like physiology (absorption of solutes and water, respiratory function, photosynthetic activity, and loss of water) and the environmental factors (e.g., moisture content, rain fall, temperature, and stresses) (Lobell & Gourdji, 2012). Hence, under such circumstances, it is crucial to enhance the agricultural productivity by using nanoparticles at different phases of plant's life cycle.

6 Role of nanoparticles in agrowaste management

A large amount of waste is produced from agricultural activities, and few of the wastes may have unacceptable smell. The decay of some of this generated waste matter may change the pH of soil; thus the indiscriminate discarding of agrowastes has emerged as a great challenge worldwide (Obi, Ugwuishiwu, & Nwakaire, 2016). Agrowastes are the crop residues that are composed of the harvested crop itself (Obi et al., 2016). The composition of these agrowastes depends mainly on the crop plants grown, prevailing natural environment and harvesting pattern (Obi et al., 2016). Every year, approximately 140 billion tons of wastes from different industries and farming areas is generated (FAO, 2011). Wastes from different industries and agriculture consist of solid wastes, atmospheric pollutants, and huge amount of contaminated water. These wastes can be minimized and/or treated by controlling different processes leading to their emission and utilization of efficient treatment techniques. Therefore

This book belongs to Central Library BADJI Mokhtar-ANNABA UNIVERSITY
Copyright Elsevier 2024

nanotechnology can be applied to remediate these wastes, thereby maintaining environmental homeostasis by controlling these pollutants (Adebisi et al., 2017; Manjunatha, Biradar, & Aladakatti, 2016) through transesterification, high temperature heating, gasification, hydrogenation, and organic matter regeneration (Fryxell & Cao, 2012). Furthermore the utilization of microbes or enzymes has also been claimed as a potential tool to minimize the wastes from different origin by converting them into beneficial products including bioplastics and biopolymers (Mostafa, Farag, Abo-dief, & Tayeb, 2018). The management of agrowastes using nanoparticles has gained attention worldwide, recently. The management of agrowastes may have minimum two fates: firstly, agricultural wastes may be converted into energy (Adebisi et al., 2017), and secondly the removal of different types of pollutants from contaminated water has been generated by agrowastes (Obi et al., 2016). Furthermore the agrowastes may be processed for organic matter generation or as a suitable source of alternative energy and the synthesis of reusable or biologically decomposable material. Therefore the agrowaste materials are economic and eco-friendly (Madurwar, Ralegaonkar, & Mandavgane, 2013). Further, some agrowastes such as almond shell (Duran, Ozdes, Gundogdu, & Senturk, 2011), peanut husk (Song, Zou, Bian, Su, & Han, 2011), sesame hull (Feng et al., 2011), oil palm fronds (Salman & Hameed, 2010), oil palm fiber (Hameed, Tan, & Ahmad, 2008), coconut husk (Tan, Ahmad, & Hameed, 2008), citrus fruit peel (Dutta, Bhattacharyya, Ganguly, Gupta, & Basu, 2011), coconut shell (Cazetta et al., 2013), *Albizia lebbeck* seed (Ahmed & Theydan, 2014), Macadamia nut endocarp (Junior et al., 2014), rice husk (Hsu et al., 2009), and bamboo (Ahmad & Hameed, 2010) could be used for the removal of different pollutants from aqueous solutions (Zhou, Zhang, & Cheng, 2015).

It has been reported that nanotechnology possesses the potential to provide efficient, cost-effective, and environmentally sustainable solutions for supplying potable water for human use and clean water for agricultural and industrial purposes (Biswas & Wu, 2005). Owing to the variable nature of nanoparticles under different environments, it is necessary to investigate the fate and bioavailability of nanoparticles in soils. Cornelis et al. (2012) studied the retention of nanoparticles in soils, wherein the dominant properties that determined the retention of AgNP in natural soil were correlated with negatively charged AgNP. AgNP was found to be adsorbed preferentially at positively charged surface sites of clay-sized minerals. The high organic carbon content in the agricultural soil is suggested to contribute to an organic surface coating, thereby resulting into nanoparticle mobility across soil, thus coming into contact with microbes. It has been reported by various studies that surface properties of the nanoparticles regulate their stability and mobility as colloidal suspensions or their adsorption, aggregation, accumulation, and deposition. It was reported that ZnO nanoparticles coexisting with dissolved species of Zn were continuously released into the soil solution to recharge the Zn ions; however, ZnO nanoparticles were removed by roots as compared with the soil treated with alginate that expedite the bioaccumulation of Zn in corn plant tissues (Zhao et al., 2012).

Leaching of Cu and Zn ions from the parent nanoparticles was reported as a function of time. Further, it has been reported that the leachate of excess and postapplication nanoparticles may accumulate over a period of time in the form of aggregates and colloids and may lead to generation of an additional anthropogenic waste or nanowaste in the agroecosystem. The nanowastes generated in the process may have the tendency to interact with beneficial soil microbes, thereby negatively influencing their survival owing to the potential toxicity of nanoparticles toward microbes. Recently a number of studies had been taken up to investigate the pattern of uptake, biological fate, and toxicity of several metal oxide nanoparticles including Al_2O_3, TiO_2, CeO_2, FeO, and ZnO (Zhang, Pei, & Wang, 2016).

This book belongs to Central Library BADJI Mokhtar-ANNABA UNIVERSITY
Copyright Elsevier 2024

The gold NPs (AuNPs), because of its intrinsic properties, may be used as transducers for several improvements in agricultural products. The AuNPs have well-known surface plasmon band that is visible around 520 nm. Moreover, AuNPs have high surface areas and distinctive physicochemical assets that can be easily tuned and thus making them ideal candidates for developing biosensing devices. Additionally, these NPs have attracted attention in biological studies owing to their low toxicity, biocompatibility, and unique optical properties. Biological tests measuring the presence or activity of selected analytes have become quicker, more sensitive, and flexible when nanoscale particles are put together. Thus the application of nanoscale particles may have numerous advantages over traditional procedures (Prasad et al., 2017).

The use of NMs in plant protection and food production is an underexplored area. It is well known that insects are the predominant pests in agricultural fields and in products under stored condition and NPs may have a key role in the control of insect pests and host pathogens (Khot et al., 2012). The recent development of a nanoencapsulated pesticide formulation has slow release properties along with enhanced solubility, specificity, permeability, and stability (Bhattacharyya, Duraisamy, Govindarajan, Buhroo, & Prasad, 2016). These features are mainly achieved through either protecting the encapsulated active ingredients from premature degradation or increasing their pest control efficacy for a longer period. Formulation of nanoencapsulated pesticides led to reduction in the dosage of pesticides and thereby minimal human exposure (Nuruzzaman et al., 2016). Thus the development of nontoxic and promising pesticide delivery systems for increasing global food production and parallelly reducing the negative environmental impacts to ecosystem (Bhattacharyya et al., 2016; Grillo, Abhilash, & Fraceto, 2016) is imperative.

Microencapsulation like nanoencapsulation is the technique used to entrap the desired chemicals for efficient delivery to the target points. Recently, few chemical companies have openly promoted nanoscale pesticides for sale as "microencapsulated pesticides." Some products from Syngenta (Switzerland) such as Karate ZEON, Subdue MAXX, Ospray's Chyella, and Penncap-M and microencapsulated pesticides from BASF may be quite fit for nanoscale applications (Gouin, 2004). Syngenta also markets some products in the Australia such as the PrimoMAXX, Banner MAXX, and Subdue MAXX. Despite they are known as microemulsions in the markets, however, they are really nanoscale emulsions. It confirms very thin interface between the term of microemulsion and nanoemulsion. This technique is commonly used for formulations of organic NPs (Gouin, 2004) containing active agrochemicals or substances of interest.

7 Unprecedented negative impacts of nanocatalysts in agriculture: Effect on soil, plant, and microorganisms

It is impossible at this point of time and stage of knowledge to make any collective judgment about the potential risks of nanotechnology in the environment. Engineered nanoparticles (ENPs) are expected to affect living organisms in different ways than larger particles of the same materials. Since they differ greatly from each other in terms of structure and properties, it is expected that they would differ also a lot in terms of toxicity. Only a limited number of ecotoxicity studies with ENPs have been conducted so far, and the data they delivered are insufficient to characterize hazard. The environmental fates of ENPs

This book belongs to Central Library BADJI Mokhtar-ANNABA UNIVERSITY Copyright Elsevier 2024

are still not well studied, and it is still uncertain how most ENPs would behave in the environment. It is essential to do more research in the fields of property characterization, environmental behavior, and more ecotoxicity studies to make ecological risk assessment (ERA) of ENPs possible. Being unaware of the potential risks associated with ENPs, it would prevent policy makers from imposing adequate regulation of ENP-containing materials. The lack of regulation can lead to widespread exposure to dangerous ENPs, which can cause substantial environmental and social problems. Nanotechnology has direct beneficial applications, but like all technologies, it may have unintended effects that can adversely impact the environment, both within the human body and in the natural ecosystem. Nanoparticles have higher surface areas than the bulk materials that can cause more damage to the human body and environment as compared with the bulk particles. Therefore concern for the potential risk to the society due to nanoparticles has attracted national and international attentions. The major problem of NMs is the nanoparticle analysis method. As nanotechnology improves, new and novel NMs are gradually developed. However, the materials vary in shape and size, which are important factors in determining the toxicity. Lack of information and methods of characterizing NMs has made existing technology extremely difficult to detect the nanoparticles in air for environmental protection. Also, information of the chemical structure is a critical factor to determine how much toxic a nanomaterial is, and minor changes of chemical functional group could drastically change its properties. Full risk assessment of the safety on human health and associated environmental impacts need to be evaluated at all stages of nanotechnology. The risk assessment should include the exposure risk and its probability of exposure, toxicological analysis, transport risk, persistence risk, transformation risk, and ability to recycle. Life cycle risk assessment is another factor that can be used to predict the environmental impacts. Good experimental design in advance of manufacturing a nanotechnology-based product can reduce the material wastes. Nanoparticles may interact with environment in many ways: it may be attached to a carrier and transported in underground water by biouptake and may interact with other contaminants of organic or inorganic origin. Possible aggregation will allow for conventional transportation to sensitive environments where the nanoparticles can break up into colloidal nanoparticles. There are several ways that make nanoparticles or nanomaterials toxic and harmful to the surrounding environment, that is, (i) hydrophobic and hydrophilic nature of nanoparticles and (ii) mobility of contaminants.

Nanotechnologies are both praised for offering potential environmental benefits and scorned for creating new environmental risks. Other factors of importance for understanding environmental impacts, such as levels of exposure and the fate and behavior of NMs in the agriculture, are also subjected to high levels of uncertainty. These uncertainties are exacerbated by current limitations of appropriate and agreed methods for testing, including basic issues such as how to detect, measure, and characterize nanomaterials (Kabir, Kumar, Kim, Yip, & Sohn, 2018), hence affecting both the reliability and the generalizability of research outcomes. In summary, there is currently very little knowledge on the characteristics, ecotoxicity, and environmental fate of the various nanomaterials in use, and effective methods to perform such type of research remain substantially underdeveloped. While research in nano(eco)toxicology remains shrouded in uncertainty, emerging evidences indicate a future threat to natural environment and human health. Most concerns are related to the engineered nanoparticles not embedded in a solid matrix. While the toxicity of free nanoparticles cannot be generalized, emerging evidences for important characteristics such as mobility, persistence, and bioaccumulation are central to environmental concern.

This book belongs to Central Library BADJI Mokhtar-ANNABA UNIVERSITY Copyright Elsevier 2024

8 Nanocatalysts in agriculture: Boon or bane

The potential of nanomaterials is clearly envisaged for agricultural practices in the form of different formulations and structures. Differing from the bulk form, the NM-based smart delivery system is released in the soil through point and nonpoint sources. The fate and transfer of these ENPs mainly include deposition, accumulation, residence, degradation, and migration. Soil atmosphere is bound to receive plenty of NPs and their by-products through either atmospheric deposition, absorption of gaseous compounds, aerosols, surface runoff, or anthropogenic activities. Due to their unique properties, they are frequently applied for increased crop production, remediation of pollutants, and detection of toxic chemicals in soil. Applicability of these NMs is well known for plant growth, germination, pathogen detection, agrochemical delivery, and residue sensing (Khot et al., 2012). In this context the use of remote nanosensors for real-time monitoring in cultivated fields, for applications such as gathering crucial information like moisture level, temperature, soil fertility, crop nutrient status, plant diseases, weeds, and insects present, can be detected and eradicated. Besides these positive benefits the ENP entry to soil and plant often becomes major obstacle for achieving sustainability in the agriculture system. The adverse effect of nanomaterials cannot be clearly elucidated from their bulk form as they behave entirely in a different manner. However, the current estimated output of nanoparticles is not considered as toxic. But in the future the limit may exceed from prescribed level and may be harmful to the environment. The low mobility, aggregation, and slow breakdown of NMs in soil play a major role in their concentration buildup rather than in air or water. Several studies have suggested the accumulation, toxicity, and transfer of these NMs into the plants and microbes. The toxicity to human, phytotoxicity, residue carryover, and bioaccumulation of engineered nanoparticles are the major issues that could not be ignored for their safe usage. The compositional features like shape, size, and surface behaviors have contributed for their inevitable threats to natural environment. Therefore, for better understanding of positive and negative impacts of ENPs, the regulatory measures should be applied at manufacturing stage, and before the commercialization of product, a proper set of experiments involving animal toxicity and exposure should be conducted. In this regard, life cycle assessment, drift model measurement, toxicokinetics, toxicodynamics, transformation, application methods, and dose should be critically reviewed for their sustainable application. However, for maximizing the benefits of these NMs for agriculture, future research should be directed for more application of biodegradable/plant-derived matrices like hemicelluloses, cellulose, lignin, chitosan, starch, albumin, lecithin, or other biodegradable polymeric carriers. Detailed information on the inclusion of advanced low-cost nanotools with smart processes, advanced materials, well dispersion and stability, photodegradability, mobility in soil, toxicity, and interaction with other matrices would be an efficient and viable option for the application of engineered NMs in sustainable agriculture.

9 Conclusion and future recommendations

Nanotechnology has revealed a great potential toward the improvement in various aspects of agroecosystems. The avenues emerged in recent decade such as nanofertilizers, nanopesticide, nanoherbicides, nanosensors, and nanocarriers have shown tremendous potential to ensure better nutrient delivery, protection from pests and weeds, and precise sensing systems to crop plants. However, we must be careful while introducing nanotechnology, owing to its unforeseen risks. Further, there are reasons to believe

This book belongs to Central Library BADJI Mokhtar-ANNABA UNIVERSITY
Copyright Elsevier 2024

potential risks associated with nanoparticles. For instance, due to the very small size, reactivity, and effective penetration ability, metal nanoparticles have the tendency to reach various intracellular and extracellular areas of the plants that may initiate a cascade of physiological processes like senescence and hamper the plant growth and reduce crop yield and productivity. A number of studies have reported toxicity of metal nanoparticles on plants. Moreover, evidences are available regarding the toxicity of nanomaterials to soil microbiota, which are a vital component of agroecosystems. This may jeopardize the agroecological balance, thereby hampering the soil nutrient cycle and thus soil fertility. However, considering the current literature, the impact of NMs on soil microbes and plants varies with species and environment. Further, most of the studies are focused on toxicological aspects of NMs due their unique properties, while researches emphasizing on the realization of positive effect of nanoparticles are still very less. Therefore more systemic studies are warranted to investigate and understand the mechanism of action of various NMs along with their interaction with biomolecules and their effect on gene regulation in crop plants and microbes inhabiting the agricultural soils.

Acknowledgments

Authors are thankful to the University Grants Commission (UGC), New Delhi, for providing financial support. Rahul Bhadouria is thankful to UGC (BSR/BL/17-18/0067) for providing Dr. D.S. Kothari fellowship for post-doctoral research.

References

Adebisi, J. A., Agunsoye, J. O., Bello, S. A., Ahmed, I. I., Ojo, O. A., & Hassan, S. B. (2017). Potential of producing solar grade silicon nanoparticles from selected agro-wastes: A review. *Solar Energy*, *142*, 68–86.

Ahmad, A. A., & Hameed, B. H. (2010). Effect of preparation conditions of activated carbon from bamboo waste for real textile wastewater. *Journal of Hazardous Materials*, *173*(1–3), 487–493.

Ahmed, M. J., & Theydan, S. K. (2014). Optimization of microwave preparation conditions for activated carbon from Albizia lebbeck seed pods for methylene blue dye adsorption. *Journal of Analytical and Applied Pyrolysis*, *105*, 199–208.

Ankamwar, B., Chaudhary, M., & Sastry, M. (2005). Gold nanotriangles biologically synthesized using tamarind leaf extract and potential application in vapor sensing. *Synthesis and Reactivity in Inorganic, Metal-Organic and Nano-Metal Chemistry*, *35*(1), 19–26.

Ansari, A. A., Singh, G. S., Lanza, G. R., & Rast, W. (Eds.), (2010). Vol. 1. *Eutrophication: Causes, consequences and control*: Springer Science & Business Media.

Baruah, S., & Dutta, J. (2009). Nanotechnology applications in pollution sensing and degradation in agriculture: A review. *Environmental Chemistry Letters*, *7*(3), 191–204.

Batsmanova, L. M., Gonchar, L. M., Taran, N. Y., & Okanenko, A. A. Using a colloidal solution of metal nanoparticles as micronutrient fertiliser for cereals, Doctoral dissertation. (2013). Sumy State University.

Benício, L. P. F., Silva, R. A., Lopes, J. A., Eulálio, D., Santos, R. M. M. D., Aquino, L. A. D., et al. (2015). Layered double hydroxides: Nanomaterials for applications in agriculture. *Revista Brasileira de Ciência do Solo*, *39*(1), 1–13.

Bernardo, M. P., Moreira, F. K., & Ribeiro, C. (2017). Synthesis and characterization of eco-friendly Ca-Al-LDH loaded with phosphate for agricultural applications. *Applied Clay Science*, *137*, 143–150.

This book belongs to Central Library BADJI Mokhtar-ANNABA UNIVERSITY

Copyright Elsevier 2024

Bhattacharyya, A., Duraisamy, P., Govindarajan, M., Buhroo, A. A., & Prasad, R. (2016). Nano-biofungicides: Emerging trend in insect pest control. In *Advances and applications through fungal Nanobiotechnology* (pp. 307–319). Cham: Springer.

Biswas, P., & Wu, C. Y. (2005). Nanoparticles and the environment. *Journal of the Air & Waste Management Association*, *55*(6), 708–746.

Bodirsky, B. L., Rolinski, S., Biewald, A., Weindl, I., Popp, A., & Lotze-Campen, H. (2015). Global food demand scenarios for the 21st century. *PLoS ONE*, *10*(11), e0139201.

Bouldin, J. L., Ingle, T. M., Sengupta, A., Alexander, R., Hannigan, R. E., & Buchanan, R. A. (2008). Aqueous toxicity and food chain transfer of quantum dots™ in freshwater algae and Ceriodaphnia dubia. *Environmental Toxicology and Chemistry*, *27*(9), 1958–1963.

Bueno, P. D. L. C., Gillerman, L., Gehr, R., & Oron, G. (2017). Nanotechnology for sustainable wastewater treatment and use for agricultural production: A comparative long-term study. *Water Research*, *110*, 66–73.

Bülbül, G., Hayat, A., & Andreescu, S. (2015). Portable nanoparticle-based sensors for food safety assessment. *Sensors*, *15*(12), 30736–30758.

Bundschuh, M., Filser, J., Lüderwald, S., McKee, M. S., Metreveli, G., Schaumann, G. E., et al. (2018). Nanoparticles in the environment: Where do we come from, where do we go to? *Environmental Sciences Europe*, *30*(1), 6.

Campos, E. V. R., De Oliveira, J. L., Da Silva, C. M. G., Pascoli, M., Pasquoto, T., Lima, R., et al. (2015). Polymeric and solid lipid nanoparticles for sustained release of carbendazim and tebuconazole in agricultural applications. *Scientific Reports*, *5*, 13809.

Cao, L., Zhang, H., Cao, C., Zhang, J., Li, F., & Huang, Q. (2016). Quaternized chitosan-capped mesoporous silica nanoparticles as nanocarriers for controlled pesticide release. *Nanomaterials*, *6*(7), 126.

Carpenter, S. R. (2005). Eutrophication of aquatic ecosystems: Bistability and soil phosphorus. *Proceedings of the National Academy of Sciences*, *102*(29), 10002–10005.

Cazetta, A. L., Junior, O. P., Vargas, A. M., Da Silva, A. P., Zou, X., Asefa, T., et al. (2013). Thermal regeneration study of high surface area activated carbon obtained from coconut shell: Characterization and application of response surface methodology. *Journal of Analytical and Applied Pyrolysis*, *101*, 53–60.

Chaturvedi, S., Dave, P. N., & Shah, N. K. (2012). Applications of nano-catalyst in new era. *Journal of Saudi Chemical Society*, *16*(3), 307–325.

Chen, H., Lin, Y., Zhou, H., Zhou, X., Gong, S., & Xu, H. (2016). Synthesis and characterization of chlorpyrifos/copper (II) schiff base mesoporous silica with pH sensitivity for pesticide sustained release. *Journal of Agricultural and Food Chemistry*, *64*(43), 8095–8102.

Chhipa, H., & Joshi, P. (2016). Nanofertilisers, nanopesticides and nanosensors in agriculture. In. *vol. 1. Nanoscience in food and agriculture* (pp. 247–282). Cham: Springer.

Chislock, M. F., Doster, E., Zitomer, R. A., & Wilson, A. E. (2013). Eutrophication: Causes, consequences, and controls in aquatic ecosystems. *Nature Education Knowledge*, *4*(4), 10.

Cifuentes, Z., Custardoy, L., de la Fuente, J. M., Marquina, C., Ibarra, M. R., Rubiales, D., et al. (2010). Absorption and translocation to the aerial part of magnetic carbon-coated nanoparticles through the root of different crop plants. *Journal of Nanobiotechnology*, *8*(1), 26.

Cornelis, G., Doolette Madeleine Thomas, C., McLaughlin, M. J., Kirby, J. K., Beak, D. G., & Chittleborough, D. (2012). Retention and dissolution of engineered silver nanoparticles in natural soils. *Soil Science Society of America Journal*, *76*(3), 891–902.

Dall'Erba, S., & Domínguez, F. (2016). The impact of climate change on agriculture in the southwestern United States: The Ricardian approach revisited. *Spatial Economic Analysis*, *11*(1), 46–66.

de Castro, G. F., Ferreira, J. A., Eulálio, D., e Moraes, A. R. F., Constantino, V. R. L., Pinto, F. G., et al. (2018). Organic-inorganic hybrid materials: Layered double hydroxides and cellulose acetate films as phosphate recovery. *Journal of Agricultural Science and Technology*, *8*(6), 360–374.

This book belongs to Central Library BADJI Mokhtar-ANNABA UNIVERSITY

Copyright Elsevier 2024

De Jong, W. H., & Borm, P. J. (2008). Drug delivery and nanoparticles: Applications and hazards. *International Journal of Nanomedicine*, *3*(2), 133.

Deodhar, G. V., Adams, M. L., & Trewyn, B. G. (2017). Controlled release and intracellular protein delivery from mesoporous silica nanoparticles. *Biotechnology Journal*, *12*(1), 1600408.

UN DESA. (2015). *World population prospects: Key findings and advance tables*.

Ditta, A., Arshad, M., & Ibrahim, M. (2015). Nanoparticles in sustainable agricultural crop production: Applications and perspectives. In *Nanotechnology and plant sciences* (pp. 55–75). Cham: Springer.

Duran, C., Ozdes, D., Gundogdu, A., & Senturk, H. B. (2011). Kinetics and isotherm analysis of basic dyes adsorption onto almond shell (*Prunus dulcis*) as a low cost adsorbent. *Journal of Chemical & Engineering Data*, *56*(5), 2136–2147.

Dutta, S., Bhattacharyya, A., Ganguly, A., Gupta, S., & Basu, S. (2011). Application of response surface methodology for preparation of low-cost adsorbent from citrus fruit peel and for removal of methylene blue. *Desalination*, *275*(1–3), 26–36.

El Hadri, H., Louie, S. M., & Hackley, V. A. (2018). Assessing the interactions of metal nanoparticles in soil and sediment matrices—A quantitative analytical multi-technique approach. *Environmental Science: Nano*, *5*(1), 203–214.

FAO. (2011). *The state of world fisheries and aquaculture 2010*. Fisheries and Aquaculture Department, editors. Rome, Italy.

Feng, Y., Yang, F., Wang, Y., Ma, L., Wu, Y., Kerr, P. G., et al. (2011). Basic dye adsorption onto an agro-based waste material–sesame hull (*Sesamum indicum* L.). *Bioresource Technology*, *102*(22), 10280–10285.

Fernandes, J. P., Almeida, C. M. R., Andreotti, F., Barros, L., Almeida, T., & Mucha, A. P. (2017). Response of microbial communities colonizing salt marsh plants rhizosphere to copper oxide nanoparticles contamination and its implications for phytoremediation processes. *Science of the Total Environment*, *581*, 801–810.

Frenk, S., Ben-Moshe, T., Dror, I., Berkowitz, B., & Minz, D. (2013). Effect of metal oxide nanoparticles on microbial community structure and function in two different soil types. *PLoS ONE*, *8*(12), e84441.

Fryxell, G. E., & Cao, G. e. (2012). *Environmental applications of nanomaterials: Synthesis, sorbents and sensors*. World Scientific.

Fukamachi, K., Konishi, Y., & Nomura, T. (2019). Disease control of *Phytophthora infestans* using cyazofamid encapsulated in poly lactic-co-glycolic acid (PLGA) nanoparticles. *Colloids and Surfaces A: Physicochemical and Engineering Aspects*, *577*, 315–322.

Galbraith, D. W. (2007). Nanobiotechnology: Silica breaks through in plants. *Nature Nanotechnology*, *2*(5), 272.

Gao, Y., Zhang, Y., He, S., Xiao, Y., Qin, X., Zhang, Y., et al. (2019). Fabrication of a hollow mesoporous silica hybrid to improve the targeting of a pesticide. *Chemical Engineering Journal*, *364*, 361–369.

Gopinath, K., Karthika, V., Gowri, S., Senthilkumar, V., Kumaresan, S., & Arumugam, A. (2014). Antibacterial activity of ruthenium nanoparticles synthesized using *Gloriosa superba* L. leaf extract. *Journal of Nanostructure in Chemistry*, *4*(1), 83.

Gouin, S. (2004). Microencapsulation: Industrial appraisal of existing technologies and trends. *Trends in Food Science & Technology*, *15*(7–8), 330–347.

Grillo, R., Abhilash, P. C., & Fraceto, L. F. (2016). Nanotechnology applied to bio-encapsulation of pesticides. *Journal of Nanoscience and Nanotechnology*, *16*(1), 1231–1234.

Grün, A. L., Manz, W., Kohl, Y. L., Meier, F., Straskraba, S., Jost, C., et al. (2019). Impact of silver nanoparticles (AgNP) on soil microbial community depending on functionalization, concentration, exposure time, and soil texture. *Environmental Sciences Europe*, *31*(1), 15.

Gutiérrez, F. J., Mussons, M. L., Gatón, P., & Rojo, R. (2011). *Nanotechnology and food industry. Scientific, health and social aspects of the food industry*. Tech, Croatia Book Chapter.

Hameed, B. H., Tan, I. A. W., & Ahmad, A. L. (2008). Optimization of basic dye removal by oil palm fibre-based activated carbon using response surface methodology. *Journal of Hazardous Materials*, *158*(2–3), 324–332.

This book belongs to Central Library BADJI Mokhtar-ANNABA UNIVERSITY

Copyright Elsevier 2024

Hristozov, D., & Ertel, J. (2009). Nanotechnology and sustainability: benefits and risks of nanotechnology for environmental sustainability. In *Vol. 22. Forum der Forschung* (pp. 161–168). Vol. 22, (pp. 161–168).

Hsu, S. T., Chen, L. C., Lee, C. C., Pan, T. C., You, B. X., & Yan, Q. F. (2009). Preparation of methacrylic acid-modified rice husk improved by an experimental design and application for paraquat adsorption. *Journal of Hazardous Materials*, *171*(1–3), 465–470.

Huang, S., Wang, L., Liu, L., Hou, Y., & Li, L. (2015). Nanotechnology in agriculture, livestock, and aquaculture in China. A review. *Agronomy for Sustainable Development*, *35*(2), 369–400.

Ihegwuagu, N. E., Sha'Ato, R., Tor-Anyiin, T. A., Nnamonu, L. A., Buekes, P., Sone, B., et al. (2016). Facile formulation of starch-silver-nanoparticle encapsulated dichlorvos and chlorpyrifos for enhanced insecticide delivery. *New Journal of Chemistry*, *40*(2), 1777–1784.

Imran, A., López-Rayo, S., Magid, J., & Hansen, H. C. B. (2016). Dissolution kinetics of pyroaurite-type layered double hydroxide doped with Zn: Perspectives for pH controlled micronutrient release. *Applied Clay Science*, *123*, 56–63.

Junior, O. P., Cazetta, A. L., Gomes, R. C., Barizão, É. O., Souza, I. P., Martins, A. C., et al. (2014). Synthesis of $ZnCl_2$-activated carbon from macadamia nut endocarp (*Macadamia integrifolia*) by microwave-assisted pyrolysis: Optimization using RSM and methylene blue adsorption. *Journal of Analytical and Applied Pyrolysis*, *105*, 166–176.

Kabir, E., Kumar, V., Kim, K. H., Yip, A. C., & Sohn, J. R. (2018). Environmental impacts of nanomaterials. *Journal of Environmental Management*, *225*, 261–271.

Kaur, M., Verma, A., Setia, H., & Toor, A. P. (2019). Comparative study on the photocatalytic degradation of Paraquat using tungsten-doped TiO_2 under UV and sunlight. In *Sustainable engineering* (pp. 145–155). Singapore: Springer.

Khan, I., Saeed, K., & Khan, I. (2017). Nanoparticles: Properties, applications and toxicities. *Arabian Journal of Chemistry*.

Khot, L. R., Sankaran, S., Maja, J. M., Ehsani, R., & Schuster, E. W. (2012). Applications of nanomaterials in agricultural production and crop protection: A review. *Crop Protection*, *35*, 64–70.

Kumaraswamy, R. V., Kumari, S., Choudhary, R. C., Pal, A., Raliya, R., Biswas, P., et al. (2018). Engineered chitosan based nanomaterials: Bioactivities, mechanisms and perspectives in plant protection and growth. *International Journal of Biological Macromolecules*, *113*, 494–506.

Kuppusamy, S., Thavamani, P., Venkateswarlu, K., Lee, Y. B., Naidu, R., & Megharaj, M. (2017). Remediation approaches for polycyclic aromatic hydrocarbons (PAHs) contaminated soils: Technological constraints, emerging trends and future directions. *Chemosphere*, *168*, 944–968.

Lal, R. (2008). Promise and limitations of soils to minimize climate change. *Journal of Soil and Water Conservation*, *63*(4), 113A–118A.

Lin, S., Reppert, J., Hu, Q., Hudson, J. S., Reid, M. L., Ratnikova, T. A., et al. (2009). Uptake, translocation, and transmission of carbon nanomaterials in rice plants. *Small*, *5*(10), 1128–1132.

Liu, Y., Lang, J., Wang, T., Jawad, A., Wang, H., Khan, A., et al. (2018). Enhanced degradation of isoproturon in soil through persulfate activation by Fe-based layered double hydroxide: Different reactive species comparing with activation by homogenous Fe (II). *Environmental Science and Pollution Research*, *25*(26), 26394–26404.

Liu, Y., Zhao, Y., Zhang, T., Chang, Y., Zou, R., Wang, S., et al. (2019). Quantum dots-based immunochromatographic strip for rapid and sensitive detection of acetamiprid in agricultural products. *Frontiers in Chemistry*, *7*, 76.

Lobell, D. B., & Gourdji, S. M. (2012). The influence of climate change on global crop productivity. *Plant Physiology*, *160*(4), 1686–1697.

Madurwar, M. V., Ralegaonkar, R. V., & Mandavgane, S. A. (2013). Application of agro-waste for sustainable construction materials: A review. *Construction and Building Materials*, *38*, 872–878.

This book belongs to Central Library BADJI Mokhtar-ANNABA UNIVERSITY

Copyright Elsevier 2024

Mani, P. K., & Mondal, S. (2016). Agri-nanotechniques for plant availability of nutrients. In *Plant nanotechnology* (pp. 263–303). Cham: Springer.

Manjunatha, S. B., Biradar, D. P., & Aladakatti, Y. R. (2016). Nanotechnology and its applications in agriculture: A review. *Journal of Farm Science*, *29*(1), 1–13.

Manoharan, R. K., & Sankaran, S. (2018). Photocatalytic degradation of organic pollutant aldicarb by non-metal-doped nanotitania: Synthesis and characterization. *Environmental Science and Pollution Research*, *25*(21), 20510–20517.

Marcelo, C. R., Lopes, R. P., Cruz, J. C., Nascimento, M. A., Silva, A. A., & Lima, C. F. (2016). Evaluation of different parameters on the acetamiprid degradation by bimetallic Fe/Ni nanoparticles. *Separation and Purification Technology*, *171*, 256–262.

Maurer-Jones, M. A., Gunsolus, I. L., Murphy, C. J., & Haynes, C. L. (2013). Toxicity of engineered nanoparticles in the environment. *Analytical Chemistry*, *85*(6), 3036–3049.

Méndez, F. B., Sánchez, D. A. M., Rangel, D. S., Landa, I. B., Haas, J. B. R., Villanueva, J. L. M., et al. (2019). Propiconazole nanoencapsulation in biodegradable polymers to obtain pesticide controlled delivery systems. *Journal of the Mexican Chemical Society*, *63*(1).

Milewska-Hendel, A., Gawecki, R., Zubko, M., Stróz, D., & Kurczynska, E. (2016). Diverse influence of nanoparticles on plant growth with a particular emphasis on crop plants. *Acta Agrobotanica*, *69*(4).

Mishra, G., Pandey, S., Dutta, A., & Giri, K. (2017). Nanotechnology applications for sustainable crop production. In *Applying nanotechnology for environmental sustainability* (pp. 164–184): IGI Global.

Mohamed, M. A., Hashim, A. F., Alghuthaymi, M. A., & Abd-Elsalam, K. A. (2018). Nano-carbon: Plant growth promotion and protection. In *Nanobiotechnology applications in plant protection* (pp. 155–188). Cham: Springer.

Mostafa, N. A., Farag, A. A., Abo-dief, H. M., & Tayeb, A. M. (2018). Production of biodegradable plastic from agricultural wastes. *Arabian Journal of Chemistry*, *11*(4), 546–553.

Mueller, N. D., Gerber, J. S., Johnston, M., Ray, D. K., Ramankutty, N., & Foley, J. A. (2012). Closing yield gaps through nutrient and water management. *Nature*, *490*(7419), 254.

Nel, A., Xia, T., Mädler, L., & Li, N. (2006). Toxic potential of materials at the nanolevel. *Science*, *311*(5761), 622–627.

Nguyen, T. T., Le, G. H., Le, C. H., Nguyen, M. B., Quan, T. T., Pham, T. T., et al. (2018). Atomic implantation synthesis of Fe-cu/SBA-15 nanocomposite as a heterogeneous Fenton-like catalyst for enhanced degradation of DDT. *Materials Research Express*, *5*(11), 115005.

Norman, S., & Hongda, C. (2013). IB IN DEPTH special section on nanobiotechnology, part 2. *Industrial Biotechnology*, *9*, 17–18.

Nsibande, S. A., & Forbes, P. B. C. (2016). Fluorescence detection of pesticides using quantum dot materials—A review. *Analytica Chimica Acta*, *945*, 9–22.

Nuruzzaman, M. D., Rahman, M. M., Liu, Y., & Naidu, R. (2016). Nanoencapsulation, nano-guard for pesticides: A new window for safe application. *Journal of Agricultural and Food Chemistry*, *64*(7), 1447–1483.

Obi, F. O., Ugwuishiwu, B. O., & Nwakaire, J. N. (2016). Agricultural waste concept, generation, utilization and management. *Nigerian Journal of Technology*, *35*(4), 957–964.

Omara, A. E. D., Elsakhawy, T., Alshaal, T., El-Ramady, H., Kovács, Z., & Fári, M. (2019). Nanoparticles: A novel approach for sustainable agro-productivity. *Environment, Biodiversity and Soil Security*, *3*(2019), 29–62.

Ortiz, I., & Velasco, A. (2019). Degradation of DDT, endrin, and endosulfan in polluted-soils by zero-valent iron (fe0) and zero-valent iron-copper (fe0-cu0) treatment. *Revista Mexicana de Ingeniería Química*, *18*(3), 875–888.

Petosa, A. R., Rajput, F., Selvam, O., Öhl, C., & Tufenkji, N. (2017). Assessing the transport potential of polymeric nanocapsules developed for crop protection. *Water Research*, *111*, 10–17.

This book belongs to Central Library BADJI Mokhtar-ANNABA UNIVERSITY

Copyright Elsevier 2024

Piao, S., Ciais, P., Huang, Y., Shen, Z., Peng, S., Li, J., et al. (2010). The impacts of climate change on water resources and agriculture in China. *Nature*, *467*(7311), 43.

Prasad, R., Bhattacharyya, A., & Nguyen, Q. D. (2017). Nanotechnology in sustainable agriculture: Recent developments, challenges, and perspectives. *Frontiers in Microbiology*, *8*, 1014.

Que, X., Tang, D., Xia, B., Lu, M., & Tang, D. (2014). Gold nanocatalyst-based immunosensing strategy accompanying catalytic reduction of 4-nitrophenol for sensitive monitoring of chloramphenicol residue. *Analytica Chimica Acta*, *830*, 42–48.

Rai, M., & Ingle, A. (2012). Role of nanotechnology in agriculture with special reference to management of insect pests. *Applied Microbiology and Biotechnology*, *94*(2), 287–293.

Rajput, V. D., Minkina, T., Sushkova, S., Tsitsuashvili, V., Mandzhieva, S., Gorovtsov, A., et al. (2018). Effect of nanoparticles on crops and soil microbial communities. *Journal of Soils and Sediments*, *18*(6), 2179–2187.

Rani, M., Shanker, U., & Jassal, V. (2017). Recent strategies for removal and degradation of persistent & toxic organochlorine pesticides using nanoparticles: A review. *Journal of Environmental Management*, *190*, 208–222.

Rastogi, A., Tripathi, D. K., Yadav, S., Chauhan, D. K., Živčák, M., Ghorbanpour, M., et al. (2019). Application of silicon nanoparticles in agriculture. *3 Biotech*, *9*(3), 90.

Rizwan, M., Ali, S., Qayyum, M. F., Ok, Y. S., Adrees, M., Ibrahim, M., et al. (2017). Effect of metal and metal oxide nanoparticles on growth and physiology of globally important food crops: A critical review. *Journal of Hazardous Materials*, *322*, 2–16.

Rodrigues, S. M., Demokritou, P., Dokoozlian, N., Hendren, C. O., Karn, B., Mauter, M. S., et al. (2017). Nanotechnology for sustainable food production: Promising opportunities and scientific challenges. *Environmental Science: Nano*, *4*(4), 767–781.

Rosbero, T. M. S., & Camacho, D. H. (2017). Green preparation and characterization of tentacle-like silver/copper nanoparticles for catalytic degradation of toxic chlorpyrifos in water. *Journal of Environmental Chemical Engineering*, *5*(3), 2524–2532.

Rosenzweig, C., Iglesias, A., Yang, X. B., Epstein, P. R., & Chivian, E. (2001). Climate change and extreme weather events; Implications for food production, plant diseases, and pests. *Global Change & Human Health*, *2*(2), 90–104.

Salman, J. M., & Hameed, B. H. (2010). Effect of preparation conditions of oil palm fronds activated carbon on adsorption of bentazon from aqueous solutions. *Journal of Hazardous Materials*, *175*(1–3), 133–137.

Scott, N., & Chen, H. (2012). Nanoscale science and engineering for agriculture and food systems. *Industrial Biotechnology*, *8*(6), 340–343.

Scrinis, G., & Lyons, K. (2007). The emerging nano-corporate paradigm: Nanotechnology and the transformation of nature, food and agri-food systems. *International Journal of Sociology of Food and Agriculture*, *15*(2), 22–44.

Sekhon, B. S. (2014). Nanotechnology in agri-food production: An overview. *Nanotechnology, Science and Applications*, *7*, 31.

Servin, A. D., De la Torre-Roche, R., Castillo-Michel, H., Pagano, L., Hawthorne, J., Musante, C., et al. (2017). Exposure of agricultural crops to nanoparticle CeO_2 in biochar-amended soil. *Plant Physiology and Biochemistry*, *110*, 147–157.

Shan, Y., Cao, L., Xu, C., Zhao, P., Cao, C., Li, F., et al. (2019). Sulfonate-functionalized mesoporous silica nanoparticles as carriers for controlled herbicide diquat dibromide release through electrostatic interaction. *International Journal of Molecular Sciences*, *20*(6), 1330.

She, Y., Hong, S., Cao, X., Wang, M., He, Y., Zheng, L., et al. (2019). A novel CdSe/ZnS quantum dots fluorescence assay based on molecularly imprinted sensitive membranes for determination of triazophos residues in cabbage and apple. *Frontiers in Chemistry*, *7*, 130.

This book belongs to Central Library BADJI Mokhtar-ANNABA UNIVERSITY

Copyright Elsevier 2024

Simonin, M., & Richaume, A. (2015). Impact of engineered nanoparticles on the activity, abundance, and diversity of soil microbial communities: A review. *Environmental Science and Pollution Research*, *22*(18), 13710–13723.

Singh, A., Bhati, A., Tripathi, K. M., & Sonkar, S. K. (2018). Nanocarbons in agricultural plants: Can be a potential nanofertilizer? In *Nanotechnology in environmental science* (pp. 153–190).

Singh, D., & Kumar, A. (2016). Impact of irrigation using water containing CuO and ZnO nanoparticles on spinach oleracea grown in soil media. *Bulletin of Environmental Contamination and Toxicology*, *97*(4), 548–553.

Smith, C. J., Shaw, B. J., & Handy, R. D. (2007). Toxicity of single walled carbon nanotubes to rainbow trout (*Oncorhynchus mykiss*): Respiratory toxicity, organ pathologies, and other physiological effects. *Aquatic Toxicology*, *82*(2), 94–109.

Song, J., Zou, W., Bian, Y., Su, F., & Han, R. (2011). Adsorption characteristics of methylene blue by peanut husk in batch and column modes. *Desalination*, *265*(1–3), 119–125.

Soni, D., Naoghare, P. K., Saravanadevi, S., & Pandey, R. A. (2015). Release, transport and toxicity of engineered nanoparticles. In *Reviews of environmental contamination and toxicology* (pp. 1–47). Cham: Springer.

Srivastava, A. K., Dev, A., & Karmakar, S. (2018). Nanosensors and nanobiosensors in food and agriculture. *Environmental Chemistry Letters*, *16*(1), 161–182.

Tan, I. A. W., Ahmad, A. L., & Hameed, B. H. (2008). Adsorption of basic dye on high-surface-area activated carbon prepared from coconut husk: Equilibrium, kinetic and thermodynamic studies. *Journal of Hazardous Materials*, *154*(1–3), 337–346.

Tang, C., Li, Y., Pun, J., Osman, A. S. M., & Tam, K. C. (2019). Polydopamine microcapsules from cellulose nanocrystal stabilized pickering emulsions for essential oil and pesticide encapsulation. *Colloids and Surfaces A: Physicochemical and Engineering Aspects*, *570*, 403–413.

Tassi, E., Giorgetti, L., Morelli, E., Peralta-Videa, J. R., Gardea-Torresdey, J. L., & Barbafieri, M. (2017). Physiological and biochemical responses of sunflower (*Helianthus annuus* L.) exposed to nano-CeO_2 and excess boron: Modulation of boron phytotoxicity. *Plant Physiology and Biochemistry*, *110*, 50–58.

Theng, B. K., & Yuan, G. (2008). Nanoparticles in the soil environment. *Elements*, *4*(6), 395–399.

Tilman, D., Balzer, C., Hill, J., & Befort, B. L. (2011). Global food demand and the sustainable intensification of agriculture. *Proceedings of the National Academy of Sciences*, *108*(50), 20260–20264.

Tilman, D., Cassman, K. G., Matson, P. A., Naylor, R., & Polasky, S. (2002). Agricultural sustainability and intensive production practices. *Nature*, *418*(6898), 671.

Tolaymat, T., Genaidy, A., Abdelraheem, W., Dionysiou, D., & Andersen, C. (2017). The effects of metallic engineered nanoparticles upon plant systems: An analytic examination of scientific evidence. *Science of the Total Environment*, *579*, 93–106.

Torney, F., Trewyn, B. G., Lin, V. S. Y., & Wang, K. (2007). Mesoporous silica nanoparticles deliver DNA and chemicals into plants. *Nature Nanotechnology*, *2*(5), 295.

Tripathi, D. K., Singh, S., Singh, S., Pandey, R., Singh, V. P., Sharma, N. C., et al. (2017). An overview on manufactured nanoparticles in plants: Uptake, translocation, accumulation and phytotoxicity. *Plant Physiology and Biochemistry*, *110*, 2–12.

Trujillo-Reyes, J., Majumdar, S., Botez, C. E., Peralta-Videa, J. R., & Gardea-Torresdey, J. L. (2014). Exposure studies of core–shell Fe/Fe_3O_4 and Cu/CuO NPs to lettuce (*Lactuca sativa*) plants: Are they a potential physiological and nutritional hazard? *Journal of Hazardous Materials*, *267*, 255–263.

Vithanage, M., Seneviratne, M., Ahmad, M., Sarkar, B., & Ok, Y. S. (2017). Contrasting effects of engineered carbon nanotubes on plants: A review. *Environmental Geochemistry and Health*, *39*(6), 1421–1439.

Wang, C., He, R., Wu, Y., Lürling, M., Cai, H., Jiang, H. L., et al. (2017). Bioavailable phosphorus (P) reduction is less than mobile P immobilization in lake sediment for eutrophication control by inactivating agents. *Water Research*, *109*, 196–206.

This book belongs to Central Library BADJI Mokhtar-ANNABA UNIVERSITY

Copyright Elsevier 2024

Wu, J., Xie, Y., Fang, Z., Cheng, W., & Tsang, P. E. (2016). Effects of Ni/Fe bimetallic nanoparticles on phytotoxicity and translocation of polybrominated diphenyl ethers in contaminated soil. *Chemosphere*, *162*, 235–242.

Xu, X., Sun, L., Bai, B., Wang, H., & Suo, Y. (2019). Interfacial assembly of mussel-inspired polydopamine@ Ag core–shell nanoparticles as highly recyclable catalyst for nitroaromatic pesticides degradation. *Science of the Total Environment*, *665*, 133–141.

Xue, Y., Wang, P., Wang, C., & Ao, Y. (2018). Efficient degradation of atrazine by BiOBr/UiO-66 composite photocatalyst under visible light irradiation: Environmental factors, mechanisms and degradation pathways. *Chemosphere*, *203*, 497–505.

Yan, S., Zhao, L., Li, H., Zhang, Q., Tan, J., Huang, M., et al. (2013). Single-walled carbon nanotubes selectively influence maize root tissue development accompanied by the change in the related gene expression. *Journal of Hazardous Materials*, *246–247*, 110–118.

Yang, J., Cao, W., & Rui, Y. (2017). Interactions between nanoparticles and plants: Phytotoxicity and defense mechanisms. *Journal of Plant Interactions*, *12*(1), 158–169.

Zaytseva, O., & Neumann, G. (2016). Carbon nanomaterials: Production, impact on plant development, agricultural and environmental applications. *Chemical and Biological Technologies in Agriculture*, *3*(1), 17.

Zhang, K., Pei, Z., & Wang, D. (2016). Organic solvent pretreatment of lignocellulosic biomass for biofuels and biochemicals: A review. *Bioresource Technology*, *199*, 21–33.

Zhao, L., Hernandez-Viezcas, J. A., Peralta-Videa, J. R., Bandyopadhyay, S., Peng, B., Munoz, B., et al. (2012). ZnO nanoparticle fate in soil and zinc bioaccumulation in corn plants (*Zea mays*) influenced by alginate. *Environmental Science: Processes & Impacts*, *15*(1), 260–266.

Zhou, Y., Zhang, L., & Cheng, Z. (2015). Removal of organic pollutants from aqueous solution using agricultural wastes: A review. *Journal of Molecular Liquids*, *212*, 739–762.

Further reading

Dwivedi, S., Saquib, Q., Al-Khedhairy, A. A., & Musarrat, J. (2016). Understanding the role of nanomaterials in agriculture. In *Microbial inoculants in sustainable agricultural productivity* (pp. 271–288). New Delhi: Springer.

García, A., Alriols, M. G., & Labidi, J. (2014). Evaluation of different lignocellulosic raw materials as potential alternative feedstocks in biorefinery processes. *Industrial Crops and Products*, *53*, 102–110.

García, A., Labidi, J., Belgacem, M. N., & Bras, J. (2017). The nanocellulose biorefinery: Woody versus herbaceous agricultural wastes for NCC production. *Cellulose*, *24*(2), 693–704.

Gil-Díaz, M., Diez-Pascual, S., González, A., Alonso, J., Rodríguez-Valdés, E., Gallego, J. R., et al. (2016). A nanoremediation strategy for the recovery of an as-polluted soil. *Chemosphere*, *149*, 137–145.

Gil-Díaz, M., Pinilla, P., Alonso, J., & Lobo, M. C. (2017). Viability of a nanoremediation process in single or multi-metal (loid) contaminated soils. *Journal of Hazardous Materials*, *321*, 812–819.

Sadeghzadeh, B. (2013). A review of zinc nutrition and plant breeding. *Journal of Soil Science and Plant Nutrition*, *13*(4), 905–927.

Sharma, V., Kumar, A., & Dhawan, A. (2012). Nanomaterials: Exposure, effects and toxicity assessment. *Proceedings of the National Academy of Sciences, India Section B: Biological Sciences*, *82*(1), 3–11.

This book belongs to Central Library BADJI Mokhtar-ANNABA UNIVERSITY

Copyright Elsevier 2024

CHAPTER

Nanotechnology for soil remediation: Revitalizing the tarnished resource

17

Mansi Bakshi, P.C. Abhilash*

Institute of Environment & Sustainable Development (IESD), Banaras Hindu University, Varanasi, India

**Corresponding author: e-mail address: mansibakshi.51@gmail.com; pca.iesd@bhu.ac.in*

1 Introduction

1.1 Soil contamination: Current scenario

Soil is an important life-supporting system and also the most vital component of terrestrial ecosystem. Apart from being an indispensable medium for plant growth and food production, soil regulates major planetary processes ensuring existences of life on earth (Abhilash, Powell, Singh, & Singh, 2012; Banwart, 2011; Hodson, 2010). These include biogeochemical cycles, water cycle, earth's climate, pollutant detoxification, biogenic gas regulation, ecosystem restoration, and biodiversity maintenance (Abhilash et al., 2013; Gil-Díaz et al., 2014). In respect to reference the terms "land" and "soil" are often used synonymously since many natural and anthropogenic activities affect both targets in nearly the same way. However, land is more than soil, while soil is an important part of land (Blum, 2002). Management of soil health is crucial not only for safeguarding food and agricultural productions but also for maintaining the balance of earth and environmental processes (Lal, 2015).

However, in the current scenario, soil contamination and degradation are a serious environmental problem that poses great challenge to agricultural productivity and food security (Lal, 2009). Soil degradation is triggered by many factors such as overgrazing, soil erosion, deforestation, decline in soil fertility, and urbanization (Clair & Lynch, 2010; Lal, 2015; León & Osorio, 2014). Apart from this, chemical pollution and contamination from heavy metals, polycyclic aromatic hydrocarbons (PAHs), pesticides, and persistent organic pollutants (POPs) have also emerged as an important factor contributing directly to degradation of soil. Excessive pesticide and fertilizer usage leads to their accumulation in soil since a large amount of these (~90%) is lost to the air during application or as runoff, and in due course of time, these chemicals make their way into the soil. Also, chemical pollutants like heavy metals released from industries degrade the land not only in the vicinity of the industrial plant but also far off (Bhatnagar, 2001; Ghormade, Deshpande, & Paknikar, 2011; Maharia, Dutta, Acharya, & Reddy, 2010; Stephenson, Coats, & Yamamoto, 2003).

Environmental risks associated with soil pollution are considered great threats to the entire ecosystem. Due to all of the aforementioned reasons and further human activities, an estimated 30% of land is

Nano-Materials as Photocatalysts for Degradation of Environmental Pollutants. https://doi.org/10.1016/B978-0-12-818598-8.00017-1
© 2020 Elsevier Inc. All rights reserved.

This book belongs to Central Library BADJI Mokhtar-ANNABA UNIVERSITY

Copyright Elsevier 2024

either degraded or contaminated, with the degradation level increasing sequentially (Abhilash et al., 2013; Huettermann, Orikiriza, & Agaba, 2009). The widespread damage to land and soil has not only raised concerns but also sparked an urgent need for remediation of these tarnished resources. Over the course of time, heavy metals, pesticides, and POPs have contaminated the soil resource to an extent that further crop production on these degraded and polluted resource has become impossible (Abhilash & Singh, 2009; Tripathi, Fraceto, & Abhilash, 2015; Zhang et al., 2013). Contaminated land not only is unsuitable for food production but also poses great risks of food chain contamination as these contaminants (many heavy metals, pesticides, and POPs) exhibit bioaccumulation and biomagnification characteristics (Gavrilescu, 2009; Lu et al., 2015; Weber et al., 2008). Consumption of crops grown on these soils can thus pose serious consequences to human health, or else, these pollutants can also enter the human body via food chain contamination. Therefore, being unsuitable for crop production, most of these contaminated and polluted lands are abandoned, causing massive loss to agricultural production. With every passing year, soils are increasingly becoming polluted and contaminated, leading to a decrease in the quantity of land available for agricultural activities. So, we are faced with the dual challenge of producing more food for a burgeoning human population on an already shrinking landscape while at the same time preventing land from further damage and restoring the already degraded land. Therefore prevention alongside remediation and restoration of this contaminated soil is the need of the hour. After remediation, this revitalized land can then be used for meeting the food and bioenergy demands of the present world.

1.2 Nanotechnology: Uses and applications in soil remediation

Nanotechnology is seen as a novel technology that is progressing speedily and spreading its application domains in all dimensions. Nanotechnology encompasses designing, measuring, and manipulating matter at the atomic, molecular, macromolecular, and micromolecular scales, such that the resulting material possesses unique and entirely different properties from the parent bulk material (Bhatt & Tripathi, 2011; Khan, Mobin, Abbas, AlMutairi, & Siddiqui, 2017). The particles generated through this are termed as engineered nanoparticles (ENPs) or simply nanoparticles (NPs). ENPs are defined as particles having at least one external dimension between 1 and 100 nm (Shi, Abid, Kennedy, Hristova, & Silk, 2011; Thuesombat, Hannongbua, Akasit, & Chadchawan, 2014). Nanotechnology finds applications in an extensive range of sectors ranging from agriculture, food production and packaging, medical diagnostic, pharmaceutical, nanobased encapsulation of pesticides, genetic material delivery in plants, drug delivery in humans, and cancer treatment to many more (De Oliveira, Campos, Bakshi, Abhilash, & Fraceto, 2014; Ghormade et al., 2011; Gogos, Knauer, & Bucheli, 2012). Apart from these, its most anticipated applications have been for remediation of environmental compartments like water and soil. These include treatment of wastewater, cleaning of groundwater, and remediation of soil contaminated with pollutants (Karn, Kuiken, & Otto, 2009; Kuiken, 2010; Rogueda & Traini, 2007; Roh, Park, Park, & Choi, 2010; Shi, Votruba, Farokhzad, & Langer, 2010).

The increasing use and application of nanobased methods, devices, or materials for environmental cleanup possibly stem from the urgent need of a technology that is cleaner, affordable, easily available, and cost-effective while at the same time quicker in delivering results without additional burden to the cleanup process in the form of residues and environmental persistence (Cai, Zhao, Yu, Rong, & Zhang, 2019; Karn et al., 2009; Yan, Lien, Koel, & Zhang, 2013). Therefore the use of nanoparticles (NPs) or nanomaterials containing nanoparticles for the remediation of soil contaminated by chemicals like heavy metals, pesticides, and POPs, which are chiefly nonbiodegradable in nature, is being widely considered. Various nanotechnology-based applications being used for soil remediation include

This book belongs to Central Library BADJI Mokhtar-ANNABA UNIVERSITY Copyright Elsevier 2024

(i) nanobased materials for conversion of heavy metals to their less toxic forms, (ii) nanomaterials for pesticide and POP degradation, (iii) nanobased sensors for pesticide residue detection in soil, and (iv) nanomaterial-assisted phytoremediation or bioremediation of contaminated soil.

NPs that are being most widely used for soil remediation include nanoscale zerovalent iron (nZVI), titanium dioxide (TiO_2), zinc oxide (ZnO), multiwalled carbon nanotubes (MWCNTs), fullerenes, bimetallic nanoparticles, and stabilized nanoparticles (Cai et al., 2019; Pan & Xing, 2012). Nanoremediation involves applications of reactive nanomaterials to the contaminated soil for either transformation or detoxification of pollutants (Karn et al., 2009; Otto, Floyd, & Bajpai, 2008; Yan et al., 2013). Nanomaterials by virtue of their size and properties possess much larger surface areas and thus higher sorption sites making them excellent absorbents (Gong et al., 2018; Khin, Nair, Babu, Murugan, & Ramakrishna, 2012). Their other useful properties include lower temperature modification, shorter interparticle diffusion distance, more tunable pore size, and different surface chemistry (Tang et al., 2014). These properties enable them to be remarkable catalysts that can enable chemical reduction and also catalysis for the mitigation of the concerned pollutants. Therefore nanomaterials have garnered much attention and are being extensively considered to remediate soil environments contaminated by the most infamous pollutants like heavy metals, chlorinated organic solvents, organochlorine pesticides, polycyclic aromatic hydrocarbons (PAHs), and polychlorinated biphenyls (PCBs) (Fig. 1).

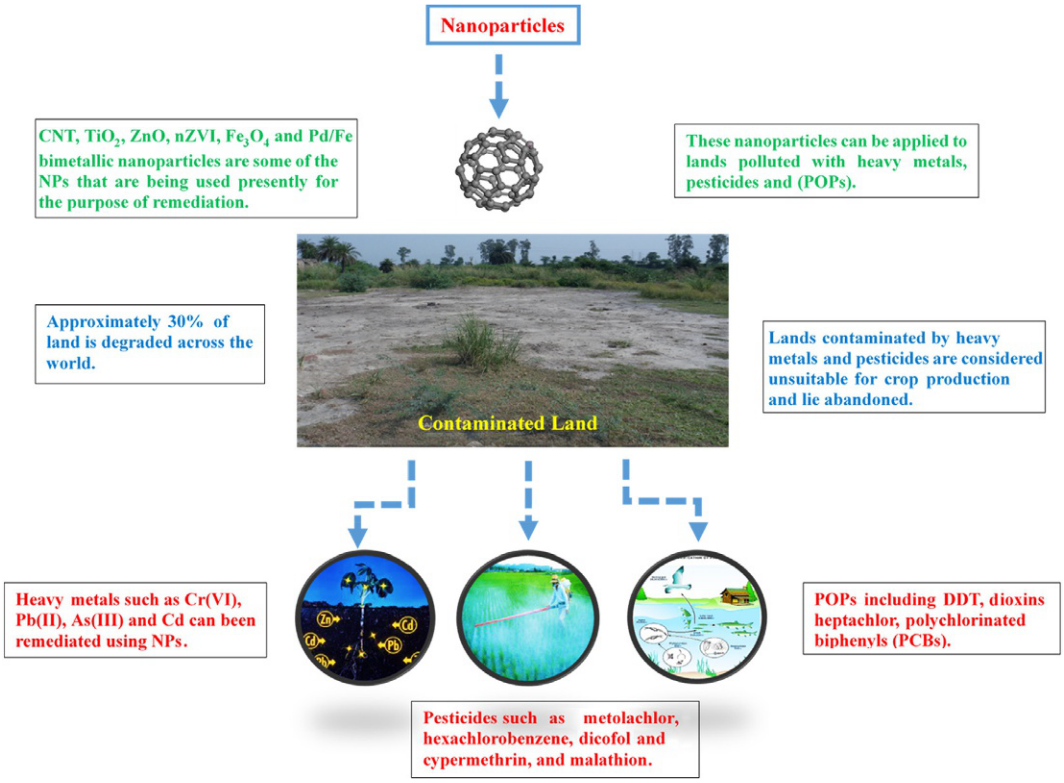

FIG. 1

The use of nanoparticles for remediation of soil contaminated with heavy metals, pesticides, and persistent organic pollutants (POPs).

This book belongs to Central Library BADJI Mokhtar-ANNABA UNIVERSITY Copyright Elsevier 2024

While the other methods of soil remediation are both in situ and ex situ, the process of nanoremediation is generally on-site without inclusion of methods like pumping up or transportation of soil. This, therefore, makes nanoremediation a cost-effective environmental remediation method (Cai et al., 2019; Jiang et al., 2018).

2 Role of nanomaterials in heavy metal removal from soil

Heavy metal by definition refers to the group of elements that have a relatively high density (>5 g/cm^3) and atomic mass (>20). From toxicity point of view, the most important heavy metals include arsenic (As), chromium (Cr), cadmium (Cd), mercury (Hg), copper (Cu), lead (Pb), cobalt (Co), zinc (Zn), manganese (Mn), nickel (Ni), and selenium (Se). Apart from these the other less toxic, lesser-known, but likewise important heavy metals include antimony (Sb), gold (Au), silver (Ag), molybdenum (Mo), barium (Ba), tungsten (W), thallium (Tl), tin (Sn), uranium (U), and vanadium (V). Heavy metals are natural components of the Earth's crust and soils, originating from weathering of soil parent material, where their concentration generally tend to remain quite low (Alloway, 2012; Bradl, 2005; Kabata-Pendias & Pendias, 2001; Violante, Cozzolino, Perelomov, Caporale, & Pigna, 2010). However, over the course of time, the external or anthropogenic inputs of many heavy metals in soils have exceeded their natural inputs from parent rock material, also known as paedogenesis. The major sources of these anthropogenic inputs are industries of paints, dyes, paper and pulp, textile mills, metal mining industries, metallurgical extractions, tanneries, agricultural fertilizers, and improper waste disposal (Castillo, Trujillo, Alonso, de Torres, & Pavón, 2013; Fayiga & Saha, 2016; Le Cloarec, Bonte, Lestel, Lefèvre, & Ayrault, 2011; Men et al., 2018; Navarro et al., 2008; Pacyna et al., 2007; Wuana & Okieimen, 2011). Apart from these, heavy metal deposition in soil may also occur due to aerosol particles generated from fossil fuel combustion and atmospherically transported over long distance from the source (Pacyna, Pacyna, & Aas, 2009; Rühling & Tyler, 2001; Wong, Li, Zhang, Qi, & Peng, 2003). Due to all the reasons mentioned above, a significant proportion of soil sites have been contaminated with heavy metals in many parts of the world, which pose great risks of toxicity to humans. Adding to these numbers, are those sites that have been historically contaminated by excessive use of heavy metals, whose toxicity was unknown earlier and which over the course of time have degraded these soils, and that are unfit for agricultural use, and this may continue for decades or even centuries, if they are not properly restored.

Many technological innovations are being explored, to clear contaminated soil from heavy metal pollution and make them suitable for agriculture and crop production. One such technique is the use of nanomaterials for the remediation of soil contaminated with heavy metals, primarily, due to their excellent capacity to immobilize or adsorb metal ions. Their high adsorption capacity makes nanoparticles (NPs) an ideal adsorbent, leading to their increasing application in the removal of heavy metal from soil (Ali, Khan, & Sajad, 2013; Cai et al., 2019; Gil-Díaz et al., 2014; Hua et al., 2012; Peikam & Jalali, 2018).

Due to its large surface area, high reactivity, and reduction capability, the most widely studied nanoparticle (NP) for the removal of both organic and inorganic pollutant from soil is nanoscale zerovalent iron (nZVI) (Fu et al., 2015; Fu et al., 2017; Lefevre, Bossa, Wiesner, & Gunsch, 2016; Li, Wang, Liang, & Zhang, 2017; Stefaniuk, Oleszczuk, & Ok, 2016; Wang, Lombi, Zhao, & Kopittke, 2016; Zou et al., 2016). Singh, Misra, and Singh (2012) reported the use of nanoscale zerovalent iron (nZVI)

This book belongs to Central Library BADJI Mokhtar-ANNABA UNIVERSITY
Copyright Elsevier 2024

for the removal of hexavalent chromium Cr(VI) in a soil contaminated by tannery waste and by its reduction to less toxic Cr(III) trivalent form. They reported that nZVI increased Cr(VI) reduction efficiency from 14.51% to 86.83% in a time span of 120 min. Gil-Díaz et al. (2014) used column experiment to test leachability of nZVI-treated and nZVI-untreated soil for remediating lead (Pb) or zinc (Zn) in an acidic soil. They found that leachates from columns that contained soil treated with nZVI had significantly lower concentrations of Pb and Zn compared with untreated soil. Pb was found to be more effectively immobilized compared with Zn. They further performed toxicity tests on bacteria *Vibrio fischeri*, on larvae of *Artemia franciscana*, and on nematode *Caenorhabditis elegans* for the evaluation of ecotoxicological effects on soil organism after nZVI treatment. Toxicity end points that included decreasing bioluminescence, reproduction, and lethality were found to be lower for nZVI-treated soils (Table 1).

In another study the authors reported that the application of nZVI was successful in reducing metal availability of arsenic (As), chromium (Cr), lead (Pb), cadmium (Cd), and zinc (Zn) in a multimetal-contaminated acidic and calcareous soil. The availability of heavy metals As, Pb, and Cr was reduced by >82%, while for Zn the reduction ranged between 31% and 75%. The lowest reduction was found for Cd, which ranged between 13% and 42% (Gil-Díaz et al., 2016).

They also reported that 10% of nanoscale zerovalent iron (nZVI) significantly reduced the uptake of arsenic (As) in a highly polluted brownfield soil by reducing the content of As in available fractions while increasing its amount in the residual fraction. The mechanism for As immobilization was attributed to the formation of adsorption complexes in the form of ferric arsenates between Fe^0 corrosion products from the nZVI's shell. Barley plants cultivated on these As-polluted soils treated with nZVI showed better development and no negative effects with respect to nutrient content and exhibited lower As uptake. Further, no adverse impacts were observed on the soil physicochemical and biological properties (Gil-Díaz, Alonso, Rodríguez-Valdés, Gallego, & Lobo, 2017).

The use of bimetallic nanoparticles and stabilizers such as starch or carboxymethyl cellulose (CMC) in the synthesis of nanomaterials has also been investigated since these have been found to increase the mobility and reactivity of NPs in soil. Virkutyte, Al-Abed, Choi, and Bennett-Stamper (2014) reported that encapsulation of TiO_2 NPs with stabilizers such as carboxymethyl cellulose greatly affected their surface chemistry and mobility in a porous medium. Madhavi et al. (2014) stabilized zerovalent iron nanoparticles with carboxymethyl cellulose (CMC) for the reduction of Cr(VI). Addition of farm yard manure (FYM) to these nanoparticles facilitated the reduction further. At an increasing loading concentration of 0.1–0.3 mg/100 g for the NPs, an increase in Cr(VI) reduction rate from 60% to 80% was recorded. The NPs had similar effects on Cr reduction rate, both individually and when combined with FYM concentration of 50–100 mg/100 g soil. The authors identified the presence of functional groups like hydroquinones in the FYM as the reason behind the improved reduction potential. These functional groups acted as major source of electron donor for the reduction of Cr(VI) to Cr(III) in soil. An and Zhao (2012) prepared carboxymethyl cellulose (CMC)-stabilized Fe-Mn binary oxide nanoparticles for As treatment in a contaminated soil. These NPs reduced the water leachable arsenic by 91%–96%. The TCLP leachability of As (III)-laden soil was reduced by 94%–98%, while that of As (III) remaining in the soil bed was reduced by 78%. Su et al. (2016) synthesized biochar-supported zerovalent iron nanoparticles (nZVI@BC) that were able to completely convert exchangeable Cr to Fe-Mn oxides and organic matter in a Cr(VI)-contaminated soil. The immobilization efficiency of Cr(VI) and total Cr was 100% and 91.94%, respectively, for a 15-day remediation period. Moreover, this biochar NP-based remediation was found to effectively improve soil pH and soil

This book belongs to Central Library BADJI Mokhtar-ANNABA UNIVERSITY Copyright Elsevier 2024

Table 1 Removal of heavy metals by different types of nanomaterials

Nanomaterial used	Target pollutant	Remarks	Reference
nZVI	Cr(VI)	Reduction of chromium from Cr(VI) to Cr(III)	Singh et al. (2012)
nZVI	Pb, Zn	Effective immobilization and reduced concentrations in leachates	Gil-Díaz et al. (2014)
nZVI	As, Cr, Pb, Cd, Zn	Reduction in metal availability	Gil-Díaz, Pinilla, Alonso, and Lobo (2016)
CMC-nZVI	Cr(VI)	Reductive immobilization of Cr(VI)	Madhavi, Prasad, Reddy, Reddy, and Gajulapalle (2014)
CMC-stabilized nZVI	Cr(VI)	Reduced Cr(VI) to Cr(III) in both water and soil	Xu and Zhao (2007)
Biochar-supported nZVI	Cr(VI)	Effective immobilization of Cr, improvement in soil pH, fertility and organic matter content	Su et al. (2016)
Bimetallic nZVI/Cu	Cr(VI)	Increase in Cr(VI) removal rate with increasing temperature	Zhu, Li, Ma, and Shang (2016)
CMC-stabilized FeS NPs	Cr(VI)	Effective immobilization of Cr(VI) via adsorption, reduction, and coprecipitation	Wang et al. (2019)
Fe(II) phosphate NPs	Pb(II)	Reduction in leachability and bioaccessibility of soil-bound Pb(II) and Cu(II)	Liu and Zhao (2007)
Ca(II) phosphate NPs	Pb(II)	In situ immobilization of Pb(II) and possible remediation of other hazardous heavy metals like Cu, Cd, Zn, and U	Liu and Zhao (2013)
CMC-stabilized Fe-Mn binary oxide NPs	As (III)	In situ immobilization of arsenite	An and Zhao (2012)
Nano-Fe/Ca/CaO	As, Cd, Pb	Total immobilization of soil heavy metals As, Cd, and Pb	Mallampati, Mitoma, Okuda, Sakita, and Kakeda (2013)
Na-zeolitic nanotuff	Cd	Immobilization and increased Cd sorption	Ghrair, Ingwersen, and Streck (2010)
Water treatment residual NPs (nWTR)	Hg, Cr	Increased metal sorption for both Hg and Cr and significant decrease in their soil release	Moharem, Elkhatib, and Mesalem (2019)
Starch-stabilized nZVI, FeS, Fe_3O_4	As	Decreased As bioaccessibility and leachability with increasing Fe/As molar ratio	Zhang, Wang, Zhao, and Pan (2010)
Al_2O_3, SiO_2, TiO_2 NPs	Zn, Cd, Ni	Reduction in metal mobility	Peikam and Jalali (2018)

fertility by increasing organic matter content and was predicted to enhance plant growth and prevent excessive Fe iron release. Zhu et al. (2016) reported that soil pH and temperature were main factors greatly influencing remediation of Cr(VI) by iron-copper bimetallic nanoparticle (nZVI/Cu). nZVI/Cu displayed high efficiency in Cr(VI) reduction at higher doses. Cr(VI) removal rate increased with increasing temperature with soil concentration of Cr(VI) dropping $<2\,mg\,L^{-1}$ in a time span of 30 min as the temperature reached 298 K and further more at 303 K.

This book belongs to Central Library BADJI Mokhtar-ANNABA UNIVERSITY
Copyright Elsevier 2024

Wang et al. (2019) applied iron sulfide nanoparticles (FeS NPs) stabilized with carboxymethyl cellulose (CMC) to remediate groundwater and soil contaminated with Cr(VI) and reported that FeS NPs immobilized Cr(VI) effectively via adsorption, reduction, and coprecipitation. Moharem et al. (2019) used water treatment residual nanoparticles (nWTR) produced during water purification process as waste in a water industry for reducing mercury (Hg) and chromium (Cr) mobility in a contaminated calcareous soil. Application of these nWTR to the contaminated soil greatly increased the metal sorption process for both Hg and Cr while significantly decreasing Hg and Cr release from the soil. An increased transformation of Hg and Cr ions occurred in the contaminated soil at the nWTR application rate of 0.3%. Both Hg and Cr formed stable complexes of $Hg(OH)_2$ and $Cr(OH)_2$, respectively. Zhang et al. (2010) prepared starch-stabilized iron-based nanoparticles that included zerovalent iron (ZVI), magnetite (Fe_3O_4), and iron sulfide (FeS). They used it for immobilization of arsenic (As) and found that an increasing Fe/As molar ratio decreased As bioaccessibility and leachability in soil. The use of these NPs for in situ arsenic immobilization was recommended in soils having a higher As and lower Fe concentration. Leachability and bioaccessibility of soil-bound Cu(II) and Pb(II) were reduced with Fe (II) phosphate nanoparticles synthesized by Liu and Zhao (2007). The same authors synthesized a new class of calcium phosphate nanoparticles that were found effective in decreasing the TCLP-leachable fraction of Pb in soil from 66% to 10% (Liu & Zhao, 2013). In both the studies the authors remarked that the NPs possessed greater mobility and greater reactivity in soils because of their small particle size and showed promising results for in situ soil remediation. These NPs were also projected to have potential for remediation of other hazardous heavy metals and radioactive nuclides such as Cu, Cd, Zn, and U. Moreover, these recommended the applications of these NPs as nanofertilizer for fulfilling the P requirements of crops while overcoming the problem of eutrophication that is often associated with the use of conventional fertilizers containing phosphate (Liu & Zhao, 2013).

Ghrair et al. (2010) synthesized Na-zeolitic nanotuff and investigated its effect on sorption of Cd. They found pH to be a strong influence on the sorption of Cd and suggested that pH and texture might influence the metal-immobilizing effect of these zeolitic nanotuff in soils. Mallampati et al. (2013) reported that treatment with nano-Fe/Ca/CaO reduced the leachate concentration lower than the standard regulatory threshold values for soil elution for heavy metals, which were $0.01\,mg\,L^{-1}$ for As, Cd, and Pb and $0.05\,mg\,L^{-1}$ for Cr. Peikam and Jalali (2018) investigated immobilization potential of Al_2O_3, SiO_2, and TiO_2 NPs in multimetal-contaminated (Zn, Cd, and Ni) calcareous and noncalcareous soils. While SiO_2 NPs were found to be most effective for immobilizing the three metals in calcareous soils, Al_2O_3 NPs showed maximum mobility reduction for Cd and Zn in the noncalcareous soils. This was attributed mainly to the high surface area of SiO_2 and high site density of Al_2O_3. Moreover, soil with high carbonate calcium content has been found to have high metal immobilization capacity as liming of soil increases its adsorption potential, thereby reducing metal bioavailability (Bradl, 2005).

3 Nanotechnology for pesticides and persistent organic pollutant (POP) remediation

3.1 Nanoremediation of pesticides and persistent organic pollutants (POPs)

The contamination of soil with pesticides and persistent organic pollutants (POPs) from anthropogenic sources leads to a complete ban of these chemical pollutants following the Stockholm Convention on Persistent Organic Pollutants (POPs) in 2004. Since then, there has been a global priority to eliminate

This book belongs to Central Library BADJI Mokhtar-ANNABA UNIVERSITY
Copyright Elsevier 2024

these pollutants from the soil through their remediation and through proper management of soil sites contaminated with these toxic chemical pollutants. Out of the 12 banned POP chemicals, which are referred to as the dirty dozen, 8 are pesticides. The other POPs include industrial solvents or chemicals and pharmaceutical (Abhilash et al., 2013; Allinson et al., 2016; Loos et al., 2009; Yang et al., 2008). POPs and many pesticides exhibit the properties of bioaccumulation and biomagnification, thereby posing great risks of food chain contamination, especially to those at the top of the food chain. Apart from this, POPs are lipophilic and can accumulate in the fatty tissue of living animals and human beings, thereby adversely affecting them with both chronic and acute effects.

Although many pesticides have been banned worldwide recently and many have been banned for decades, the threats posed by them tend to remain even after years of abandoning their usage. It is because the soil, on which they were once used directly or indirectly, continues to be contaminated by their residues as they take several years to degrade due to their persistent nature. Also, POPs can circulate globally by means of evaporation and deposition and get deposited at sites far from their original source and contaminate it. Therefore remediation of these pollutants becomes essential if one needs to revitalize the land for agricultural purpose and bioenergy production. Nanoparticles are also being widely investigated for their possible role in degradation of pesticides and POPs. The process associated with the degradation of pesticide pollutant is photocatalysis (Fig. 2). In the process, nanoparticles act as catalyst in the presence of light and undergo reaction with chemical pollutants, i.e., pesticides and POPs. These nanophotocatalysts convert the harmful chemicals present in these pollutants into simpler and harmless molecules such as CO_2, N_2, and H_2O. So far nanoscale titanium dioxide (TiO_2) and zinc oxide (ZnO) are considered as good photocatalysts (Fujishima et al., 2008).

Yu et al. (2007) studied the degradation of three organochlorine pesticides α-, β-, γ-, and δ-hexachlorobenzene; dicofol; and cypermethrin through photocatalysis by nano-TiO_2. TiO_2 enabled photolytic degradation of these pesticides on its surface by attracting peroxide or hydroxyl radicle and electron transfer. Rui, Jingguo, Jianyu, Lin, and Kangguo (2010) reported photocatalytic degradation of organophosphorus and carbamate pesticides found in the leaves of tomato plants along with soil at a rate of 15%–30% using nano-TiO_2 doped with rhenium (Re^{+3}). Same nanomaterial was capable of degrading carbofuran at a rate of 55%, a rate 30% higher than natural degradation. In addition, the

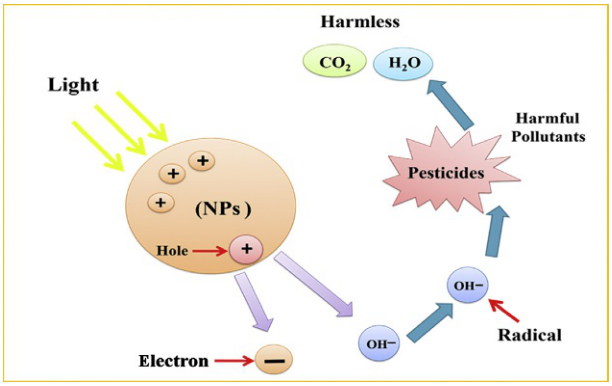

FIG. 2

The process of photocatalytic degradation with the use of nanoparticles.

This book belongs to Central Library BADJI Mokhtar-ANNABA UNIVERSITY
Copyright Elsevier 2024

photocatalytic activity of (modified) TiO_2 nanomaterial was found to reduce half-lives of pesticides, without losing its effectiveness (Gogos et al., 2012). Restivo, Órfão, Armenise, Garcia-Bordejé, and Pereira (2012) used multiwalled carbon nanotubes (MWCNTs) as catalysts for the catalytic ozonation of metolachlor (MTLC), a widely used herbicide. The use of a carbon catalyst, greatly increased MTLC mineralization along with decreasing its toxicity. Further, application of carbon nanofibers grown on a structured support was regarded as a potential solution for the complete mineralization of metolachlor, which otherwise was capable of producing several harmful by-products such as organic acids and aromatic compounds.

El-Temsah, Sevcu, Bobcikova, Cernik, and Joner (2016) investigated the degradation effect of nanoscale zerovalent iron (nZVI) on DDT in a soil spiked with it and on a historically contaminated soil and aged contaminated soil. They found the degradation rate to be 50% in spiked soil and 24% in aged contaminated soil. In another study, they examined the ecotoxicological effects of nZVI on soil organisms like collembolan (*Folsomia candida*) and ostracods (*Heterocypris incongruens*) with conclusion that while considering nZVI for remediation the risks posed by it on soil biota should be taken into consideration (El-Temsah & Joner, 2013). Tilston, Collins, Mitchell, Princivalle, and Shaw (2013) investigated the use of nanoscale zerovalent iron (nZVI) for the remediation of organochlorine contaminated environment. They reported reduction in the activity of chloroaromatic mineralizing microorganisms and perturbation to soil bacterial community composition after nZVI addition. Fouad and Mohamed (2011) synthesized semiconductor nanoparticles with different metal core-shell nanocomposites such as TiO_2, Au/TiO_2, ZnO, and Au/ZnO to be used as catalysts for the photodegradation of malathion. The use of nanocomposite with a metal core and semiconductor combination enhanced the photocatalytic activity that accelerated the degradation of malathion in a time-dependent order. A study by Gu, Dong, Kong, Zheng, and Li (2012) investigated the effect of nano-TiO_2 (anatase) on the photocatalytic degradation of phenanthrene, a polycyclic aromatic hydrocarbon (PAH). The half-life of phenanthrene was reduced from 46 to 31 h when the TiO_2 loading was 0 and 4 wt%. The authors reported that, while TiO_2 significantly accelerated the degradation process on the soil surfaces, factors such as H_2O_2 concentration, light intensity, and humic acid further enhanced the process of degradation (Table 2).

Chen et al. (2014) comparatively studied the use of nZVI and Pd/Fe bimetallic nanoparticles for in situ remediation of soils contaminated with PCBs. They reported that, compared with nZVI, Pd/Fe bimetallic nanoparticles gave more rapid and complete hydrodechlorination of 2,2,4,4,5, 5-hexachlorobiphenyl, probably achieved by Pd loading. They also inferred that soil properties like clay and sand content promoted the catalytic activity of Pd thereby improving PCBs degradation rate. A lower clay content and a higher sand content stimulated greater removal efficiency of PCBs while soil organic matter retarded the process of hydrodechlorination. Yuan et al. (2012) investigated the remediation of a clayed soil contaminated by pentachlorophenol (PCP) using CMC-stabilized nano-Pd/Fe. PCP in soil was dechlorinated to phenol by the electrokinetic transport mechanism exhibited by nano-Pd/Fe. Similarly, Fan et al. (2013) synthesized xanthan gum–stabilized nano-Pd/Fe and investigated their electrokinetic transport kinetics for the remediation of soil contaminated with PCBs. The surfactants increased the solubility and enhanced the degradation rate of PCBs in the soil. Paknikar et al. (2005) investigated the catalytic dechlorination of lindane, an organochlorine pesticide using an integrated nanobiotechnological approach that comprised the use of FeS nanoparticles followed by microbial degradation. The stabilized nanoparticles were found to degrade 5 mg L^{-1} of lindane with 94% efficiency in a time span of 8 h. The remaining residual lindane and its partially degraded

This book belongs to Central Library BADJI Mokhtar-ANNABA UNIVERSITY
Copyright Elsevier 2024

Table 2 Nanomaterials used for pesticides and persistent organic pollutant (POP) degradation

Nanomaterial	Target pesticide	Remarks	Reference
MWCNTs	Metolachlor	Catalytic ozonation leading to pesticide mineralization	Restivo et al. (2012)
Nanoscale zerovalent iron (nZVI)	DDT	Complete oxidation and enhanced electron release leading to reduction of pesticide	El-Temsah et al. (2016)
	Aroclor 1242, PCB	Reduction in the activity of chloroaromatic mineralizing microorganisms	Tilston et al. (2013)
	Organochlorine pesticides and PCBs	Transformation and detoxification of chlorinated organic solvents	Pan and Xing (2012)
TiO_2, Au/TiO_2, ZnO, and Au/ZnO	Malathion	Catalytic photodegradation	Fouad and Mohamed (2011)
Nano-TiO_2-coated film	Organochlorine pesticides—α-, β-, γ-, and δ-hexachlorobenzene; dicofol; and cypermethrin	Hydroxyl radical and electron transfer enabled photolytic degradation of pesticides on TiO_2 surface	Yu et al. (2007)
Anatase TiO_2	Phenanthrene (PAHs)	Degradation by TiO_2 along with H_2O_2, light intensity, and humic acid	Gu et al. (2012)
Rhenium (Re^{+3})-doped nano-TiO_2	Carbofuran	Photocatalytic degradation of the pesticide	Rui et al. (2010)
CMC-stabilized nano-Pd/Fe	Pentachlorophenol (PCP)	Dechlorination to phenol	Yuan, Long, Xie, Liao, and Tong (2012)
nZVI and Pd/Fe bimetallic NPs	Polychlorinated biphenyls (PCBs)	Hydrodechlorination of the pesticide	Chen et al. (2014)
Xanthan gum–stabilized nano-Pd/Fe	Polychlorinated biphenyls (PCBs)	Solubilization of pesticide	Fan et al. (2013)
Bimetallic iron (BioCAT slurry)	Pentachlorophenol	90% Degradation of pesticide	Dien, De Windt, Buekens, and Chang (2013)
FeS NPs	Lindane	Degradation of pesticide and its metabolites with 94% efficiency	Paknikar, Nagpal, Pethkar, and Rajwade (2005)

intermediates alongside the stabilizing polymer were further completely degraded after a subsequent microbiological treatment in 1 h. Thus the authors were completely able to remove 5 mg L^{-1} of lindane in a time span of 9 h. Dien et al. (2013) synthesized bimetallic iron (BioCAT slurry) biocomposite by coating biologically encapsulated nanoparticle agents onto the particle surface of ZVI containing palladium nanoparticles for degradation of pentachlorophenol, a widely used organochlorine pesticide.

This book belongs to Central Library BADJI Mokhtar-ANNABA UNIVERSITY
Copyright Elsevier 2024

After 21 days of treatment, this bimetallic iron was found to degrade 90% of pentachlorophenol in a sandy soil at a dose of 600-mg BioCAT slurry/kg soil.

3.2 Nanotechnology-based biosensing systems for pesticide residue detection

Although at present nanoparticles and nanomaterial-based sensors or nanosensor systems are at their beginning stage of research, they have been anticipated to hold great promises in the field of environmental remediation and agriculture. Biosensors, incorporated with nanomaterials, have diverse applications in monitoring and detection of pesticides; toxic chemicals; contaminants in the form of pathogens, odor-creating bacteria, and other microbes; and other toxic materials, both in field and in production units (Baruah & Dutta, 2009). Nanosensors can thus significantly contribute toward an overall increased soil health and productivity by offering wide range of services, one of which is pesticide residue detection. Apart from this, nanosensors are currently being used in the food manufacturing industries for pathogen detection, toxins and chemicals in food, thus helping in the prevention of foodborne illness.

The widespread use of persistent pesticides for the elimination of pests and improvement of agricultural productivity globally has severely contaminated groundwater and soil at various places, resulting in various health hazards to nontarget species like humans and animals. Use of pesticides has also led to the development of resistance by pest for these chemicals while also resulted in killing of their natural enemies, further making their control extremely difficult. There are about 1045 chemicals reported by the Food and Drug Administration (FDA) as pesticide residues (FDA, 2005). Nanosensors offer sensitive and on-site detection of pesticide residues in soil, water, and agriculture products. Hence they have attracted considerable attention as a rapid and effective field monitoring tool compared with the conventional methods of pesticide residue detection such as liquid chromatography, gas chromatography (GC), high-performance liquid chromatography (HPLC), and mass spectroscopy, which albeit have a great efficiency and exhibit great discriminability for pesticides but are time consuming, expensive, sophisticated, and unsuited for field analysis of multiple samples, while nanosensors offer higher sensitivity, great selectivity, quick responses, lower detection limits, and small sizes (Liu, Yuan, Yue, Zheng, & Tang, 2008).

Based on their sensing mechanism, nanosensing techniques can be divided into three main types. These are (a) the inhibition of cholinesterases, (b) immunoassays, and (c) organophosphorus hydrolase (OPH) (Liu et al., 2008). Most of the sensors being developed for the detection of pesticide residues, especially for pesticides like organophosphate and carbamate, are acetylcholinesterase (AChE)-based electrochemical sensors. Both these pesticides are widely used in many countries and are extremely toxic to acetylcholinesterase (AChE), a primary enzyme responsible for the functioning of the central nervous system in humans. Being a specific molecular target of organophosphate and carbamate pesticides, the inhibition of acetylcholinesterase activity has been increasingly used to develop human biological marker for the early detection of poisoning resulting from exposure to these pesticides (Kumar, Kim, & Deep, 2015; Liu et al., 2008). In a before and after incubation process, pesticides being inhibitors of these enzymes, can be determined by measuring the kinetic performance of the initial velocity of the reaction that is catalyzed by AChE. The reaction follows the equation given in the succeeding text:

$$\text{Acetylcholine} + H_2O \xrightarrow{\text{AChE}} \text{acetic acid} + \text{choline} \tag{1}$$

This book belongs to Central Library BADJI Mokhtar-ANNABA UNIVERSITY
Copyright Elsevier 2024

The response in these devices is sensitive and easy to measure while showing a dose-dependent behavior to pollutant exposure. However, the instability of the enzymes is a primary limitation of developing sensitive and stable AChE and OPH-based biosensors (Songa & Okonkwo, 2016). However, nanoparticles owing to their unique properties have been shown to act as substrates for enzyme immobilization, thus making them stable and not losing their activity. Many ongoing researches are aimed at successfully exploiting the property of acetylcholinesterase by immobilizing and stabilizing it with various nanoparticles to ensure high enzymatic activity, stability, and sensitivity of the biosensor systems based on them for the detection of organophosphates.

Su et al. (2008) reported the use of a silicon-based nanocomplex, that is, gold nanoparticle–coated silicon nanowires. The high electrical conductivity of this nanocomplex, that is, AuNPs/SiNWs alongside its high compatibility with the enzyme, led to a significantly enhanced performance of the sensor that detected dichlorvos, an organophosphate pesticide even at the lowest concentration of 8 ng/L. Similarly, Wang, Shi, She, Mu, and Lee (2010) developed a surface-enhanced Raman scattering sensor made of Ag nanoparticle–coated silicon nanowire arrays for the detection of insecticide carbaryl. They found significantly high sensitivity of the current substrate for the detection of carbaryl even at the lowest concentrations like 10^{-7} mol/L (0.02 ppm). The sensor was highly sensitive and stable toward the detection of carbaryl and also offered great reproducibility. Liu et al. (2011) developed a biosensor based on immobilizing acetylcholinesterase on 3-carboxyphenylboronic/reduced graphene oxide–gold nanocomposite modified electrode for the detection of pesticides organophosphorus and carbamate. The successful immobilization was possible owing to high activity by the specific binding between the boronic acid group of 3-carboxyphenylboronic and the glycosyl of acetylcholinesterase. The biosensor exhibited good sensitivity owing to excellent electron transfer properties of gold NPs. Further a reduced graphene oxide enhanced the electrochemical response by promoting electron transfer reaction.

Cesarino, Moraes, Lanza, and Machado (2012) developed a sensor based on immobilization of cholinesterase in a core-shell modified glassy electrode of multiwalled carbon nanotubes (MWCNTs) and polyaniline for the quantification of carbamate pesticides in apples, cabbage, and broccoli. This MWCNT/PANI/AChE-based biosensor exhibited detection limits of 1.4 mol/L for carbaryl and 0.95 mol/L for methomyl. Wu et al. (2013) developed a sensor consisting of a reduced graphene oxide and nafion nanocomposite for AchE immobilization for monitoring dichlorovos, a toxic organophosphate. The sensor displayed high sensitivity, good selectivity, wide linear range between 5.0 and 100 ng/mL and 1.0–20 μg/mL, low detection limit of 2.0 ng/mL, good stability, and reproducibility. Dong, Fan, Qiao, Ai, and Xin (2013) fabricated a biosensor by immobilizing AChE on multiwalled carbon nanotube/chitosan nanocomposites modified glassy carbon electrode for the detection of methyl parathion. This method combined electrochemical reduction of Ellman's reagent DTNB with AChE inhibition. An inhibition effect in the activity of AChE, followed by a change in electrochemical reduction response of DTNB, was the detection point for methyl parathion. Simonian, Good, Wang, and Wild (2005) used a conjugation of organophosphate hydrolase (OPH) with gold nanoparticles incubated with a fluorescent enzyme inhibitor or decoy, for the detection of organophosphate paraoxon. After introducing different paraoxon concentrations to the OPH-nanoparticle-conjugate-decoy mixtures, normalized ratio of fluorescence intensities was measured. The highest sensitivity of paraoxon was obtained at near equimolar levels of decoys and OPH-gold NP conjugates (Table 3).

While the application domain of nanomaterial-based sensing for pesticide residue detection is vast, there are few issues that need to be addressed for their successful applications. These include (i) the

This book belongs to Central Library BADJI Mokhtar-ANNABA UNIVERSITY
Copyright Elsevier 2024

Table 3 Nanoenabled sensors used for pesticide residue detection

Nanomaterial used	Target analyte	Remarks	Reference
Au NP-coated Si nanowires	Dichlorvos	Enhanced enzymatic activity and increased electron communication	Su et al. (2008)
Ag NP-coated Si nanowires	Carbaryl	Surface-enhanced Raman scattering sensor	Wang et al. (2010)
AChE/RGO-Au nanocomposite	Organophosphate and carbamate	Enhanced electrochemical response due to electron transfer reaction	Liu et al. (2011)
MWCNT/PANI/AChE	Carbaryl and methomyl (carbamate)	Modified with polyaniline in a core-shell structure	Cesarino et al. (2012)
Er-GRO-nafion nanocomposite	Dichlorovos (organophosphate)	High sensitivity, good selectivity, low detection range	Wu et al. (2013)
MWCNT-chitosan nanocomposites	Methyl parathion	Combined electrochemical reduction of Ellman's reagent (DTNB) with AChE inhibition	Dong et al. (2013)
Organophosphate hydrolase (OPH)-conjugated Au NPs	Paraoxon	Greatest sensitivity at equimolar levels OPH-gold nanoparticle and decoys	Simonian et al. (2005)

availability of the nanomaterials that are sensitive to residues of the most commonly used pesticides, (ii) ease of nanosensor fabrication techniques and instrumentation, (iii) detection at trace level with the desired reliability and repeatability, (iv) manufacturing cost, and (v) environmental risks associated with nanomaterial exposure to the soil surroundings (Khot, Sankaran, Maja, Ehsani, & Schuster, 2012). Another evolving trend is the manufacture of smart nanomaterials and nanopesticides that would act both as source of pesticide and analytical sensor for detection. This could entirely eliminate the need of biosensors for pesticide residue detection in soil. Also a nanomaterial that could both work as an efficient release system for the delivery of materials like pesticide and fertilizers and also indicate deficiency of the nutrients in soil by indicator mechanism like change in color is also highly desirable. It could work as an advanced alert system for farmers to decide upon the dosage, rate, and frequency of pesticide being used (Khot et al., 2012).

4 Role of nanotechnology for enhancing phytoremediation and bioremediation

Phytoremediation involves the use of plants to remove, degrade, or clean environmental compartments such as soil, sediment, and water. Along with plants, rhizospheric microbial fauna associated with them are also used for cleaning these polluted resources (Cunningham, Berti, & Huang, 1995; Cunningham, Shann, Crowley, & Anderson, 1997; Pilon-Smits, 2005; Raskin, Smith, & Salt, 1997). The potential of many plant species such as tomato, sunflower, willow, poplar tree, Chinese cabbage, sunbeam, and alfalfa has been explored for phytoremediation of soils contaminated with pollutant, and many of these

This book belongs to Central Library BADJI Mokhtar-ANNABA UNIVERSITY Copyright Elsevier 2024

plants have been found to be good phytoremediators (Mitton, Miglioranza, Gonzalez, Shimabukuro, & Monserrat, 2014). Phytoremediation employs the same principles that are used by plants and microbes in nature for degradation and sequestration of organic and inorganic pollutants (Negri & Hinchman, 2000). Various phytoremediation techniques used for soil pollution include phytovolatilization, phytoextraction, phytodegradation, phytostabilization, and rhizodegradation (Song et al., 2019). Phytovolatilization involves absorption and transformation of pollutants into volatile forms by plants and their transportation to leaves and further transpiration by them. It may also involve degradation of pollutants into volatile products (Sakakibara, Watanabe, Inoue, Sano, & Kaise, 2010). Phytoextraction includes the use of plants for extracting and accumulating pollutants in their tissues (Bhargava, Carmona, Bhargava, & Srivastava, 2012; Raskin & Ensley, 2000). The process of phytodegradation involves direct degradation of organic pollutants by plants through their enzymatic activities (McCutcheon & Schnoor, 2003). Phytostabilization is the in situ immobilization of pollutants by plant roots and occurs in the rhizosphere rather than the plant. Phytostabilization aims at reducing pollutant mobility through root adsorption and complex formation or precipitation within the rhizosphere, so that the possibility of pollutant entering groundwater or food chain is reduced (Jadia & Fulekar, 2009). Biodegradation of organic pollutants by microbes in their rhizosphere upon facilitation by plants is known as phytostimulation or rhizodegradation (McCutcheon & Schnoor, 2003).

For a long time the use of phytoremediation techniques for environmental cleanup has received widespread attention. Phytoremediation technology has been anticipated to yield benefits like increasing soil organic carbon through carbon sequestration, stimulation of microbial activity, soil stabilization, and biofuel or fiber production (Abhilash, Jamil, & Singh, 2009; Vamerali, Bandiera, & Mosca, 2010; Ali et al., 2013). However, phytoremediation techniques usually need long time, often several years, to provide positive outcomes. Moreover, its applications are limited by weather conditions, quality of soil, and phytotoxicity of pollutant (Song et al., 2019). In recent years, use of phytoremediation in combination with different technologies like microbial bioremediation and nanotechnology has gained momentum due to increased efficiency and cost-effectiveness (Gerhardt, Gerwing, & Greenberg, 2017). Nanotechnology is being increasingly considered a reasonable and effective method for removing environmental contaminants, due to their quick mode of action and on-site remediation (Gong et al., 2018; Wang et al., 2016). Nanoparticles have been shown to potentially influence the fate, behavior, and uptake of pollutants in phytoremediation systems (Abhilash et al., 2012). Moreover, the combined use of nanoparticles along with soil microbes and plants is being extensively investigated due to their anticipated higher degradation potential as compared with the removal of pollutant with an individual technology.

Nanophytoremediation involves the use of both nanotechnology and phytotechnology for cleaning soil contaminated with pollutants (Fig. 3). The most widely studied nanomaterials are carbon-based nanomaterials, closely followed by metal and metal oxide nanomaterials (Chen et al., 2017; Gong et al., 2009). Carbon nanotubes, owing to their large specific surface area, have demonstrated excellent adsorption capacity for various pollutants, particularly toward hydrophobic organic pollutants (Pan & Xing, 2008; Song et al., 2017). These organic compounds laden with carbon nanoparticles could act as excellent carriers of contaminant, especially organic pollutants, and dramatically change their fate and transport in the environment (Hofmann & Von der Kammer, 2009). Fullerenes were found to enhance trichloroethylene uptake in cottonwood (*Populus deltoides*). In related experiments conducted with a bush plant, Redosier dogwood, similar results were observed owing to similar xylem structures of the two plant species (Ma & Wang, 2010). C_{60} fullerene reportedly altered the accumulation and potential

This book belongs to Central Library BADJI Mokhtar-ANNABA UNIVERSITY
Copyright Elsevier 2024

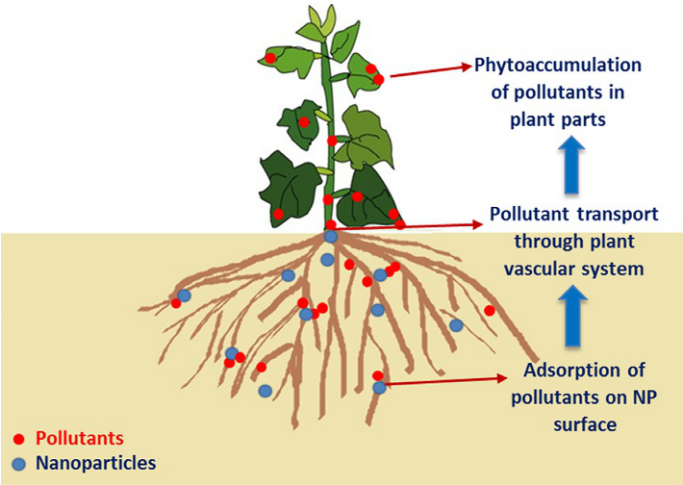

FIG. 3

The use of nanotechnology for enhancing the phytoremediation of pollutants in soil.

toxicity of dichlorodiphenyldichloroethylene (p,p′-DDE), a DDT metabolite by three plants *Cucurbita pepo* (zucchini), *Glycine max* (soybean), and *Solanum lycopersicum* (tomato).

Upon fullerene exposure the root and total plant DDE concentration for all the plant species increased significantly with the uptake ranging between 30% and 65% (De La Torre-Roche et al., 2012). This study pointed out that nanomaterials may have varied impacts on different plant species and their phytoremediation potential of contaminated soil. Such points were further investigated by another study in which four plants, namely, *Zea mays* (corn), *S. lycopersicum* (tomato), *C. pepo* (zucchini), and *G. max* (soybean), were used to remediate chlordane along with DDT and its metabolites (DDx) by the application of multiwalled carbon nanotubes (MWCNTs) and C_{60}. The authors reported that pesticide uptake and accumulation varied between 21% and 80% depending on species used and nanomaterial concentration. While C_{60} treatment completely suppressed DDx uptake in corn and tomato plants, it increased chlordane accumulation in tomato and soybean to 34.9% (De La Torre-Roche et al., 2013). The impacts of nonfunctionalized and amino-functionalized MWCNT were investigated on coexistent of chlordanes and DDE accumulation in lettuce (*Lactuca sativa* L.) by Hamdi, De La Torre-Roche, Hawthorne, and White (2015). Pesticide availability was significantly influenced by the presence of different types of CNT. While nonfunctionalized CNT decreased the pesticide content in root and shoot by 88% and 78%, respectively, the decrease by amino-functionalized CNT effects was only 57% and 23% in the roots and shoots, respectively. The coexposure of CNT resulted in significant decreases in bioavailability of pesticide residues, thereby efficiently minimizing the contamination of edible lettuce tissues.

An increase in root and shoot length was observed in edible plants of wheat, soybean, corn, and alfalfa after treatment with CeO_2 and ZnO NPs, anticipating the role of nanotechnology in significantly enhancing phytoremediation efficiency (López-Moreno, de la Rosa, Hernández-Viezcas, Peralta-Videa, & Gardea-Torresdey, 2010). Jiamjitrpanich, Parkpian, Polprasert, and Kosanlavit (2013) conducted a nanophytoremediation study for evaluating the effectiveness of nZVI in influencing the

This book belongs to Central Library BADJI Mokhtar-ANNABA UNIVERSITY Copyright Elsevier 2024

uptake of trinitrotoluene (TNT) and its metabolites by plant *Panicum maximum* from a TNT-contaminated soil. The study supported the fact that the combination of nanotechnology with phytotechnology resulted in higher accumulation of TNT in plant roots. The uptake of TNT from the soil was more effective in the presence of nZVI than that without nZVI, particularly, at concentration of 500 mg/kg. Ni/Fe bimetallic nanoparticles were found to decrease the translocation of polybrominated diphenyl ethers (PBDEs) and its phytotoxicity to Chinese cabbage in a contaminated soil after 3 days of soil culture experiments (Wu, Xie, Fang, Cheng, & Tsang, 2016).

The possible role of iron oxide nanoparticles (Fe NPs) on wheat plants grown in a soil contaminated by heavy metal cadmium (Cd) was studied by Hussain et al. (2019). The application of 20 ppm of Fe NPs mitigated the adverse impacts of Cd by increasing plant growth rate, photosynthetic activity, antioxidant enzymes, and Fe uptake reducing the Cd concentration in plants. Wheat plant morphological parameters such as photosynthetic pigments and dry biomass of shoots, roots, spike husks, and grains were enhanced by exogenous application of Fe NPs (Table 4).

Wang et al. (2014) studied remediation of Cr(VI)-contaminated soil by nanoscale zerovalent iron stabilized with sodium carboxymethyl cellulose (CMC-stabilized nZVI) and reported that they

Table 4 Use of nanotechnology along with plant species and microbes for pollutant removal

Nanomaterial used	Target pollutant	Species	Remarks	Reference
Fe NPs	Cd	Wheat	Reduction in Cd concentration and adverse effects, increase in plant growth, photosynthesis, antioxidant enzymes	Hussain et al. (2019)
CMC-stabilized nZVI	Cr(VI)	Rape, Chinese cabbage	Reduction in Cr leachability and bioaccessibility by 82% and 58%	Wang, Fang, Kang, and Tsang (2014)
Citrate-coated magnetite NPs	Cr(VI)	Wheat, oat, sorghum	Metal toxicity mitigation	López-Luna et al. (2016)
TiO_2 NPs	Pb	Rice	Reduction in Pb bioaccumulation in rice tissues but accumulation of NPs in rice roots	Cai et al. (2017)
Fullerene	Trichloroethylene	Cottonwood	Elevated TCE concentration in plant tissues	Ma and Wang (2010)
C_{60} fullerene	p,p′-DDE	Zucchini, soybean, tomato	30%–65% Increase in pollutant uptake by the three species	De La Torre-Roche et al. (2012)
MWCNT	Chlordane, DDT	Zucchini, soybean, tomato, corn	Pesticide uptake and accumulation varied by plants species between 21% and 80%	De La Torre-Roche et al. (2013)

This book belongs to Central Library BADJI Mokhtar-ANNABA UNIVERSITY
Copyright Elsevier 2024

Table 4 Use of nanotechnology along with plant species and microbes for pollutant removal—cont'd

Nanomaterial used	Target pollutant	Species	Remarks	Reference
MWCNT	Chlordanes and DDE	Lettuce	The presence of CNT significantly influenced pesticide availability, Decreased the root and shoot pesticide content by 88% and 78%, respectively	Hamdi et al. (2015)
nZVI	Trinitrotoluene (TNT)	*Panicum maximum*	Higher uptake and accumulation of TNT in plant roots in the presence of nZVI	Jiamjitrpanich et al. (2013)
Fe_3O_4 NPs	2,4-Dichlorophenoxyacetic acid (2,4-D)	Soil indigenous microbes	Higher degradation efficiency of herbicide with combined treatment compared with individual treatments	Fang, Si, Tian, Zhang, and Zhou (2012)
CMC-Pd/nFe^0	γ-HCH	*Sphingomonas sp.* NM05	Synergistic effect on γ-HCH degradation	Singh, Manickam, Mudiam, Murthy, and Misra (2013)
Ni/Fe bimetallic nanoparticles	Polybrominated diphenyl ethers	Chinese cabbage	Decrease in translocation of PBDEs	Wu et al. (2016)

significantly enhance Cr immobilization by reducing Cr leachability and bioaccessibility by 82% and 58%, respectively. However, the remediation exerted inhibitory effects on plants rape (*Brassica campestris* L.) and Chinese cabbage (*B. pekinensis*) grown on the soil. The negative impacts on plants like lowered germination rate, germination retardation, and decreased root biomass were attributed to the physicochemical properties of nZVI. However, after 1 month, the phytotoxicity test was repeated on the plants, and an improvement in the cultivation was observed for both plants. This indicated that such remediation using nZVI could gradually restore the soil quality, thereby permitting its reuse in planting. Meanwhile, López-Luna et al. (2016) investigated toxicity mitigation of Cd(II) and Cr(VI) by wheat seedlings in the presence of citrate-coated magnetite NPs. They observed that the mitigation of heavy metal toxicity by these NPs favored wheat seedling growth. However, when magnetite was added, the predicted toxicity was higher than the observed value, showing an interactive infraadditive or antagonistic effect. The individual and mixed toxicity of Cd and Cr were significantly alleviated due to the phytoavailability attenuation with magnetite NPs. Cai et al. (2017) investigated the effect of four types of TiO_2 NPs of varied anatase and rutile form on lead (Pb) bioaccumulation by rice seedlings. They found that, while TiO_2 NPs were able to effectively reduce the bioaccumulation of Pb in tissues of rice, the particles themselves accumulated in roots of rice with a concentration of >80%, thereby posing potential risk to food safety.

This book belongs to Central Library BADJI Mokhtar-ANNABA UNIVERSITY Copyright Elsevier 2024

As far as bioremediation is concerned, few studies have reported the role of nanoparticles alongside microorganisms in promoting remediation of contaminated land. Fang et al. (2012) reported that the degradation of 2,4-dichlorophenoxyacetic acid (2,4-D), a herbicide in soils by Fe_3O_4 NPs combined with soil indigenous microbes, displayed a higher and more efficient degradation potential. This combination was more effective that the treatment that employed individual technology with NPs or microbes alone. A similar integrated nanobiotechnique was used by Singh et al. (2013) for the degradation of γ-HCH in soil. They stabilized Pd/Fe^0 bimetallic nanoparticles ($CMC\text{-}Pd/nFe^0$) along with a microbial strain of *Sphingomonas sp*. NM05 for pesticide degradation. The authors reported that the integration of microbial cells and nanoparticles had a synergistic effect on γ-HCH degradation. Therefore the amalgamation of nanotechnology with phytoremediation and bioremediation could result in two-way beneficial impacts on both the remediation of harmful pollutants from soil and on plant growth.

5 Hopes, uncertainties, and future research needs

Although nanotechnology offers a plethora of possibilities and is seen as a promising endeavor for remediation of pollutants in soil, there is a certain body of evidences that indicate that applications of nanoparticles also produce some uncertainties and risks (Ju-Nam & Lead, 2008; Maynard et al., 2006; Nowack & Bucheli, 2007; Oberdörster, Oberdörster, & Oberdörster, 2005). The potential promises of nanotechnology and the threats that it may pose are being widely debated. One cannot deny the fact that the use of nanoparticles for soil remediation will no doubt lead to their release in the environment and ecosystem. As soil forms the indispensable medium of agriculture and food production, therefore, the possibility of the nanoparticle transport through the food chain, that is, reaching the human body via the crops grown on NP-treated soil, is seriously debated making people more reluctant toward using NPs for soil remediation. But one cannot also comprehend that the possible outcomes are bound to be detrimental. There are numerous possibilities that need to explored and answered. Currently, there are no international law and policy regarding nanotechnology, manufactured nanomaterials, and their release into the environment (Ganzleben & Hansen, 2012; Stander & Theodore, 2011; Wiek, Gasser, & Siegrist, 2009). The complexity of the soil system and the use of various types of nanoparticles ranging from metal oxide- to carbon-based also complicate the situation further, limiting our understanding of nanoparticle behavior in natural system. A detailed life cycle assessment (LCA) of each and every nanoparticles/materials either in bulk form or in nanoform is also essential for ensuring the safety of these materials.

In conclusion, while nanotechnology is seen as a beneficial replacement for current practices due to the countless benefits it offers, one should be cautious about the possible threats that it may pose on soil. Nanoremediation shows promising potential for reducing the overall costs and time required for cleaning up contaminated sites on large scale. They are also effective for on-site remediation, thereby eliminating the need for transportation, treatment, and soil disposal after remediation. Before the usage and applications of nanoparticles on a massive scale, full-scale ecosystem studies with proper long-term evaluation are needed for preventing any potential adverse environmental effects that might be caused by them.

This book belongs to Central Library BADJI Mokhtar-ANNABA UNIVERSITY
Copyright Elsevier 2024

Acknowledgments

The authors are thankful to the director of Institute of Environment and Sustainable Development. Mansi Bakshi is thankful to the University Grants Commission, New Delhi, for awarding UGC-NET-SRF.

References

Abhilash, P. C., Dubey, R. K., Tripathi, V., Srivastava, P., Verma, J. P., & Singh, H. B. (2013). Remediation and management of POPs-contaminated soils in a warming climate: Challenges and perspectives. *Environmental Science and Pollution Research*, *20*(8), 5879–5885.

Abhilash, P. C., Jamil, S., & Singh, N. (2009). Transgenic plants for enhanced biodegradation and phytoremediation of organic xenobiotics. *Biotechnology Advances*, *27*(4), 474–488.

Abhilash, P. C., Powell, J. R., Singh, H. B., & Singh, B. K. (2012). Plant–microbe interactions: Novel applications for exploitation in multipurpose remediation technologies. *Trends in Biotechnology*, *30*(8), 416–420.

Abhilash, P. C., & Singh, N. (2009). Pesticide use and application: An Indian scenario. *Journal of Hazardous Materials*, *165*(1–3), 1–12.

Ali, H., Khan, E., & Sajad, M. A. (2013). Phytoremediation of heavy metals—Concepts and applications. *Chemosphere*, *91*(7), 869–881.

Allinson, G., Allinson, M., Bui, A., Zhang, P., Croatto, G., Wightwick, A., et al. (2016). Pesticide and trace metals in surface waters and sediments of rivers entering the corner inlet marine National Park, Victoria, Australia. *Environmental Science and Pollution Research*, *23*(6), 5881–5891.

Alloway, B. J. (Ed.), (2012). *Vol. 22. Heavy metals in soils: Trace metals and metalloids in soils and their bioavailability*. Springer Science & Business Media.

An, B., & Zhao, D. (2012). Immobilization of As (III) in soil and groundwater using a new class of polysaccharide stabilized Fe–Mn oxide nanoparticles. *Journal of Hazardous Materials*, *211*, 332–341.

Banwart, S. (2011). Save our soils. *Nature*, *474*(7350), 151.

Baruah, S., & Dutta, J. (2009). Nanotechnology applications in pollution sensing and degradation in agriculture: A review. *Environmental Chemistry Letters*, *7*(3), 191–204.

Bhargava, A., Carmona, F. F., Bhargava, M., & Srivastava, S. (2012). Approaches for enhanced phytoextraction of heavy metals. *Journal of Environmental Management*, *105*, 103–120.

Bhatnagar, V. K. (2001). Pesticides pollution: Trends and perspectives. *ICMR Bulletin*, *31*(9), 87–88.

Bhatt, I., & Tripathi, B. N. (2011). Interaction of engineered nanoparticles with various components of the environment and possible strategies for their risk assessment. *Chemosphere*, *82*(3), 308–317.

Blum, W. E. (2002). Environmental protection through sustainable soil management, a holistic approach. In *Advances in geoecology: vol. 35. Sustainable land management—Environmental protection–A soil physical approach* (pp. 1–8).

Bradl, H. B. (2005). Sources and origins of heavy metals. In *Vol. 6. Interface Science and Technology* (pp. 1–27): Elsevier.

Cai, F., Wu, X., Zhang, H., Shen, X., Zhang, M., Chen, W., et al. (2017). Impact of TiO_2 nanoparticles on lead uptake and bioaccumulation in rice (*Oryza sativa* L.). *NanoImpact*, *5*, 101–108.

Cai, C., Zhao, M., Yu, Z., Rong, H., & Zhang, C. (2019). Utilization of nanomaterials for in-situ remediation of heavy metal (loid) contaminated sediments: A review. *Science of the Total Environment*, *662*, 205–217.

Castillo, M. A., Trujillo, I. S., Alonso, E. V., de Torres, A. G., & Pavón, J. C. (2013). Bioavailability of heavy metals in water and sediments from a typical Mediterranean Bay (Málaga Bay, region of Andalucía, southern Spain). *Marine Pollution Bulletin*, *76*(1–2), 427–434.

This book belongs to Central Library BADJI Mokhtar-ANNABA UNIVERSITY

Copyright Elsevier 2024

Cesarino, I., Moraes, F. C., Lanza, M. R., & Machado, S. A. (2012). Electrochemical detection of carbamate pesticides in fruit and vegetables with a biosensor based on acetylcholinesterase immobilised on a composite of polyaniline–carbon nanotubes. *Food Chemistry*, *135*(3), 873–879.

Chen, X., Yao, X., Yu, C., Su, X., Shen, C., Chen, C., et al. (2014). Hydrodechlorination of polychlorinated biphenyls in contaminated soil from an e-waste recycling area, using nanoscale zerovalent iron and Pd/Fe bimetallic nanoparticles. *Environmental Science and Pollution Research*, *21*(7), 5201–5210.

Chen, M., Zeng, G., Xu, P., Zhang, Y., Jiang, D., & Zhou, S. (2017). Understanding enzymatic degradation of single-walled carbon nanotubes triggered by functionalization using molecular dynamics simulation. *Environmental Science: Nano*, *4*(3), 720–727.

Clair, S. B. S., & Lynch, J. P. (2010). The opening of Pandora's box: Climate change impacts on soil fertility and crop nutrition in developing countries. *Plant and Soil*, *335*(1–2), 101–115.

Cunningham, S. D., Berti, W. R., & Huang, J. W. (1995). Phytoremediation of contaminated soils. *Trends in Biotechnology*, *13*(9), 393–397.

Cunningham, S. D., Shann, J. R., Crowley, D. E., & Anderson, T. A. (1997). Phytoremediation of contaminated water and soil. In E. L. Kruger, T. A. Anderson, & J. R. Coats (Eds.), *Phytoremediation of soil and water contaminants. ACS symposium series 664* (pp. 2–19). Washington, DC: American Chemical Society.

De La Torre-Roche, R., Hawthorne, J., Deng, Y., Xing, B., Cai, W., Newman, L. A., et al. (2013). Multiwalled carbon nanotubes and C60 fullerenes differentially impact the accumulation of weathered pesticides in four agricultural plants. *Environmental Science & Technology*, *47*(21), 12539–12547.

De La Torre-Roche, R., Hawthorne, J., Deng, Y., Xing, B., Cai, W., Newman, L. A., et al. (2012). Fullerene-enhanced accumulation of p, p′-DDE in agricultural crop species. *Environmental Science & Technology*, *46*(17), 9315–9323.

De Oliveira, J. L., Campos, E. V. R., Bakshi, M., Abhilash, P. C., & Fraceto, L. F. (2014). Application of nanotechnology for the encapsulation of botanical insecticides for sustainable agriculture: Prospects and promises. *Biotechnology Advances*, *32*(8), 1550–1561.

Dien, N. T., De Windt, W., Buekens, A., & Chang, M. B. (2013). Application of bimetallic iron (BioCAT slurry) for pentachlorophenol removal from sandy soil. *Journal of Hazardous Materials*, *252*, 83–90.

Dong, J., Fan, X., Qiao, F., Ai, S., & Xin, H. (2013). A novel protocol for ultra-trace detection of pesticides: Combined electrochemical reduction of Ellman's reagent with acetylcholinesterase inhibition. *Analytica Chimica Acta*, *761*, 78–83.

El-Temsah, Y. S., & Joner, E. J. (2013). Effects of nano-sized zero-valent iron (nZVI) on DDT degradation in soil and its toxicity to collembola and ostracods. *Chemosphere*, *92*(1), 131–137.

El-Temsah, Y. S., Sevcu, A., Bobcikova, K., Cernik, M., & Joner, E. J. (2016). DDT degradation efficiency and ecotoxicological effects of two types of nano-sized zero-valent iron (nZVI) in water and soil. *Chemosphere*, *144*, 2221–2228.

Fan, G., Cang, L., Qin, W., Zhou, C., Gomes, H. I., & Zhou, D. (2013). Surfactants-enhanced electrokinetic transport of xanthan gum stabilized nanoPd/Fe for the remediation of PCBs contaminated soils. *Separation and Purification Technology*, *114*, 64–72.

Fang, G., Si, Y., Tian, C., Zhang, G., & Zhou, D. (2012). Degradation of 2, 4-D in soils by Fe 3 O 4 nanoparticles combined with stimulating indigenous microbes. *Environmental Science and Pollution Research*, *19*(3), 784–793.

Fayiga, A. O., & Saha, U. K. (2016). Arsenic hyperaccumulating fern: Implications for remediation of arsenic contaminated soils. *Geoderma*, *284*, 132–143.

FDA. (2005). *Glossary of pesticide chemicals*. Available at: http://www.fda.gov/downloads/Food/FoodSafety/FoodContaminantsAdulteration/Pesticides/ucm114655.pdf. Accessed 31 January 2011.

Fouad, D. M., & Mohamed, M. B. (2011). Studies on the photo-catalytic activity of semiconductor nanostructures and their gold core–shell on the photodegradation of malathion. *Nanotechnology*, *22*(45), 455705.

This book belongs to Central Library BADJI Mokhtar-ANNABA UNIVERSITY

Copyright Elsevier 2024

Fu, R., Yang, Y., Xu, Z., Zhang, X., Guo, X., & Bi, D. (2015). The removal of chromium (VI) and lead (II) from groundwater using sepiolite-supported nanoscale zero-valent iron (S-NZVI). *Chemosphere*, *138*, 726–734.

Fu, R., Zhang, X., Xu, Z., Guo, X., Bi, D., & Zhang, W. (2017). Fast and highly efficient removal of chromium (VI) using humus-supported nanoscale zero-valent iron: Influencing factors, kinetics and mechanism. *Separation and Purification Technology*, *174*, 362–371.

Fujishima, A., Zhang, X., & Tryk, D. A. (2008). TiO_2 photocatalysis and related surface phenomena. *Surface Science Reports*, *63*(12), 515–582.

Ganzleben, C., & Hansen, S. F. (2012). *Environmental exposure to nanomaterials—Data scoping study: Final report* (193 pp.). Brussels: Milieu Ltd.

Gavrilescu, M. (2009). Behaviour of persistent pollutants and risks associated with their presence in the environment—Integrated studies. *Environmental Engineering and Management Journal*, *8*(6), 1517–1531.

Gerhardt, K. E., Gerwing, P. D., & Greenberg, B. M. (2017). Opinion: Taking phytoremediation from proven technology to accepted practice. *Plant Science*, *256*, 170–185.

Ghormade, V., Deshpande, M. V., & Paknikar, K. M. (2011). Perspectives for nano-biotechnology enabled protection and nutrition of plants. *Biotechnology Advances*, *29*(6), 792–803.

Ghrair, A. M., Ingwersen, J., & Streck, T. (2010). Immobilization of heavy metals in soils amended by nanoparticulate zeolitic tuff: Sorption-desorption of cadmium. *Journal of Plant Nutrition and Soil Science*, *173*(6), 852–860.

Gil-Díaz, M., Alonso, J., Rodríguez-Valdés, E., Gallego, J. R., & Lobo, M. C. (2017). Comparing different commercial zero valent iron nanoparticles to immobilize As and Hg in brownfield soil. *Science of the Total Environment*, *584*, 1324–1332.

Gil-Díaz, M., Ortiz, L. T., Costa, G., Alonso, J., Rodríguez-Membibre, M. L., Sánchez-Fortún, S., et al. (2014). Immobilization and leaching of Pb and Zn in an acidic soil treated with zerovalent iron nanoparticles (nZVI): Physicochemical and toxicological analysis of leachates. *Water, Air, & Soil Pollution*, *225*(6), 1990.

Gil-Díaz, M., Pinilla, P., Alonso, J., & Lobo, M. C. (2016). Viability of a nanoremediation process in single or multi-metal (loid) contaminated soils. *Journal of Hazardous Materials*, *321*, 812–819.

Gogos, A., Knauer, K., & Bucheli, T. D. (2012). Nanomaterials in plant protection and fertilization: Current state, foreseen applications, and research priorities. *Journal of Agricultural and Food Chemistry*, *60*(39), 9781–9792.

Gong, X., Huang, D., Liu, Y., Peng, Z., Zeng, G., Xu, P., et al. (2018). Remediation of contaminated soils by biotechnology with nanomaterials: Bio-behavior, applications, and perspectives. *Critical Reviews in Biotechnology*, *38*(3), 455–468.

Gong, J. L., Wang, B., Zeng, G. M., Yang, C. P., Niu, C. G., Niu, Q. Y., et al. (2009). Removal of cationic dyes from aqueous solution using magnetic multi-wall carbon nanotube nanocomposite as adsorbent. *Journal of Hazardous Materials*, *164*(2–3), 1517–1522.

Gu, J., Dong, D., Kong, L., Zheng, Y., & Li, X. (2012). Photocatalytic degradation of phenanthrene on soil surfaces in the presence of nanometer anatase TiO2 under UV-light. *Journal of Environmental Sciences*, *24*(12), 2122–2126.

Hamdi, H., De La Torre-Roche, R., Hawthorne, J., & White, J. C. (2015). Impact of non-functionalized and amino-functionalized multiwall carbon nanotubes on pesticide uptake by lettuce (*Lactuca sativa* L.). *Nanotoxicology*, *9*(2), 172–180.

Hodson, M. E. (2010). The need for sustainable soil remediation. *Elements*, *6*(6), 363–368.

Hofmann, T., & Von der Kammer, F. (2009). Estimating the relevance of engineered carbonaceous nanoparticle facilitated transport of hydrophobic organic contaminants in porous media. *Environmental Pollution*, *157*(4), 1117–1126.

Hua, M., Zhang, S., Pan, B., Zhang, W., Lv, L., & Zhang, Q. (2012). Heavy metal removal from water/wastewater by nanosized metal oxides: A review. *Journal of Hazardous Materials*, *211*, 317–331.

This book belongs to Central Library BADJI Mokhtar-ANNABA UNIVERSITY

Copyright Elsevier 2024

Huettermann, A., Orikiriza, L. J., & Agaba, H. (2009). Application of superabsorbent polymers for improving the ecological chemistry of degraded or polluted lands. *Clean: Soil, Air, Water*, *37*(7), 517–526.

Hussain, A., Ali, S., Rizwan, M., Rehman, M. Z. U., Qayyum, M. F., Wang, H., et al. (2019). Responses of wheat (*Triticum aestivum*) plants grown in a Cd contaminated soil to the application of iron oxide nanoparticles. *Ecotoxicology and Environmental Safety*, *173*, 156–164.

Jadia, C. D., & Fulekar, M. H. (2009). Phytoremediation of heavy metals: Recent techniques. *African Journal of Biotechnology*, *8*, 6.

Jiamjitrpanich, W., Parkpian, P., Polprasert, C., & Kosanlavit, R. (2013). Trinitrotoluene and its metabolites in shoots and roots of Panicum maximum in nano-phytoremediation. *International Journal of Environmental Science and Development*, *4*(1), 7.

Jiang, D., Zeng, G., Huang, D., Chen, M., Zhang, C., Huang, C., et al. (2018). Remediation of contaminated soils by enhanced nanoscale zero valent iron. *Environmental Research*, *163*, 217–227.

Ju-Nam, Y., & Lead, J. R. (2008). Manufactured nanoparticles: An overview of their chemistry, interactions and potential environmental implications. *Science of the Total Environment*, *400*(1–3), 396–414.

Kabata-Pendias, A., & Pendias, H. (2001). *Trace elements in soils and plants.* Boca Raton, FL: CRC Press.

Karn, B., Kuiken, T., & Otto, M. (2009). Nanotechnology and in situ remediation: A review of the benefits and potential risks. *Environmental Health Perspectives*, *117*(12), 1813–1831.

Khan, M. N., Mobin, M., Abbas, Z. K., AlMutairi, K. A., & Siddiqui, Z. H. (2017). Role of nanomaterials in plants under challenging environments. *Plant Physiology and Biochemistry*, *110*, 194–209.

Khin, M. M., Nair, A. S., Babu, V. J., Murugan, R., & Ramakrishna, S. (2012). A review on nanomaterials for environmental remediation. *Energy & Environmental Science*, *5*(8), 8075–8109.

Khot, L. R., Sankaran, S., Maja, J. M., Ehsani, R., & Schuster, E. W. (2012). Applications of nanomaterials in agricultural production and crop protection: A review. *Crop Protection*, *35*, 64–70.

Kuiken, T. (2010). Cleaning up contaminated waste sites: Is nanotechnology the answer? *Nano Today*, *5*(1), 6–8.

Kumar, P., Kim, K. H., & Deep, A. (2015). Recent advancements in sensing techniques based on functional materials for organophosphate pesticides. *Biosensors and Bioelectronics*, *70*, 469–481.

Lal, R. (2009). Soil degradation as a reason for inadequate human nutrition. *Food Security*, *1*(1), 45–57.

Lal, R. (2015). Restoring soil quality to mitigate soil degradation. *Sustainability*, *7*(5), 5875–5895.

Le Cloarec, M. F., Bonte, P. H., Lestel, L., Lefèvre, I., & Ayrault, S. (2011). Sedimentary record of metal contamination in the Seine River during the last century. *Physics and Chemistry of the Earth, Parts A/B/C*, *36* (12), 515–529.

Lefevre, E., Bossa, N., Wiesner, M. R., & Gunsch, C. K. (2016). A review of the environmental implications of in situ remediation by nanoscale zero valent iron (nZVI): Behavior, transport and impacts on microbial communities. *Science of the Total Environment*, *565*, 889–901.

León, J. D., & Osorio, N. W. (2014). Role of litter turnover in soil quality in tropical degraded lands of Colombia. *The Scientific World Journal*, *2014*.

Li, S., Wang, W., Liang, F., & Zhang, W. X. (2017). Heavy metal removal using nanoscale zero-valent iron (nZVI): Theory and application. *Journal of Hazardous Materials*, *322*, 163–171.

Liu, T., Su, H., Qu, X., Ju, P., Cui, L., & Ai, S. (2011). Acetylcholinesterase biosensor based on 3-carboxyphenylboronic acid/reduced graphene oxide–gold nanocomposites modified electrode for amperometric detection of organophosphorus and carbamate pesticides. *Sensors and Actuators B: Chemical*, *160*(1), 1255–1261.

Liu, S., Yuan, L., Yue, X., Zheng, Z., & Tang, Z. (2008). Recent advances in nanosensors for organophosphate pesticide detection. *Advanced Powder Technology*, *19*(5), 419–441.

Liu, R., & Zhao, D. (2007). In situ immobilization of Cu (II) in soils using a new class of iron phosphate nanoparticles. *Chemosphere*, *68*(10), 1867–1876.

This book belongs to Central Library BADJI Mokhtar-ANNABA UNIVERSITY

Copyright Elsevier 2024

Liu, R., & Zhao, D. (2013). Synthesis and characterization of a new class of stabilized apatite nanoparticles and applying the particles to in situ Pb immobilization in a fire-range soil. *Chemosphere*, *91*(5), 594–601.

Loos, R., Gawlik, B. M., Locoro, G., Rimaviciute, E., Contini, S., & Bidoglio, G. (2009). EU-wide survey of polar organic persistent pollutants in European river waters. *Environmental Pollution*, *157*(2), 561–568.

López-Luna, J., Silva-Silva, M. J., Martinez-Vargas, S., Mijangos-Ricardez, O. F., González-Chávez, M. C., Solís-Domínguez, F. A., et al. (2016). Magnetite nanoparticle (NP) uptake by wheat plants and its effect on cadmium and chromium toxicological behavior. *Science of the Total Environment*, *565*, 941–950.

López-Moreno, M. L., de la Rosa, G., Hernández-Viezcas, J. A., Peralta-Videa, J. R., & Gardea-Torresdey, J. L. (2010). XAS corroboration of the uptake and storage of CeO_2 nanoparticles and assessment of their differential toxicity in four edible plant species. *Journal of Agricultural and Food Chemistry*, *58*(6), 3689.

Lu, Y., Song, S., Wang, R., Liu, Z., Meng, J., Sweetman, A. J., et al. (2015). Impacts of soil and water pollution on food safety and health risks in China. *Environment International*, *77*, 5–15.

Ma, X., & Wang, C. (2010). Fullerene nanoparticles affect the fate and uptake of trichloroethylene in phytoremediation systems. *Environmental Engineering Science*, *27*(11), 989–992.

Madhavi, V., Prasad, T. N. V. K. V., Reddy, B. R., Reddy, A. V. B., & Gajulapalle, M. (2014). Conjunctive effect of CMC–zero-valent iron nanoparticles and FYM in the remediation of chromium-contaminated soils. *Applied Nanoscience*, *4*(4), 477–484.

Maharia, R. S., Dutta, R. K., Acharya, R., & Reddy, A. V. R. (2010). Heavy metal bioaccumulation in selected medicinal plants collected from Khetri copper mines and comparison with those collected from fertile soil in Haridwar, India. *Journal of Environmental Science and Health. Part. B, Pesticides, Food Contaminants, and Agricultural Wastes*, *45*(2), 174–181.

Mallampati, S. R., Mitoma, Y., Okuda, T., Sakita, S., & Kakeda, M. (2013). Total immobilization of soil heavy metals with nano-Fe/Ca/CaO dispersion mixtures. *Environmental Chemistry Letters*, *11*(2), 119–125.

Maynard, A. D., Aitken, R. J., Butz, T., Colvin, V., Donaldson, K., Oberdörster, G., et al. (2006). Safe handling of nanotechnology. *Nature*, *444*(7117), 267.

McCutcheon, S. C., & Schnoor, J. L. (2003). Overview of phytotransformation and control of wastes. In *Phytoremediation: Transformation and control of contaminants* (pp. 1–58). New York: Wiley.

Men, C., Liu, R., Xu, F., Wang, Q., Guo, L., & Shen, Z. (2018). Pollution characteristics, risk assessment, and source apportionment of heavy metals in road dust in Beijing, China. *Science of the Total Environment*, *612*, 138–147.

Mitton, F. M., Miglioranza, K. S., Gonzalez, M., Shimabukuro, V. M., & Monserrat, J. M. (2014). Assessment of tolerance and efficiency of crop species in the phytoremediation of DDT polluted soils. *Ecological Engineering*, *71*, 501–508.

Moharem, M., Elkhatib, E., & Mesalem, M. (2019). Remediation of chromium and mercury polluted calcareous soils using nanoparticles: Sorption–desorption kinetics, speciation and fractionation. *Environmental Research*, *170*, 366–373.

Navarro, M. C., Pérez-Sirvent, C., Martínez-Sánchez, M. J., Vidal, J., Tovar, P. J., & Bech, J. (2008). Abandoned mine sites as a source of contamination by heavy metals: A case study in a semi-arid zone. *Journal of Geochemical Exploration*, *96*(2–3), 183–193.

Negri, M. C., & Hinchman, R. R. (2000). The use of plants for the treatment of radionuclides. In *Phytoremediation of toxic metals: Using plants to clean up the environment*. New York: Wiley-Interscience.

Nowack, B., & Bucheli, T. D. (2007). Occurrence, behavior and effects of nanoparticles in the environment. *Environmental Pollution*, *150*(1), 5–22.

Oberdörster, G., Oberdörster, E., & Oberdörster, J. (2005). Nanotoxicology: An emerging discipline evolving from studies of ultrafine particles. *Environmental Health Perspectives*, *113*(7), 823–839.

Otto, M., Floyd, M., & Bajpai, S. (2008). Nanotechnology for site remediation. *Remediation Journal*, *19*(1), 99–108.

This book belongs to Central Library BADJI Mokhtar-ANNABA UNIVERSITY

Copyright Elsevier 2024

Pacyna, J. M., Pacyna, E. G., & Aas, W. (2009). Changes of emissions and atmospheric deposition of mercury, lead, and cadmium. *Atmospheric Environment*, *43*(1), 117–127.

Pacyna, E. G., Pacyna, J. M., Fudala, J., Strzelecka-Jastrzab, E., Hlawiczka, S., Panasiuk, D., et al. (2007). Current and future emissions of selected heavy metals to the atmosphere from anthropogenic sources in Europe. *Atmospheric Environment*, *41*(38), 8557–8566.

Paknikar, K. M., Nagpal, V., Pethkar, A. V., & Rajwade, J. M. (2005). Degradation of lindane from aqueous solutions using iron sulfide nanoparticles stabilized by biopolymers. *Science and Technology of Advanced Materials*, *6*(3–4), 370–374.

Pan, B., & Xing, B. (2008). Adsorption mechanisms of organic chemicals on carbon nanotubes. *Environmental Science & Technology*, *42*(24), 9005–9013.

Pan, B., & Xing, B. (2012). Applications and implications of manufactured nanoparticles in soils: A review. *European Journal of Soil Science*, *63*(4), 437–456.

Peikam, E. N., & Jalali, M. (2018). Application of three nanoparticles (Al_2O_3, SiO_2 and TiO_2) for metal-contaminated soil remediation (measuring and modeling). *International Journal of Environmental Science and Technology*, 1–14.

Pilon-Smits, E. (2005). Phytoremediation. *Annual Review of Plant Biology*, *56*, 15–39.

Raskin, I., & Ensley, B. D. (2000). *Phytoremediation of toxic metals*. John Wiley and Sons.

Raskin, I., Smith, R. D., & Salt, D. E. (1997). Phytoremediation of metals: Using plants to remove pollutants from the environment. *Current Opinion in Biotechnology*, *8*(2), 221–226.

Restivo, J., Órfão, J. J. M., Armenise, S., Garcia-Bordejé, E., & Pereira, M. F. R. (2012). Catalytic ozonation of metolachlor under continuous operation using nanocarbon materials grown on a ceramic monolith. *Journal of Hazardous Materials*, *239*, 249–256.

Rogueda, P. G., & Traini, D. (2007). The nanoscale in pulmonary delivery. Part 1: Deposition, fate, toxicology and effects. *Expert Opinion on Drug Delivery*, *4*(6), 595–606.

Roh, J. Y., Park, Y. K., Park, K., & Choi, J. (2010). Ecotoxicological investigation of CeO_2 and TiO_2 nanoparticles on the soil nematode *Caenorhabditis elegans* using gene expression, growth, fertility, and survival as endpoints. *Environmental Toxicology and Pharmacology*, *29*(2), 167–172.

Rühling, Å., & Tyler, G. (2001). Changes in atmospheric deposition rates of heavy metals in Sweden a summary of nationwide Swedish surveys in 1968/70–1995. *Water, Air and Soil Pollution: Focus*, *1*(3–4), 311–323.

Rui, Z., Jingguo, W., Jianyu, C., Lin, H., & Kangguo, M. (2010). Photocatalytic degradation of pesticide residues with RE^{3+}-doped nano-TiO_2. *Journal of Rare Earths*, *28*, 353–356.

Sakakibara, M., Watanabe, A., Inoue, M., Sano, S., & Kaise, T. (2010). Phytoextraction and phytovolatilization of arsenic from as-contaminated soils by *Pteris vittata*. In *Proceedings of the annual international conference on soils, sediments, water and energy, Vol. 12* (p. 26). 1.

Shi, J., Abid, A. D., Kennedy, I. M., Hristova, K. R., & Silk, W. K. (2011). To duckweeds (*Landoltia punctata*), nanoparticulate copper oxide is more inhibitory than the soluble copper in the bulk solution. *Environmental Pollution*, *159*(5), 1277–1282.

Shi, J., Votruba, A. R., Farokhzad, O. C., & Langer, R. (2010). Nanotechnology in drug delivery and tissue engineering: From discovery to applications. *Nano Letters*, *10*(9), 3223–3230.

Simonian, A. L., Good, T. A., Wang, S. S., & Wild, J. R. (2005). Nanoparticle-based optical biosensors for the direct detection of organophosphate chemical warfare agents and pesticides. *Analytica Chimica Acta*, *534*(1), 69–77.

Singh, R., Manickam, N., Mudiam, M. K. R., Murthy, R. C., & Misra, V. (2013). An integrated (nano-bio) technique for degradation of γ-HCH contaminated soil. *Journal of Hazardous Materials*, *258*, 35–41.

Singh, R., Misra, V., & Singh, R. P. (2012). Removal of Cr (VI) by nanoscale zero-valent iron (nZVI) from soil contaminated with tannery wastes. *Bulletin of Environmental Contamination and Toxicology*, *88*(2), 210–214.

This book belongs to Central Library BADJI Mokhtar-ANNABA UNIVERSITY

Copyright Elsevier 2024

Song, B., Xu, P., Chen, M., Tang, W., Zeng, G., Gong, J., et al. (2019). Using nanomaterials to facilitate the phytoremediation of contaminated soil. *Critical Reviews in Environmental Science and Technology*, *49*(9), 791–824.

Song, B., Zeng, G., Gong, J., Liang, J., Xu, P., Liu, Z., et al. (2017). Evaluation methods for assessing effectiveness of in situ remediation of soil and sediment contaminated with organic pollutants and heavy metals. *Environment International*, *105*, 43–55.

Songa, E. A., & Okonkwo, J. O. (2016). Recent approaches to improving selectivity and sensitivity of enzyme-based biosensors for organophosphorus pesticides: A review. *Talanta*, *155*, 289–304.

Stander, L., & Theodore, L. (2011). Environmental implications of nanotechnology—An update. *International Journal of Environmental Research and Public Health*, *8*(2), 470–479.

Stefaniuk, M., Oleszczuk, P., & Ok, Y. S. (2016). Review on nano zerovalent iron (nZVI): From synthesis to environmental applications. *Chemical Engineering Journal*, *287*, 618–632.

Stephenson, G. R., Coats, J. R., & Yamamoto, H. (2003). Pesticide use and world food production: Risks and benefits. In *Expert Committee on Weeds Comité d'experts en malherbologie* (p. 9).

Su, H., Fang, Z., Tsang, P. E., Zheng, L., Cheng, W., Fang, J., et al. (2016). Remediation of hexavalent chromium contaminated soil by biochar-supported zero-valent iron nanoparticles. *Journal of Hazardous Materials*, *318*, 533–540.

Su, S., He, Y., Zhang, M., Yang, K., Song, S., Zhang, X., et al. (2008). High-sensitivity pesticide detection via silicon nanowires-supported acetylcholinesterase-based electrochemical sensors. *Applied Physics Letters*, *93*(2), 023113.

Tang, W. W., Zeng, G. M., Gong, J. L., Liang, J., Xu, P., Zhang, C., et al. (2014). Impact of humic/fulvic acid on the removal of heavy metals from aqueous solutions using nanomaterials: A review. *Science of the Total Environment*, *468*, 1014–1027.

Thuesombat, P., Hannongbua, S., Akasit, S., & Chadchawan, S. (2014). Effect of silver nanoparticles on rice (*Oryza sativa* L. cv. KDML 105) seed germination and seedling growth. *Ecotoxicology and Environmental Safety*, *104*, 302–309.

Tilston, E. L., Collins, C. D., Mitchell, G. R., Princivalle, J., & Shaw, L. J. (2013). Nanoscale zerovalent iron alters soil bacterial community structure and inhibits chloroaromatic biodegradation potential in Aroclor 1242-contaminated soil. *Environmental Pollution*, *173*, 38–46.

Tripathi, V., Fraceto, L. F., & Abhilash, P. C. (2015). Sustainable clean-up technologies for soils contaminated with multiple pollutants: Plant-microbe-pollutant and climate nexus. *Ecological Engineering*, *82*, 330–335.

Vamerali, T., Bandiera, M., & Mosca, G. (2010). Field crops for phytoremediation of metal-contaminated land. A review. *Environmental Chemistry Letters*, *8*(1), 1–17.

Violante, A., Cozzolino, V., Perelomov, L., Caporale, A. G., & Pigna, M. (2010). Mobility and bioavailability of heavy metals and metalloids in soil environments. *Journal of Soil Science and Plant Nutrition*, *10*(3), 268–292.

Virkutyte, J., Al-Abed, S. R., Choi, H., & Bennett-Stamper, C. (2014). Distinct structural behavior and transport of TiO_2 nano-and nanostructured particles in sand. *Colloids and Surfaces A: Physicochemical and Engineering Aspects*, *443*, 188–194.

Wang, Y., Fang, Z., Kang, Y., & Tsang, E. P. (2014). Immobilization and phytotoxicity of chromium in contaminated soil remediated by CMC-stabilized nZVI. *Journal of Hazardous Materials*, *275*, 230–237.

Wang, T., Liu, Y., Wang, J., Wang, X., Liu, B., & Wang, Y. (2019). In-situ remediation of hexavalent chromium contaminated groundwater and saturated soil using stabilized iron sulfide nanoparticles. *Journal of Environmental Management*, *231*, 679–686.

Wang, P., Lombi, E., Zhao, F. J., & Kopittke, P. M. (2016). Nanotechnology: A new opportunity in plant sciences. *Trends in Plant Science*, *21*(8), 699–712.

Wang, X. T., Shi, W. S., She, G. W., Mu, L. X., & Lee, S. T. (2010). High-performance surface-enhanced Raman scattering sensors based on Ag nanoparticles-coated Si nanowire arrays for quantitative detection of pesticides. *Applied Physics Letters*, *96*(5), 053104.

This book belongs to Central Library BADJI Mokhtar-ANNABA UNIVERSITY

Copyright Elsevier 2024

Weber, R., Gaus, C., Tysklind, M., Johnston, P., Forter, M., Hollert, H., et al. (2008). Dioxin-and POP-contaminated sites—Contemporary and future relevance and challenges. *Environmental Science and Pollution Research*, *15*(5), 363.

Wiek, A., Gasser, L., & Siegrist, M. (2009). Systemic scenarios of nanotechnology: Sustainable governance of emerging technologies. *Futures*, *41*(5), 284–300.

Wong, C. S. C., Li, X. D., Zhang, G., Qi, S. H., & Peng, X. Z. (2003). Atmospheric deposition of heavy metals in the Pearl River Delta, China. *Atmospheric Environment*, *37*(6), 767–776.

Wu, S., Huang, F., Lan, X., Wang, X., Wang, J., & Meng, C. (2013). Electrochemically reduced graphene oxide and Nafion nanocomposite for ultralow potential detection of organophosphate pesticide. *Sensors and Actuators B: Chemical*, *177*, 724–729.

Wu, J., Xie, Y., Fang, Z., Cheng, W., & Tsang, P. E. (2016). Effects of Ni/Fe bimetallic nanoparticles on phytotoxicity and translocation of polybrominated diphenyl ethers in contaminated soil. *Chemosphere*, *162*, 235–242.

Wuana, R. A., & Okieimen, F. E. (2011). Heavy metals in contaminated soils: A review of sources, chemistry, risks and best available strategies for remediation. *ISRN Ecology*, *2011*, 1–20.

Xu, Y., & Zhao, D. (2007). Reductive immobilization of chromate in water and soil using stabilized iron nanoparticles. *Water Research*, *41*(10), 2101–2108.

Yan, W., Lien, H. L., Koel, B. E., & Zhang, W. X. (2013). Iron nanoparticles for environmental clean-up: Recent developments and future outlook. *Environmental Science: Processes & Impacts*, *15*(1), 63–77.

Yang, X., Wang, S., Bian, Y., Chen, F., Yu, G., Gu, C., et al. (2008). Dicofol application resulted in high DDTs residue in cotton fields from northern Jiangsu province, China. *Journal of Hazardous Materials*, *150*(1), 92–98.

Yu, B., Zeng, J., Gong, L., Zhang, M., Zhang, L., & Chen, X. (2007). Investigation of the photocatalytic degradation of organochlorine pesticides on a nano-TiO_2 coated film. *Talanta*, *72*(5), 1667–1674.

Yuan, S., Long, H., Xie, W., Liao, P., & Tong, M. (2012). Electrokinetic transport of CMC-stabilized Pd/Fe nanoparticles for the remediation of PCP-contaminated soil. *Geoderma*, *185*, 18–25.

Zhang, X., Wang, H., He, L., Lu, K., Sarmah, A., Li, J., et al. (2013). Using biochar for remediation of soils contaminated with heavy metals and organic pollutants. *Environmental Science and Pollution Research*, *20*(12), 8472–8483.

Zhang, M., Wang, Y., Zhao, D., & Pan, G. (2010). Immobilization of arsenic in soils by stabilized nanoscale zero-valent iron, iron sulfide (FeS), and magnetite (Fe_3O_4) particles. *Chinese Science Bulletin*, *55*(4–5), 365–372.

Zhu, F., Li, L., Ma, S., & Shang, Z. (2016). Effect factors, kinetics and thermodynamics of remediation in the chromium contaminated soils by nanoscale zero valent Fe/Cu bimetallic particles. *Chemical Engineering Journal*, *302*, 663–669.

Zou, Y., Wang, X., Khan, A., Wang, P., Liu, Y., Alsaedi, A., et al. (2016). Environmental remediation and application of nanoscale zero-valent iron and its composites for the removal of heavy metal ions: A review. *Environmental Science & Technology*, *50*(14), 7290–7304.

Further reading

Adriano, D. C. (2001). Arsenic. In *Trace elements in terrestrial environments* (pp. 219–261). New York, NY: Springer.

Burris, K. P., & Stewart, C. N., Jr. (2012). Fluorescent nanoparticles: Sensing pathogens and toxins in foods and crops. *Trends in Food Science & Technology*, *28*(2), 143–152.

Zeng, R., Wang, J., Cui, J., Hu, L., & Mu, K. (2010). Photocatalytic degradation of pesticide residues with RE3+-doped nano-TiO2. *Journal of Rare Earths*, *28*, 353–356.

Zhao, X., Hilliard, L. R., Mechery, S. J., Wang, Y., Bagwe, R. P., Jin, S., et al. (2004). A rapid bioassay for single bacterial cell quantitation using bioconjugated nanoparticles. *Proceedings of the National Academy of Sciences*, *101*(42), 15027–15032.

This book belongs to Central Library BADJI Mokhtar-ANNABA UNIVERSITY

Copyright Elsevier 2024

CHAPTER

Overview of nanomaterials synthesis methods, characterization techniques and effect on seed germination

18

Somenath Das[a], Arpan Mukherjee[b], Gereraj Sengupta[a], Vipin Kumar Singh[a]
Department of Botany, Centre of Advanced Study (CAS), Institute of Science, Banaras Hindu University, Varanasi, India[a]
Institute of Environment and Sustainable Development, Banaras Hindu University, Varanasi, India[b]

1 Introduction

Today, nanotechnology has emerged as one of the advanced and fastest developing technology with its significant contribution in agriculture (Kumar, Gupta, Dixit, Mishra, & Srivastava, 2019), food technology (Wu et al., 2019), and drug delivery (Vangijzegem, Stanicki, & Laurent, 2019). Nanoparticle size may range between one and thousand nanometers and possess variable electronic and physicochemical properties such as greater surface-to-volume ratio, higher quantum effect, and surface reactivity (Albanese, Tang, & Chan, 2012). Since 2008, brief definition of nanoparticle includes any object/particle carrying all of its three dimensions reduced up to 100 nm or less (nanoobject). On the other hand, nanomaterials could have any external or internal structure at nanometer scale. Hence, nanomaterials can be categorized as nanolayers (with one dimension at nanometer range), nanowires, nanofibers, carbon nanotubes (two dimension at the nanometer scale), and nanoparticles (all the three dimensions at the nanoscale) (Paul & Robeson, 2008). Nanoparticles have been regarded as to act like a bridge between molecular structure of atoms and bulk materials.

Currently, various physical, chemical, and biological techniques have been used to synthesize the nanomaterials. The expensive and large amount of chemical application in physicochemical methods of nanomaterial synthesis has limited their commercial application. On the other hand, biological techniques relying on microbial actions and plant-derived extracts or chemical for nanomaterial synthesis has attracted the researchers worldwide. Apart from the synthesis, characterization of nanomaterials is another important aspect in the area of nanotechnology. In this context, different sensitive analytical techniques have come into existence to precisely evaluate nanomaterial exposure at the environmental state. Different methods available for nanoparticle detection and characterizations are electron microscopy (scanning and transmission electron microscopy), atomic force microscopy (AFM), energy electron loss spectroscopy (EELS), X-ray microscopy (XRM), size exclusion chromatography, multiangle laser light scattering (MALLS) chromatography, capillary electrophoresis, hydrodynamic

Nano-Materials as Photocatalysts for Degradation of Environmental Pollutants. https://doi.org/10.1016/B978-0-12-818598-8.00018-3
© 2020 Elsevier Inc. All rights reserved.

This book belongs to Central Library BADJI Mokhtar-ANNABA UNIVERSITY
Copyright Elsevier 2024

chromatography (HDC), field-flow fractionation (FFF) chromatography, dynamic light scattering (DLS) spectroscopy, photon correlation spectroscopy (PCS), laser-induced breakdown (LIB), laser-induced fluorescence (LIF), Fourier transform infrared spectroscopy (FTIR), UV-visible spectroscopy, nuclear magnetic resonance (Zou et al., 2019), X-ray photoelectrons (XPS) (Bauer et al., 2019), X-ray diffraction (XRD) (Meva et al., 2019), X-ray absorption spectroscopy (XAS) (Wattanawikkam, Kansaard, & Pecharapa, 2019), single-particle mass spectrophotometry (SPMS) (Yu, Ying, Gao, & Long, 2019), inductively coupled plasma emission spectroscopy (ICP-MS) (Itabashi, Mizukami, Taniguchi, Nishifuji, & Kamiya, 2019), matrix-assisted laser desorption ionization spectroscopy, thermogravimetric analysis (TGA) (Ali, Ovens, Starosta, & Gates, 2019), electrophoretic mobility, and zeta potential. Existing techniques with diverse elemental composition may provide size separation from 1 nm to several micrometers.

In the present era, humans are frequently exposed to nanoparticles due to their effective use as food additive, packaging substances, and in cosmetics (Duncan, 2011). In addition, different intended and unintended origins of nanoparticles may affect human body through food chain, food web, and drinking water. There are several reports on nanoparticle toxicity based on their long-term effects, excessive bioaccumulation, and adverse effect on food chain. Toxicity and behavior of nanoparticles are greatly affected by surface charge, aggregation states, elemental composition, and structure and shape of the nanoparticle (Borm et al., 2006; Chau, Wu, & Yen, 2007). There are several predicted pathways for nanoparticle absorption and translocation in the plant body. The aboveground parts such as leaves and shoots are directly exposed and act as sink for nanoparticle deposition. In addition, absorption of nanoparticle may also occur through rhizomatous portion, roots, and mycorrhizal parts of roots. Outer surface of epidermal cells, fruits, and leaves are covered by cuticle and could actively minimize the nanoparticle deposition and permeation properties (Domínguez, Heredia-Guerrero, & Heredia, 2011). Nanoparticle may induce excess reactive oxygen species (ROS) generation and subsequent changes in DNA, RNA, solubility, and aggregation of biomolecules. Due to nanometric size, it can easily cross tissue junction and cause mutation in nuclear and mitochondrial DNA (Donaldson & Stone, 2003).

Seed serves as the primary unit for the establishment of most of the plant species existing on Earth and is the prime basis of current day agricultural practices. Assessment of seed germination under the influence of nanoparticles is one of the most widely used and inexpensive techniques for determining the beneficial or toxicological impacts associated with their application in modern agriculture. Nanoparticles may affect the germination property of seeds and root elongation (Scherer et al., 2019) with varied particle size. TiO_2 nanoparticles and bentonite (a natural clay material) have been reported to cause effective inhibition of transpiration and hydraulic conductivity with reduction in pore size of cell wall of maize roots from 6.6 to 3 nm (Asli & Neumann, 2009). So far, numerous reports are available indicating both useful and harmful effects of nanoparticles on growth, reproduction, and seed germination potency in higher plants. Zheng, Hong, Lu, and Liu (2005) reported an alteration in nitrate reductase activity in silicon and titanium oxide nanoparticle-treated *Glycine max* (soybean) plants and inhibition of seed germination and seedling growth. Lin and Xing (2007) observed nonphytotoxic effect of zinc oxide- and carbon nanotube-treated cucumber, lettuce, rapeseed, and corn seeds within specific days of interval. Recent finding of Das et al. (2019) has exhibited nonphytotoxic effect of *Coriandrum sativum* essential oil-loaded nanoparticles on 6-month-stored rice seeds with negligible effects on the emergence of plumule and radical.

This book belongs to Central Library BADJI Mokhtar-ANNABA UNIVERSITY
Copyright Elsevier 2024

The present article has been prepared to deal with different methods (physical, chemical, and biological) of nanoparticle synthesis and varied characterization techniques. Further the sequential effect of nanoparticles on germination of seeds and mechanistic mode of action has also been described.

2 Methods of nanomaterial synthesis

Based on varieties of preparation techniques, nanoparticles, nanocapsules, and nanospheres have been developed. Polymer-based nanoparticles are rapidly expanding and acting as promising vehicle for manipulation in conducting materials, electronics, photonics, sensors, drug delivery, and associated biotechnological applications (Lombardo, Kiselev, & Caccamo, 2019). The major factors for the preparation of nanoparticles are the selection of nontoxic, nonantigenic, biodegradable, and biocompatible polymers. Some of the natural polymers for synthesis of nanoparticles include albumin, sodium alginate, gelatin, starch, β-cyclodextrin, and chitosan (Esfanjani & Jafari, 2016). However, commonly used synthetic polymers are polyvinyl alcohol, polyanhydrides, polylactides, polyglycolides, polyacrylic acid, polyethylene glycol, poly-N-vinyl pyrrolidone, polycyanoacrylates, polyorthoesters, poly(malic acid), polyglutamic acid, polycaprolactone, and polymethyl methacrylate. Different methods have been employed for synthesis of nanoparticles; among them, nanoprecipitations, salting out, dialysis, emulsification, solvent evaporation, and supercritical fluid technology are commonly used. There are different physical, chemical, and green biological methods for successful synthesis of nanoparticles. Preparation of nanoparticles mainly involves two steps, emulsification and precipitation. Evaporation-based condensation and laser ablation are the prominent physical approaches for nanoparticle synthesis.

Physical method for nanoparticle preparation occasionally involves long-term inhalation toxicity studies and calibration devices (Jung, Oh, Noh, Ji, & Kim, 2006). Nanoparticles are also synthesized by laser ablation metallic bulk materials in homogenized solution phase (Mafuné, Kohno, Takeda, Kondow, & Sawabe, 2000). Silver nanospheroides, carbon nanotubes, and colloidal particles are prepared by laser ablation techniques without any agglomeration.

Chemical methods of nanoparticle synthesis includes reduction reaction by organic and inorganic agents. Several commonly used reducing substrates, namely, ascorbate, Tollen's reagent, sodium borohydride, N,N-dimethylformamide, and elemental hydrogen, are currently being used for synthesis of metal nanoparticles (Iravani, Thota, & Crans, 2018). In chemical reduction method, different polymeric components such as polyvinylpyrrolidone, polymethacrylate acid, and polyvinyl alcohol are effectively used as protective agents for providing stability to synthesized nanoparticle. Kim et al. have observed the synthesis of spherical silver nanoparticles with moderate dispersity following the modified injection precursor method.

Microemulsion or colloidal nanodispersions are thermodynamically stable dispersion formed by chemical reaction of nanomaterials. Based on the Brownian motion of the formed droplets, particles collide with each other to form fused dimer (Lopez-Quintela, 2003). Metal nanoparticles may also be synthesized by electrochemical and irradiation methods. Different monodisperse silver nanospheroides have also been synthesized by active participation of modified electrodes of zeolite with specific electrochemical reduction. Others include laser irradiation-based metal nanoparticle synthesis with short-term photosensitization at different intervals.

This book belongs to Central Library BADJI Mokhtar-ANNABA UNIVERSITY Copyright Elsevier 2024

Microwave-assisted synthesis of nanoparticles has been characterized with narrow range sizes, consistent yielding of nanomaterials, and higher degree of crystallization without any agglomeration of formed particles. Yin, Yamamoto, Wada, and Yanagida (2004) have developed techniques for size-controlled silver nanoparticle synthesis from aqueous solution of trisodium citrate and silver nitrate by using formaldehyde as a reducing agent. For preparation of metal nanoparticles, gamma irradiation and radiolysis of silver ions with ethylene glycol could serve as an important parameter for successful adjustment of pH.

One of the simplest methods for silver nanoparticle synthesis is Tollen's method, which includes reduction of Tollen's reagent (Ag $[NH_3]_2$) by aldehyde group of molecules. Tollen's method is characterized by reduction of silver ions by saccharides (in the presence of NH_3) and subsequent development of silver hydrosol and silver nanoparticles (Kvitek et al., 2008). Different concentrations of NH_3 (0.005–0.20 M) and pH (11.5–13.0) were used for nanoparticle synthesis, and average size range of nanoparticles was recorded between 25 and 450 nm. Stabilization of the formed particles was done by different detergents and surfactants such as sodium dodecyl sulfate (SDS), polyvinyl pyrrolidone (PVP 360), Tween80, and Tween 20 (Soukupová, Kvítek, Panáček, Nevěčná, & Zbořil, 2008).

Sol-gel is one of the promising method for colloidal nanoparticle synthesis with the involvement of two different phases, namely, sol (solid particles in liquid) and gel (polymers in liquid) leading to the formation of discrete particle network. Zinc and other metal nanoparticle have been synthesized by this technique, and different physical parameters such as temperature, moisture, time of efflux, and drying methodology have been optimized based on the particle size. Gonçalves et al. (2013) observed that the size of different cadmium and selenium nanoparticles may depend on calcination temperature with advanced optoelectronic parameters.

Varieties of metal oxide nanoparticles such as lithium iron oxide, iron oxide, and cadmium oxide nanoparticles have been synthesized by hydrothermal synthesis with two different phases of colloidal system. Platinum nanoparticle was synthesized by hydrothermal process exhibiting significant electrocatalytic efficiency (Du et al., 2014). Promising results of luminescence with fabricated hydrophilic nanoparticle suggest their excellent utilizations in biological sections after toxicity test (Ma, Chen, & Li, 2015). Hydrothermal methods are robust and one of the fastest growing process for synthesis of zirconium, strontium, cobalt, silver, iron, and lanthanum nanoparticles with different hydrothermal oxides.

Polyol process of nanoparticle synthesis involves polyethylene glycol as reactant solvent and varying concentration of nitrate ions to produce stable complexes with controlled size and established heating exclusion for size-specific crystallinity of nanoparticles. Kim, Lim, Lee, and Xia (2008) synthesized polycrystalline cupric oxide nanoparticles with polyvinyl pyrrolidine as precursor components. Types of polyol are a major determining factor for the size and texture of nanoparticles. Two different types of polyols such as ethylene glycol and 1,2-polypropelene glycol with single mesocrystal have been used for the development of secondary structures with lower kinetic energy (Cheng, Xu, & Gu, 2011).

Biological agent-based metallic nanoparticle synthesis is categorized into bioreduction and biosorption process. Several researchers have focused on nongreen physicochemical methods of nanoparticle synthesis, while involvement of bacteria, fungi, plant extracts, and plant bioactive components involves the green synthesis of nanoparticles and provides sustainable, resourceful, and cheap method for nanoparticle preparation. Bar et al. (2009) synthesized homogenized (10–20 nm) silver nanoparticle by using the extract of *Jatropha curcas*. Synthesis of silver nanoparticle through molecular reduction of

This book belongs to Central Library BADJI Mokhtar-ANNABA UNIVERSITY Copyright Elsevier 2024

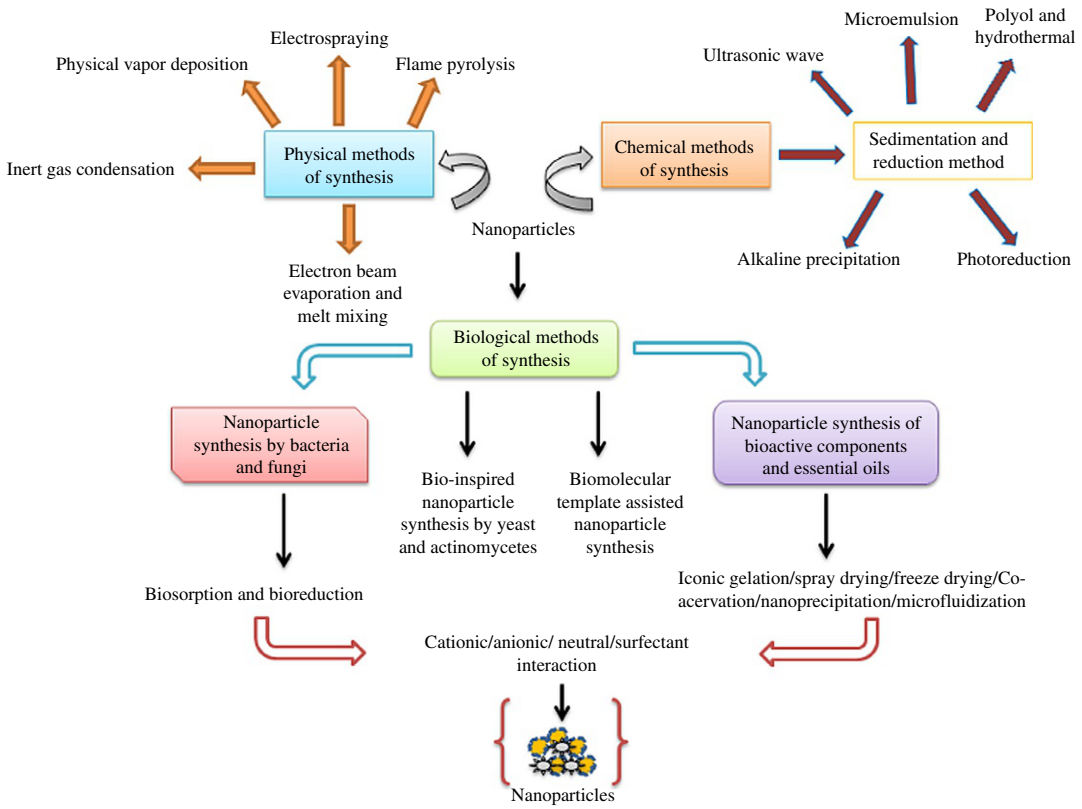

FIG. 1

Different methods of nanoparticle synthesis.

Ag^{2+} ions involving the seed extract of *Medicago sativa* was reported to have spherical to oval nanoparticles (Lukman, Gong, Marjo, Roessner, & Harris, 2011). Mukherjee et al. (2001) observed the synthesis of gold nanoparticles using *Verticillium* spp. for modified electronic applications. Species of *Fusarium* have actively participated in the synthesis of cadmium sulfide, molybdenum sulfide, lead sulfide, and zinc sulfide with appropriate concentration of inorganic salts in the media. Recent studies have focused on the synthesis of silver nanoparticle via biosorption involving the spp. of *Lactobacillus*, *Enterococcus*, *Pediococcus*, and *Pentosacues* with wide-scale industrial relevance. Some of the physical, chemical, and biological approaches used for nanoparticle synthesis are presented in Fig. 1.

3 Characterization techniques for nanoparticles

The increasing interest on nanotechnology has played significant role in characterizing nanoparticles with health and associated environmental impact. Several studies have been tried for nanoparticle characterization in a reliable and robust way. Different physicochemical methods have been used

This book belongs to Central Library BADJI Mokhtar-ANNABA UNIVERSITY Copyright Elsevier 2024

for the determination of shape, size, structure, and chemical composition of nanoparticles. The growing interest in this field is due to the fact that the nanoscale materials are endowed with much more features as compared with their bulk counterpart and these enhanced features are given by its high surface-to-volume ratio. As a result the nanoscale material shows a mounting growth trend in reactivity at its molecular level. The features that distinguish the nanostructures from its bulk counterpart include optical, mechanical, chemical, and electronic properties (Thanh, Maclean, & Mahiddine, 2014). Due to rapid increase in interest in the field, much stress has been given toward the synthesis of these nanostructures, which may include mechanical, chemical, and biobased methods of synthesis (Koczkur, Mourdikoudis, Polavarapu, & Skrabalak, 2015). Currently, numerous additional nanomaterials have been reported to be synthesized in huge amount than few years before, which is much essential for the development of more exact and acceptable protocols, which would help them for their proper characterization. But unfortunately, several times, these characterizations remain incomplete due to the shortcomings that these are too small in size and are produced in quite less quantities in laboratory conditions, as compared with the bulk ones. In addition, the multidisciplinary aspects of nanoscience and nanotechnology do not empower the researchers to have a proper and easy access to a wide scale of characterization facilities. It has therefore become necessary for in-depth characterization of nanoparticles, necessitating an all-inclusive approach, with the help of combinative techniques in a much complemented manner. So, for the study or characterization of a particular parameter of nanoparticle, it is very important to know both sides of a coin, that is, the strength and limitation of individual techniques to have a proper approach toward the use of a single technique or a combination of different techniques to give decisive and dependable information.

With the context of the preceding text, few methods or techniques have been described broadly for the characterization of nanoparticles. For instance, a single technique may be used specifically for studying a particular property, or sometimes, more than one technique may be used in combination with study the same in much better way (Kim, Connor, Song, Kuykendall, & Yang, 2004). Different techniques may be studied further in a comparative way to pick out the most appropriate technique for analyzing a definite parameter by considering factors such as cost, simplicity, precision, their availability, nondestructive nature, selectivity, and affinity toward certain compositions or materials.

Variable physicochemical, optical, and ferromagnetic techniques for nanoparticle characterization include microscopy-based techniques, namely, atomic force microscopy (AFM), scanning electron microscopy (SEM), transmission electron microscopy (TEM), and scanning tunneling microscopy (STM), which give information on the surface morphology of nanoparticles, its size, and crystal structure. Further, vibrating sample magnetometer (VSM), ferromagnetic resonance (FMR), X-ray magnetic circular dichroism (XMCD), thermogravimetric analysis (TGA), secondary ion mass spectrophotometry (SIMS), and electron energy loss spectroscopy (EELS) are key techniques specialized for quick examination of atomic information, surface plasmon reaction, phase aggregation, 3-D tomography, and particle homogeneity. Many more techniques based on scattering of light such as X-rays, spectroscopy, electron backscatter diffraction (EBSD), magnetic force microscopy (MFM), and tunable resistive pulse sensing (TRPS) positively concentrate on nanoparticle motion, growth kinetics, superlattice structure, and colloidal chemistry. Brief description of commonly used characterization techniques with major information is mentioned in the section in the succeeding text and in Table 1.

This book belongs to Central Library BADJI Mokhtar-ANNABA UNIVERSITY Copyright Elsevier 2024

Table 1 Different parameters and instrumental techniques for characterization of nanoparticles.

Parameters for characterization	Characterization techniques	Major informations	References
Shape and external structure	Scanning electron microscopy (SEM), transmission electron microscopy (TEM), atomic force microscopy (AFM), matrix-assisted laser desorption ionization (MALDI), inductively coupled plasma emission spectroscopy (ICP-MS), and UV-visible spectroscopy	Size of nanoparticle, nanoparticle concentration, elemental composition, and size distribution	Tiede et al. (2008), Peters et al. (2011), Patra and Baek (2014)
Elemental composition and oxidation state	Nuclear magnetic resonance (NMR), inductively coupled plasma optical emission spectrometry (ICP-OES), X-ray absorption spectroscopy (XAS), electron energy loss spectroscopy, and X-ray photoelectron spectroscopy	Density, arrangement, elemental composition, and tomography	Cosandey, Su, Sina, Pereira, and Amatucci (2012), Suleiman, Hu, Peng, and Huang (2009), Mourdikoudis, Pallares, and Thanh (2018)
Optical visualization	UV-visible spectroscopy, scanning transmission electron microscopy (STEM), dynamic light scattering (DLS), electron dispersion, and ferromagnetic resonance (FMR)	Surface composition, surface charge, density, dispersion of nanoparticles, and structural defects	Mourdikoudis et al. (2018), Hoo, Starostin, West, and Mecartney (2008), Lacava et al. (2001)
State of agglomeration	Differential scanning colorimetry (DSC), differential light scattering, cryogenic transmission electron microscopy (CR-TEM), and electron backscatter diffraction (EBSD)	Crystal lattice, particle visualization in 3D format, aggregation, and agglomeration of nanoparticles	Castelli, Puglia, Sarpietro, Rizza, and Bonina (2005), Jores et al. (2004), El-Deab (2009)
Magnetic characterization	High-temperature scanning SCQUID microscopy, magnetic force microscopy (MFM), X-ray magnetic circular dichroism (XMCD), and vibrating sample magnetometer (VSM)	Interior location of nanoparticles, imaging with magnetic moments, atomic information at the bulk plasmon resonance	Sun et al. (2002), Schreiber et al. (2008), Bellucci, Cataldo, Tagliaferro, Giorcelli, and Micciulla (2019), Gupta and Wells (2004)

Continued

This book belongs to Central Library BADJI Mokhtar-ANNABA UNIVERSITY

Copyright Elsevier 2024

Table 1 Different parameters and instrumental techniques for characterization of nanoparticles—cont'd

Parameters for characterization	Characterization techniques	Major informations	References
Crystallization and ligand binding	Extended X-ray absorption fine structure (EXAFS), X-ray diffraction (XRD), secondary ion mass spectrometry (SIMS), thermogravimetric analysis (TGA), small-angle neutron scattering (SANC), and electron diffraction	Colloidal chemistry, crystal particles, order/disorder atomic transformation, homogeneity, and phase alteration	Frenkel, Yevick, Cooper, and Vasic (2011), Kim et al. (2007), Zhu et al. (2015)
Concentration, density, and particle properties	Resonant mass measurement (RMM), tunable resistive pulse sensing (TRPS), percutaneous transluminal angioplasty (PTA), single-particle inductively coupled plasma emission spectroscopy (SP-ICP-MS), and high-resolution transmission electron microscopy (HR-TEM)	Polycrystalline, nanocrystalline, and amorphous nature of nanoparticles, surface spin, atomic composition, and elemental distribution	Sikora, Shard, and Minelli (2016), Bomila, Suresh, and Srinivasan (2019), Golchin, Farahany, Khojasteh, Soleimanifar, and Ardeshirylajimi (2019)
Matricular dispersion, hydrodynamic radius, and micelle macromolecular concentration	Fluorescence correlation spectroscopy (FCS), dynamic light scattering (DLS), absorption spectroscopy, atomic force microscopy (AFM), and scanning tunneling microscopy (STM)	Roughness, density, surface topology, surface reaction, magnetic defects, and electron valence density	Jungjohann et al. (2019), Centrone, Hu, Jackson, Zerbi, and Stellacci (2007), Hoo et al. (2008)
Surface charge, symmetry, and functional groups of nanoparticles	Fourier transform infrared spectroscopy (FTIR), matrix-assisted laser desorption ionization (MALDI), size exclusion chromatography (SEC), Mossbauer, and X-ray magnetic circular dichroism (XMCD)	Electronic state-binding energy of nanoparticle, functional group analysis, peak broadening, heterogeneity, and intensity turbidity	Dabrzalska et al. (2016), Fauth, Goering, Schütz, and Kuhn (2004), Bootz, Russ, Gores, Karas, and Kreuter (2005)
Particle growth kinetics, thickness, and surface area	Liquid transmission electron microscopy (L-TEM), small-angle X-ray scattering (SACS), nuclear magnetic resonance (NMR), cryogenic transmission electron microscopy (cryo-TEM), liquid nuclear magnetic resonance (L-NMR), and Brunauer-Emmett-Teller surface area analysis	Superlattice nanoparticle growth mechanistic, magnetic, and self-assembled particle aggregation	Cheng, Wang, Chen, and Bao (2005), Zhang and Tsapatsis (2011), Neto, Diniz, and de Oliveira (2013); Zou et al., 2019

This book belongs to Central Library BADJI Mokhtar-ANNABA UNIVERSITY

Copyright Elsevier 2024

3.1 Microscopic techniques

Different microscopic techniques have been utilized to learn the shape and surface structures of nanoparticles. Brief description of commonly used microscopic methods is described in the section in the succeeding text.

3.1.1 Electron microscopic methods: Transmission electron microscopy (TEM), scanning electron microscopy (SEM), and low-voltage electron microscopy (LVEM)

The method is used for obtaining two-dimensional images of nanoparticle, and it works on the principle of scattering of electrons. Transmission and scanning electron microscopy are the two most accepted and approved techniques most frequently used for direct or indirect characterization of the surface and structural properties of nanomaterials (Egerton, 2008). Use of these two techniques depends upon the kind of information to be obtained. They basically differ in their surface sensitivity (Zhang, Wang, Liu, Chen, & Liu, 2003). TEM basically helps in understanding the differences between the particles present at the surface and in bulk material (Derrien, Hassoun, Panero, & Scrosati, 2007). It helps in analyzing the morphological aspects of crystal and crystalline electrode materials that may include oxides (Chen, 2007; Alloyeau et al., 2009), metals (Mayhew, Mühlfeld, Vanhecke, & Ochs, 2009), and electrochemically used metal nanopowders (Braun, Cho, Pikul, King, & Zhang, 2012; Song, Park, Alamgir, Cho, & Liu, 2011).

SEM is another important method for nanoparticle characterization to decipher varied size, shape, crystal organization, composition, and electrical conductivity of nanoparticles. SEM helps not only in determining the morphological aspects but also in obtaining the composition of the nanomaterials studied. SEM attached with energy-dispersive X-ray spectroscopy (EDX) critically examines different metal morphologies and conducts the analysis of chemical composition of nanoparticles (Zhang, Liu, Shen, & Gurunathan, 2016). Major limitation of SEM is not restricted to not only the determination of internal structure but also the degree of purity and particle aggregations; however, for easy recognition up to 10 nm, high resolution is essential required.

In comparison with TEM, SEM does not need extensive preparation of specimen, and it does not impart much restriction on the size of the specimen (Shimizu & Mitani, 2009). Moreover, both SEM and TEM have several variants such as scanning transmission electron microscopy (STEM), Z-contrast transmission electron microscopy (Z-TEM), high-resolution transmission electron microscopy (HR-TEM), environmental scanning electron microscopy (E-SEM), and wet scanning electron microscopy (Wet-SEM), which actively participate in shape and surface characterization of nanoemulsions, nanogels, and metal nanoparticles. E-SEM and Wet-SEM technology directly use nonmodified and wet samples with capsular forms (Tiede et al., 2008).

3.1.2 Scanning probe microscopy: Atomic force microscopy (AFM) and scanning tunneling microscope (STM)

AFM is utilized for the investigation of aggregation, way of dispersion, and surface topography of nanoparticles with piezoelectric properties throughout the specimen in X-, Y-, and Z-directions. The tip of AFM is mounted over cantilever to direct the forces or molecular interaction with surface of the specimens. Laser-attached photodetector measures the deflection and particle structures as image complexing arrays (Xia, Biswas, Li, & Brueck, 2004). Major limitation of AFM includes

This book belongs to Central Library BADJI Mokhtar-ANNABA UNIVERSITY Copyright Elsevier 2024

overestimation in lateral dimensions with respect to cantilever. However, Li and Lindsay (1991) proposed nanoparticle role as important calibration standard for AFM imaging.

A variant of AFM is scanning tunneling microscopy (STM) that helps in determining the electronic and topographic structures of specimens at the atomic levels. It is useful in the field of microelectronics, biology, and materials science (Claridge, Schwartz, & Weiss, 2011). STM characterizes nanosuspensions in liquid and gaseous conditions at high vacuum pressure.

4 X-ray methods: X-ray photoelectron spectroscopy (XPC) and X-ray diffractometry (XRD)

Comparable size of the atoms with the aid of X-ray wavelength (0.01–10 nm) provides a method suitable for analyzing and probing the atomic and molecular structure of different nanoparticle samples. X-rays have the ability to penetrate deeper inside the sample specimen, and hence they are supposed to provide information related to the surface structures and the bulk material. This method is further divided into X-ray photoelectron spectroscopy (XPS) and X-ray diffraction (XRD).

XPS is generally used to gather local binding information of nanoparticles under high vacuum conditions. XPS is also called as electron spectroscopy for chemical analysis (ESCA) and provides quantitative, qualitative, and speciation information for sensor analysis (Titus, Samuel, & Roopan, 2019). In this technique, beams of synchrotron radiations pass through nanoparticles and atomize it. Pressure in the vacuum chamber is maintained at 10^{-6} mbar. Irradiation of X-ray causes changes in electron profile of nanoparticles and alteration in kinetic energy based on binding efficiency of C=O, C-O, C-S, -NH2, and P=S macromolecules (Sun, Li, Cao, Zhang, & Wang, 2006).

XRD is one of the important analytical techniques for measuring crystallinity, amorphousness, and particle sizes of various groups of nanoparticles (Mallikarjuna et al., 2011). It follows different diffraction patterns based on the diffracted beam quality throughout nanoparticle. XRD generally works on Bragg's law with wide angle X-ray scattering. It provides structural, crystal, and atomic fingerprint of different nanoparticles with standard diffraction pattern. The diffraction pattern is focused on photographic plate with specific angle dispersion (Banala, Nagati, & Karnati, 2015).

5 Spectroscopic analysis

Different spectroscopic techniques with modified electron and light supplies are used for characterization of fabricated nanoparticles based on local density of photonomic state and spatial resolution nanoparticle sample. An overview of different spectroscopic methods for nanoparticle characterization is discussed in the following section.

5.1 UV-visible spectroscopy

UV-visible spectroscopy is a commonly used fast, easy, and sensitive technology for characterization of colloidal nanoparticles with respect to specific wavelength of light. It also involves the oscillation of nanoparticles through surface plasmon resonance and electromagnetic waves. It allows the information of aggregation, stabilization, and surface interaction of nanoparticles with absolute involvement of

This book belongs to Central Library BADJI Mokhtar-ANNABA UNIVERSITY Copyright Elsevier 2024

standard calibration curve (Das, Nath, Chakdar, Gope, & Bhattacharjee, 2009). Different absorption bands assigned for specific surface plasmon are observed at the size ranges of 2–500 nm. Nanoparticles prepared through biological methods have specific surface plasmon resonance peak, which maintain their stability up to 12 months after preparation.

5.2 Dynamic light scattering (DLS)

DLS also called photon correlation spectroscopy (PCS) is a commonly used technique for the determination of particle size mainly for colloidal nanoparticles using radiation scattering technology. It is used to measure the size of nanoparticles in the range of 2–500 nm. Measurement of light scattering depends on Rayleigh scattering of colloidal nanoparticles. Size measured through DLS techniques is commonly greater than SEM and TEM measurement due to the involvement of Brownian motion. DLS especially works on monomodal samples, while for bimodal samples accuracy cannot be detected for diameter of particles. For bimodal samples the ratio of size has been reported to fall within the range from 2:1 to 3:1 (Hoo et al., 2008).

5.3 Fourier transform infrared spectroscopy (FTIR)

FTIR is a frequently used spectroscopic technique for identification of different molecular functional groups involving chemical bonds and vibrational frequencies of nanoparticles. Vibrational transitions based on infrared irradiations are directly measured through qualitative and quantitative analysis. Significant results for surface binding of nanoparticles with specific polymers may vary depending on the adsorption of functional group ligands (Rana, Philip, & Raj, 2010). Furthermore, FTIR confirms the covalent interaction of functional groups with specific signal-to-noise ratio. Attenuated total reflectance (ATR) FTIR is specifically concerned with the toxic effect of metals, carbon nanoparticles, and quantum dots. FTIR microspectroscopy is a microscope-attached spectroscopic technique used for replica stamping. Absorbance intensity of different bands varies upon transmittance, and ATR FTIR depends on the thickness and bulk property of nanoparticles (Mudunkotuwa, Al Minshid, & Grassian, 2014). Major advantages of FTIR are higher accuracy and stability, more signal-to-noise ratio, and significant energy throughput in the nanoparticles.

6 Nanoparticle filtration techniques

Stability of nanoparticles depends on their molecular structure associated with surrounding physicochemical parameters. Aggregation, storage, and residence property of nanoparticles may influence their uptake and transport behavior. Commonly used filtration technique for separation, fractionation, and characterization of nanoparticles are field-flow fractionation (FFF), cloud point extraction (CPE), cross-flow filtration (CFF), ultracentrifugation, and ultrafiltration. FFF is similar to HPLC and characterizes nanoparticles based on their sedimentation pressure, hydraulic pressure, and electrical conductivity. Schimpf, Caldwell, and Giddings (2000) reported FFF as flexible separation technique, which measures the nanoparticle with size ranging from 1 nm to 100 μm. Combined utilization of FFF with ICP-MS and UV-visible spectroscopy could help in quantitative determination of the size of metallic nanoparticle. FFF is possibly coupled with different separation channels and detected

This book belongs to Central Library BADJI Mokhtar-ANNABA UNIVERSITY Copyright Elsevier 2024

through several multidetector approaches. CPE is performed by the addition of specific surfactants with colloidal nanoparticles (López-Serrano, Olivas, Landaluze, & Cámara, 2014). At higher concentration of surfactants, nanoparticles produce micelle-like structure with involvement of nonpolar materials at the outer side. For the separation of silver nanoparticles, density is a major factor, which accelerates centrifugation-based separation procedure. Separation of nanoparticles through CFF causes major changes in diffusion coefficient involving proper polarization and dead-end filtration. Ultracentrifugation is one of the versatile nanoparticle separation technologies with particle size ranging between 25 kDa and 1.5 mDa.

So far, different chromatographic techniques have been used for separation of nanoparticles. Varied prefractionation methods for separation of nanoparticles include size exclusion chromatography (SEC), ion-exchange chromatography (IEC), hydrodynamic chromatography (HDC), and high-performance liquid chromatography (HPLC). In chromatography, separation of nanoparticles is based on the interaction of ionic charges, polarity, hydrophobic interaction, and molecular mass of the samples. Size exclusion and ion-exchange chromatography are practically used for separation and characterization of food nanoparticles (Luykx, Peters, van Ruth, & Bouwmeester, 2008). Tiede et al. (2008) reported separation of nanoparticles in food and agricultural industries by using hydrodynamic chromatography (HDC) based on the hydrodynamic diameter of nanoparticles. Shape and size of nanoparticles are detected through HDC attached UV-visible spectroscopy with specific standard calibration curve.

7 Characterization of magnetic features of nanoparticles

Magnetic properties of nanoparticles are based on the differences in orbital motion atomic current loop magnetic behavior with basic diamagnetism, ferromagnetism, antiferromagnetism, ferrimagnetism, and paramagnetism responses (Faraji, Yamini, & Rezaee, 2010). Different superparamagnetism phases are developed during fluctuation of temperature and dynamic crystallographic orientations. Commonly used techniques for measurement of magnetic properties of nanoparticles include vibrating sample magnetometry (VSM), SQUID magnetometry, and nuclear magnetic resonance (NMR).

VSM is used to measure the magnetic correlation of metal nanoparticles in between the field of −3 and 3 T. The superparamagnetic plateau and VSM saturation magnetization curve estimate the surface spin, magnetic ordering, and magnetic anisotropic energy (Yan, FitzGerald, Crawford, & Mefford, 2019). SQUID magnetometry commonly monitors the remnant magnetization based on the range of higher to lower temperatures with significant blocking temperature and demagnetization imperfection of nanoparticles (Lee, Jeong, Shin, Kim, & Kim, 2004).

8 Effect of nanomaterials on seed germination

The agriculture majorly relied on the quality of seeds, vigor, and productivity. In other words, seeds are the strong foundation for present-day agricultural practices and hence for human survival. Approximately, 75% of calories in human food are obtained from seeds (Sreenivasulu & Wobus, 2013). Most importantly, seeds are essentially required for the multiplication of diverse plants not able to regenerate in a vegetative manner. Thus seeds are the hidden plants serving as the parents for new plants.

This book belongs to Central Library BADJI Mokhtar-ANNABA UNIVERSITY
Copyright Elsevier 2024

Generally, seed is surrounded by a covering called seed coat encircling endosperm and embryo. Germination of seed is an important step during the establishment of plant in a given environmental condition. The mechanism of seed germination may be categorized into three distinct phases: (1) water absorption (imbibition), (2) induction or lag phase, and (3) root emergence (Rajjou et al., 2012). Seed germination as a complicated process may be distinguished into three main parts: (i) fast movement of water, enhancement in respiration rate, energy generation, and commencement of breakdown of stored materials; (ii) rapid mobilization of molecules, reduction in respiratory activity, and uptake of water; and (iii) reorganization of accumulated molecules into chemical forms necessary for the development of embryonal axis (Bewley, Bradford, Hilhorst, and Nonogaki, 2013). For decades, numbers of techniques have been employed to enhance the seed biological activity in changing environmental conditions, and seed germination has been utilized as an important parameter to evaluate the toxicity of chemicals intended for agricultural applications. Most of the seeds have been reported to germinate upon the commencement of favorable environmental conditions. However, seeds of some plant species do not germinate even under the favorable conditions reported for germination. This phenomenon is scientifically described as dormancy. Worldwide the recent developments in nanotechnology have considerably affected the agricultural productivity (Achari & Kowshik, 2018). However, the wide application of nanotechnology in the agriculture sector is very much limited because of complexity of agriculture ecosystems. Integration of nanotechnology in the seed science may enhance the germination, vigor, and productivity under optimal environmental conditions. In this context, synthesis of nanomaterials and their priming with seeds could have potential benefits on different physiological processes of plants including improved seed germination (Raja et al., 2019) and vigor. Nevertheless, there is raising concerns among researchers pertaining to the unintentional hazardous impacts of nanomaterials on humans and other life forms once released into the natural environment (Das et al., 2017; Verma et al., 2018). Their negative impacts on soil microbial system (Avila-Arias, Nies, Gray, & Turco, 2019), soil nutrient availability (Duncan & Owens, 2019), and soil-inhabiting arthropods (Bouguerra et al., 2019) and annelids (Bourdineaud et al., 2019; Lapied, Moudilou, Exbrayat, Oughton, & Joner, 2010) may lead to reduced crop productivity and detrimental consequences on natural ecosystem. Therefore the development of state-of-art technologies for the determination of their minute quantity in a given environmental matrix would be helpful in mitigating the impacts of nanomaterials. The application of nanomaterials in the agriculture sector should be based on multiple experimental investigations under laboratory and field conditions directed toward toxicological assessment to better understand their fate, hazardous impacts, and behavior.

Both positive and negative outcomes of nanomaterial application on seed germination have been documented. Some of the important findings associated with impact of nanomaterials on seed germinations are presented here.

The good germination of cow pea (*Vigna unguiculata*) seeds soaked with copper nanoparticle at a concentration equivalent to 100 ppm as compared with iron and zinc oxide nanoparticle is documented by Suriyaprabha, Sreeja, Prabu, Prabu, and Rajendran (2018). At first day, 100-ppm concentration of copper oxide nanoparticle resulted into hundred percent seed germination, whereas treatment with other concentrations (500, 1000, and 2000 ppm) could not lead to complete germination at day 1. At the second day after seed treatment, the hundred percent germination was exhibited by copper oxide and zinc oxide nanoparticle at 500 and 1000 ppm, respectively. For iron oxide nanoparticles the full germination of all treated seeds was observed at 500-ppm concentration on the third day. The increase in concentration of zinc oxide and iron oxide nanoparticles up to 1000 ppm was directly correlated with

This book belongs to Central Library BADJI Mokhtar-ANNABA UNIVERSITY
Copyright Elsevier 2024

coleoptile growth. Overall, seeds treated with selected nanoparticle demonstrated positive influence on the length of coleoptiles as compared with control sets. The improved coleoptile growth was reported for nanoparticle-treated sets and ascribed to the transport of nanoparticles inside the seed. Entry and storage of synthesized nanoparticle inside the seed were confirmed through X-ray photoelectron spectroscopy (XPS).

Effect of different concentrations of zinc oxide nanoparticle on wheat seed germination is recently presented (Du, Yang, Peng, Liang, & Mao, 2019). The bulk material ($ZnSO_4 \cdot 7H_2O$) was found to exert more inhibitory impact on seed germination, root, and shoot length along with dry matter at higher concentration as compared with their nanoparticulate forms. Further the bulk material was noticed to induce structural deformity and modulation of enzymic activities than reported for zinc oxide nanomaterials. The rate of seed germination was considerably reduced at higher dose of zinc oxide nanoparticles (1000 ppm), whereas at concentration below 200 ppm there was insignificant impact. Further, ZnO treatment had no apparent effect on germination potential and germination index.

Zhang et al. (2015) have described the negligible impacts of ZnO nanoparticles on maize seed germination at concentration equivalent to 1000 ppm. The differences in the biological effects of nanoparticles may be due to differing sensitivity of different plant species and the size of seeds selected. The ionic form of zinc at 100-ppm concentration was able to inhibit the germination of cucumber seeds, while negligible impact of ZnO nanoparticles on germination was documented.

Effect of copper oxide nanoparticles on germination of lettuce and carrot seed was represented by Margenot et al. (2018). Copper oxide nanoparticle concentration around 800 ppm could not exert inhibitory effect on germination of selected seed. Although CuO nanoparticle at a concentration equivalent to 40 ppm negatively affected the seed germination, the effects were insignificant. Contrary to this the bulk copper at concentration around 5.0 ppm and higher caused reduced germination of seeds of both plants. This study leads to the fact that the release of copper ions from nanoparticle had no inhibitory action on seed germination showing contrasting results with those reported by earlier workers (Dimkpa et al., 2012; Shaw & Hossain, 2013; Stampoulis, Sinha, & White, 2009; Tang et al., 2013). Such differences in the outcomes regarding the seed germination may result from (i) the interaction of CuO nanoparticles with seed surface and alleviation of copper toxicity and (ii) inhibitory effects of chloride ions present in copper chloride. The toxicity of nanoparticles could also be affected by the seed coat characteristics such as thickness and chemical composition.

Globally, there is rapid upsurge in the application of silver nanoparticles in the medicine (as antiviral, antibacterial, antifungal, etc.), food technology, and agriculture because of potential benefits to human society. Reduction in germination index of *Allium cepa* seeds caused by silver nanoparticle is mentioned in the literature (Scherer et al., 2019). The pronounced effect in terms of reduced germination index of *Allium cepa* was, however, documented for particle with size 10 nm. The effect on seed germination has been represented to be affected by the nanoparticle concentrations and sensitivity of particular plant seeds. Studies by different workers have reached to the conclusion that the effect on seed germination imposed by nanoparticle could not be considered as the only parameter for determining the toxicity to plant system (Stampoulis et al., 2009).

Currently the impact of nanomaterials on biological systems is a challenging issue. Since the physicochemical attributes of nanomaterials are very much different to parent compound, they could be envisaged to put forth considerable effects on natural ecosystems and human health. Because of size below 100 nm, at least in one dimension, they are able to traverse the biological membranes easily. Adhikari, Kundu, Biswas, Tarafdar, and Rao (2012) have demonstrated the impact of CuO

This book belongs to Central Library BADJI Mokhtar-ANNABA UNIVERSITY Copyright Elsevier 2024

nanoparticles having size lower than 50 nm on soybean and chick pea seed germination. The CuO nanoparticle had no inhibitory effect on germination at a concentration equivalent to 2000 ppm, while 200 ppm of copper ions alone suppressed seed germination indicating the differences in chemical characteristics of bulk and nanostructured material. Further the CuO nanoparticle retarded the root growth at 500-ppm concentration suggesting the direct interaction of nanoparticle with root surface as a mechanism of inhibition of root elongation. Seed coat might adsorb the sufficient amount of CuO nanoparticle and thus may minimize the associated phytotoxic impacts of germination.

There are multiple reports indicating the application of engineered nanomaterials as pesticides and fungicides and as nanofertilizers to control the loss of stored seeds caused by insect and fungal pathogens and to enhance the crop productivity, respectively. Further, engineered nanomaterials could have regulatory impact on seed germination (Khodakovskaya, De Silva, Biris, Dervishi, & Villagarcia, 2012) and growth of different plant species. Under these scenarios the metal engineered nanomaterials should be evaluated for their toxicity to seed germination and seedling growth. Wang et al. (2019) have described the negligible effect of titanium dioxide (TiO_2) nanoparticles on wheat seed germination at a dose of 50 and 500 mg kg^{-1}. Insignificant toxicity to seed germination could be considered for application of TiO_2 in agricultural practices; however, further phytotoxicity tests based on root and shoot growth and biomass must be conducted to validate its future exploitation.

To date, large numbers of carbohydrate-based nanoparticles have been used in food and agriculture indicating its suitability. The effect of chitosan nanoparticle on germination of wheat seed is currently published (Li et al., 2019). The comparative analysis of effect of chitosan nanoparticle and chitosan on seed germination was examined in the range of 1–100 ppm concentration. The study revealed positive influence of chitosan nanoparticle on seed germination and seedling growth at lower concentration (5 ppm) as compared with chitosan (50 ppm). Improved seed germination and seedling growth rendered by chitosan nanoparticle was ascribed to the considerable adsorption of nanoparticles on seed as confirmed through energy-dispersive spectroscopy (EDS) and confocal laser scanning microscopy (CLSM). The improved seed germination was attributed to the smaller size and larger surface area of chitosan nanoparticles. The stimulatory effect of chitosan nanoparticles on seed germination has also been reported for *Zea mays*, *Brassica rapa*, and *Pisum sativum* (Nakasato, Pereira, Oliveira, Oliveira, & Fraceto, 2017). Some of the nanoparticles and their impact on seed germination are presented in Table 2.

9 Mechanism of nanoparticle action

Nanoparticles get entry inside the seed during the imbibition of water. Some of the nanoparticles may also tend to adsorb on the surface of seed coat. Transport of nanoparticles into seeds generally occurs via the void spaces present in parenchymatous tissues and has been proposed to assist in its movement toward cotyledons (Lee et al., 2010; Ma et al., 2010). Surface adsorption via seed coat may restrict either the positive or negative influence of nanoparticles on seed germination, seedling emergence, length of radicle and plumule, fresh weigh, antioxidant enzymatic activities (Movafeghi et al., 2018), and important physiological processes including photosynthesis and respiration. Entry, surface binding, accumulation, and effects of nanoparticles on cellular processes are presented in Fig. 2.

So far, no definite mechanism regarding the potential mechanism of action of nanoparticles has been proposed. The negative consequences of nanomaterial actions as proposed by different workers

This book belongs to Central Library BADJI Mokhtar-ANNABA UNIVERSITY Copyright Elsevier 2024

Table 2 Some examples of effect of different nanomaterials on seed germination.

S. No.	Nanoparticles (NPs)	Plant seed	Remarks	References
1.	CoO	*Zea mays*, *Avena sativa*, *Lycopersicon lycopersicum*, and *Brassica oleracea*	Significant inhibition in percent seed germination of *Lycopersicon lycopersicum* at 1000 mg kg^{-1} nanomaterial; no significant effect on seed germination of *Zea mays*, *Avena sativa* and *Brassica oleracea*	Bouguerra et al. (2019)
2.	ZnO	Peanut	Positive influence on seed germination	Prasad et al. (2012)
3.	ZnO	Pomegranate	Improvement in seed germination	Davarpanah, Tehranifar, Davarynejad, Abadía, and Khorasani (2016)
4.	ZnO	Rye grass	Inhibition of seed germination at 200 mg L^{-1} concentration	Nhan et al. (2015)
5.	ZnO	*Brassica pekinensis*	Nanoparticle did not impose negative effect on seed germination rate up to 80-mg L^{-1} concentration	Xiang et al. (2015)
6.	ZnO	*Vigna radiata*	Improved seed germination after 4 hours treatment with nanoparticles	Jayarambabu, Kumari, Rao, and Prabhu (2014)
7.	ZnO	Eggplant	Nanoparticle displayed inhibitory effect on seed germination in MS medium, while positive effect on seed germination was recorded in soil system; with increase in concentration of ZnO NPs in MS media, percent seed germination was negatively affected, whereas in soil system amended with increasing doses of NPs, there was increase in percent seed germination	Thunugunta et al. (2018)
8.	ZnO, TiO_2, CuO, Ag	*Avena sativa* and *Trifolium alexandrinum*	Treatment was done at 750, 1000, and 1250 mg of NPs per kilogram of seeds; low concentration was able to increase seed germination except NPs of TiO_2 and CuO	Maity et al. (2018)

This book belongs to Central Library BADJI Mokhtar-ANNABA UNIVERSITY
Copyright Elsevier 2024

Table 2 Some examples of effect of different nanomaterials on seed germination—cont'd

S. No.	Nanoparticles (NPs)	Plant seed	Remarks	References
			in berseem; at lower concentration (750 mg kg^{-1}), different types of NP treatment resulted into complete seed germination of oat, while only Ag NPs could enhance the seed germination in berseem	
9.	Ag	*Lolium multiflorum*, *Panicum virgatum*, *Carex lurida*, *Carex scoparia*, *Carex vulpinoidea*, *Carex crinita*, *Eupatorium fistulosum*, *Phytolacca americana*, *Scirpus cyperinus*, *Lobelia cardinalis*, *Juncus effusus*	Gum arabic–coated Ag NPs significantly retarded the growth of *Scirpus cyperinus*, *Juncus effusus*, *Phytolacca americana* in pure culture experiment. No effect on germination was recorded for other seeds	Yin, Colman, McGill, Wright, and Bernhardt (2012)
10.	TiO_2	*Triticum aestivum*	Improved seed germination at lower concentration; higher concentration suppressed the seed germination; lower concentration of TiO_2 reduced the germination times; reduction in seed germination time at 10 ppm was ascribed to the facilitated water absorption rendered by nano-TiO_2	Feizi, Moghaddam, Shahtahmassebi, and Fotovat (2012)
11.	TiO_2	*Linum usitatissimum, Solanum lycopersicum and Vigna radiata*	Treatment with NPs having size 15-nm reduced seed germination and root biomass after; low concentration of NPs displayed weak phytotoxicity as compared with higher concentration; for root biomass synthesis the higher concentration of NPs (15 nm TiO_2) was less toxic as compared with lower concentration; treatment with TiO_2 having size equivalent to 25 and 32 nm represented stimulatory effect on seed germination and root growth	Clément, Hurel, and Marmier (2013), Singh et al. (2016)

Continued

This book belongs to Central Library BADJI Mokhtar-ANNABA UNIVERSITY

Copyright Elsevier 2024

Table 2 Some examples of effect of different nanomaterials on seed germination—cont'd

S. No.	Nanoparticles (NPs)	Plant seed	Remarks	References
12.	TiO_2	Switch grass (*Panicum virgatum*)	TiO_2 at 2.5% concentration reduced the mean seed germination by approximately 50% as compared with control sets; the concentration below 2.5% did not exert negative effect on seed germination	Boykov, Shuford, and Zhang (2018)
13.	Nano Fe^0 and Ag	Ryegrass, barley, and flax	Nanozerovalent iron (nZVI) and Ag NP suppressed the germination at 250 and 10 ppm, respectively; complete suppression of seed germination was recorded at 1000–2000 ppm of nZVI; in soil system, there was minimal effect on toxicity; for sandy soil, nZVI at a concentration equivalent to 750 and 1500 ppm absolutely retarded the germination of flax and ryegrass, correspondingly, while nZVI applied at a concentration of 1500 ppm resulted into 13% germination of barley seeds; the inhibitory effects of seed germination in clay soils were low at the nZVI concentration used for sandy soil	El-Temsah and Joner (2012)
14.	Hydroxyapatite	*Solanum lycopersicum*	No inhibitory action over seed germination with rise in concentration (2–2000 ppm) of hydroxyapatite was detected	Marchiol et al. (2019)
15.	Cu_2O	*Lycopersicum esculentum*	Low concentration (20 ppm) had stimulatory effect on seed germination; beyond 20-ppm-reduced seed germination was noticed	Ananda, Shobha, Shashidhara, and Mahadimane (2019)
16.	Chitosan	*Oryza sativa*	Treatment with chitosan nanoparticle improved the seed germination in rice and could be regarded as germination elicitor; with increase in concentration of nanoparticle, a number of	Divya, Vijayan, Nair, and Jisha (2019)

This book belongs to Central Library BADJI Mokhtar-ANNABA UNIVERSITY
Copyright Elsevier 2024

Table 2 Some examples of effect of different nanomaterials on seed germination—cont'd

S. No.	Nanoparticles (NPs)	Plant seed	Remarks	References
			germinated seeds were noticed to be reduced in definitive test; the synthesized nanoparticles were nonphytotoxic to rice seeds; highest percent germination was found at 1-mg mL^{-1} concentration of nanoparticle; IC_{50} value of chitosan nanoparticle was around 5 mg mL^{-1}	
17.	TiO_2	*Foeniculum vulgare*	Seed germination index was enhanced after treatment with NPs at low concentration; 14 days incubation at 60-ppm concentration of NPs displayed improvement in seed germination; NPs at 40-ppm concentration improved the germination duration up to 31.8% as compared with control ones	Feizi, Kamali, Jafari, and Moghaddam (2013)
18.	SiO_2	*Lycopersicum esculentum*	Application of NPs caused stimulatory effects on seed germination attributes; the optimum favorable concentration for enhancement of seed germination and time for seedling emergence was recorded at 8 g L^{-1}; enhanced seed attributes like germination and time of seed germination were ascribed to be the resultant of absorption and deployment of NPs by seeds	Siddiqui and Al-Whaibi (2014)
19.	Monometallic and bimetallic nanoparticles based on Ag, Au, and Cu	*Silybum marianum*	Nanoparticle treatment significantly enhanced the germination; maximum positive influence was recorded for suspension of silver nanoparticles; mean germination rate of all tested seed was higher than 85%	Khan, Zaka, Abbasi, and Shah (2016)

Continued

This book belongs to Central Library BADJI Mokhtar-ANNABA UNIVERSITY

Copyright Elsevier 2024

Table 2 Some examples of effect of different nanomaterials on seed germination—cont'd

S. No.	Nanoparticles (NPs)	Plant seed	Remarks	References
20.	Multiwalled carbon nanotube, Al, Al_2O_3, Zn, and ZnO	*Raphanus sativus*, *Brassica napus*, *Lolium multiflorum*, *Lactuca sativa*, *Zea mays*, and *Cucumis sativus*	Only Zn-based nanoparticle affected the seed germination in *Lolium multiflorum* and *Zea mays*	Lin and Xing (2007)
21.	Ag, Cu, Au	*Eruca sativa*	Seed germination determined at 42 days revealed optimum positive response for Ag NPs; complete seed germination was observed only for Ag NPs; Ag NPs enhanced the root length, shoot length, and seed vigor index	Zaka, Abbasi, Rahman, Shah, and Zia (2016)
22.	Amine-modified polystyrene and TiO_2	Lettuce	Significant reductions in root and shoot length after exposure to amine-modified polystyrene and TiO_2 were recorded; sulfate-modulated polystyrene did not result into inhibitory effects	Kibbey and Strevett (2019)
23.	Al_2O_3, CuO	*Solanum lycopersicon*	Seed germination was not affected after treatment with NPs. 2000 ppm of CuO NPs suppressed the root and stem growth was considerably minimized (~60%) as compared with control sets	Ahmed, Khan, and Musarrat (2018)
24.	CuO	*Hordeum sativum*	NPs suppressed seed germination by 23% as compared with control ones; decrement in root and shoot growth was recorded as 64.1% and 8.4%, respectively, after 7 days; at fourth week, relative reductions in root and shoot growth were determined as 35.3% and 9.9%, correspondingly	Rajput et al. (2018)
25.	TiO_2, ZnO, Al_2O_3, and CuO	*Raphanus sativus*, *Cucumis sativus*, *Solanum lycopersicon*, and *Medicago sativa*	Inhibition in seed germination after treatment with different NPs; increase in root and shoot growth after treatment with TiO_2 up to certain concentrations; treatment with ZnO NPs and CuO NPs displayed inhibitory effects on root and shoot length	Ahmed, Rizvi, Zaidi, Khan, and Musarrat (2019)

This book belongs to Central Library BADJI Mokhtar-ANNABA UNIVERSITY
Copyright Elsevier 2024

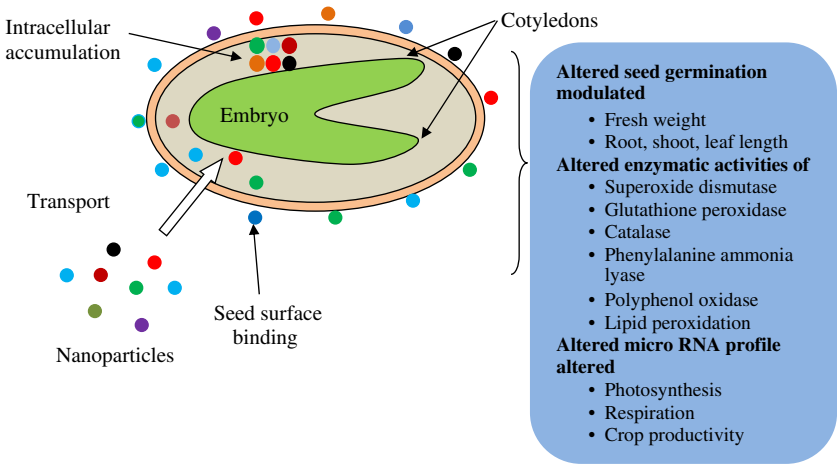

FIG. 2

Entry, surface binding, accumulation, and effects of nanoparticles on cellular processes.

are concerned with (i) very low size of NPs facilitating easy entry inside cell and transportation to different parts of cellular organisms (Ma, Lü, & Huang, 2011; Yin et al., 2012), (ii) increase in contents of NPs in organisms at higher trophic levels rendered by biological magnification (Judy, Unrine, & Bertsch, 2011), and (iii) large amount accumulation in cellular system due to nondegradability (Yoo-iam, Chaichana, & Satapanajaru, 2014). Studies have shown the potential of accumulated nanoparticles in provoking DNA breakage in plant systems and hence modification in genome integrity (Santos et al., 2010), a promising field of future experimental investigation in the discipline of agriculture sciences. Moreover, the presence of nanoparticles may induce the enhanced expression of stress-related genes (Khodakovskaya et al., 2009), enhanced production of reactive oxygen species (ROS) (Das et al., 2018), and deformation in chromosome morphology (Castiglione, Giorgetti, Geri, & Cremonini, 2011). Conclusively the impact of nanoparticles may be directly related with profound modulations at structural, biochemical, genetic, and physiological level (Rico, Peralta-Videa, & Gardea-Torresdey, 2015). Numerous experimental facts regarding the chemical behavior, transport, and cycling of nanoparticles in natural ecosystem are still unanswered. In this context, knowledge concerned with the entry pathway of NPs, contribution of cell walls during uptake, and effect of NPs on important plant physiological processes especially photosynthesis and respiration still needs in-depth investigation.

10 Conclusion

Engineered nanomaterials synthesized through numerous physicochemical and biological techniques have revolutionized the field of agriculture. Improvement in the nanomaterial characterization tools like SEM, XRD, FTIR, TEM, and XPS and quantification techniques in the field of nanotechnology would be beneficial to identify even the minute quantity of engineered nanomaterials present in a given

This book belongs to Central Library BADJI Mokhtar-ANNABA UNIVERSITY Copyright Elsevier 2024

environmental matrix. Seeds are the foundation for the emergence of new offsprings of different plant species. The exploitation of nanomaterial-based weedicides, fungicides, insecticides, and pesticides has contributed significantly in the management of stored seed losses resulting from insect pests and fungal pathogens. Application of nanomaterials under field condition may improve the seed germination and seedling growth along with the breakage of dormancy. In spite of numbers of advantageous effects associated with the application of nanomaterials in the field of agricultural productivity, the negative effects associated with exploitation of nanomaterial application on seed germination has also been documented. Such differential effect on germination of seeds of different plant species caused by nanomaterial application has been attributed to result from the size of nanoparticles and sensitivity of particular seeds, as well as composition and thickness of seed coat. The toxicity of nanomaterials during the field-scale application may restrict its wide applicability for the purpose of enhancing agricultural productivity. Safety assessment of engineered nanomaterials in a system other than the nontarget including biological ones in which they are submitted should be critically examined to avoid the negative consequences on natural ecosystem. Studies regarding their fate and behavior in the natural environmental conditions including soil and water environment would help understand the management of nanomaterials with possible toxicological significance. Effect of different nanomaterials on seed germination and seedling growth is one of the primary criteria for determining the phytotoxicity of engineered nanostructured materials; nevertheless, this assay on seed system is not enough for determining the toxicity to plant and other biological entities.

Acknowledgment

Authors are extremely thankful to the head of Department of Botany, Banaras Hindu University, Varanasi, and the director of Institute of Environment and Sustainable Development, Banaras Hindu University, for providing necessary facilities.

References

Achari, G. A., & Kowshik, M. (2018). Recent developments on nanotechnology in agriculture: Plant mineral nutrition, health, and interactions with soil microflora. *Journal of Agricultural and Food Chemistry*, *66*, 8647–8661.

Adhikari, T., Kundu, S., Biswas, A. K., Tarafdar, J. C., & Rao, A. S. (2012). Effect of copper oxide nano particle on seed germination of selected crops. *Journal of Agricultural Science and Technology A*, *2*(6A), 815.

Ahmed, B., Khan, M. S., & Musarrat, J. (2018). Toxicity assessment of metal oxide nano-pollutants on tomato (*Solanum lycopersicon*): A study on growth dynamics and plant cell death. *Environmental Pollution*, *240*, 802–816.

Ahmed, B., Rizvi, A., Zaidi, A., Khan, M. S., & Musarrat, J. (2019). Understanding the phyto-interaction of heavy metal oxide bulk and nanoparticles: Evaluation of seed germination, growth, bioaccumulation, and metallothionein production. *RSC Advances*, *9*(8), 4210–4225.

Albanese, A., Tang, P. S., & Chan, W. C. (2012). The effect of nanoparticle size, shape, and surface chemistry on biological systems. *Annual Review of Biomedical Engineering*, *14*, 1–16.

Ali, R. F., Ovens, J., Starosta, K., & Gates, B. D. (2019). Novel defect-fluorite pyrochlore sodium niobate nanoparticles: Solution-phase synthesis and radiation tolerance analysis. *Nanoscale*, *11*(12), 5489–5498.

This book belongs to Central Library BADJI Mokhtar-ANNABA UNIVERSITY Copyright Elsevier 2024

Alloyeau, D., Ricolleau, C., Oikawa, T., Langlois, C., Le Bouar, Y., & Loiseau, A. (2009). Comparing electron tomography and HRTEM slicing methods as tools to measure the thickness of nanoparticles. *Ultramicroscopy*, *109*, 788–796.

Ananda, S., Shobha, G., Shashidhara, K. S., & Mahadimane, V. (2019). Nano-cuprous oxide enhances seed germination and seedling growth in *Lycopersicum esculentum* plants. *Journal of Drug Delivery and Therapeutics*, *9*(2), 296–302.

Asli, S., & Neumann, P. M. (2009). Colloidal suspensions of clay or titanium dioxide nanoparticles can inhibit leaf growth and transpiration via physical effects on root water transport. *Plant, Cell & Environment*, *32*, 577–584.

Avila-Arias, H., Nies, L. F., Gray, M. B., & Turco, R. F. (2019). Impacts of molybdenum-, nickel-, and lithium-oxide nanomaterials on soil activity and microbial community structure. *Science of the Total Environment*, *652*, 202–211.

Banala, R. R., Nagati, V. B., & Karnati, P. R. (2015). Green synthesis and characterization of *Carica papaya* leaf extract coated silver nanoparticles through X-ray diffraction, electron microscopy and evaluation of bactericidal properties. *Saudi Journal of Biological Sciences*, *22*, 637–644.

Bar, H., Bhui, D. K., Sahoo, G. P., Sarkar, P., Pyne, S., & Misra, A. (2009). Green synthesis of silver nanoparticles using seed extract of *Jatropha curcas*. *Colloids and Surfaces A: Physicochemical and Engineering Aspects*, *348*(1–3), 212–216.

Bauer, P. S., Amenitsch, H., Baumgartner, B., Köberl, G., Rentenberger, C., & Winkler, P. M. (2019). In-situ aerosol nanoparticle characterization by small angle X-ray scattering at ultra-low volume fraction. *Nature Communications*, *10*, 1122.

Bellucci, S., Cataldo, A., Tagliaferro, A., Giorcelli, M., & Micciulla, F. (2019). X-ray absorption and magnetic circular dichroism in CVD grown carbon nanotubes. *Materials*, *12*, 1073.

Bewley, J. D., Bradford, K. J., Hilhorst, H. W. M., & Nonogaki, H. (2013). Germination. In *Seeds—Physiology of development, germination and dormancy* (3rd ed., pp. 133–181). New York: Springer.

Bomila, R., Suresh, S., & Srinivasan, S. (2019). Synthesis, characterization and comparative studies of dual doped ZnO nanoparticles for photocatalytic applications. *Journal of Materials Science*, *30*, 582–592.

Bootz, A., Russ, T., Gores, F., Karas, M., & Kreuter, J. (2005). Molecular weights of poly (butyl cyanoacrylate) nanoparticles determined by mass spectrometry and size exclusion chromatography. *European Journal of Pharmaceutics and Biopharmaceutics*, *60*, 391–399.

Borm, P. J., Robbins, D., Haubold, S., Kuhlbusch, T., Fissan, H., Donaldson, K., et al. (2006). The potential risks of nanomaterials: A review carried out for ECETOC. *Particle and Fibre Toxicology*, *3*, 1–35.

Bouguerra, S., Gavina, A., da Graça Rasteiro, M., Rocha-Santos, T., Ksibi, M., & Pereira, R. (2019). Effects of cobalt oxide nanomaterial on plants and soil invertebrates at different levels of biological organization. *Journal of Soils and Sediments*, 1–17.

Bourdineaud, J. P., Štambuk, A., Šrut, M., Radić Brkanac, S., Ivanković, D., Lisjak, D., et al. (2019). Gold and silver nanoparticles effects to the earthworm Eisenia fetida–the importance of tissue over soil concentrations. *Drug and Chemical Toxicology*, 1–18.

Boykov, I. N., Shuford, E., & Zhang, B. (2018). Nanoparticle titanium dioxide affects the growth and microRNA expression of switchgrass (*Panicum virgatum*). *Genomics*. https://doi.org/10.1016/j.ygeno.2018.03.002.

Braun, P. V., Cho, J., Pikul, J. H., King, W. P., & Zhang, H. (2012). High power rechargeable batteries. *Current Opinion in Solid State and Materials Science*, *16*, 186–198.

Castelli, F., Puglia, C., Sarpietro, M. G., Rizza, L., & Bonina, F. (2005). Characterization of indomethacin-loaded lipid nanoparticles by differential scanning calorimetry. *International Journal of Pharmaceutics*, *304*, 231–238.

Castiglione, M. R., Giorgetti, L., Geri, C., & Cremonini, R. (2011). The effects of nano-TiO_2 on seed germination, development and mitosis of root tip cells of *Vicia narbonensis* L. and *Zea mays* L. *Journal of Nanoparticle Research*, *13*(6), 2443–2449.

This book belongs to Central Library BADJI Mokhtar-ANNABA UNIVERSITY

Copyright Elsevier 2024

Centrone, A., Hu, Y., Jackson, A. M., Zerbi, G., & Stellacci, F. (2007). Phase separation on mixed-monolayer-protected metal nanoparticles: A study by infrared spectroscopy and scanning tunneling microscopy. *Small*, *3*, 814–817.

Chau, C. F., Wu, S. H., & Yen, G. C. (2007). The development of regulations for food nanotechnology. *Trends in Food Science and Technology*, *18*, 269–280.

Chen, H. (2007). Expression and purification of the recombinant HBcAg core particles derived from methyltrophic *Pichia pastoris*, and TEM and AFM of the core particles and their natural aggregates. *Journal of Electron Microscopy*, *56*, 235–242.

Cheng, Y., Wang, Y., Chen, D., & Bao, F. (2005). Evolution of single crystalline dendrites from nanoparticles through oriented attachment. *The Journal of Physical Chemistry B*, *109*, 794–798.

Cheng, C., Xu, F., & Gu, H. (2011). Facile synthesis and morphology evolution of magnetic iron oxide nanoparticles in different polyol processes. *New Journal of Chemistry*, *35*, 1072–1079.

Claridge, S. A., Schwartz, J. J., & Weiss, P. S. (2011). Electrons, photons, and force: Quantitative single-molecule measurements from physics to biology. *ACS Nano*, *5*, 693–729.

Clément, L., Hurel, C., & Marmier, N. (2013). Toxicity of TiO_2 nanoparticles to cladocerans, algae, rotifers and plants—Effects of size and crystalline structure. *Chemosphere*, *90*(3), 1083–1090.

Cosandey, F., Su, D., Sina, M., Pereira, N., & Amatucci, G. G. (2012). Fe valence determination and Li elemental distribution in lithiated $FeO_{0.7}F_{1.3}$/C nanocomposite battery materials by electron energy loss spectroscopy (EELS). *Micron*, *43*, 22–29.

Dabrzalska, M., Benseny-Cases, N., Barnadas-Rodríguez, R., Mignani, S., Zablocka, M., Majoral, J. P., et al. (2016). Fourier transform infrared spectroscopy (FTIR) characterization of the interaction of anti-cancer photosensitizers with dendrimers. *Analytical and Bioanalytical Chemistry*, *408*, 535–544.

Das, D., Datta, A. K., Kumbhakar, D. V., Ghosh, B., Pramanik, A., & Gupta, S. (2018). Nanoparticle (CdS) interaction with host (*Sesamum indicum* L.)—Its localization, transportation, stress induction and genotoxicity. *Journal of Plant Interactions*, *13*(1), 182–194.

Das, D., Datta, A. K., Kumbhakar, D. V., Ghosh, B., Pramanik, A., Gupta, S., et al. (2017). Assessment of photocatalytic potentiality and determination of ecotoxicity (using plant model for better environmental applicability) of synthesized copper, copper oxide and copper-doped zinc oxide nanoparticles. *PLoS ONE*, *12*(8), e0182823.

Das, R., Nath, S. S., Chakdar, D., Gope, G., & Bhattacharjee, R. (2009). Preparation of silver nanoparticles and their characterization. *Journal of Nanotechnology*, *5*, 1–6.

Das, S., Singh, V. K., Dwivedy, A. K., Chaudhari, A. K., Upadhyay, N., Singh, P., et al. (2019). Encapsulation in chitosan-based nanomatrix as an efficient green technology to boost the antimicrobial, antioxidant and in situ efficacy of *Coriandrum sativum* essential oil. *International Journal of Biological Macromolecules*, *133*, 294–305.

Davarpanah, S., Tehranifar, A., Davarynejad, G., Abadía, J., & Khorasani, R. (2016). Effects of foliar applications of zinc and boron nano-fertilizers on pomegranate (*Punica granatum* cv. Ardestani) fruit yield and quality. *Scientia Horticulturae*, *210*, 57–64.

Derrien, G., Hassoun, J., Panero, S., & Scrosati, B. (2007). Nanostructured Sn–C composite as an advanced anode material in high-performance lithium-ion batteries. *Advanced Materials*, *19*, 2336–2340.

Dimkpa, C. O., McLean, J. E., Latta, D. E., Manangón, E., Britt, D. W., Johnson, W. P., et al. (2012). CuO and ZnO nanoparticles: Phytotoxicity, metal speciation, and induction of oxidative stress in sand-grown wheat. *Journal of Nanoparticle Research*, *14*, 1125.

Divya, K., Vijayan, S., Nair, S. J., & Jisha, M. S. (2019). Optimization of chitosan nanoparticle synthesis and its potential application as germination elicitor of *Oryza sativa* L. *International Journal of Biological Macromolecules*, *124*, 1053–1059.

Domínguez, E., Heredia-Guerrero, J. A., & Heredia, A. (2011). The biophysical design of plant cuticles: An overview. *The New Phytologist*, *189*, 938–949.

This book belongs to Central Library BADJI Mokhtar-ANNABA UNIVERSITY

Copyright Elsevier 2024

Donaldson, K., & Stone, V. (2003). Current hypotheses on the mechanisms of toxicity of ultrafine particles. *Annali dell'Istituto Superiore di Sanità*, *39*, 405–410.

Du, J. J., Chen, C., Gan, Y. L., Zhang, R. H., Yang, C. Y., & Zhou, X. W. (2014). Facile one-pot hydrothermal synthesis of Pt nanoparticles and their electrocatalytic performance. *International Journal of Hydrogen Energy*, *39*, 17634–17637.

Du, W., Yang, J., Peng, Q., Liang, X., & Mao, H. (2019). Comparison study of zinc nanoparticles and zinc sulphate on wheat growth: From toxicity and zinc biofortification. *Chemosphere*, *227*, 109–116.

Duncan, T. V. (2011). Applications of nanotechnology in food packaging and food safety: Barrier materials, antimicrobials and sensors. *Journal of Colloid and Interface Science*, *363*, 1–24.

Duncan, E., & Owens, G. (2019). Metal oxide nanomaterials used to remediate heavy metal contaminated soils have strong effects on nutrient and trace element phytoavailability. *Science of the Total Environment*, *678*, 430–437.

Egerton, R. F. (2008). Electron energy-loss spectroscopy in the TEM. *Reports on Progress in Physics*, *72*, 016502.

El-Deab, M. S. (2009). On the preferential crystallographic orientation of Au nanoparticles: Effect of electrodeposition time. *Electrochimica Acta*, *54*, 3720–3725.

El-Temsah, Y. S., & Joner, E. J. (2012). Impact of Fe and Ag nanoparticles on seed germination and differences in bioavailability during exposure in aqueous suspension and soil. *Environmental Toxicology*, *27*(1), 42–49.

Esfanjani, A. F., & Jafari, S. M. (2016). Biopolymer nano-particles and natural nano-carriers for nano-encapsulation of phenolic compounds. *Colloids and Surfaces B: Biointerfaces*, *146*, 532–543.

Faraji, M., Yamini, Y., & Rezaee, M. (2010). Magnetic nanoparticles: Synthesis, stabilization, functionalization, characterization, and applications. *Journal of the Iranian Chemical Society*, *7*, 1–37.

Fauth, K., Goering, E., Schütz, G., & Kuhn, L. T. (2004). Probing composition and interfacial interaction in oxide passivated core-shell iron nanoparticles by combining X-ray absorption and magnetic circular dichroism. *Journal of Applied Physics*, *96*, 399–403.

Feizi, H., Kamali, M., Jafari, L., & Moghaddam, P. R. (2013). Phytotoxicity and stimulatory impacts of nanosized and bulk titanium dioxide on fennel (*Foeniculum vulgare* Mill). *Chemosphere*, *91*(4), 506–511.

Feizi, H., Moghaddam, P. R., Shahtahmassebi, N., & Fotovat, A. (2012). Impact of bulk and nanosized titanium dioxide (TiO_2) on wheat seed germination and seedling growth. *Biological Trace Element Research*, *146*(1), 101–106.

Frenkel, A. I., Yevick, A., Cooper, C., & Vasic, R. (2011). Modeling the structure and composition of nanoparticles by extended X-ray absorption fine-structure spectroscopy. *Annual Review of Analytical Chemistry*, *4*, 23–39.

Golchin, A., Farahany, T. Z., Khojasteh, A., Soleimanifar, F., & Ardeshirylajimi, A. (2019). The clinical trials of mesenchymal stem cell therapy in skin diseases: An update and concise review. *Current Stem Cell Research & Therapy*, *14*, 22–33.

Gonçalves, G., Vila, M., Portolés, M. T., Vallet-Regi, M., Gracio, J., & Marques, P. A. A. (2013). Nano-graphene oxide: A potential multifunctional platform for cancer therapy. *Advanced Healthcare Materials*, *2*, 1072–1090.

Gupta, A. K., & Wells, S. (2004). Surface-modified superparamagnetic nanoparticles for drug delivery: Preparation, characterization, and cytotoxicity studies. *IEEE Transactions on Nanobioscience*, *3*, 66–73.

Hoo, C. M., Starostin, N., West, P., & Mecartney, M. L. (2008). A comparison of atomic force microscopy (AFM) and dynamic light scattering (DLS) methods to characterize nanoparticle size distributions. *Journal of Nanoparticle Research*, *10*, 89–96.

Iravani, S., Thota, S., & Crans, D. (2018). Methods for preparation of metal nanoparticles. In *Metal nanoparticles: Synthesis and applications in pharmaceutical sciences* (pp. 15–32). John Wiley & Sons.

Itabashi, D., Mizukami, K., Taniguchi, S., Nishifuji, M., & Kamiya, H. (2019). Sulfur-free surfactant for carbide nanoparticle characterization in steel using asymmetric flow field-flow fractionation hyphenated inductively coupled plasma-mass spectrometry. *Analytical Science*, 19P087.

Jayarambabu, N., Kumari, B. S., Rao, K. V., & Prabhu, Y. T. (2014). Germination and growth characteristics of mungbean seeds (*Vigna radiata* L.) affected by synthesized zinc oxide nanoparticles. *International Journal of Current Engineering and Technology*, *4*(5), 3411–3416.

This book belongs to Central Library BADJI Mokhtar-ANNABA UNIVERSITY

Copyright Elsevier 2024

Jores, K., Mehnert, W., Drechsler, M., Bunjes, H., Johann, C., & Mäder, K. (2004). Investigations on the structure of solid lipid nanoparticles (SLN) and oil-loaded solid lipid nanoparticles by photon correlation spectroscopy, field-flow fractionation and transmission electron microscopy. *Journal of Controlled Release*, *95*, 217–227.

Judy, J. D., Unrine, J. M., & Bertsch, P. M. (2011). Evidence for biomagnification of gold nanoparticles within a terrestrial food chain. *Environmental Science & Technology*, *45*, 776–781.

Jung, J. H., Oh, H. C., Noh, H. S., Ji, J. H., & Kim, S. S. (2006). Metal nanoparticle generation using a small ceramic heater with a local heating area. *Journal of Aerosol Science*, *37*, 1662–1670.

Jungjohann, K. L., Wheeler, D. R., Polsky, R., Brozik, S. M., Brozik, J. A., & Rudolph, A. R. (2019). Liquid-cell scanning transmission electron microscopy and fluorescence correlation spectroscopy of DNA-directed gold nanoparticle assemblies. *Micron*, *119*, 54–63.

Khan, M. S., Zaka, M., Abbasi, B. H., & Shah, A. (2016). Seed germination and biochemical profile of *Silybum marianum* exposed to monometallic and bimetallic alloy nanoparticles. *IET Nanobiotechnology*, *10*(6), 359–366.

Khodakovskaya, M. V., De Silva, K., Biris, A. S., Dervishi, E., & Villagarcia, H. (2012). Carbon nanotubes induce growth enhancement of tobacco cells. *ACS Nano*, *6*(3), 2128–2135.

Khodakovskaya, M., Dervishi, E., Mahmood, M., Xu, Y., Li, Z., Watanabe, F., et al. (2009). Carbon nanotubes are able to penetrate plant seed coat and dramatically affect seed germination and plant growth. *ACS Nano*, *3*(10), 3221–3227.

Kibbey, T. C., & Strevett, K. A. (2019). The effect of nanoparticles on soil and rhizosphere bacteria and plant growth in lettuce seedlings. *Chemosphere*, *221*, 703–707.

Kim, F., Connor, S., Song, H., Kuykendall, T., & Yang, P. (2004). Platonic gold nanocrystals. *Angewandte Chemie International Edition*, *43*, 3673–3677.

Kim, M. H., Lim, B., Lee, E. P., & Xia, Y. (2008). Polyol synthesis of Cu_2O nanoparticles: Use of chloride to promote the formation of a cubic morphology. *Journal of Materials Chemistry*, *18*, 4069–4073.

Kim, Y. P., Oh, E., Oh, Y. H., Moon, D. W., Lee, T. G., & Kim, H. S. (2007). Protein kinase assay on peptide-conjugated gold nanoparticles by using secondary-ion mass spectrometric imaging. *Angewandte Chemie International Edition*, *46*, 6816–6819.

Koczkur, K. M., Mourdikoudis, S., Polavarapu, L., & Skrabalak, S. E. (2015). Polyvinylpyrrolidone (PVP) in nanoparticle synthesis. *Dalton Transcations*, *44*, 17883–17905.

Kumar, A., Gupta, K., Dixit, S., Mishra, K., & Srivastava, S. (2019). A review on positive and negative impacts of nanotechnology in agriculture. *International Journal of Environmental Science and Technology*, *16*(4), 2175–2184.

Kvitek, L., Panáček, A., Soukupova, J., Kolář, M., Večeřová, R., Prucek, R., et al. (2008). Effect of surfactants and polymers on stability and antibacterial activity of silver nanoparticles (NPs). *Journal of Physical Chemistry C*, *112*, 5825–5834.

Lacava, L. M., Lacava, B. M., Azevedo, R. B., Lacava, Z. G. M., Buske, N., Tronconi, A. L., et al. (2001). Nanoparticle sizing: A comparative study using atomic force microscopy, transmission electron microscopy, and ferromagnetic resonance. *Journal of Magnetism and Magnetic Materials*, *225*, 79–83.

Lapied, E., Moudilou, E., Exbrayat, J. M., Oughton, D. H., & Joner, E. J. (2010). Silver nanoparticle exposure causes apoptotic response in the earthworm *Lumbricus terrestris* (Oligochaeta). *Nanomedicine*, *5*(6), 975–984.

Lee, S. J., Jeong, J. R., Shin, S. C., Kim, J. C., & Kim, J. D. (2004). Synthesis and characterization of superparamagnetic maghemite nanoparticles prepared by coprecipitation technique. *Journal of Magnetism and Magnetic Materials*, *282*, 147–150.

Lee, C. W., Mahendra, S., Zodrow, K., Li, D., Tsai, Y. C., Braam, J., et al. (2010). Developmental phytotoxicity of metal oxide nanoparticles to *Arabidopsis thaliana*. *Environmental Toxicology and Chemistry*, *29*(3), 669–675.

Li, R., He, J., Xie, H., Wang, W., Bose, S. K., Sun, Y., et al. (2019). Effects of chitosan nanoparticles on seed germination and seedling growth of wheat (*Triticum aestivum* L.). *International Journal of Biological Macromolecules*, *126*, 91–100.

This book belongs to Central Library BADJI Mokhtar-ANNABA UNIVERSITY

Copyright Elsevier 2024

Li, Y., & Lindsay, S. M. (1991). Polystyrene latex particles as a size calibration for the atomic force microscope. *The Review of Scientific Instruments*, *62*, 2630–2633.

Lin, D., & Xing, B. (2007). Phytotoxicity of nanoparticles: Inhibition of seed germination and root growth. *Environmental Pollution*, *150*, 243–250.

Lombardo, D., Kiselev, M. A., & Caccamo, M. T. (2019). Smart nanoparticles for drug delivery application: Development of versatile nanocarrier platforms in biotechnology and nanomedicine. *Journal of Nanomaterials*, 1–26. Article ID: 3702518.

Lopez-Quintela, M. A. (2003). Synthesis of nanomaterials in microemulsions: Formation mechanisms and growth control. *Current Opinion in Colloid and Interface Science*, *8*, 137–144.

López-Serrano, A., Olivas, R. M., Landaluze, J. S., & Cámara, C. (2014). Nanoparticles: A global vision. Characterization, separation, and quantification methods. Potential environmental and health impact. *Analytical Methods*, *6*, 38–56.

Lukman, A. I., Gong, B., Marjo, C. E., Roessner, U., & Harris, A. T. (2011). Facile synthesis, stabilization, and anti-bacterial performance of discrete Ag nanoparticles using *Medicago sativa* seed exudates. *Journal of Colloid and Interface Science*, *353*, 433–444.

Luykx, D. M., Peters, R. J., van Ruth, S. M., & Bouwmeester, H. (2008). A review of analytical methods for the identification and characterization of nano delivery systems in food. *Journal of Agricultural and Food Chemistry*, *56*, 8231–8247.

Ma, Y., Chen, M., & Li, M. (2015). Hydrothermal synthesis of hydrophilic NaYF4: Yb, Er nanoparticles with bright upconversion luminescence as biological label. *Materials Letters*, *139*, 22–25.

Ma, Y., Kuang, L., He, X., Bai, W., Ding, Y., Zhang, Z., et al. (2010). Effects of rare earth oxide nanoparticles on root elongation of plants. *Chemosphere*, *78*(3), 273–279.

Ma, J., Lü, X., & Huang, Y. (2011). Genomic analysis of cytotoxicity response to nanosilver in human dermal fibroblasts. *Journal of Biomedical Nanotechnology*, *7*, 263–275.

Mafuné, F., Kohno, J. Y., Takeda, Y., Kondow, T., & Sawabe, H. (2000). Structure and stability of silver nanoparticles in aqueous solution produced by laser ablation. *The Journal of Physical Chemistry B*, *104*, 8333–8337.

Maity, A., Natarajan, N., Vijay, D., Srinivasan, R., Pastor, M., & Malaviya, D. R. (2018). Influence of metal nanoparticles (NPs) on germination and yield of oat (*Avena sativa*) and berseem (*Trifolium alexandrinum*). *Proceedings of the National Academy of Sciences, India Section B: Biological Sciences*, *88*(2), 595–607.

Mallikarjuna, K., Narasimha, G., Dillip, G. R., Praveen, B., Shreedhar, B., Lakshmi, C. S., et al. (2011). Green synthesis of silver nanoparticles using Ocimum leaf extract and their characterization. *Digest Journal of Nanomaterials and Biostructures*, *6*, 181–186.

Marchiol, L., Filippi, A., Adamiano, A., Degli Esposti, L., Iafisco, M., Mattiello, A., et al. (2019). Influence of hydroxyapatite nanoparticles on germination and plant metabolism of tomato (*Solanum lycopersicum* L.): Preliminary evidence. *Agronomy*, *9*(4), 161.

Margenot, A. J., Rippner, D. A., Dumlao, M. R., Nezami, S., Green, P. G., Parikh, S. J., et al. (2018). Copper oxide nanoparticle effects on root growth and hydraulic conductivity of two vegetable crops. *Plant and Soil*, *431*(1-2), 333–345.

Mayhew, T. M., Mühlfeld, C., Vanhecke, D., & Ochs, M. (2009). A review of recent methods for efficiently quantifying immunogold and other nanoparticles using TEM sections through cells, tissues and organs. *Annals of Anatomy*, *191*, 153–170.

Meva, F. E. A., Ntoumba, A. A., Kedi, P. B. E., Tchoumbi, E., Schmitz, A., Schmolke, L., et al. (2019). Silver and palladium nanoparticles produced using a plant extract as reducing agent, stabilized with an ionic liquid: sizing by X-ray powder diffraction and dynamic light scattering. *Journal of Materials Research and Technology*, *8*, 1991–2000.

Mourdikoudis, S., Pallares, R. M., & Thanh, N. T. (2018). Characterization techniques for nanoparticles: Comparison and complementarity upon studying nanoparticle properties. *Nanoscale*, *10*, 12871–12934.

This book belongs to Central Library BADJI Mokhtar-ANNABA UNIVERSITY

Copyright Elsevier 2024

Movafeghi, A., Khataee, A., Abedi, M., Tarrahi, R., Dadpour, M., & Vafaei, F. (2018). Effects of TiO_2 nanoparticles on the aquatic plant *Spirodela polyrrhiza*: Evaluation of growth parameters, pigment contents and antioxidant enzyme activities. *Journal of Environmental Sciences*, *64*, 130–138.

Mudunkotuwa, I. A., Al Minshid, A., & Grassian, V. H. (2014). ATR-FTIR spectroscopy as a tool to probe surface adsorption on nanoparticles at the liquid–solid interface in environmentally and biologically relevant media. *Analyst*, *139*, 870–881.

Mukherjee, P., Ahmad, A., Mandal, D., Senapati, S., Sainkar, S. R., Khan, M. I., et al. (2001). Fungus-mediated synthesis of silver nanoparticles and their immobilization in the mycelial matrix: A novel biological approach to nanoparticle synthesis. *Nano Letters*, *1*, 515–519.

Nakasato, D. Y., Pereira, A. E. S., Oliveira, J. L., Oliveira, H. C., & Fraceto, L. F. (2017). Evaluation of the effects of polymeric chitosan/tripolyphosphate and solid lipid nanoparticles on germination of *Zea mays*, *Brassica rapa* and *Pisum sativum*. *Ecotoxicology and Environmental Safety*, *142*, 369–374.

Neto, B. A. D., Diniz, J. R., & de Oliveira, A. L. (2013). Ionic liquid effect probed by nuclear magnetic resonance: NMR approaches to catalytic reactions performed in ionic liquids. *Current Organic Chemistry*, *17*, 273–282.

Nhan, L. V., Ma, C., Rui, Y., Liu, S., Li, X., Xing, B., et al. (2015). Phytotoxic mechanism of nanoparticles: Destruction of chloroplasts and vascular bundles and alteration of nutrient absorption. *Scientific Reports*, *5*, 11618.

Patra, J. K., & Baek, K. H. (2014). Green nanobiotechnology: Factors affecting synthesis and characterization techniques. *Journal of Nanomaterials*, *2014*, 219.

Paul, D. R., & Robeson, L. M. (2008). Polymer nanotechnology: Nanocomposites. *Polymer*, *49*, 3187–3204.

Peters, R., ten Dam, G., Bouwmeester, H., Helsper, H., Allmaier, G., vd Kammer, F., et al. (2011). Identification and characterization of organic nanoparticles in food. *Trends in Analytical Chemistry*, *30*, 100–112.

Prasad, T., Sudhakar, P., Sreenivasulu, Y., Latha, P., Munaswamy, V., Reddy, K. R., et al. (2012). Effect of nanoscale zinc oxide particles on the germination, growth and yield of peanut. *Journal of Plant Nutrition*, *35*, 905–927.

Raja, K., Sowmya, R., Sudhagar, R., Moorthy, P. S., Govindaraju, K., & Subramanian, K. S. (2019). Biogenic ZnO and Cu nanoparticles to improve seed germination quality in blackgram (*Vigna mungo*). *Materials Letters*, *235*, 164–167.

Rajjou, L., Duval, M., Gallardo, K., Catusse, J., Bally, J., Job, C., et al. (2012). Seed germination and vigor. *Annual Review of Plant Biology*, *63*, 507–533.

Rajput, V., Minkina, T., Fedorenko, A., Sushkova, S., Mandzhieva, S., Lysenko, V., et al. (2018). Toxicity of copper oxide nanoparticles on spring barley (Hordeum sativum distichum). *Science of the Total Environment*, *645*, 1103–1113.

Rana, S., Philip, J., & Raj, B. (2010). Micelle based synthesis of cobalt ferrite nanoparticles and its characterization using Fourier transform infrared transmission spectrometry and thermogravimetry. *Materials Chemistry and Physics*, *124*, 264–269.

Rico, C. M., Peralta-Videa, J. R., & Gardea-Torresdey, J. L. (2015). Chemistry, biochemistry of nanoparticles, and their role in antioxidant defense system in plants. In *Nanotechnology and plant sciences* (pp. 1–17). Cham: Springer.

Santos, A. R., Miguel, A. S., Tomaz, L., Malhó, R., Maycock, C., Patto, M. C. V., et al. (2010). The impact of CdSe/ZnS quantum dots in cells of Medicago sativa in suspension culture. *Journal of Nanbiotechnology*, *8*(1), 24.

Scherer, M. D., Sposito, J. C., Falco, W. F., Grisolia, A. B., Andrade, L. H., Lima, S. M., et al. (2019). Cytotoxic and genotoxic effects of silver nanoparticles on meristematic cells of *Allium cepa* roots: A close analysis of particle size dependence. *Science of the Total Environment*, *660*, 459–467.

Schimpf, M. E., Caldwell, K., & Giddings, J. C. (Eds.), (2000). *Field-flow fractionation handbook*: John Wiley & Sons.

Schreiber, S., Savla, M., Pelekhov, D. V., Iscru, D. F., Selcu, C., Hammel, P. C., et al. (2008). Magnetic force microscopy of superparamagnetic nanoparticles. *Small*, *4*, 270–278.

This book belongs to Central Library BADJI Mokhtar-ANNABA UNIVERSITY

Copyright Elsevier 2024

Shaw, A. K., & Hossain, Z. (2013). Impact of nano-CuO stress on rice (*Oryza sativa* L.) seedlings. *Chemosphere*, *93*, 906–915.

Shimizu, K., & Mitani, T. (2009). *New horizons of applied scanning electron microscopy. Vol. 45*. Springer Science & Business Media.

Siddiqui, M. H., & Al-Whaibi, M. H. (2014). Role of nano-SiO_2 in germination of tomato (*Lycopersicum esculentum* seeds Mill.). *Saudi Journal of Biological Sciences*, *21*(1), 13–17.

Sikora, A., Shard, A. G., & Minelli, C. (2016). Size and ζ-potential measurement of silica nanoparticles in serum using tunable resistive pulse sensing. *Langmuir*, *32*, 2216–2224.

Singh, P., Singh, R., Borthakur, A., Srivastava, P., Srivastava, N., Tiwary, D., et al. (2016). Effect of nanoscale TiO_2-activated carbon composite on *Solanum lycopersicum* (L.) and *Vigna radiata* (L.) seeds germination. *Energy, Ecology and Environment*, *1*(3), 131–140.

Song, M. K., Park, S., Alamgir, F. M., Cho, J., & Liu, M. (2011). Nanostructured electrodes for lithium-ion and lithium-air batteries: The latest developments, challenges, and perspectives. *Materials Science and Engineering*, *72*, 203–252.

Soukupová, J., Kvítek, L., Panáček, A., Nevěčná, T., & Zbořil, R. (2008). Comprehensive study on surfactant role on silver nanoparticles (NPs) prepared via modified Tollens process. *Materials Chemistry and Physics*, *111*, 77–81.

Sreenivasulu, N., & Wobus, U. (2013). Seed-development programs: A systems biology-based comparison between dicots and monocots. *Annual Review of Plant Biology*, *64*, 189–217.

Stampoulis, D., Sinha, S. K., & White, J. C. (2009). Assay-dependent phytotoxicity of nanoparticles to plants. *Environmental Science & Technology*, *43*, 9473–9479.

Suleiman, J. S., Hu, B., Peng, H., & Huang, C. (2009). Separation/preconcentration of trace amounts of Cr, Cu and Pb in environmental samples by magnetic solid-phase extraction with Bismuthiol-II-immobilized magnetic nanoparticles and their determination by ICP-OES. *Talanta*, *77*, 1579–1583.

Sun, S., Anders, S., Hamann, H. F., Thiele, J. U., Baglin, J. E. E., Thomson, T., et al. (2002). Polymer mediated self-assembly of magnetic nanoparticles. *Journal of the American Chemical Society*, *124*, 2884–2885.

Sun, Y. P., Li, X. Q., Cao, J., Zhang, W. X., & Wang, H. P. (2006). Characterization of zero-valent iron nanoparticles. *Advances in Colloid and Interface Science*, *120*, 47–56.

Suriyaprabha, R., Sreeja, K. A., Prabu, M., Prabu, P., & Rajendran, V. (2018). Bioaccumulation of transition metal oxide nanoparticles and their influence on early growth stages of *Vigna unguiculata* seeds. *BioNanoScience*, *8*(3), 752–760.

Tang, Y. J., Wu, S. G., Huang, L., Head, J., Chen, D., & Kong, I. C. (2013). Phytotoxicity of metal oxide nanoparticles is related to both dissolved metals ions and adsorption of particles on seed surfaces. *Journal of Petroleum & Environmental Biotechnology*, *3*(4), 126.

Thanh, N. T., Maclean, N., & Mahiddine, S. (2014). Mechanisms of nucleation and growth of nanoparticles in solution. *Chemical Reviews*, *114*, 7610–7630.

Thunugunta, T., Reddy, A. C., Seetharamaiah, S. K., Hunashikatti, L. R., Chandrappa, S. G., Kalathil, N. C., et al. (2018). Impact of zinc oxide nanoparticles on eggplant (*S. melongena*): Studies on growth and the accumulation of nanoparticles. *IET Nanobiotechnology*, *12*(6), 706–713.

Tiede, K., Boxall, A. B., Tear, S. P., Lewis, J., David, H., & Hassellöv, M. (2008). Detection and characterization of engineered nanoparticles in food and the environment. *Food Additives and Contaminants*, *25*, 795–821.

Titus, D., Samuel, E. J. J., & Roopan, S. M. (2019). Nanoparticle characterization techniques. In *Green synthesis, characterization and applications of nanoparticles* (pp. 303–319): Elsevier.

Vangijzegem, T., Stanicki, D., & Laurent, S. (2019). Magnetic iron oxide nanoparticles for drug delivery: Applications and characteristics. *Expert Opinion on Drug Delivery*, *16*(1), 69–78.

Verma, S. K., Das, A. K., Patel, M. K., Shah, A., Kumar, V., & Gantait, S. (2018). Engineered nanomaterials for plant growth and development: A perspective analysis. *Science of the Total Environment*, *630*, 1413–1435.

This book belongs to Central Library BADJI Mokhtar-ANNABA UNIVERSITY

Copyright Elsevier 2024

Wang, Y., Jiang, F., Ma, C., Rui, Y., Tsang, D. C., & Xing, B. (2019). Effect of metal oxide nanoparticles on amino acids in wheat grains (*Triticum aestivum*) in a life cycle study. *Journal of Environmental Management*, *241*, 319–327.

Wattanawikkam, C., Kansa-ard, T., & Pecharapa, W. (2019). X-ray absorption spectroscopy analysis and photocatalytic behavior of $ZnTiO_3$ nanoparticles doped with Co and Mn synthesized by sonochemical method. *Applied Surface Science*, *474*, 169–176.

Wu, C., Zhu, Y., Wu, T., Wang, L., Yuan, Y., Chen, J., et al. (2019). Enhanced functional properties of biopolymer film incorporated with curcurmin-loaded mesoporous silica nanoparticles for food packaging. *Food Chemistry*, *288*, 139–145.

Xia, D., Biswas, A., Li, D., & Brueck, S. R. (2004). Directed self-assembly of silica nanoparticles into nanometer-scale patterned surfaces using spin-coating. *Advanced Materials*, *16*, 1427–1432.

Xiang, L., Zhao, H. M., Li, Y. W., Huang, X. P., Wu, X. L., Zhai, T., et al. (2015). Effects of the size and morphology of zinc oxide nanoparticles on the germination of Chinese cabbage seeds. *Environmental Science and Pollution Research*, *22*(14), 10452–10462.

Yan, Z., FitzGerald, S., Crawford, T., & Mefford, O. T. (2019). *Synthesis and characterization of multi-dopant ferrite magnetic nanoparticles with designed structures; 2019*. https://tigerprints.clemson.edu›grads_symposium.

Yin, L., Colman, B. P., McGill, B. M., Wright, J. P., & Bernhardt, E. S. (2012). Effects of silver nanoparticle exposure on germination and early growth of eleven wetland plants. *PLoS ONE*, *7*(10), e47674.

Yin, H., Yamamoto, T., Wada, Y., & Yanagida, S. (2004). Large-scale and size-controlled synthesis of silver nanoparticles under microwave irradiation. *Materials Chemistry and Physics*, *83*, 66–70.

Yoo-iam, M., Chaichana, R., & Satapanajaru, T. (2014). Toxicity, bioaccumulation and biomagnification of silver nanoparticles in green algae (Chlorella sp.), water flea (*Moina macrocopa*), blood worm (Chironomus spp.) and silver barb (*Barbonymus gonionotus*). *Chemical Speciation and Bioavailability*, *26*, 257–265.

Yu, R. J., Ying, Y. L., Gao, R., & Long, Y. T. (2019). Confined nanopipette sensing: from single molecules, single nanoparticles, to single cells. *Angewandte Chemie International Edition*, *58*(12), 3706–3714.

Zaka, M., Abbasi, B. H., Rahman, L. U., Shah, A., & Zia, M. (2016). Synthesis and characterisation of metal nanoparticles and their effects on seed germination and seedling growth in commercially important *Eruca sativa*. *IET Nanobiotechnology*, *10*(3), 134–140.

Zhang, X. F., Liu, Z. G., Shen, W., & Gurunathan, S. (2016). Silver nanoparticles: Synthesis, characterization, properties, applications, and therapeutic approaches. *International Journal of Molecular Sciences*, *17*, 1534.

Zhang, X., & Tsapatsis, M. (2011). Mesoporous silica nanoparticles from a clear sol and their transformation to lamellar silicalite-1 particles and films. *Microporous and Mesoporous Materials*, *138*, 239–242.

Zhang, J., Wang, Z. L., Liu, J., Chen, S., & Liu, G. Y. (2003). *Self-assembled nanostructures. Vol. 2*. Springer Science & Business Media.

Zhang, R., Zhang, H., Tu, C., Hu, X., Li, L., Luo, Y., et al. (2015). Phytotoxicity of ZnO nanoparticles and the released Zn (II) ion to corn (*Zea mays* L.) and cucumber (*Cucumis sativus* L.) during germination. *Environmental Science and Pollution Research*, *22*, 11109–11117.

Zheng, L., Hong, F., Lu, S., & Liu, C. (2005). Effect of nano-TiO_2 on strength of naturally aged seeds and growth of spinach. *Biological Trace Element Research*, *104*, 83–91.

Zhu, Y., Zhou, W., Ran, R., Chen, Y., Shao, Z., & Liu, M. (2015). Promotion of oxygen reduction by exsolved silver nanoparticles on a perovskite scaffold for low-temperature solid oxide fuel cells. *Nano Letters*, *16*, 512–518.

Zou, D., Jin, L., Wu, B., Hu, L., Chen, X., Huang, G., et al. (2019). Rapid detection of Salmonella in milk by biofunctionalised magnetic nanoparticle cluster sensor based on nuclear magnetic resonance. *International Dairy Journal*, *91*, 82–88.

This book belongs to Central Library BADJI Mokhtar-ANNABA UNIVERSITY

Copyright Elsevier 2024

Further reading

Fissan, H., Ristig, S., Kaminski, H., Asbach, C., & Epple, M. (2014). Comparison of different characterization methods for nanoparticle dispersions before and after aerosolization. *Analytical Methods*, *6*, 7324–7334.

Fournier, S. B., Kallontzi, S., Fabris, L., Love, C., & Stapleton, P. A. (2019). Effect of gestational age on maternofetal vascular function following single maternal engineered nanoparticle exposure. *Cardiovascular Toxicology*, *19*(4), 321–333.

Lesniak, A., Salvati, A., Santos-Martinez, M. J., Radomski, M. W., Dawson, K. A., & Åberg, C. (2013). Nanoparticle adhesion to the cell membrane and its effect on nanoparticle uptake efficiency. *Journal of the American Chemical Society*, *1*(35), 1438–1444.

Lin, P. C., Lin, S., Wang, P. C., & Sridhar, R. (2014). Techniques for physicochemical characterization of nanomaterials. *Biotechnology Advances*, *32*, 711–726.

Xia, I. F., Cheung, J. S., Wu, M., Wong, K. S., Kong, H. K., Zheng, X. T., et al. (2019). Dietary chitosan-selenium nanoparticle (CTS-SeNP) enhance immunity and disease resistance in zebrafish. *Fish & Shellfish Immunology*, *87*, 449–459.

This book belongs to Central Library BADJI Mokhtar-ANNABA UNIVERSITY

Copyright Elsevier 2024

This page intentionally left blank

This book belongs to Central Library BADJI Mokhtar-ANNABA UNIVERSITY

Copyright Elsevier 2024

Index

Note: Page numbers followed by *f* indicate figures and *t* indicate tables.

A

Acidic dye, 174–175
Activated carbon (AC)
  pesticides degradation, 162–163
  semiconductor nanoparticles, 247–248
Activated carbon fibers (ACF), 248
Adsorption process, for pesticides degradation, 165
Advanced oxidation processes (AOPs), 42, 92, 143–144, 149–150, 245–246
AEC. *See* Anion exchange capacity (AEC)
AgBr-α-$NiMoO_4$ composite, 73
Ag-doped TiO_2, 69
Ag nanoparticle-loaded TiO_2/MWCNT composites, 252
Ag_3PO_4/CQD nanocomposites, 263
Agroecosystems, nanocatalysts for
  fate and transport, 330–331
  fertilizers, 327–329
  potential benefits, 327–329, 328*f*
  soil, plant and microorganisms, 332, 334–335
Ag-ZnO-$La_2O_2CO_3$ hydrotalcites, 86–87
Anatase, 69
Animal husbandry, antibiotic usage for, 198
Anion exchange capacity (AEC), 82–83
Anodization, 310–311
Antibiotic ciprofloxacin (CIP) degradation, 69
Antibiotic-resistant bacteria (ARBs). *See* Antibiotic-resistant genes (ARGs)
Antibiotic-resistant genes (ARGs)
  acquired resistance mechanisms, 201–202
  directional evolutionary effect, 199, 201*f*
  human health, 202
  intrinsic resistance mechanisms, 200–201
  nanomaterials
    degradation, 206
    detection, 205
  wastewater treatment methods, 202–204, 203–204*t*
Antibiotics, 195–196
  classification, 196, 196–197*t*, 211–212, 213*f*
  consumption, 212
  definition, 211–212
  degradation
    heterogeneous photocatalysis, 225–236
    sunlight action, 212–224
  environmental concerns, 211
  environmental percolation, 198
  mechanism of action, 196, 196–197*t*
  microbial communities, 199
  percolation, into environment, 198
  pollutants
    animal husbandry, 198
    degradation, 206
    detection, 205
    directional evolutionary effect, 199, 201*f*
    environmental consequences, 199, 200*t*
    mitigation, nanomaterials in, 205–206
    pharmaceutical consumption, 196–197
    sources, 196–198
AOPs. *See* Advanced oxidation processes (AOPs)
Aquatic pollution. *See* Water pollution
Atomic force microscopy (AFM), 379–380
Azo dye, 174–175

B

Ball milling method, 290–291
Basic dye, 174–175
BET. *See* Brunauer-Emmett-Teller (BET) approach
Biochar-supported zerovalent iron nanoparticles (nZVI@BC), 349–350
Biodegradable pesticides, 156
Biodiversity, pesticides effects on, 159–160
Biological treatment, pesticides degradation, 165–166
Biopesticides, 157
Bisphenol A (BPA), 21–23
$BiVO_4$ photocatalyst, for wastewater treatment, 73
Brookite, 69
Brucite, 81
Brunauer-Emmett-Teller (BET) approach, 105
Bulk graphitic carbon nitride, 281

C

Caffeine degradation, 86–87
Carbamate insecticides, 156
Carbon-based nanomaterials, 147
Carbon black (CB), 265
Carbon nanofibers (CNFs), 264–265
Carbon nanotubes (CNTs)
  phytoremediation, 358–359
  semiconductor nanoparticles, 250–252
Carbon quantum dots (CQDs), 262–263
Carbon-supported semiconductor photocatalysis
  activated carbon, 247–248
  carbon black, 265
  carbon nanofibers, 264–265

This book belongs to Central Library BADJI Mokhtar-ANNABA UNIVERSITY
Copyright Elsevier 2024

Carbon-supported semiconductor photocatalysis *(Continued)*
carbon nanotubes, 250–252
carbon quantum dots, 262–263
fullerene, 248–250
graphene, 252–262
graphitic carbon nitride, 265–266
macro-/micromaterials, 246–247
mesoporous carbon, 248
nanomaterials, 246–247
Carboxymethyl cellulose (CMC)-stabilized Fe-Mn binary oxide nanoparticles, 349–350
Cation exchange capacity (CEC), 82–83
Cd-based metal-organic frameworks, 114–115
CdS-based photocatalysts, environmental pollutants degradation, 136–137
CdSe/TiO_2-based PEC system, 26–28
CdS/TiO_2 nanoparticle decorated CNFs, 265
CEC. *See* Cation exchange capacity (CEC)
Ce-doped zinc oxide nanorods, photocatalytic activity of, 179
Cefazolin, photodegradation of, 223
Cephalexin
photodegradation, 223
UV-vis spectra for, 212, 214*f*
Chemical oxygen demand (COD) removal, 136–137
Chemical treatment, pesticides removal
advanced oxidation process, 164
Fenton process, 164
UV and UV/H_2O_2 process, 164–165
Chlorpyrifos, 154
Ciprofloxacin, UV-vis spectra for, 212, 214*f*
Clay-based photocatalysts, 73
Clay particles, pesticides degradation, 162
Cloud point extraction (CPE), 381–382
Coagulation method, 16–17
Co- and Ni-based metal-organic frameworks, 109–111
Colloidal nanodispersions, 373
Colorant. *See* Dyes
Compound parabolic concentrator (CPC) photoreactor model, 318
Compound parabolic reactors (CPC), 74
Concoction oxygen request (COD) examinations, 318
Conventional synthesis, 97–98
Core-shell nanocatalysts, 325
Cross-flow filtration (CFF), 381–382

D

2,4-Dichlorophenoxy acetic (2,4-D), 153
Direct photolysis, 212–214
Disperse dyes, 174–175
Doped semiconductors, 3
coprecipitation, 4
hydrothermal and solvothermal synthesis, 5
sol–gel synthesis, 4
Dyes
classification, 174–176, 174*f*
degradation, kinetic parameters, 109–111, 111*t*
photoreactor, 313–316
sources, 173
waste water treatment processes, 176
Dynamic light scattering (DLS), 381

E

EDC. *See* Endocrine disruptive compounds (EDC)
Electrochemical synthesis, of MOFs, 99
Electrospinning, 309–310, 310*f*
Emerging contaminate technology (ECT), 316
Emerging organic pollutants (EOPs), 79–80
Endocrine disruptive compounds (EDC), 67
Energy-dispersive X-ray analysis (EDAX/EDX), 106
Engineered nanomaterials (ENMs), 195, 206–207, 330
Engineered nanoparticles (ENPs), 329, 334–335, 346
Environmental scanning electron microscopy (E-SEM), 379
EOPs. *See* Emerging organic pollutants (EOPs)

F

Fat-soluble pesticides, 159
Fe-based metal-organic frameworks, 72, 108–109
Fe/Co/Ni-based graphene composites, 18–21
Fenton process, for pesticides degradation, 164
Fe_2O_3/CQD nanocomposites, 263
Field emission scanning electron microscope (FESEM), 106, 107*f*
Field-flow fractionation (FFF), 381–382
Fourier transform infrared spectroscopy (FTIR), 381
Fullerene (C_{60})
phytoremediation, 358–359
semiconductor nanoparticles, 248–250

G

Gas adsorption measurements, 105
Gold nanoparticle–coated silicon nanowires, 356
Gold nanoparticles (AuNPs), 334
Granulated activated carbon (GAC), 248
Graphene, 70, 252–262
Graphene-based materials, photocatalytic degradation of, 70–71
Graphene-based nanostructures, 18–25
Fe/Co/Ni-based graphene composites, 18–21
metal-/nonmetal (N)-based graphene nanocomposites, 25
(Zn/Ti/W/Ce)O-based graphene composites, 21–25
Graphene-based photocatalyst composites
adsorptivity enhancer, 257–258
light absorption range, 257

This book belongs to Central Library BADJI Mokhtar-ANNABA UNIVERSITY
Copyright Elsevier 2024

photoelectron mediator and acceptor, 255–257
photosensitizer/photon absorber, 259–260
photothermal effect, 260
selective adsorption, 258–259
semiconductor photocatalysts
catalytically active sites, 261–262
defect density reduction, 260–261
entire system, optimization of, 262
functions, 260
heterojunction interaction, 262
synthesis, 253–255
Graphene oxide, 18, 25
Graphitic carbon nitride (GCN, g-C_3N_4)
bulk materials, 281
literature records, 279, 280*f*
modification strategies, 280
nanosheets, 287–294
bottom-up method, 294, 295–296*t*
top-down method, 291, 292–293*t*
one-dimensional nanostructures, 285–287
QDs, 281–285
semiconductor nanoparticles, 265–266
shortcomings, 279–280
size and shape control synthesis, 280–281, 282*f*, 285–287, 291
synthetic challenges, 297, 299
three-dimensional nanostructures, 294–297
visible-light absorption, 279–280
Graphitic carbon nitride quantum dots, 281–285, 283–284*t*

H

Heterogeneous Fenton degradation, 18–19
Heterogeneous photocatalysis, 16–17, 43*f*, 92, 145, 147–148, 177
antibiotics degradation, 225–236
petrochemical pollutants, 136–137
pharmaceutical waste treatment, 147–148
supportive carbon materials, 246–247, 246*f*
Highest occupied molecular orbital (HOMO), 104, 115–116
High-resolution transmission electron microscopy (HR-TEM), 106, 107*f*, 379
HOMO. *See* Highest occupied molecular orbital (HOMO)
Homogeneous photocatalysis, 16–17, 176
Household gray water, purification of, 317
Human, pesticides effects on, 159
Humic acids, 28–31
Hydrogenotitanate nanotubes (HNT), 250
Hydrotalcite compounds. *See* Layered double hydroxides
Hydrotalcite, pharmaceutical compounds photodegradation, 79–80
adsorption process, 80
advanced oxidation processes, 80
general formula of, 83
materials used in, 80
of pharmaceuticals, 85–88
preparation of, 83–84
anion exchange, 83–84
coprecipitation, 83, 84*f*
reconstruction, 84
structure of, 81–83
Hydrothermal/solvothermal synthesis, 5

I

Imidazole
structure, 182
tautomerism, 182, 183*f*
Imidazole framework-based metal oxide photocatalyst
applications, 186, 186*f*
challenges, 187
physicochemical properties, 179–181
preparation, 182–186
X-ray crystal structure, 182, 183*f*
Indirect photolysis, 212
Intercalation-exfoliation method, 289–290
International Union of Pure and Applied Chemistry (IUPAC), 105
Iron oxide nanoparticles (Fe NPs), 360, 360–361*t*
Iron sulfide nanoparticles, 351
IUPAC. *See* International Union of Pure and Applied Chemistry (IUPAC)

L

Langmuir-Hinshelwood kinetic model, 225–229
Layered double hydroxides (LDHs), 85–86, 88, 326
Ligand-to-metal charge transfer (LMCT) mechanism, 93
Light expanded clay aggregate (LECA), 136–137
Lowest unoccupied molecular orbital (LUMO), 104, 115–116

M

Mechanochemical synthesis, of MOFs, 99–100
Mesoporous carbon, 248
Metal-based nanocatalysts, 324–327
Metal-fullerene/TiO_2 composites, 249
Metal/metal oxide nanoparticles, 146
Metal-/nonmetal (N)-based graphene nanocomposites, 25
Metal-organic frameworks (MOFs), 18–19, 91–108
Cd-based, 114–115
characterizations, 100–108
electron microscopy, 106
nitrogen adsorption-desorption isotherms, 105
photoluminescence spectroscopy, 107–108
powder X-ray diffraction, 101
single-crystal X-ray diffraction, 101–102
thermogravimetric analysis, 102–104

This book belongs to Central Library BADJI Mokhtar-ANNABA UNIVERSITY
Copyright Elsevier 2024

Metal-organic frameworks (MOFs) *(Continued)*
ultraviolet–visible diffuse reflectance spectroscopy, 104
X-ray photoelectron spectroscopy, 106–107
Co- and Ni-based, 109–111
design considerations, 96–97
Fe-based, 108–109
organic pollutants, photocatalytic degradation of, 116
solar active photocatalytic degradation, of pharmaceuticals, 71–73
synthesis strategies, 97–100
conventional, 97–98
electrochemical, 99
mechanochemical, 99–100
microwave-assisted, 98
sonochemical, 100
Zn-based, 96–97, 111–114
Methicillin-resistant *Staphylococcus aureus* (MRSA), 202
Microencapsulated pesticides, 334
Microwave-assisted (MW) synthesis, 98, 374
Mo-doped TiO_2 nanoparticles, 8
MOFs. *See* Metal-organic frameworks (MOFs)
MoS_2/TiO_2 composite, 70
Multilayer turning circle reactor (MLRDR), 313, 313*f*

N

Nanocarbon catalysts, 326
Nanocatalysts
in agriculture
fate and transport, 330–331
fertilizers, 327–329
potential benefits, 327–329, 328*f*
soil, plant and microorganisms, 332, 334–335
carbon materials, 326
core-shell, 325
layered double hydroxides, 326
metal-based, 324–327
polymers, 327
quantum dots, 327
silica, 325
Nanomaterials, 305–306
antibiotic pollution mitigation
degradation, 206
detection, 205
categories, 371
seed germination, 382–385, 386–390*t*
synthesis methods, 373–375, 375*f*
biological method, 374–375
chemical method, 373
physical method, 373
Nano Na-zeolitic tuff, 351
Nanoparticles
action mechanism, on seed germination, 385–391
agrowaste management, 332–334
characterization techniques, 375–380, 377–378*t*
definition of, 371
filtration techniques, 381–382
magnetic properties, 382
microscopic techniques, 379–380
spectroscopic analysis, 380–381
wastewater treatment
drawbacks, 46
immobilization, advantages, 46–47
removal of organic pollutant using, 43, 44–45*t*, 46–47
X-ray methods, 380
Nanophotocatalysts, 146
Nanophytoremediation, 358–360, 359*f*
Nanoremediation
persistent organic pollutants (POPs), 351–355
pesticides, 351–355
Nanoscale zerovalent iron (nZVI), phytoremediation, 349, 353, 359–361
Natural dyes, 174–175, 175*f*
N-doped TiO_2, 70
Nitrogen adsorption-desorption isotherms, 105

O

One-dimensional graphitic carbon nitride, 285–287, 287*t*
One-dimensional photocatalyst structure, 309–311
Orange-G azo dye degradation, 23–25
Organic linkers, 96
Organic pollutants. *See also* Dyes
degradation methods of, 16–17
degradation, ZnO-based photocatalysts, 134–135
Organochlorine insecticides, 157
Organophosphorus pesticides, 154, 156
Ozone–ultraviolet (O_3/UV) photocatalytic oxidation, 28–31

P

PCA. *See* Photocatalytic activity (PCA) evaluation
Pd nanoparticles @ MIL-100(Fe) nanocomposite, 71
Persistent pesticides, 156
Personal care products, 144–145
Pesticides, 15–16, 153–154
chemically related
biopesticide, 157
carbamate, 156
organochlorine insecticides, 157
organophosphate, 156
pyrethroid, 157
sulfonylurea herbicides, 157
chemical treatment, pesticides removal (*see* Chemical treatment, pesticides removal)
degradation methods, 161–162, 161–162*f*
activated carbon, 162–163

This book belongs to Central Library BADJI Mokhtar-ANNABA UNIVERSITY
Copyright Elsevier 2024

adsorption, 165
biological treatment, 165–166
clays, 162
photocatalysis, 167–168
zeolites and polymeric materials, 163
entry to animals
dermal entry, 154
oral entry, 154–155
respiratory entry, 155
harmful effects, 158–161
on biodiversity, 159–160
on human, 159
soil contamination, 160–161
insecticides types
biodegradable, 156
persistent, 156
residue detection, nanoenabled sensors used for, 356, 357*t*
usage in India, 157–158
Petrochemical industry, 127–128
Petrochemical pollutants
biological degradation/treatment, 131
chemical degradation/treatment, 131
environmental stress, 129, 129*f*
heterogeneous photocatalysts, 136–137
petrochemical industry, 127–128
photo catalysis, principles and kinetic concepts of, 131–133
photocatalyst, 133–134, 133–134*t*
physical degradation/treatment, 131
solid wastes, 129
toxicity spread, 129–130
UV/visible light-driven photocatalysts, 134–135
Pharmaceuticals, 15–16, 144–145. *See also* Antibiotics
antibiotics, 196–197
categories of, 211
photodegradation, 145
Pharmaceutical waste
health effects of, 66–67
in water resources, 65–66
Pharmaceutical waste treatment, 143–144
carbon-based nanomaterials, 147
degradation pathways for, 145–146
heterogeneous photocatalysis, 147–148
metal/metal oxide nanoparticles, 146
nanophotocatalysts, 146
nanotechnology for, 145
and personal care products, 144–145
photodegradation of, 145
semiconductor nanophotocatalyst, 148–149
zeolites nanoparticles, 147
Phenol pollutants degradation, 136–137
Phenoxy herbicides, 160
Phosphate-functionalized MWCNT-TiO_2 composites, 251–252
Photocatalysis
antibiotics degradation, nanomaterials, 230–236, 232–236*t*
carbon modification (*see* Carbon-supported semiconductor photocatalysis)
categories, 176–177
definition, 176–177, 245–246
degradation mechanism, 68–69
materials used in, 80
pesticides degradation, 167–168
pollutant degradation, 176–181
process, schematic of, 177, 177*f*
semiconductor nanoparticles, 307
Photocatalytic activity (PCA) evaluation, 48, 55–56*t*
catalyst dosing effect, 53
light intensity effect, 54
organic pollutant effect, 53
pH effect, 53
photocatalytic efficiency, 52
photoreactor, 52
temperature effect, 54
Photoelectrocatalysis mechanism, 26–31
Photoelectrochemical technique, 25–31
Photo-Fenton reaction, 19–20, 19*f*
Photoluminescence spectroscopy, 107–108
Photoreactors
drugs, 316–317
dye, 313–316
organic and microorganism, 317–318
Photoremediation, 306–307
Physisorption isotherms, types of, 105
Phytodegradation, 357–358
Phytoextraction, 357–358
Phytoremediation, 357–362
Phytostabilization, 357–358
Phytostimulation, Rhizodegradation
Phytotoxicity, 385, 391–392
Phytovolatilization, 357–358
PNCs. *See* Polymer-based nanocomposites (PNCs)
Polyhydroxylated fullerene (PHF), 248–249
Polymer-based nanocomposites (PNCs), 48, 50–51*t*, 52
characterization of, 52
microscopic techniques, 52
spectroscopic techniques, 52
surface modification, 54
ligand exchange technique, 54
synthetic polymers, grafting of, 57
thermal analysis, 52
Polymeric carbon nitride. *See* Graphitic carbon nitride (GCN, g-C_3N_4)
Polymeric nanomaterials, 327
Polyol process, 374
Polyoxometalates (POMs), 25

This book belongs to Central Library BADJI Mokhtar-ANNABA UNIVERSITY

Copyright Elsevier 2024

Powder X-ray diffraction (PXRD), 101
PXRD. *See* Powder X-ray diffraction (PXRD)
Pyrethroid, 157

Q

Quantum dots (QDs), 327
  graphitic carbon nitride, 281–285, 283–284*t*
  nanocatalysts, 327

R

Reactive dyes, 174–175
Reactive oxygen species (ROS), 177–178, 177*f*, 212–215, 214*f*, 315–316
Reduced graphene oxide (rGO), 70–71
Remediation, 306
Reverse micelles, 7–8
rGO. *See* Reduced graphene oxide (rGO)
Rhizodegradation, 357–358
Rhodamine B, photocatalytic degradation of, 21–23, 248
Rhodium–antimony-codoped TiO_2 nanorods and titanate nanotube (RS-TONR/TNT) composite, 28–31
Rutile, 69

S

SBU. *See* Secondary building units (SBU)
Scanning electron microscopy (SEM), 106, 379
Scanning tunneling microscopy (STM), 380
SCXRD. *See* Single-crystal X-ray diffraction (SCXRD)
Sealed condensation approach, 294–297, 297*f*
Sea urchin-like 3D g-C_3N_4 structure, 294–297, 297*f*
Secondary building units (SBU), 96
Seed germination, nanomaterials effect on, 382–385
  assessment, 372
SEM. *See* Scanning electron microscopy (SEM)
Semiconductor-based nanocomposites, 168
Semiconductor nanoparticles, 143–144, 307
Semiconductor nanophotocatalyst, 148–149
Semiconductor photocatalysis
  advantages, 92
  drawbacks, 92–93
  role of, 68
Semiconductor photocatalysts, 16–17, 43
Sewage contamination, 25
Side-glowing optical fibers (SOFs), 70–71
Silica nanomaterials, 325
Single-crystal X-ray diffraction (SCXRD), 101–102
SOFs. *See* Side-glowing optical fibers (SOFs)
Soil contamination, pesticides effects on, 160–161
Soil microorganisms, antibiotic pollutants, 199, 200*t*
Soil remediation, nanotechnology for
  bioremediation, 357–362
    heavy metal removal, 348–351, 350*t*
    hopes and uncertainties, 362
    pesticides and persistent organic pollutants
      biosensing systems, 355–357
      nanomaterials used for, 353, 354*t*
      photocatalytic degradation, 352–353, 352*f*
    phytoremediation, 357–362
    uses and applications, 346–348
Solar active photocatalytic degradation, of pharmaceuticals
  graphene-based materials, 70–71
  mechanism, 68–69
  metal-organic frameworks, 71–73
  novel composites, 73
  titania-based materials, 69–70
Solar photocatalyst reactor, 317
Sol–gel synthesis, 374
  doped photocatalysts, preparation of, 4
  petrochemical pollutants, 136–137
Solvent-exfoliated graphene (SEG), 260–261
Solvothermal/hydrothermal method, 97–98
Solvothermal/nonsolvothermal method, 97–98
Sonochemical synthesis, 6–7, 100
SQUID magnetometry, 382
Sulfamethoxazole, UV-vis spectra for, 212, 214*f*
Sulfonylurea herbicides, 157
Sulfur dyes, 174–175
Sunlight, antibiotic degradation by, 212–224, 216–221*t*
  environmental implications, 224–225
  natural waters, 215–223, 223*f*
  pH, 224
  photosensitizers, 223–224
Synthetic dyes, 15–16, 174–175, 175*f*

T

TEM. *See* Transmission electron microscopy (TEM)
Ternary copper indium disulfide, 21–23
Tetracycline removal, 72
TGA. *See* Thermogravimetric analysis (TGA)
Thermal oxidative etching, 288–289, 288*f*
Thermogravimetric analysis (TGA), 102–104, 103*f*
Three-dimensional graphitic carbon nitride, 294–297, 298*t*
Three-dimensional photocatalyst structure, 312
Ti-changed volcanic cinders (TVA), 313–314
TiO_2-coated activated carbon, 247
TiO_2/CQDs nanocomposites, 263
TiO_2-rGO composite, 70–71
TiO_2/SiO_2-supported CNFs, 264
Titanium dioxide (TiO_2), 134–135
  nanoparticle, 26–28
  photocatalysis, 179
    antibiotics degradation, 225–230, 226–228*t*
    antibiotics transformation stages, 229, 229*f*

This book belongs to Central Library BADJI Mokhtar-ANNABA UNIVERSITY
Copyright Elsevier 2024

carbon nanotubes (CNTs), 250–252
fullerene, 249–250
limitations, 230
photocatalytic degradation, 69–70
Tollen's method, 374
Total organic carbon (TOC) removal, 136–137
Transmission electron microscopy (TEM), 106, 379
Two-dimensional photocatalyst structure, 311–312

U

Ultrasonic liquid exfoliation method, 289
Ultraviolet–visible diffuse reflectance spectroscopy (DRS), 104
UTSA-38 photocatalyst, 114
UV and UV/H_2O_2 process, for pesticides degradation, 164–165
UV/visible light-driven photocatalysts, 134–135
UV-visible spectroscopy, 380–381

V

Vat dyes, 174–175
Vertical gradient freeze growth (VGFG) method, 285–287, 286*f*
Vibrating sample magnetometry (VSM), 382

W

Wastewater management. *See also* Pharmaceutical waste treatment
Wastewater treatment. *See also* Solar active photocatalytic degradation, of pharmaceuticals
biological treatment, 41–42
conventional methods, 39–41, 41*t*
global water usage, 39, 40*f*
photocatalysis, 42–45
principles of, 42–45
scope of, 74
photocatalytic activity evaluation (*see* Photocatalytic activity evaluation)
polymer as support, 47
polymeric substrates, 47
different methods for supporting nanoparticles on, 48–51
solar photocatalyst reactor for, 317
support system
nanocomposites, synthesis of, 48, 49*t*
NPs drawbacks, in powder form, 46
NPs immobilization, advantages, 46–47
photocatalytic activity, 48
polymer, 47
polymer-based nanocomposites, 48, 50–51*t*
polymeric substrates, 47
waterborne disease, 39
Wastewater treatment plants (WWTPs), 195, 198
Water oxidation method, 16–17
Water pollution, 168, 173
Water-soluble pesticides, 159
Water treatment residual nanoparticles (nWTR), 351
Wet scanning electron microscopy (Wet-SEM), 379
Wide bandgap (WBG) photocatalysts, 1

X

XPS. *See* X-ray photoelectron spectroscopy (XPS)
X-ray absorption fine structure (XAFS) spectroscopy, 101
X-ray diffraction (XRD), 380
X-ray photoelectron spectroscopy (XPS), 106–107, 380

Z

Z-contrast transmission electron microscopy (Z-TEM), 379
Zeolites
nanoparticles, 147
pesticides degradation, 163
Zeolitic imidazole framework (ZIF)-based metal oxides, 184–187, 185*f*, 188*f*
Zero-dimensional photocatalyst structure, 308–309
Zinc oxide (ZnO)
imidazole-derived nanoparticles
crystal structure and TEM image, 184, 185*f*
synthesis, 184, 184*f*
photocatalysts, organic pollutants degradation, 134–135
ZnAl-chloride hydrotalcite, 87–88
Zn-based metal-organic frameworks, 96–97, 111–114
Zn-Fe carbonate hydrotalcite, 86, 88
Zn/Fe hydrotalcite, 87
ZnO/GO nanocomposite, 21–23, 24*t*
$ZnSnO_3$ hollow nanospheres, 70

This book belongs to Central Library BADJI Mokhtar-ANNABA UNIVERSITY
Copyright Elsevier 2024

This page intentionally left blank

This book belongs to Central Library BADJI Mokhtar-ANNABA UNIVERSITY

Copyright Elsevier 2024

Nano-Materials as Photocatalysts for Degradation of Environmental Pollutants

CHALLENGES AND POSSIBILITIES

EDITED BY
PARDEEP SINGH
ANWESHA BORTHAKUR
P.K. MISHRA
DHANESH TIWARY

Explores recent developments in degradation of organic pollutants using various kind of heterogeneous catalysts

Nano-Materials as Photocatalysts for Degradation of Environmental Pollutants: Challenges and Possibilities contains both practical and theoretical aspects of environment management through the process of photodegradation by using various heterogeneous catalysts. However, an emphasis has been made on trends and probable new catalysts, which works on solar energy. The main focus is on the degradation of harmful pollutants like petrochemicals, crude oils, dyes, and xenobiotic pharmaceutical waste and other common pollutants. The chapters incorporate both theoretical and practical aspects, and the information therein could be used as a basis for further study.

This book is useful for the undergraduate or university students, teachers, and researchers, especially those working in the areas of photocatalysis through heterogeneous catalysts. Primary audiences are chemical engineers, environmental engineers and scientists, scholars working on the management of hazardous waste, scientists working in the fields of materials science, and civil engineers working on wastewater treatment.

Key Features

- Reviews recents trend in photodegradation of organic pollutants
- Includes many degradation mechanisms of organic pollutants using various catalysts
- Includes examples for the degradation of organic pollutants from various sources, for example, pharmaceuticals, dyes, and pesticides
- Discusses the effect of nanocatalysts on soil, plants, and the ecosystem

Pardeep Singh, assistant professor, Department of Environmental Studies, PGDAV College, University of Delhi, New Delhi, India

Anwesha Borthakur, Marie Skłodowska Curie postdoctoral fellow, Katholieke Universiteit Leuven (KU Leuven), Parkstraat, Leuven, Belgium

P.K. Mishra, professor and head, Department of Chemical Engineering and Technology, Indian Institute of Technology (BHU), Varanasi, India

Dhanesh Tiwary, professor and head, Department of Chemistry, Indian Institute of Technology, Banaras Hindu University, Varanasi, India

ISBN 978-0-12-818598-8
9 780128 185988

ELSEVIER elsevier.com/books-and-journals

This book belongs to Central Library BADJI Mokhtar-ANNABA UNIVERSITY

Copyright Elsevier 2024